



PICES  
6TH  
ANNUAL MEETING

1997. 10. 14-10. 26

제6차 북태평양해양과학총회논문집 (I)



.....  
P I C E S

해 양 수 산 부

**PICES**  
**6TH**  
**ANNUAL MEETING**

**1997. 10. 14 - 10. 26**

**제6차 북태평양해양과학총회논문집( I )**

**P I C E S**

**해 양 수 산 부**

**KOREAN MINISTRY OF MARITIME AFFAIRS & FISHERIES**

# 발 간 사

북태평양해역은 해양환경이나 해양자원면에서 우리 나라나 미국, 일본 등 연안국가에게는 매우 중요한 해역이며 주요 해양국간에 해양자원개발의 각축전이 전개되고 있는 곳이기도 합니다. 동 해역의 연안국들은 90년 12월 12일 북태평양해양과학기구(PICES)헌장을 채택하고 생물자원, 해양환경, 기후변동 및 생태계전반에 걸친 연구활동을 촉진시키고 활발한 정보교환 등을 통한 해양과학 발전을 위해 정부차원에서 협력하기로 한 바 있습니다. 이에 따라 92년 3월 24일 캐나다, 미국, 일본, 중국 등 4개국 회원국이 이 기구에 가입하였고 러시아가 5번째 회원국으로, 그리고 우리 나라는 95년 7월 6번째 회원국으로 가입하였습니다.

그간 우리 나라를 비롯한 여러 회원국의 많은 해양과학자들이 PICES 총회에서 좋은 논문을 많이 발표하여 이 지역의 해양과학발전에 크게 이바지하여 왔습니다. 더욱이 지난해에는 부산 해운대에서 해양수산부 주관으로 제6차 총회를 개최하여 한국 해양과학의 면모를 과시하기도 하였습니다.

해양수산부에서는 세계 해양과학자들의 이러한 귀중한 논문들을 모아 우리 나라의 해양과학자는 물론 해양수산분야에 종사하는 모든 분들에게 널리 배포하여 해양과학의 발전을 통한 해양산업의 번영에 기여했으면 하는 바램으로 이를 한 권의 책으로 엮어내게 되었습니다. 아무쪼록 이 한권의 책이 우리 나라 해양과학 연구에 좋은 참고자료가 되었으면 합니다.

1998년 8월

해 양 수 산 부

국제협력관 안 국 전

## 제 6 차 PICES 총회 위원회별 발표논문

구 분	Poster	Oral	Invited	Total
BASS Symposium (해분해역 심포지엄)	3	0	9	12
POC Papers (물리해양 및 기후위원회)	2	6	1	9
POC Topic (물리해양 및 기후위원회)	12	27	1	40
BIO & FIS Topic (생물해양위 & 수산과학위원회)	7	10	1	18
BIO Papers (생물해양위원회)	2	9	0	11
FIS & BIO Topic(수산과학위 & 생물해양위원회)	2	13	1	16
FIS Papers (수산과학위원회)	17	8	0	25
MEQ Topic & Papers (해양환경위원회)	11	14	0	25
BIO & MEQ (생물해양위 & 해양환경위원회)	7	15	2	24
Total	62	102	15	179

# I. Table of Contents

1. BASS Symposium(BASS(Basin Scale Study) 심포지움) .....	5
Ecosystem dynamics in the eastern and western gyres of the subarctic Pacific-lower trophic modelling(아북극 태평양의 외해인 동부와 서부 권역에서의 생태계 역학 연구 - 하위 영양단계 모델) .....	
	7
Possible differences in structure at lower trophic levels of ecosystems in the eastern and western subarctic Pacific(Abstract)(동·서부 아북극 태평양 생태계에서 유추 가능한 하위 영양단계 생물들의 구조적 차이점 연구(요약문)) .....	
	10
2. POC Papers(물리해양분과) .....	15
Time scale of tracer diffusion in the North Pacific intermediate layer(북태평양 중간층에서 추적자 확산의 시간 규모) .....	
	17
Retrospective analysis of sea surface wind fields over the North Pacific during the period of 1899~1995(1899~1995 기간동안 북태평양상 해표면 바람장의 소급적 분석) ...	
	27
Diagnostic calculation of the North Pacific circulation based on a seasonal climatic data(계절적 기후자료에 근거한 북태평양 순환의 진단 계산) .....	
	32
No evidence for large interannual variations in oceanic carbon uptake(해양탄소 흡수에 있어서의 대형 경년변동의 미확인) .....	
	44
3. POC Topic(물리해양분과) .....	53
Seasonal variability of currents in the area of eastern Sakhalin(사할린 동쪽 해역에서 해류의 계절 변동) .....	
	55
Salt ice and dense water production in the northern Okhotsk Sea coastal polynyas in winter 1995~1996(1995~1996 겨울 북쪽 오후츠크해 연안 비빙결수권에서 염빙과 무거운 해수의 생성) .....	
	70
Some features of mesoscale and small scale water dynamics in the southern Okhotsk sea seen by the ers-1 synthetic aperture radar(ERS-1 합성 개구 레이더에 의해 관측된 남쪽 오후츠크해에서의 중규모 및 소규모 해양역학의 몇 가지 특징) .....	
	78
Mechanisms of influence of coastal and shelf waters on the open sea bioproductivity (외해역 생물생산에 미치는 연안과 대륙붕 해수의 영향 미케니즘) .....	
	84
Present status on NEAR-GOOS real time data base at the Japan Meteorological Agency(일본 기상청의 NEAR-GOOS 실시간 데이터 베이스 현황) .....	
	114
Some oceanographic features of the Okhotsk Sea derived from historical hydrographic observations(역사적인 해양특성관측치로부터 유추된 오후츠크해의 몇가지 해양학적 특징) .....	
	120
Thermal structure of the north-western Japan Sea(East Sea) upper layer : climate and variability(북서 동해 상층의 온도 구조 : 기후와 변동) .....	
	124

4. BIO & FIS Topic(생물해양분과 및 수산과학분과) ..... 131

Importance of micronektonic fishes as revealed from the stomach analysis of neon flying squid, *Ommastrephes bartrami* in the northwestern North Pacific(북태평양의 북서부에 서식하는 빨강오징어(*Ommastrephes bartrami*)의 위내용물 분석으로 나타난 미세유영생물의 중요성) ..... 133

Daily and seasonal feeding dynamics of the two myctophid species, *Stenobrachius leucopsarus* and *S. nannochir* in the mesopelagic zone of Bering Sea.(베링해 중층에 서식하는 2종의 샛비늘치류(*Stenobrachius leucopsarus*와 *S. nannochir*)의 일별·계절별 섭식 연구) ..... 143

Stable carbon and nitrogen isotope ratios of mesopelagic micronekton and their prey (중층 서식 미세유영생물과 그들의 먹이에서 측정된 안정 동위원소 탄소와 질소의 비율) ..... 157

Feeding habits and diel vertical migration patterns of the three dominant myctophid fishes in the western subarctic and transitional Pacific(서부 아북극 태평양과 경계 지역에 서식하는 샛비늘치류(myctophid fish) 3종의 섭식 특징과 일별 수직 회유 경로) ..... 169

Stomach contents of Dall's poropises in the north Pacific ocean(북태평양에 서식하는 돌고래 Dall's poropises의 위 내용물 분석) ..... 173

Distribution and stomach contents of *Maurollicus muelleri* in the Japan Sea(East Sea) (동해(일본해)에 서식하는 엘통이(*Maurollicus muelleri*)의 분포와 위 내용물 분석) ..... 182

Distribution and relative abundance of some micronektonic fishes in the Aleutian Basin(알류산 해분에 서식하는 몇몇 미세 유영생물 어류의 분포와 상대 풍도 조사) ... 188

Community ecology of juvenile pollock(*Theragra chalcogramma*) and other midwater taxa in the eastern Bering Sea during August-October 1987(1987년 8~10월에 동부 베링해에 서식하는 명태(*Theragra chalcogramma*) 미성어와 다른 중층 서식 종의 군집 생태 연구) ..... 201

Predation on micronekton by demersal fishes(저어류에 의한 미세 유영생물의 포식 조사) ..... 214

5. BIO Papers(생물해양분과) ..... 219

Distributional characters of salps in relation to oceanographic condition in the Korean waters(한반도 주변의 해양환경에 따른 살파(salps)의 분포 특징) ..... 221

Long-term change in zooplankton biomass in the Korean waters(한반도 수괴에서 동물플랑크톤 생물량의 장기 변동 조사) ..... 229

The effect of changing environmental regimes on Japanese common squid, *Todarodes pacificus* populations: a possible scenario(일본 오징어(*Todarodes pacificus*) 군집에 미치는 환경 변화 효과 예측) ..... 238

Comparison of zooplankton communities between the central and western subarctic Pacific Ocean(중앙 태평양과 서부 아북극 태평양 사이의 동물플랑크톤 군집 구조 비교) ..... 247

Interannual-interdecadal variations in zooplankton biomass, chlorophyll concentration and physical environment in the subarctic Pacific and Bering Sea(아북극 태평양과 베링해의 물리 환경과 동물플랑크톤 생물량, 엽록소 농도의 시간에 따른 변화 조사) ...	254
West-east comparison of seasonal variation in phytoplankton biomass in the subarctic North Pacific Ocean(아북극 북태평양의 서부와 동부에서 식물플랑크톤 생물량의 비교) .....	264
Life cycles of <i>Neocalanus flemingeri</i> and <i>N. plumchrus</i> (Calanoida, Copepoda) in the western subarctic Pacific(서부 아북극 태평양에 서식하는 <i>Neocalanus flemingeri</i> 와 <i>N. plumchrus</i> 의 생활사) .....	269

## II. Table of Contents

### 6. FIS & BIO Topic(수산과학 및 생물해양분과) ..... 283

An estimation of spawning grounds of skipjack in the tropical western Pacific using and OGCM(OGCM을 이용한 열대 서부 태평양에 서식하는 가다랭이(skipjack)의 산란장 조사) .....	285
Variations of fish community structure in the Yellow Sea and the Bohai Sea(황해와 발해만에 서식하는 어류 군집 구조 변이) .....	287
Mechanisms of the seasonal variation of chlorophyll in the North Pacific : A study using an ecosystem model embedden in the ocean general circulation model(북태평양의 계절별 엽록소 변이 기작 : 일반 해양 순환 모델에 기초한 생태계 모델을 사용) .....	297
Changes associated with the 1989~90 ocean climate shift and effects of British Columbia steelhead( <i>O. mykiss</i> ) populations(British Columbia 지역에서 발생한 1989~90년 해양의 기후변동과 무지개송어(Steelhead, <i>O. mykiss</i> )에 미친 영향) .....	303
Use of fluorescent probes for biochemical monitoring of environmental contamination (생화학적 형광 probes를 이용한 환경오염) .....	315

### 7. FIS Papers(수산과학분과) ..... 319

Distribution and stock condition of major groundfishes in the East China Sea and the Yellow Sea from bottom trawl survey(동중국해와 황해에서 저층 트롤에 의해 행해진 주요 저서어종의 군집상태와 분포 조사) .....	321
Results from the 1997 echo integration and midwater trawl survey for the Bering Sea walleye pollock by the R/V Pusan 851(1997년 조사선 부산 851호에 의해 행해진 베링해 명태의 중층 트롤과 음향 조사 결과) .....	333
Results of the Bering Sea walleye pollock survey by the Korean R/V Pusan 851 during May-June 1997(1997년 5~6월 동안 조사선 부산 851호에 의해 조사된 베링해	

명태 조사사업의 결과) .....	359
Distribution and migration of blue crab <i>Portunus trituberculatus</i> in Korean waters (한반도 수역에서 꽃게( <i>Portunus trituberculatus</i> )의 분포와 이동경로) .....	363
Growth and mortality of blue crab <i>Portunus trituberculatus</i> in the East China Sea (동중국해에 서식하는 꽃게( <i>Portunus trituberculatus</i> )의 성장과 사망률 조사) .....	371
<b>8. MEQ Topic &amp; Papers(해양환경분과) .....</b>	<b>379</b>
A comprehensive assessment of the impacts of contaminants on fish from an urban waterway(도시 하수로부터의 오염물질이 어류에 미치는 영향 평가) .....	381
Mariculture and the environment : The importance of water movements Satoru Toda National Research Institute of Aquaculture, Fishery Agency Tamaki, Watarai, Mie 519-04 Japan(양식과 환경 : 해수이동의 중요성(일본 미에현 사토루 토다 국립양식 연구소)) .....	386
<b>9. BIO &amp; MEQ(생물해양 및 해양환경분과) .....</b>	<b>395</b>
The harmful algal blooms in shrimp ponds in North China(중국 북부지방의 새우양식지(養殖池)에서의 유해조류의 대발생) .....	397
Recent red tides in Kunsan inner harbor- 'The Kunsan type red tide' (최근 군산내항에서 발생한 적조-군산형 적조) .....	411
<b>10. 기타 .....</b>	<b>419</b>
PICES WG-10 bibliography for the circulation of the Japan/East Sea and adjacent waters(동해 및 그 주변해의 해수 순환에 관한 문헌목록(PICES Working Group-10)) ...	421
The climate variations in the Japan/East Sea(동해(일본해)에서의 기후변동) .....	439
PICES WG-10 Report : Circulation and ventilation in the Japan/East Sea and its adjacent areas(PICES Working Group-10 (동해/주변해의 해수순환실무그룹) 보고서 : 동해와 그 주변해에서의 해수 순환) .....	450
North Pacific Marine Science Organization(PICES) (북태평양해양과학기구(PICES)) .....	456
NPTT Working Group Report-JGOFS Korea Programme(한국 JGOFS (전세계해양 물질순환연구) 프로그램-북태평양 Task Team 실무그룹 보고서) .....	463
Revised PICES CCCC agenda-implementation panel meeting(수정된PICES-CCCC 사업계획 실행위 회의) .....	498



# 1. BASS Symposium

## (BASS(Basin Scale Study)심포지움)

Ecosystem dynamics in the eastern and western gyres of the subarctic Pacific-lower trophic modelling(아북극 태평양의 외해인 동부와 서부 권역에서의 생태계 역학 연구-하위 영양단계 모델) ..... 7

Possible differences in structure at lower trophic levels of ecosystems in the eastern and western subarctic Pacific(Abstract)(동·서부 아북극 태평양 생태계에서 유추 가능한 하위 영양단계 생물들의 구조적 차이점 연구(요약문)) ..... 10

## Ecosystem Dynamics in the Eastern and Western Gyres of the Subarctic Pacific - Lower Trophic Modelling -

Michio J. Kishi+ and Bruce Frost++

+ Hokkaido University ++ University of Washington

Our obligation is to review numerical models in subarctic Pacific focused on the lower trophic model. We divide papers roughly into two types. One is diagnostic model and the other is deterministic model. Glover et al.(1994), Obata et al.(1996), Behrenfeld and Falkowski(1997) and Longhurst (1995) belong to the former and Kawamiya et al.(1995,1997), Evans and Garcon (1997), Yoshimori et al.(1995), Fasham et al.(1990) and Kawamiya(1997) belong to the latter.

Glover et al.(1994) and Obata(1996) are fundamentally based on the same idea. At first they define the mixed layer depth from Levitus data. In Glover et al.(1994) they used N-P-Z model to get steady state solution in a mixed layer which is a function of total nitrogen derived from winter time mixed layer depth. There cannot be found the clear difference between the east and the west in Northern Pacific (NP) phytoplankton distribution in their model.

In Obata et al.(1996) they used satellite data to get light condition. They pointed out the difference between the east and the west of NP is the timing of the month when MLD becomes shallower than critical depth, that is, it is a good condition to spring bloom.

Behrenfeld and Falkowski(1997)'s model is mainly based on satellite data. Their results of primary production map show the same order between the east and the west in NP although rather high values appears mainly at the east side.

Longhurst (1995) divided all oceans into many provinces based on mainly physical structure adding the knowledge of CZCS data. According his calcification, NP is divided into two parts, i.e., the east and the west.

Next we want to review the deterministic model. One dimensional models

have been developed by many researchers and adapted in many ocean points. If we focus on NP region, Kawamiya et al.(1995,1997), Evans and Garcon (1997), Yoshimori et al.(1995) made a one dimensional models. Kawamiya et al.(1995,1997) used their KKWS model and pointed out the HNLC in station Papa is explained by high grazing pressure. Yoshimori et al.(1995) used Frank's NPZD model to explain the spring bloom at Sanriku region (Eastern NP) and concluded the shallow surface mixed layer caused early days of spring bloom at the station near Hokkaido.

Three dimensional model containing the seasonal variation of phytoplankton were developed by Fasham et al.(1990) and Kawamiya(1997). Especially, Kawamiya(1997) focused on the regional characteristics of seasonal variation of phytoplankton in NP region. Based on the numerical experiment he divided the NP into seven domain. The difference of phytoplankton seasonal variation between the east and the west of NP is caused by the depth of mixed layer. i.e., whether strong spring bloom exist or not depend on whether strong deepening of mixed layer in March occurs or not.

## *References*

- Behrenfeld M.J., and P.G. Falkowski (1997) Photosynthetic rates derived from a satellite-based chlorophyll concentration. *Limnol.Oceanogr.*,42, 1-20.
- Evans, G.T. And V.C. Garcon ed. (1997) One-dimensional models of water column biochemistry. -Report of workshop held in Toulouse, France, 1995. JGOFS Report.
- Fasham, M.J.R., H.W.Ducklow and S.M.Mckelvie (1990) A nitrogen based model of plankton dynamics in the oceanic mixed layer. *J.Mar.Res.*, 48, 591-6339.
- Glover, D.V., J.S. Wroblewski and C.R.McClain (1994) Dynamics of the transition zone in coastal zone color scanner - sensed ocean color in the North Pacific during oceanographic spring. *J. Geophys. Res.*, 99, c4, 7501-7511.
- Kawamiya,M., M.J.Kishi, Y. Yamanaka and N. Suginoara (1995) An ecological-physical coupled model applied to station Papa. *Jour. Oceanogr.*, 51, 635-664.
- Kawamiya,M. (1997) Mechanisms of the seasonal variation of chlorophyll in the north Pacific : A study using an ecosystem model embedded in an ocean general circulation model. Ph.D.Thesis, University of Tokyo. (Part of which will be submitted to JGR)
- Kawamiya,M., M.J.Kishi, Y. Yamanaka and N. Suginoara (1997) Obtaining

reasonable results in different oceanic regimes with the same ecological-physical coupled model. *Jour. Oceanogr.*, 53, 397-402.

Longhurst,A.(1995) Seasonal cycles of pelagic production and consumption. *Prog. Oceanogr.*,36, 77-167.

Obata,A., J. Ishizaka and M. Endoh (1996) Global verification of critical depth theory for phytoplankton bloom with climatological in situ temperature and satellite ocean color data. *J. Geophys. Res.*, 101,C9,20657-20667.

Yoshimori,A., J. Ishizaka, T. Kono, H.Kasai, H.Saito, M.J.Kishi and S.Taguchi (1995) Modelling of spring bloom in the western subarctic Pacific (off Japan) with observed vertical density structure. *Jour. Oceanogr.*, 51,471-488.

6AM1997-SB12

## Possible differences in structure at lower trophic levels of ecosystems in the eastern and western subarctic Pacific (Abstract)

Akira Taniguchi

Laboratory of Aquatic Ecology, School of Agriculture, Tohoku University, Sendai 981, Japan

It has been commonly said that net-zooplankton such as copepods, euphausiids, amphipods, pteropods, tunicates and hydromedusae are main herbivores which control productivity of phytoplankton from the top and also control productivity of pelagic fish populations from the bottom over the subarctic Pacific. However, an apparent predominance of microzooplankton as major grazers is recently reported from the eastern part of the subarctic Pacific, or in the Gulf of Alaska, where standing stock of net-zooplankton is particularly small, while that of macronutrients is relatively large. This makes a striking contrast to the situation in the western part or in the Oyashio region, where standing stock of net-zooplankton is fairly large but nutrient stocks are very small. In the latter region, ratio of microzooplankton to net-zooplankton in biomass is not very high, around 5-15% and iron precipitation from the air is said to enhance the phytoplankton growth.

The Bering Sea north of Aleutian Chain and the sea area south of the chain are likely to make another contrasting pair. In the southern area, rich nutrient stock seems to be left unused by relatively smaller biomass of net-zooplankton as well as of phytoplankton. This situation is essentially the same with that seen in the Gulf of Alaska. On the other hand, the Bering Sea reveals the nature of the most productive sea areas, as seen in the Oyashio region. Namely, biomasses of both zooplankton and phytoplankton are large and relative biomass of microzooplankton is not high. However, there can be seen the essential difference between the Bering Sea and the Oyashio region: while nutrient stock is very large in the Bering Sea (largest among the subarctic Pacific), it is very low (lowest among the subarctic Pacific) in the Oyashio region. Then, the following two points can be

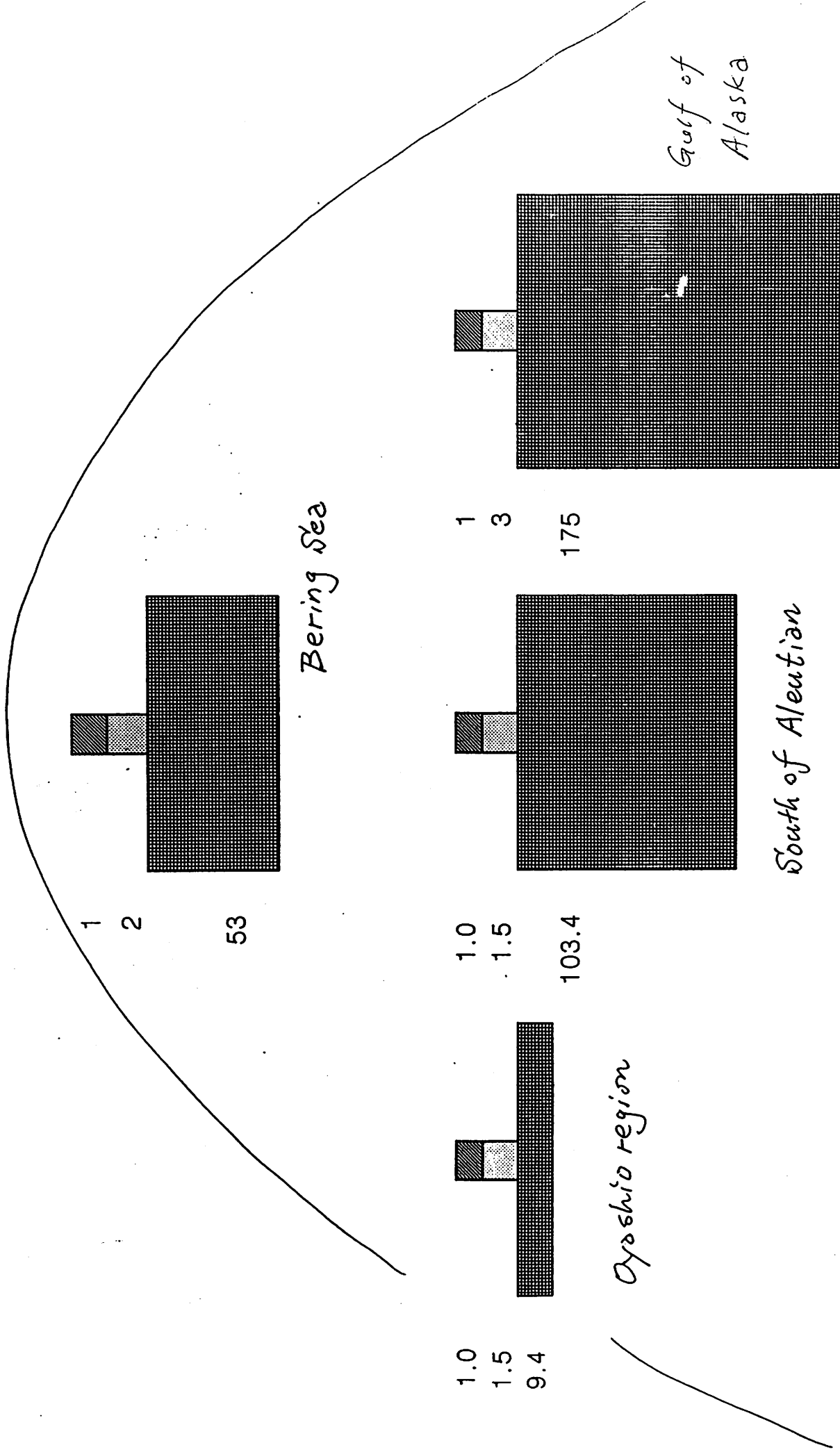
indicated by this fact, i.e., (1) transfer efficiency from nutrients through net-zooplankton is highest in the Oyashio region, and (2) carrying capacity of the rest sea areas, particularly of the Bering Sea, can be expanded to large extent in future. To explore this high potential productivity of the ocean by artificial ways, we must carefully identify so-called key factor or mechanism that controls phytoplankton productivity in individual sea areas of the subarctic Pacific.

Table 1. Average values of stocks of nitrate-nitrogen, phytoplankton chlorophyll a and net zooplankton wet weight (>330 um) in surface layer of different open sea areas of the subarctic Pacific in summer. Equivalent carbon weight of each stock is also given.

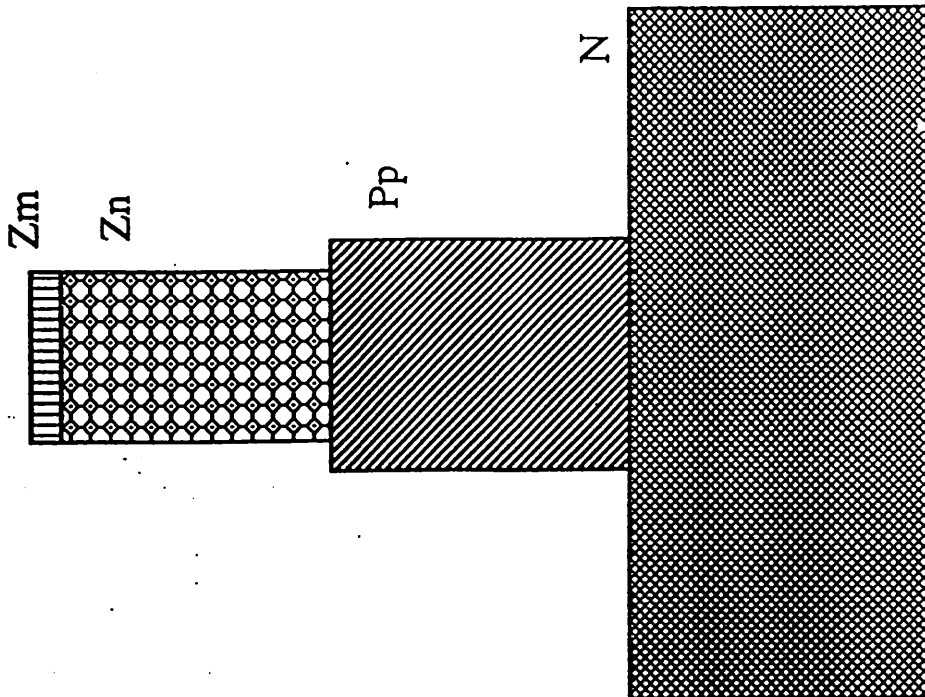
Sea area (Reference)	NO <sub>3</sub> <sup>a)</sup> (uM)(mgC m <sup>-3</sup> )	Phytoplankton <sup>b)</sup> (ugChl l <sup>-1</sup> )(mgC m <sup>-3</sup> )	Net zooplankton <sup>c)</sup> (mgWW m <sup>-3</sup> )(mgC m <sup>-3</sup> )
Bering Basin (2,4)	15 1193	0.9 45	450 22.5
South of Aleutian (2,4)	13 1034	0.3 15	200 10.0
Gulf of Alaska (1)	11 875	0.3 15	100 5.0
Oyashio (3,4)	2 159	0.5 25	340 17.0

Conversion factors to carbon weight: a) 12x106/16, b) 50, c) 0.05  
 Reference: 1 Frost (1983), 2 Motoda and Minoda (1974), 3 Saito (1996),

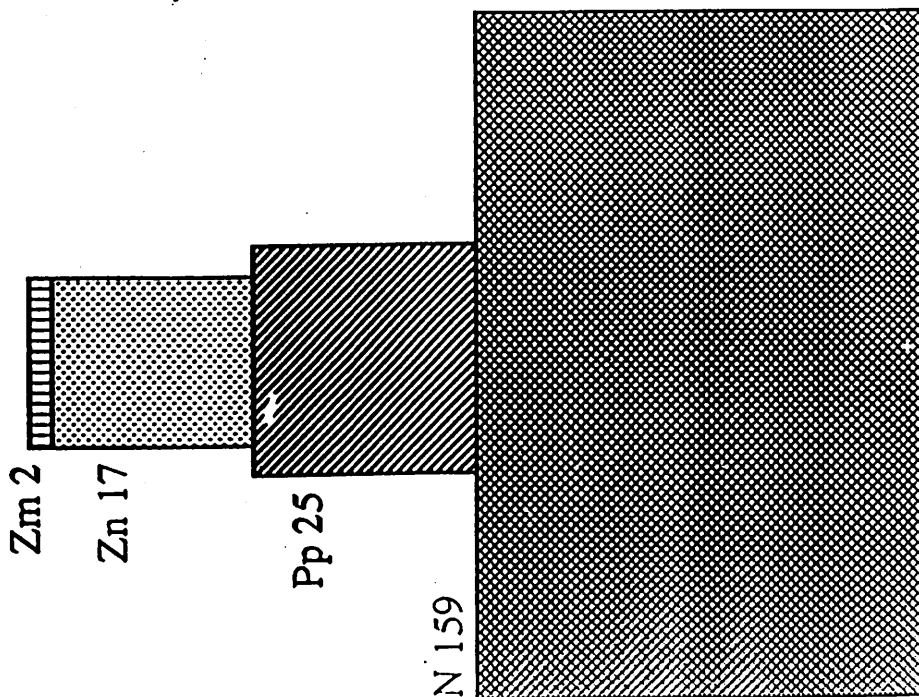
4 Taniguchi (1972)







Predation



## 2. POC Papers(물리해양분과)

- Time scale of tracer diffusion in the North Pacific intermediate layer  
(북태평양 중간층에서 추적자 확산의 시간 규모) ..... 17
- Retrospective analysis of sea surface wind fields over the North Pacific  
during the period of 1899~1995(1899~1995 기간동안 북태평양상 해표  
면 바람장의 소급적 분석) ..... 27
- Diagnostic calculation of the North Pacific circulation based on a seasonal  
climatic data(계절적 기후자료에 근거한 북태평양 순환의 진단 계산) ... 32
- No evidence for large interannual variations in oceanic carbon uptake  
(해양탄소 흡수에 있어서의 대형 경년변동의 미확인) ..... 44

# Time scale of tracer diffusion in the North Pacific intermediate layer\*

M.Endoh, G.Yamanaka and Y.Kitamura

Meteorological Research Institute  
Nagamine 1-1, Tsukuba, 305 Japan

e-mail: endoh@mri-jma.go.jp  
fax : +81-298-55-1439

## 1. Introduction

The North Pacific intermediate layer is characterized by North Pacific Intermediate Water (NPIW), which is a water mass known for its well-defined salinity minimum at around  $26.8 \sigma_\theta$ . Fresh NPIW has been considered to come from the subarctic surface layer, the freshest area in the North Pacific. In other words, the North Pacific intermediate layer is connected to the subarctic surface. The sea surface temperature in the subarctic North Pacific has been noted to correlate clearly with climate change over a decade-scale timescale, by the analysis of both observed data [Tanimoto *et al.*, 1994] and coupled model data [Yukimoto *et al.*, 1996]. The subarctic gyre is also regarded as a possible sink for green-house gases such as CO<sub>2</sub> [Tsunogai *et al.*, 1993] and chlorofluorocarbons (CFCs) [Warner *et al.*, 1996]. These results suggest that the North Pacific intermediate layer is associated with climate through the subarctic surface. To understand how the North Pacific climate change affects the ocean interior, it is necessary to clarify how subarctic waters spread into this intermediate layer and to examine its relevant timescale.

CFCs and idealized passive tracers are often used to analyze ocean circulation obtained in the OGCM. Dissolved CFCs are useful for the validation of ocean model processes. England [1994] studied the sensitivity of the simulated CFC distributions to the model parameterization of air-sea CFC fluxes. Robitaille and Weaver [1995] and England [1995a] examined different formulations of subgrid-scale mixing, comparing the simulated CFC distributions to observations.

Idealized passive tracers are also useful for visualization of path of water spreading. For example, Cox [1985] used a passive tracer with radioactive decay with half-life of 12.3 years (tritium) to make a distinction between ventilated and unventilated regions in the OGCM. Idealized passive tracers are also used to estimate ventilation timescale of water spreading. As an example, England [1995b] employed "age tracer", where age is defined as time taken for water at the sea surface to arrive at the ocean interior in complete diffusion and advection balance.

Firstly we present flow and density fields obtained in the OGCM and paths of NPIW spreading (Yamanaka *et al.* [1997a]). Then, the paths are revealed by tracer experiments using tritium-type tracers with radioactive decay. Then, we estimate timescale of NPIW spreading using conservative tracer having a distinct temporal peak of source (Yamanaka *et al.* [1997b]).

## 2. NPIW and Intermediate Layer Circulation in the OGCM

### a. Ocean circulation model

---

\*The present paper is based on Yamanaka *et al.* [1997b].

The OGCM we used has a North Pacific domain from 10°N to 60°N, and 120°E to 110°W, with realistic bottom topography and continental boundary. The grid spacing is 2° longitude by 1° latitude with 28 vertical levels. The effect of mesoscale eddies is taken into account implicitly by subgrid-scale mixing schemes [Gent and McWilliams, 1990]. Isopycnal, diapycnal, and isopycnal thickness diffusivity coefficients are treated as constant at  $5 \times 10^3 \text{ m}^2/\text{s}$ ,  $5 \times 10^{-5} \text{ m}^2/\text{s}$ , and  $5 \times 10^3 \text{ m}^2/\text{s}$ . The model is forced at the sea surface by the annual mean climatological wind stress [Hellerman and Rosenstein, 1983] and perpetually by winter climatology of temperature and salinity [Levitus, 1982]. Surface temperature and salinity are imposed by the Newtonian restoring term with a constant of  $(10 \text{ days})^{-1}$ . At the southern boundary along 10°N and the deeper levels below 2000 m, temperature and salinity are restored toward Levitus climatology with a constant of  $(15 \text{ days})^{-1}$  and  $(360 \text{ days})^{-1}$  to represent water masses of South Pacific origin. In the Okhotsk and Bering Seas, temperature and salinity are restored to the climatological value with a constant of  $(15 \text{ days})^{-1}$  to represent high density water mass formation. The model was integrated to equilibrium.

### b. Simulated NPIW and intermediate layer circulation

Results of NPIW simulation are presented in Figures 1 and 2. Figure 1a shows simulated salinity distribution along 180°E with the observed [Levitus, 1982] salinity distribution for reference (Figure 1b). Figure 2 shows simulated salinity and velocity distributions at  $26.8 \sigma_\theta$ .

Simulated salinity along 180°E (Figure 1a) demonstrates a low salinity tongue (33.9-34.3 psu) which extends southward at intermediate depths. This salinity minimum is located at around  $26.8 \sigma_\theta$ . Simulated salinity at  $26.8 \sigma_\theta$  (Figure 2a) shows the low salinity water (33.5-34.4 psu) throughout the North Pacific north of 15°N and the lowest salinity in the Okhotsk Sea. Isopycnal mixing was found to be important in the low salinity water spreading, and NPIW representation depends on isopycnal diffusivity.

We also found that the modeled NPIW has two fresh water sources with sensitivity experiments. For the upper intermediate layer ( $26.4\text{-}26.7 \sigma_\theta$ ), the source is in the northwestern subarctic surface, where precipitation maintains low salinity [Oberhuber, 1988]. For the lower intermediate layer ( $26.8\text{-}27.4 \sigma_\theta$ ), the source is in the subsurface Okhotsk Sea, where high density water mass formation occurs due to brine rejection through sea-ice formation and due to vertical mixing near the Kurile Islands [Kitani, 1973; Talley, 1991].

The general pattern of the intermediate layer circulation is clockwise in mid latitudes (Figure 2b). The boundary current leaves the west coast east of Japan and flows eastward, corresponding to the Kuroshio Extension in upper layer circulation. A major portion of the eastward flow turns southward in the eastern North Pacific at 160°W-140°W.

We used these flow and density fields to calculate passive tracer advection and diffusion in the following experiments.

### 3. Tracer experiments for origins of fresh water in NPIW

We introduce an idealized passive tracer having a uniform or localized source function, and examine fresh water spreading from the two source regions of the modeled NPIW.

To obtain a steady state, a tracer has a sink term due to radioactive collapse such as tritium. Tracers are governed by the following advective-diffusive equation;

$$\frac{\partial Tr}{\partial t} + \mathbf{u} \cdot \nabla Tr = -\lambda Tr + \nabla \cdot (\mathbf{K} \nabla Tr) \quad (1)$$

$\lambda$  is a constant  $(50 \text{ years})^{-1}$  corresponding to the radioactive collapse rate. Isopycnal, diapycnal and isopycnal thickness diffusivity coefficients are treated as  $5 \times 10^3 \text{ m}^2/\text{s}$ ,  $5 \times 10^{-5} \text{ m}^2/\text{s}$ , and  $5 \times 10^3 \text{ m}^2/\text{s}$ , the same values as used in the OGCM.

We found that the modeled NPIW has two fresh water sources: the northwestern subarctic surface and the subsurface Okhotsk Sea (Yamanaka *et al.* [1997a]). Therefore, we set up two corresponding experiments, cases A and B. In case A, surface tracer concentration is restored to a value of  $Tr=1$  with a constant of  $(10 \text{ days})^{-1}$  in the subarctic gyre where the surface density is greater than  $26.0 \sigma_\theta$ . In case B, the tracer concentration is restored to a value of  $Tr=1$  with a constant of  $(10 \text{ days})^{-1}$  from the surface to the bottom in the Okhotsk Sea. Eq. (1) is integrated until the steady state from an initial condition is  $Tr=0$  everywhere.

In case A, the tracer concentration decreases with density in the intermediate layer (Figure 3). At  $26.4 \sigma_\theta$  (Figure 3a), the highest tracer concentration is found in the northwest subarctic gyre where this density surface outcrops, and spreads south clockwise. At  $26.8$  and  $27.2 \sigma_\theta$  (Figures 3b and 3c), tracer concentrations are extremely low because the Okhotsk Sea outflow is not included. Tracer concentration at  $30^\circ\text{N}$  (Figure 3d) shows a core of highly concentrated tracers in the subsurface layer between  $170^\circ\text{W}$  and  $150^\circ\text{W}$  where the subsurface CFC maximum is observed. An intensified southward flow is also seen (Figure 2b), indicating that the high concentrated tracers are transported primarily by this southward advection in the upper intermediate layer.

In case B, tracers in the intermediate layer originate from the Okhotsk Sea (Figure 4). At  $26.4 \sigma_\theta$  (Figure 4a), tracers spread clockwise as in case A. In deeper surfaces ( $26.8 \sigma_\theta$  and  $27.2 \sigma_\theta$ ), the high tracer concentration in the Okhotsk Sea spreads southeastward (Figures 4b and 4c). Tracer concentrations at  $30^\circ\text{N}$  (Figure 4d) show that two tracer cores appear in the eastern part ( $170^\circ\text{W}$ - $150^\circ\text{W}$ ) of the upper layer ( $26.2$ - $26.6 \sigma_\theta$ ) and in the western part ( $150^\circ\text{E}$ - $170^\circ\text{E}$ ) of the lower layer ( $26.8$ - $27.4 \sigma_\theta$ ). The eastern tracer core corresponds to the high concentration in case A, which originates from the sea surface in the Okhotsk Sea, and spreads south clockwise as in case A. The highly concentrated western tracer core originates from the Okhotsk Sea subsurface, and spreads southeastward. The maximum density surface where the western core is located (roughly  $27.6 \sigma_\theta$ ) is presumably determined by the depth of the outflowing strait between the Okhotsk Sea and North Pacific.

These results indicate two pathways for tracers originating from fresh water sources of the modeled NPIW entering the subtropical gyre. For the upper intermediate layer ( $26.4$ - $26.7 \sigma_\theta$ ), tracers spread clockwise from the outcropping area. For the lower intermediate layer ( $26.8$ - $27.4 \sigma_\theta$ ), tracers spread southeastward from the Okhotsk Sea.

#### 4. Time scale of NPIW spreading

The ratio of CFC-11 and CFC-12 concentration in the atmosphere increases monotonically with time before the mid 1970s. Since this ratio in sea water is conserved while CFC-bearing water is mixed with CFC-free water, the ratio assumes one obtained at the sea surface (*the CFC-ratio apparent age*). Warner *et al.* [1996] discussed timescale of NPIW spreading, using the CFC ratio apparent age calculated from observed CFCs distributions. The CFC-ratio apparent age does not, however, apply to recently ventilated water because the CFC-11/CFC-12 ratio in the atmosphere since 1975 has remained almost constant.

In this section, alternatively, we introduce two dye tracers whose ratio in the atmosphere increases linearly with time. This idealization of time dependency of source makes estimate of the apparent age valid uniform in time. The *tracer-ratio apparent age* is not, however, conserved when tracer-bearing surrounding waters are mixed. We propose more appropriate estimate of NPIW spreading timescale, using *dye tracer with a distinct temporal peak*. Finally, we examine water spreading sensitivity to source timescales.

##### a. Apparent age derived from passive tracer ratio

Assume two dye tracers whose concentration ( $T_i$ ,  $i=1, 2$ ) obeys an advective-diffusive equation with no source and no sink term in the ocean interior, i.e.,

$$\frac{\partial T_i}{\partial t} + \mathbf{u} \cdot \nabla T_i = \nabla \cdot (\mathbf{K} \nabla T_i) \quad (i=1, 2) \quad (2)$$

Assumed source functions of these tracers increase with time, e.g.,  $T_1=a*t$  and  $T_2=b*t^2$  (Figure 9a), where  $a$  and  $b$  are constants independent of time. Thus, the ratio of the two source tracers,  $T_2/T_1=(b/a)t$ , is a linear function of time (Figure 9b).

We also assume the subarctic sea surface ( $\sigma_\theta > 26.0$ ) is a source region and specify the source function there. In the Okhotsk Sea, large vertical diffusivity ( $A_{HV}=8 \times 10^{-4} \text{ m}^2/\text{s}$ ) is used to represent high density water mass formation. Isopycnal, diapycnal, and isopycnal thickness diffusivity coefficients are the same as the OGCM. Eq. (2) is integrated for 100 years.

The *tracer-ratio apparent ages* are calculated from the ratio of the two tracer concentrations after 50 years of integration, and presented on the three isopycnal surfaces (26.4, 26.8, and 27.2  $\sigma_\theta$ ) (Figure 5). With this tracer, it is possible to determine age for recently ventilated waters, for example, in the northwestern Pacific where the CFC ratios are near the modern (post-1975) ratio. At 26.4  $\sigma_\theta$ , the tracer-ratio apparent age counted from the outcrop to the southern subtropical gyre is 10-12 years. At 26.8  $\sigma_\theta$ , the age is about 4 years outside the Okhotsk Sea and 12-16 years at the southern subtropical gyre. The region of small ages extends southeastward from the Okhotsk Sea to the south, as suggested by the spreading path at this density. At 27.2  $\sigma_\theta$ , the age is about 8 years outside the Okhotsk Sea and 18-24 years at the southern subtropical gyre.

The tracer-ratio apparent age we introduced above is not conserved, however, when tracer-bearing waters are mixed. Figure 11 shows ratio apparent ages averaged over the three isopycnal surfaces (26.4, 26.8, and 27.2  $\sigma_\theta$ ) as a function of the period from the initial state; ratio apparent ages increase with elapsed time. Due to surrounding tracer-bearing water from different sources, estimated ratio apparent age becomes older as the integration period increases. This indicates that the tracer-ratio apparent age is not an appropriate measure of age of water.

#### b. Tracer with a distinct peak

We propose an alternative method to estimate a timescale of water spreading. We suppose passive tracers with a temporally varying source. When the source function peaks at a particular moment, it is reasonable to assume that the time required for the peak to appear as a maximum of the tracer concentration in the ocean may be an appropriate response time of water spreading. This timescale is called "peak-to-peak age".

The time sequence of source function of tracer considered is given in Figure 6. The source concentration increases linearly with time for the first 5 years, then decreases linearly with time for the next 5 years, becoming zero by year 10. The source function has a 10-year timescale. The peak-to-peak age is defined as a time-lag between the observed and source peaks. The source function is given at the subarctic surface ( $\sigma_\theta > 26.0$ ). In the Okhotsk Sea, large vertical diffusivity ( $A_{HV}=8 \times 10^{-4} \text{ m}^2/\text{s}$ ) is used to represent high density water mass formation.

The peak-to-peak age at the three isopycnal surfaces derived after 50 years of integration are presented in Figure 7. At 26.4  $\sigma_\theta$  (Figure 7a), the peak of tracer concentration starts from the outcropping area in the subarctic gyre, and extends southeastward. The timescale required for tracers to expand throughout the basin is estimated at about 6 years. At 26.8  $\sigma_\theta$  (Figure 7b), the peak starts from the Okhotsk Sea and extends southeastward with an 8-year timescale. At 27.2  $\sigma_\theta$  (Figure 7c), a general pattern is similar to that at 26.8  $\sigma_\theta$  for a 15-year timescale. Peak-to-peak age thus increases with density (Figure 7), reflecting the difference in spreading mechanisms between the upper intermediate layer (advection) and the lower intermediate layer (diffusion).

The peak-to-peak age has an apparent gap between the subtropical gyre west of 150°E and east of 150°E. The northeastward western boundary current is considered to cause such age distribution.

West of 150°E, southward water spreading is hindered by the transport of the northeastward western boundary current (Figure 2b), delaying the peak time in the western subtropical gyre.

### c. Sensitivity of water spreading to source's timescale

Salinity at 26.8  $\sigma\theta$  is known to indicate decadal year-to-year variations [Qiu and Joyce, 1992], but has no significant seasonal variation [Masuzawa, 1950] along 137E. The temporal evolution of NPIW spreading may depend on the timescale of the source function. We examine the sensitivity of water spreading at 26.8  $\sigma\theta$  to different timescales of the source function. Source functions with two different timescales (1 year and 20 years) are assumed in addition to the source function with a timescale of 10 years.

Figure 8 shows distributions of peak amplitude of the tracer at 26.8  $\sigma\theta$  (the salinity minimum layer) in response to the temporally varying source with three different timescales (little change was seen in the peak-to-peak age between cases). The amplitude is normalized by a source peak. When the source timescale is 1 year (Figure 8a), the amplitude of the peak in the open North Pacific is less than 0.1. The peak amplitude greater than 0.1, is restricted to near the Okhotsk Sea. When the source timescale is 10 years (Figure 8b), the amplitude is 0.1-0.3 in the open North Pacific. When the source timescale is 20 years (Figure 8c), the amplitude further increases as much as 0.1-0.4. Such results indicate that, as the source timescale increases, the peak amplitude increases, i.e., the source signal with a longer timescale can be transmitted further into the intermediate layer. This is explained as follows; in the lower intermediate layer (26.8  $\sigma\theta$ ), waters are carried mainly by isopycnal diffusion. A lower frequency signal has time to reach the ocean interior before being diffused. Thus, diffusion allows the intermediate layer to operate as a low-pass time filter. The source signal whose timescale is 1 year appears only negligibly at 26.8  $\sigma\theta$  (Figure 8a), coinciding with the observation that the salinity at 26.8- $\sigma\theta$  apparently has no significant seasonal variation [Masuzawa, 1950].

## 5. Summary

A time scale associated with the intermediate layer circulation in the North Pacific is estimated with a 3-dimensional tracer model driven by the water velocity and density fields obtained in an OGCM simulation of NPIW (North Pacific Intermediate Water). Tracer with a distinct temporal peak is imposed at the sea surface of the Okhotsk sea and the subarctic ocean (winter  $\delta > 26.0\sigma\theta$ ).

(1) Tracer is quickly mixed to the deep Sea of Okhotsk and outflows along with fresh and dense water ( $>26.7\sigma\theta$ ), and diffuses southeastward along the isopycnal surface to the lower part of NPIW. It takes 15-20 years for the significant peak of the tracer to reach the middle of the basin (~20N).

(2) On the other hand, along the density surface which seasonally outcrops to the sea surface in the Okhotsk sea and the northwestern subarctic sea ( $26.7\sigma\theta > \delta > 26.0\sigma\theta$ ), the tracer is carried eastward mostly by the Kuroshio extension flow to the upper part of NPIW. It takes 5~10 years for the tracer peak to reach the interior of the North Pacific (~20N).

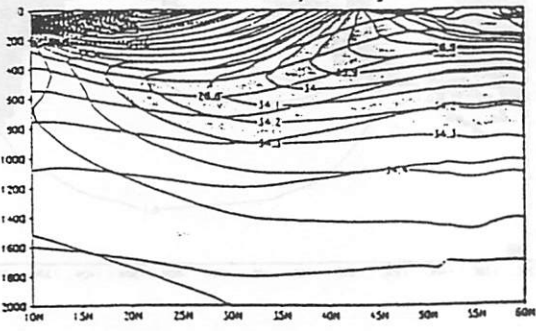
It is noted that the present time scale defined by the period between the source peak to the local peak is shorter than the time required for the diffusive equilibrium ( $>300$  years) and the apparent age (10~30 years). The apparent age is estimated from ratio of tracers with different source history, where mixing with the surrounding old water is counted.

## References

- Cox, M. D., An eddy resolving numerical model of the ventilated thermocline, *J. Phys. Oceanogr.*, 15, 1312-1324, 1985.
- England, M., V. Garçon, and J. Minster, Chlorofluorocarbon uptake in a world ocean model I: sensitivity to the surface gas forcing, *J. Geophys. Res.*, 99, 25215-25233, 1994.
- England, M., Using chlorofluorocarbons to assess ocean climate models, *Geophys. Res. Lett.*, 22, 3051-3054, 1995a.
- England, M., The age water and ventilation timescales in a global ocean model, *J. Phys. Oceanogr.*, 25, 2756-2777, 1995b.
- Gent, P. R., and J. C. McWilliams, Isopycnal mixing in ocean general circulation models, *J. Phys. Oceanogr.*, 20, 150-155, 1990.
- Hellerman, S., and M. Rosenstein, Normal monthly wind stress over the World Ocean with error estimates, *J. Phys. Oceanogr.*, 13, 1093-1104, 1983.
- Kitani, K., An oceanographic study of the Okhotsk Sea- Particularly in regard to cold waters-, *Bull. Far Seas Fish. Res. Lab.*, 9, 45-77, 1973.
- Levitus, S., *Climatological atlas of the World Ocean*, NOAA Prof. Pap., 13, U. S. Dep. of Commerce, Washington, DC, 173 pp, 1982.
- Masuzawa, J., On the intermediate water in the southern Sea of Japan, *The Oceanographic Magazine*, 2, 137-144, 1950.
- Oberhuber, J. M., An atlas based on the "COADS" data set: The budgets of heat, buoyancy, and turbulent kinetic energy at the surface of global ocean, *Max-Planck-Institute for Meteorology, Report*, 15, 199 pp, 1988.
- Qiu B., and T. Joyce, Interannual variability in the mid- and low-latitude western North Pacific, *J. Phys. Oceanogr.*, 22, 1062-1079, 1992.
- Robitaille, D. Y., and A. J. Weaver, Validation of sub-grid-scale mixing schemes using CFCs in a global ocean model, *Geophys. Res. Lett.*, 22, 2917-2920, 1995.
- Talley, L. D., An Okhotsk Sea water anomaly: implications for ventilation in the North Pacific, *Deep-Sea Res.*, 38, S171-190, 1991
- Tanimoto Y., N. Iwasaka, K. Hanawa, and Y. Toba, Characteristic variations of sea surface temperature with multiple time scales in the North Pacific, *J. Climate*, 6, 1153-1160, 1993.
- Tsunogai S., T. Ono, and S. Watanabe, Increase in total carbonate in the western North Pacific Water and a hypothesis on the missing sink of anthropogenic carbon, *J. Oceanogr.*, 49, 305-315, 1993.
- Warner, M. J., J. L. Bullister, D. P. Wisegarver, R. H. Gammon, and R. F. Weiss, Basin-wide distributions of chlorofluorocarbons CFC-11 and CFC-12 in the North Pacific: 1985-1989, *J. Geophys. Res.*, 101, 20525-20542, 1996.
- Yamanaka, G., Y. Kitamura, and M. Endoh, Formation of North Pacific Intermediate Water in an MRI ocean general circulation model. Part I: Isopycnal mixing and marginal sea fresh water, *submitted to J. Geophys. Res.*, 1997a
- Yamanaka, G., Y. Kitamura, and M. Endoh, Formation of North Pacific Intermediate Water in an MRI ocean general circulation model. Part II: Passive tracer experiments, *submitted to J. Geophys. Res.*, 1997b.
- Yukimoto S., M. Endoh, Y. Kitamura, A. Kitoh, T. Motoi, A. Noda, and T. Tokioka, Interannual and interdecadal variabilities in the Pacific in an MRI coupled GCM, *Climate Dynamics*, 12, 667-683, 1996.

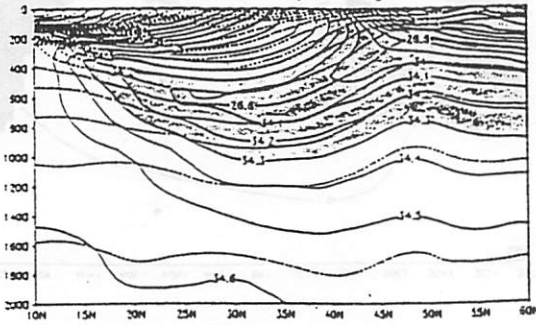


Simulated salinity along 180E



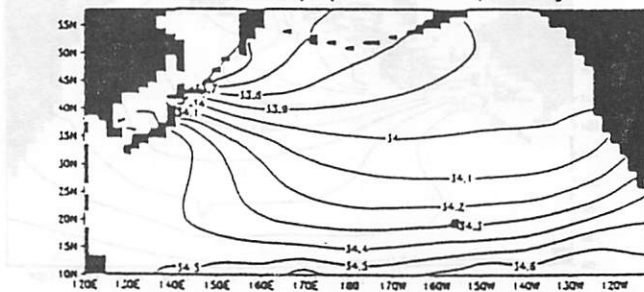
(a)

Observed salinity along 180E

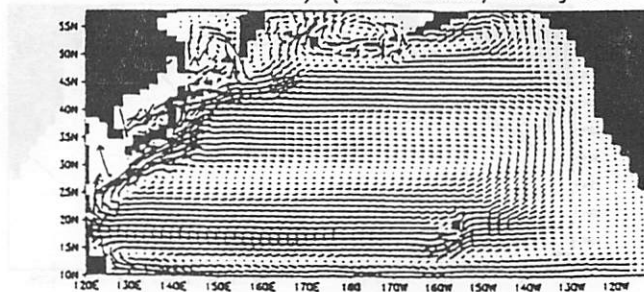


(b)

Simulated salinity (Control Run) along 26.8



Simulated velocity (Control Run) along 26.8



0.04

Figure 1. Salinity distribution (solid lines) along 180°E for (a) observed [Levitus, 1982] and (b) simulated. Isopycnals are indicated by dashed lines. Contours are drawn at 0.1 psu intervals for salinity and 0.2  $\sigma\theta$  for potential density. Shaded areas denote regions where salinity is less than 34.3 psu.

Figure 2. (a) Simulated salinity at 26.8  $\sigma\theta$  (b) Simulated velocity at 26.8  $\sigma\theta$ . Contours are drawn at 0.1 psu intervals for salinity. Vector scaling is in m/s.

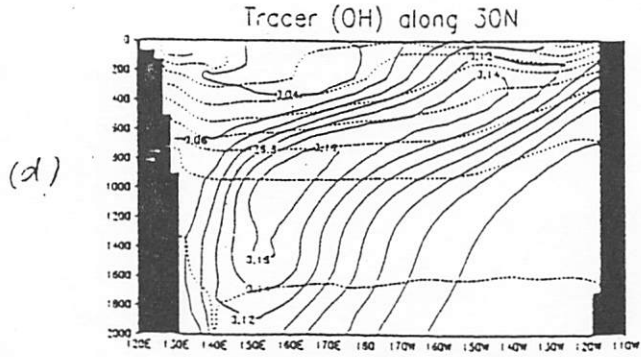
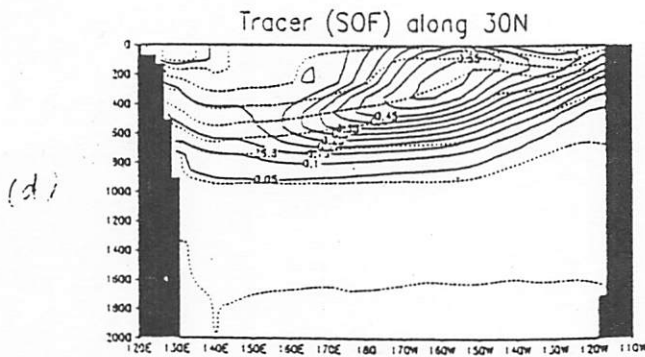
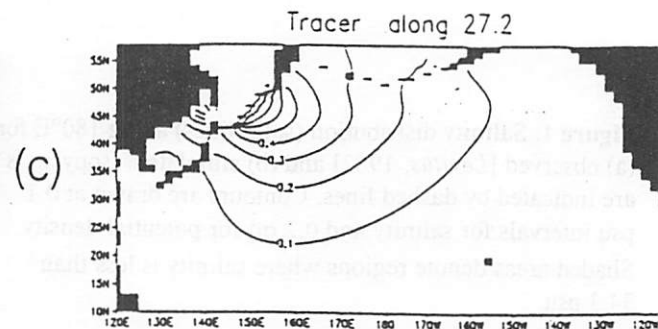
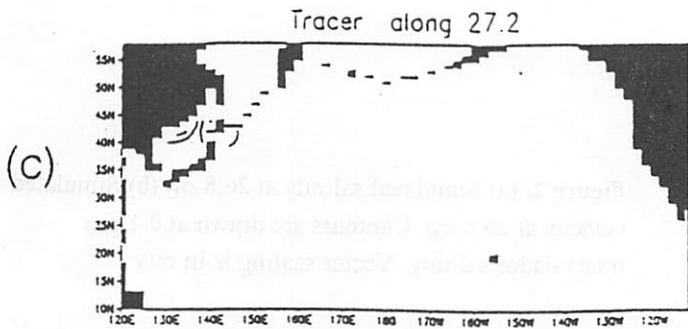
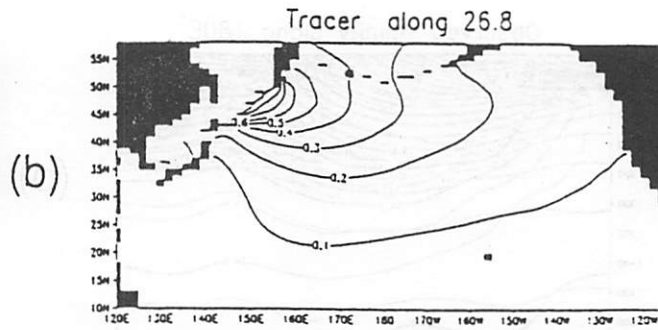
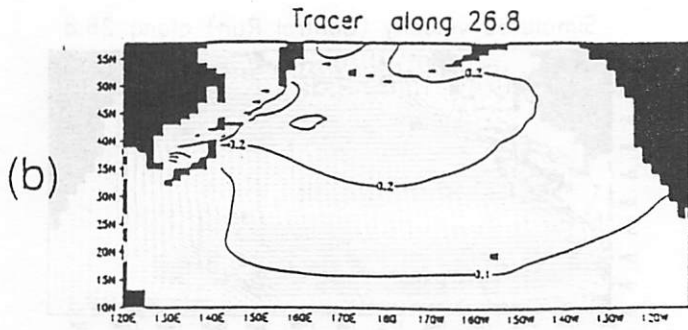
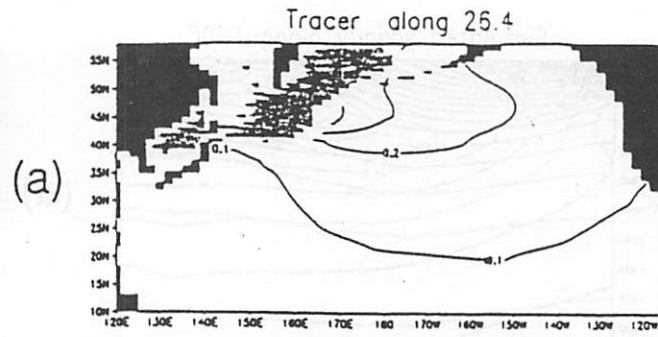
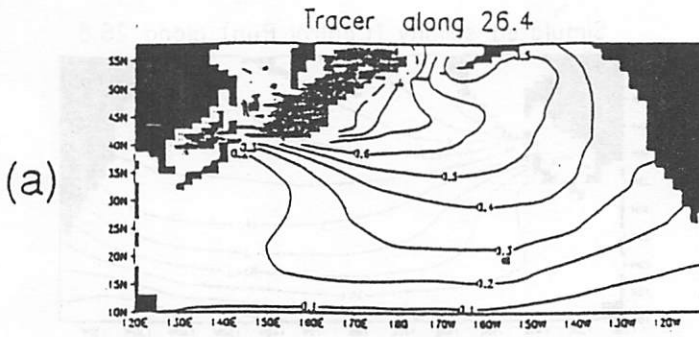
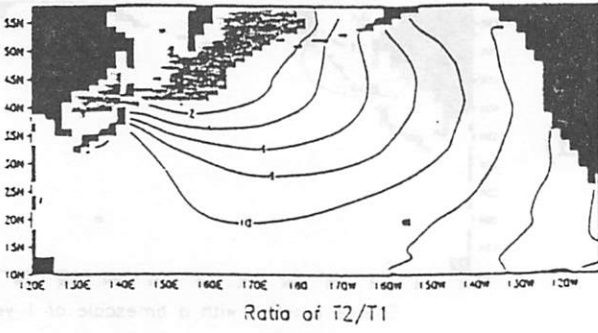


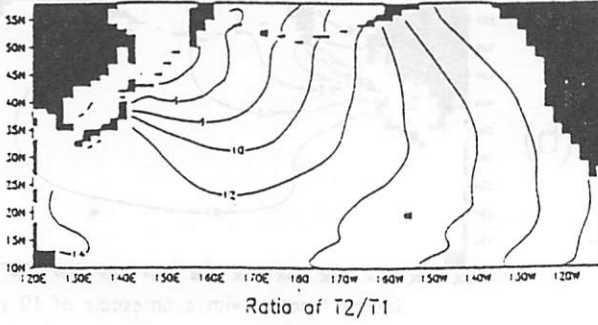
**Figure 3.** Concentrations of simulated tritium-type tracer with radioactive decay in case A (the source is given in the subarctic surface) for (a)  $26.4 \sigma_\theta$ , (b)  $26.8 \sigma_\theta$ , (c)  $27.2 \sigma_\theta$ , and (d)  $30^\circ\text{N}$ . Tracers are indicated in arbitrary units. Contours are drawn at 0.1 intervals. Shaded areas denote regions where the isopycnal outcrops. In a meridional map, isopycnals in the Control Run are indicated by dashed lines at  $0.4 \sigma_\theta$  intervals.

**Figure 4.** Concentrations of simulated idealized tritium-type tracer in case B (the source is given in the Okhotsk Sea) for (a)  $26.4 \sigma_\theta$ , (b)  $26.8 \sigma_\theta$ , (c)  $27.2 \sigma_\theta$ , and (d)  $30^\circ\text{N}$ . Tracers are indicated in arbitrary unit. Contours are drawn at 0.1 intervals. Shaded areas denote regions where the isopycnal outcrops. In a meridional map, isopycnals in the Control Run are indicated by dashed lines at  $0.4 \sigma_\theta$  intervals.

Apparent age (Years) along 26.4



Apparent age (Years) along 26.8



Apparent age (Years) along 27.2

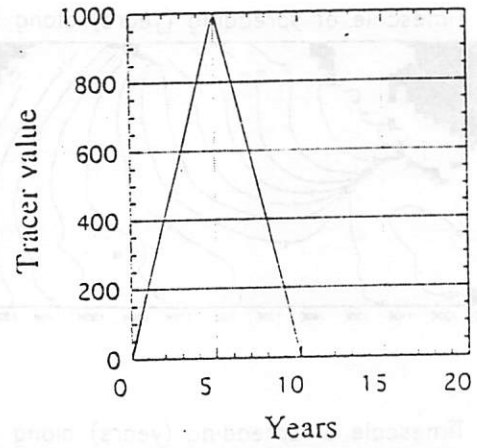
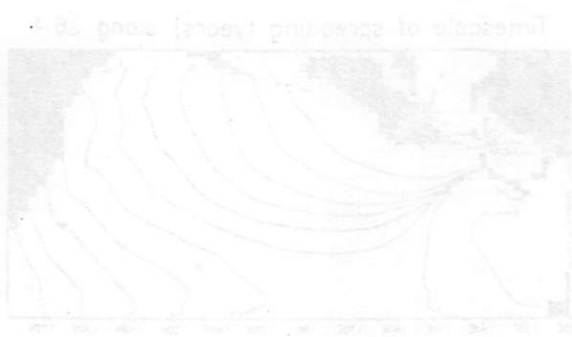
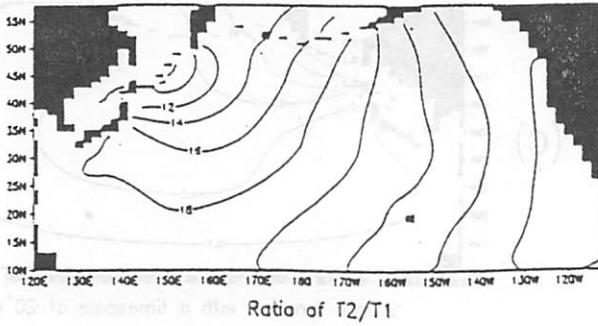


Figure 6. Time series of source function with timescale of 10 years.

Figure 5. Apparent ages (in years) calculated from the ratio of the two dye tracers ( $T_1$  and  $T_2$ ) after 50 years of integration on isopycnals (a)  $26.4 \sigma_\theta$ , (b)  $26.8 \sigma_\theta$ , and (c)  $27.2 \sigma_\theta$ . Shaded areas denote regions where the isopycnal outcrops.

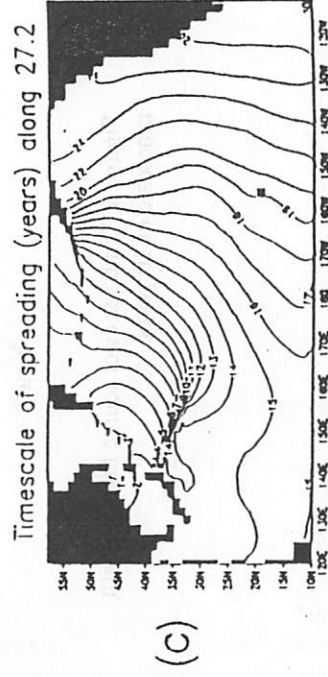
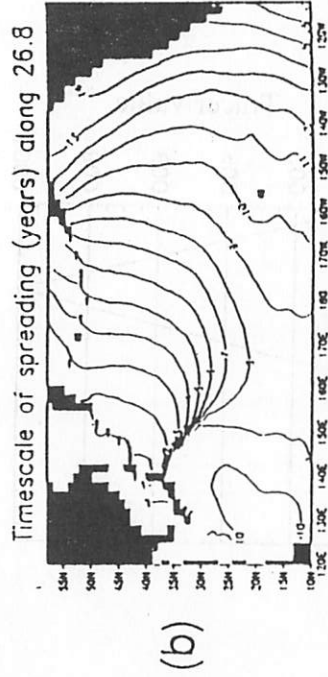
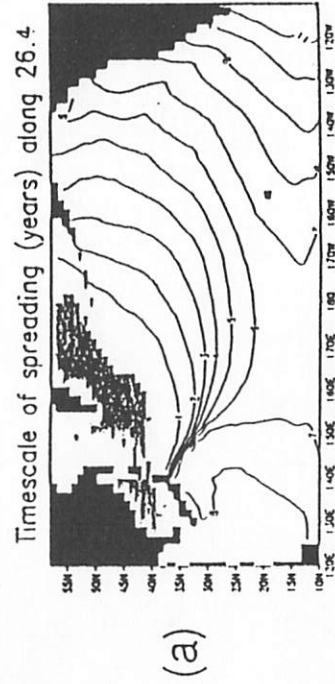


Figure 7. Timescale of spreading (in years) in response to the source function in Figure 13 on isopycnals (a) 26.4  $\sigma\theta$ , (b) 26.8  $\sigma\theta$ , and (c) 27.2  $\sigma\theta$ . Shaded areas denote regions where the isopycnal outcrops.

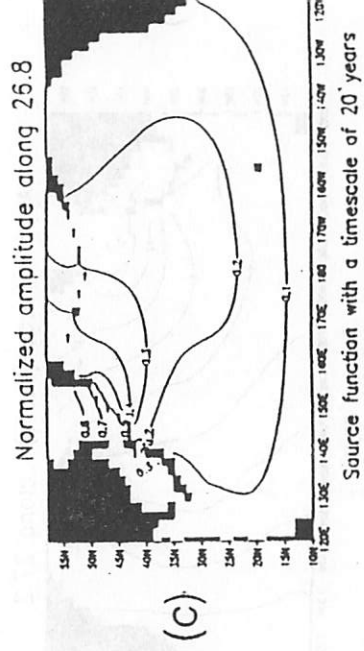
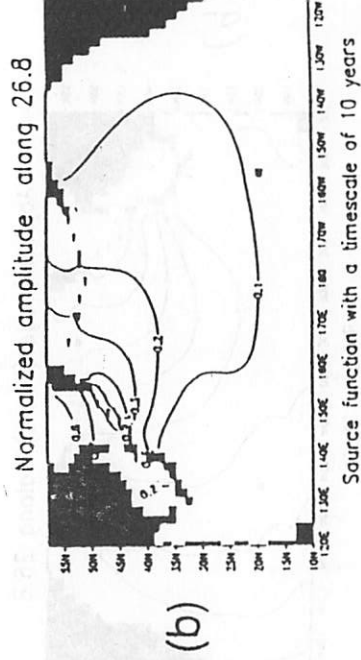
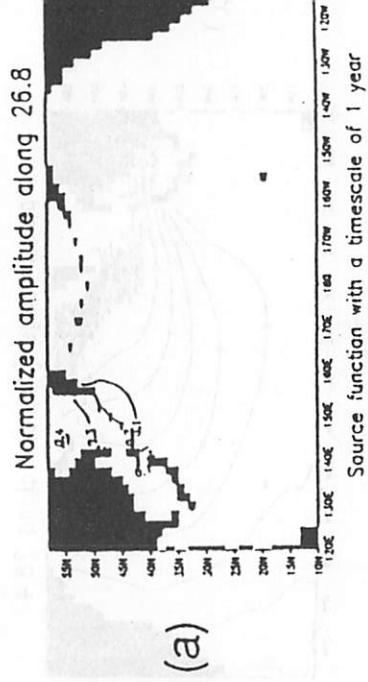


Figure 8. Amplitude of tracer concentration peak at 26.8  $\sigma\theta$  in response to source function with a timescale of (a) 1 year, (b) 10 years, and (c) 20 years. The peak amplitude is normalized by that of the source function. Tracers are indicated in arbitrary unit. Contours are drawn at 0.1 intervals.

## Retrospective Analysis of Sea Surface Wind Fields over the North Pacific during the Period of 1899- 1995

Kimio Hanawa<sup>1</sup> and Tamaki Yasuda<sup>1,2</sup>

1. Department of Geophysics, Graduate School of Science, Tohoku University  
Aoba-ku, Sendai 980-77, Japan
2. Meteorological Research Institution, Japan Meteorological Agency,  
Nagamine, Tsukuba 305, Japan

### Extended Abstract

Sea surface wind (SSW) fields over the North Pacific are reconstructed using sea level pressure (SLP) fields (Trenberth's Corrected Yearly- Monthly Northern Hemisphere SLP, version 010.1) for the period of 97 years from 1899 to 1995.

The reconstruction method is purely empirical as follows. First, monthly climatologies of SSW using winds of the Comprehensive Ocean- Atmosphere Data Set (COADS) and of SLP averaged for ten years from 1981 through 1990 are computed (Fig. 1). Then, monthly anomalies of both SSW and SLP fields during the ten years are calculated (Fig. 2). Under the assumption of a geostrophic balance, geostrophic winds are computed using monthly SLP anomalies (Fig. 3). Comparing those with monthly COADS SSW anomalies, two adjustment factors of the reduction coefficient and the correction angle are estimated for four seasons (Fig. 4: Fig. 5: Table 1). Adopting these adjustment factors for the calculated geostrophic winds, corrected wind anomalies for the rest of the period are calculated. The total wind fields are then obtained as the sum of wind anomalies and COADS SSW climatologies (Fig. 6). When we regard the COADS SSWs as the reference fields, the errors of reconstructed SSWs are estimated to be less than 1 m/s in magnitude (Fig. 7: Fig. 8: Table 2). Since the mean height of the anemometers installed in the merchant vessels during 1980s is approximately 35 m, reconstructed winds are further adjusted to that at the standard height of 10 m.

Time series of the reconstructed wind speeds in the westerlies region shows decadal to multidecadal scale variation: in 1920s through 1940s, westerlies strengthened compared with the rest of the period (Fig. 9). In the same region, wind speeds are also compared to those derived from COADS SSWs. As pointed by the previous researchers, COADS SSWs show the increasing trend at least from 1950s to the present (Fig. 10).

(This paper has been submitted to *Journal of Atmospheric and Oceanic Technology*.)

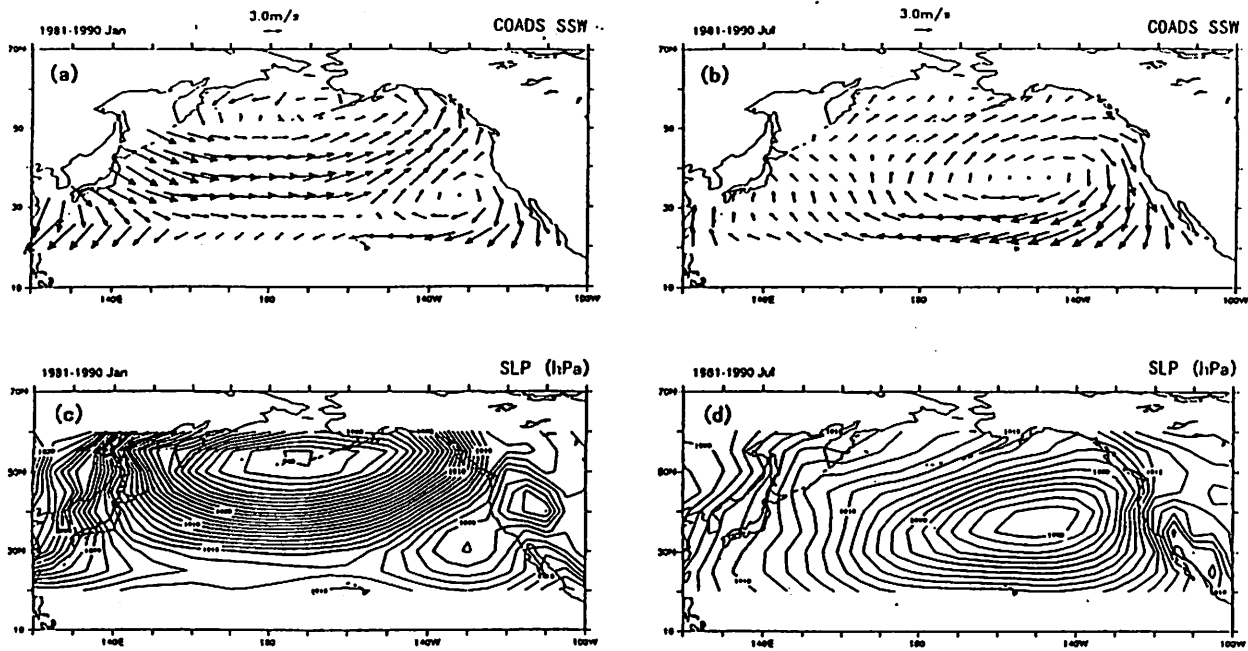


**Fig. 1.** Climatologies of SSW fields of January (a) and July (b): ten-year averages from 1981 to 1990 and those of SLP fields of January (c) and July (d). The raw data of SSWs are COADS.

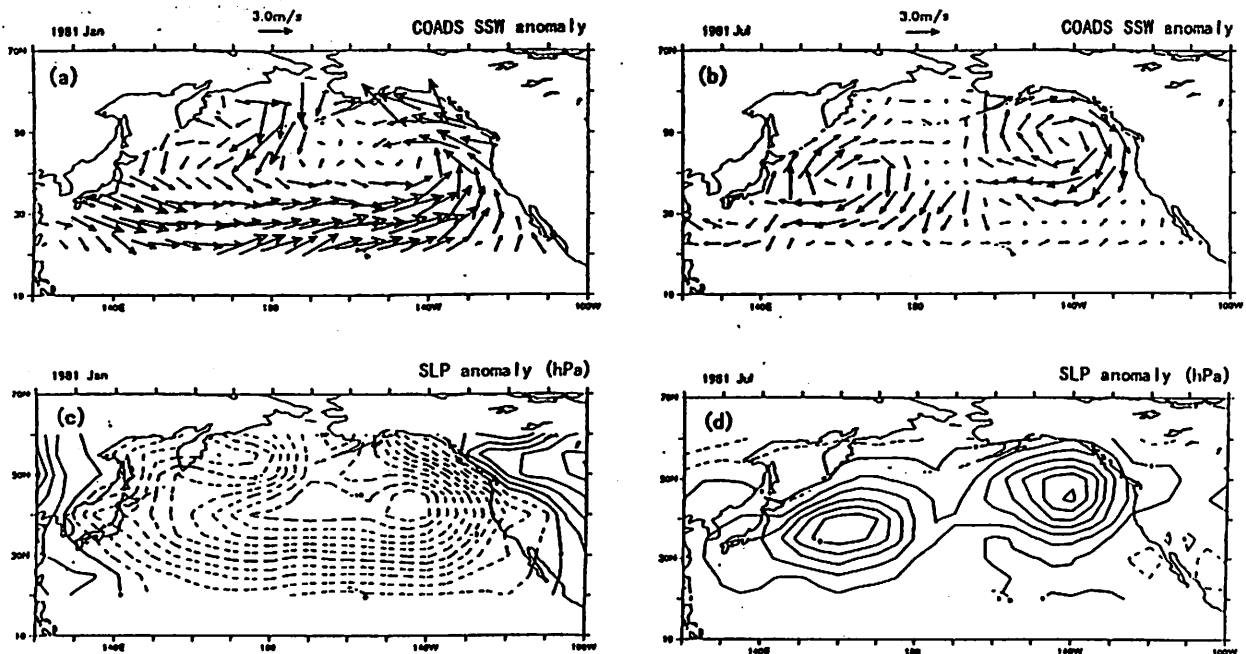


**Fig. 2.** Anomaly fields of SSW of January (a) and July (b) 1981, and those of SLP ((c) and (d)).

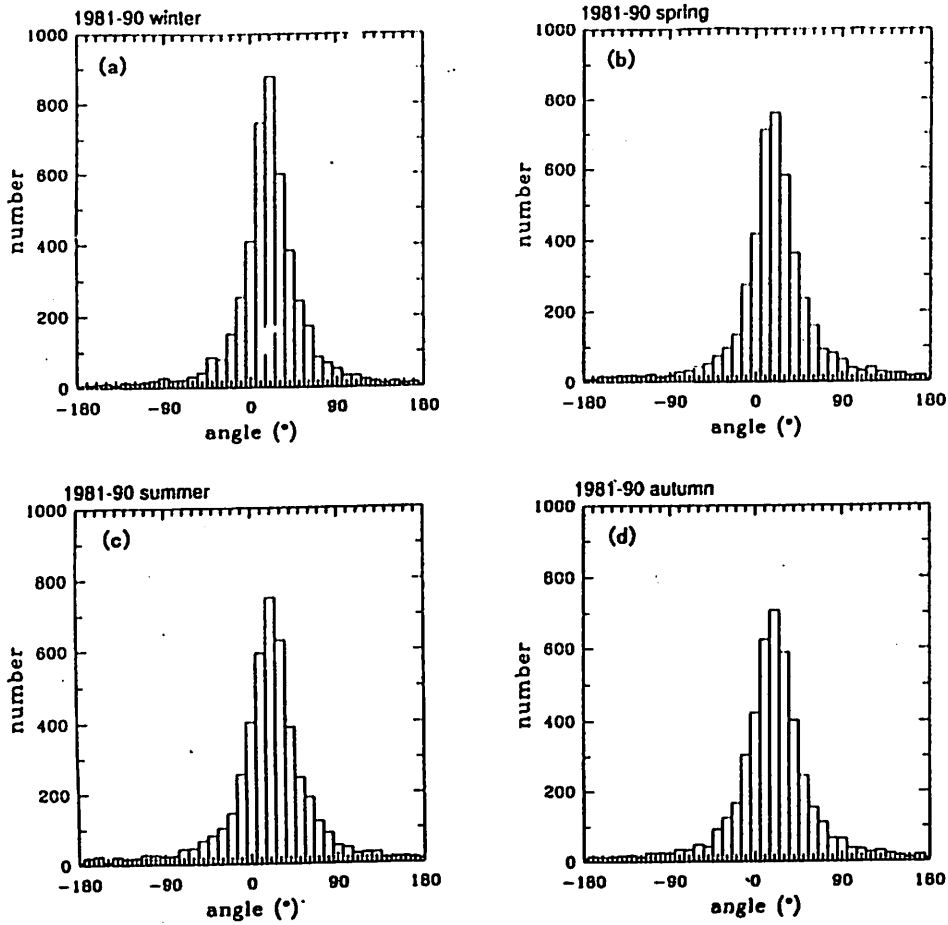


**Fig. 5.** Frequency distribution of angle differences between COADS SSW anomaly vectors and calculated GW anomaly vectors. Sample number is the same as Fig. 4. The bin of angle is ten degrees such as -5 to +5, +5 to +15 and so on.

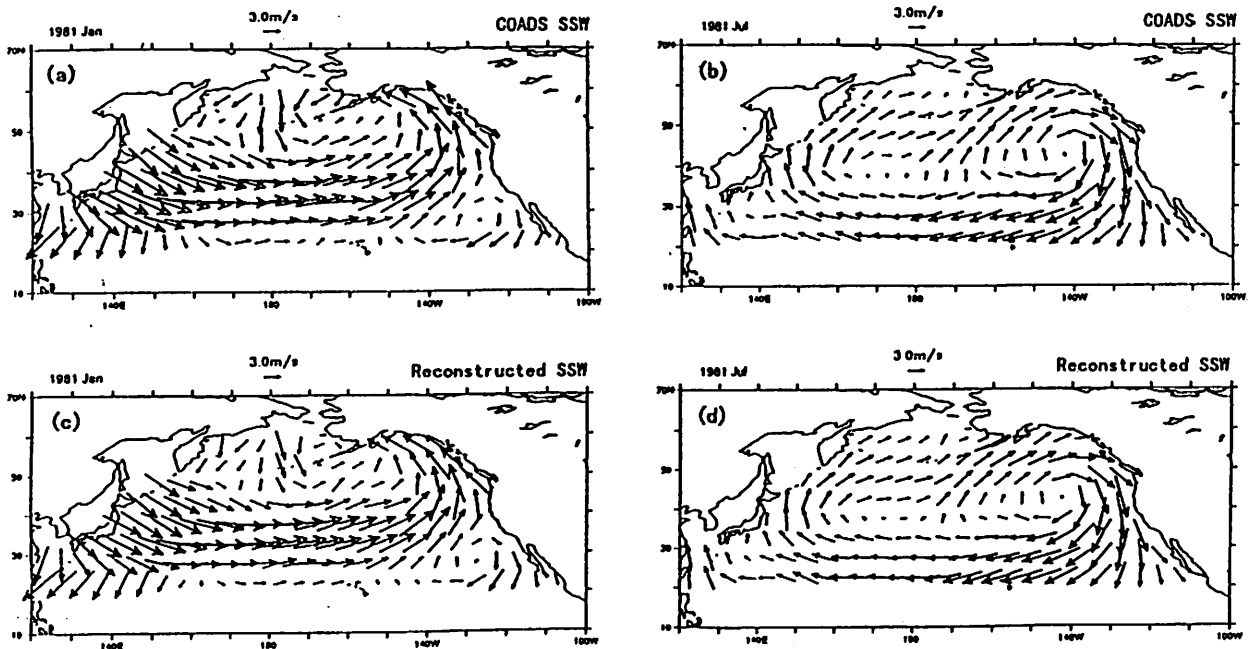


**Fig. 6.** COADS SSW fields of January (a) and July (b) 1981, and those of the finally reconstructed SSW fields ((c) and (d)).

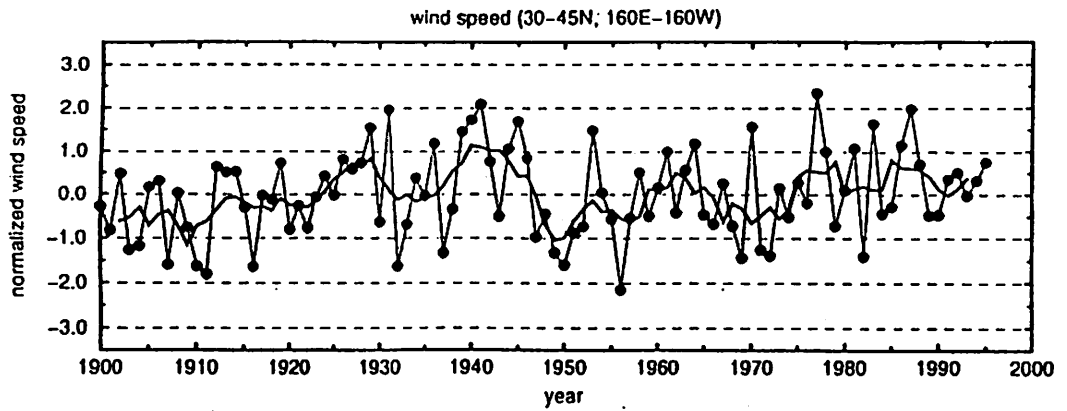


**Fig. 9.** Time series of wintertime westerlies wind speeds averaged in the area of 30N-45N and 160E-160W from 1900 to 1995. Thick solid line denotes 5-year running mean. The origin of vertical axis is the mean wind speed of 4.27 m/s during 96 years and unit is normalized by the standard deviation of 1.20 m/s.

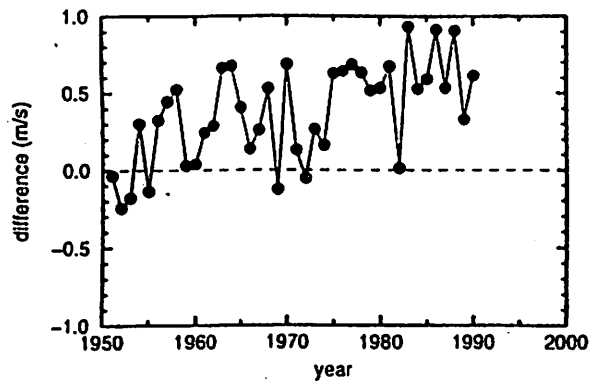


**Fig. 10.** Time series of difference of wintertime westerlies wind speeds between the reconstructed SSWs and COADS SSWs from 1950 to 1990, in the same region as Fig. 9. Please note that since the COADS SSWs are those at the height greater than the standard height of 10 m, while the reconstructed SSWs are at 10-m height, there is some bias between the two.



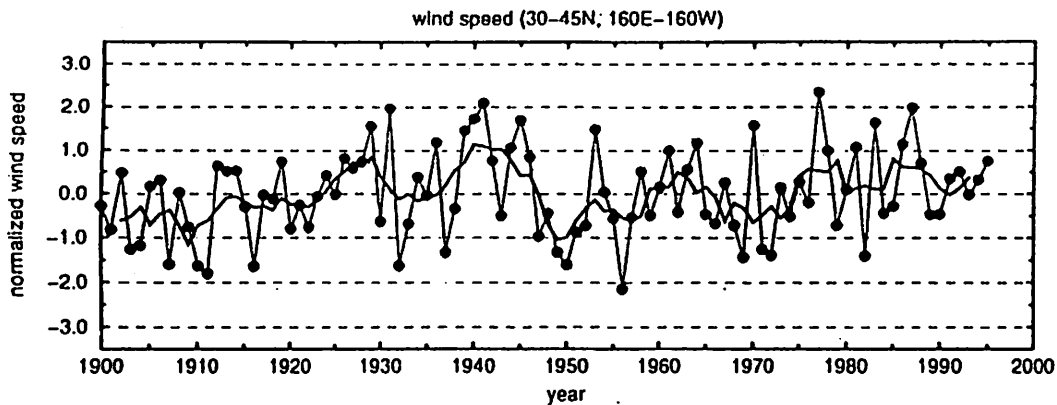


Fig. 9. Time series of wintertime westerlies wind speeds averaged in the area of 30N-45N and 160E-160W from 1900 to 1995. Thick solid line denotes 5-year running mean. The origin of vertical axis is the mean wind speed of 4.27 m/s during 96 years and unit is normalized by the standard deviation of 1.20 m/s.

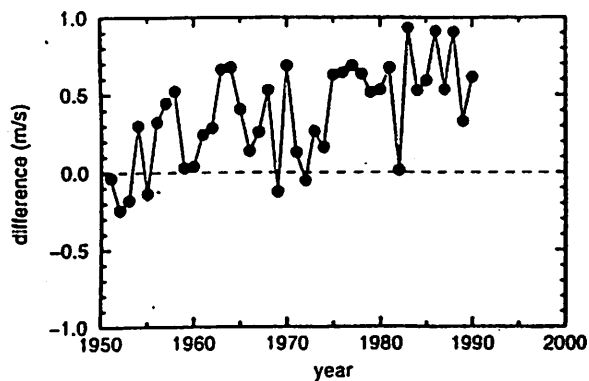


Fig. 10. Time series of difference of wintertime westerlies wind speeds between the reconstructed SSWs and COADS SSWs from 1950 to 1990, in the same region as Fig. 9. Please note that since the COADS SSWs are those at the height greater than the standard height of 10 m, while the reconstructed SSWs are at 10-m height, there is some bias between the two.

# Diagnostic Calculation of the North Pacific Circulation Based on a Seasonal Climatic Data

*Prof., Dr. Victor Kuzin, Dr. Valery Moiseev*

Novosibirsk Computing Center Siberian Division RAS,  
RUSSIA

The reconstruction of the velocity fields on the basis of the hydrophysical fields distributions (T&S) with the use of some mathematical relations is the classical problem of oceanography. The first of the series of the methods dealing with the solving this problem was the dynamical method of Zubov, Mamaev, 1956, Defant, 1961. This method played an important role in the estimates of currents for many regions of the World Ocean. Nevertheless this techniques has a well-known disadvantage connected with determining the "zero" surface or absolute velocity. In this connection any efforts in the direction of the diagnostic theory development with the use of more complete models were encouraged. These are the computations of Sarkysian, 1966, Cox, 1975, Holland, Hirshman, 1983. One of the problems arising at the diagnostic stage is unbalanceness of the climatic data, especially in the tropical zone. Filtering of the climatic fields do not lead to the appropriate results. One of the approaches which has to overcome this problem is the "robust" technique used by Sarmiento, Bryan, 1982. They include the sources to the prognostic heat and salt equations which controls the deviations from the "initial" climatic data. This was also done by Fujio, Imasato, 1991 for the study of the deep Pacific circulation.

The present study follows another approach suggested by Demin, Sarkysian, 1992, Ezer, Mellor, 1994, who used the additional adjustment calculations after the diagnostic step with the use of the prognostic primitive equations without any sources. The criteria for the adjustment period is the kinetic energy and potential enstrophy behaviour.

The object of the study of the present paper of the North Pacific hydrophysical characteristics and its seasonal variations according to the climatic data. The Novosibirsk Computing Center North Pacific Circulation Model based on the finite element technique was used for the calculations of the currents, mass and heat fluxes.

## Model and Numerical Technique

A primitive equations of the ocean thermodynamics is used with the traditional Boussinesq, hydrostatics and "rigid-lid" approximations. The model is formulated in the spherical coordinates. The basin includes the tropical zone up to 30 S. The T&S seasonally averaged climatic fields from Levitus Climatic Atlas,1994, was used at the surface and the "liquid" southern boundary. Hellesman,Rosenstein,1983 wind-stress was set at the sea surface. At the "solid" boundaries no-flux condition for heat and salt as well as free-slip conditions for the momentum equations were used.

The spatial resolution on E-type grid is  $1^{\circ}2'$  deg. with respect to the horizontal coordinates and with 18 vertical nonuniform standard levels.

The numerical technique based on the finite element approach with splitting has been developed by Kuzin,1985 and applied to the North' pacific basin in the work by Kuzin, Moiseev,1995.

The main aspects of the numerical technique is as follows.

a) Momentum equations. The algorithm is based on the traditional idea of separations of the external and the internal modes. The external mode equations are reformulated as a vorticity equation in terms of the integral-stream function. For the internal mode the system of equations which is similar to the initial system is solved. Discretization of the equations was carried out on the basis of the piece-wise interpolating functions with the use of the "mass-lumping" technique. For the advective terms the finite element version of the up-stream scheme was used. With respect to time the implicit scheme was used. The pressure gradient terms as well as some part of the advective terms integrated by the vertical were treated in the explicit manner. For all other terms Crank-Nicholson scheme was used with the block Zeidel iterative procedure.

b) Heat and Salt equations. First, the equation is split by the cross-sections of the "chess" grid and then the quasi-two-dimensional problems are discretized by piece-wise finite elements at each section with the mass and energy conservation laws. At each time step an additional wise-coordinate splitting is used on the basis of the Crank-Nicholson scheme which allows construction the completely implicit algorithm.

c) Hydrostatic equation. Discretisation is done on the staggered grid for different characteristics in the manner which leads to the correct transformation of the potential energy to the kinetic energy and vice versa. As a result the model in the discrete form in adiabatic conditions conserve the first momentum (mass, heat, salt ) and the total energy.

## Numerical experiments and results

Numerical experiment has been carried out for seasons. The initial moment the seasonal temperature, salinity fields are prescribed.

The diffusivity and viscosity coefficient are as follows: coefficient of the horizontal viscosity  $A_L = 5 \cdot 10^6 \text{ cm}^2 / \text{s}$  ; coefficient of the vertical viscosity  $A_V = 10^2 \text{ cm}^2 / \text{s}$  ; coefficient of the horizontal diffusivity  $\mu = 2 \cdot 10^6 \text{ cm}^2 / \text{s}$  ; coefficient of the vertical diffusivity  $\nu = 10 \text{ cm}^2 / \text{s}$  ; bottom drag coefficient  $R = 10^{-7} \text{ s}^{-1}$ .

For the diagnosis stage 3-D momentum equations were calculated for each season during 50 days period of the model time.

For the analysis of the results three zones are selected: A (30 N - 60 N), B (10N - 30 N), C (10 S - 10 N). Then the seasonal values of the integral stream function (ISF) was subtracted from the annual mean value. The results show remarkable seasonal variations of the maxima of the integral stream function for selected zones. The peaks of variations are observed for the winter and the summer seasons. The variations of the subpolar and subtropical gyres and subpolar front is caused by the interaction between the Siberian High and the Aleutian Low which dominates in this region. The seasonal deviations in the A- and C- zones are positively correlated, whereas they are in the antiphase with the variations in B- zone. The value of the annual mean mass transport for the subpolar and subtropical gyres are 20 sv and 45sv respectively. So, the Kuroshio integral mass transport varies from the summer to the winter season from value 63 sv to 28 sv.

The results of the 3D velocity diagnosis are appropriate enough for extratropical zones, however for the tropical basin the circulation, meridional circulation, integral heat fluxes and some other characteristics are rather disinformative because of the inconsistency of the density field and the diagnostic model. To avoid this problem the short-range prognostic calculations for seventy five-day periods with a primitive equation model were done for each season. This procedure, as it was mentioned above, is alternative to the robust technique and allows the balance of hydrophysical fields and leads to some improvement of the hydrological characteristics. Let us consider the process of adjustment as well as the changes which it causes on the example of the autumn season. For this purpose four regions were selected: equatorial (5 S - 5 N), tropical (5 N -10 N), subtropical (10 N -30 N) and subpolar (30 N - 60 N). On the pictures of the kinetic energy for each regions one can see that the period of stabilization is very short for subtropical and subpolar regions both for the diagnostic

and adjustment modes (Figs 1b,c). It is less than fifteen days. For the tropical regions the period of diagnostic stabilization is slightly more than fifteen days whereas adjustment need more than thirty days (Fig. 1 a). As concerns the equatorial region, the behaviour is extremely different (Figs 2 a-d). Diagnostic stabilisation at the deepest levels is reached after forty days. The adjustment processes last three months. One can see that there are some oscillations during the adjustment period in this region. This process not been analysed in detail yet, but all the above mentioned features are specific for each season. The results of adjustment for velocity fields at depths 100 m and 5000 m are presented at the Fig. 3.

Now let us turn to the discussion of the hydrological characteristics for the other seasons and their specific features. At the Figs. 4,5 the pictures of the winter and summer circulation are presented at the depths 50, 150, 1200 and 5000 m. The joint features of circulation in all of the seasons are the presence of the subpolar, subtropical and tropical system of circulation with strong intra-tropical countercurrents and equatorial undercurrent which is began to form. The Oyashio and Kuroshio with the recirculation zones are well expressed, although are not so intensive and narrow. At the layers deeper than 1200 m there arise a system of undercurrents shifted relatively the main current by the latitude. The main difference between the winter and summer circulation is that for all levels of the Northern hemisphere the currents in winter are more intensive.

Finally let us discuss such important characteristic as the meridional heat transport which play the key role in the atmosphere-ocean joint climatic system. Fig. 6 represents the transformation of the components of the heat flux for autumn during the adjustment period. The results shows the significant ordering and increasing of the heat flux for the layers 0-100 and 100-900 m (Fig. 6). This is caused by improving of the balance in the hydrophysical fields after adjustment. The similar processes are specific for the all other seasons. The results are in agreement with the estimates known from the literature (Talley, 1984). The seasonal variations presented in the Fig. 7 indicate that in summer the maximal values of the northward heat flux increased and shifted to the south what is in accordance with the estimates of Levitus, 1987.

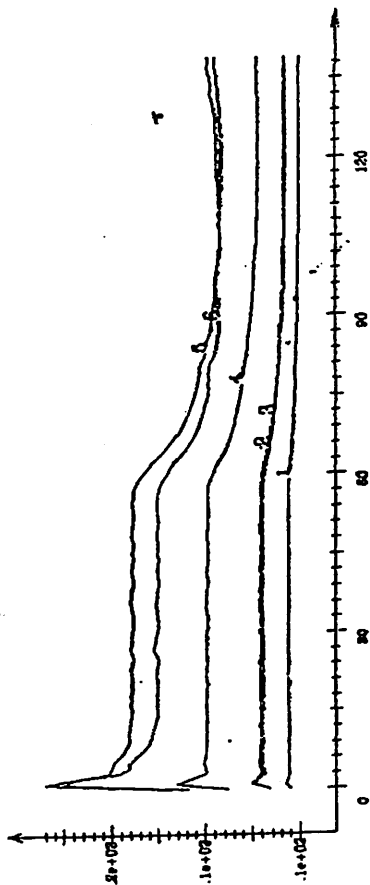
This work was supported by Russian Foundation of Fundamental Research Grant No 95-05-65953.

## REFERENCES

1. Kuzin V.I., Moiseev V.M. North Pacific diagnostic circulation model. // Bull. Novosibirsk Comp. Center, Series: Numerical Modelling in Atmosphere, Ocean and Environment Studies, NCC Publisher Novosibirsk, 1995, pp. 13- 30.

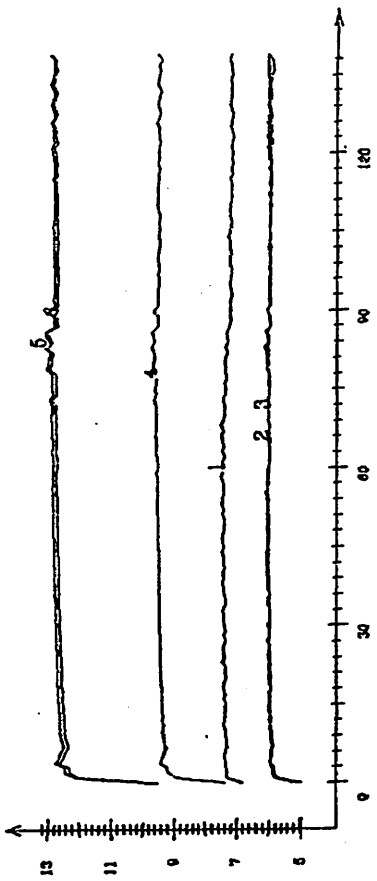
2. Defant A. *Physical Oceanography*. 1961, Pergamon Press, Oxford, Part I: 745 p., Part II: 606 p.
3. Zubov K.K., Mamaev O.I. *Dynamical method for sea current calculations*. 1956, Hydrometeoizdat.
4. Sarkysian A.S. *The basis for the sea currents calculation*. 1966, Hydrometeoizdat, p. 123.
5. Cox M.D. *A baroclinic numerical model of the World Ocean: preliminary results*, - In: *Numerical Models of Ocean Circulation*. 1975, NAS, Washington, D.C., p. 107-120.
6. Holland W.R., Hirschman A.D. *A numerical calculation of the circulation of the North Atlantic Ocean*. 1983, *J. Phys. Oceanogr.*, v. 13, pp. 1093-1104.
7. Sarmiento J.L., K.Bryan. *An ocean transport model for the North Atlantic*. 1982, *J. Geoph. Res.*, v. 87, pp. 394-408.
8. Demin Yu.L., Sarkysian A.S. *General conditions of the first stage of the numerical models intercalibration*. In/ *Num. Methods and Results of the Calculations of the Atlantic Ocean Circulation*. 1992, pp. 5-12.
8. Fujio S., Imasato N. *Diagnostic Calculation for Circulation and Water Mass Movement in Deep Pacific*. 1991, *J. Geoph. Res.*, V. 96, No C1, pp. 759-774.
9. Levitus S. *Climatological Atlas of the World Ocean*. // *Environmental Res. Lab., Geophys. Fluid Dynamics Lab., Princeton, N.J. Rockville, Md December, 1982*.
10. Hellerman S., Rosenstein M. *Normal monthly wind-stress over the World Ocean with error estimates*. // *J. Phys. Oceanogr.*, v. 13, No 7, 1983, pp. 1093 - 1104.
11. Kuzin V.I. *Finite Element Method in the Oceanic Processes Modelling*. Novosibirsk, 1985, p. 190.
12. Levitus S. *Meridional Ekman Heat Fluxes for the World Ocean and Individual Ocean Basin* // *J. Phys. Oceanogr.*, 1987, v. 17, p. 1484 - 1506.
13. Talley L.D. *Meridional heat transport in the Pacific Ocean*. // *J. Phys. Oceanogr.*, 1984, v. 14, p. 232 - 241.

a)



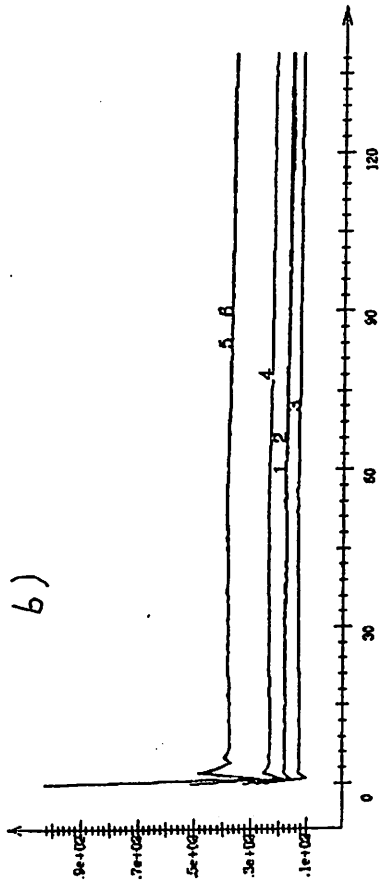
Kinetic energy (.5N-10N)  
 MAX=.28e+03 MIN=.13e+02 Levels =1 -6 Day =.1400e+03  
 Autumn

c)



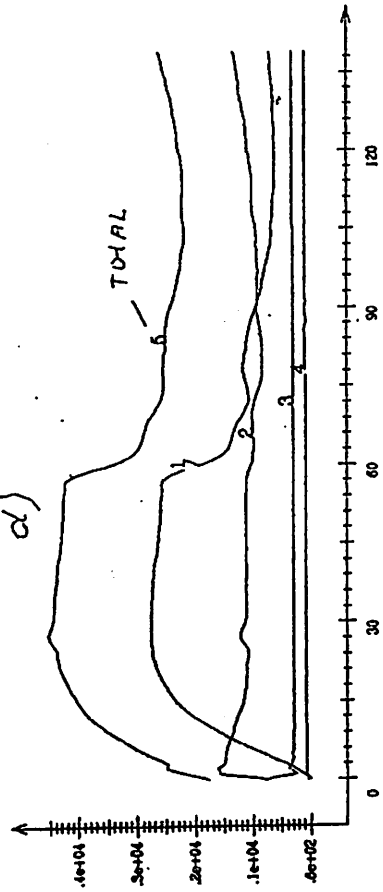
Kinetic energy (30N-60N)  
 MAX=.13e+02 MIN=.45e+01 Levels =1 -6 Day =.1400e+03  
 Autumn

b)



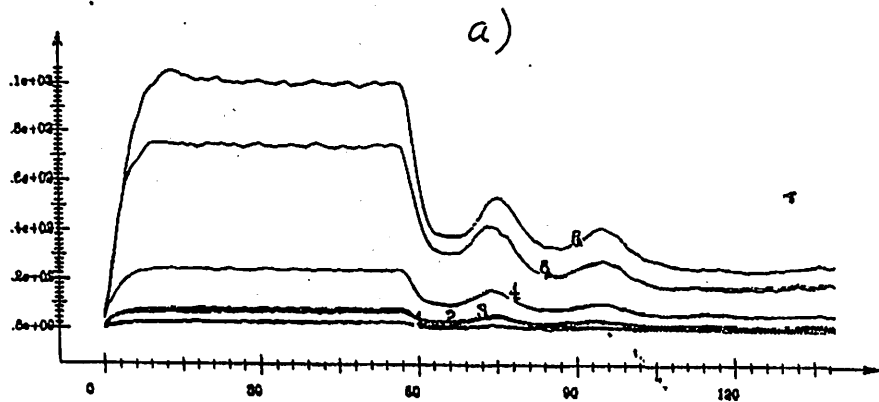
Kinetic energy (10N-30N)  
 MAX=.11e+03 MIN=.13e+02 Levels =1 -6 Day =.1400e+03  
 Autumn

d)

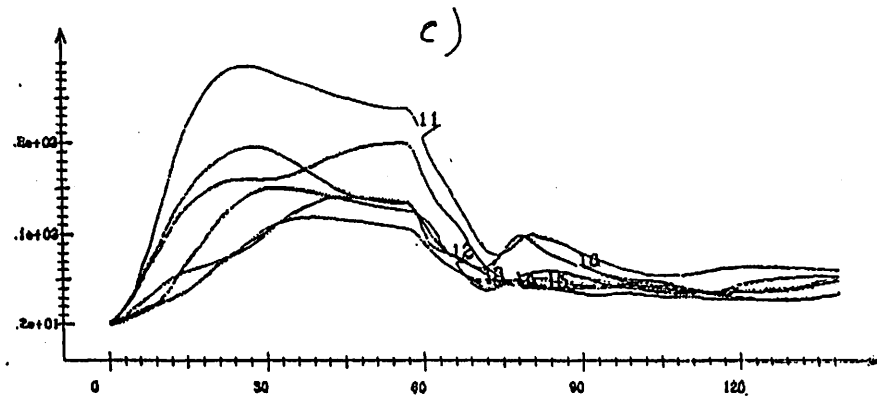


Kinetic energy in the regions  
 MAX=.46e+04 MIN=.58e+02 Day =.1400e+03  
 Autumn

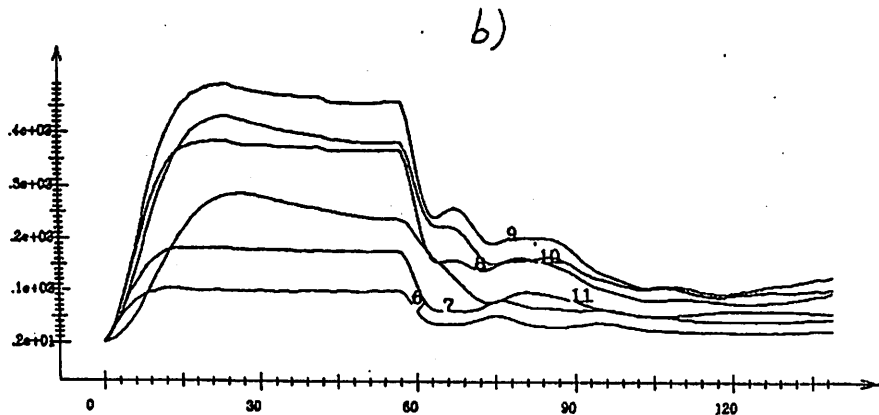
Fig.1.



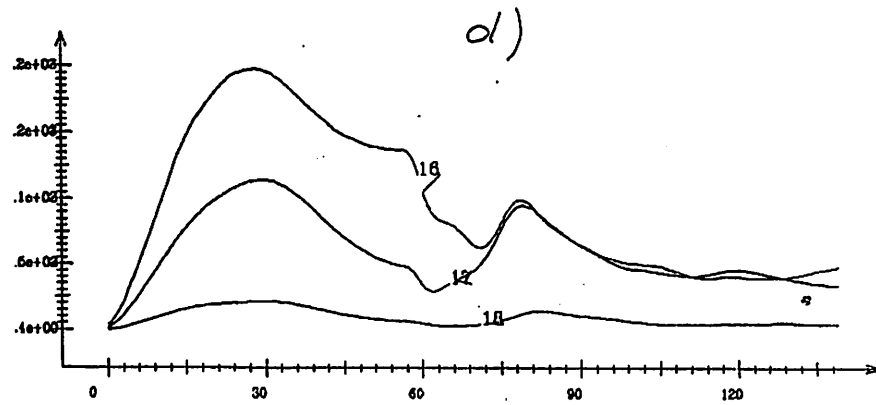
Kinetic energy (.5S-.5N)  
MAX=.11e+03 MIN =.75e+00 Levels =1 -6 Day =.1400e+03  
Autumn



Kinetic energy (.5S-.5N)  
MAX=.29e+03 MIN =.16e+01 Levels =11 -16 Day =.1400e+03  
Autumn



Kinetic energy (.5S-.5N)  
MAX=.49e+03 MIN =.23e+01 Levels =6 -11 Day =.1400e+03  
Autumn



Kinetic energy (.5S-.5N)  
MAX=.20e+03 MIN =.36e+00 Levels =16 -18 Day =.1400e+03  
Autumn



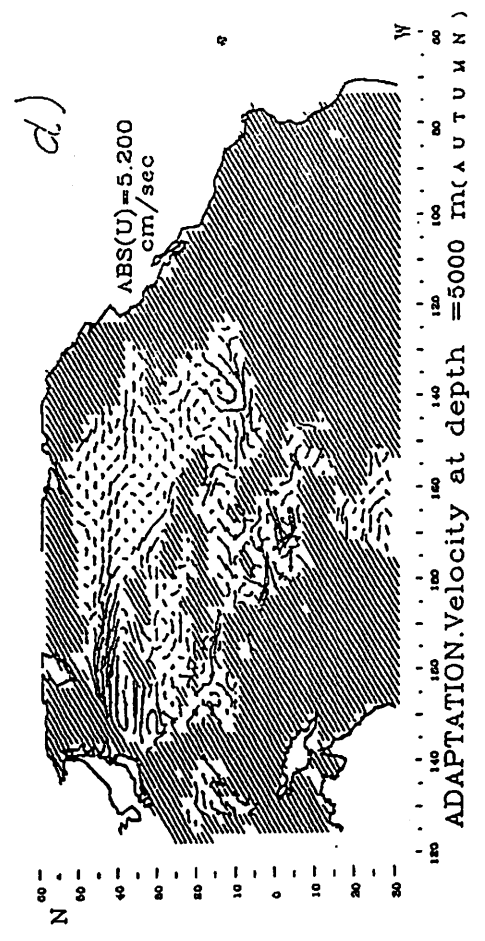
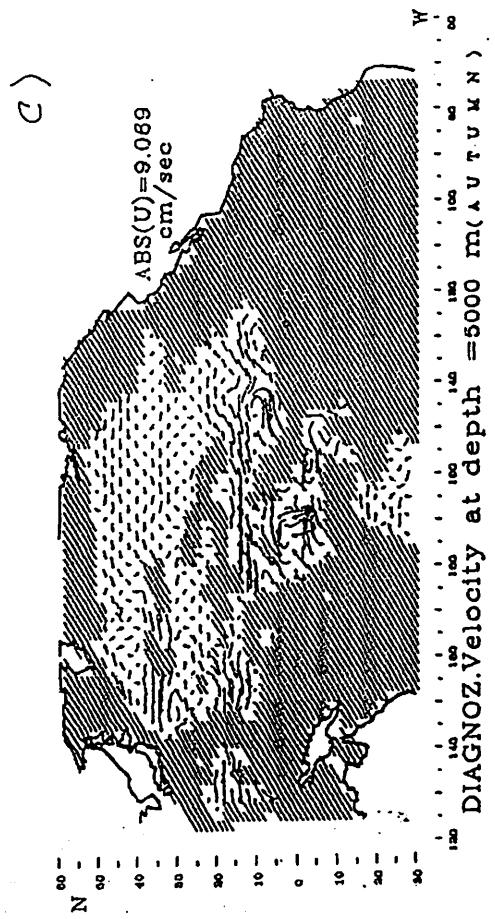
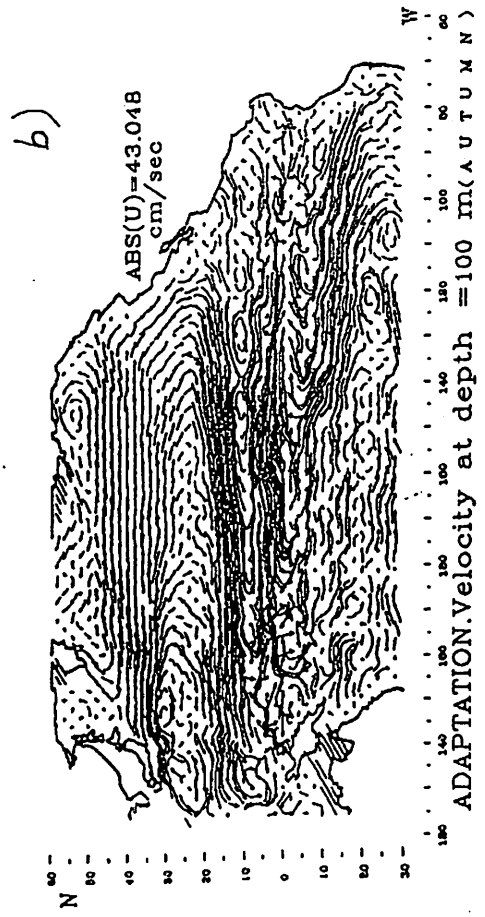
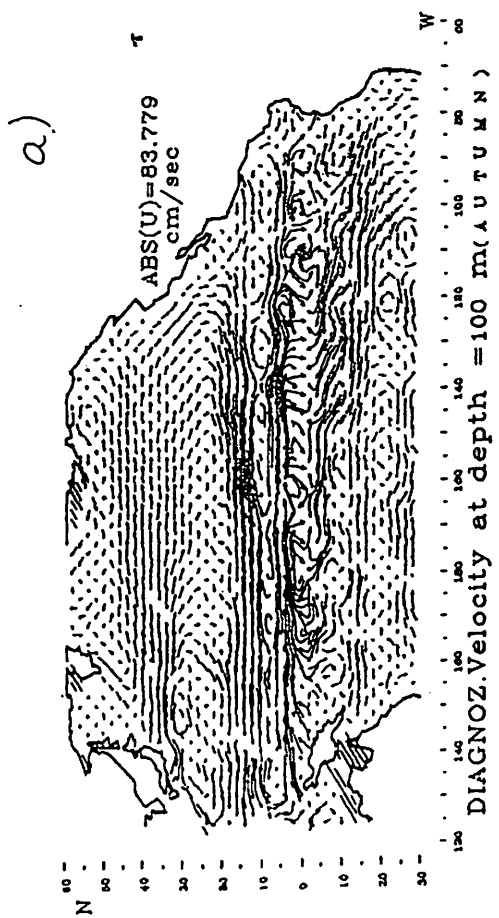


Fig.3.

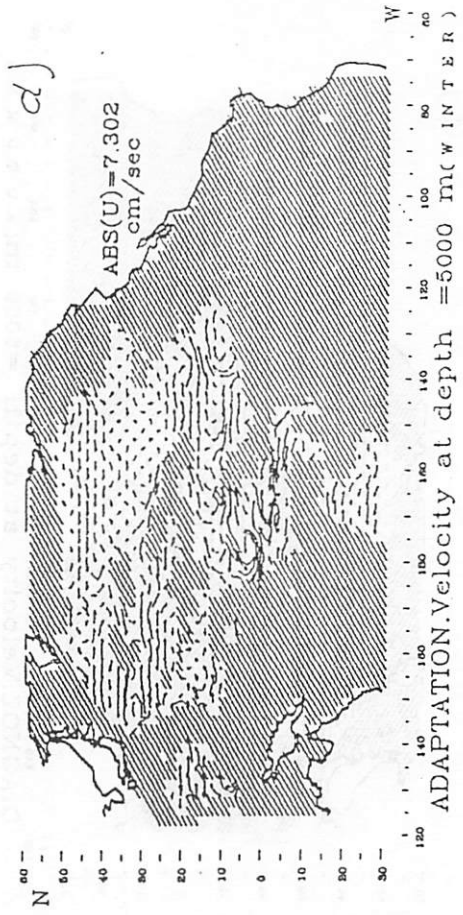
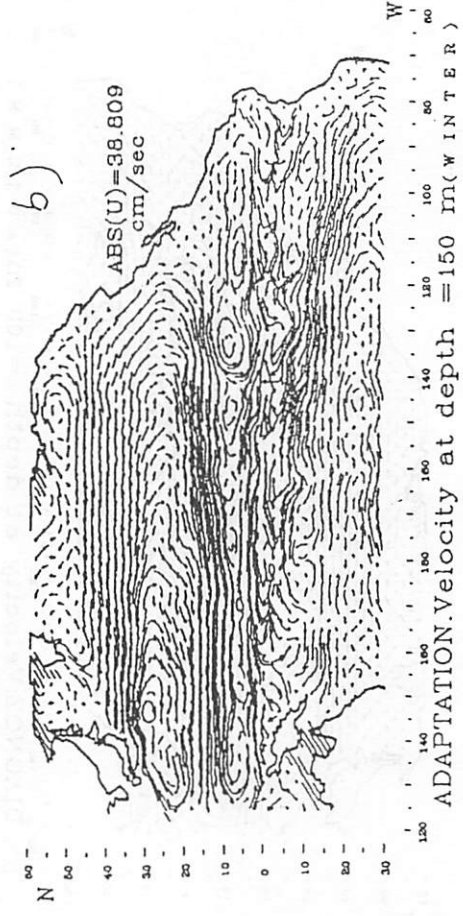
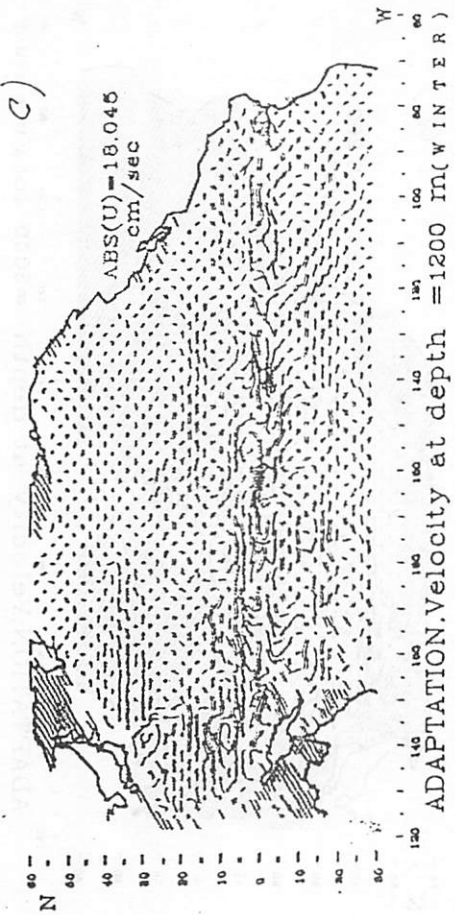
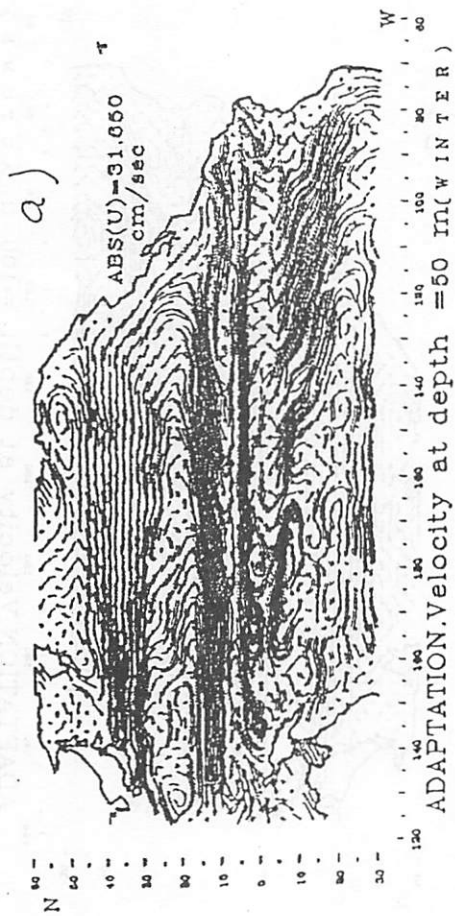


Fig.4.

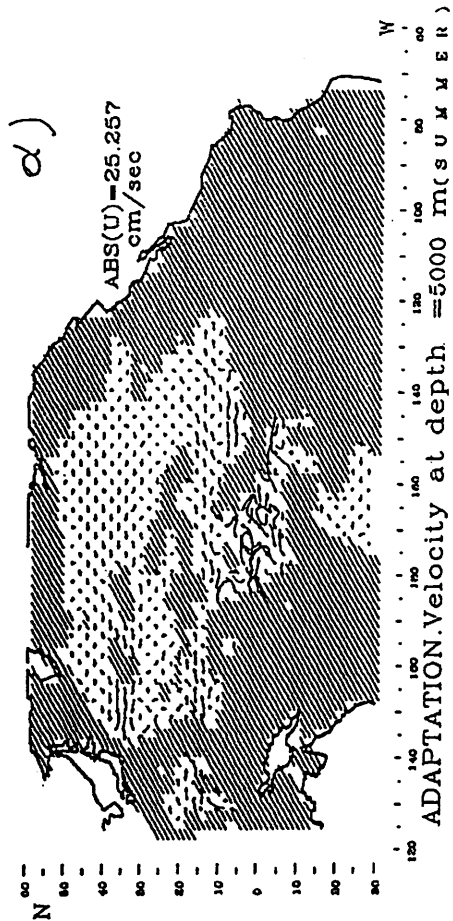
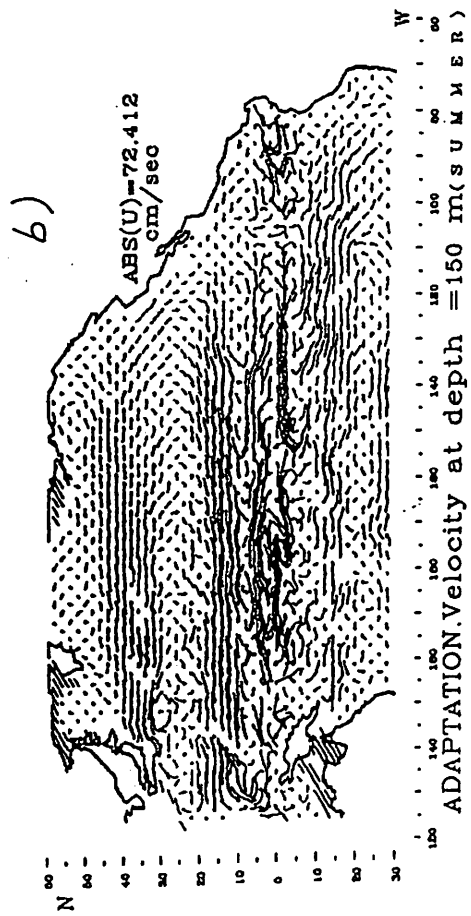
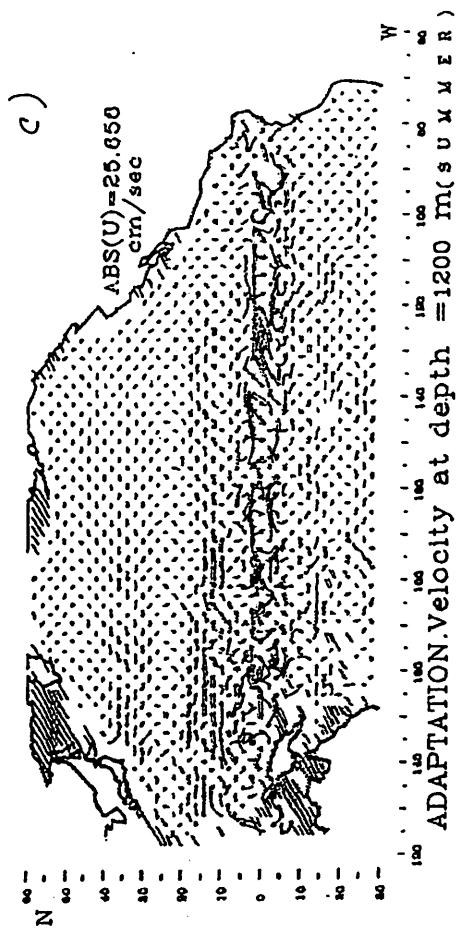
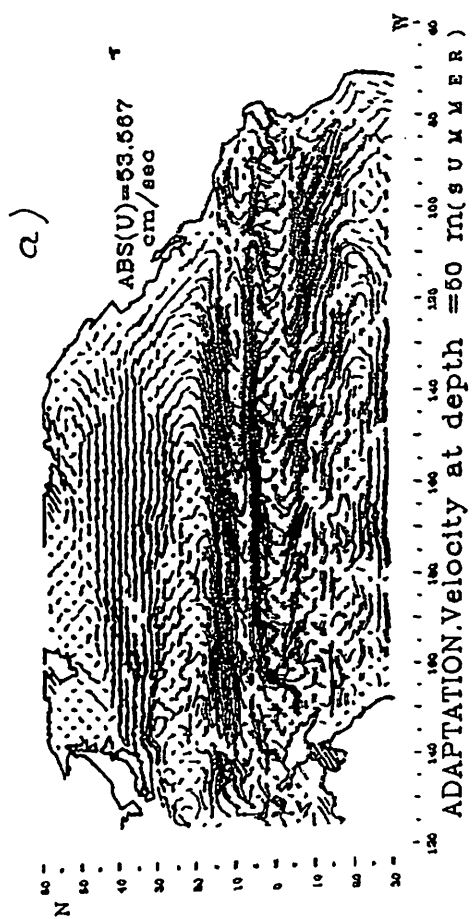
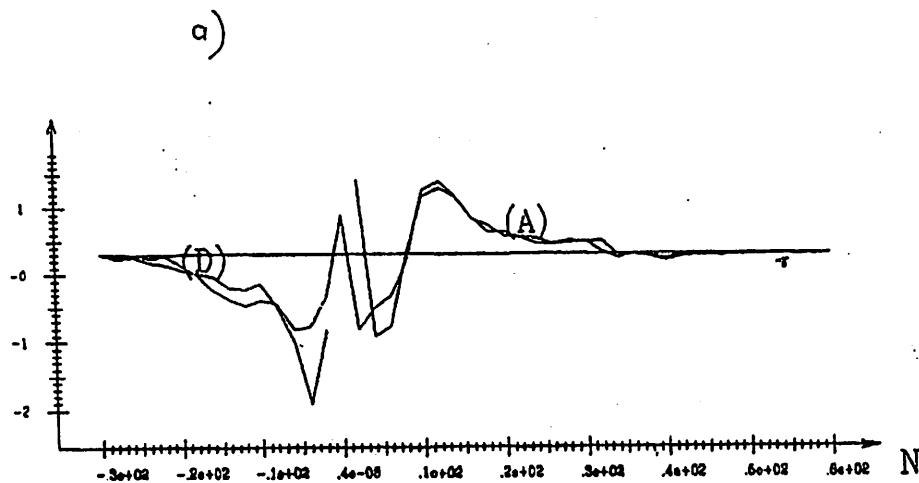
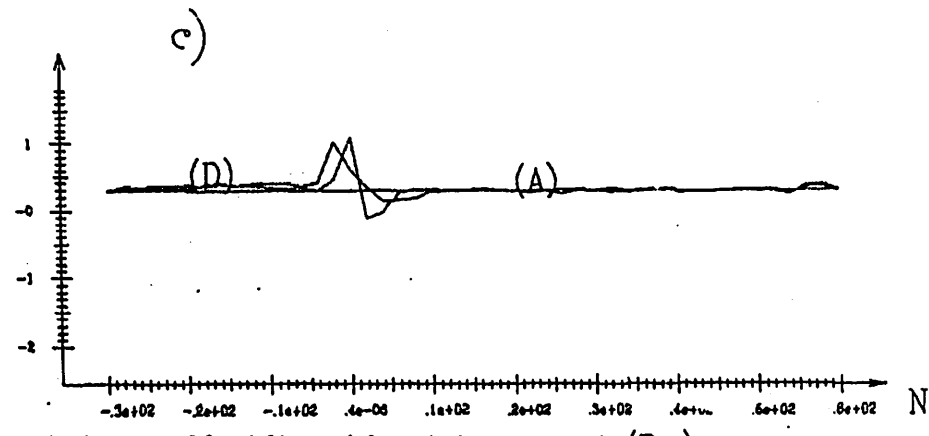


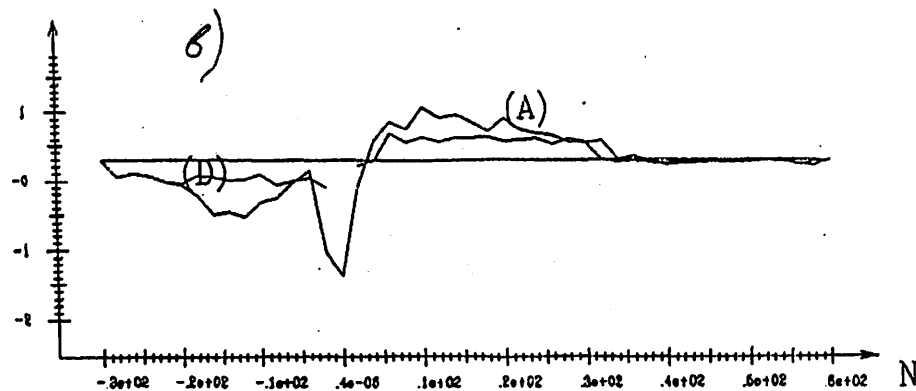
Fig. 5.



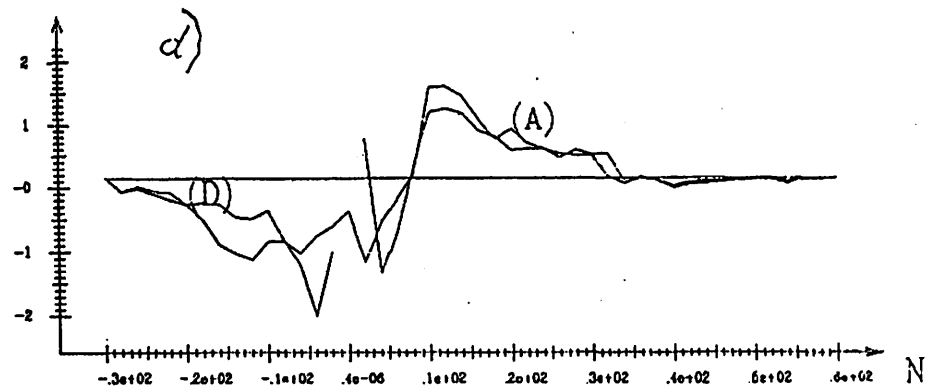
Autumn. Meridional heat transport (Pw).  
 (D)-Diagnoz;(A)-Adaptation. Levels (m)0 -100  
 MAX =.15e+01 MIN =-.23e+01



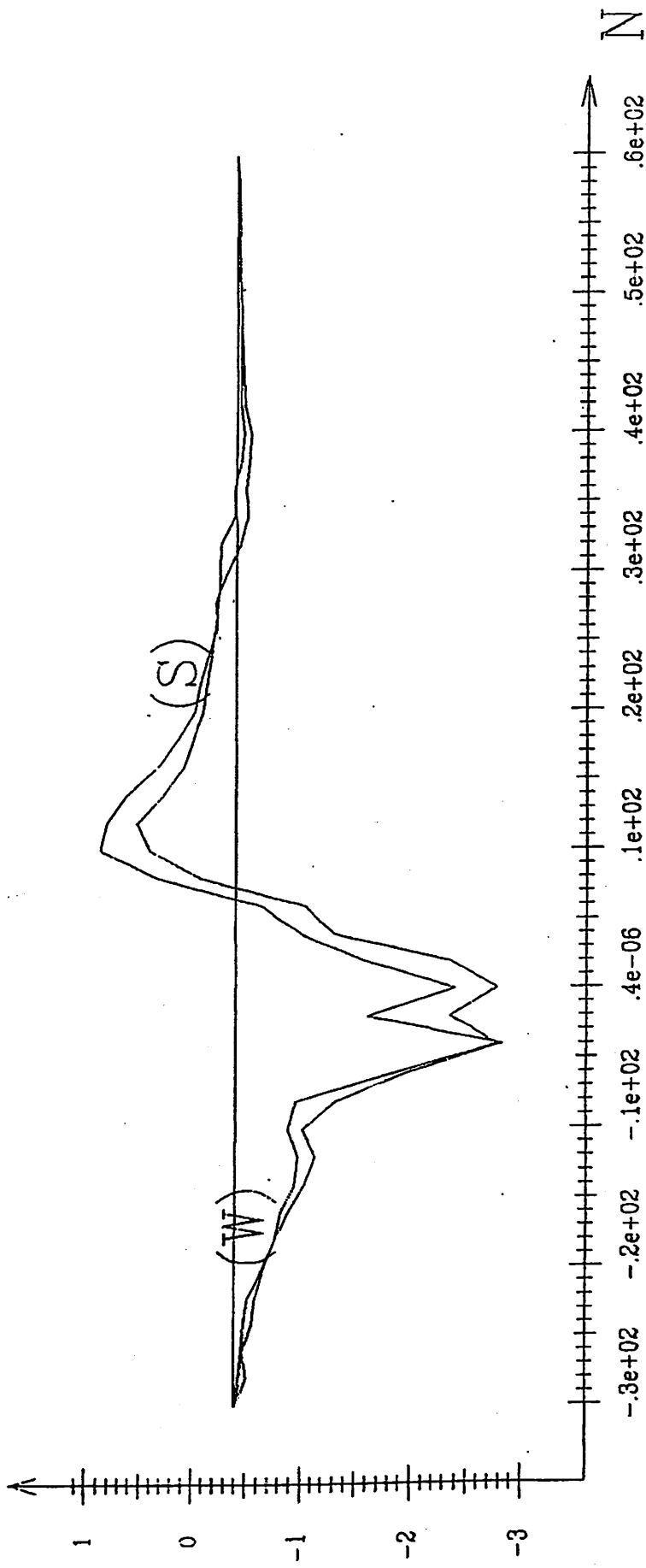
Autumn. Meridional heat transport (Pw).  
 (D)-Diagnoz;(A)-Adaptation. Levels (m)900 -5000  
 MAX =.15e+01 MIN =-.23e+01



Autumn. Meridional heat transport (Pw).  
 (D)-Diagnoz;(A)-Adaptation. Levels (m)100 -900  
 MAX =.15e+01 MIN =-.23e+01



ADAPTATION. Autumn. Meridional heat transport (Pw).  
 (D)-Diagnoz;(A)-Adaptation. Levels (m)0 -5000  
 MAX =.20e+02 MIN =-.22e+01



ADAPTATION. Meridional heat transport (Pw)

(W) - Winter; (S) - Summer. Levels (m) 0 -100

MAX = .15e+01 MIN = -.26e+01

No Evidence for Large Interannual Variations  
In Oceanic Carbon Uptake

By

Kitack Lee<sup>1</sup>, Rik Wanninkhof<sup>2</sup>, Taro Takahashi<sup>3</sup>,  
Scott Doney<sup>4</sup>, and Richard A. Feely<sup>5</sup>

<sup>1</sup>Rosenstiel School of Marine and Atmospheric Science/CIMAS,

University of Miami

4600 Rickenbacker Cswy., Miami, FL 33149

Email: [lee@aoml.noaa.gov](mailto:lee@aoml.noaa.gov) Tel: 305-361-4389 Fax: 305-361-4392

<sup>2</sup>Atlantic Oceanographic and Meteorological Laboratory, NOAA, Miami, FL 33149

<sup>3</sup>Lamont-Doherty Earth Observatory of Columbia University, Palisades, NY 10964

<sup>4</sup>Climate and Global Dynamics, NCAR, Box 3000, Boulder, CO 80307

<sup>5</sup>Pacific Marine Environmental Laboratory, NOAA, Seattle, WA 98115

<sup>1</sup>To whom correspondence should be addressed

submitted to *Nature*

September 29, 1997

Changes in atmospheric CO<sub>2</sub> and <sup>13</sup>CO<sub>2</sub> growth rates suggest that terrestrial and oceanic carbon uptakes vary by 2 to 4 giga tons (Gt) C yr<sup>-1</sup> on interannual time scales<sup>1,2</sup>. Here we estimate the interannual variability of sea-air CO<sub>2</sub> partial pressure differences ( $\Delta p\text{CO}_2 = p\text{CO}_{2\text{SW}} - p\text{CO}_{2\text{AIR}}$ ) using regionally varying seasonal correlations between  $p\text{CO}_{2\text{SW}}$  and sea surface temperature (SST). Intrinsic in our study is the assumption that variations in SST capture the interannual variations of  $p\text{CO}_{2\text{SW}}$ . Variations in oceanic carbon uptake are then computed with an empirical wind speed-gas exchange dependence together with monthly mean wind speed and SST fields for the period between 1982 and 1995. The calculated interannual variability of 0.3 Gt C yr<sup>-1</sup> ( $2\sigma$ ) is an order of magnitude less than inferred from the atmospheric record. Our results suggest that changes in CO<sub>2</sub> uptake by the terrestrial biosphere are probably the main cause of year-to-year variations in the rate of atmospheric CO<sub>2</sub> increase.

Double deconvolution calculations<sup>1,2</sup> using changes in concentration of atmospheric CO<sub>2</sub> and its stable carbon isotope ratio ( $\delta^{13}\text{C}$ ) suggest that oceanic sinks have interannual variability on the order of 3 Gt C ( $2\sigma$ ) from 1982 to 1992 (Fig. 1). However, this conclusion is drawn from atmospheric observations alone and no independent verification utilizing oceanic measurements has been made to date. Such verification is singularly difficult because of spatial and temporal variability in sea-air CO<sub>2</sub> fluxes and lack of global observations on seasonal time scale.

Recently Takahashi *et al.*<sup>3</sup> constructed a monthly mean global distribution of  $\Delta p\text{CO}_2$  for a non-El Niño year using approximately  $2.5 \times 10^5$  measurements made during about 250 expeditions over the past 20 years. Because of the spatial and temporal sparseness of observations, the multi-year data were normalized to 1990 and interpolated onto  $4^\circ \times 5^\circ$  grids and on a monthly time scale using the surface transport field of the Princeton/GFDL General Circulation Model<sup>4</sup>. Sea-air CO<sub>2</sub> fluxes ( $F$ ) were determined by multiplying the sea-air partial pressure difference ( $\Delta p\text{CO}_2$ )<sup>3</sup> with the monthly mean gas transfer velocity ( $k$ ) and solubility ( $K_0$ ):  $F = k K_0 \Delta p\text{CO}_2$ . The gas transfer velocity was calculated from an empirical relationship with wind speed<sup>5</sup>.

Here we estimate the interannual variability in oceanic carbon uptake for the period from 1982 to 1995 utilizing this monthly global climatology of  $\Delta p\text{CO}_2$ <sup>3</sup> and global records<sup>6</sup> of monthly mean wind speed and SST anomalies from the 1990 observations (Fig. 2a). Sea-air CO<sub>2</sub> fluxes can be decomposed into a kinetic ( $k$ ) and a thermodynamic component ( $K_0 \Delta p\text{CO}_2$ ). We assume that the kinetic variability is accounted for by wind speed variations and the thermodynamic variability by SST variations through regional  $p\text{CO}_{2\text{SW}}$ -SST relationships.

The seasonal variations of  $p\text{CO}_{2\text{SW}}$  are controlled primarily by changes in temperature ( $\partial \ln p\text{CO}_{2\text{SW}} / \partial t \approx 0.042$ ) and total CO<sub>2</sub> concentrations ( $\partial \ln p\text{CO}_{2\text{SW}} / \partial \ln \text{TCO}_2 \approx 8$  for tropical and 12 for polar waters). The effects of changes in TCO<sub>2</sub> and SST on  $p\text{CO}_{2\text{SW}}$  are roughly of equal importance but often act in opposite directions. Changes in  $p\text{CO}_{2\text{SW}}$  due to the production of biogenic CaCO<sub>3</sub> are generally small with the exception of coccolithophore blooms in temperate and subpolar seas<sup>7</sup>. Three general trends in the  $p\text{CO}_{2\text{SW}}$ -SST relationship are found in the world oceans (Table 1)<sup>8-17</sup>. In high latitude oceans, the total CO<sub>2</sub> (TCO<sub>2</sub>) increases during seasonal cooling due to the convective mixing of deep waters rich in CO<sub>2</sub>. Thus, the potential lowering of  $p\text{CO}_{2\text{SW}}$  by cooling is opposed and sometimes overtaken by increases due to elevated TCO<sub>2</sub>. Photosynthesis, which reduces  $p\text{CO}_{2\text{SW}}$ , is governed by irradiance which, in turn, affects SST and influences the vertical stability of upper layers of the ocean. Therefore, the observed  $p\text{CO}_{2\text{SW}}$ -SST relationships at high latitude vary seasonally and geographically over a wide range from  $-6\%^\circ\text{C}^{-1}$  in winter to  $+4\%^\circ\text{C}^{-1}$  in summer<sup>8,12</sup>. In temperate and tropical oceans where the mixed layer is thin and vertical mixing is weak, the  $p\text{CO}_{2\text{SW}}$ -SST relationship<sup>12</sup> is seasonally less variable and is positive ranging from  $+1$  to  $+4\%^\circ\text{C}^{-1}$ . In

the Eastern Equatorial Pacific where  $p\text{CO}_{2\text{SW}}$  is controlled by the rate and depth of upwelling, the distribution of  $p\text{CO}_{2\text{SW}}$  is to a large extent controlled by El-Niño/Southern Oscillation (ENSO) event<sup>15,17</sup>. Changes in  $p\text{CO}_{2\text{SW}}$  are strongly inversely correlated with changes in SST. Although the mechanism controlling  $p\text{CO}_{2\text{SW}}$  differs for different regions and seasons, changes in  $p\text{CO}_{2\text{SW}}$  are well correlated with SST variations.

Two different approaches are used to construct global  $\Delta p\text{CO}_2$  maps for individual years between 1982 and 1995. In the first technique, we determine least squares linear fits of monthly climatological  $p\text{CO}_{2\text{SW}}$  and SST values<sup>3</sup> of 1990 for each pixel ( $4^\circ \times 5^\circ$ ) for three seasonal periods, January through April, May through August, and September through December. However, the  $p\text{CO}_{2\text{SW}}$ -SST relationship for the Eastern Equatorial Pacific of  $-6\%^\circ\text{C}^{-1}$  was obtained from measurements made during both the warm and cold phase of the ENSO<sup>15,17</sup>, since the climatology of  $p\text{CO}_{2\text{SW}}$  excludes measurements made during El Niño years. These relationships were then used to calculate the monthly anomalies in  $\Delta p\text{CO}_2$  using the differences between monthly mean SST of 1990 and the observed monthly SST from the NCEP/NCAR reanalysis<sup>6</sup> for each pixel (case 1 in Fig. 2a). A basic premise in this approach is that the same factors that govern seasonal variations in  $p\text{CO}_{2\text{SW}}$  control the interannual variations as well.

The second approach is to use regional  $p\text{CO}_{2\text{SW}}$ -SST relationships reported in numerous published papers<sup>8-17</sup> (case 2 in Fig. 2a). The  $p\text{CO}_{2\text{SW}}$ -SST relationships obtained with the two methods are in good agreement, when seasonal relationships for each pixel are averaged annually over the areas listed in Table 1. The average uptake for 1982-1995 and interannual variability of oceanic carbon uptake obtained for the two methods is similar as well (Fig. 2a).

Since the  $p\text{CO}_{2\text{SW}}$ -SST relationships are by no means exact, sensitivity studies were performed by adjusting the regional relationships by 50% in such a way to maximize and minimize global oceanic carbon uptake. For a maximum uptake scenario (case 3 in Fig. 2a), the  $p\text{CO}_{2\text{SW}}$ -SST relationship for the Eastern Equatorial Pacific was increased by 50% from  $-6\%^\circ\text{C}^{-1}$  to  $-9\%^\circ\text{C}^{-1}$ , whereas  $p\text{CO}_{2\text{SW}}$ -SST relationships for the rest of the oceans were decreased by 50%. For a minimum oceanic uptake (case 4 in Fig. 2a), the opposite condition to case 3 was used. The largest sensitivity to the variations of the  $p\text{CO}_{2\text{SW}}$ -SST relationship, with peak-to-peak difference of 0.4-0.6 Gt C yr<sup>-1</sup>, is found during the large ENSO events (1982-1983 and 1986-1987), whereas the sensitivity is generally smaller during the La Niña events (1984-1985 and 1989).

Most of the variations in oceanic carbon uptake from 1982 to 1989 can be attributed to changes in  $\text{CO}_2$  flux in the eastern equatorial Pacific alone (Fig. 2b). However, the smaller variability in SST in the equatorial Pacific during the 1990s results in significantly smaller variations in the equatorial efflux.

The interannual variations in wind speeds account for less than 10% of the total variations in oceanic carbon uptake except for 1982-1983 and 1986-1987 when strong El Niño events took place. Wind speed anomalies that are predominantly in equatorial regions during the El Niño periods account for 20-30% of the annual oceanic uptake anomalies.

There is good general agreement with sparse interannual observations except that variability in the Eastern Equatorial Pacific is less in our modeled results. Feely *et al.*<sup>17</sup> suggest that approximately  $0.3 \pm 0.2$  Gt C was released to the atmosphere from the Eastern Equatorial Pacific ( $10^\circ\text{N}$ - $10^\circ\text{S}$ ,  $80^\circ\text{W}$ - $135^\circ\text{E}$ ) in 1992,  $0.6 \pm 0.3$  Gt C in 1993, and  $0.7 \pm 0.3$  Gt C in 1994, while our results give the equatorial effluxes of 0.3 Gt C, 0.4 Gt C, and 0.5 Gt C, respectively. An average of observed  $\text{CO}_2$  fluxes (moles C m<sup>-2</sup>) in the Bermuda Atlantic Time-Series (BATS) site<sup>16</sup> ( $31^\circ 50\text{N}$ ,  $64^\circ 10\text{W}$ ) were  $-0.8 \pm 0.3$  ( $1\sigma$ ) moles C m<sup>-2</sup>yr<sup>-1</sup> for a period from 1989 to 1995, while our results give an average flux of  $-1.0 \pm 0.2$  ( $1\sigma$ ) for the same period. At Ocean Station P<sup>18</sup> ( $50^\circ\text{N}$ ,  $145^\circ\text{W}$ ) in the eastern subarctic Pacific, an average  $\text{CO}_2$  flux was  $-0.8 \pm 0.3$  ( $1\sigma$ ) moles C m<sup>-2</sup>yr<sup>-1</sup> over the six



years period from 1973 to 1978. Our modeled oceanic uptake at the same location is  $-1.3 \pm 0.2$  ( $1\sigma$ ) moles C  $m^{-2}yr^{-1}$  over the period between 1982 and 1995.

The sharp contrast between our modeled oceanic carbon uptake variations and those determined from atmospheric double deconvolution calculations can be caused by several factors. Partitioning of carbon between land biosphere and ocean is sensitive to biases in the limited atmospheric  $\delta^{13}C$  record, with an uncertainty of  $\pm 0.015\%$  in  $\delta^{13}C$ , resulting in an error of  $\pm 1$  Gt C  $yr^{-1}$  in partitioning<sup>1</sup>. Interannual changes in growth rates of C3 and C4 plants which have different fractionation factors for photosynthesis ( $\delta^{13}C = -10$  to  $-15\%$  for C4 and  $-25$  to  $-30\%$  for C3) would cause errors in assessments of terrestrial and oceanic carbon uptakes based on atmospheric observations<sup>19,20</sup>. Our method might depress the amplitude of interannual carbon uptake variability. The  $\Delta pCO_2$  climatology<sup>3</sup> smooths the mesoscale variability in local observations, because of normalization of 20 years of data to the virtual year 1990, and because of interpolation of data in space and time by a lateral transport model. The simple  $pCO_{2SW}$ -SST relationships might not capture variability in the fresh water fluxes particularly in the Equatorial Pacific. During ENSO events, low salinity surface water with low  $\Delta pCO_2$  (due to enhanced rainfall) moves from the Western Equatorial Pacific into the Central and Eastern Equatorial Pacific<sup>21</sup>. The eastward movement of fresh water lenses causes a decrease of  $\Delta pCO_2$  in the Central Pacific, which may be partially compensated by higher  $\Delta pCO_2$  in the western-most Equatorial Pacific due to influx of saltier waters<sup>22,23</sup>.

Atmospheric deconvolution models<sup>1,2</sup> suggest that environmental factors such as ENSO events have a large influence on the interannual variability in oceanic carbon uptake. Our results show the same, but the magnitude of the interannual variability in our oceanic carbon uptake is much smaller. Updates in the atmospheric deconvolutions show smaller interannual variability but still significantly larger than we estimate<sup>24</sup>. The use of the  $pCO_{2SW}$ -SST relationship is a first step in estimating interannual variations in global sea-air  $CO_2$  fluxes. Recent work using 3-D global circulation model by Le Quéré *et al.*<sup>25</sup> also suggested that the interannual variability in oceanic carbon uptake is significantly smaller than inferred from changes in atmospheric  $CO_2$  and  $\delta^{13}C$  and that most of the variability is in the Eastern Equatorial Pacific. In the future, the use of satellite-derived observations of ocean color and SST along with ground truthing should improve temporal and spatial extrapolations of  $pCO_{2SW}$  fields and thus increase our confidence of estimates of interannual variability in oceanic carbon uptake.

## REFERENCES

1. Francey, R.J., Tans, P.P., Allison, C.E., Enting, I.G., White, J.W.C. and Trollier, M. Changes in oceanic and terrestrial carbon uptake since 1982, *Nature*, 373, 326-373 (1995).
2. Keeling, C.D., Whorf, T.P., Wahlen, M. and Plicht, J.V. Interannual extremes in the rate of rise of atmospheric carbon dioxide since 1980, *Nature*, 375, 666-670 (1995).
3. Takahashi, T., Feely, R.A., Weiss, R., Wanninkhof, R.H., Chipman, D.W., Sutherland S.C. and Takahashi, T.T. Global air-sea flux of  $CO_2$ : An estimate based on measurements of sea-air  $pCO_2$  difference, *Proc. Natl. Acad. Sci.*, 94, 8292-8299 (1997)
4. Cox, M.D. A primitive, 3-dimensional model of the ocean, *GFDL Ocean Group Tech. Rep. 1*, 143 pp., Geophys. Fluid Dyn. Lab., Princeton Univ., Princeton (1984).
5. Wanninkhof, R. Relationship between wind speed and gas exchange over the ocean, *J. Geophys. Res.*, 97, 7373-7382 (1992).
6. Kalnay, E., Kanamitsu, M., Kistler, R., Collins, W., Deaven, D., Gandin, L., Iredell, M., Saha, S., White, G., Janowiak, J., Mo, K.C., Ropelewski, C., Leetmaa, A., Reynolds, R. and Jenne, R. The NCEP/NCAR 40-year reanalysis project, *Bull. Amer. Meteor. Soc.*, 77, 437-471 (1996).

7. Balch, W.M., Holligen, P.M., Ackleson, S.G. and Voss, K.J. Biological and optical properties of mesoscale coccolithophore blooms in the Gulf of Main. *Limnol. Oceanogr.*, 36, 629-643 (1991).
8. Watson, A.J., Robinson, C., Robinson, J.E., Williams, P.J.B. and Fasham, M.J.R. Spatial variability in the sink for atmospheric carbon dioxide in the North Atlantic. *Nature*, 350, 50-53 (1991).
9. Poisson, A., Metzl, N., Brunet, C., Schauer, B., Bres, B., Ruiz-Pino, D. and Louanchi, F. Variability of sources and sinks of CO<sub>2</sub> in the Western Indian and Southern Oceans during the year 1991. *J. Geophys. Res.*, 98, 22759-22778 (1993).
10. Stephens, M.P., Samuels, G., Olson, D.B. and Fine, R.A. Sea-air flux of CO<sub>2</sub> in the North Pacific using shipboard and satellite data. *J. Geophys. Res.*, 100, 13571-13583 (1995).
11. Metzl, N., Poisson, A., Louanchi, F., Brunet, C., Schauer, B. and Bres, B. Spatio-temporal distributions of air-sea fluxes of CO<sub>2</sub> in the Indian and Antarctic oceans. *Tellus*, 47B, 56-69 (1995).
12. Takahashi, T., Olafsson, J., Goddard, J.G., Chipman, D.W. and Sutherland, S.C., Seasonal variation of CO<sub>2</sub> and nutrients in the high-latitude surface oceans: a comparative study. *Global Biogeochem. Cycles*, 7, 843-878 (1993).
13. Tans, P.P., Fung, I.Y. and Takahashi, T. Observational constraints on the global atmospheric CO<sub>2</sub> budget. *Science*, 247, 1431-1438 (1990).
14. Inoue, H.Y., Matsueda, H., Ishii, M., Fushimi, K., Hirota, M., Asanuma, I. and Takasugi, Y. Long-term trend of the partial pressure of carbon dioxide (pCO<sub>2</sub>) in surface waters of the western North Pacific, 1984-1993. *Tellus*, 47B, 391-413 (1995).
15. Landrum, L.L., Gammon, R.H., Feely, R.A., Murphy, P.P., Kelly, K.C., Cosca, C.E. and Weiss, R.F. North Pacific Ocean CO<sub>2</sub> disequilibrium for spring through summer, 1985-1989. *J. Geophys. Res.*, 101, 28539-28555 (1996).
16. Bates, N.R., Takahashi, T., Chipman, D.W. and Knap, A.H. Variability of pCO<sub>2</sub> on diel to seasonal timescales in the Sargasso Sea. *J. Geophys. Res.* (in the press).
17. Feely, R.A., Wanninkhof, R., Takahashi, T. and Tans, P. The role of the equatorial Pacific sea-air exchange fluxes on the atmospheric CO<sub>2</sub> growth rate during and after the 1991-94 ENSO event, (in preparation).
18. Wong, C.S. and Chan, Y.-H. Temporal variations in the partial pressure and flux of CO<sub>2</sub> at ocean station P in the Subarctic Northeast Pacific Ocean. *Tellus*, 43B, 206-223 (1991).
19. Ciais, P., Tans, P.P., Trolier, M., White, J.W.C. and Francey, R.J. A large Northern Hemisphere terrestrial CO<sub>2</sub> sink indicated by the <sup>13</sup>C/<sup>12</sup>C ratio of atmospheric CO<sub>2</sub>. *Science*, 1098-1102 (1995).
20. Field, C.B., Berry, J.A., Denning, A.S., Fung, I.Y., Randerson, J.T., Tans, P. and Tucker, C.J. C4 photosynthesis, atmospheric <sup>13</sup>C, and the distribution of carbon sink between land and ocean, Fifth International Carbon Dioxide Conference, 97 CO<sub>2</sub> Extended Abstract, Cairns, Queensland, Australia (1997).
21. Feely, R.A., Wanninkhof, R., Cosca, C.E., Murphy, P.P., Lamb, M.F. and Steckley, M.E. CO<sub>2</sub> distribution in the Equatorial Pacific during the 1991-1992 ENSO event. *Deep-Sea Res. II*, 42, 365-386 (1995).
22. Fushimi, K. Variation of carbon dioxide partial pressure in the Western North Pacific surface water during the 1982/83 El Niño event. *Tellus*, 39B, 214-227 (1987).
23. Takahashi, T., Chipman, D.W., Goddard, J., Mathieu, G. and Ma, L. Carbon dioxide in the surface water of the western equatorial Pacific Ocean, Proceedings of US-PRC international TOGA symposium, 511-539 (1988).
24. Piper, S.C., Keeling, C.D., Wahlen, M. and Plicht, H.V. Temporal and spatial variations in terrestrial biospheric and oceanic sources and sinks of CO<sub>2</sub> since the early 1980s. Fifth International Carbon Dioxide Conference, 97 CO<sub>2</sub> Extended Abstract, Cairns, Queensland, Australia (1997).

25. Le Quéré, C., Orr, J.C. and Monfray, P. Modelling the interannual variability of the air-sea flux of carbon for the year 1979-1993, Fifth International Carbon Dioxide Conference, 97 CO<sub>2</sub> Extended Abstract, Cairns, Queensland, Australia (1997)

#### ACKNOWLEDGEMENT

This work was supported by the NOAA's Oceanic Atmosphere Carbon Exchange Study (OACES). We thank Kenneth Masarie and Thomas Conway of NOAA-CMDL for providing regional climatology of CO<sub>2</sub> dry mixing ratios in air for 1982-1995.

Table 1 The regional pCO <sub>2SW</sub> -SST relationships			
Oceans	Case #1 PCO <sub>2SW</sub> -SST <sup>#</sup>	Case #2 PCO <sub>2SW</sub> -SST <sup>*</sup>	N <sup>§</sup>
North Atlantic and Pacific (40°N-70°N)	-2 ± 2.7% <sup>&amp;</sup>	-4% (-4%) <sup>8,12</sup>	142
Subtropical gyres (40°S-40°N)	1.5 ± 2.4%	1 to 4% (2.5%) <sup>10,12,13,14,15,16</sup>	912
Central and Eastern Pacific (10°N-10°S, 80°W-150°W)	-6% <sup>@</sup>	-4 to -7% (-6%) <sup>15,17</sup>	69
Southern Ocean (40°S-70°S)	-1.7 ± 2.1%	-1.5% (-1.5%) <sup>9,11,12,13</sup>	508

# The pCO<sub>2SW</sub>-SST relationships were derived from climatological pCO<sub>2SW</sub> and SST values<sup>3</sup> for each 4°×5° pixel in 1990 and averaged over the annual cycle for the areas listed in column 1.

\* Literature values of pCO<sub>2SW</sub>-SST relationships from measurements made during various seasons. Values in parenthesis were used for calculation for case 2 in Figure 2.

& The standard deviations (S.D) for the climatological pCO<sub>2SW</sub>-SST relationships averaged over the entire region. For case 1, seasonal pCO<sub>2SW</sub>-SST relationships for individual grid boxes were used, and the S.D. presented here does not reflect the uncertainty in oceanic carbon uptake.

@ Literatures values<sup>15,17</sup> were used for the Eastern Equatorial Pacific, since the climatology<sup>3</sup> of pCO<sub>2SW</sub> does not include measurements made during El Niño years.

§ Number of grid boxes in the regions.

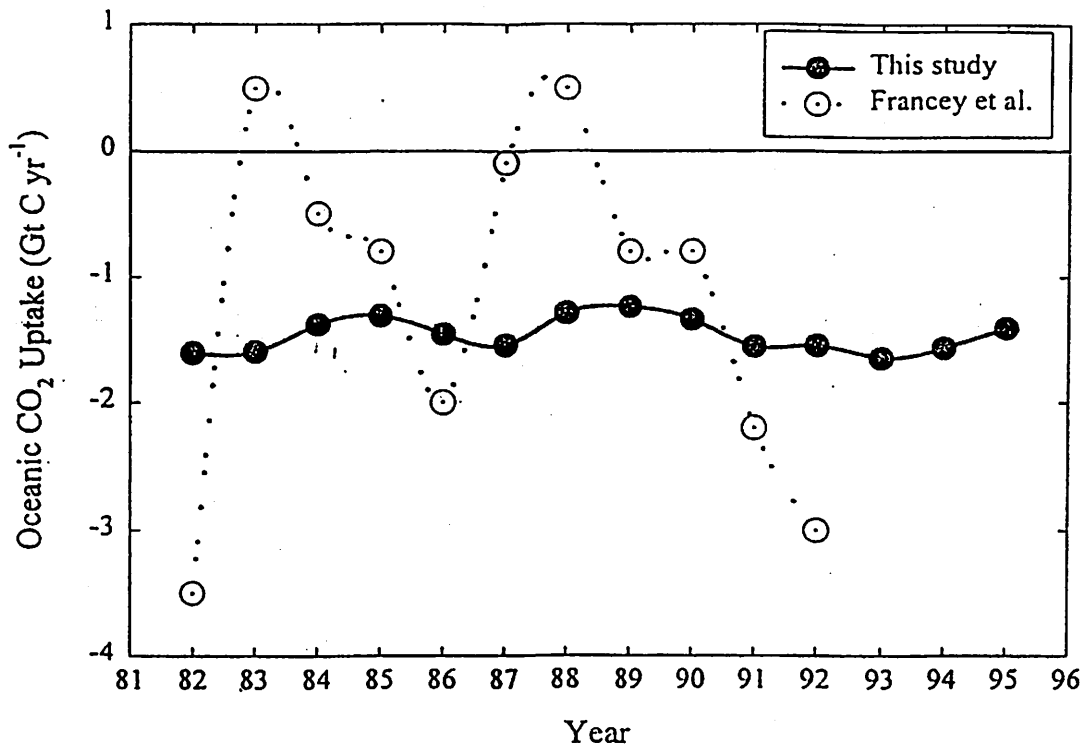


FIG. 1 Interannual variability of oceanic CO<sub>2</sub> uptake (1982-1995) obtained from this study (for case 1 in Fig. 2) compared with the results from Francey *et al.*<sup>1</sup>.

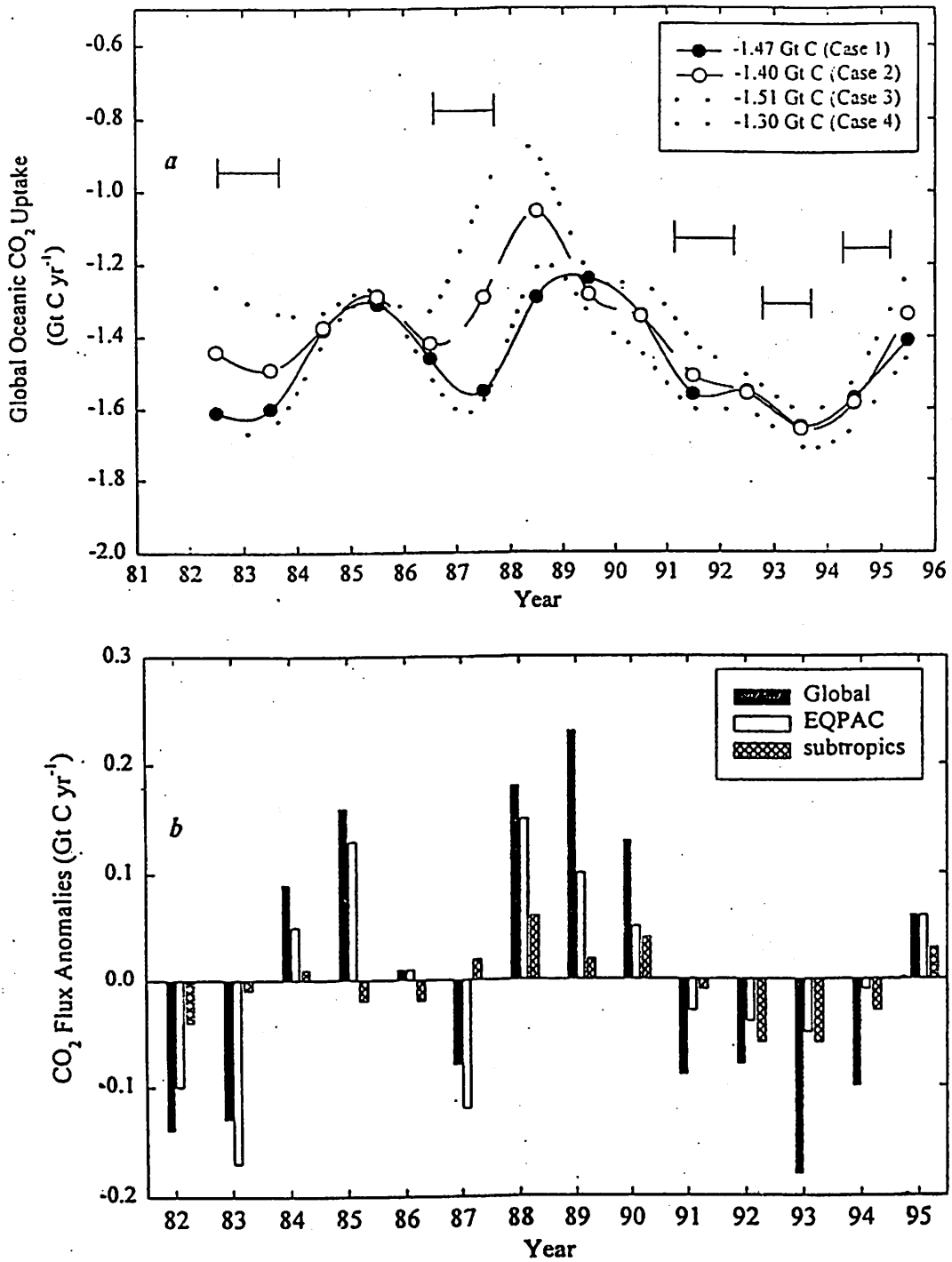


FIG. 2 *a*, Global oceanic uptakes from 1982 to 1995 for 4 different scenarios discussed in the text. Horizontal bars indicate times of El Niño events. The 14-year mean global oceanic uptakes for four different scenarios are listed in the legend. The curves are spline fits. *b*, Annual flux anomalies for the globe, the Eastern Equatorial Pacific (EQPAC), and subtropical oceans calculated from the results of case 1. The flux anomalies are differences from a 14-year average of  $-1.47$  Gt C for the globe, of  $0.3$  Gt C for EQPAC and of  $-0.9$  Gt C for subtropical gyres.

### 3. POC Topic(물리해양분과)

Seasonal variability of currents in the area of eastern Sakhalin(사할린 동쪽 해역에서 해류의 계절 변동) .....	55
Salt ice and dense water production in the northern Okhotsk Sea coastal polynyas in winter 1995~1996(1995~1996 겨울 북쪽 오후츠크해 연안 비빙결수권에서 염빙과 무거운 해수의 생성) .....	70
Some features of mesoscale and small scale water dynamics in the southern Okhotsk sea seen by the ers-1 synthetic aperture radar(ERS-1 합성 개구 레이더에 의해 관측된 남쪽 오후츠크해에서의 중규모 및 소규모 해양 역학의 몇 가지 특징) .....	78
Mechanisms of influence of coastal and shelf waters on the open sea bioproductivity(외해역 생물생산에 미치는 연안과 대륙붕 해수의 영향 메커니즘) .....	84
Present status on NEAR-GOOS real time data base at the Japan Meteorological Agency(일본 기상청의 NEAR-GOOS 실시간 데이터 베이스 현황) .....	114
Some oceanographic features of the Okhotsk Sea derived from historical hydrographic observations(역사적인 해양특성관측치로부터 유추된 오후츠크해의 몇가지 해양학적 특징) .....	120
Thermal structure of the north-western Japan Sea(East Sea) upper layer : climate and variability(북서 동해 상층의 온도 구조 : 기후와 변동) ...	124

# **SEASONAL VARIABILITY OF CURRENTS IN THE AREA OF EASTERN SAKHALIN**

*Budaeva V. D\*, Makarov V.G\*\*, Gavrilevsky A.V.\**

*\*Far Eastern Regional Hydrometeorological Research Institute, Vladivostok, Russia*

*\*\* Pacific Oceanological Institute of The Far Eastern Branch The Russian Academy of Sciences, Vladivostok, Russia*

The eastern Sakhalin shelf is characterized by a complex spatial-temporal variability of sea water circulation, current fields, hydrological properties and their vertical distribution. It is conditioned by combined activity of multiple factors resulting in variability of shelf waters regime: atmospheric effects and intensive water exchange with open sea zones; inhomogeneous velocity field of tidal currents facilitating vortex formations, effects of the Amur water discharge [1-5].

Modern perceptions of sea water circulation in the area of the eastern Sakhalin shelf are based on calculations fulfilled with the help of dynamic method. The conclusion on prevailing cyclonic character of coastal circulation is conventionally referred to warm and cold seasons. However, due to relatively shallow sea in the area of the eastern Sakhalin shelf zone and its considerable meridional stretching the circulation there is much influenced by strong local winds of monsoon type. Under specific baric situations these winds can transform the global sea level gradient, and the structure of coastal currents. These real situations are not accounted in calculations based on dynamic method.

Instrumental observations over currents in the area of the eastern Sakhalin are not numerous. They can be only used for local forecasting of short-period variability of currents. Thus, one way to understand variability of stationary currents on so great area is numerical calculations with the help of modern diagnostic models.



For calculations the improved version of three-dimensional linear diagnostic model of the Ekman type [6] developed for coastal deeper areas of Sakhalin was used. For the distinguished wind situations this model was applied to forecast sea water circulation and three-dimensional field of currents in the coastal Sakhalin are over the grid with  $20 \times 20$  minutes approximation of the calculated area. A number of nodal points of the grid - 282; maximal depth in the area under study - 3 200 m.

To investigate the structure of sea water circulation and three-dimensional field of currents in the area of eastern Sakhalin between  $43^{\circ}50'$ - $54^{\circ}30'$  N, shoreline and  $146^{\circ}00'$  W the deep sea oceanographic observations collected in 1947-1995, and typical wind situations for summer and autumn were used. As the field  $\Psi$  is sensitive to errors in values  $\rho$  in deep sea below 1 500 m the density was assumed constant. Integral water transport through the La Perouse and Kunashir Straits are set in accordance with [7]. Coefficient of vertical turbulent exchange was assumed constant and was accordingly given as  $10^2$  ( $\text{cm}^2 \cdot \text{sec}^{-1}$ ).

Gridal representation of seafloor topography was obtained from bathymetric maps and numerical massive data of National Geophysical Data Center (NOAA, US).

### ***Results of numerical modeling and their discussion***

Appendix I demonstrates the results of numerical calculations of sea water circulation and nontidal surface current fields on the eastern Sakhalin shelf for the most characteristic for summer and autumn wind situations. From the Figures one can see that sea water circulation structure and current fields on the eastern Sakhalin shelf observed in summer differ a lot from the ones observed in autumn. The main differences are manifested in changing vector of integral water transport in the area of shallow waters and internal shelf edge. In summer under prevailing *south* directed winds (basic wind type in

summer) surface sea water circulation looks like an intensively meandering flow north-east directed, with a system of vortices on its lateral boundaries in the north and south of the area under study. The tendency of changing current vectors is well pronounced in the shelf zone of north-eastern Sakhalin. It is manifested in generation of north directed flows blocking the East Sakhalin Current in surface layers and shifting its axis seaward. In eastern Terpeniye Bay sea water surge is observed; warm waters from the Sea of Japan actively penetrate northward along the south-eastern Sakhalin coasts. Prevailing speeds of surface currents make up 15-30 cm/sec, maximal speed - 50 cm/sec. (Appendix I, Fig.1). One should mention that in summer, even at weak south directed winds, the East Sakhalin Current on the north-eastern Sakhalin shelf in surface layers is not an integral stream. As a relatively uniform stream, southward directed along the outside shelf edge it is observed beyond 200 m isobath to the east of 144° W.

Under stable *south-western* winds (another summer wind type characteristic of the northern part of model area) the north directed flow with 5-15 m/sec speed is observed only on the shelf between Terpeniye and Yelizaveta Capes. In the area under study at large north-east and east directed transport of surface water is predominant.

The activity of south-east and east directed winds is accompanied by broadening and intensifying northern coastal flow in shelf zone of north-eastern Sakhalin coasts. Its speeds on sea surface are 15-30 cm/sec. Prevalence of winds with eastern constituent also causes sea water surge along south-eastern coasts of Sakhalin and generation of north-western flows in the La Perouse Strait forcing the Soya Current to go down.

Surface currents' reaction to stable western and north-western winds is manifested in principle changes in summer circulation scheme. Well pronounced is the flow of general south (south-east) direction, whose intensification is observed in the shelf zone of north-eastern Sakhalin coasts,

along Terpeniye Cape traverse ( $> 50$  cm/sec). One should point out that, unlike other situations, directions of surface and near bottom currents in this zone coincide. This is characteristic of autumn velocity profile. In case of west and south-west directed winds the ebb of sea water along the south-eastern Sakhalin coasts was observed. Speeds of surface currents were 10-15 cm/sec.

Notable changes in general summer scheme of currents are observed in case of *southern* and *south-western* winds. (Appendix I, Fig.2). The data available support the assumption that in the northern part of the area under study, upon open sea water washing shelf edge, the current diverges: part of water at  $53^{\circ} - 54^{\circ}$ N deviates north-eastward and at Yelizaveta Cape traverse blocks the penetration of the deluded Amur water; the main stream turns south-westward (southward) and, on its way along the north-eastern coasts of Sakhalin, enters Terpeniye Bay. On the shelf of south-eastern Sakhalin, when southern and south-eastern winds prevail, in the direction of surface along-shoreline currents the south-western mode prevails. Dynamically active zones, where surface current speeds exceed 50 cm/sec, are observed in the areas of capes. Weak southern winds do not cause notable transformation of summer current field on the shelf of eastern Sakhalin : the schemes of surface currents for this very case and situations "summer-calm" are much alike.

In autumn the East Sakhalin Current is maximally developed and is south-east and south-south-east directed. Under stable western and south-western winds (prevailing wind type for autumn) its transport increases considerably as well as the surge of surface water (most active under south-western winds) near shoreline. For the field of integral sea water circulation one should point out the formation of two wind-generated vortices. In the northern part it is cyclonic, in the southern part it is anticyclonic. This type of wind circulation is characterized by complex vertical structure of currents in the southern part of the area, it is mainly two-layer: compensational flows are north

directed, their speed at 100 m horizon makes up 5-10 cm/sec (Appendix I, Fig.3).

Under stable southern and south-western winds (second important wind type for autumn) the general transport of surface waters is north-east directed; current system both surface and in deep sea is mainly anticyclonic (Appendix I, Fig.4), consequently it causes the shift of the East Sakhalin Current's axis to the shelf edge, which is not observed in its western branch at Terpeniye Cape traverse, as well as generation of great anticyclonic eddy to the east of Yelizaveta Cape. Surge of sea water in the eastern Terpeniye Bay blocks penetration of open sea water into the bay (however, in autumn, in case of weak southern winds, as well as in case of calm the open sea waters, the western branch of the East Sakhalin Current, enter the eastern Terpeniye Bay). Prevailing speeds of surface currents under stable southern and south-western winds make up 20-40 cm/sec with maximal velocities to be over 50 cm/sec. Near bottom the intensity of currents in this bay gets considerably weaker, in the direction of currents the northern and north-western mode prevails.

Under stable northern winds intensification of southern flows is observed; sea water ebb takes place in the eastern Terpeniye Bay, as well as, consequent, activation of the western branch of East Sakhalin Current. In autumn, under weak northern winds, the general character of water circulation on the shelf of eastern Sakhalin remains the same, but its intensity changes.

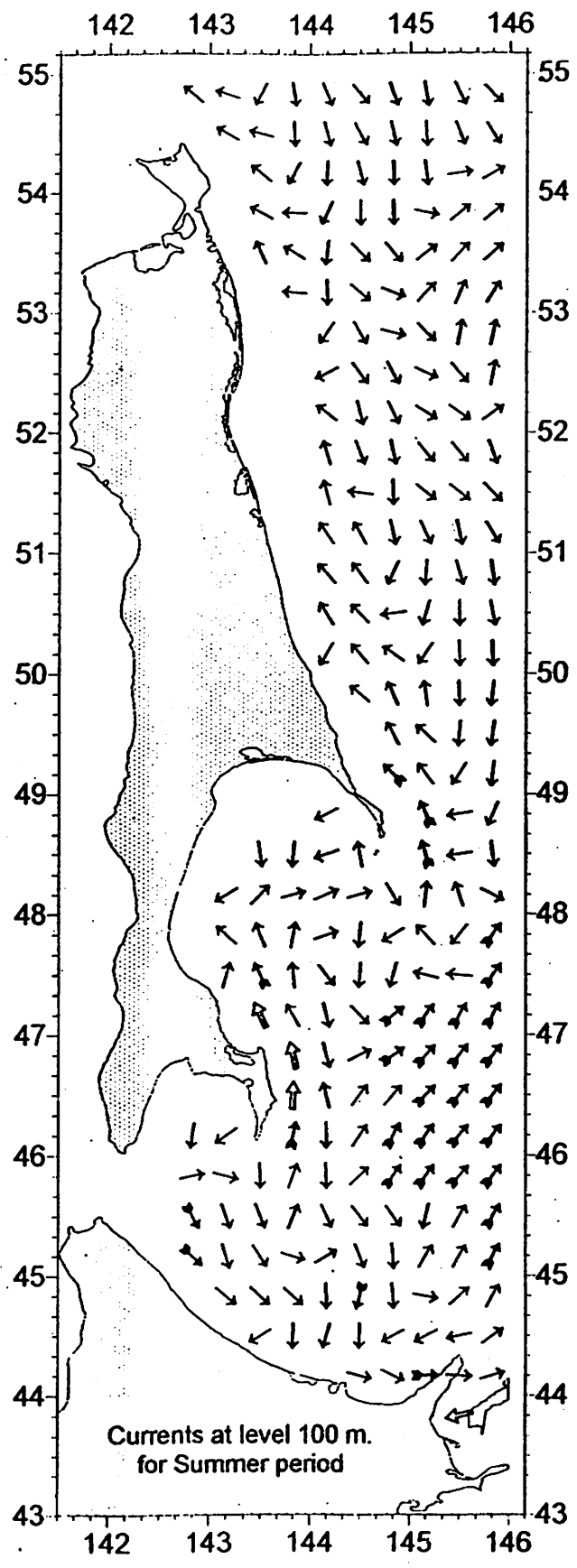
In autumn, under prevailing winds with south-eastern constituent the general transport of surface waters is mainly realized north-westward, that is toward shoreline. Near south-eastern shores of Sakhalin and in the western La Perouse Strait the surge of waters is observed. It causes sea level gradient decrease between the Seas of Japan and Okhotsk. Durable influence of north-eastern and eastern winds can change the sign of sea level gradient in the La Perouse Strait and western surface current in the strait, blocking the Soya

Current. These situations are characterized by well-distinguished two-layer vertical structure of currents on the shelf of eastern Sakhalin. Maximal speeds of surface currents may reach 50 cm/sec. and more in Aniva and Terpeniye Bays.

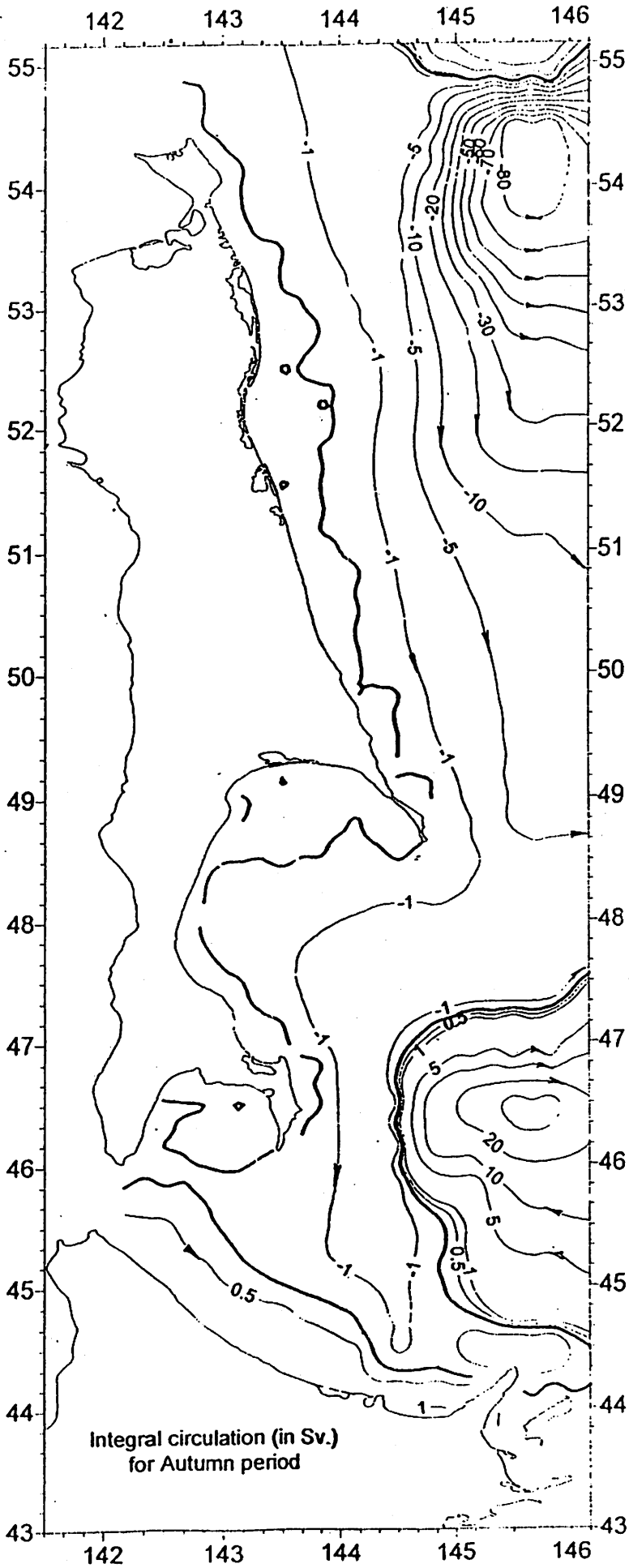
*According to model calculations fulfilled for the shelf of eastern Sakhalin the field of currents there is dynamic and considerably dependent on characteristics of wind situation type. For regime monsoon winds observed on the shelf of eastern Sakhalin two general types of sea water circulation can be conventionally distinguished: summer and "winter" (autumn). Summer horizontal structure of currents is characterized by shifting of the East Sakhalin Current's axis to the shelf edge and generating of drifting northern currents with prevailing northern and north-eastern modes in surface sea water. Autumn structure is characterized by intensification of southern flows and prevalence of southern and south-eastern modes in the vectors of surface currents. Summer integral water transport to the north does not exceed 0.2-0.3 Sv, in autumn transport of the East Sakhalin makes up about - 1-2 Sv.*

## **References**

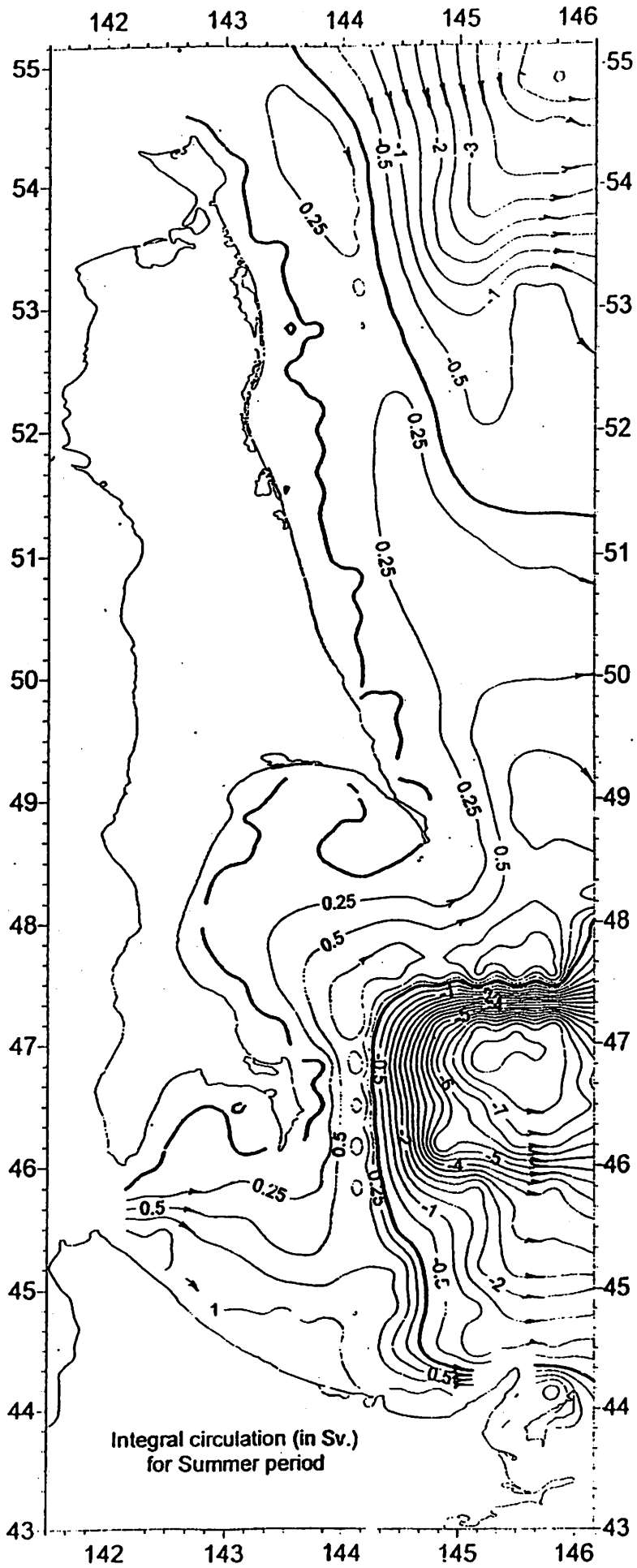
1. Leonov A.K. Regional oceanography.- L.: Hydrometeoizdat , 1960, P. 1.
2. Moroshkin K.V. New scheme of surface currents in the Sea Okhotsk-  
Oceanology. 1964. N. 4, PP. 641-643.
3. Moroshkin K.V. Water masses of the Sea Okhotsk.-M.: Science. 1966. 66 p.
4. Hydrometeorology and hydrochemistry of seas. Sea of Okhotsk. Vol. IX.  
Issue 2.  
Hydrochemical conditions and oceanological principles of biological  
productivity  
formation.- L.: Hydrometeoizdat . 1993, 167 pages.
5. Budaeva V.D. Regularities of oceanological conditions formation in the  
coastal fishery  
areas of Sakhalin.- Dr. Sc. (Geography) Thesis.- M.: preprint SOI, 1981, 25  
pages.
6. Budaeva V.D., Makarov V.G. Melnikova I.Yu. Diagnostic modeling of  
stationary current in Aniva Bay and La Perouse Strait. Proceedings.  
FERHRI. 1980, issue 87, pp.66-78.
7. Sekine Y.A. A barotropic model for the wind -driven circulation in the in  
the Okhotsk Sea. -Bull. Fac. Bioresources, Mie Univ., N. 3, pp. 25-29:

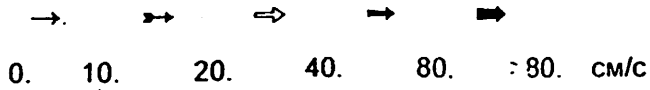
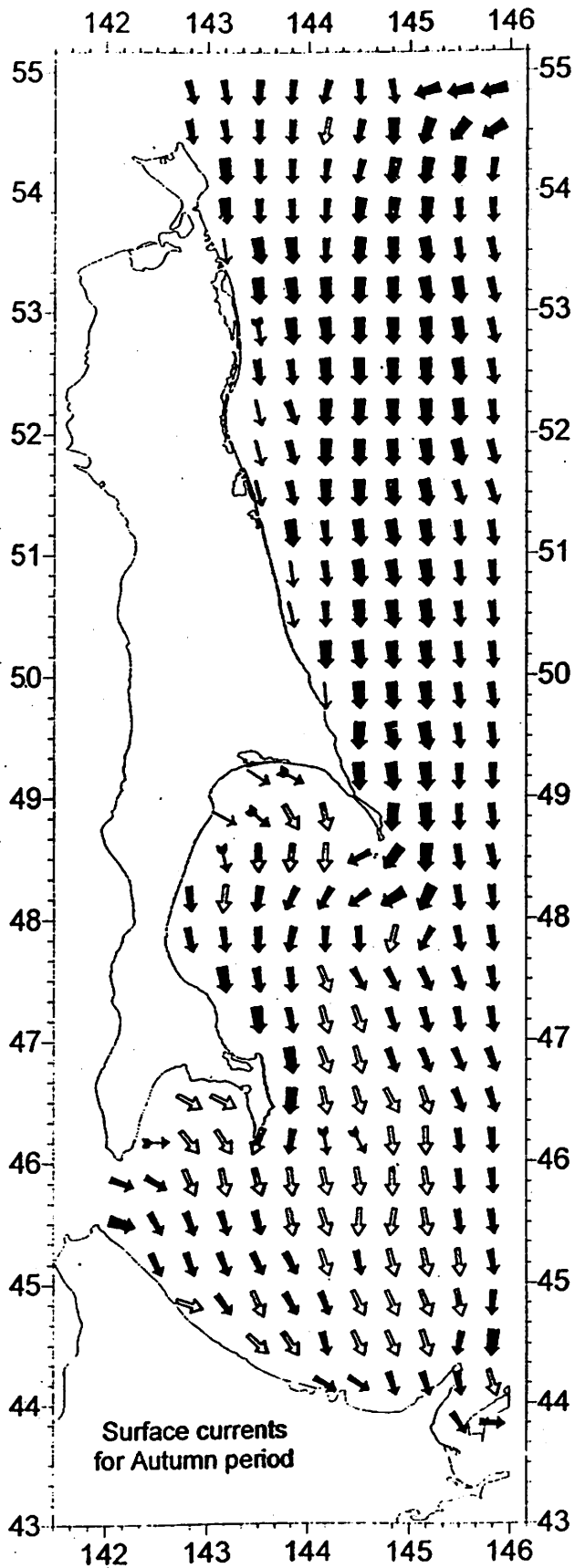


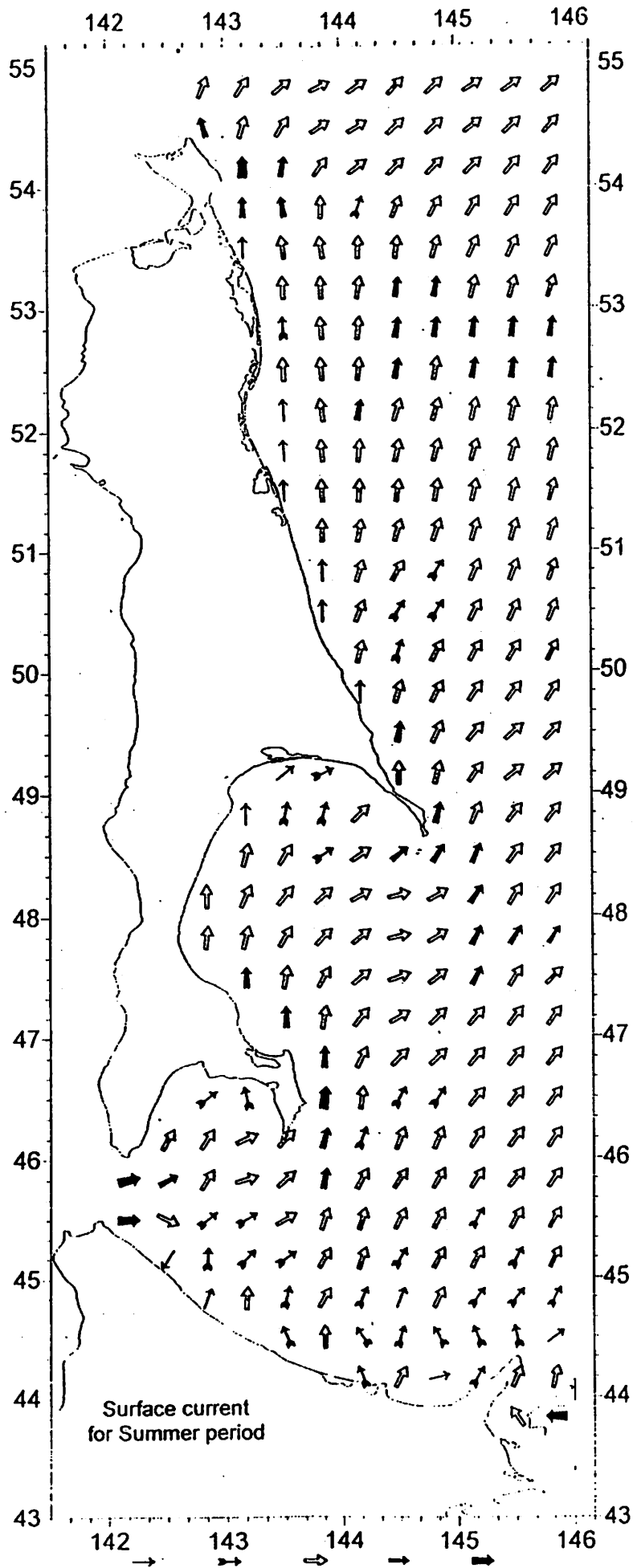
Currents at level 100 m.  
for Summer period

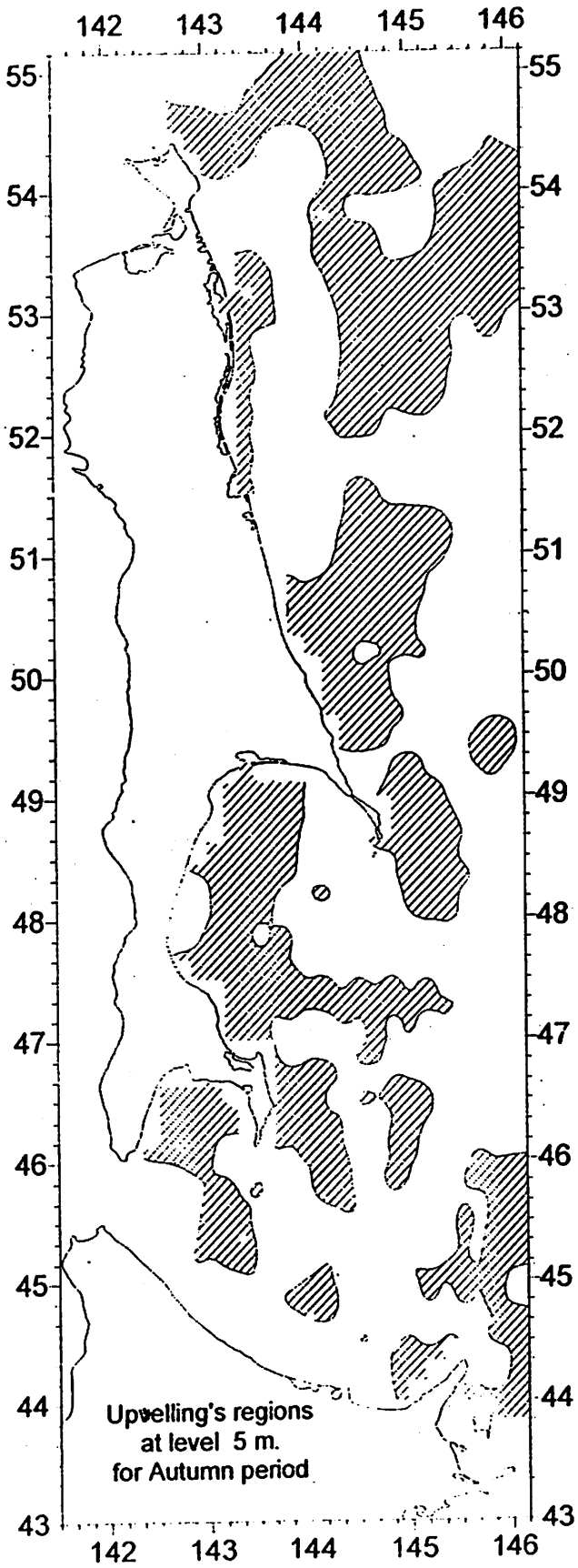


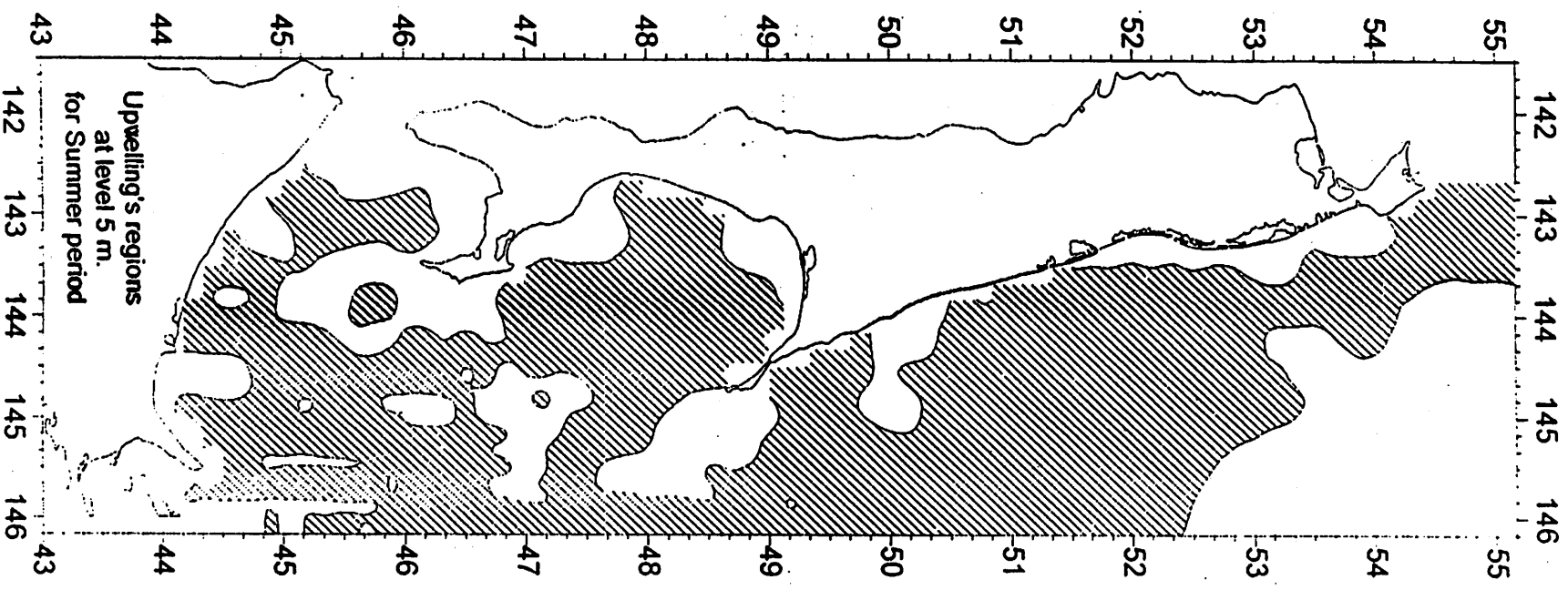




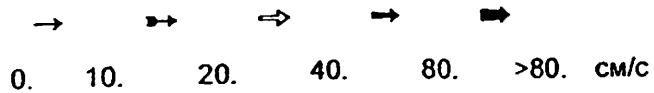
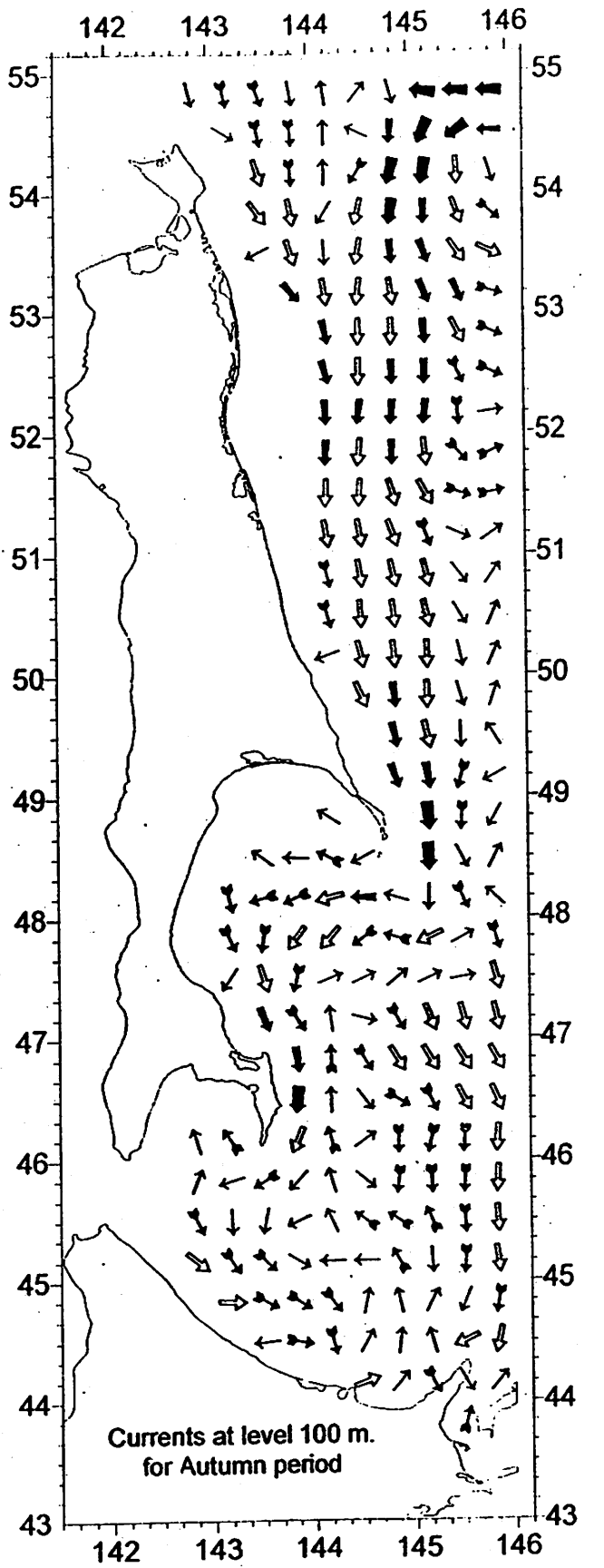








Upwelling's regions  
at level 5 m.  
for Summer period



**Salt ice and dense water production in the northern Okhotsk Sea  
coastal polynyas in winter 1995-1996**

S. V. Gladyshev

Pacific Oceanological Institute, Russian Academy of Sciences  
43 Baltiyskaya St. Vladivostok 690041, Russia

## **1. Introduction**

The broad northern Okhotsk Sea shelf is the main ventilation site for North Pacific Intermediate Water. This high-latitude overturning is an important North Pacific part of the global thermohaline circulation widely distributed over shelves of the Arctic and Antarctic Seas. Salt is redistributed and dense water forms during brine rejection from sea ice growth in coastal polynyas. Salty plumes emanate from ice crystals and sink to the bottom, slightly mixing with surrounding waters. As a result, a cold and saline bottom lens is formed with a salinity which can exceed the overrunning by 1-2.5 psu. According to Cavalieri and Martin (1994), the total productivity of arctic polynyas is 0.7-1.2 Sv, and more than a half of this dense water is produced by the Gulf of Anadyr polynya and polynyas near Cape Lisburn, located on the shelf of the Canadian Arctic Basin. The dense shelf bottom water mixes with slope water and forms a cold arctic halocline in the Arctic Basin. Okhotsk Sea coastal polynyas are the most productive. Alftis and Marin (1987) (hereafter AM) have estimated their average volume flow rate as 0.5 Sv and have suggested this transport is strong enough to freshen and cool of the North Pacific Intermediate Water because there is extensive exchange between the Okhotsk Sea and North Pacific waters through the Kuril Arc. AM have also indirectly estimated ice and salt production in northern Okhotsk Sea shelf polynyas using bulk formulae to calculate atmospheric fluxes in winter.

The main purposes of this report are to describe the thermohaline structure of cold saline bottom lenses on the northern Okhotsk Sea shelf and to re-exam the results of AM based on a detailed CTD survey carried out in 1996.

## **2. Data**

The CTD observations were taken with an NBIS Mark-3 CTD over the northern Okhotsk Sea shelf during 30 May-22 June 1996. Station locations were offshore from the 100-m isobath (Fig. 1). Salinity data were calibrated with the salinity of bottle sample water with an accuracy of 0.01 psu. Raw data were interpolated in 1-db and were smoothed by a 5 point running average.

### 3. Northern Okhotsk Sea cold pool

Extremely severe winters with low temperatures and high winds are the main cause of the seasonally forming and anomalous southern ice cover, which usually spreads over 70% of the Okhotsk Sea. Winter convection occurs in the upper 150-200 m layer and completely mixes the whole water column over the 100-300 km wide northern Okhotsk Sea shelf. Waters with temperature near freezing exist under the ice, every year renewing the huge shelf cold pool (Fig. 1a). However, waters are stratified quite rapidly in the bottom layer through the recovering coastal polynyas. According to Yakunin (1997), these polynyas exist as a quasi-stationary feature along the northern Okhotsk Sea coast from Tauiskaya Guba to Ayan due to off-shore north-northwestern winds that remove ice from the coast. The polynyas are localized in the coastal area near Okhotsk City during warm winters. Strong negative buoyancy flux and tidal mixing homogenize bottom salinity, decreasing horizontal salinity gradients between coastal and outer shelf waters in winter-spring (Fig. 1b). In summer-fall the most dense bottom water usually occurs in the northwestern part of the northern Okhotsk Sea shelf and Sakhalin Bay, which is somewhat far from the polynyas region (Kitani, 1973 and Fig. 1c). This suggests that brine water is removed by quasi-stationary cyclonic current from places of formation. Bottom density clearly shows general cyclonic circulation over the northern Okhotsk Sea shelf that transfers the dense water along isobaths westward and west-southward. High vertical density gradients on the upper boundary of the bottom dense lenses (bottom cold halocline) and small-scale hollows and canyons of the bottom relief prevent a rapid mixing of the brine rejected water. Thus, the dense lenses occur over the northern Okhotsk Sea shelf bottom throughout most of the year.

### 4. Structure of the bottom brine water

Applying T-S analysis, it is easy to recognize the brine rejected water on T-S curves as «cold tails» parallel to the freezing line (Fig. 2). Bottom temperature increases off-shore therefore the end of the «cold tail» rises away from salinity axis on T-S curves of the middle and outer shelf water. The most remarkable feature of all T-S curves is a fold point that divides them into two parts. Structure of the brine rejected water on the northern Okhotsk Sea shelf were defined using this point. In this case, the fold point on the T-S curve marks an upper boundary of the dense bottom lens and a length of the «cold tail» from the fold point defines the salinity difference between a winter mixed layer and brine water. Some T-S curves, especially for stations at the edges of the brine lenses and in the Sakhalin Bay, have an intermittent «cold tail» due to strong horizontal tidal mixing. In this case, it is difficult to recognize the fold point for this T-S curves,



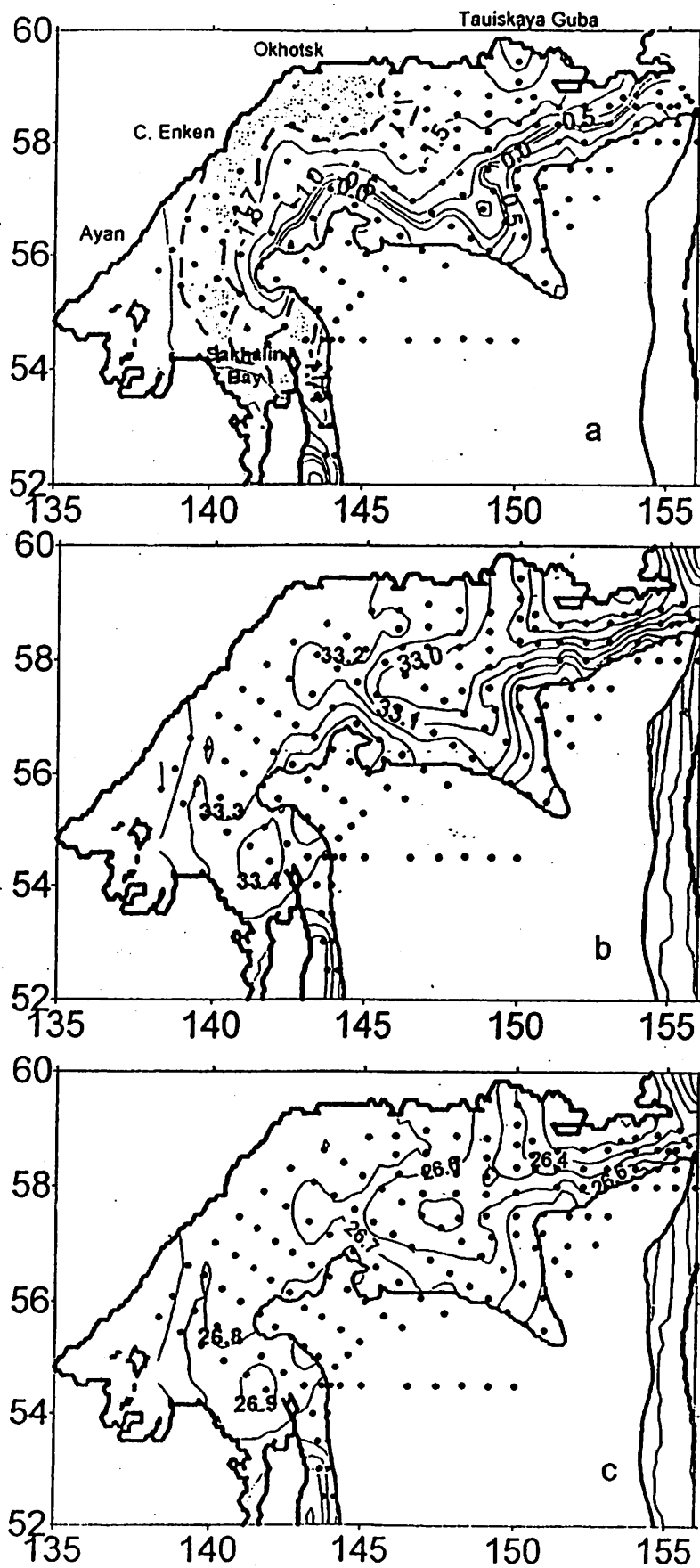


Fig. 1 Distribution of the bottom temperature (a), salinity (b) and density (c) in the northern Okhotsk Sea shelf in May-June 1996. Shaded area is a region with temperature lower than  $-1.7^{\circ}\text{C}$

therefore subjectively, the highest temperature of the brine water was taken  $-1.5^{\circ}\text{C}$ . The results of this analysis are shown on Fig. 3. Generally, brine water occurred at 100-150 m depths between Pyagin and Shimdt Peninsulas and had a salinity of 32.67-33.54 psu (potential density  $26.28-27.0 \sigma_{\theta}$ ) in June 1996 although it was formed closer to the shore (probably near 50 m isobath or shallower). Thus, the dense water moved slowly across the shelf to satisfy quasi-geostrophic balance with westward along-shelf current. According to our estimates, the speed of the cross-shelf component of this flow was 1-2 cm/s.

The brine water from the Tauiskaya polynya formed as a separate bottom lens with the lowest salinity and highest temperature (region I on Fig. 3). The maximum lens thickness was 60 m, and the maximum salinity difference between the brine and winter mixed water was 0.2 psu. This lens was located near the shelf break and potentially could have mixed with slope water of the Tinro Deep, but it was the lowest candidate to ventilate the densest Okhotsk Sea Intermediate Water. The largest bottom lens occurred along the northern shelf of the Okhotsk Sea between Khmitevskii Peninsula and Cape Enken (region II on Fig. 3). This lens had the same maximum thickness but a greater maximum difference ( $>0.3$  psu) between brine bottom and winter mixed water than the Tauiskaya lens. Its maximum cross-shelf width was greater than 125 km. The southern edge of this lens was not near the outer shelf boundary, but this coastal area is a potential power source for ventilation of the Okhotsk Sea Intermediate Water. The northern lens of the dense water was connected with the northwestern lens by a narrow neck near Cape Enken. This lens had the highest thickness ( $>80$  m) and the lowest salinity difference between the core of this lens and winter mixed layer ( $<0.2$  psu) (region III on Fig. 3). It seems that this lens was a strongly modified part of the northern lens removed by quasi-stationary currents in this region and a little quantity of the brine water formed on the northwestern shelf during winter 1995-1996. Sakhalin Bay looked like trap for the brine water because it stored and intensively mixed with Deryugin Deep slope water there (region IV on Fig. 3). The lens of the brine water became fractured and located at the shelf break region. This mixing appeared to be an effective mechanism for Okhotsk Sea Intermediate Water formation. Salinity of some separate lenses exceeded the salinity of the surrounding water by more than 0.6 psu and its temperature was near  $-1.5^{\circ}\text{C}$ . Part of this water spread to the south as the East-Sakhalin current along the eastern Sakhalin shelf. According to our estimates, density-driven circulation might be 7-8 cm/s to drag dense bottom water along isobath.

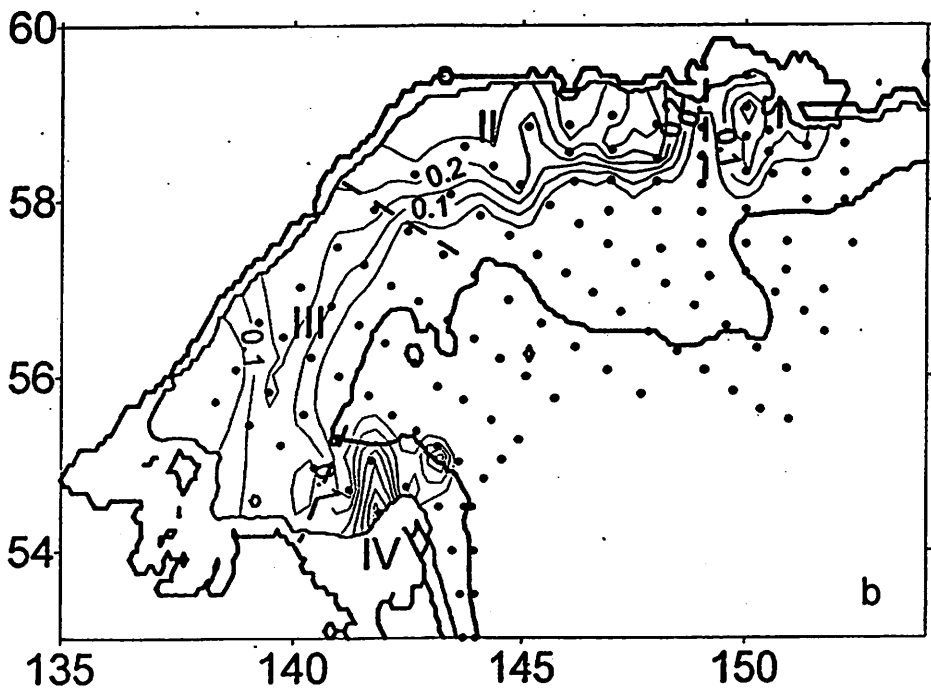
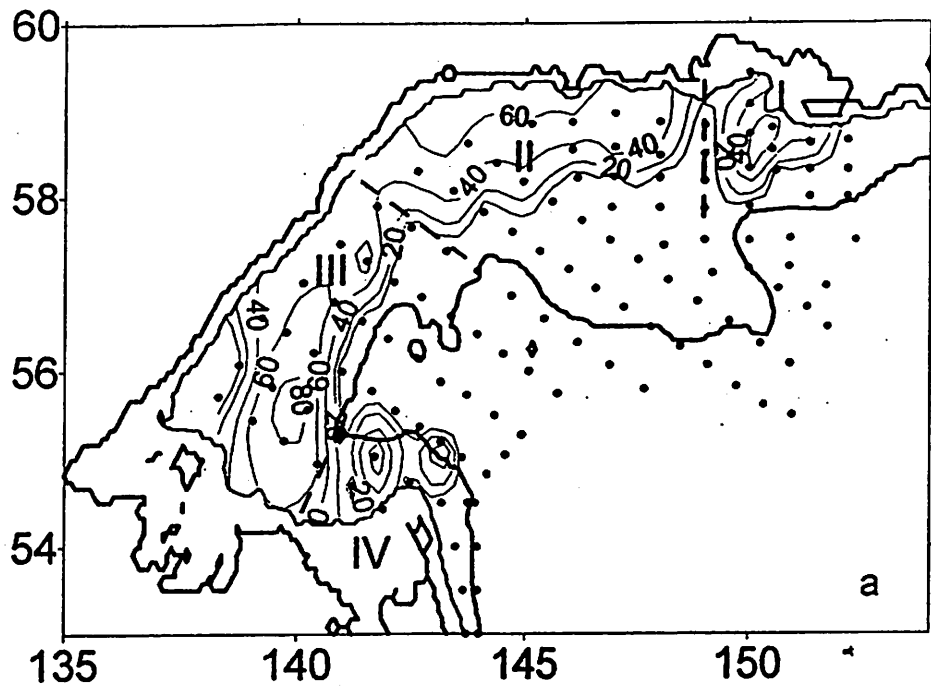


Fig. 3 Lens thickness(m) (a) and salinity difference (psu) between winter mixed and brine waters (b) in the northern Okhotsk Sea shelf in May-June 1996

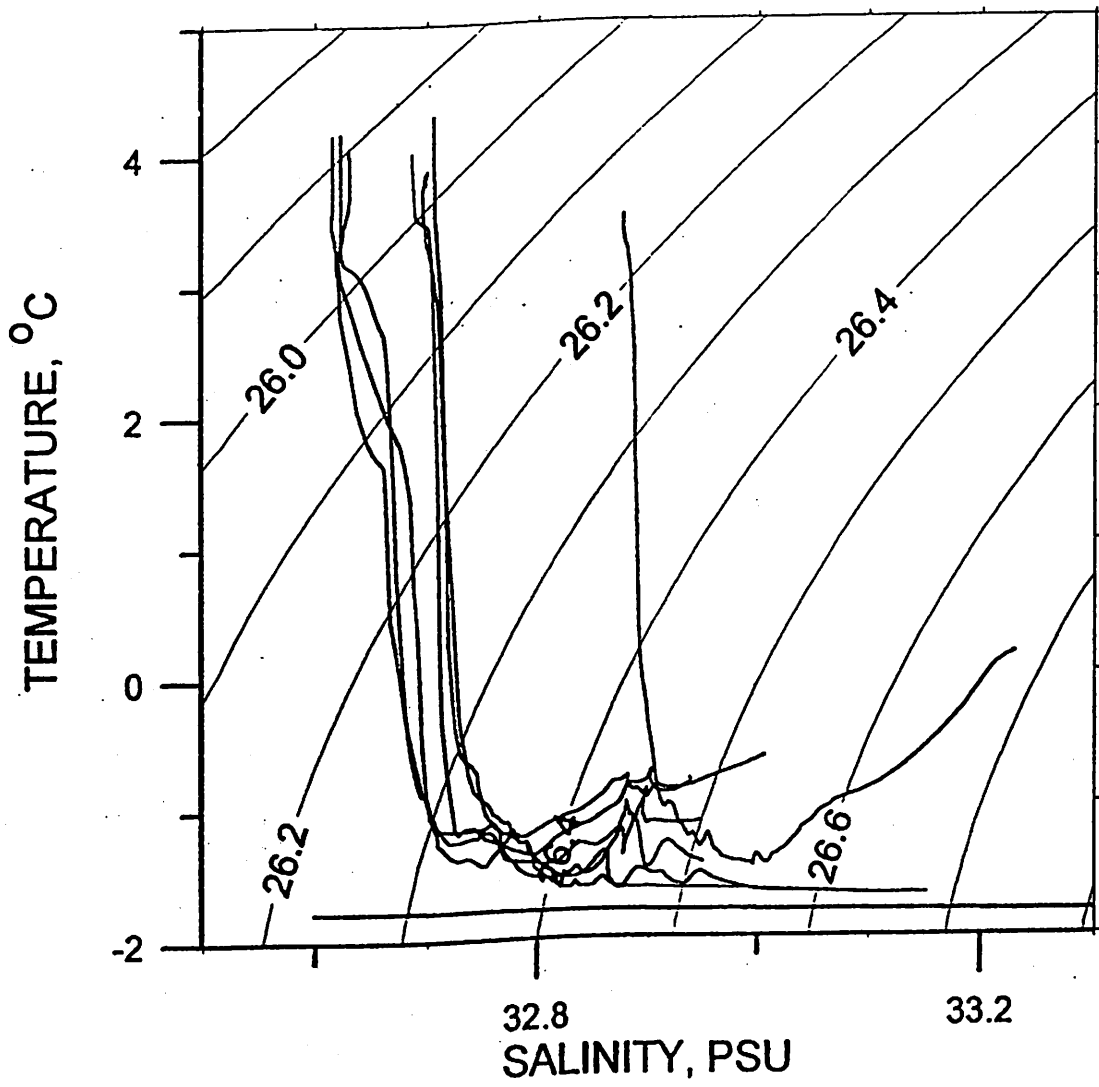


Fig. 2 T-S curves of the northern Okhotsk Sea shelf water

## 5. Estimates of brine water salt and ice productions

Mild winters in the 1990s, when seasonal ice cover in the Okhotsk Sea was reportedly below a long-term average, led to a dramatic decrease of dense water formation at coastal polynyas. We calculated volumes of water of different densities with temperatures lower  $-1.5^{\circ}\text{C}$  directly from observations. Considering, that we dealt only with June remnants of the brine shelf water, our estimates are lower than the actual volumes during late winter-early spring 1996. The results are shown in Table 1. Much less water with densities more than  $26.8 \sigma_{\theta}$  were formed in the coastal polynyas than was predicted by AM. Thus, Okhotsk Sea Intermediate Water at these densities has become warmer and saltier during recent years. Estimates of the cumulative salt and ice production were made using the equations

$$M = \rho_w \times V \times \Delta S \times 10^{-3}, \quad V_L = M / (\rho_L \times S_L \times 10^{-3}),$$

where  $M$  is cumulative salt production,  $\rho_w$  and  $\rho_L$  are densities of water and ice ( $0.92 \times 10^3 \text{ kg m}^{-3}$ ), respectively,  $S_L$  is an ice salinity (4 psu),  $\Delta S$  is salinity difference between the salinity of the brine and winter mixed water (strength of the bottom cold halocline), and  $V$  and  $V_L$  are volumes of water and ice, respectively. Calculations were made assuming two different onshore boundaries, located along the 10m and 50m isobaths (indexes 10 and 50 in Table 2), because the onshore boundary of the brine water is unknown from our dataset. Comparing of our results with the results of the AM for their warm year shows that cumulative salt production was overestimated by more than (by) two times and cumulative ice production was underestimated by less than three times by these authors. The former difference is due to the crude salinity approximation used by AM and the latter due to disadvantages of the bulk formulae and the inaccuracy of the initial atmospheric data. According to our estimates, if ice produced in the coastal polynyas during winter 1995-1996 will be evenly distributed over the northern shelf of the Okhotsk Sea, then the thickness of the shelf ice will approximately double. Thus, the northern coastal Okhotsk Sea polynyas are the power source of seasonal ice in the Okhotsk Sea. Since the northern shelf occupies 22% of the total Okhotsk Sea area the recent decrease of the Okhotsk Sea ice cover may be due to short periods of polynya occurrence in winter because remarkable warming was not observed in the atmosphere.

Table 1. Estimates of annual production and annually averaged volume flow rate of the brine shelf water ( $T < -1.5^{\circ}\text{C}$ ) in the northern Okhotsk Sea shelf in winter 1995-1996

Potential density, $\sigma_{\theta}$	Square, $\text{m}^2$	Volume, $\text{m}^3$	Average thickness, m	Annual average flow rate, Sv
> 26.6	$1.12 \cdot 10^{11}$	$0.72 \cdot 10^{13}$	64	0.23
> 26.7	$0.93 \cdot 10^{11}$	$0.38 \cdot 10^{13}$	41	0.12
> 26.8	$0.23 \cdot 10^{11}$	$0.06 \cdot 10^{13}$	25	0.02
> 26.9	$0.03 \cdot 10^{11}$	$0.008 \cdot 10^{13}$	25	< 0.01

Table 2. Estimates of annual brine water ( $V_w$ ) cumulative salt (S) cumulative ice ( $V_L$ ) productions and seeming average shelf ice thickness addition ( $H_L$ ) due to northern coastal Okhotsk Sea polynyas occurrence in winter 1995-1996

	$V_w$ 10/50 ( $\text{m}^3$ )	S 10/50 (kg)	$V_L$ 10/50 ( $\text{m}^3$ )	$H_L$ 10/50 (m)	Q (Sv)
this work	$1.14 \cdot 10^{13}$	$1.17 \cdot 10^{12}$	$3.18 \cdot 10^{11}$	0.94	0.36
this work	$1.08 \cdot 10^{13}$	$1.11 \cdot 10^{12}$	$3.02 \cdot 10^{11}$	0.89	0.34
AM 1987	0.4-0.8 $\cdot 10^{13}$	$2.51 \cdot 10^{12}$	$1.18 \cdot 10^{11}$	-	0.1-0.3

## SOME FEATURES OF MESOSCALE AND SMALL SCALE WATER DYNAMICS IN THE SOUTHERN OKHOTSK SEA SEEN BY THE ERS-1 SYNTHETIC APERTURE RADAR

*Vyacheslav Lobanov\**, *Leonid Mitnik\** and *Nafanail Bulatov\*\**

\* - *Pacific Oceanological Institute, Far Eastern Branch of Russian Academy of Sciences, Vladivostok 690041 Russia*

\*\* - *Pacific Research Institute of Fisheries and Oceanography (TINRO), Vladivostok 690600 Russia*

**Abstract.** Synthetic aperture radar (SAR) images obtained from the ERS-1 satellite in spring of 1995 were analyzed together with NOAA AVHRR imagery, weather maps and hydrographic CTD data to study oceanic phenomena in the southern Okhotsk Sea by their surface manifestation. The backscatter difference that causes the SAR signatures of the ocean surface are related to changes of water mass properties, natural surfactants concentration, atmospheric boundary layer stability and current shear. Distinguishing features of anticyclonic rings and the Soya Warm Current are common when the wind is 2-10 m/s and seem to be associated with a modulation of the surface capillary-gravity waves by the current shear. Some small-scale features of circulation were also detected due to the surface films just after period of ice melting, which correlates with biological activity. Spatially organized vortex structures of 7-10 km in diameter with a strong current shear were found at peripheral parts of the rings. Rough bottom topography and strong tidal currents in the area of Kuril Islands are responsible for formation of rips, wakes and headland vortices, packets of internal waves. Pattern of the shear fronts at the SAR images varies with a tidal phase. However the main areas of tidal energy dissipation seem to be stable and are tightly related to the bottom topography. Spatial structure of tidal flow and new fine details of the surface water circulation are discussed.

### 1. INTRODUCTION

Among the different kinds of satellite measurements the radar data have their benefit by providing useful information on phenomena and processes both in the upper layer of the sea and in the boundary layer of the atmosphere independent of clouds. Intensity of reflected radar signal depends on a surface roughness and indicates the phenomena which affect wave spectra. Apart the wind other oceanic phenomena such as internal waves, eddies and fronts were found in the synthetic aperture radar (SAR) images because they are associated with variable surface currents, natural surfactants, instability of atmospheric boundary layer which modulate the surface roughness (e.g. Fu and Holt, 1982; Alpers, 1995; Nilsson and Tildesley, 1995). The C band SAR of the European Space Agency (ESA) ERS-1 satellite operates at a wavelength of 5.6 cm at incidence angle of about 19-26 degrees and provides images with a spatial resolution of about 25 m and a swath width of 100 km. These data were analyzed to study mesoscale and small scale oceanic phenomena in southern part of the Okhotsk Sea in spring period of 1995.

The main features of water dynamics in the area are associated with the Soya Warm Current flowing along Hokkaido and Kuril Islands, the East Sakhalin Current carrying drifting ice and cold fresh waters southward and mesoscale anticyclonic eddies located over the Kuril Basin (Moroshkin, 1968; Kuzmina and Sklyarov, 1984; Wakatsuchi and Martin, 1992). Strong tidal currents over rough bottom

topography at the Kuril Islands produce inhomogeneous water mass distribution. Spring period is also characterized by fast change of hydrographic and biological conditions in the area cause by sea ice melting and intense radiate heating of the surface layer. Manifestation of these processes in the radar backscatter pattern of the ERS-1 SAR images is discussed below.

### 2. THE DATA

During the period from 19 April to 9 June 1995 the 42 ERS-1 SAR images over the southern Okhotsk Sea were obtained under the research grant from the ESA. They provide 3 coverages of the area as indicated at Fig. 1 which not only allowed to identify phenomena but also to trace their evolution. NOAA AVHRR data, weather maps, maps of bathymetry, hydrographic observations of R/V Akademik M.A.Lavrentyev were also used in the analysis.

### 3. MESOSCALE EDDIES

The main features of water dynamics in the area may be illustrated by NOAA AVHRR IR image for 8 May, 1995, at 03:05 UTC (Fig. 2 and 3). Warm water of the Soya Current is visible along the coast of Hokkaido and Kunashir Island, cold water filaments of the East Sakhalin Current and anticyclonic eddies of 80-150 km in diameter (A, B, C) are located over the Kuril Basin. Sea surface temperature contrast

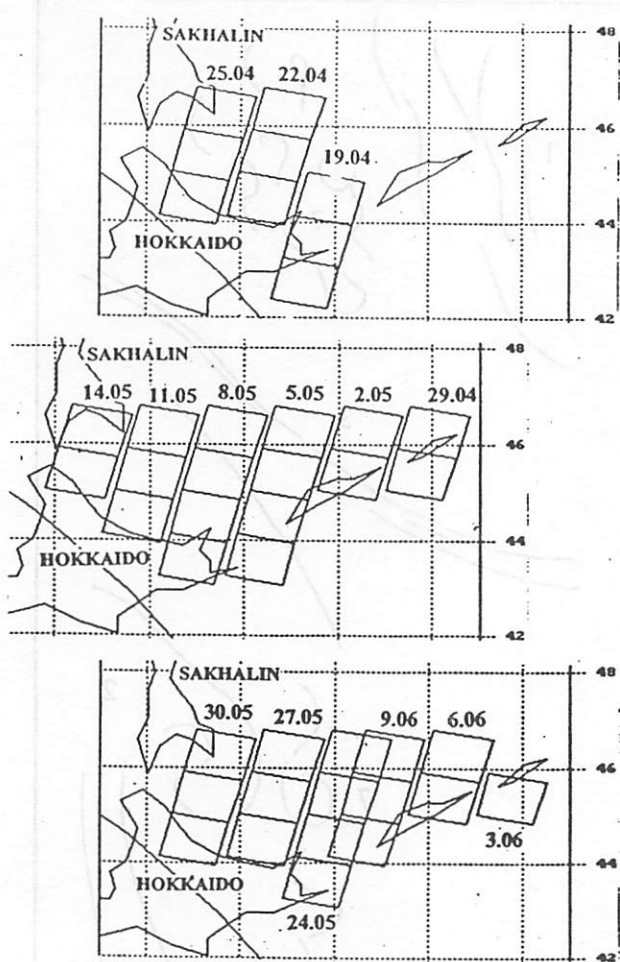


Figure 1. Location of the ERS-1 SAR frames obtained in the period 19 April - 9 June 1995.

estimated by the IR image are of 3-4°C at the edge of the Soya Warm Current and of 0.5-2.0°C at the cold streamers inside the eddies. Surface currents derived from the analysis of IR images pairs for 4-9 May by the "temperature markers" technique demonstrated that the eddies A and B are prominent anticyclonic circulation features with currents of 25-40 cm/s. Maximum velocities (up to 50 cm/s) are observed at the jets between the eddies. Flow of the Soya warm current was of: 10-15 (cm/s). The latter might be underestimated as direct current measurements showed mean speeds of 89-97 cm/s for the surface layer (Aota et al., 1988).

The ERS-1 SAR images were taken about two hours before the IR image (Fig. 4). Cloudless weather and wind speed below 5-7 m/s (northern periphery of anticyclone) was favorable for indication of ocean dynamics using both thermal and radar signatures (Fig. 5). The lighter areas of the radar pattern correspond to the higher backscatter and sea surface roughness. Eastern part of the eddy A (1) and western cyclonic part of the dipole eddy structure C (2) are depicted by the curvilinear bands of high and

low intensity. Jet streamer (3) between eddy C and A is pronounced well. Boundary of the Soya warm current (4) and cyclonic eddies (5) off Siretoko Cape (6) are demonstrated at Fig. 11.

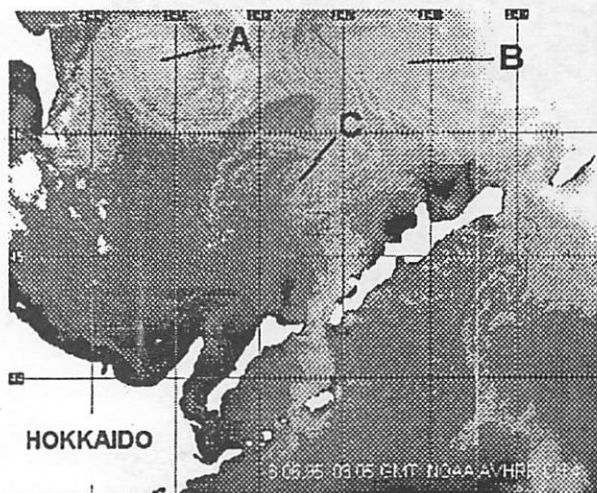


Figure 2. NOAA AVHRR infrared image of the southern Okhotsk Sea for 8 May 1995, 03:05 UTC. Dark areas correspond to warmer water. Large anticyclonic eddies labeled by A, B and C are discussed in text.

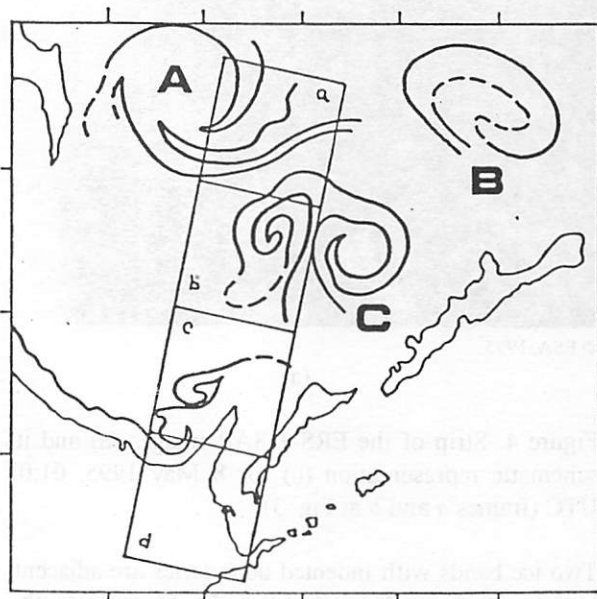
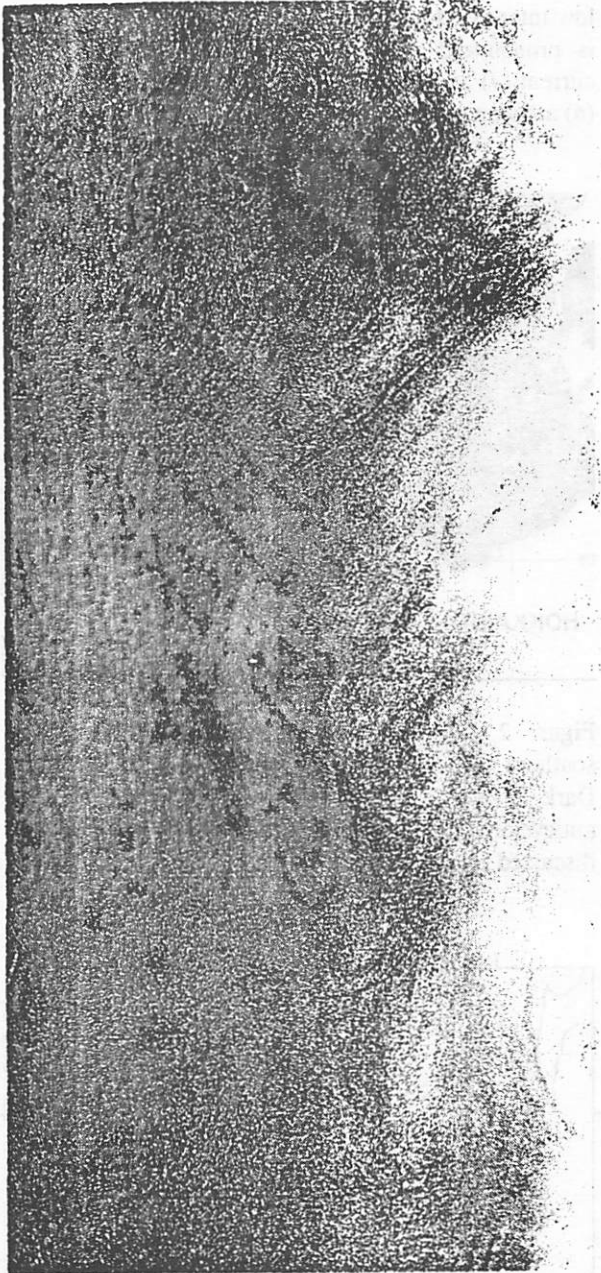


Figure 3. Schematic representation of the infrared image of Fig. 2. Rectangles indicate location of the ERS-1 SAR frames for 8 May 1995, 01:07 UTC shown at Fig. 4 and 11.

The eddy A was also seen earlier in the field of drifting ice at NOAA AVHRR visible image for 25 April, 1995 at 03:47 UTC (Fig. 6) and ERS-1 SAR image for 22 April, 1995 at 01:11 UTC (Figure 7).



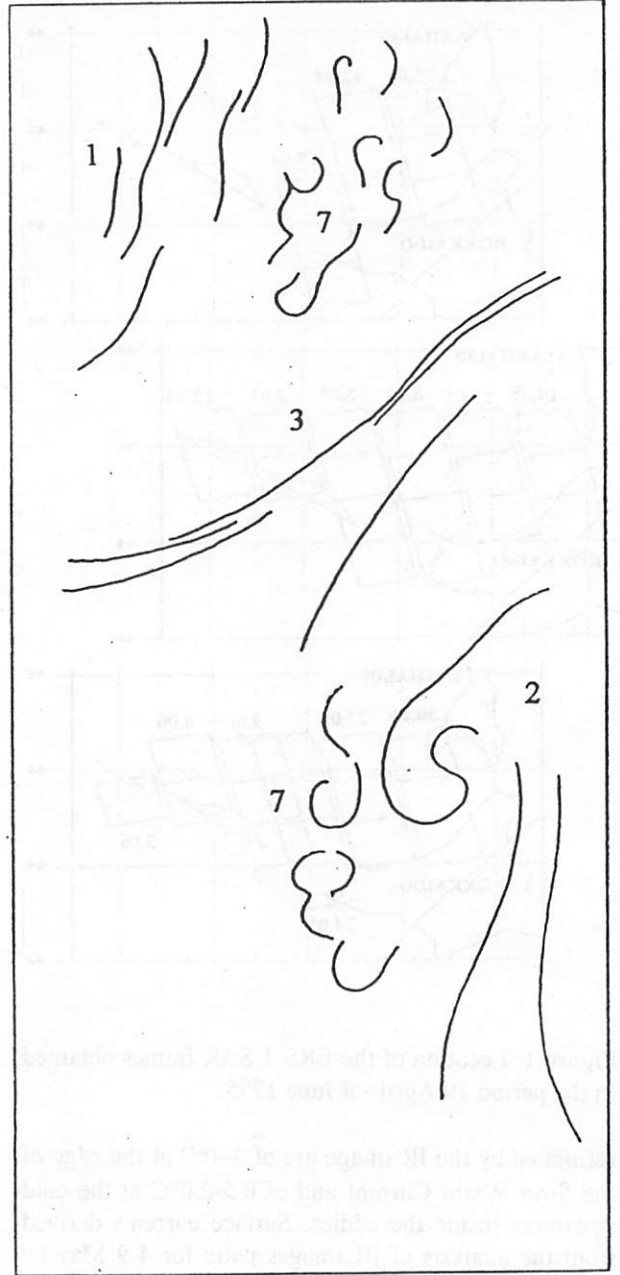


© ESA, 1995

(a)

Figure 4. Strip of the ERS-1 SAR images (a) and its schematic representation (b) for 8 May 1995, 01:07 UTC (frames *a* and *b* at Fig. 3).

Two ice bands with indented boundaries are adjacent to the central circular part of the eddy from the south. SAR swath crossed nondeep cyclone centered at about 47 N, 147E (the synoptic chart is not shown). Wind speed over the area was about 5 m/s. The ice eddy and band under consideration have detectable brightness contrast on NOAA-14 AVHRR visible images for the end of April. Then the ice contrasts both on visible and radar images decrease because of thawing ice and snow and decrease of ice concentration.



(b)

Another ERS-1 SAR image of the eddy A was obtained on 27 May, 1995 (Fig. 8). The eddy signature characterized by the spatially organized concentric curvilinear or arcuate bands of high and low intensity changing to the chopped-like mottled features at the very central part of the eddy. This signature also repeats for the eddy B at SAR image for 6 June, 1995 and may be explained by convergent flow inside an anticyclonic eddy. Comparing SAR images for 22 April and 27 May we can find the eddy A drifted about 50 km southward. This corresponds to drift velocity of 50 km / 35 days or 1.6  $cm/s$  which is typical for mesoscale eddies (Olson, 1991).

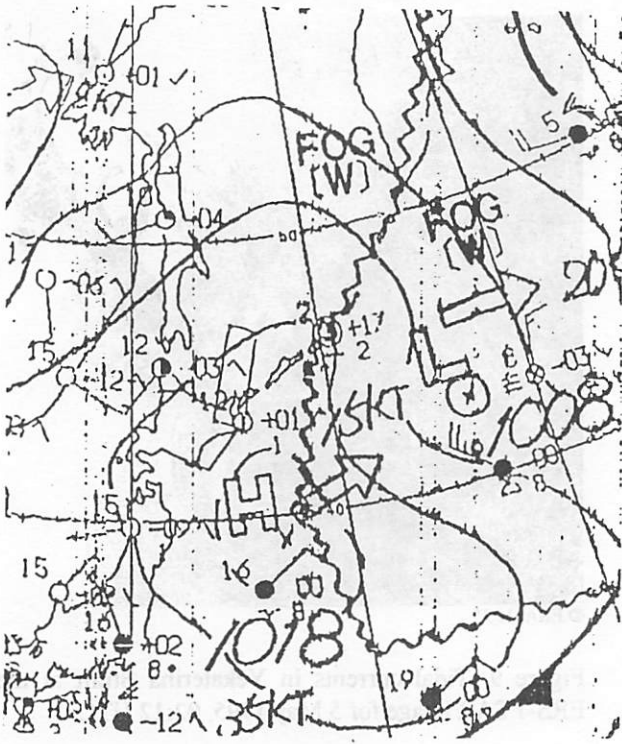


Figure 4. Surface analysis chart for 8 May 1995, 00:00 UTC by Japan Meteorological Agency.

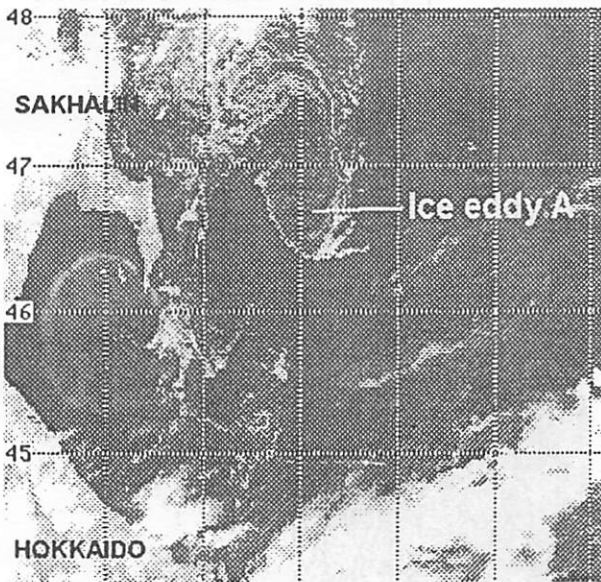
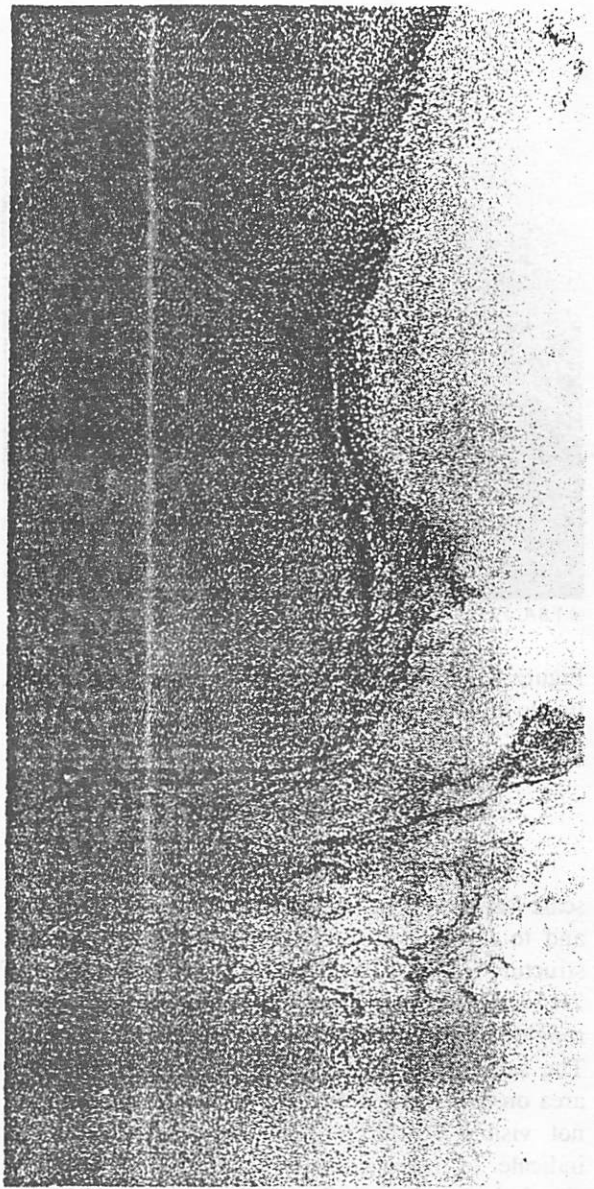
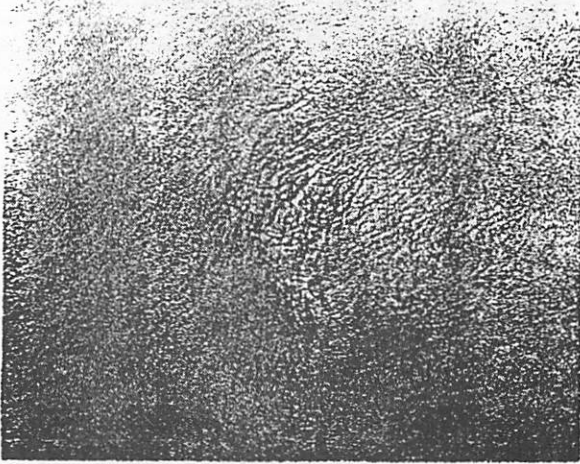


Figure 6. Eddy A as a sea ice eddy at the NOAA AVHRR visual image for 25 April 1995, 03:47 UTC.



© ESA, 1995

Figure 7. ERS-1 SAR image of the sea ice eddy A for 22 April 1995, 01:11 UTC.



© ESA, 1995

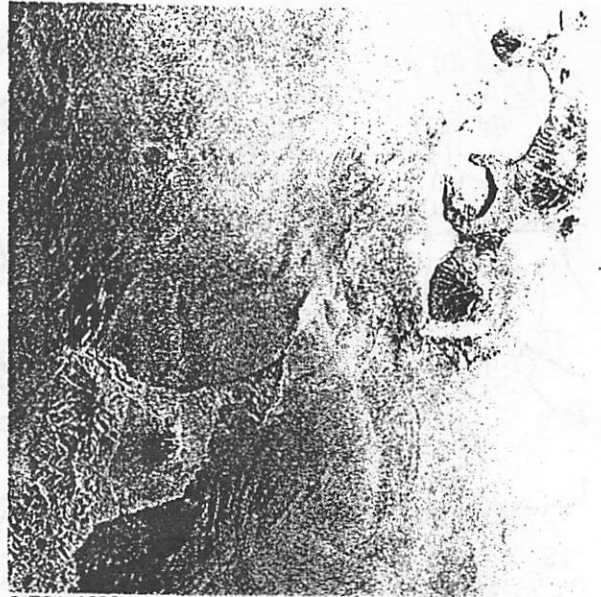
Figure 8. Central part of the eddy A on ERS-1 SAR image for 27 May 1995, 01:10 UTC.

#### 4. SMALL SCALE FEATURES

Fig. 4 demonstrates an existence of small scale features (7) just to the east of the edge of eddy A and to the west of cyclonic part of the mushroom structure C. These small features have a dimension of 7-15 km and pretty sharp contrast of the sea surface roughness which corresponds to high current shear. The same features were also observed at the same area on SAR images for 24 May. This structures are not visible at the infrared images however they indicate to intense small scale process of water circulation at the periphery of mesoscale eddies that should be further investigated.

#### 5. TIDAL FLOW IN THE KURIL STRAITS

Tides and rough bottom topography around the islands play an important role in local hydrography. In spring period irregular tides of with a dominant semidiurnal fluctuation are dominant in the area. Tidal currents can reach velocity up to 5-8 knots in shallow straits (Bogdanov, 1968; Luchin, 1996). Maximum currents are usually proceeds sea level extrema by 1/4 period for shallow straits (Luchin, 1996). The SAR images taken at different stage of tide show complicated pattern of tidal flow (Fig. 9 and 10). Outflowing phase of tide (current directed from the Okhotsk Sea) is demonstrated at Fig. 9. The flow directed into the Okhotsk Sea is shown at the SAR image for 19 April (the figure is



© ESA, 1995

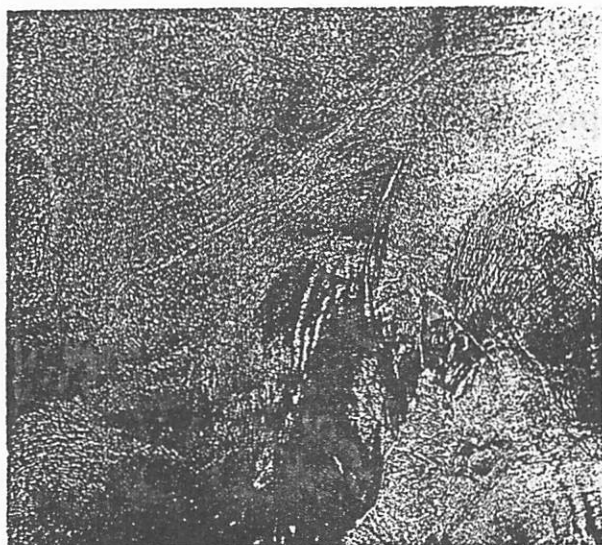
Figure 9. Tidal currents in Yekaterina Strait at the ERS-1 SAR image for 5 May 1995, 02:12 UTC.

omitted). The distinguishing curved feature of high and low intensity corresponds to the current shear zones and rips area can be seen along 30-50 km off the strait. Breaking of tidal waves at the shelf and strong tidal currents in the straits are responsible for formation of rips, packets of internal waves, current

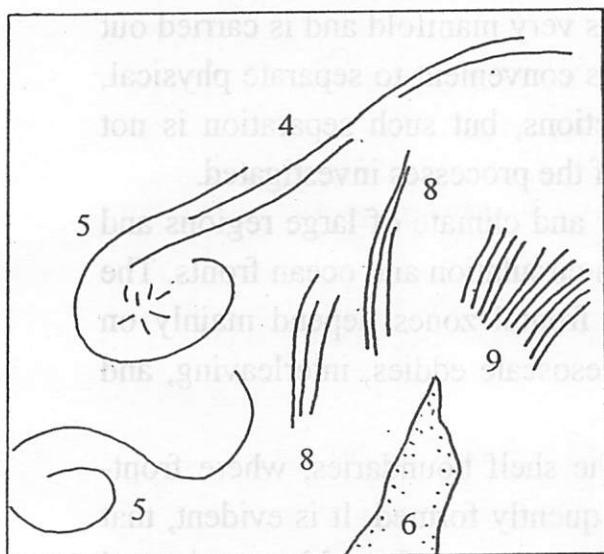


© ESA, 1995

Figure 10. ERS-1 SAR image for 6 June 1995, 00:51 UTC showing dynamic features associated with tidal currents in Friz Strait.



(a)



(b)

Figure 11. Internal waves and mesoscale eddies on the ERS-1 SAR image for 8 May 1995, 01:08 UTC (fragment of the frame *c* at Fig.3)

shear fronts and headland vortices. Permanent area of high surface roughness locates at the south-western edge of Island (Fig. 10). This area was also reported by observations of the airborne radar (Etkin et al., 1989).

## 6. INTERNAL WAVES

Spring period in the Okhotsk Sea is characterized by a freshening of the surface waters due to the sea ice thawing and intense radiate heating which leads to a formation of well developed pycnocline in the vertical stratification. According to CTD observations

by R/V Akademik M.A.Lavrentyev in April May 1997 the pycnocline was observed at the depths of 10-30 m which provides favourable conditions for manifestation of the internal waves at the sea surface. Various systems of internal waves generated by an interaction of semidiurnal tide with intended shelf edge are clearly seen at Fig. 11. Long soliton-like systems (8) are propagating to the west of Siretoko Cape (6) while well developed linear system of waves of about 1 km length is seen east of the cape (9).

## 7. CONCLUSION

It was found that main mesoscale features of water dynamics of the southern Okhotsk Sea such as anticyclonic eddies and the Soya Warm Current meanders are visible on ERS-1 SAR images. Their manifestation is mostly due to dynamical effects, while some small scale eddies were depicted by filaments of different surfactants concentration.

Small scale coherent structures of 7-15 km were found at the periphery of large eddies. Sharp contrast of surface roughness indicate strong current shear and intense water dynamics at such scales.

SAR data allowed to examine horizontal structure of tidal flow through the Kuril Straits. Actual pattern of tidal flow and water exchange between the Okhotsk Sea and Pacific is an important problem of physical oceanography and climatic studies. It is expected for further studies that series of ERS SAR images could be of use in solving this problem.

*Aknowlegement.* We thank the ESA for providing the ERS SAR images, Dr. Ming-Kuang Hsu (NTOU, Keelung, Taiwan) for collaboration in data acquisition and processing, Mr.A.Aleksanin (IACP, Vladivostok, Russia) for processing the NOAA AVHRR images and Dr. V.Luchin (FERHRI, Vladivostok, Russia) for providing tidal data and discussions.

# Mechanisms of influence of coastal and shelf waters on the open sea bioproductivity

V.V.Navrotsky, T.A.Zadonskaya  
Pacific Oceanological Institute, Vladivostok  
E-mail: [navr@online.vladivostok.ru](mailto:navr@online.vladivostok.ru)  
Fax : +7 4232 31 25 73

## Introduction

The bioproductivity of marginal seas is to high degree determined by land-ocean interactions. This interaction is very manifold and is carried out on a large range of scales. It is sometimes convenient to separate physical, chemical and biological kinds of interactions, but such separation is not always productive, depending on scales of the processes investigated.

Large-scale interactions define weather and climate of large regions and form the most important features of ocean circulation and ocean fronts. The biological characteristics in the oceanic frontal zones depend mainly on such dynamical processes as currents, mesoscale eddies, interleaving, and they have been studied for long time.

Less investigated are processes near the shelf boundaries, where front-like structures of most parameters are frequently formed. It is evident, that inertial and tidal motions, as well as vertical motions forced by continental slope, are important for biological processes, but complex observations in these zones are scarce. Special attention should be given here to internal waves and small-scale turbulence.

Next to the boundary between land and ocean the most important become physical, chemical and biological processes caused by transport of terrigene matter by run-off and by air flows from land. But again the role of specific mechanisms depends on scales and distance from shore. We will be discussing here two cases: 1) Small runoff and small depths (down to 20-30m). 2) Large runoff and arbitrary depths.

In the first case the interaction between land and ocean waters begins practically from zero depths, and essential input in the process comes from

sea-weeds. Their role in purification of contaminated land waters, especially in poorly ventilated bays, is difficult to overestimate. From the other side, sea-weeds are very useful for many purposes, and studying conditions of their life is necessary for needs of production.

### Oceanological conditions and sea-weeds

The observations analyzed were made on 65 stations in 2 bays and on 28 stations along the open shore (Fig.1,2,3). Parameters measured form two groups. Abiotic parameters were depth, currents at surface, 5 m and 10m (or bottom), temperature T, salinity S, light intensity E, pH, oxigen O<sub>2</sub>, dissolved carbon C, nitrites NO<sub>2</sub>, nitrates NO<sub>3</sub>, phosphates PO<sub>4</sub>, suspended matter Sm. Biotic parameters were number of leaves Fn, overall weight of maternal leaves Wm, length of leaves L, root mean square lengths DL, sometimes width of leaves W and coefficient of variability  $K=DL/L$ .

Spatial distribution of environmental parameters in different periods was related to runoff and to the character of propagation of river waters. Measurements of currents were made to explain the form and characteristics of zosteria fields, but now we are looking for some generalized laws, not going onto details (they were needed for prediction and of production).

Very detailed measurements of light intensity at different depths were made (Fig.4), but it soon became clear, that at depths of the investigated sea-weeds fields light is not a limiting factor (light intensity diminished typically 8-12 times from surface to bottom), though concentrations of suspended matter were high in both bays.

In At Table 1 a matrix of correlation coefficients between abiotic parameters for all measurements is presented. The main interrelations are clearly seen, and they were the base for factor analysis (Table 2 and Fig.5). About 50% of general variability are due to the first factor (T, S, O<sub>2</sub>, pH, Sm tend to it), the rest is spread slowly diminishing over other parameters. After varimax rotation we can see, that depth H, carbon and phosphates tend to the second factor. All observations split into two groups. In the left group a linear relation between factors can be seen, in the right one their effects are independent.

We calculated , first, T-S regression (Fig.6), and then regression of T of all other parameters (Fig.7). We can see a distinct grouping due to time shift, but inside the each period of time the distributions of observations along the regression lines are rather monotonous.

Analyzing the sea-weeds parameters, we came to conclusion, that the most sensitive (and hence the most informative) statistical characteristics for lengths of leaves are probability distribution densities. They change drastically while moving from the bays to the open poligones, though the mean values are not very different. More uniform distributions in bays mean higher stability of these populations.

In Table 3 the matrix of correlation coefficients between all pairs of parameters is presented. The mean weight  $W_m$  is positively correlated with T, pH, O<sub>2</sub>, negatively with S<sub>m</sub>. The number of leaves has also negative correlation with S<sub>m</sub>. The length of leaves has positive correlation with T, pH, O<sub>2</sub>, and negative with S<sub>m</sub>.

Factor analysis of these observations (Fig.12, Table 4) has shown, that 95 % of variability is due to three factors (compare with 7 factors for separately analyzed abiotic parameters). The first factor is responsible for 70 % of variability. If we have a look at the distribution of parameters on the plane of the first two factors, we can see, that the main input in the first factor is made by pH, O<sub>2</sub>, T, PO<sub>4</sub>.

From factor analysis for each stage and region of observations we concluded, that interrelations between parameters change with time and space, so that it is practically useless to look for good predictability on the base of correlations between any two specific parameters. So we formed a group of 6 abiotic parameters and a group of 6 biotic parameters. Two canonical variables were formed as linear combinations of all parameters in each group with requirement that correlation between the variables should be maximum. As a result, two first modes of such canonical correlations show rather good and stable linear relation between the combinations of abiotic and biotic parameters.

Our conclusions are as follows:

- 1) Sea-weeds in bays have much better conditions, than in the open sea coastal zone.
- 2) The main negative factor for sea-weeds is suspended matter, which

effects directly through mudding, as its correlation with light is rather small. (The best conditions in the bay Jight were just due to large runoff of biogenic elements simultaneously with high current velocities).

3) No one of the parameters observed is determinative, as their relative role changes with time and space. But factor and canonical correlation analysis have shown, that two generalized variables can be formed, which can be used to determine the sea-weeds characteristics rather well through linear relations.

### Estuarian frontal zones

The influence of large rivers on processes in marginal seas and shelf zones is now very essential as from production so from ecological points of view (see, for example, Mallin, Paerl, 1994; Laprise, Dodson, 1994; Moffat, Jones, 1993; Taylor, 1993; Laprise, Dodson, 1993; Donaghay, Rines, Sieburth, 1992).

Our investigations differ from mentioned above and many others in that they were made in estuaries of big rivers of Asia, Africa and Europe, namely, Amour, Hangzhou, Mecong, Nile, Elba. Comparison of results of such observations may help to reveal as universal so specific laws of the processes investigated.

From investigations of last 10-15 years we know, that: 1) The matter carried out by river runoff into a sea does not distribute uniformly by processes of horisontal and vertical mixing. In coastal zones fronts of all parameters are formed, and these fronts have their footprints in bottom sediments. 2) In the frontal zones very active biochemical and biological processes are going on, in which a large amount of new organic matter is produced. This organic matter includes terrigene matter in its life cycle, substantially changing its migration ability.

Consequently, investigation of such parameters as primary production, pigment concentration, biomass and structure of plancton is necessary to forecast bioproductivity and ecosystem state in shelf zones and adjoining parts of seas.

In Table 4 some average characteristics of the five rivers and results of our measurements are given. The difference between background and



frontal values of all characteristics is clearly seen.

In the following figures we can see the position of these zones and their relation to the process of river and sea waters mixing. It's necessary to take into account two circumstances: 1) The boundary between waters is inclined due to density differences.

2) The boundary position changes under influence of tides, runoff and winds.

In Fig. 13 the position of maximum primary productivity and zooplankton biomass

in the by-estuarine zone of Amour river is given. They coincide with salinity changes from 5 to 12 ‰ and show the frontal zone 10–15 miles wide.

In Fig. 14, 15 are shown distributions of salinity, primary production, and zooplankton biomass for Hangzhou river. It's easy to see, that the zone of maximum salinity gradient, that is river and sea water mixing, is the zone of maximum productivity, forming front of both hydrological and biological characteristics.

Analogous picture is seen in the Mecong estuary (Fig. 16, 17, 18).

It is important to note, that substantial rebuilding of the plankton community follows the salinity change and biomass increase. As an example, the relative part of copepodes increases from 30% to 80% from the front zone of the Mecong estuary to the open sea.

Thus, the influence of river runoff on bioproductivity characteristics is not confined only to a mixing zone, but can be followed up to deep waters.

In Fig. 19, 20 the distribution of biological characteristics in by-estuarine zone of Nile is shown. Because of small runoff and influence of the Red Sea waters, we practically can't find the salinity front, but maximum and front of biological characteristics is analogous to those observed in the Asian rivers.

For Elba the distributions of salinity, primary production and zooplankton are shown in Fig. 21. We can see not only the general distribution of biomass, but also the relative change of 4 main groups of zooplankton. The width of frontal zone here is minimum (5 miles) comparing to the rivers shown earlier, and that is due to lower runoff and lower tides comparing to the Far-Eastern rivers.

If we follow farther from shore, we should take into account, in

addition to tides, processes confined to shelf boundary and continental slope: eddies, currents, internal waves, cross-boundary topography dependent vertical motions. As a rule, some kind of front along shelf and marginal sea boundaries is formed. In these fronts the mean gradients of chemical and biological characteristics are not so high as in the previous cases, but that is just due to larger scales and higher intensity of mixing processes, which extend the influence of land on biology far from the coast. Investigation of dynamical processes in this region is the objective of special investigation and special paper, but it's evident, that detailed complex measurements on sections from shore to deep sea are needed to describe all important effects and especially to forecast all positive and negative consequences for ocean bioproductivity and its ecosystems.

Conclusions for that part of the paper:

- 1) High values of primary and secondary production are confined to the zone of mixing between river and sea waters. They form a hydrobiological front with width and intensity depending on season and hydromorphological characteristics of the aquatory (especially on the range of tidal movements of river-sea front).
- 2) The estuarine waters are mesotrophic and eutrophic ones.
- 3) The chlorophil concentration is poorly correlated to primary production and seems not to be its indicator in estuarine waters.
- 4) While moving from river to sea, changes in concentration and structure of the plancton community take place, that are different for tropical and subtropical estuaries.
- 5) The chlorophil concentration and primary production grow from subarctic to tropical latitudes, but the relative biomass of zooplankton diminishes.

## Conclusions

1. Sea-weeds form the first barrier between land and ocean waters. They have much better conditions in bays, than in open sea coastal zones, and that defines the special attention, that should be given to preservation of the large and small bays ecosystems.
2. The main negative factor for sea-weeds is suspended matter, which affects directly through mudding of sea-weeds fields.
3. No one of environmental parameters is determinative, as their relative role changes with time and place. But with help of canonical correlations two generalized variables can be formed and used to determine the sea-weeds characteristics through linear relations.
4. High values of primary and secondary production in estuaries are confined to zones of mixing between river and sea waters. They form the hydrobiological front with width and intensity depending on season and hydromorphological characteristics of aquatory.
5. The estuarine waters are mesotrophic and eutrophic ones.
6. The chlorophil concentration is poorly correlated to primary production and seems not to be its indicator in estuarine waters.
7. With distance from shore, changes in concentration and structure of zooplankton community take place, that are different for tropical and subtropical estuaries.
8. The chlorophil concentration and primary production grow from subarctic to tropical latitudes, but relative biomass of zooplankton diminishes.

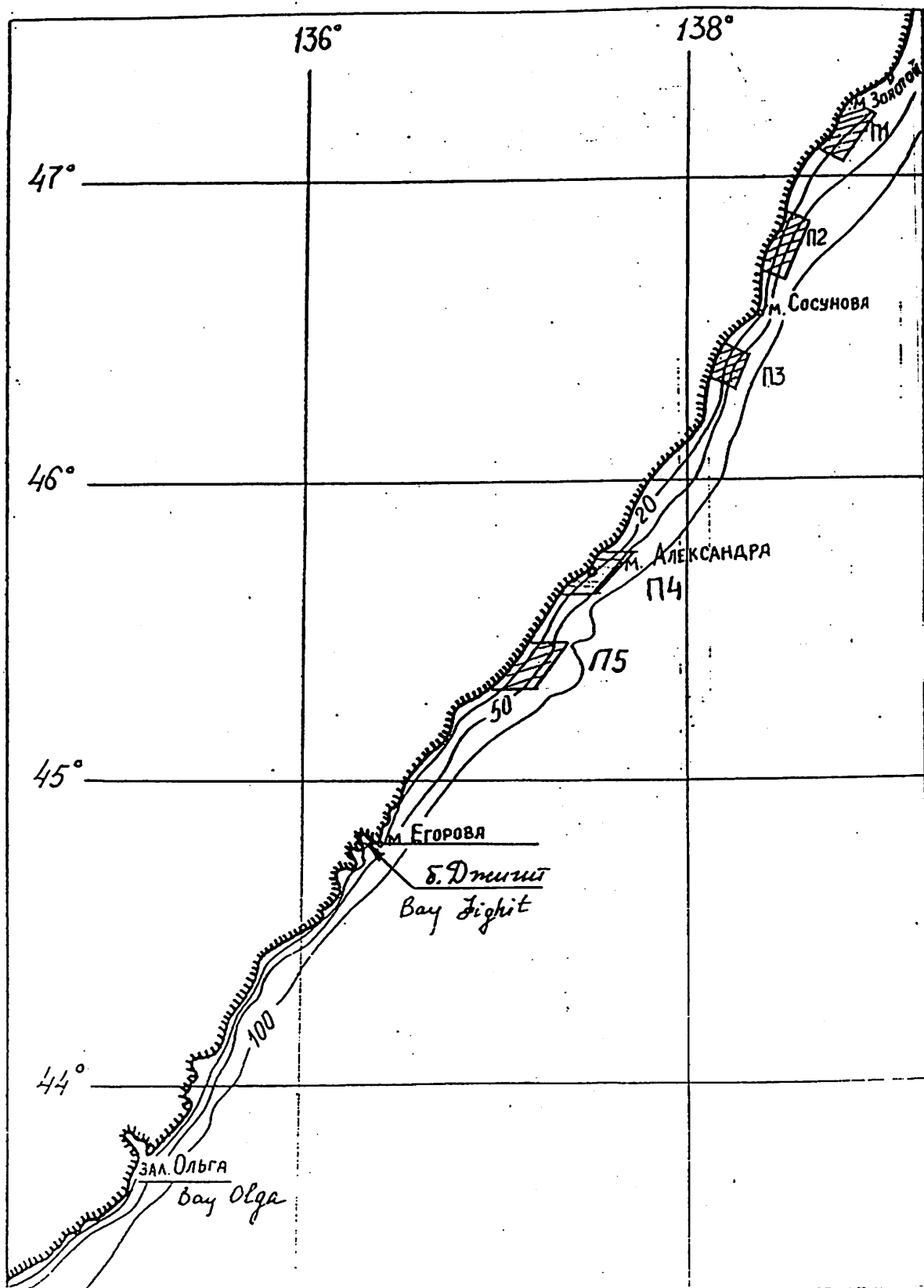






Рис. 1. Расположение районов работ: полигоны открытого моря П1-П5, б.Дмитри, в.Ольга.

*Fig. 1. The regions of sea-weeds observations in the Japanese sea.*

УСЛОВНЫЕ ОБОЗНАЧЕНИЯ:  - ПЕСОК sand  
 - ПЕСОК, ИЛ sand, silt  
 - ИЛ silt  
 - ПОЛЕ ЗОСТЕРЫ zostera field

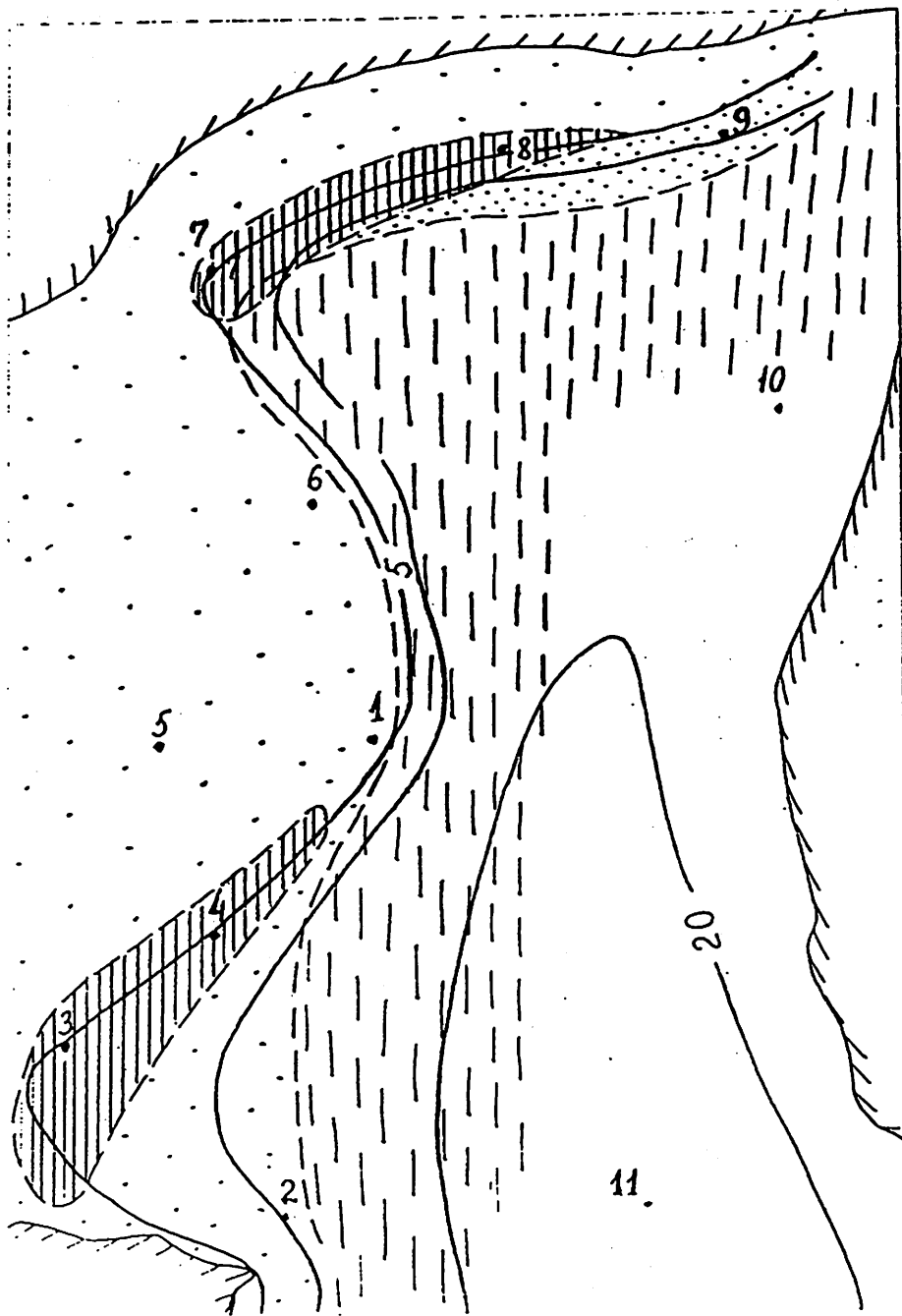


Рис. 2. Положение стенок и поля zostera в заливе.

Fig. 2. Observation points and Zostera fields in the Bay Olga.

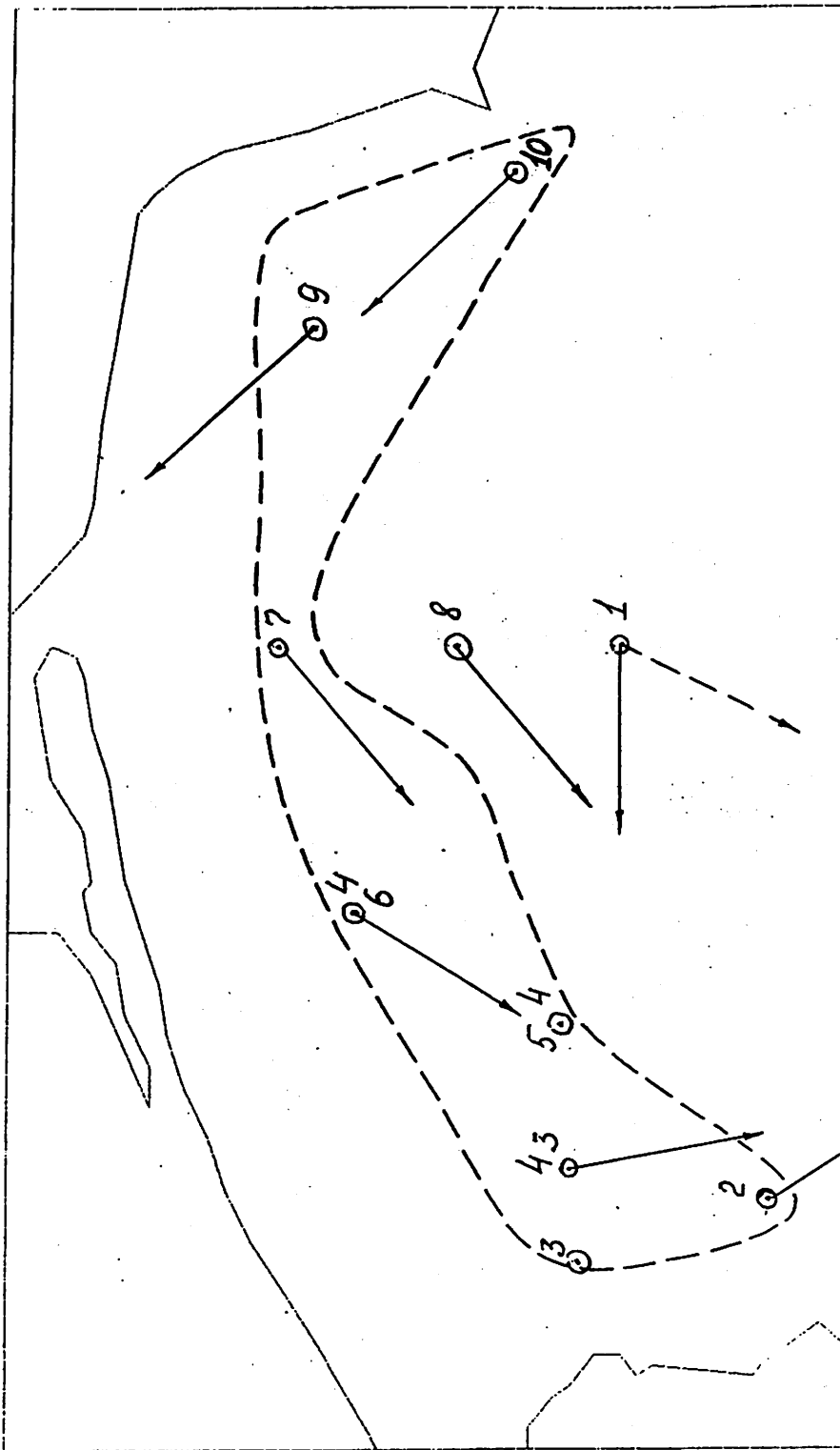


Рис. 70. Течения в б. Джигит (3. II. 91 г.).

*Fig. 3 Currents in the Bay Jigit.*

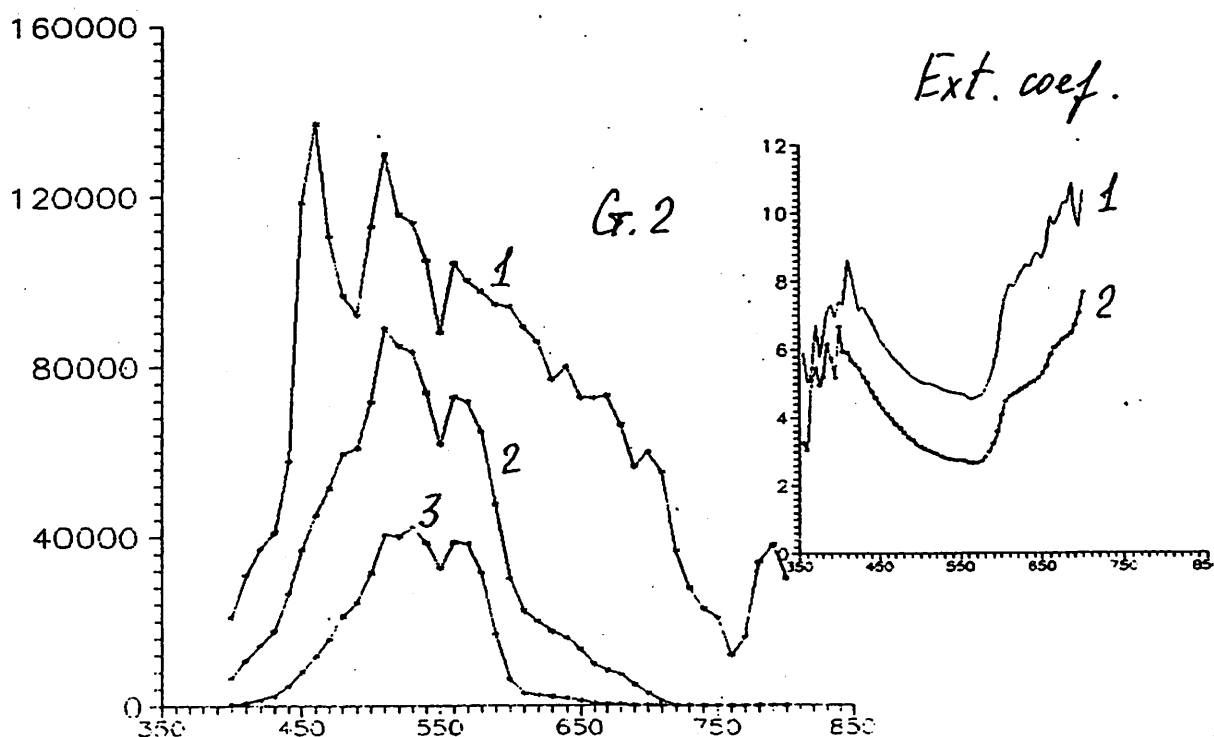
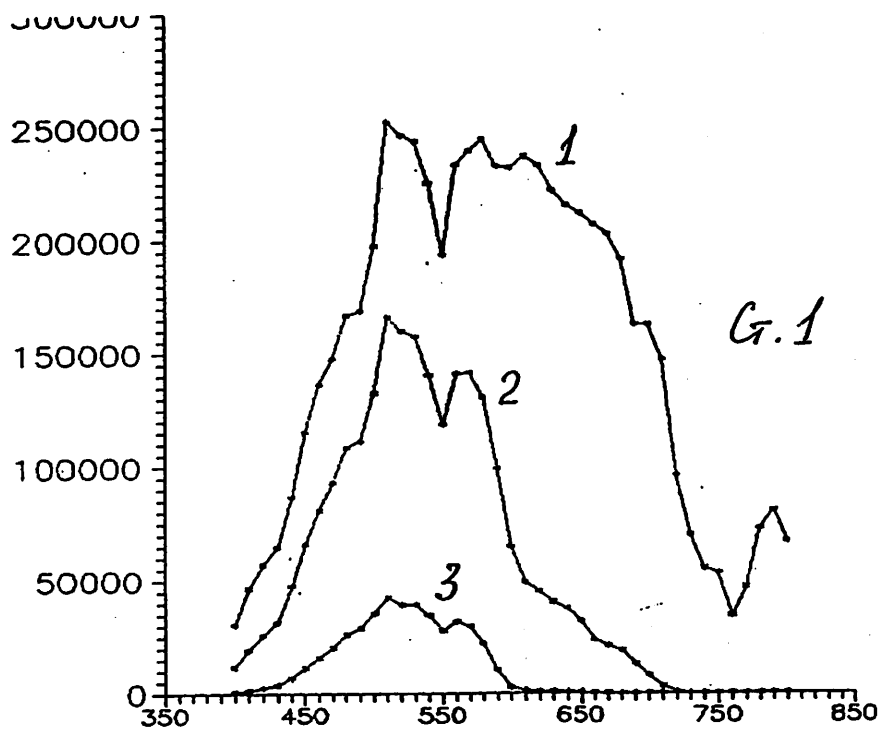


Рис. 122,а. Спектры светового потока на станциях в б.джигит на поверхности (1), 5 м (2), дне (3) по измерениям на первом этапе. на врезках даны спектры коэффициентов затухания от поверхности по п/н для соответствующих станций.

Fig.4. Spectra of light and ~~ext. coef.~~ at surface, 5 m.

интегральная матрица коэффициентов корреляции по измерениям  
в б. Ольга, б. Джигит и, на полигонах в районах обитания водорослей.

Sample Correlations

	H	T	S	O2	pH	NO2
H	1.0000	-.2361	.2425	-.1989	-.2122	.1545
T	-.2361	1.0000	-.2535	.9383	.9491	-.1081
S	.2425	<b>-.8535</b>	1.0000	-.7392	-.7253	.2347
O2	-.1989	<b>.9383</b>	-.7392	1.0000	.9688	.0203
pH	-.2122	<b>.9491</b>	-.7253	<b>.9688</b>	1.0000	.0448
NO2	.1545	-.1081	.2347	.0203	.0448	1.0000
NO3	.1390	-.1838	.2752	-.1574	-.1055	.6722
PO4	.4287	-.5038	.3939	-.4229	-.4837	.1130
Sm	.1848	<b>-.8442</b>	.5870	<b>-.3398</b>	<b>-.8830</b>	-.0795
C	-.4768	.4329	-.4392	.4397	.4579	-.1896
dSh	.4900	-.5824	.5835	-.4836	-.4806	.1972
dEO	.1177	-.4581	.4967	-.3386	-.3352	.1128

	NO3	PO4	Sm	C	dSh	dEO
H	.1390	.4287	.1848	-.4768	.4900	.1177
T	-.1838	-.5038	-.8442	.4329	-.5824	-.4581
S	.2752	.3939	.5870	-.4392	.5835	.4967
O2	-.1574	-.4229	-.3398	.4397	-.4836	-.3386
pH	-.1055	-.4837	-.8830	.4579	-.4806	-.3352
NO2	.6722	.1130	-.0795	-.1396	.1972	.1128
NO3	1.0000	.1118	-.0727	-.0429	.2221	.3291
PO4	.1118	1.0000	.4627	-.4316	.3535	.2120
Sm	-.0727	.4627	1.0000	-.4331	.3903	.2437
C	-.0429	-.4316	-.4331	1.0000	-.3221	-.1348
dSh	.2221	.3535	.3903	-.3221	1.0000	.1741
dEO	.3291	.2120	.2437	-.1348	.1741	1.0000

Table 1. Correlation coefficients  
for all measurements



VARIMAX ROTATED FACTOR MATRIX

Variable/Factor	1	2	3	4
C:A1.H	0.01194	<u>0.98195</u>	0.23067	0.05114
C:A1.T	<u>0.92583</u>	-0.19214	-0.25778	-0.10589
C:A1.S	<u>-0.73714</u>	0.19381	0.34697	0.26115
C:A1.O2	<u>0.93910</u>	-0.12151	-0.18963	-0.02102
C:A1.pH	<u>0.95031</u>	-0.16986	-0.14893	0.02495
C:A1.NO2	<u>0.03142</u>	0.15729	-0.00432	0.91513
C:A1.NO3	-0.06041	-0.01716	0.21758	0.88426
C:A1.PO4	-0.40287	<u>0.59944</u>	0.09525	0.03513
C:A1.Sm	<u>-0.89254</u>	0.18352	0.04787	-0.14315
C:A1.C	0.43756	<u>-0.70550</u>	0.23149	-0.12558
C:A1.d3a	-0.31380	0.42134	0.74983	0.10246
C:A1.d3c	-0.25232	-0.06096	0.89963	0.14336

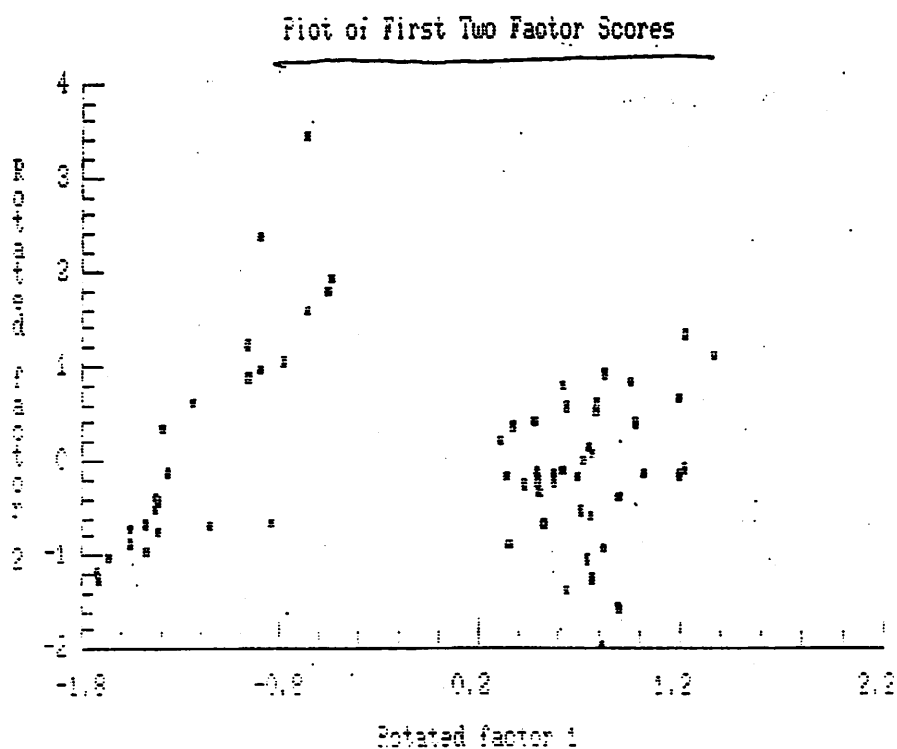


Рис. 162. Распределение наблюдений на плоскости первых двух параметров после вращения (по суммарным данным).

Fig. 5.

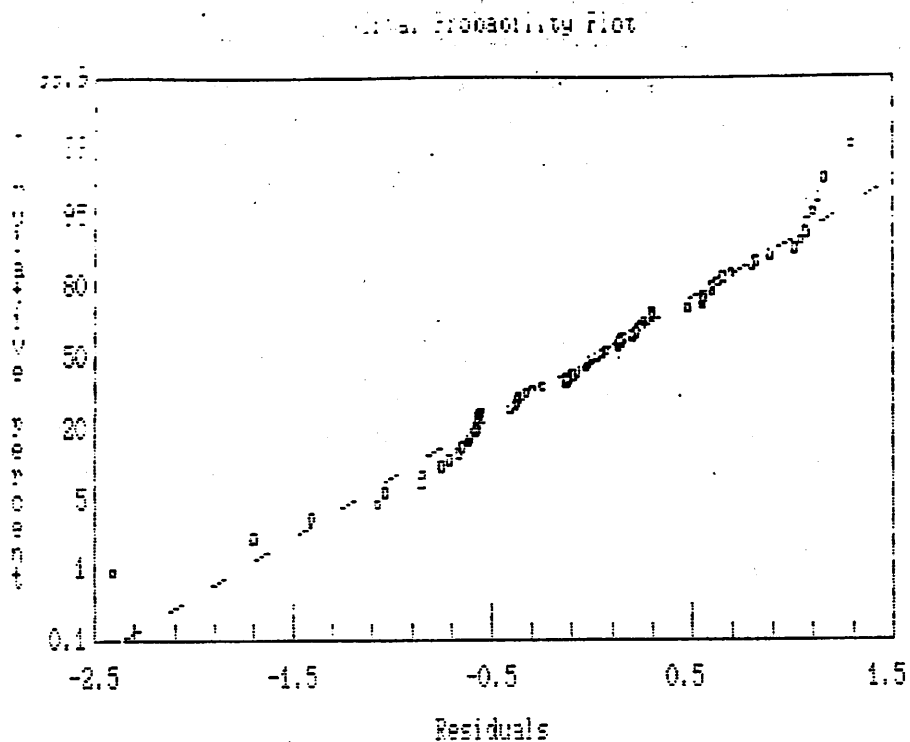


Рис. 166. Функция распределения остаточных отклонений от уравнения регрессии (масштаб по оси x логарифмический).  
Component Residual Plot for C:NI.1

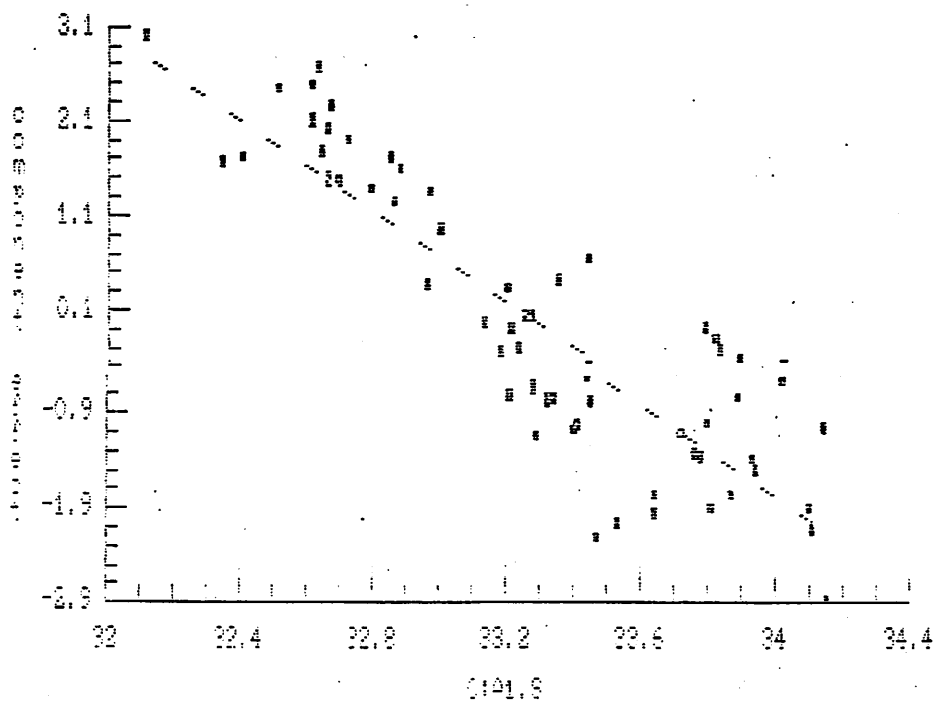


Рис. 167. Связь температуры и солености по уравнению регрессии.

Fig. 6. T-S regression

Model fitting results for: C:A1.T

Independent variable	coefficient	std. error	t-value	sig.level
CONSTANT	75.092277	11.745192	6.3921	0.0000
C:A1.S	-2.423254	0.203559	-7.9823	0.0000
C:A1.O3	0.253392	0.155149	1.5251	0.1327
C:A1.pH	2.482591	0.709204	3.5055	0.0009
C:A1.PC4	-0.057471	0.051771	-1.1101	0.2715
C:A1.9m	-0.180191	0.076528	-2.3513	0.0221
C:A1.dEH	-0.202905	0.092198	-2.1997	0.0318

R-SQ. (ADJ.) = 0.8624 SE= 0.778561 MAE= 0.585109 Durbin= 1.071  
 Previous: 0.0000 0.000000 0.000000 0.0000  
 55 observations fitted, forecast(s) computed for 0 missing val. of dep. var.

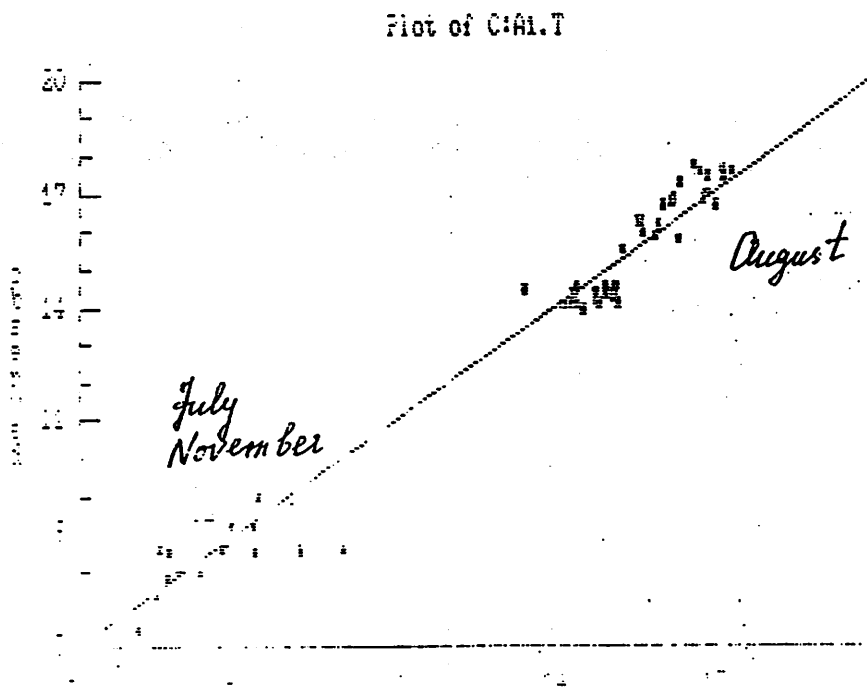
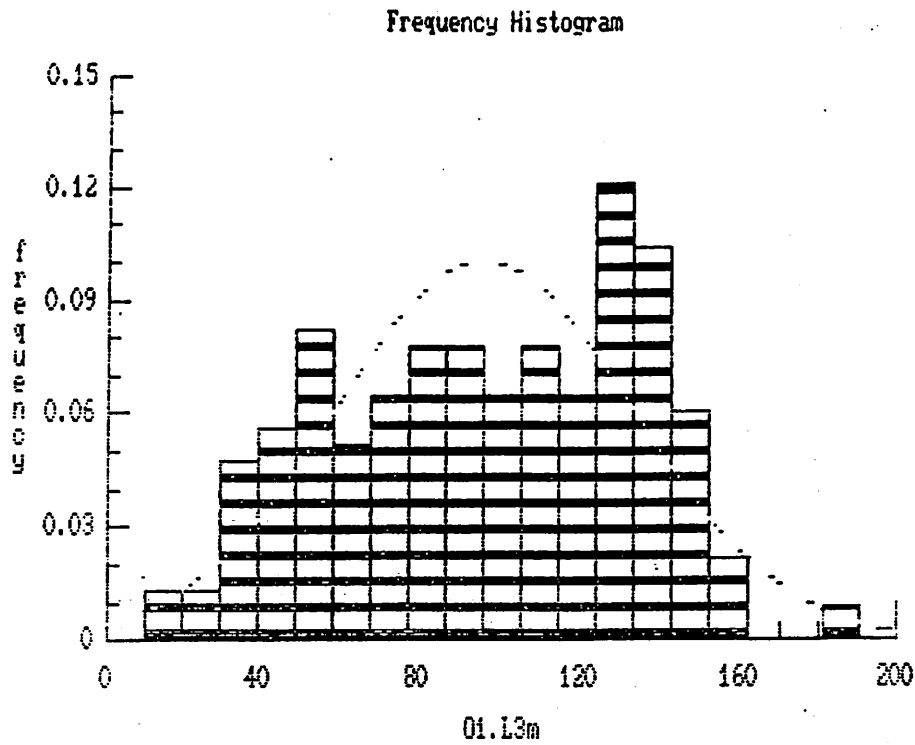


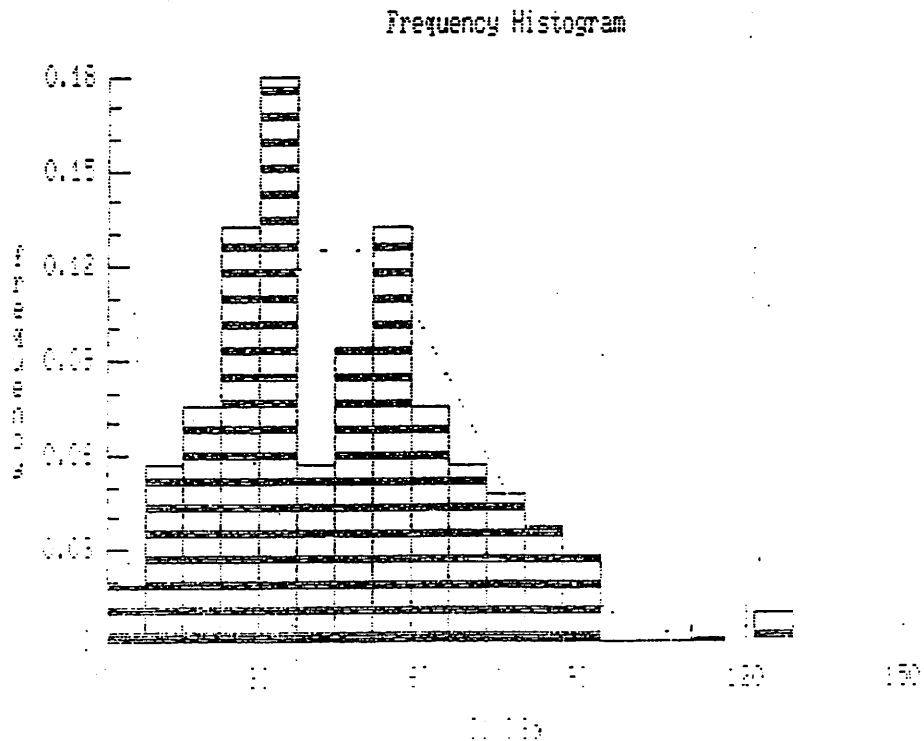
Рис. 7. Соотношение наблюдаемых и предсказанных по уравнению регрессии значений температур (суммарные данные).

Fig. 7. Linear regression for T (summarized over three stages)



*mat.*

Chisquare = 44.39 with 13 d.f. Sig. level = 2.64399E-5



*d.*

Chi-square = 10.111 with 5 d.f. Sig. level = 0.047310

рис. 10. Гистограммы относительного распределения длин листьев на станции в б. Ольга.

*Fig. 10. Histograms for lengths of leaves (b. Olga)*

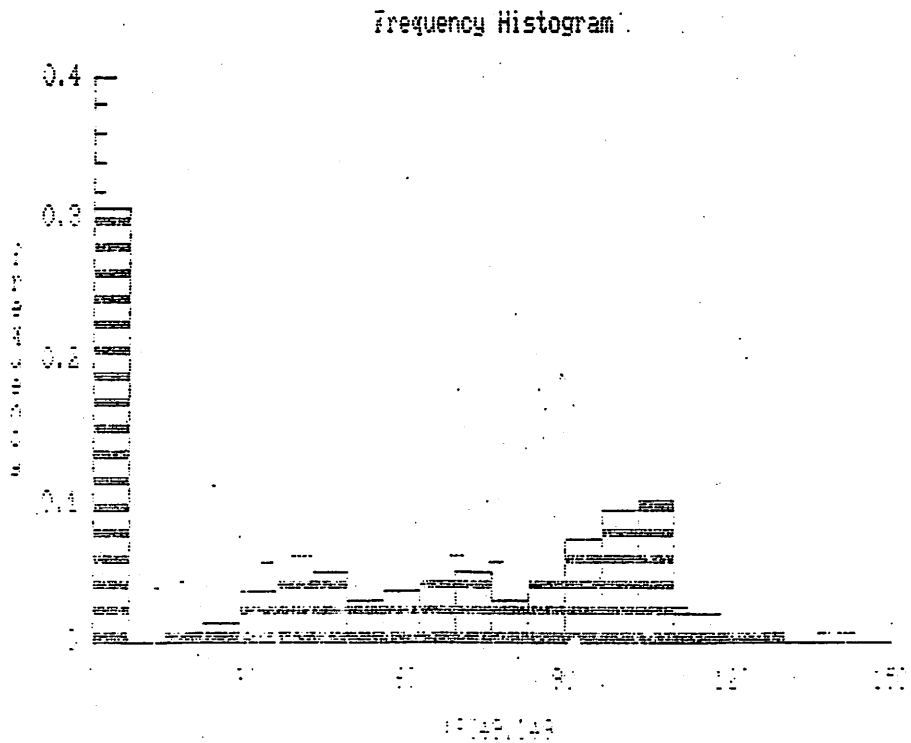
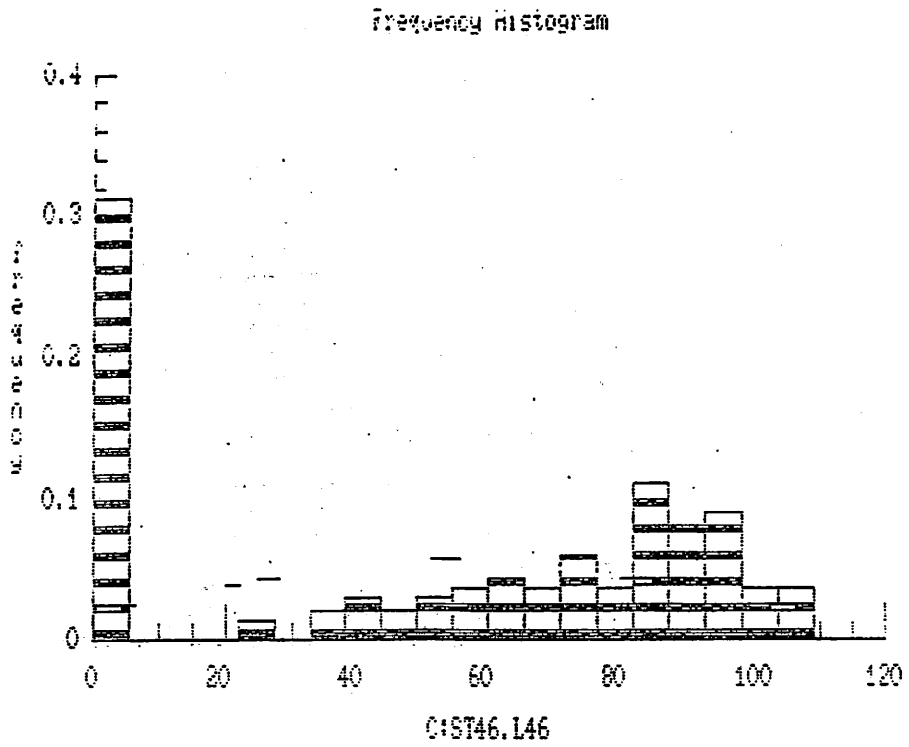


Рис. 170, 1.

Fig. 11. Histograms for lengths of leaves  
(open sea)

**Матрица коэффициентов взаимных корреляций  
между параметрами.**

Sample Correlations

	T	S	NO3	O2	pH	Sm
T	1.0000	-.8741	-.2386	.9733	.9599	-.8175
S	-.8741	1.0000	.3406	-.7750	-.7241	.7017
NO3	-.2386	.3406	1.0000	-.1807	-.1071	-.0644
O2	.9733	-.7750	-.1807	1.0000	.9840	-.7846
pH	.9599	-.7241	-.1071	.9840	1.0000	-.7954
Sm	-.8175	.7017	-.0644	-.7846	-.7954	1.0000
dEh	-.1402	.0313	.1022	-.1662	-.1528	.0895
Wm	.5728	-.2394	-.0118	.6617	.6925	-.5072
Fn	.2338	-.0407	.2453	.3012	.3030	-.5392
L	.5837	-.2975	-.2319	.6402	.6737	-.4223
DL	.6021	-.2515	-.1591	.6890	.7160	-.4155
Kv	.3588	.0142	.1115	.4834	.4852	-.2112

	dEh	Wm	Fn	L	DL	Kv
T	-.1402	.5728	.2338	.5837	.6021	.3588
S	.0313	-.2394	-.0407	-.2975	-.2515	.0142
NO3	.1022	-.0118	.2453	-.2319	-.1591	.1115
O2	-.1662	.6617	.3012	.6402	.6890	.4834
pH	-.1528	.6925	.3030	.6737	.7160	.4852
Sm	.0895	-.5072	-.5392	-.4223	-.4155	-.2112
dEh	1.0000	-.1739	-.1947	.0273	-.0649	-.2333
Wm	-.1739	1.0000	.6078	.8966	.9330	.5544
Fn	-.1947	.6078	1.0000	.7205	.6673	.2313
L	.0273	.8966	.7205	1.0000	.8571	.3373
DL	-.0649	.9330	.6673	.8571	1.0000	.3172
Kv	-.2333	.5544	.2313	.3373	.3172	1.0000

Table 3

Table 4. Собственные значения и факторная матрица  
для измеренных параметров.

Variable	Communality	Factor	Eigenvalue	Percent Var	Cum Percent
C:RR12.Wm	0.93603	1	6.26145	69.6	69.6
C:RR12.L	0.95598	2	1.55529	17.3	86.9
C:RR12.DL	0.98605	3	.67501	7.5	94.4
C:RR12.T	0.99259	4	.27037	3.0	97.4
C:RR12.S	0.96933	5	.13576	1.5	98.9
C:RR12.O2	0.98562	6	.07169	.8	99.7
C:RR12.pH	0.98628	7	.01762	.2	99.9
C:RR12.Sm	0.82400	8	.00959	.1	100.0
C:RR12.PO4	0.69435	9	.00429	.0	100.0

## Factor Matrix

Variable/Factor	1	2	3	4
C:RR12.Wm	0.78936	0.55208	0.14136	-0.09664
C:RR12.L	0.79917	0.54595	-0.10313	0.00626
C:RR12.DL	0.81203	0.57085	-0.03469	0.06004
C:RR12.T	0.94369	-0.29979	0.04904	0.10957
C:RR12.S	-0.73302	0.60798	0.12502	-0.11349
C:RR12.O2	0.95325	-0.16466	0.14631	0.16342
C:RR12.pH	0.95842	-0.11143	0.15876	0.11223
C:RR12.Sm	-0.79104	0.33994	-0.28996	0.41413
C:RR12.PO4	-0.67780	0.10965	0.70318	0.14727

Plot of First Two Factor weights

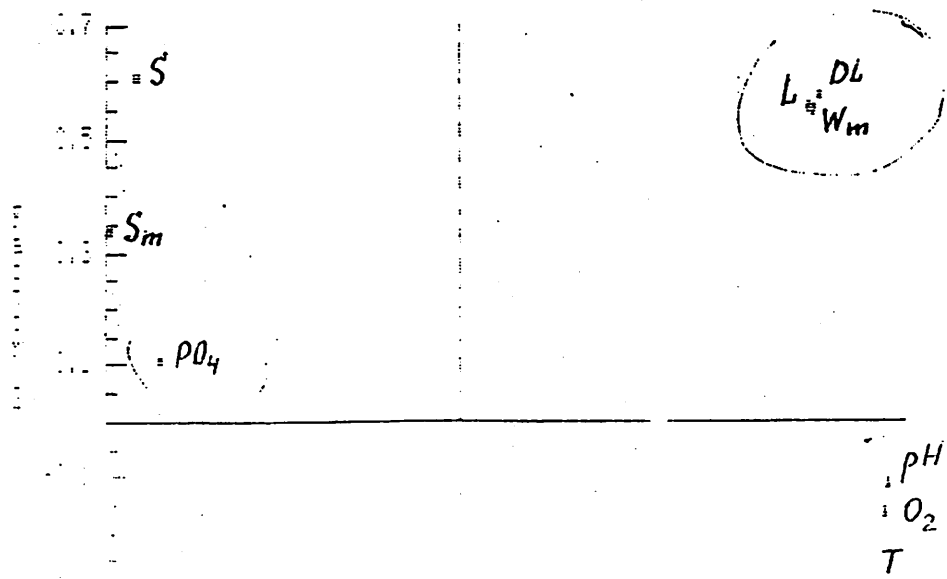


Рис. 101. Распределение параметров на плоскости  
первых двух факторов.

Table 4

	Sedimentation, t/km <sup>2</sup>	Run-off volume, km <sup>3</sup>	Photic layer thickness, m	Width of frontal zone, mile	Primary production, mg C/m <sup>3</sup> h		Chlorophyll A, mg Chl/m <sup>3</sup>		Zooplankt. biomass, mg/m <sup>3</sup>	
					Front zone	Back gr.	Front zone	Back gr.	Front zone	Back gr.
Amur	135.1	350	11	10-15	16.0-37.0	2.5-7.0	8.0-10.0	0.7-2.0	300-500	100-200
Yangtze	273.5	690	6	30	20.0-25.0 1.5-2.0	5.0-10.0 0.7-1.0	3.0-4.0 0.6-0.7	1.0-1.5 0.3	1400-1600 200-300	800-1000 20-100
Mekong	209.3	387	2-10	25-30	6.0-8.0 5.0-8.0	2.0-3.0 0.5-2.0	1.2-1.7 0.8-1.1	0.5 0.4-0.2	1500-2000 300-500	1000-100-200
Nile	371.0	39		10-12	0.3-0.6 2.0-6.0	<0.3 <2.0	0.2	0.1	200-500	50
Elba			5-6	5	1.5-2.2 18.0-20.0	2.0-1.3 4.0-10.0	0.6-1.6 2.0-4.0	1.0-1.0 4.0	150	10



Sakhalinsky bay - river Amur

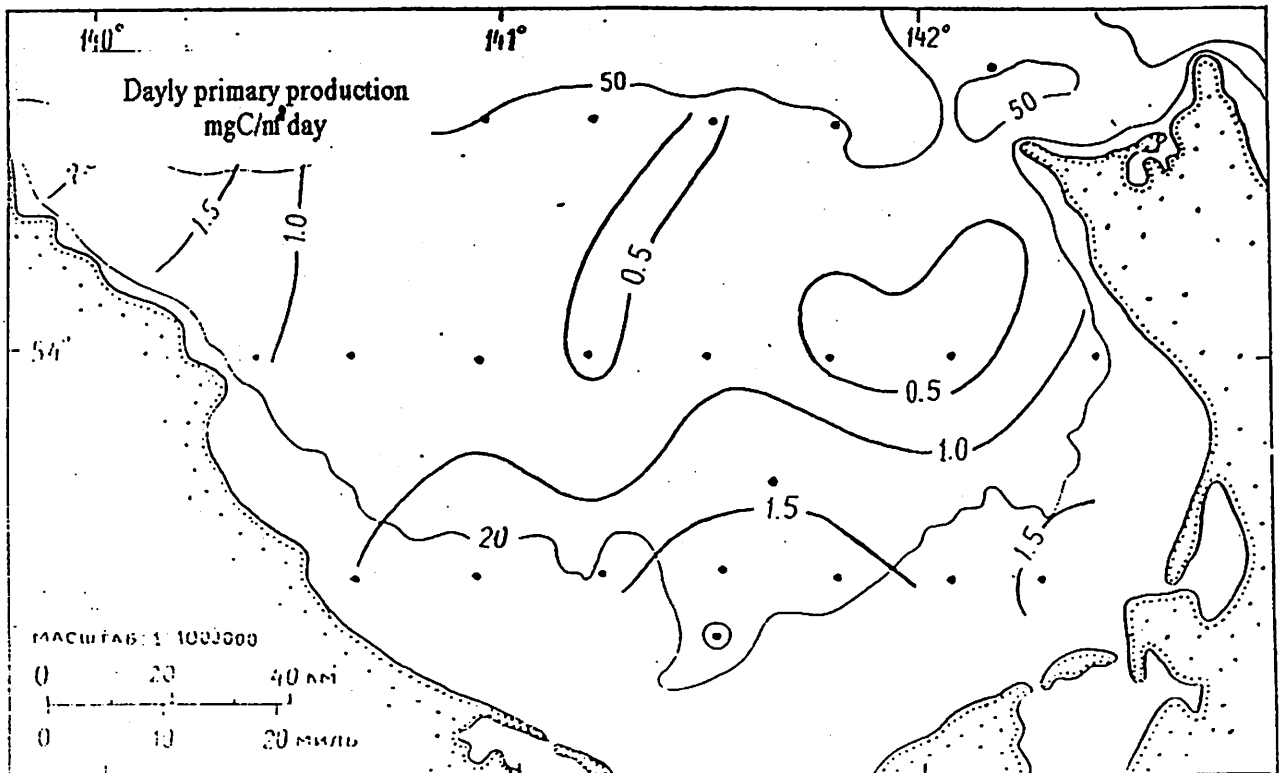
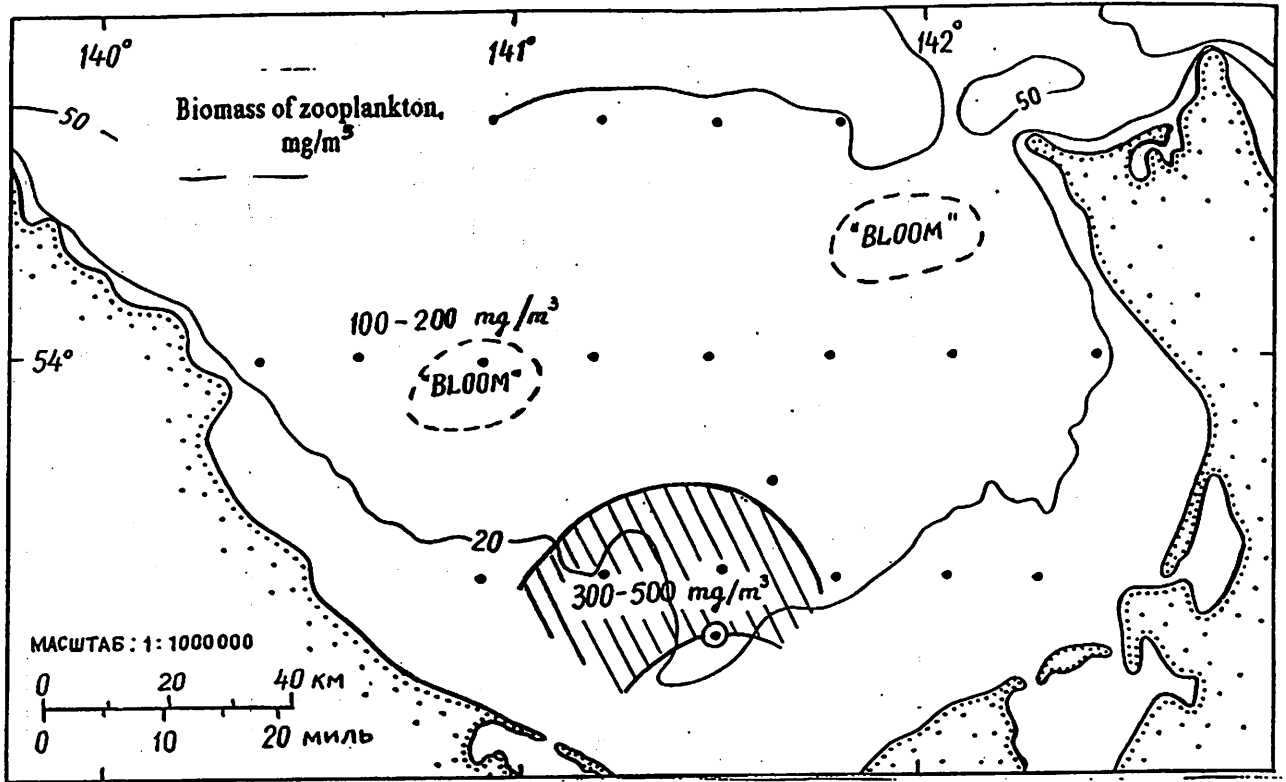


Fig. 13

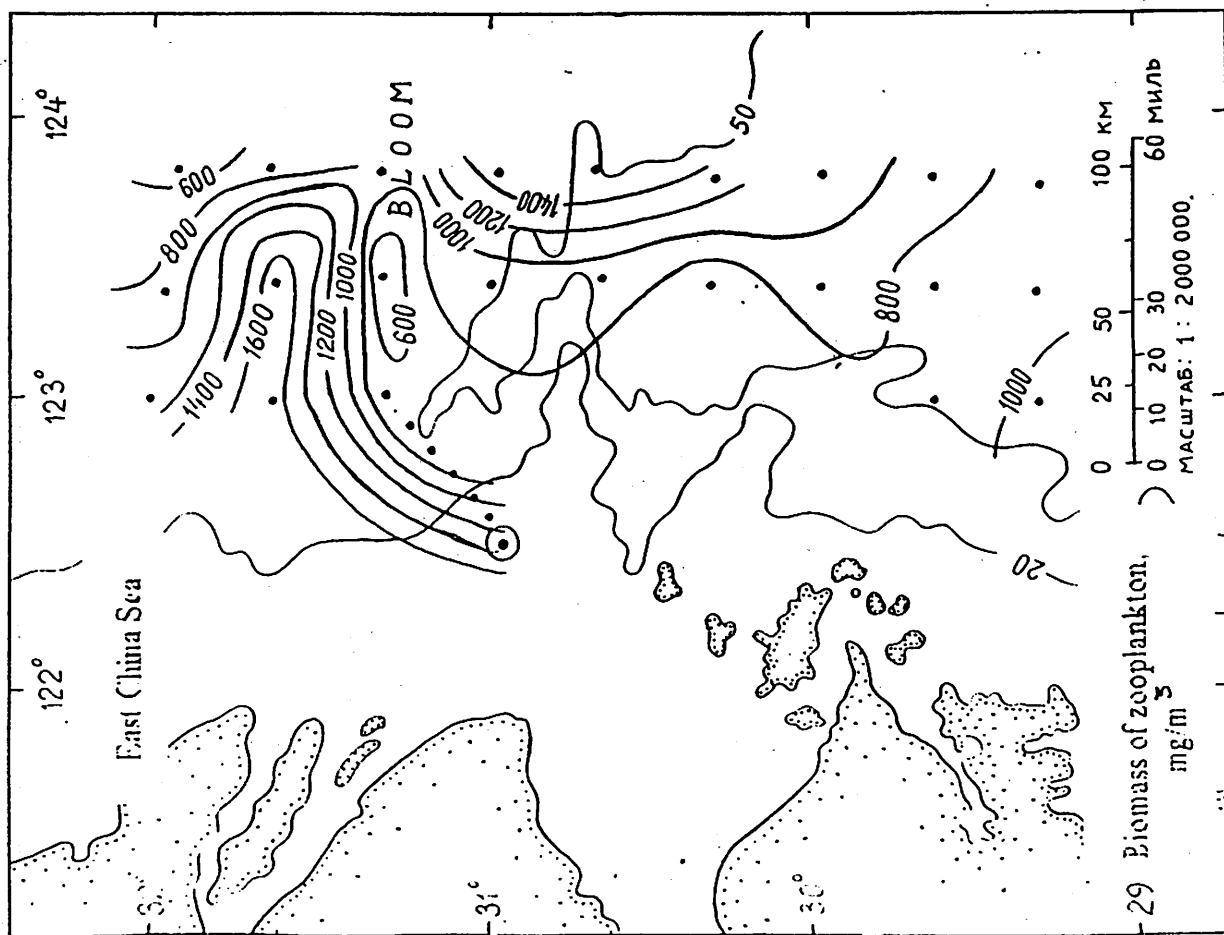
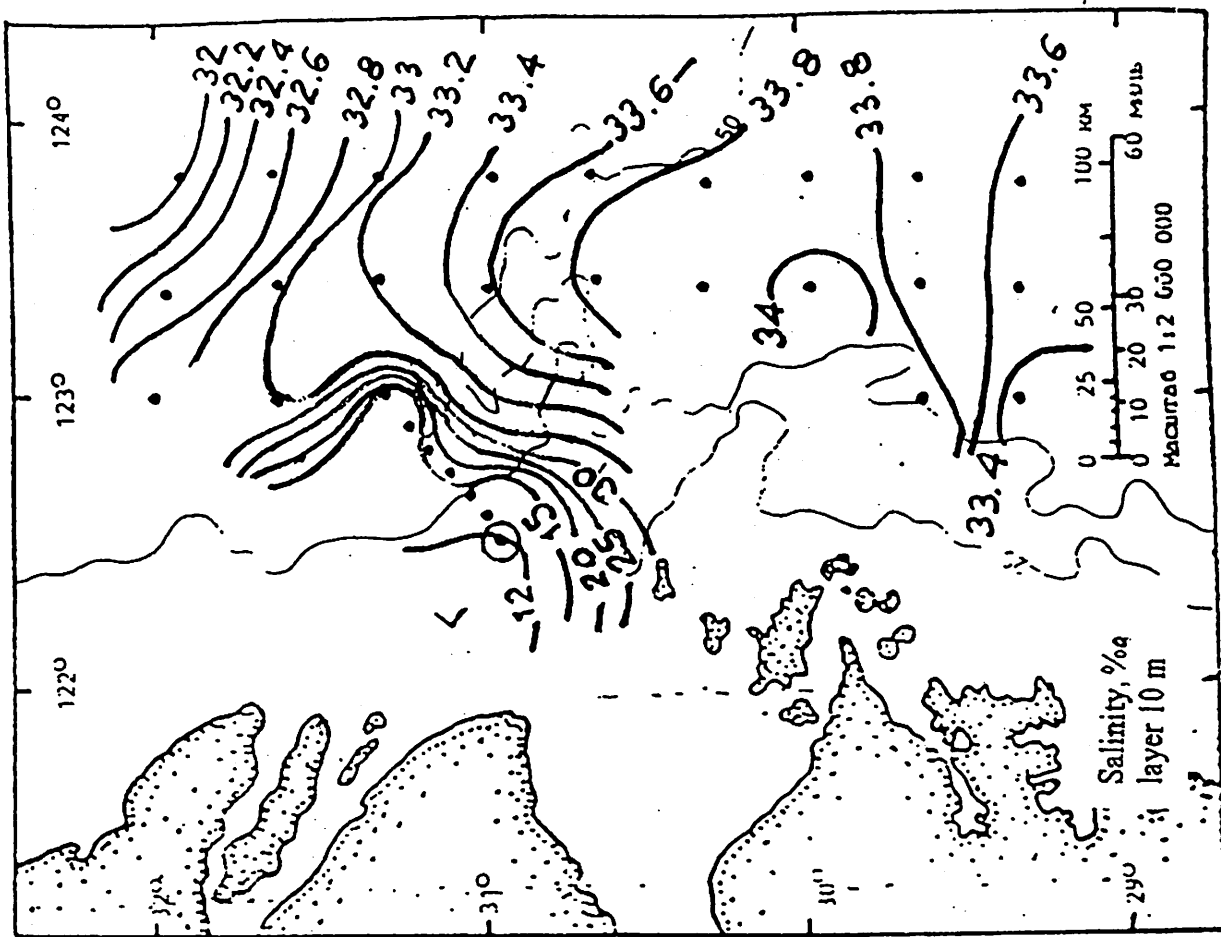
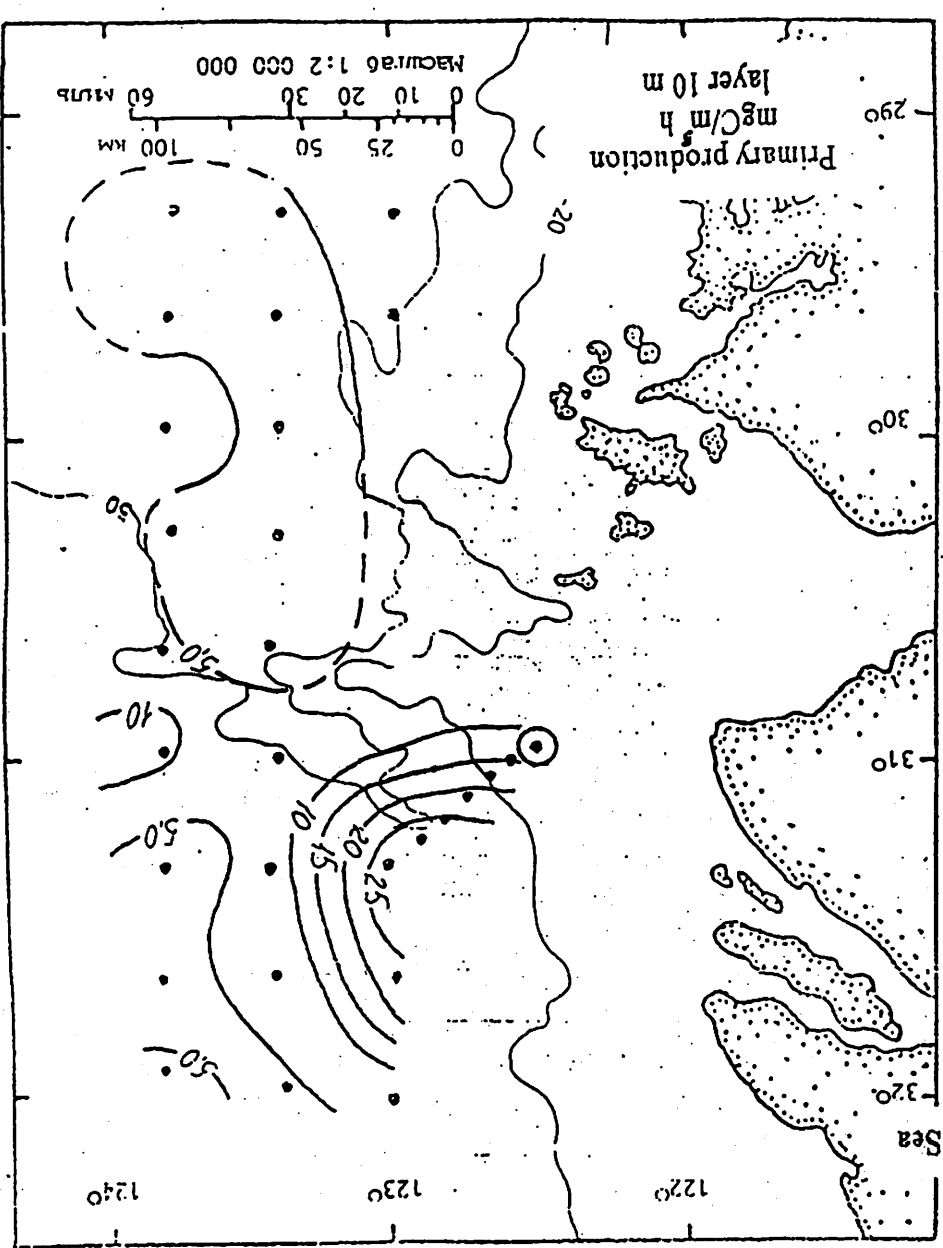
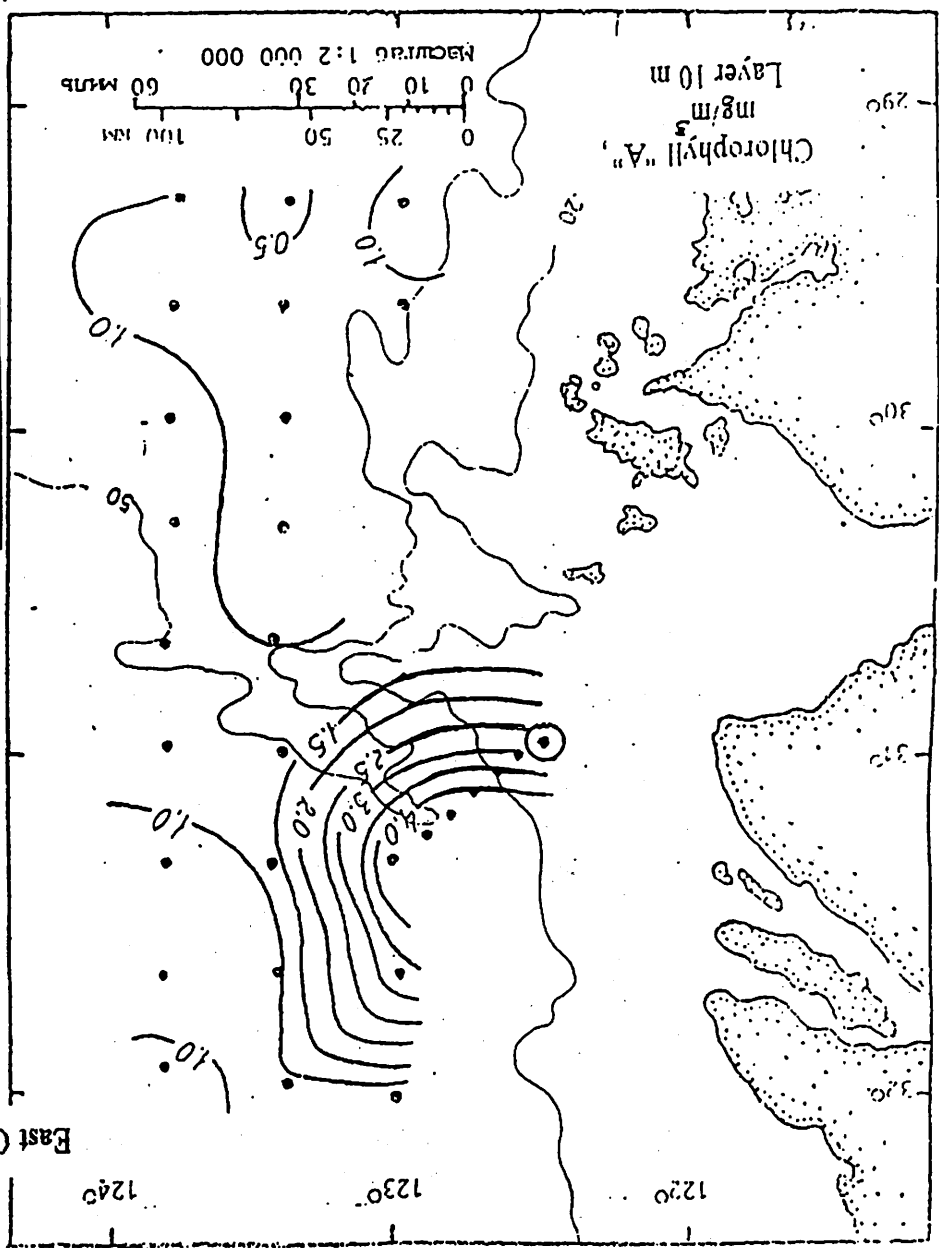
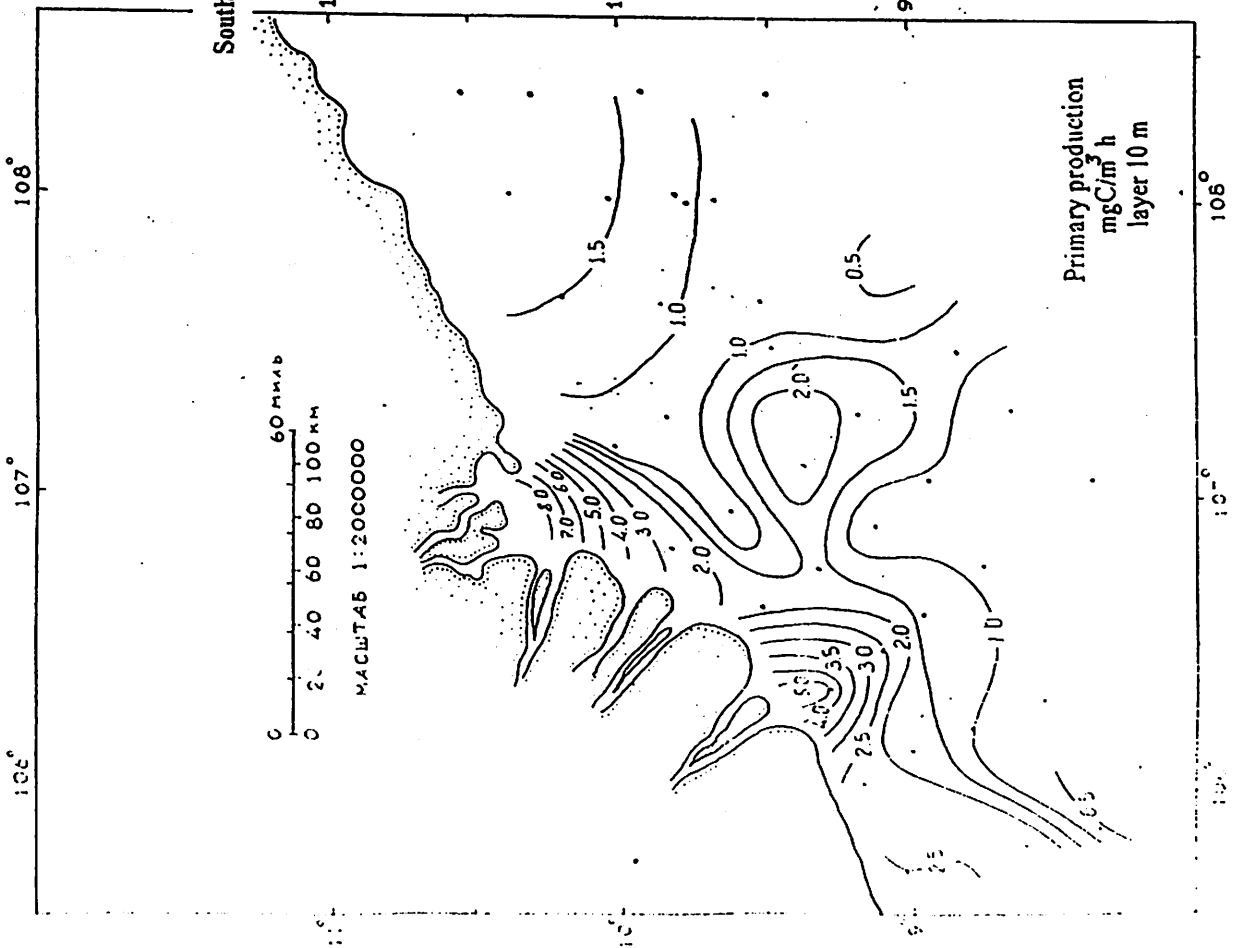
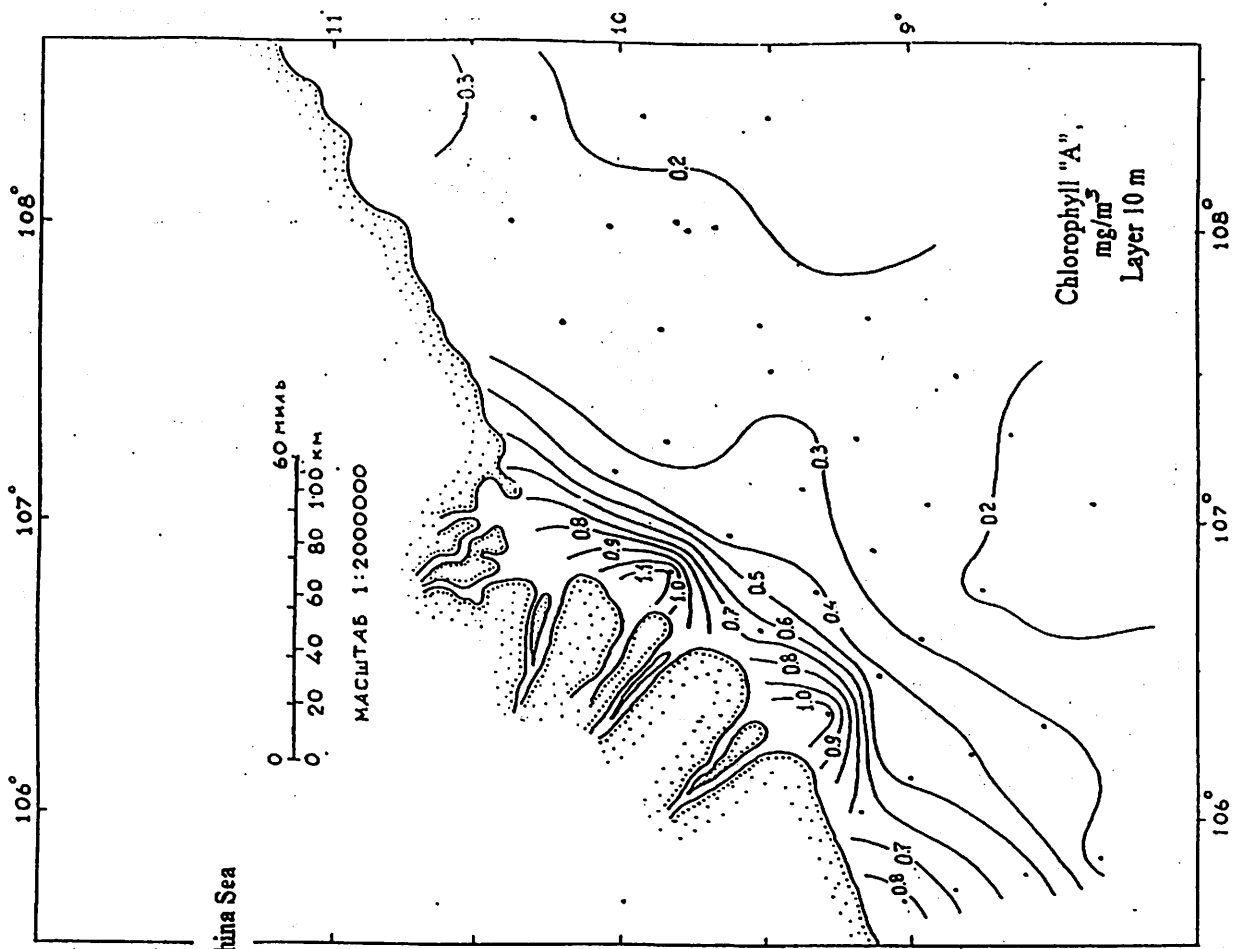


Fig. 14





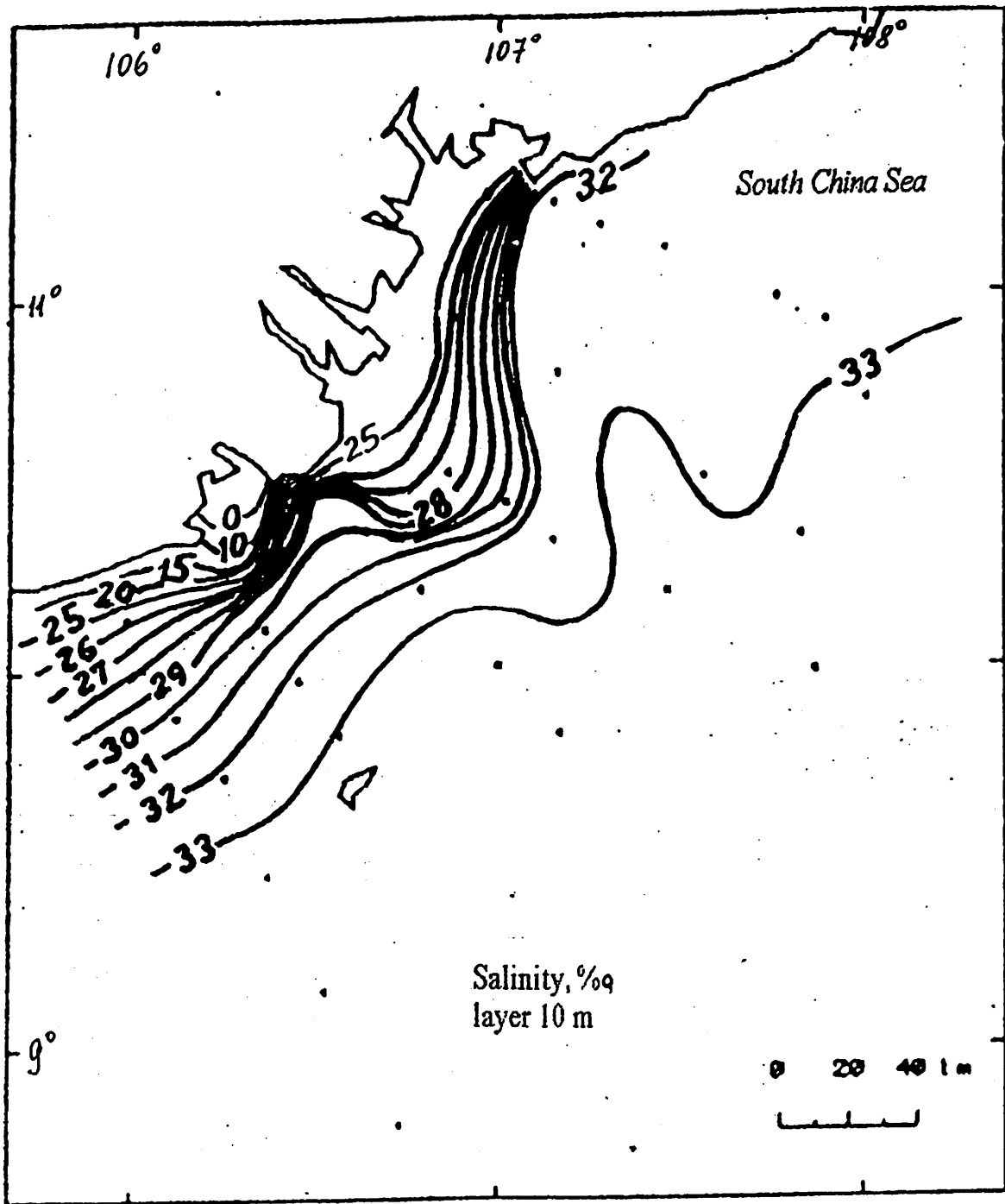
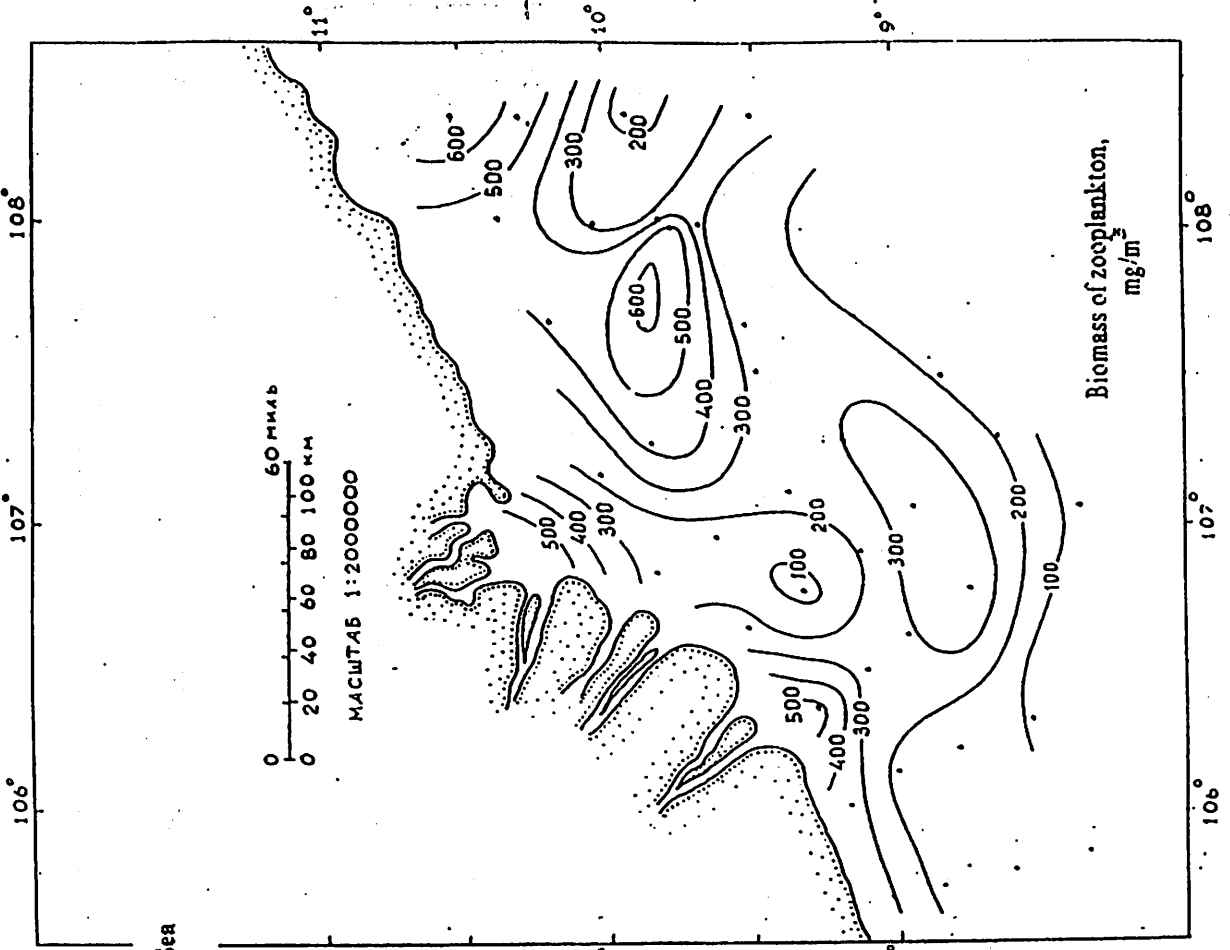


Fig. 17



South China Sea

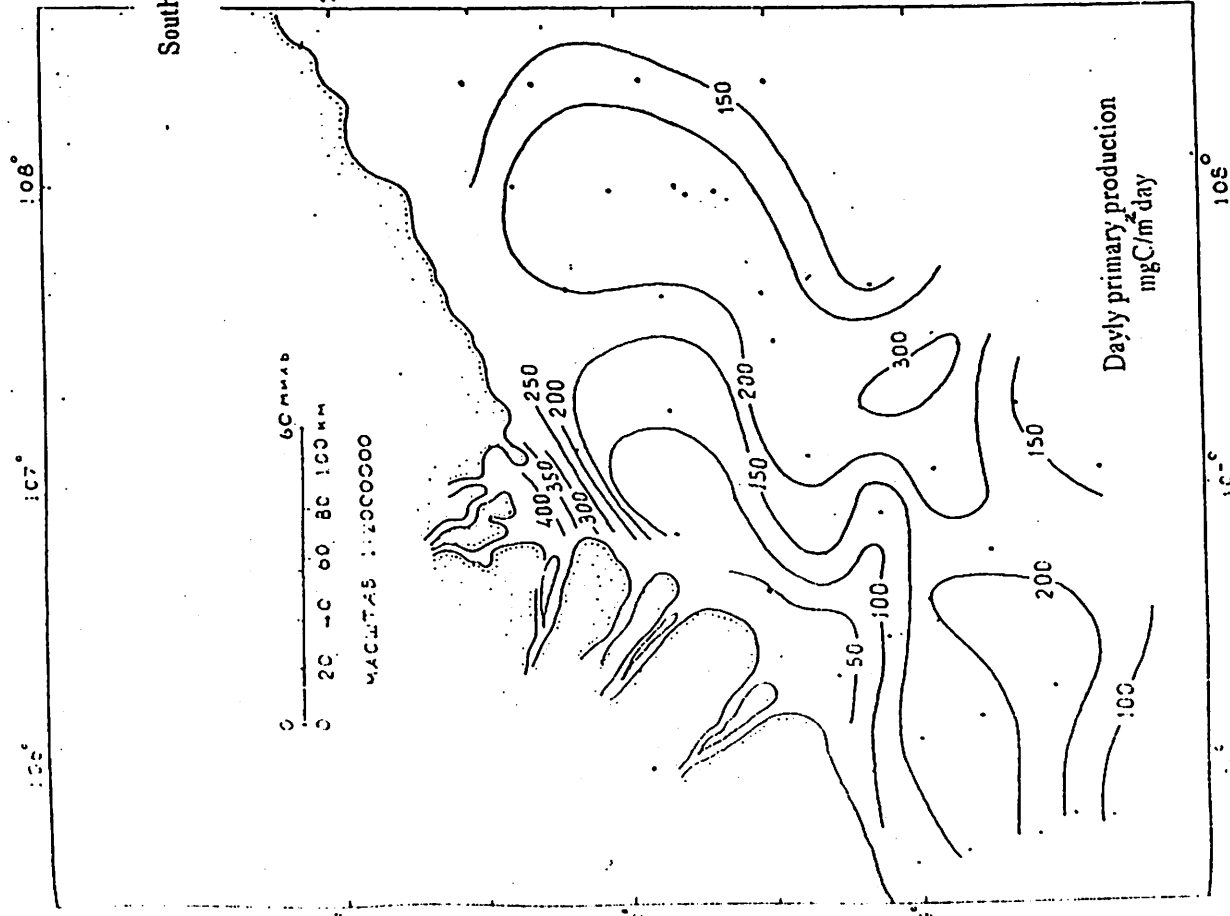
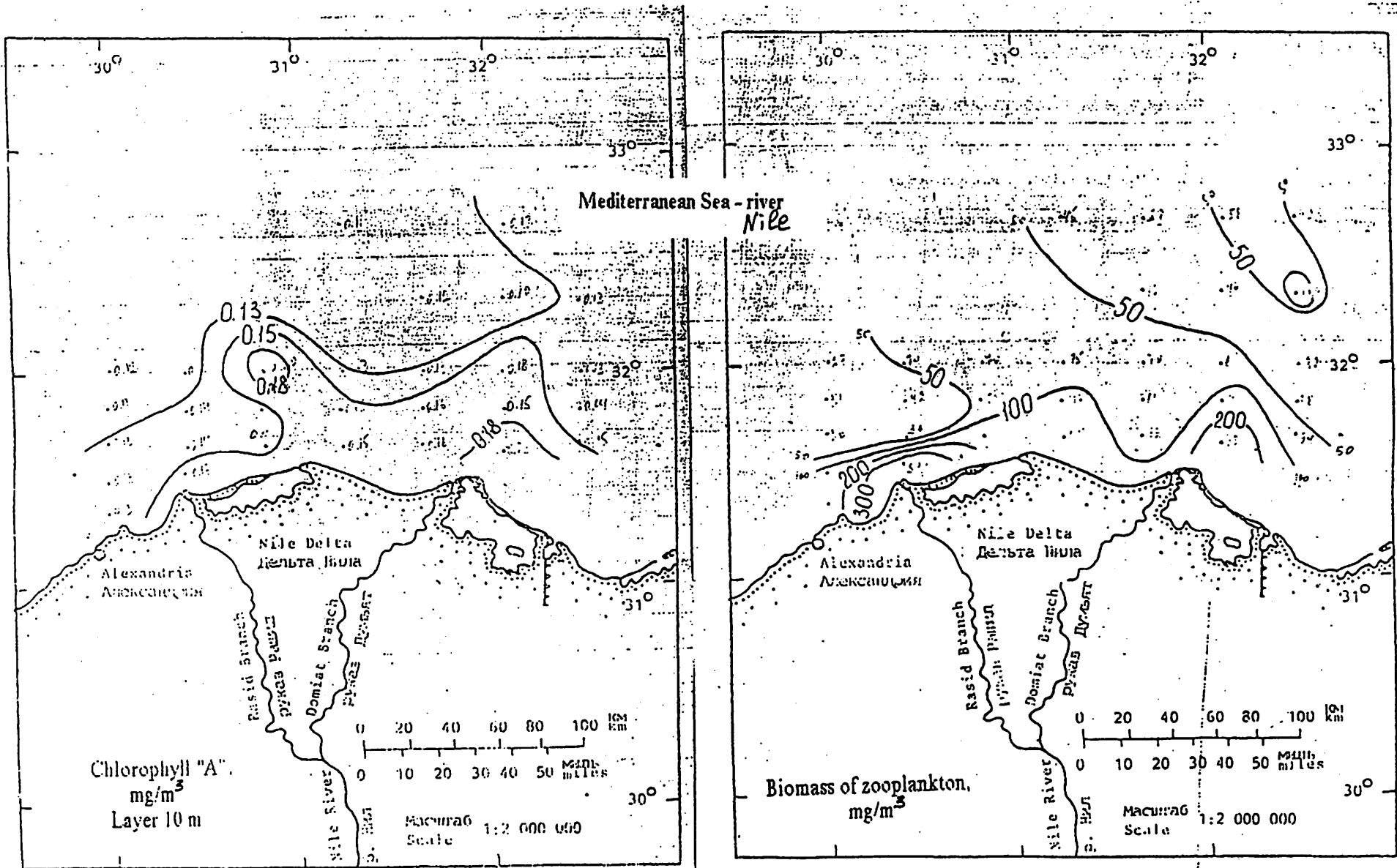


Fig. 19



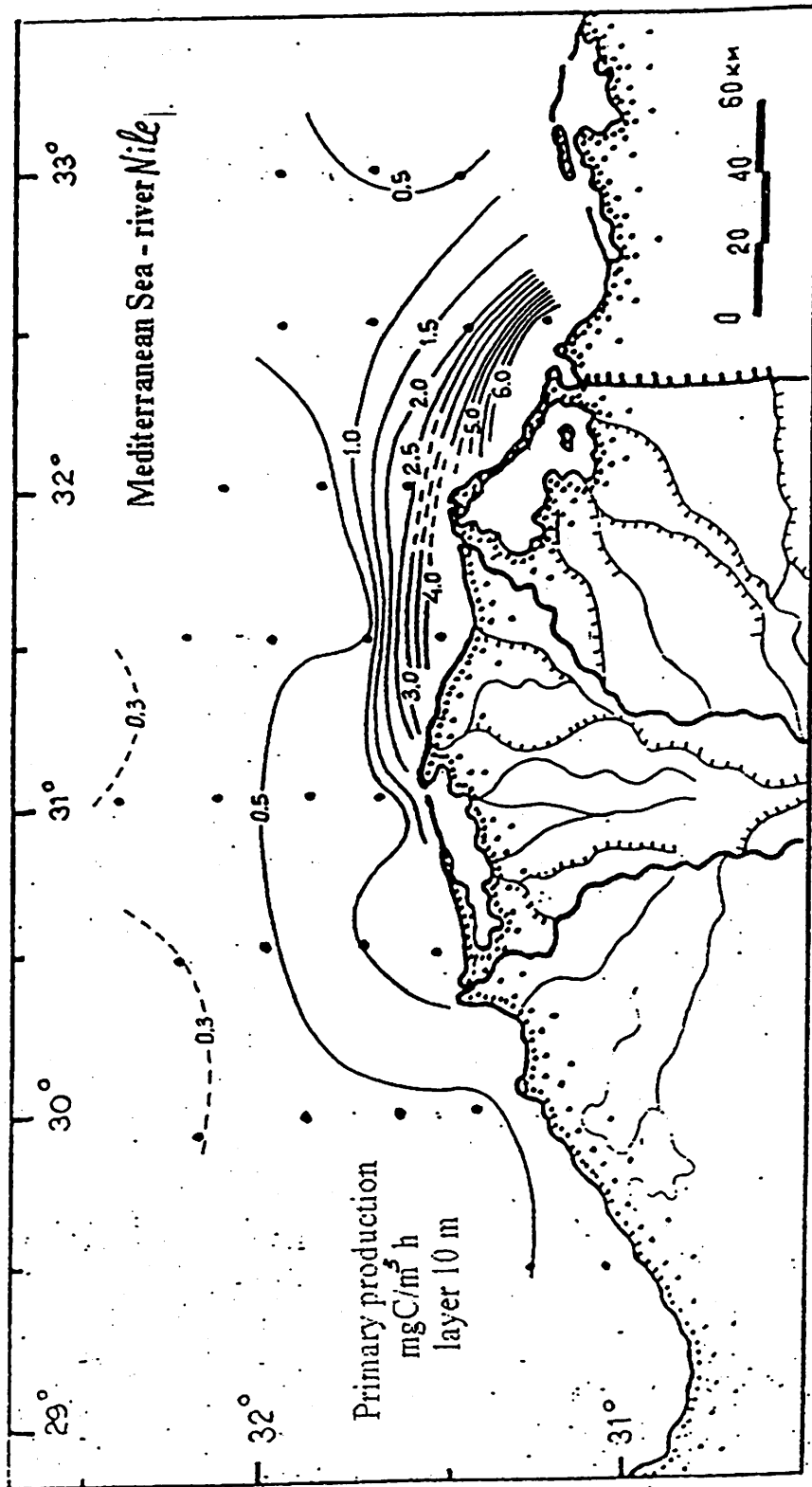


Fig. 2D



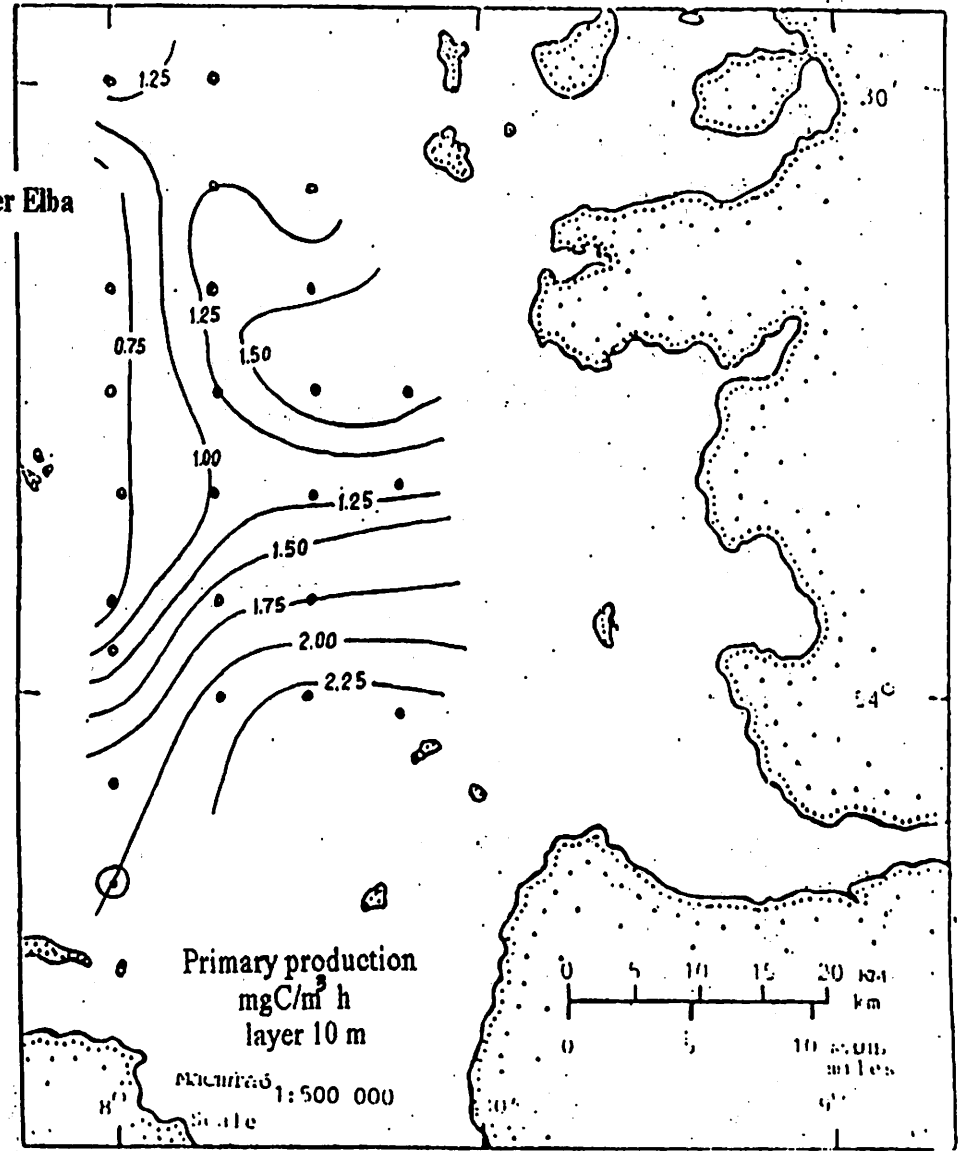
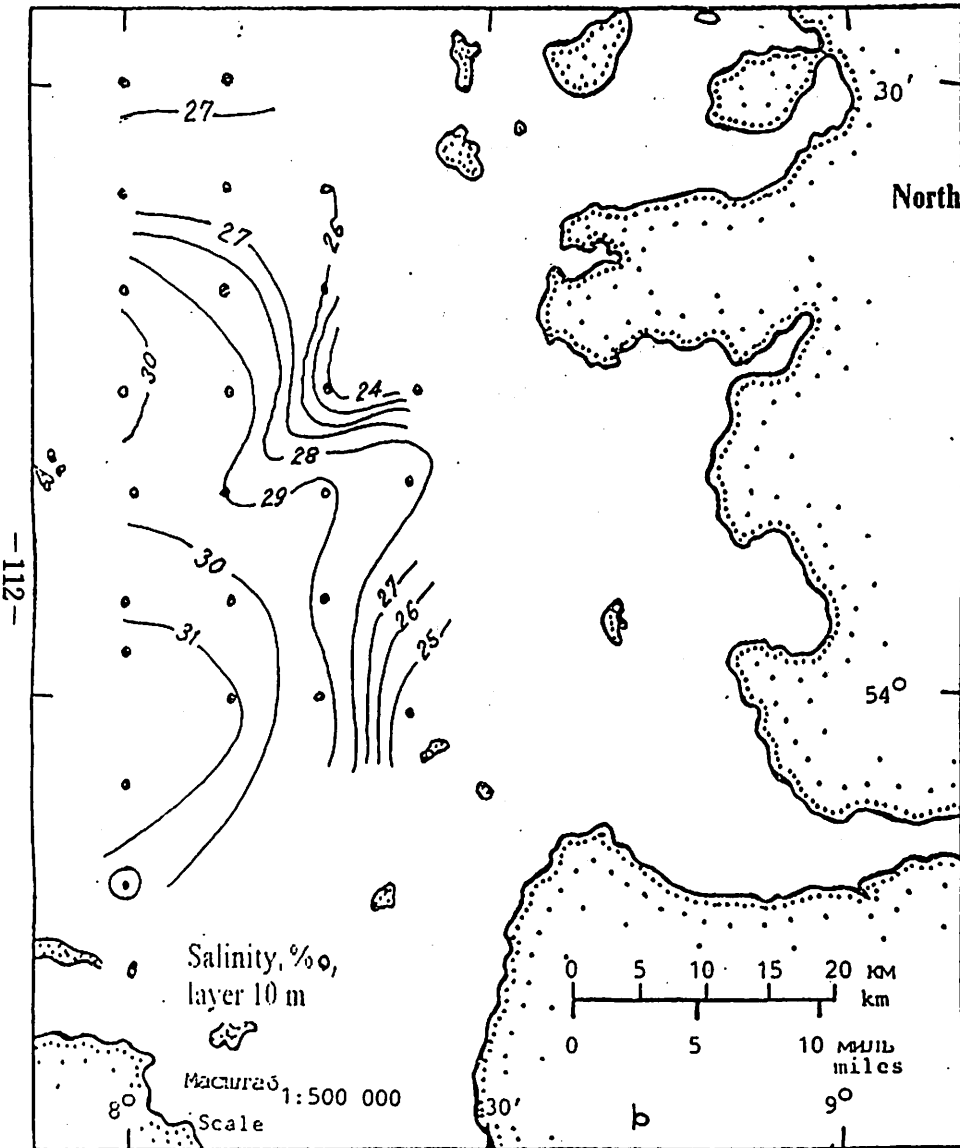


Fig. 2021

North Sea - river Elba

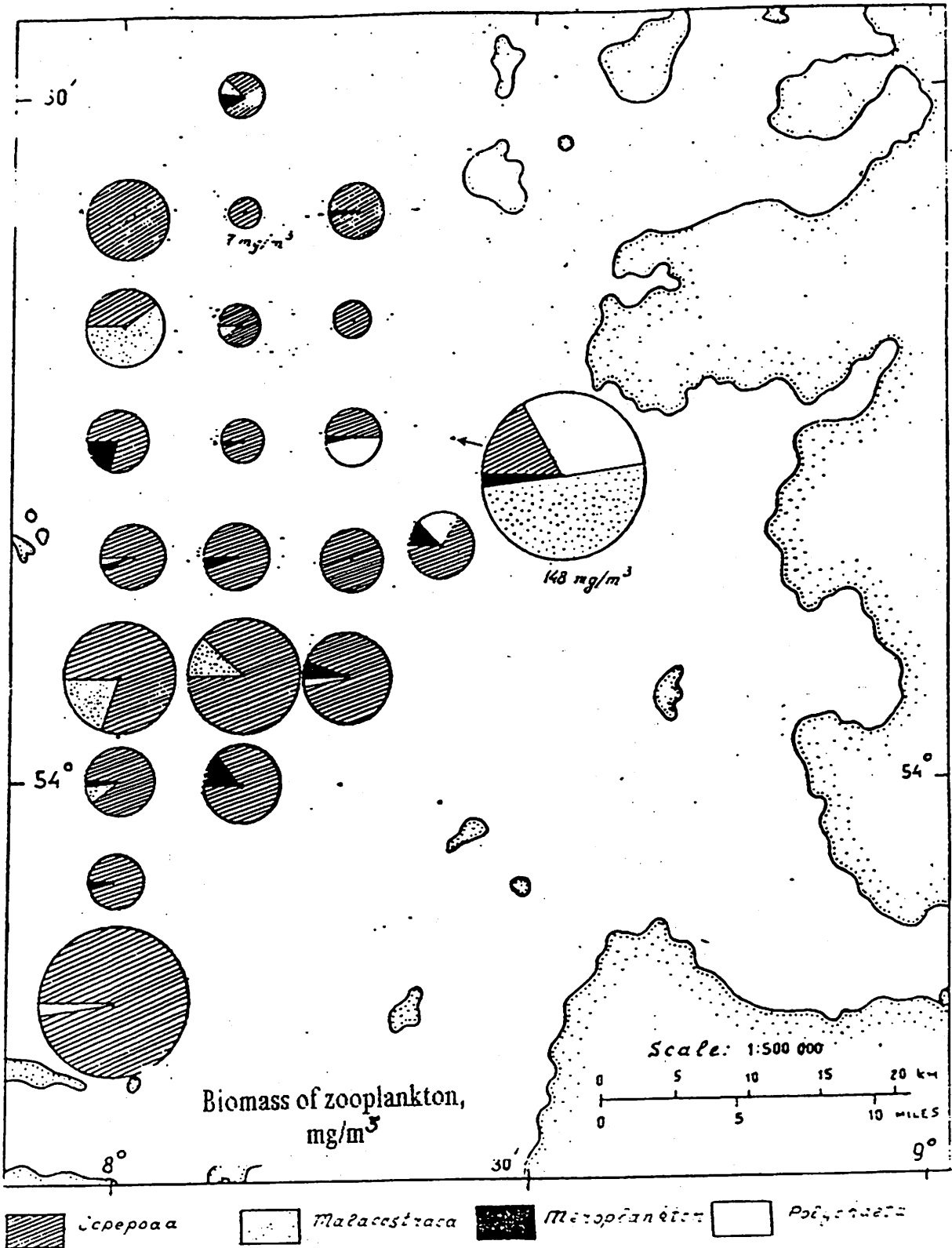


Fig. 22

Present Status on NEAR-GOOS Real Time Data Base  
at the Japan Meteorological Agency

*Takashi Yoshida, Naoyuki Hasegawa and Yukio Kurihara*  
*Climate and Marine Department*  
*Japan Meteorological Agency*  
*1-3-4, Otemachi, Chiyoda-ku*  
*100 Tokyo, Japan*  
*email: yoshida@hq.kishou.go.jp*

In 1993, UNESCO endorsed the establishment of a GOOS regional pilot activity in the North East Asian region. After through consideration by experts, IOC/WESTPAC adopted the North East Asian Regional GOOS (NEAR-GOOS) as its project and established the NEAR-GOOS Coordinating Committee to look after the project. The Committee adopted an Implementation Plan for the Initial Phase of NEAR-GOOS, as well as an Operation Manual for the NEAR-GOOS Data Exchange. As described in these documents, in the initial phase, NEAR-GOOS will concentrate its effort on the establishment of a system to exchange existing oceanographic data and products among the four participating country, namely China, Japan, Republic of Korea and Russian Federation, both in the real time and delayed mode.

According to the Implementation Plan and the Operation Manual, a data exchange system was established. The system now consists of Real Time Data Base (RTDB), Delayed Mode Data Base and Associated Data Bases, which are linked with each other via the Internet. The Japan Meteorological Agency (JMA), which operates a Regional Telecommunication Hub under the Global Telecommunication System (GTS), is responsible for the operation of RTDB. The main function of RTDB is collecting oceanographic data and providing them to users. More than 1,000 data are downloaded from GTS and transferred to RTDB everyday. Any organization can be registered as a user with the minimal formalities defined in the Operational Manual. The registered users can obtain the data via ftp (or ftp capability in the WWW browsers). The RTDB server provides the WWW homepage (<http://goos.kishou.go.jp>) for registered and non registered users. Within this home page, one can look at the description of the data base, the list of the available data, the Operational Manual and so on; however, the section to obtain the real data is password protected and only accessible to the registered users.

As emphasized in the Implementation Plan, distribution of oceanographic data in real-time is essential for improving operational ocean service activities. Therefore, as the most effective way of data distribution in real-time, organizations which carry out oceanographical observations are encouraged to transmit their data on board to meteorological centers via INMARSAT or coastal radio stations in the WMO International Code Forms such as SHIP, BATHY and TRACKOB. National Fisheries Research Institutes of Japan have contributed to an increase in the real-time data by reporting them from research vessels since last year. Otherwise oceanographic services and research organizations are encouraged to provide their data to RTDB by opening their own data server for access by others including RTDB. If they do not have such a server, they could ftp their data to RTDB server, and JMA takes care of the data for the use by others. First direct input of the data via the Internet was made in June 1997 from FERHRI of Russian Federation.

Thirty days after collection, all data are transferred to the Delayed Mode Data Base

operated by the Japan Oceanographic Data Center.

As a daily mapping product, results of a high resolution daily sea surface temperature (SST) analysis in seas adjacent to Japan by JMA are available on RTDB. SST grid point values of 0.25 x 0.25 degree resolution between 20N to 50N from 110E to 160E are operationally determined everyday in an optimal interpolation method. Thirty-years mean daily SST field is used as the first guess field of the analysis. Analysis increment for each grid point is given as a weighted sum of the deviations between the first guess field and AVHRR observations of NOAA satellite and ship and buoy *in situ* observations. The error statistics of the first guess fields are determined based on the satellite observations for 32 months. Any interested persons can look at the images of the analysis and registered users can get the grid point values.

If we have good knowledge on the oceanographic processes and have good access to the real time observational data required to monitor those processes, more useful ocean service products could be provided. NEAR-GOOS are expected to promote the data/product exchange and the researches needed for such activities and to contribute to better ocean services.

File Edit View Go Bookmarks Options Directory Window Help

Back Forward Home Reload Images Open Print Find

Location:

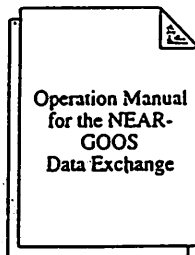
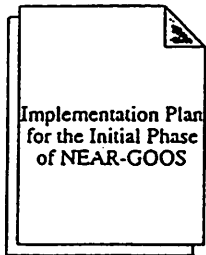
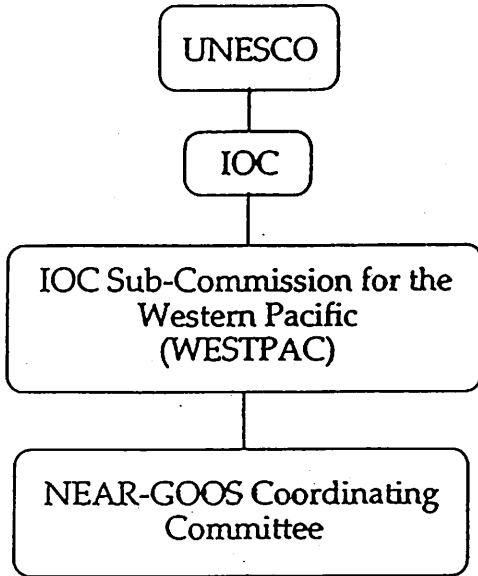
What's New What's Cool Handbook Net Search Net Directory

## NEAR-GOOS REALTIME DATABASE

You can obtain or input oceanographical data using this database. In order, however, to be authorized to have access to the database, you need to have your account by applying to NEAR-GOOS Real Time Database Operator. The database contains the data collected at the Japan Meteorological Agency (JMA) through Global Telecommunication System (GTS) of the World Meteorological Organization and the data that the participating institutes have contributed. The data which have been resided in the Real Time Data Base for 30 days are transferred to the Delayed Mode Data Base and maintained for your access.

- o [Access to Data](#)
- o [JMA Daily SST Analysis Chart](#)
- o [Registration to the Data Base](#)
- o [List of Available Data Files](#)
- o [Operation Manual](#)
- o [Manual on Codes of WMO](#)
- o [News on Database](#)
- o [Associate Data Bases](#)
- o [Home](#)

## Managing Mechanism



### Goals of NEAR-GOOS

- (i) to improve ocean services in the region
- (ii) to provide data and information useful in the mitigation of the effects of natural disasters caused by waves, storm surges, and sea-ice
- (iii) to increase the efficiency of fishing vessels
- (iv) to provide information useful in pollution monitoring
- (v) to monitor parameters useful to mariculture, particularly with regard to harmful algal blooms
- (vi) to provide information on the health of the coastal zone for recreation purposes
- (vii) to provide data sets required for data assimilation, modeling and forecasting

(extracts from the Implementation Plan)

### NEAR-GOOS Data Policy

The NEAR-GOOS data should be accessible, free of charge, to all users who are interested in obtaining data from and contributing data to the data bases.

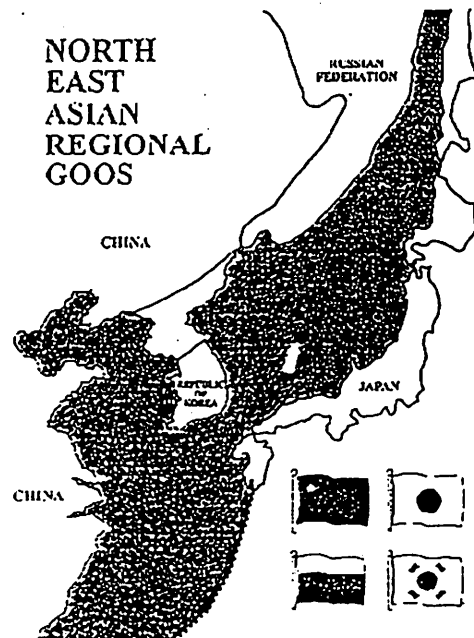
To ensure the security of the bases and to maintain effective utilization of data base, registration is necessary.

(extracts from the Operational Manual)

IOC at UNESCO, Paris

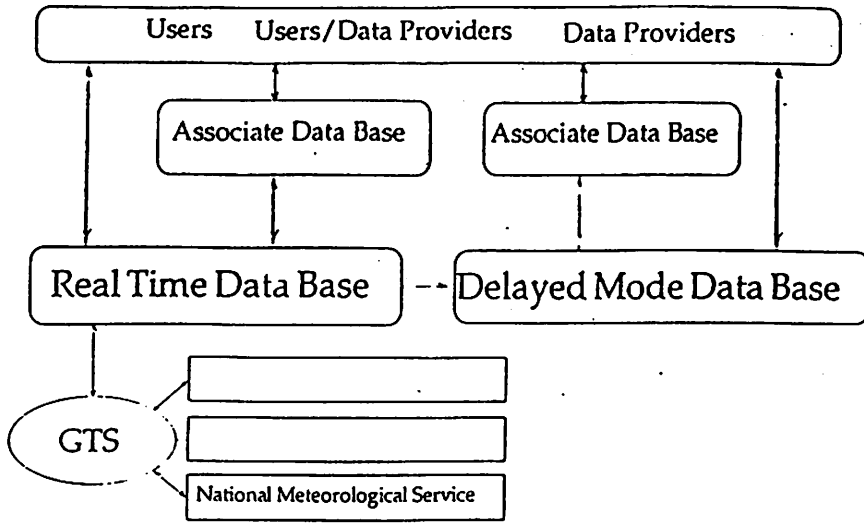
## NEAR-GOOS

An Operational Demonstration of the North-East Asian Regional GOOS.

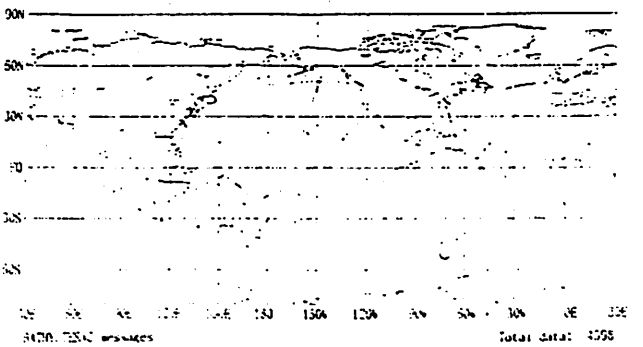
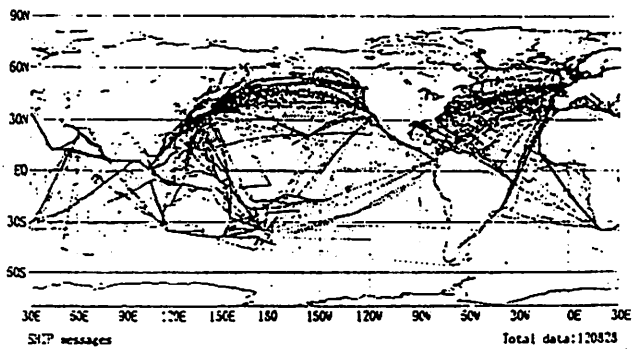
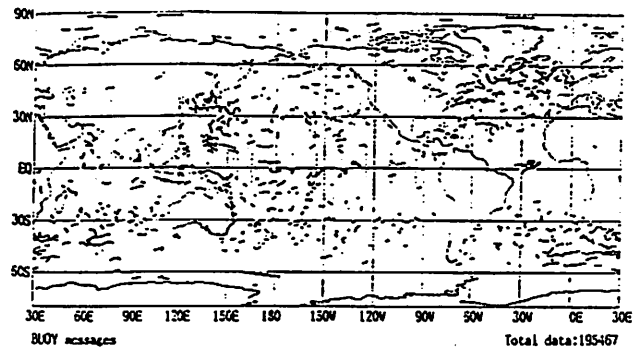
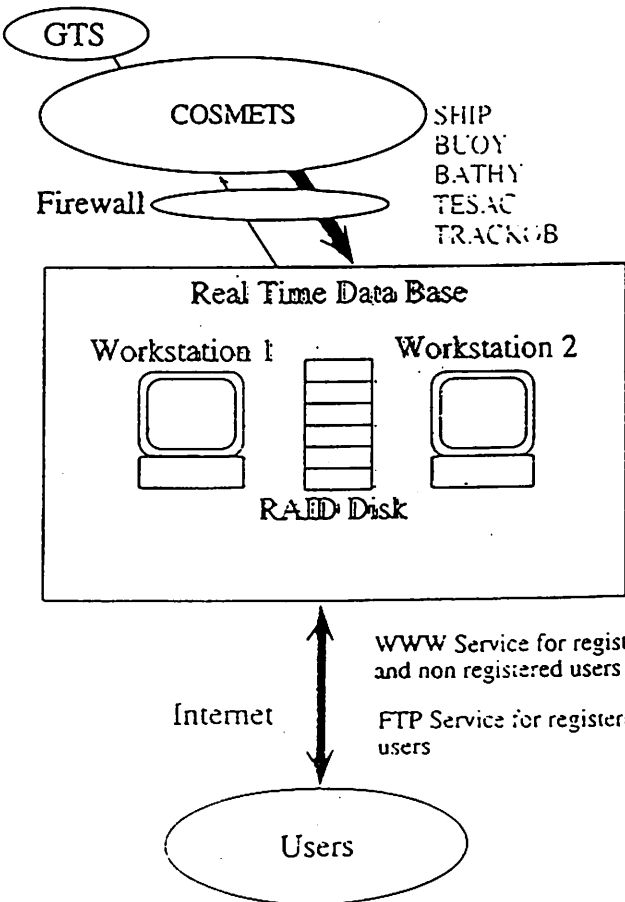


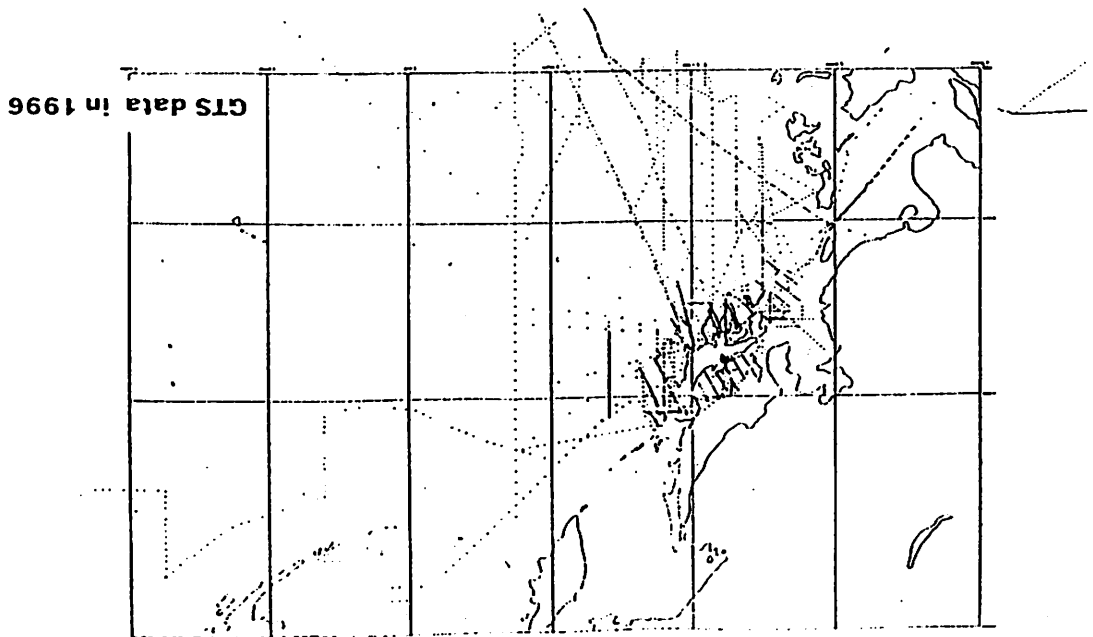
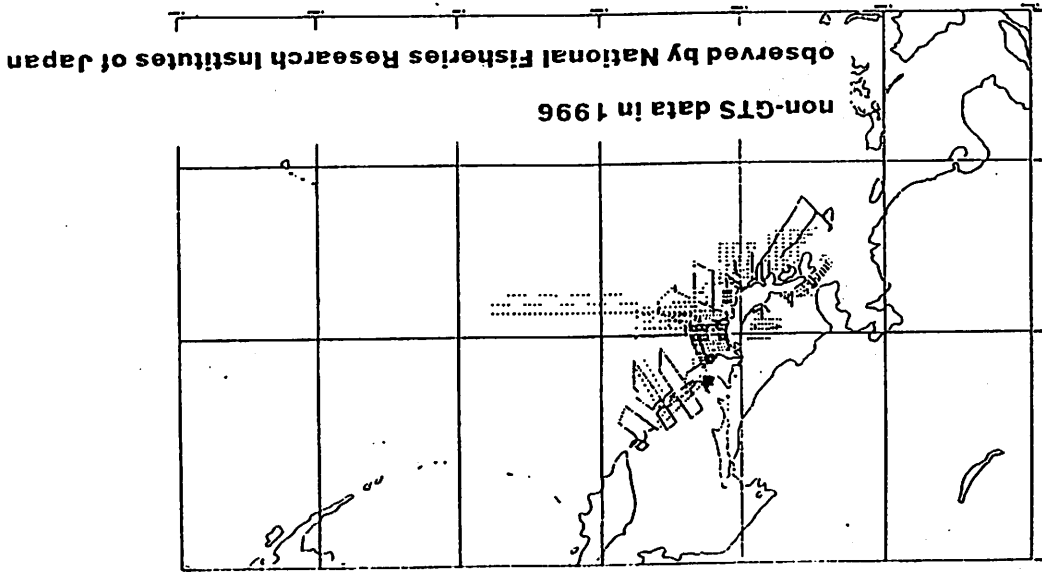
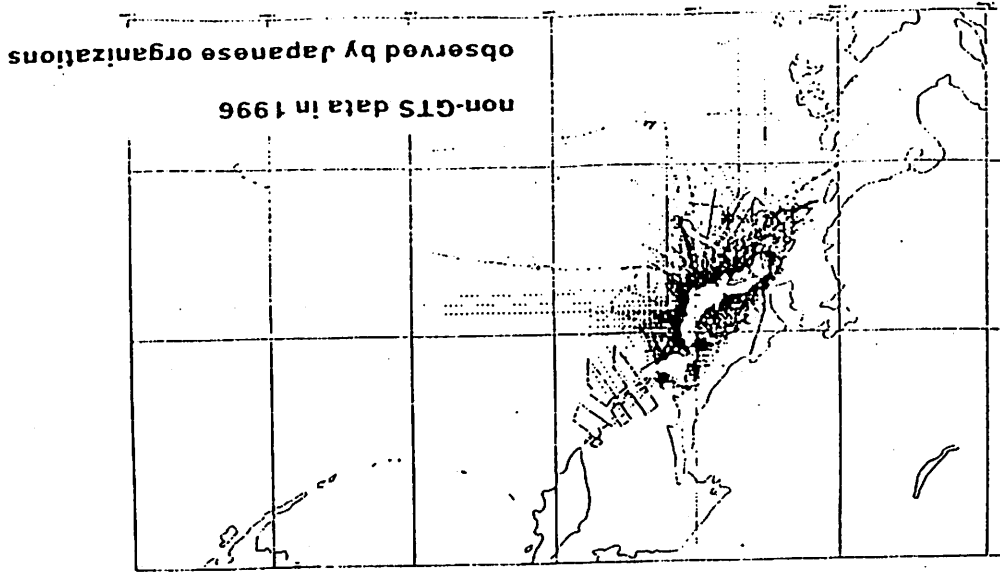
### Functions of Real Time Data Base

- Data Collection
- Format Translation
- Quality Control
- Data Provision

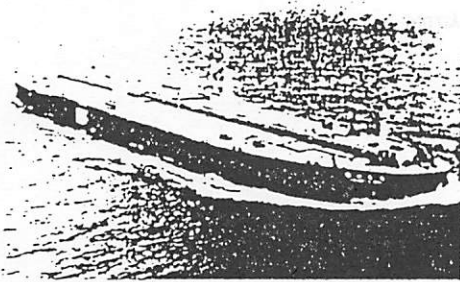


Data Flow



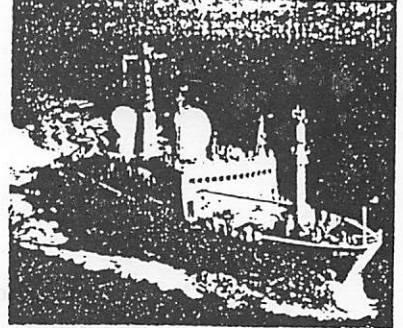


# Ship of Opportunity Programme (SOOP)

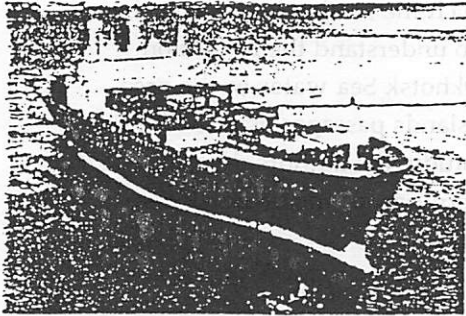
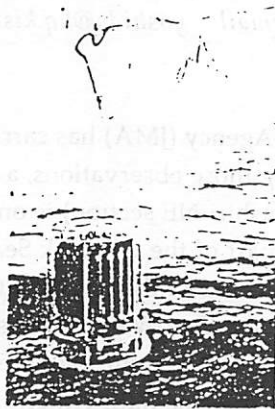


Kashimasan-maru

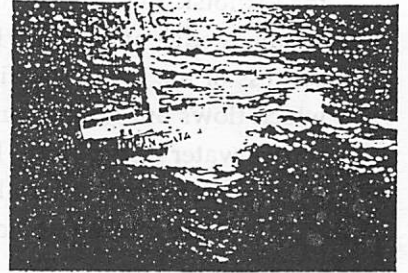
Keifu Maru



Ocean Data Buoy



Wellington-maru



## BATHY

CTD (Recorder Unknown) 01 August 1996 0111 UTC Latitude Longitude

JJYY 01086 0111/ 13815 14350

88888	83099	00255	13254	34190	73156	99901
00144	88106	99902	41091	71074	99903	21064
30067	46047	99904	45030	90034	99905	14038
57033	90040	99906	05051	99907	64047	99908
31035	99910	00033	66666	23313		

JDWX=

Surface, 25.5°C      13m 25.4°C

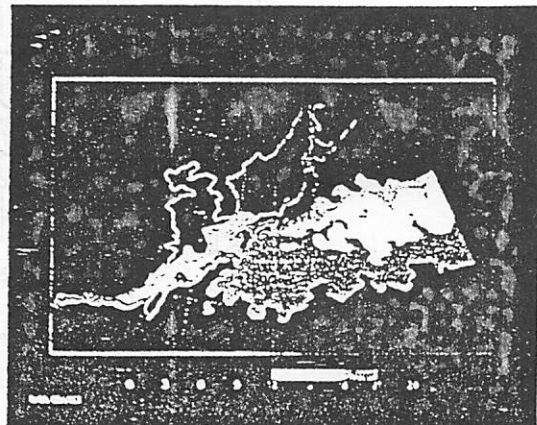
241m 9.1°C      Surface Current 330° 1.3knots

File Edit View Go Bookmarks Options Directory Window Help

Location: <http://goos.kishou.go.jp/cgi-bin/display1>

What's New | What's Cool | Handbook | Net Search | Net Directory | Software

## JMA SST Analysis on Mar10



## SHIP

1st Day of the Month, 06UTC Longitude Meteorological Observation

JJRQ 01064 99355 11458

41598	22008	10270	20248	40155	58008	70300
81232	22223	02272	20301	32113	40704	50603

30254=

SST (Bucket) = 27.2°C      Swells



## Some Oceanographic Features of the Okhotsk Sea Derived from Historical Hydrographic Observations

*Takashi Yoshida and Koichi Ishikawa*  
*Oceanographical Division*  
*Japan Meteorological Agency*  
*1-3-4, Otemachi, Chiyoda-ku*  
*100 Tokyo, Japan*  
*email: yoshida@hq.kishou.go.jp*

### Introduction

The Japan Meteorological Agency (JMA) has carried out hydrographic observations in the Okhotsk Sea since 1940's. Among those observations, a hydrographic section from off Abashiri to the station at 47.5N, 151E (Abashiri-NE section) is one of few repeat hydrographic sections in the Okhotsk Sea. The southern part of the Okhotsk Sea, in which the section lays along the southern edge of the Kuril Basin, is one of the important areas to understand the formation process of the North Pacific Intermediate Water because the Okhotsk Sea water in the area, which flows out to the North Pacific Ocean through the Kuril Islands passages, is one of the source water of the North Pacific Intermediate Water. In this study, the authors describe the average status and variability of water properties in the southern part of the Okhotsk Sea based on the hydrographic data along the Abashiri-NE section.

### Data

R/V Kofu Maru of the Hakodate Marine Observatory carried out hydrographic observations every one degree longitude along Abashiri-NE section (figure 1) in summer during thirteen years period from 1971 to 1983. Water sampling and temperature and depth measurement from surface to the depth of 1200 or 1500 meters were performed with Nansen bottles and reversing thermometers. Salinity, dissolved oxygen (O<sub>2</sub>), and inorganic phosphate (PO<sub>4</sub>) were determined for all the samples. The data have been distributed by the yearly publication entitled "The results of Marine Meteorological and Oceanographical Observations" and are available in WDCA archives.

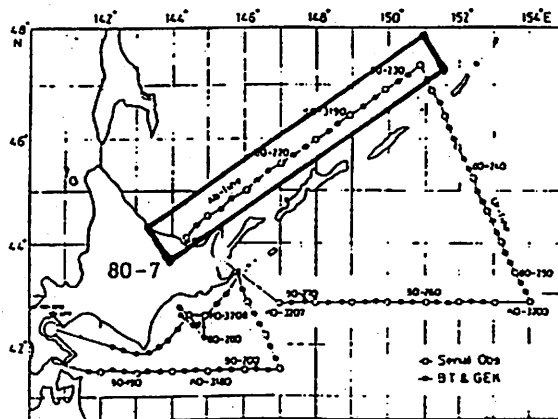


Figure 1. Station chart (after Oceanographic Observation report of the Hakodate Marine Observatory, vol 18, no. 3, 1980)

**Average status and variabilities**

In order to eliminate possible contamination of seasonal change, the authors used the data obtained only in June and July during the ten-year period from 1973 to 1982. Values of the four elements (T, S, O<sub>2</sub> and PO<sub>4</sub>) at the standard depths were calculated by interpolation first, and ten-year average and standard deviation for each standard depth and station was calculated from the interpolated values.

The average temperature field (figure 2) shows a warm summer surface layer over a sharp thermocline at 20 to 30 meters. Below the thermocline, there is a temperature minimum layer centered at 100 meters except for the station just off Hokkaido coast (144.5E), where warm Soya Current Water occupies. Water of the temperature minimum layer is the coldest at 145E and 148E, and the water of the temperature minimum layer between the two stations is relatively warm. The relatively warm water is accompanied with large temperature variability, and it means appearances of the Soya Current Water at 146E and 147E. Temperature variability is large in the warm summer surface layer and that of sea surface at 144.5E (3.2C) is comparable to those observed along 41.5N PH-line in the south of Hokkaido, where intrusions of Oyashio cold water and warm core rings make complicated temperature distribution. Temperature variability is relatively small at the other stations (2-3C), though it is larger than those observed in subtropical region (0.5-1C) and tropical region (less than 0.5C) along 137E.

The average salinity field (figure 3) shows saline Soya Current Water at 144.5E as seen in the temperature field. At all stations, surface water is less saline (less than 32.5). Salinity rapidly increase to 33 from surface to the depth of 50 meters and it gradually increase to 34.2 at the depth of 1000 meters. Salinity variability field shows similar pattern as in the temperature variability field.

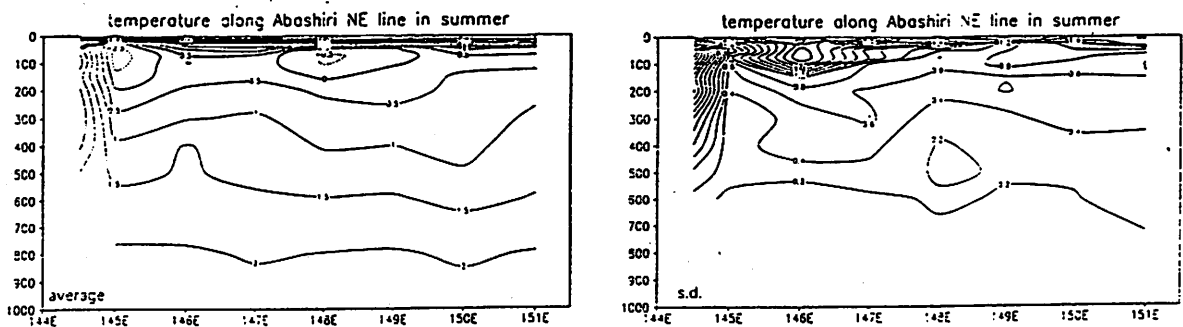


Figure 2. Ten-year average and standard deviation of temperature (degree C) along Abashiri-NE section

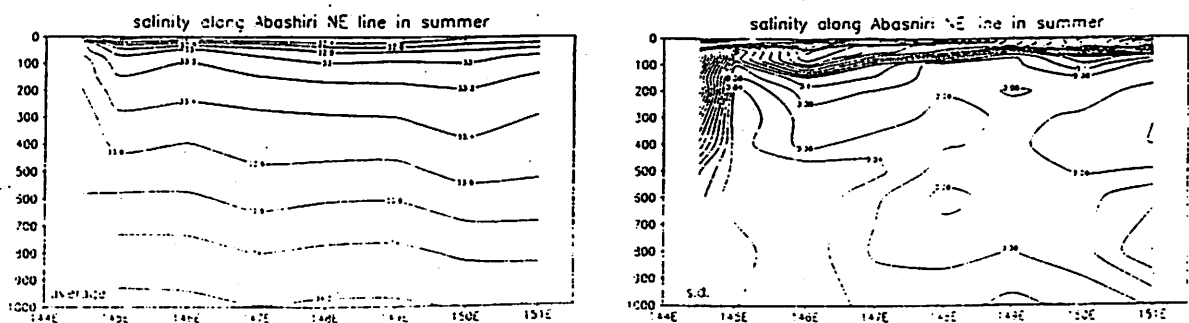


Figure 3. As with for figure 2 but for salinity (psu)

Apart from those features picked up from the distribution of temperature and salinity, an anomalous feature is found in the distributions of O<sub>2</sub> and PO<sub>4</sub> (figures 4 and 5). A large variability, which is accompanied with relatively rich O<sub>2</sub> and poor PO<sub>4</sub>, is found in both O<sub>2</sub> and PO<sub>4</sub> distributions in the layer of 200 to 600 meters at 146E and 147E. It means appearances of rich O<sub>2</sub> and poor PO<sub>4</sub> water in the layer and the appearances are clearly found in O<sub>2</sub> and PO<sub>4</sub> vertical profiles show in figure 6 and 7. Richness in O<sub>2</sub> and poorness in PO<sub>4</sub> in a water means that the water has been affected by surface convecting process. Therefore, the rich O<sub>2</sub> and poor PO<sub>4</sub> water must be transported from surface to the layer of 200 to 600m.

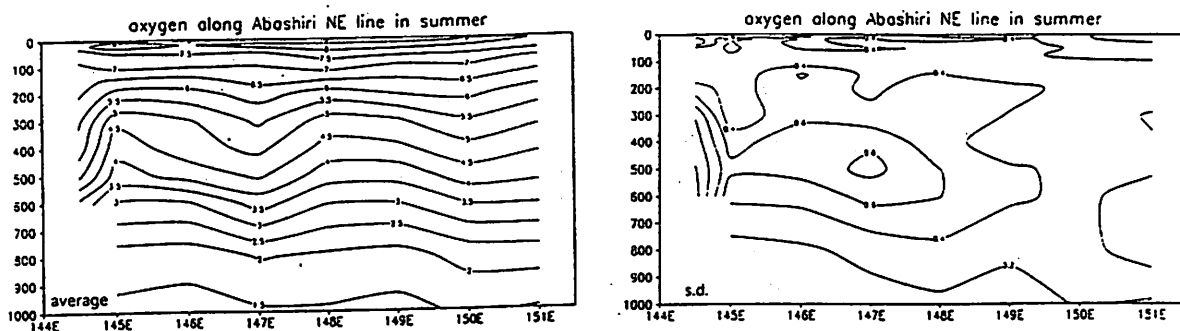


Figure 4. As with for figure 2 but for dissolved oxygen (ml/l)

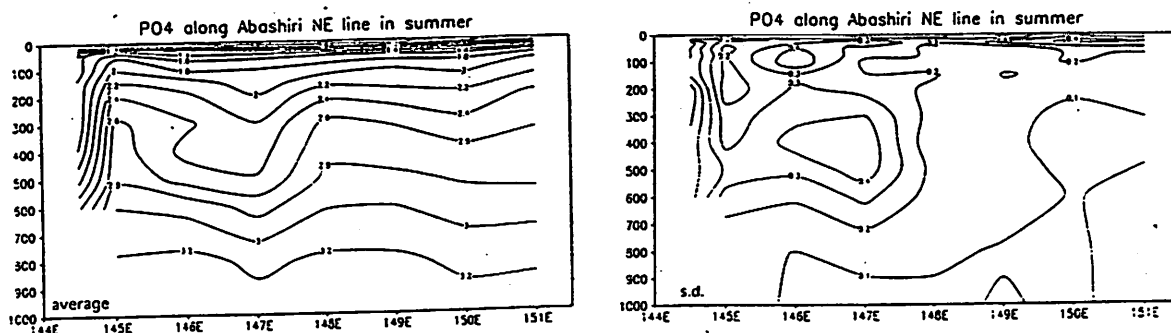


Figure 5. As with for figure 2 but for inorganic phosphate ( $\mu$ g-at/l)

#### Source of the rich O<sub>2</sub> and poor PO<sub>4</sub> water

The authors propose the Soya Current Water in spring, which Takizawa (1982) called the Forerunner of the Soya Warm Water, as a possible source of the rich O<sub>2</sub> and poor PO<sub>4</sub> water because of the similarity of water properties between the two waters. In O<sub>2</sub>-density and PO<sub>4</sub>-density profiles (figure 8 and 9), in which a profile observed by Seifu-Maru in the northern Japan Sea (42N, 139.7E) on March 2, 1967 is superimposed, the rich O<sub>2</sub> and poor PO<sub>4</sub> waters are plotted between the profiles of the Okhotsk Water and that of the Japan Sea Water in density around 26.8 sigma-t. The northern Japan Sea Water in density around 26.8 sigma-t is just correspond to the surface mixed layer water in cold season which can flow into the Okhotsk Sea over shallow Soya Straits. It means that the Japan Sea Water flowed into the Okhotsk Sea through the Soya Straits could be a source of the rich O<sub>2</sub> and poor PO<sub>4</sub> water found in the layer of 200 to 600 meters at 146E and 147E by assuming its movement along density 26.8 sigma-t surface.

Apart from those features picked up from the distribution of temperature and salinity, an anomalous feature is found in the distributions of O<sub>2</sub> and PO<sub>4</sub> (figures 4 and 5). A large variability, which is accompanied with relatively rich O<sub>2</sub> and poor PO<sub>4</sub>, is found in both O<sub>2</sub> and PO<sub>4</sub> distributions in the layer of 200 to 600 meters at 146E and 147E. It means appearances of rich O<sub>2</sub> and poor PO<sub>4</sub> water in the layer and the appearances are clearly found in O<sub>2</sub> and PO<sub>4</sub> vertical profiles show in figure 6 and 7. Richness in O<sub>2</sub> and poorness in PO<sub>4</sub> in a water means that the water has been affected by surface convecting process. Therefore, the rich O<sub>2</sub> and poor PO<sub>4</sub> water must be transported from surface to the layer of 200 to 600m.

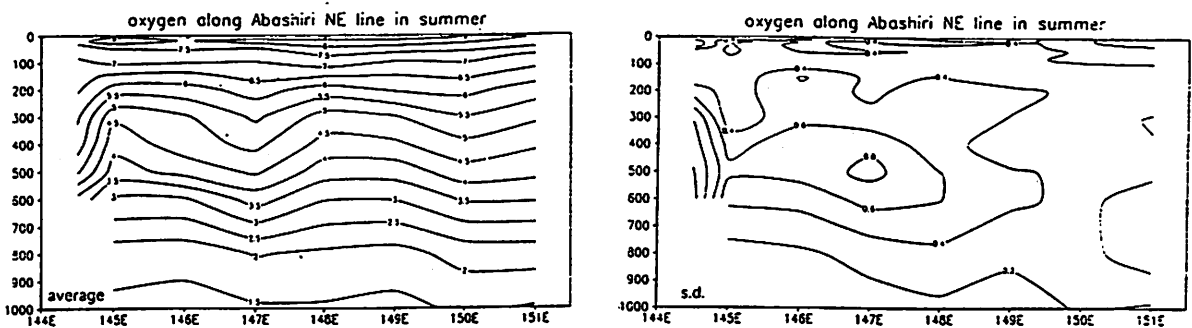


Figure 4. As with for figure 2 but for dissolved oxygen (ml/l)

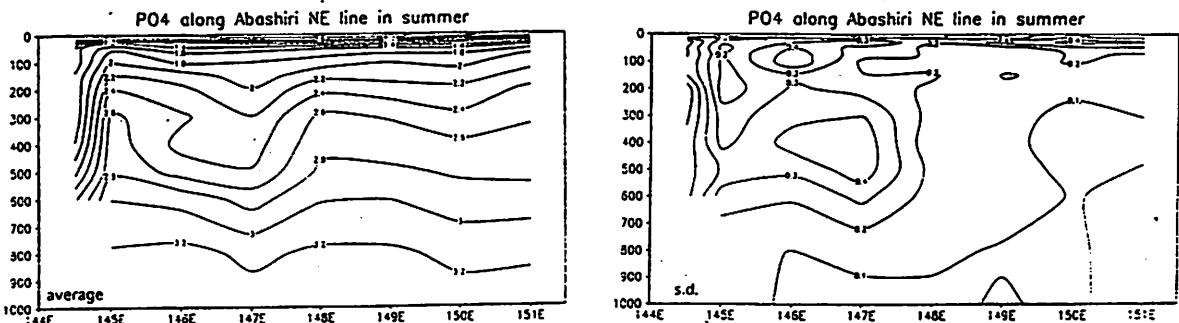


Figure 5. As with for figure 2 but for inorganic phosphate ( $\mu$ g-at/l)

#### Source of the rich O<sub>2</sub> and poor PO<sub>4</sub> water

The authors propose the Soya Current Water in spring, which Takizawa (1982) called the Forerunner of the Soya Warm Water, as a possible source of the rich O<sub>2</sub> and poor PO<sub>4</sub> water because of the similarity of water properties between the two waters. In O<sub>2</sub>-density and PO<sub>4</sub>-density profiles (figure 8 and 9), in which a profile observed by Seifu-Maru in the northern Japan Sea (42N, 139.7E) on March 2, 1967 is superimposed, the rich O<sub>2</sub> and poor PO<sub>4</sub> waters are plotted between the profiles of the Okhotsk Water and that of the Japan Sea Water in density around 26.8 sigma-t. The northern Japan Sea Water in density around 26.8 sigma-t is just correspond to the surface mixed layer water in cold season which can flow into the Okhotsk Sea over shallow Soya Straits. It means that the Japan Sea Water flowed into the Okhotsk Sea through the Soya Straits could be a source of the rich O<sub>2</sub> and poor PO<sub>4</sub> water found in the layer of 200 to 600 meters at 146E and 147E by assuming its movement along density 26.8 sigma-t surface.

# THERMAL STRUCTURE OF THE NORTH-WESTERN JAPAN SEA UPPER LAYER: CLIMATE AND VARIABILITY

Yury I. ZUENKO, Yury V. NOVIKOV

Pacific Fisheries Research Centre (TINRO), Vladivostok, Russia

The north-western part of the Japan Sea (Russian and N.Korean EEZ between 39-45 N) is situated at the boundary between two planetar climatic zones: subtropic and subarctic. That's why its water regime is very complex, especially in summer. Northern part of the aquatory is influenced by subarctic processes as winter convection, autumn storm mixing, freezing, dense water formation on the shelf, etc. Its southern part is influenced by subtropic waters intrusions with branches and meanders of warm currents. Different mechanisms produce a set of water masses. Naturally, all processes in different water masses have a certain peculiarities, and when one tries to study any process in the Sea (a biological process for example), the nature of water mass where the process occurs should be taken into consideration.

To understand the water structure of upper 200 m layer we used the temperature and salinity data obtained by Russian and Japanese research vessels in the last decade (1985-1996). The majority of data had been collected in April-October, so this period was investigated. The data were averaged in squairs approximately 20x20 n.miles (20x30 minutes) for 10-days periods. Water masses were determined as quasi-homogeneous zones divided by thermal fronts. Surface fronts position was defined on satellite infra-red images had been obtained in AVHR regime from NOAA satellites. Fronts at other horizons were determined as the zones of hightened horizontal gradients of temperature on the charts of temperature distribution. Horizons between 20-40 m wasn't analysed because temperature distribuion on them was distorted by thermocline topography.

Three kinds of fronts were identificated: Primorje Current Front and two frontal divisions of Polar front - northern (NPF) and southern (SPF) ones. Several quasi-homogeneous zones (corresponding to surface water masses) were distinguished between fronts in surface laver. They were identificated as: Coastal, Shelf (or Primorje Current, the coldest), Subarctic,

Subtropic transformed, and Subtropic (the warmest). The similar nomenclature of water masses and fronts was suggested for subsurface layer below the thermocline, but Subarctic Subsurface water mass was absent there and substituted by the Japan Sea Proper Water (Fig.1,2).

2-layers vertical water structure was usual round the year with the exclusion of limited convective area in winter. Combined vertically, the surface and subsurface water masses form several types of vertical water structure. Typical temperature profiles, values of upper quasi-homogeneous layer thickness and thermocline mean gradient were determined for 6 types of vertical structure which were the most usual for the investigated part of the Sea. Example of these profiles is presented at Fig.3 and in Tab.1.

Table 1

Climatic characteristics of main types of vertical water structure for late August

type	water masses S / SS	temperature at horizons								thermocline	
		0	20	30	50	75	100	150	200	depth	grad.
Subtropic	ST/ST	21.6	20.4	15.8	11.9	7.6	6.5	2.9	2.1	31	0.4
Subtr.trans.	ST/STT	22.1	12.5	7.9	4.3	2.5	2.1	1.3	1.2	23	0.5
Interfrontal	STT/STT	20.6	14.4	8.2	5.0	3.6	2.6	1.5	0.8	22	0.6
Interfr.tr.	STT/JSP	21.0	11.0	5.9	2.5	1.4	1.1	0.7	0.7	23	0.7
Subarctic	SA/JSP	19.5	9.4	5.7	2.8	1.6	1.4	0.9	0.8	20	0.6
Shelf	PC/JSP	15.7	7.4	4.7	3.0	2.1	1.9	1.6	1.5	15	0.5

Note: water masses: ST - Subtropic;  
 STT - Subtropic transformed;  
 SA - Subarctic;  
 PC - Primorye Current;  
 JSP - Japan Sea Proper Water;  
 S - surface;  
 SS - subsurface.

The profiles were determined for each 10-days period from early April to late October. Considerable seasonal variation was observed in all structural zones. Sea surface temperature was the warmest in August-September, subsurface temperature - in early

October (Fig.4). The thickness of upper quasi-homogeneous layer was minimal in the middle of summer and rose in autumn. Thermocline gradient was the sharpest in late summer and weakened in autumn (Tab.2).

Table 2

Terms of extremal climate values of temperature and thermocline parameters during April-October for different types of structure

type of structure	highest temperature		UQL minimal	max.thermocline	
	SST	50-100 m	100-200 m thickness	depth	gradient
Subtropic	mid.Sep.	ear.Oct.	ear.Oct.	ear.June	lat.Oct. ear.Sep.
Subtr.trans.	mid.Aug.	ear.Oct.	ear.Oct.	mid.Aug.	lat.Oct. ear.Aug.
Interfrontal	lat.Aug.	ear.Oct.	ear.Oct.	mid.Aug.	lat.Oct. mid.Aug.
Interfr.tr.	lat.Aug.	ear.Oct.	ear.Oct.	ear.Aug.	lat.Oct. mid.Aug.
Subarctic	lat.Aug.	ear.Oct.	ear.Oct.	mid.Aug.	lat.Oct. mid.Sep.
Shelf	ear.Sep.	lat.Sep.	ear.Oct.	lat.Aug.	lat.Oct. lat.July

Temperature anomalies of different water masses didn't change coherent, although periods were marked when negative (1986-1987) or positive (1988-1990; 1993-1995) anomalies had dominated at sea surface.

Arrangement of the zones of certain types of vertical structure changes seasonally as well - the main reason was the variability of Polar front position. Three sectors were determined with coherent fluctuations of fronts: westward from 132-133 E, eastward from 135-137 E and central one. These sectors are supposed to correspond to warm currents' branches. Real-time images show that in many cases these branches, especially western and central ones, were formed by meso-scale anticyclonic eddies with diameter 50-150 km (Fig.5). So, the fluctuations could be related with these eddies movement.

Mean positions of NPF and SPF were determined for each 10-days period. Seasonal and year-to-year variability of frontal lines position and shape was investigated for surface fronts. Because of warm currents' advection strengthening both SPF and NPF shifted northward during spring-summer and returned southward in autumn (Fig.6). The northeast position of both fronts observed

usually in late August for western and central branches and in middle August for their eastern branch. Real position of fronts in every sector relative to the climatic position was classified as "abnormally northern", "normal", and "abnormally southern" in order to have approximately 1/3 of "normal" situations. According to certain warm currents' branches activity, 6 types of frontal lines at sea surface were observed (Tab.3), Fig.7).

Table 3

Types of NPF line

type & characteristic	position in sectors			periods of observation	NN obs.
	west	central	east		
S (weak advection)	as(n)	as(n)	as	05-07.86;07.88;09.95;10.93	10
M (normal advection)	n	n	n	04.87; 06.87; 07.88; 05.91	5
E (east stress)	n	n	an	09.88; 04.90	4
C (central stress)	n	an	n(as)	10.87; 08.90; 09.96	4
W (west stress)	an	n(an)	n	08-09.86;05.87;05.88;10.95	10
WE (east & west strengthening)	an	n(as)	an	08.88;05.89;10.91;07.94, 06.96	6
N (strong advection)	an	an	an	06.88; 04-07.90; 07.92	5

Notes: 1. an - abnormally northern position; n - normal position; as - abnormally southern position.

2. Types of SPF line are similar to presented NPF' types but the data for SPF line are less numerous because of its position at periphery of investigated area.

Thus, the variability of thermal structure in the north-western part of the Japan Sea isn't coherent. Although seasonal variation of temperature is similar in all structural zones, the parameters of temperature profiles change differently because of different mechanism of formation. Year-to-year variations of temperature aren't coherent for different water masses. Shifts of Polar front divisions' lines are similar in seasonal cycle, but three sectors of these lines have a peculiar year-to-year variability that leads to changes of Polar front shape. It means that large-scale estimations of water condition cannot be used for meso-scale studies, and a researcher should examine the state of certain water mass, certain fragment of front.



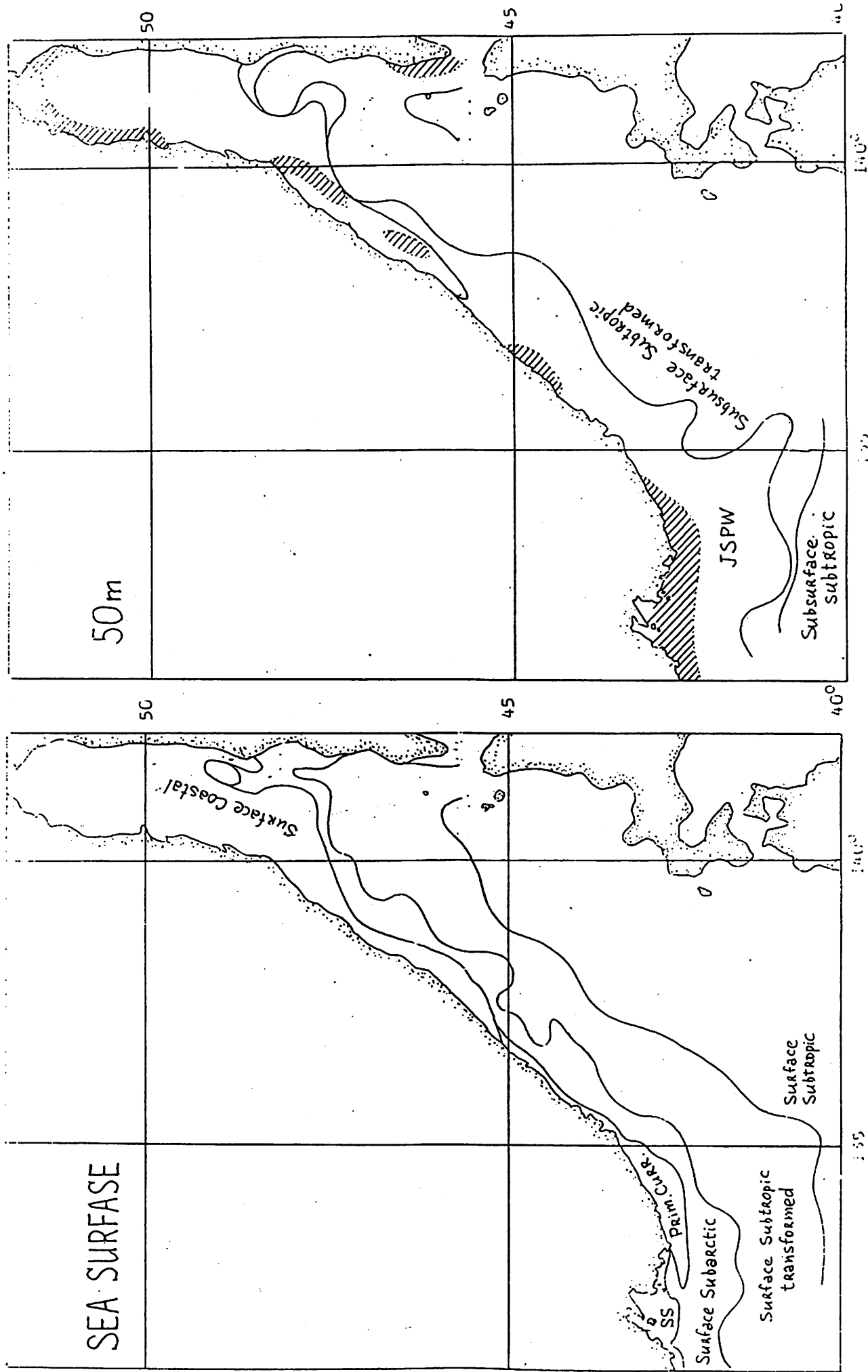


Fig.1. An example of surface (left) and subsurface (right) water masses arrangement in August, 1990 (r/v "Prof.Kizevetter")  
 Subsurface shelf water mass area is shaded.

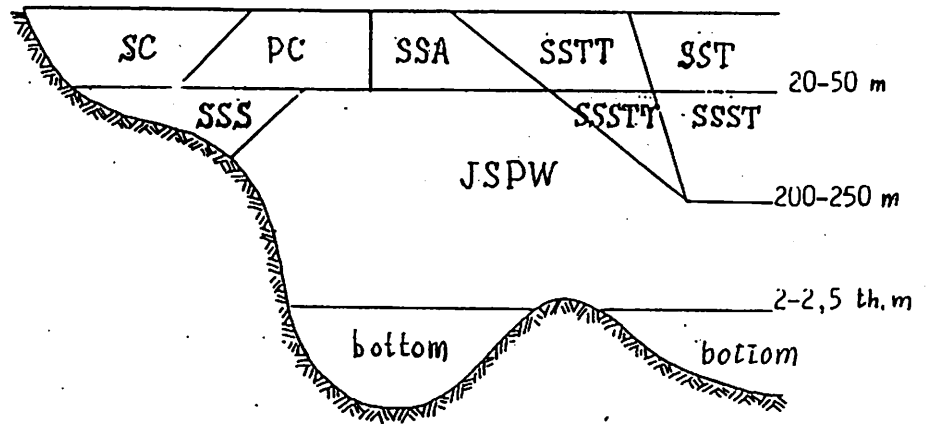


Fig.2. Sceme of water masses arrangement on a section across the shelf of Primorye

Water masses: SC - Surface Coastal; PC - Primorye Current;  
 SSA - Surface Subarctic; SST - Surface Subtropic;  
 SSTT - Surface Subtropic transformed;  
 SSS - Subsurface Shelf; SSST - Subsurface Subtropic;  
 SSSTT - Subsurface Subtropic transformed;  
 JSPW - Japan Sea Proper Water

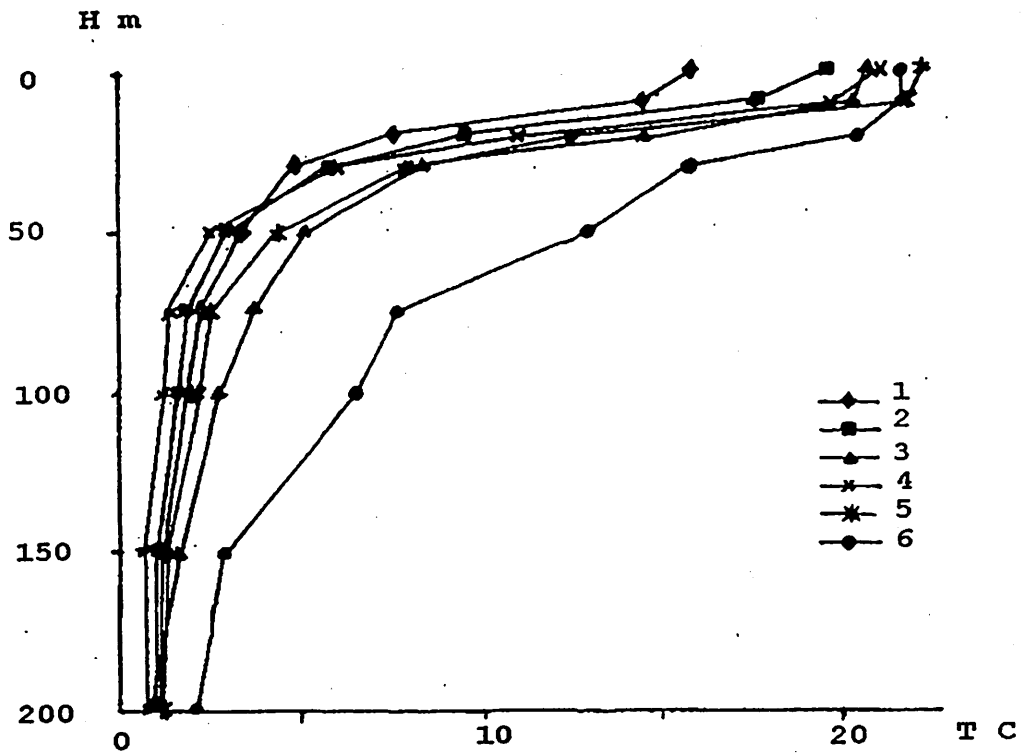


Fig.3 Climatic profiles of temperature for types of vertical water structure in August

- 1 - Primorye Current
- 2 - Subarctic
- 3 - Interfrontal
- 4 - Interfrontal transformed
- 5 - Subtropic transformed
- 6 - Subtropic

## 4. BIO & FIS Topic (생물해양분과 및 수산과학분과)

Importance of micronektonic fishes as revealed from the stomach analysis of neon flying squid, <i>Ommastrephes bartrami</i> in the northwestern North Pacific(북태평양의 북서부에 서식하는 빨강오징어( <i>Ommastrephes bartrami</i> )의 위내용물 분석으로 나타난 미세유영생물의 중요성) .....	133
Daily and seasonal feeding dynamics of the two myctophid species, <i>Stenobrachius leucopsarus</i> and <i>S. nannochir</i> in the mesopelagic zone of Bering Sea.(베링해 중층에서 서식하는 2종의 샛비늘치류( <i>Stenobrachius leucopsarus</i> 와 <i>S. nannochir</i> )의 일별·계절별 섭식 연구) .....	143
Stable carbon and nitrogen isotope ratios of mesopelagic micronekton and their prey(중층 서식 미세유영생물과 그들의 먹이에서 측정된 안정 동위원소 탄소와 질소의 비율) .....	157
Feeding habits and diel vertical migration patterns of the three dominant myctophid fishes in the western subarctic and transitional Pacific(서부 아북극 태평양과 경계지역에 서식하는 샛비늘치류(myctophid fish) 3종의 섭식 특징과 일별 수직 회유경로) .....	169
Stomach contents of Dall's poropises in the north Pacific ocean(북태평양에 서식하는 돌고래 Dall's poropises의 위 내용물 분석) .....	173.
Distribution and stomach contents of <i>Maurolicus muelleri</i> in the Japan Sea(East Sea)(동해(일본해)에 서식하는 엘통이( <i>Maurolicus muelleri</i> )의 분포와 위 내용물 분석) .....	182
Distribution and relative abundance of some micronektonic fishes in the Aleutian Basin(알류산 해분에 서식하는 몇몇 미세 유영생물 어류의 분포와 상대 풍도 조사) .....	188
Community ecology of juvenile pollock( <i>Theragra chalcogramma</i> ) and other midwater taxa in the eastern Bering Sea during August-October 1987(1987년 8~10월에 동부 베링해에 서식하는 명태( <i>Theragra chalcogramma</i> ) 미성어와 다른 중층 서식 종의 군집생태 연구) .....	201
Predation on micronekton by demersal fishes(저어류에 의한 미세 유영생물의 포식 조사) .....	214

# Importance of micronektonic fishes as revealed from the stomach analysis of neon flying squid, *Ommastrephes bartrami* in the northwestern North Pacific

Yasushi Arimoto and Akito Kawamura  
(Faculty of Bioresources, Mie University)

## Introduction

Cephalopods are voracious predators that feed on a wide variety of live prey (Rodhouse and Nigmatullin, 1996). Further, pelagic cephalopods are important both to commercial fisheries and as a prey of marine mammals, sea birds and large oceanic fishes (Seki, 1993b). Therefore, pelagic cephalopods play important role in the trophic relations within the oceanic ecosystems (Rodhouse and Nigmatullin, 1996). In this context, the determination of their food spectrum is a prerequisite knowledge in understanding the structure of pelagic food webs.

Neon flying squid, *Ommastrephes bartrami*, is one of the dominant species in the epipelagic waters of the subtropical and subpolar seas (Yatsu and Watanabe, 1996). In the North Pacific, *O. bartrami* undertakes extensive seasonal north-south migrations. Juveniles of this species, are considered to be recruited between winter and spring in subtropical regions, and migrate to feeding grounds near the Subarctic Boundary regions from May to August as they grow (Murata, 1990).

In warmer waters over the transitional zone and subtropics, younger individuals are preyed upon by the animals such as swordfishes, blue sharks, sperm whales, and northern elephant seals (Seki, 1993b). Ironically, neither the knowledge on the prey items of *O. bartrami* nor its role in oceanic ecosystems are still poorly documented. Since stomach contents of cephalopods are normally minced into small fragments and are often well digested, most of the prey can be classified only into broad taxonomical categories. *O. bartrami* feeds on the small fish such as myctophids, stomiiformes, saury, sardines as well as squid species such as *Watasenia scintillans*, *Onychoteuthis* spp., *O. bartrami* and planktonic crustaceans such as euphausiids, and amphipods (Naito et al., 1977; Seki, 1993a, 1993b; Shevtsov, 1972).

The present study aims to elucidate the predator-prey relationships between *O. bartrami* and micronektonic fishes in the subtropical and

transitional regions of the northwestern North Pacific.

## Materials and methods

A total of 701 neon flying squid were sampled at 21 stations between June and July of 1994 aboard the research vessel *Kaiun maru* in the northwestern North Pacific (Fig. 1). The locations of stations were determined by mapping the T-S fields down to 400m which were obtained simultaneously by the other four research vessels. CTD casts were made at each one-degree of latitude and longitude in the area, 38°-42°N and 170°E-166°W. The exploratory fishing (= sampling) stations were occupied in the area of tongue-like northward intrusions of warm water found by the grid observations. These intrusions of warm water were indicated by the meandering of 9-10°C isotherms at 200m. CTD cast down to 400m was conducted again at each worked station.

Squids were collected at night using automatic squid jigging machine. The attacked depth by the squids was less than 200m. Up to 40 individuals were selected randomly from the over night catches, and their stomachs were collected. Dorsal mantle length (DML) was measured to the nearest millimeters and total weight was to the nearest grams. Sex and sexual maturity, immature or mature, were recorded according to the maturation level proposed by Murakami *et al.* (1981). The stomach samples were frozen at -60°C.

In the laboratory, whole stomachs were fixed in a 10% phosphate-buffered formalin solution and then transferred within 24 h to 80% ethyl alcohol for preservation and storage. Whole stomach contents were extracted and weighed to the nearest 0.1 grams, and sorted into identifiable groups (fish, squid, crustaceans, pteropods, and unidentified items). Fish otoliths were used for identifying the species.

## Results

### 1. Oceanographic condition

Figure 1 shows sampling locations together with the temperature (°C) field at 200m depth during the sampling period. The tongue-like intrusions of warm water indicated by the northward meandering of 9-10°C isotherms were observed in 172°-174°E, 176°-178°E, 178°W- 180°, between 175°-177°

W, and around 172°W. For the convenience, the station groups, Stn. 1-2, 3-6, 7 & 10-11, 8-9, 12-14, 15 -19, 20-21 are called fishing ground A, B, C, D, E, F, and G, respectively.

Figure 2 shows vertical sections of salinity (PSU) along, (a) 172°W, (b) 176°W, (c) 179°W, (d) 176°30'E, and (e) 172°E. The surface, and particularly the subsurface distribution of the 34.0 isohalines provide Subarctic Boundary (Favorite *et al.*, 1976). The 34.0 isohalines were observed in the north of 40°N at (a)~(e) lines. Being based on the definition of oceanic boundaries in the North Pacific, all sampling stations were located in the subtropical domain, although fishing grounds B, D, F, and G were located close to the Subarctic Boundary.

## 2. Biological characteristic

Figure 3 shows the percentage frequencies of the dorsal mantle length (DML) for males and females of 701 neon flying squids from which the stomachs were collected. The DML ranged from 206 to 500 mm (Ave.=396mm, SD=45.5). Squids smaller than 300 mm in DML occurred at the fishing grounds A and E. Most of samples were female, and the number of males was only 11 individuals (1.6%). All these squids were at the stage of reproductively immature. The division of *O. bartrami* population into four sub-groups with different body types is based on mantle length composition. The groups have been designated extra large (LL), large (L), small (S), and extra small (SS), and the larger sized groups lead both the northward and southward migrations (Murata, 1990). The LL group are all comprised of only by female individuals (Murakami *et al.*, 1981). These catch composition suggested to be comprised of by the LL and L groups migrating northward.

## 3. Composition of stomach contents

Fish and cephalopods were the major food categories and comprised 92.3% and 73.2% of the stomachs containing food, respectively (Table 1). A small number of crustaceans belonging to phronimidae amphipods, pteropods belonging to cavolinidae, and unidentifiable remains were also recorded.

The food fish species were identified being based on otoliths remained in the stomachs. The species were mainly composed of myctophids and Pacific saury, and so on. The food cephalopods species was identified as *O. bartrami* from the characteristics of arms and tentacles in fresh condition. The

cannibalized *O. bartrami* found in 47 stomachs. The reason for this cannibalism is possibly due to feeding on the arms and tentacles of other individuals which were torn off during jigging. Other cephalopods were usually well digested but remained several varieties of small beaks and tentacular hooks. These remains were probably from micronektonic or young squids belonging to Gonatidae, Onychoteuthidae, and Enopteuthidae. The results strongly suggested that the micronektons, especially micronektonic fishes, were the most important prey item among all for *O. bartrami* in their feeding grounds.

#### 4. Preyed fish species

Table 2 shows the frequency and minimum estimated number of the prey fish species occurred in 623 stomachs. Fish otoliths remained in the stomachs were composed of at least 18 fish species belonging to four families. In myctophidae, the subtropical species and the subarctic-transitional species were five and 10 species, respectively. Of these, 11 were the species perform nocturnal vertical migration. The dominant species over the whole fishing grounds in terms of both frequency and quantity were *Diaphus theta*, followed by *Ceratoscopelus warmingi*, *Electrona rissoi*, *Bathylagus ochotensis*, and *Cololabis saira*. Therefore, these five species were considered to be the main diet for *O. bartrami* during the summer.

Figure 4 shows the composition of the prey fish species by fishing grounds. Six species, *D. theta*, *E. rissoi*, *C. warmingi*, *Protomyctophum crockeri*, *B. ochotensis*, and *C. saira* were the major fish preys and comprise more than 10% in terms of both the relative percentage of frequency and percentage of the estimated number. *E. rissoi* was common in the fishing grounds(A, B, C) located in the area of west longitudes, while *C. warmingi* was in the fishing grounds C and in the E, F in the area of east longitudes. But, *D. theta* was dominant species only in the fishing grounds located close to the Subarctic Boundary. Therefore, *D. theta* was considered to be the most important prey fish for *O. bartrami* stay close to the Subarctic Boundary.

#### 5. Quantity of the fish prey

Table 3 shows the average of stomach fullness in *O. bartrami*. The stomach fullness was expressed by the percentage of the weight of the stomach contents to the body weight. The average of stomach fullness was 0.87%, but



this figure includes contamination caused by cannibalism. Therefore, when the stomachs containing cannibalized squids were excluded, the average of stomach fullness becomes 0.69%.

Table 4 shows an estimation of micronektonic fish biomass preyed upon by *O. bartrami*. The estimations were based on the weight of prey fish and the stock size of *O. bartrami* in the North Pacific. Using the catch and effort data for Korean drift gillnet fishery in the North Pacific west of 161°W, Gong *et al.* (1985) estimated the stock size of *O. bartrami* to be  $322 \times 10^6$  to  $469 \times 10^6$  individuals. The monthly average body weight of *O. bartrami* was approximately 1 kg (1.3-0.9 kg) (Gong *et al.*, 1985), the weight based stock size may be converted  $322 \times 10^3$  to  $469 \times 10^3$  metric tons. Based on the average of stomach fullness, 0.69%, the weight of stomach contents for the whole stock is estimated as 2222 to 3236 metric tons.

Seki (1993b) analyzed the stomach composition of 37 *O. bartrami* captured in gillnets near the North Pacific Subarctic Boundary, and found that the proportion by weight of the fish prey in the stomach contents was to be 68%. Usually, ommastrephid squids have been estimated to feed twice a day (Kubodera, 1991). Then, the amount of fish preyed upon by the *O. bartrami* are estimated to be 3039 to 4426 metric tons per day.

When the limited ability of the gillnet which could not cover the deeper layer habitats of *O. bartrami* is taken into consideration, the actual stock size in the North Pacific would be more larger than estimated stock size (Gong *et al.* 1985). Therefore, it might be reasonable to suppose that the quantity of fish preyed upon *O. bartrami* would become more larger than our estimates.

The mesopelagic fish stocks have been estimated to be  $50 \times 10^6$  metric tons over the Kuroshio system and transitional area of the North Pacific (Gjøsaeter and Kawaguchi, 1980). The above mentioned the quantity of fish preyed upon by *O. bartrami* per day suggests to be 0.006-0.009% consumption of the micronektonic mesopelagic fish stock per day. Considering that the main habitats of *O. bartrami* during migrating and feeding period from May to February extend over the transitional area, the quantity of micronektonic fish preyed upon by *O. bartrami* during 10 months would be equivalent to 1.8-2.7% of the total stocks of mesopelagic fishes.

## References

- Favorite, F., A. J. Dodimead and K. Nasu., 1976. Oceanography of the subarctic Pacific region, 1960-1971. Bull. Int. North Pacific Fish. Comm., 33, 1-187.
- Gjøsaeter, J. and K. Kawaguchi., 1980. A review of the world resources of mesopelagic fish. FAO Fish. Tech. Pap., 193: 151pp.
- Gong, Y. and J. Y. Lim and Y. H. Hur., 1985. Study on the abundance of flying squid, *Ommastrephes bartrami* (LeSueur) in the North Pacific. Bull. Fish. Res. Dev. Agency, 34, 127-132.
- Kubodera, T., 1991. Physiology and ecology of squid. in K. Nasu, T. Okutani and M. Ogura eds., The squid. Seizando, Tokyo, pp. 33-67.
- Murakami, K., Y. Watanabe and J. Nakata., 1981. Growth, distribution and migration of flying squid (*Ommastrephes bartrami*) in the North Pacific. Res. Inst. N. Pac. Fish. Hokkaido Univ., Spe. Vol., 161-179.
- Murata, M., 1990. Oceanic resources of squids. Mar. Behav. Physiol., 18, 19-71.
- Naito, M., K. Murakami and T. Kobayashi., 1977. Growth and food habit of oceanic ssquid (*Ommastrephes bartrami*, *Onychoteuthis borealijaponicus*, *Beryteuthis magister* and *Gonatopsis borealis*) in the western subarctic Pacific region. Res. Inst. N. Pac. Fish. Hokkaido Univ., Spe. Vol., 339-351.
- Osako, M. and M. Murata., 1983. Stock assessment of cephalopod resources in the northwestern Pacific. FAO Fish. Tech. Paper, 231, 55-144.
- Rodhouse, P. G. and Ch. M. Nigmatullin., 1996. Role as consumers. Phil. Trans. R. Soc. Lond. B., 351, 1003-1022.
- Seki, M. P., 1993a. Trophic relationships of *Ommastrephes bartramii* during winter migrations to subtropical waters north of the Hawaiian Islands. in T. Okutani, R. K. O'Dor and T. Kubodera eds., Recent advances in cephalopod fisheries biology, Tokai Univ. Press, Tokyo, pp. 523-529.
- Seki, M. P., 1993b. The role of the neon flying squid, *Ommastrephes bartrami*, in the North Pacific pelagic food web. INPFC Bull., 53, 207-215.
- Shevtsov, G. A., 1972. Feeding habits of the squid *Ommastrephes bartrami* Leseur in the Kurile-Hokkaido region. Hydrobiol. Jor., 8(3), 77-80.
- Yatsu, A. and T. Watanabe., 1996. Interannual variability in neon flying squid abundance and oceanographic conditions in the Central North Pacific, 1982-1992. Bull. Nat. Res. Inst. Far Seas Fish., 33, 123-138.

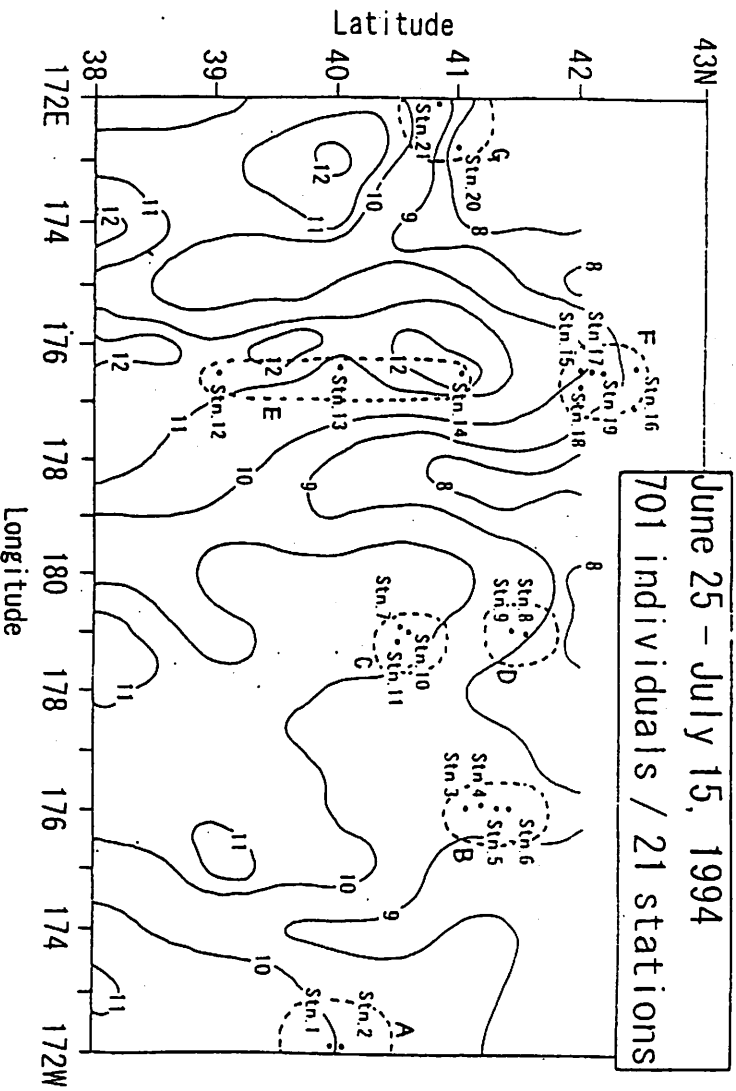



Fig. 1. Sampling locations with the temperature (°C) at 200m depth during June-July of 1994 in the northwest North Pacific.  Fishing ground; A(Stn.1-2), B(Stn.3-6), C(Stn.7 & Stn.10-11), D(Stn.8-9), E(Stn.15-19), F(Stn.20-21).

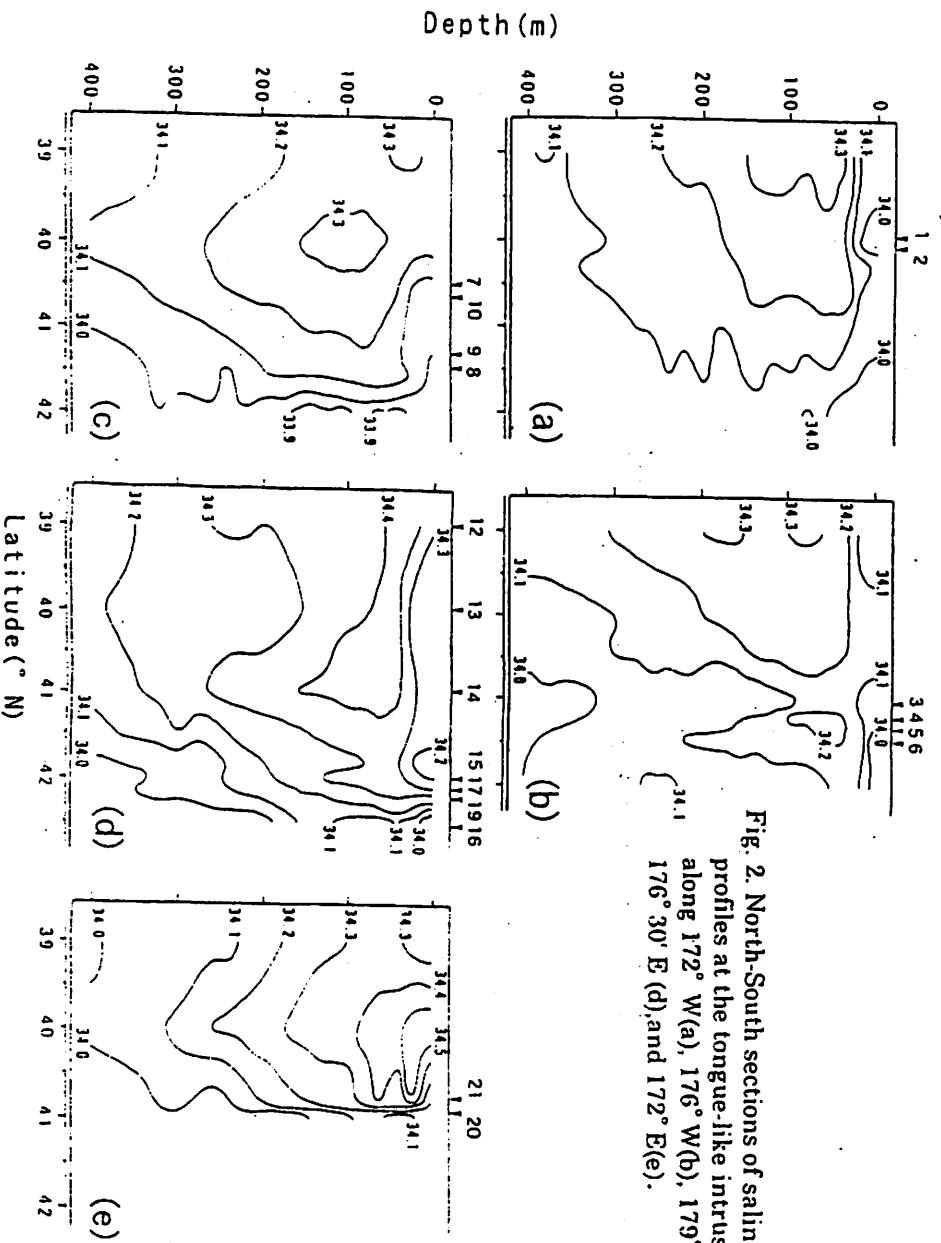


Fig. 2. North-South sections of salinity profiles at the tongue-like intrusions along 172° W(a), 176° W(b), 179° W(c), 176° 30' E (d), and 172° E(e).

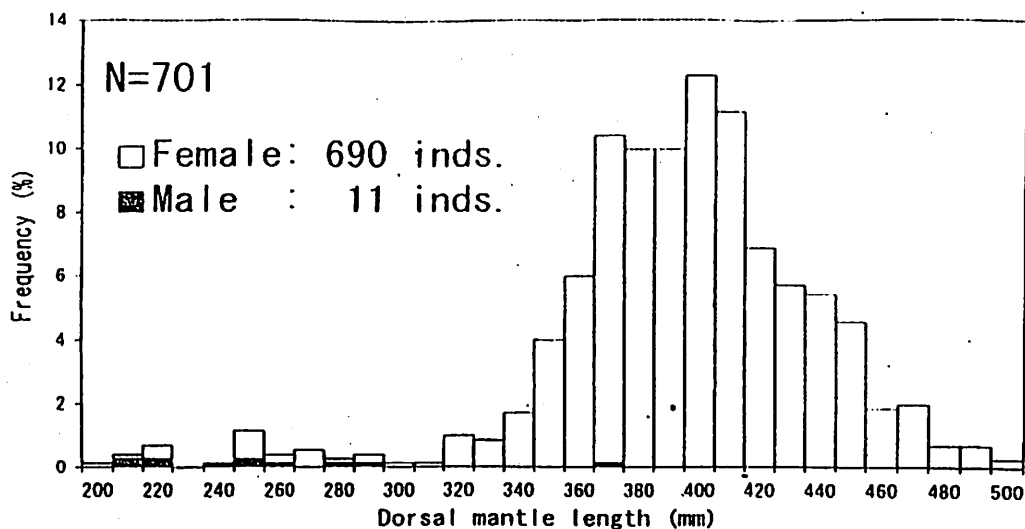


Fig. 3. Percentage frequency distributions of dorsal mantle length of *Ommastrephes bartrami*.

Table 1. Food categories in *Ommastrephes bartrami*

Food category	Frequency	Percentage frequency*
Pisces	623	92.3
Cephalopods	494	73.2
Crustaceans	70	10.4
Pteropods	20	3.0
Unidentified	4	0.6
<b>Stomach containing food</b>	<b>675</b>	<b>100.0</b>
Empty stomach	26	
Examined stomach	701	

\* Percentage of each food category to the total number of food - containing - stomachs.

Table 2. Composition of the prey fish species

Prey item	Vertical migration pattern	Frequency	Percentage frequency	Estimated No. of prey fish*	% of estimated No. of prey fish
<b>Family Myctophidae</b>					
<b>Subtropical species</b>					
<i>Ceratoscopelus warmingi</i>	N	201	32.3	387	16.3
<i>Diaphus gigas</i>	N	4	0.6	4	0.2
<i>Diaphus kuroshio</i>	N	32	5.1	33	1.4
<i>Electrona rissoi</i>	N	143	23.0	257	10.8
<i>Notoscopelus resplendens</i>	N	1	0.2	9	0.1 >
<b>Subarctic and transitional species</b>					
<i>Diaphus theta</i>	N	205	32.9	574	24.2
<i>Lampanyctus regalis</i>	NM	37	5.9	36	1.5
<i>Lampanyctus simulator</i>	?	37	5.9	41	1.7
<i>Notoscopelus japonicus</i>	N	7	1.1	1	0.4
<i>Protomyctophum crockeri</i>	N	52	8.3	90	3.8
<i>Protomyctophum thompsoni</i>	NM	6	1.0	4	0.2
<i>Stenobrachius leucopsarus</i>	N, NM	31	5.0	33	1.4
<i>Stenobrachius nannochir</i>	NM	17	2.7	15	0.6
<i>Symphotophorus californiensis</i>	SM	60	9.5	71	3.0
<i>Tarletonbeania taylora</i>	SM	43	6.9	79	3.3
<b>Family Bathylagidae</b>					
<i>Bathylagus ochotensis</i>	? (80-300m)	167	26.8	209	8.8
<b>Family Phosichthyidae</b>					
<i>Ichthyorhynchus elongatus</i>	?	55	8.8	58	2.4
<b>Family Scomberesocidae</b>					
<i>Colubus sairu</i>	? (0-80m)	105	16.9	184	7.6
Unidentified fish		270	43.3	284	12.0
<b>No. of stomachs containing fish</b>		<b>623</b>	<b>100.0</b>		
<b>Estimated total No. of fish</b>				<b>2369</b>	<b>100.0</b>

\* The half of the total number of otoliths.

M: Migratory species. NM: Non migratory species. SM: Surface migratory species.

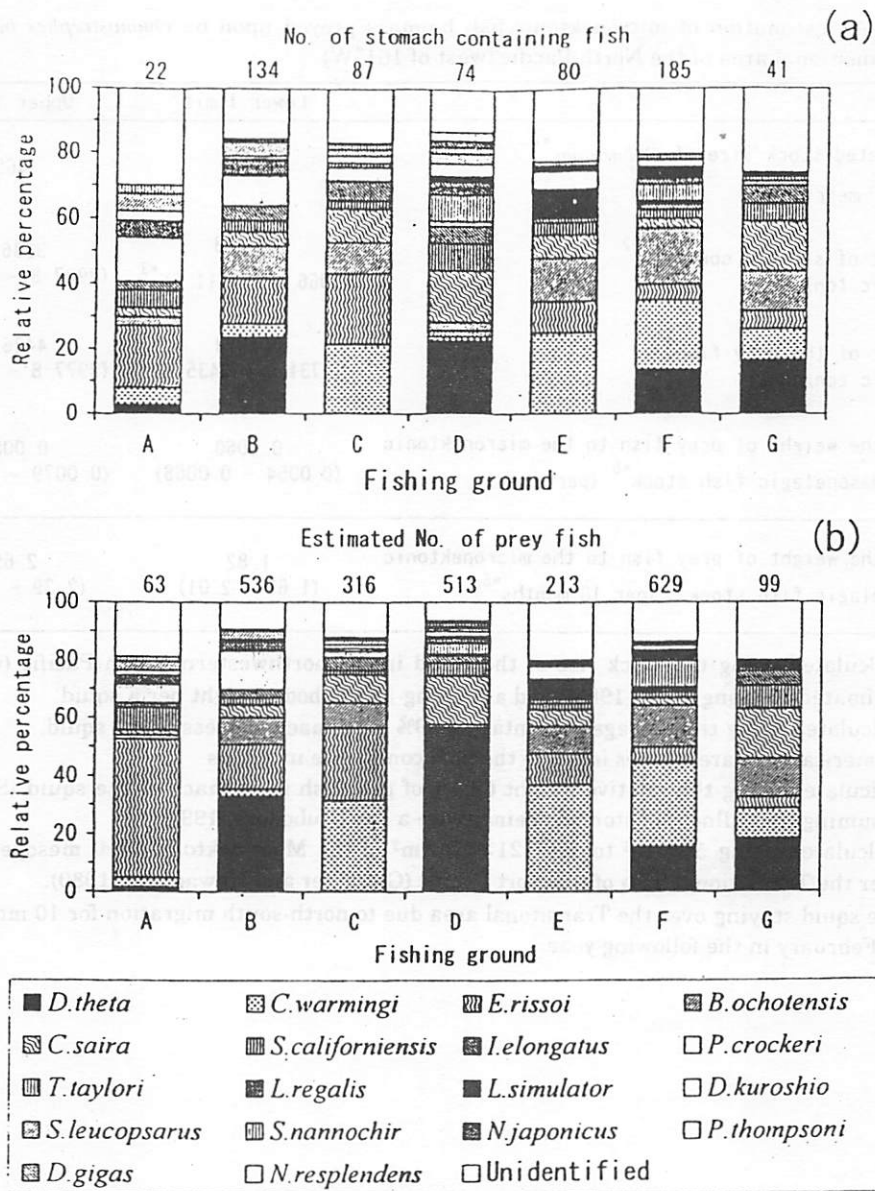


Fig. 4. Composition of the prey fish species by fishing grounds.  
 (a): showing as relative percentage of frequency.  
 (b): showing as relative percentage of the estimated number of prey fish.

Table 3. Average of stomach fullness in *Ommastrephes bartrami*.

	The stomachs containing <i>O.bartrami</i> in fresh condition included	The stomachs containing <i>O.bartrami</i> in fresh condition excluded
No. of stomachs examined	701	654
No. of stomachs containing <i>O.bartrami</i> in fresh condition	47	
Average of stomach fullness* (%)	0.87	0.69
95% confidence interval	0.74 - 1.00	0.62 - 0.76

\* Stomach fullness (%) =  $SCW / (BW - SCW) \times 100$   
 SCW: stomach contents weight (g)  
 BW: body weight (g)

Table 4. An estimation of micronektonic fish biomass preyed upon by *Ommastrephes bartrami* in the Transitional area of the North Pacific (west of 161°W)

	Lower limit	Upper limit
Estimated stock size of <i>O. bartrami</i> <sup>*1</sup> ( $\times 10^3$ metric ton)	322	469
Weight of stomach contents <sup>*2</sup> (metric ton)	2221.8 (1966.4 - 2511.6) <sup>*3</sup>	3236.1 (2907.8 - 3658.2)
Weight of the prey fish <sup>*4</sup> (metric ton/ day)	3039.4 (2731.0 - 3435.8)	4426.9 (3977.8 - 5004.4)
% of the weight of prey fish to the micronektonic and/ mesopelagic fish stock <sup>*5</sup> (per day)	0.0060 (0.0054 - 0.0068)	0.0088 (0.0079 - 0.0100)
% of the weight of prey fish to the micronektonic mesopelagic fish stock <sup>*5</sup> (per 10 months <sup>*6</sup> )	1.82 (1.63 - 2.01)	2.65 (2.39 - 2.93)

- \*1: Calculated using the stock size of the squid in the northwestern North Pacific (west of 161°W) estimated by Gong *et al.* (1985), and assuming 1Kg of body weight per a squid.
- \*2: Calculated using the average percentage 0.69% of stomach fullness of the squid.
- \*3: Numericals in parentheses indicate the 95% confidence intervals.
- \*4: Calculated using the relative weight 68.4% of prey fish in stomach of the squid (Seki, 1993), and assuming the fullness of stomach being twice a day (Kubodera, 1991).
- \*5: Calculated using  $50 \times 10^6$  tonnes/ $121 \times 10^5$  Km<sup>2</sup> of the Micronektonic and/ mesopelagic fish stock over the Transitional area of the Nort Pacific (Gjøsaeter and Kawaguchi, 1980).
- \*6: The squid staying over the Transitional area due to north-south migration for 10 months from May to February in the following year.

Daily and seasonal feeding dynamics of the two myctophid species,  
*Stenobrachius leucopsarus* and *S. nannochir*, in the mesopelagic  
zone of the Bering Sea.

Balanov A.A.

Institute of Marine Biology RAS, Vladivostok

Mesopelagic organisms form an important and integral component of pelagic communities of the World Ocean. Nekton of the mesopelagic zone plays a substantial role in the transport and redistribution of organic matter from the nutrient - rich surface to the oligotrophic deep waters of the ocean (Vinogradov, 1968; Parin, 1968; Hopkins and Baird, 1977).

Myctophids play an important role in the mesopelagic community of the North Pacific Ocean and the Bering Sea. *Stenobrachius leucopsarus* and *S. nannochir* are the most abundant mikronektonic and myctophid fishes in the mesopelagic zone of the Bering Sea. They markedly dominate in terms of wet biomass among the other mesopelagic fishes in the Bering Sea (83.1% - 200-500 m and 52.4% - 500-1000 m)(Balanov, 1995).

Feeding ecology of mesopelagic fishes of the Bering Sea and north-west Pacific was discussed in some recent publications (Balanov, 1994; Balanov et al., 1994; Balanov, 1995; Balanov et al., 1995).

The present paper surveys the daily and seasonal dynamics of feeding of dominant mesopelagic fishes of the Bering Sea - *S. leucopsarus* and *S. nannochir*.

## MATERIALS AND METHODS

Specimens were sampled during a complex expedition aboard research vessels of the Pacific Research Institute of Fisheries and

Oceanography during the summer- winter period of 1989-1990 (Fig. 1).. Samples were taken in 1-hour oblique tows from three layers: 0 - 200 m, the upper mesopelagic (200-500m) and the lower mesopelagic (500-1000 m). Trawlings were made using pelagic trawls without a closing device (Balanov, Il'inskyi, 1992).

The material sampled on different dates, places and different times of the day was pooled and analysed over a 24-h cycle at 4-h intervals. The sampling and processing procedures were those described by Gogbatenko, Il'inskyi, (1991). The feeding index was estimated as the ratio of the weight of consumed prey to the total body weight of the fish, multiplied by 10000. All investigated fishes were immature.

A total of 2631 stomachs were examined. We investigated medium-sized fish (7-10 cm) most abundant on all depths (Balanov, 1994).

## RESULTS

**Composition of prey.** *S. leucopsarus* and *S. nannochir* are zooplankton feeders. Stomachs of the inhabitants of the upper 0-1000 m layer contained animals of 17 taxonomic groups (Table 1). The greatest diversity of prey was observed in the stomachs of *S. leucopsarus* from the upper and lower mesopelagic zone (20 species). In stomachs of *S. nannochir* there were found only 17 for the former layer, and 10 species for the later (Balanov et al., 1995).

The dominant prey in the diet of *S. leucopsarus* were: *Thysanoessa longipes* (Euphausiacea), *Calanus cristatus*, *Eucalanus bumgii*, *Pareuchaeta japonica* (Copepoda). *S. nannochir* consumed primarily



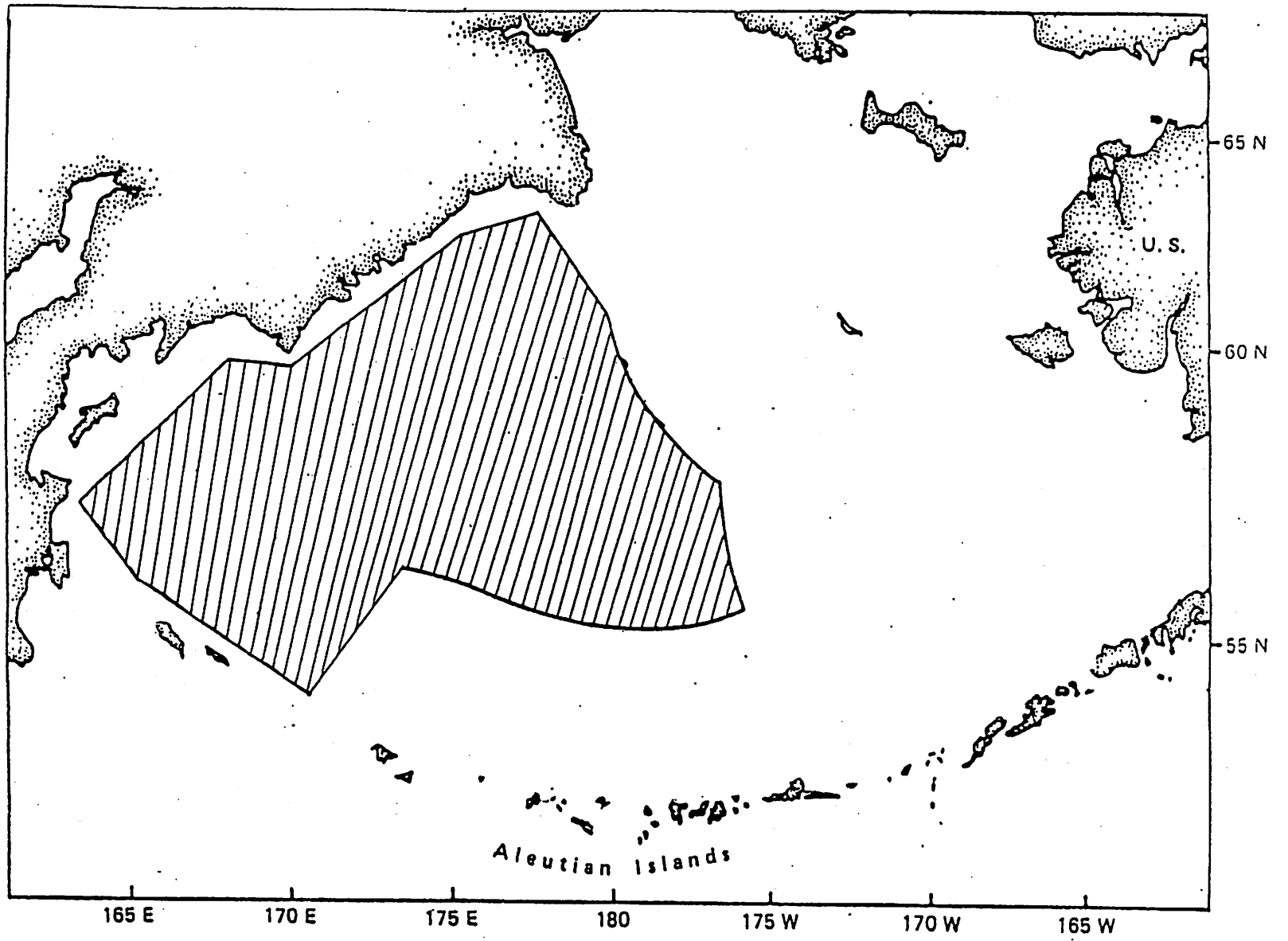


Fig. 1. Region where material was collected in the Bering Sea

Table 1

Diet composition and ratio (percent by weight) for most abundant myctophids in the Bering Sea, upper - (1) and lower mesopelagic zone (2).

Dietary items	S. leucopsarus		S. nannochir	
	1	2	1	2
Euphausiacea	35.4	0.5	-	8.6
Thysanoessa				
longipes	34.3	0.5	-	-
Other euphausiacea	1.1	-	-	8.6
Copepoda	49.2	83.5	84.2	73.8
Calanus cristatus	17.1	50.1	10.0	27.7
C. plunchrus	2.9	4.5	5	1.8
Eucalanus bungii	7.6	3.0	-	-
Gaetanus intermedius	6.1	4.1	-	-
Pareuchaeta japonica	11.5	3.3	50.0	1.0
Candacia columbiae	1.5	3.2	-	3.3
Metridia pacifica	1.9	12.6		
Heterorhabdus			-	0.2
robustoides	-	-	-	5.3
Other copepoda	0.6	2.7	14.0	22.5
Amphipoda	4.9	0.4	13.0	-
Parathemisto pacifica	3.8	0.1	13.0	-
Other amphipoda	1.1	0.3	-	-
Chaetognata	0.7	1.3	-	0.3
Parasagitta elegans	0.7	1.3	-	0.3
Pteropoda	-	-	-	0.3
Limacina helicina	-	-	-	0.3
Ostracoda	1.2	-	2.8	0.2
Appendicularia	+	0.6	-	-
Oicopleura				
labrodoriensis	+	0.6	-	-
Coelenterata	3.2	8.9	-	+
Ctenofora	0.3	-	-	-
Polychaeta	0.6	-	-	-
Decapoda	4.2	1.7	-	8.9
Cephalopoda	0.3	-	-	+
Pisces	-	-	-	8.3
Total number of fishes	1025	771	100	735

copepods - *C. cristatus*, *Metridia pecifica* and *P. japonica* (Balanov et al., 1995).

**Diel dynamics of feeding and digesting.** *S. leucopsarus* is an active vertical migrant ascending to the epipelagic zone at night. This species stayed in the epipelagic zone for 8 h (23 to 07h) in summer and 14h (17 to 07h) in autumn and winter. The feeding index increased during the night (maximal at 02 to 04 h), and the proportion of empty stomachs decreased. The feeding index of *S. leucopsarus* in the epipelagic zone was maximal in summer and autumn and smallest in winter (Fig. 2). In the upper mesopelagic layer, *S. leucopsarus* exhibited two feeding peaks, between 22 and 02 h and between 14 and 16 h (summer and winter). In autumn this species showed only one feeding peak (22 to 02 h). The proportion of empty stomachs from 18 to 06 h decreased, and it progressively increased from 06 to 18 h. The greatest amount of freshly ingested food was found during the period when feeding indices were maximal, in all seasons. In the lower mesopelagic area, the feeding index of *S. leucopsarus* was extremely low and it remained at the same level all day. Feeding index of that layer was maximal in winter (Fig. 2).

*S. nanochir* showed two feeding maxima in the upper mesopelagic zone at 22 to 02 and 10 to 14 h, during which time the share of freshly ingested prey was high. In the lower mesopelagic zone, this species ate very little, and freshly ingested food was seldom found in the stomachs in all seasons (Fig. 3).

**Diel dynamics of the species composition of freshly ingested prey.** Predominant prey organisms in the stomachs of *S. leucopsarus* in winter were euphausiids (*T. longipes*). In the upper mesopelagic area, predominant freshly ingested prey in the stomachs of this species

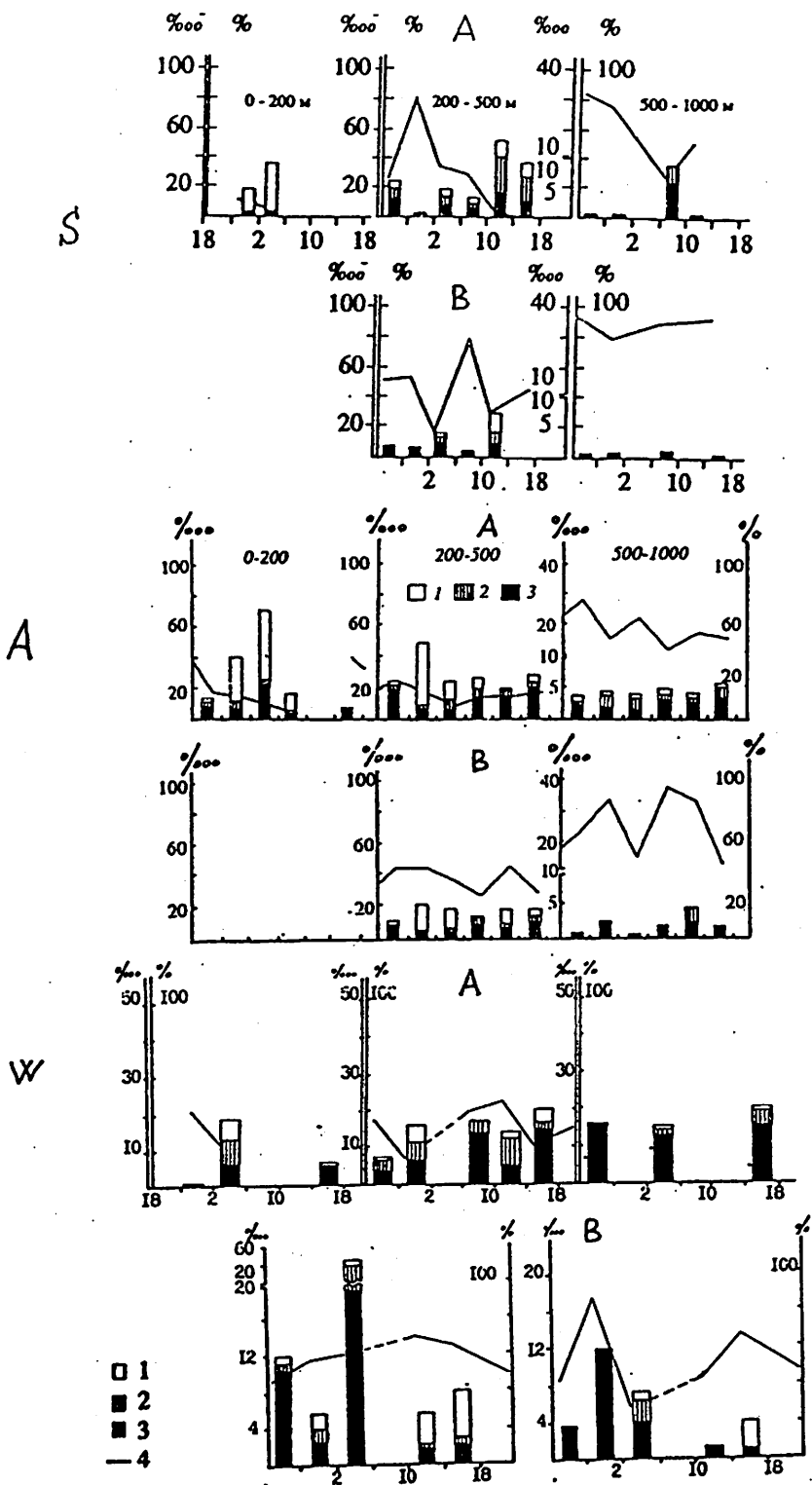


Fig. 2. Diel dynamics of feeding of *S. leucopsarus* (A) and *S. nannochir* (B) at the Bering Sea. The degree of digestion of food: (1) fresh, (2) moderately digested, (3) highly digested. Line (4) indicates the proportion of empty stomachs. S - summer, A - autumn, W - winter. Abscissa - time of day; ordinate - index of stomachs fullness.

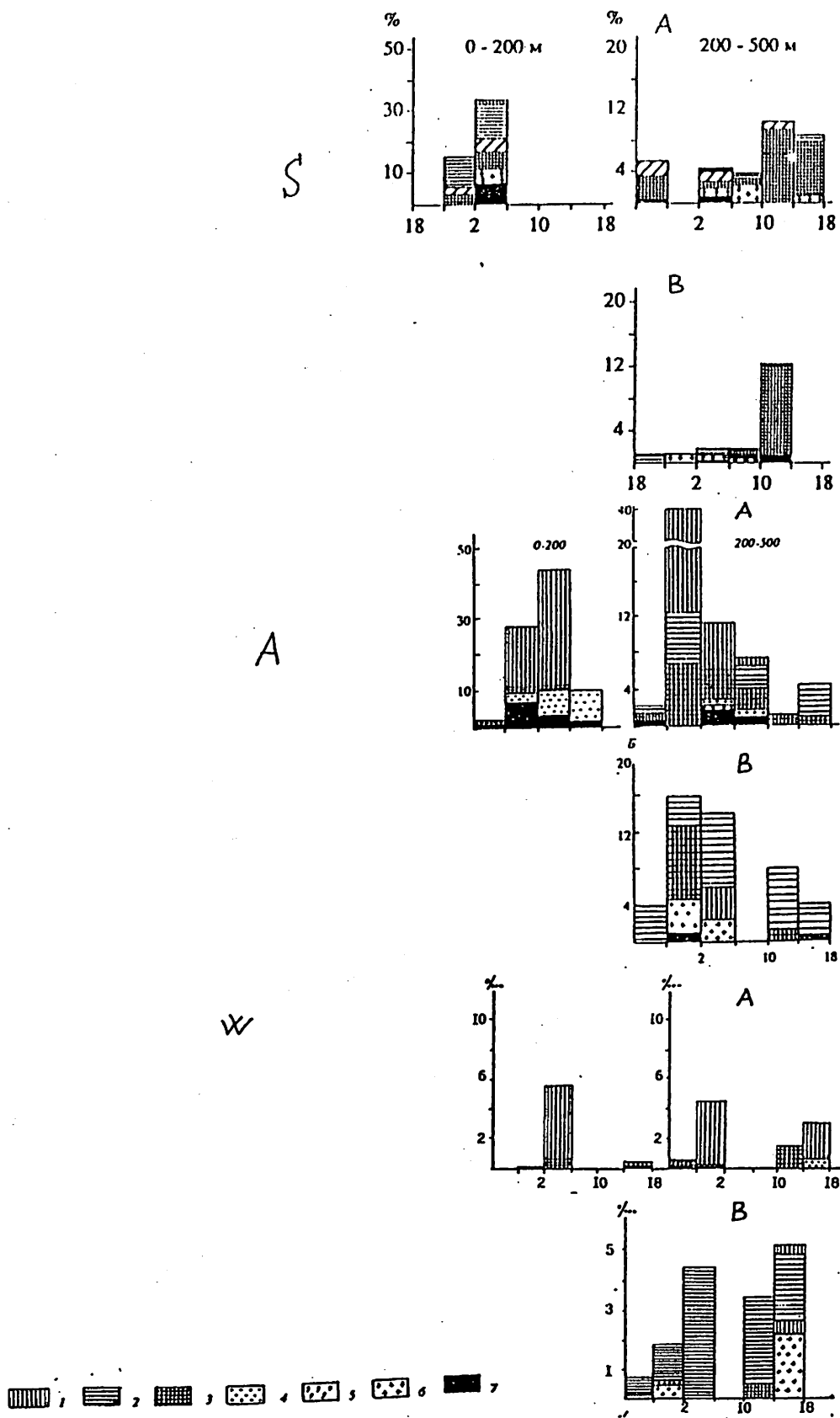


Fig. 3. Diel dynamics of prey composition in freshly ingested food in stomachs of *S. leucopsarus* (A) and *S. nannochir* (B) at the Bering Sea. (1) Euphausiacea, (2) *C. cristatus*, (3) other copepoda, (4) *P. pacifica*, (5) *O. labrodoriensis*, (6) Coelenterata, (7) other species. S - summer, A - autumn, W - winter. Abscissa - time of day; ordinate - index of stomachs fullness.

between 22 to 06 h and between 10 to 22 h in summer was a complex of copepods (*P. japonica*, *M. pacifica*, *G. intermedius*), while in autumn, *C. cristatus* and a complex of copepods ('other copepods'); in winter *T. longipes* and 'other copepods'(most abundant *P. japonica*) prevailed (Fig. 3).

Predominant freshly ingested prey in the stomachs of *S. nannochir* in the upper mesopelagic zone were *M. pacifica* and "other copepods" in summer, and *C. cristatus* in autumn and winter (Fig. 3).

## DISCUSSION

The few studies on the periodicity of feeding of northern Pacific mesopelagic fishes have revealed no distinct rhythms in the food consumption of *S. leucopsarus* (Tyler, Percy, 1975; Cailliet, Ebeling, 1990). Our results suggest that the most common myctophids of the Bering Sea show pronounced diel dynamics of feeding, which are retained during different seasons. In both investigated fishes, there are two feeding peaks: one at night from 22 to 04 h (epipelagic(only *S. leucopsarus*) and upper mesopelagic layers), , and the other during the day (upper mesopelagic layer), from 10-to 16 h. No distinct feeding rhythms were found in the lower mesopelagic area. This, together with the high percentage of empty stomachs and high degree of food digestion, points to the low feeding rates in this layer. The predominance of freshly ingested prey, the low proportion of digested food, and clear feeding rhythms support the assumption that the epipelagic (0-200 m) and upper mesopelagic layers (200-500 m) are the main trophic zones of the fish studied (Balanov, 1994).

A variety of foraging strategies of mesopelagic fishes are known. Active migrants feed during the night in the epipelagic zone, while poor migrants consume food during the day and at night in the mesopelagic area. Some active migrants can stay in the mesopelagic zone during the day and at night and feed there (Pearcy et al., 1979, Roe, Badcock, 1984).

It was found that *S. leucopsarus* as an active diel vertical migrant, feeding both in epipelagic (night) and mesopelagic (night and day) zones of the Bering Sea, while nonmigratory *S. nannochir* feeds only in the deep layers both during daytime and night.

Migratory *S. leucopsarus* shows more clear variation in feeding habits than poor migrant *S. nannochir*. The most abundant preys for *S. leucopsarus* are copepods in summer, euphausiids in autumn and copepods and euphausiids in winter (Fig. 4). *S. nannochir* mainly feeds on copepods in all seasons (Fig. 5). The feeding indices of this species at epipelagic and upper mesopelagic layers were maximal in summer and autumn and minimal in winter. Feeding index of the *S. leucopsarus* at lower mesopelagic zone was highest in winter (Fig.6). Feeding indices of the *S. nannochir* were roughly the same in all investigated seasons (Fig. 7) (Balanov et al., 1994; 1995).

Daily and seasonal changes in the feeding habits of both species are closely related to the distribution patterns of the main prey organisms such as copepods and euphausiids, in the northwest Pacific. *C. cristatus* and *E. bungii*, which are dominant during spring and summer in surface waters, migrate to mesopelagic depths in the late summer and autumn. *P. japonica*, *M. pacifica* and "other copepods" are interzonal species and quite common at mesopelagic depth (Vinogradov, 1954; 1968; Sekiguchi, 1975; Marchaseva, Raszhivin, 1992). *T. longipes* is very abundant in the plankton of the Bering Sea in fall; they attain high

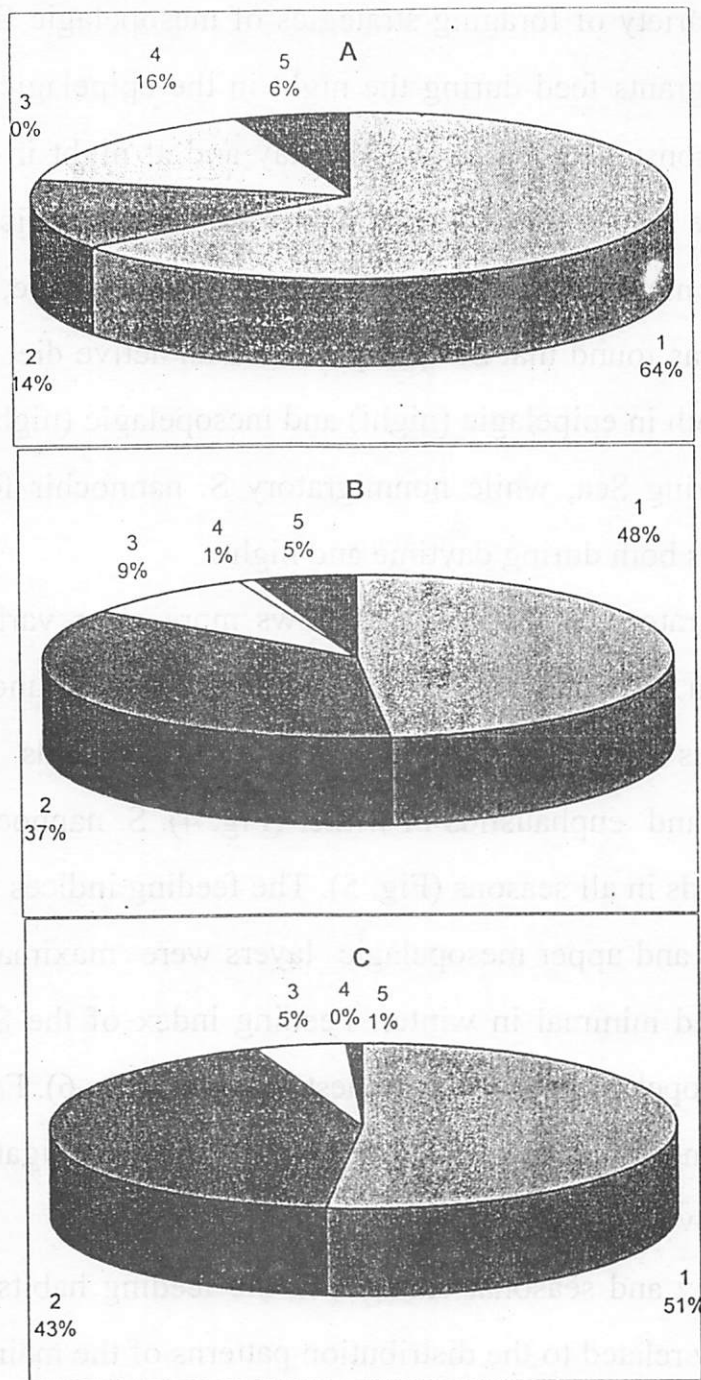


Fig. 4. Seasonal dynamics of dominant group of zooplankton in stomachs of *S. leucopsarus* at upper mesopelagic zone of the Bering Sea. A - summer, B - autumn, C - winter. 1-Copepoda, 2-Euphausiacea, 3 - Amphipoda, 4-Coelenterata, 5-other groups.



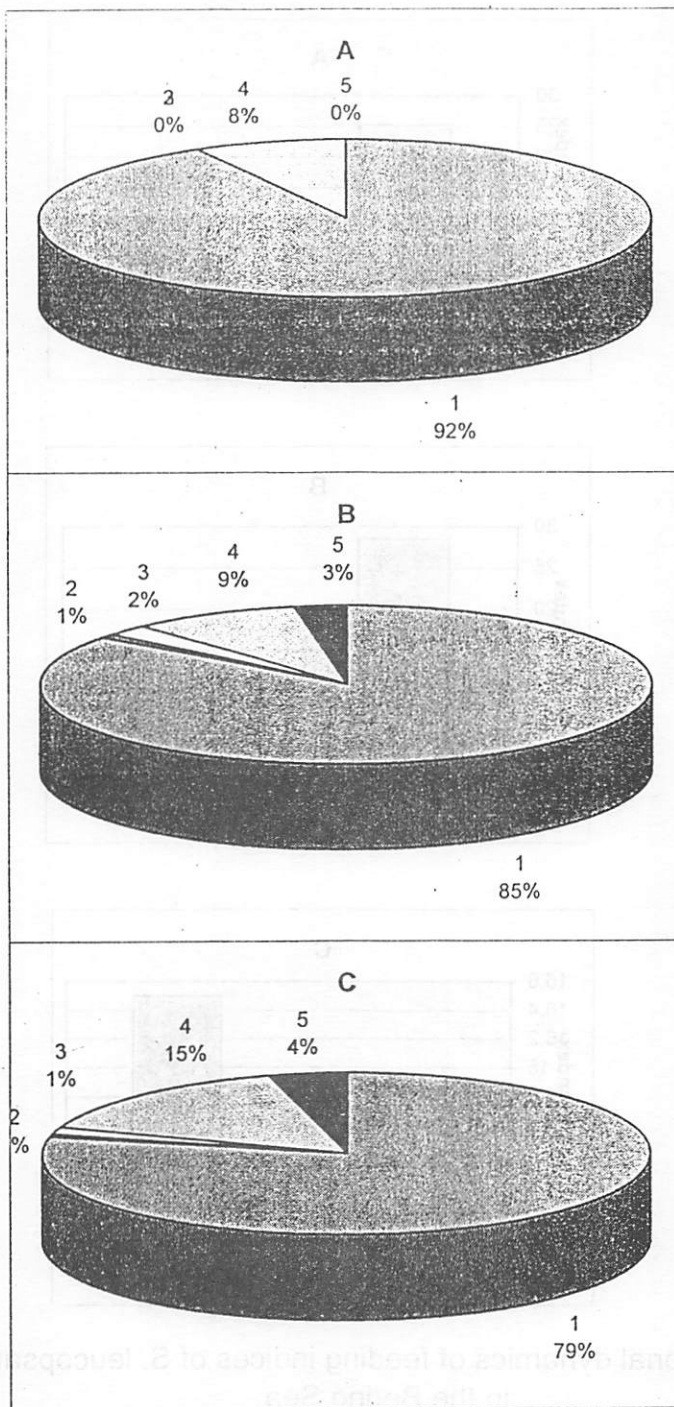


Fig. 5. Seasonal dynamics of dominant group of zooplankton in stomachs of *S. nanochir* at upper mesopelagic zone of the Bering Sea. A - summer, B - autumn, C - winter. 1-Copepoda, 2-Euphausiacea, 3-Amphipoda, 4-Coelenterata, 5-other groups

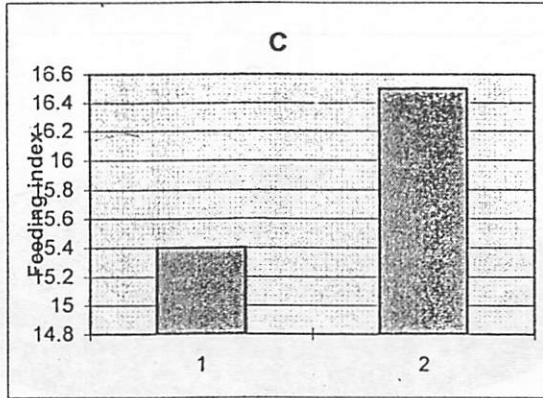
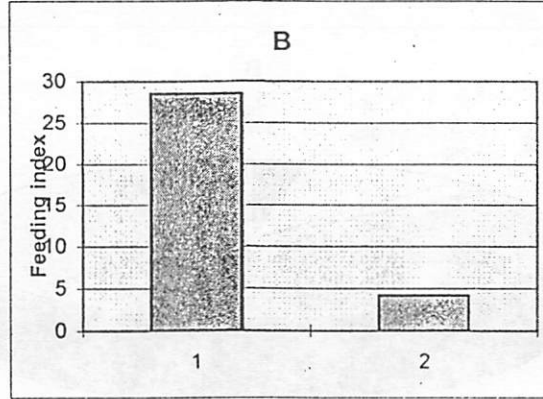
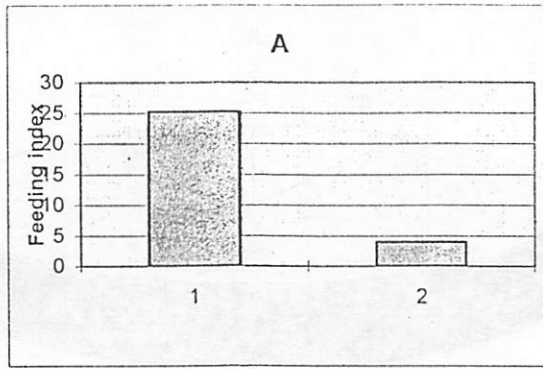


Fig. 6. Seasonal dynamics of feeding indices of *S. leucopsarus* in the Bering Sea.

A - summer, B - autumn, C - winter. 1- upper mesopelagic zone  
2 - lower mesopelagic zone

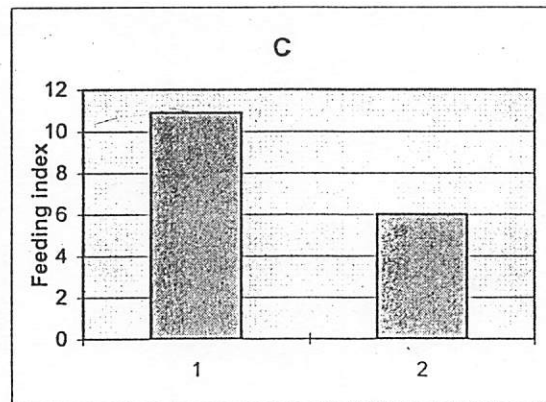
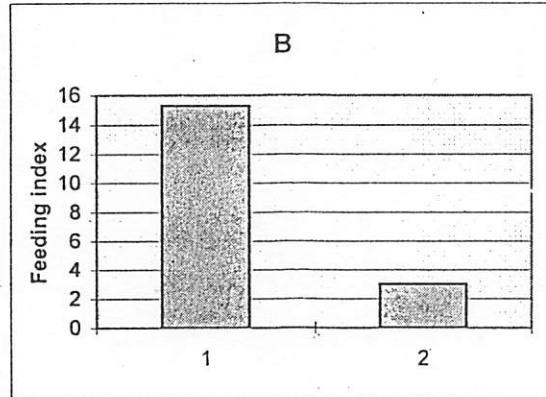
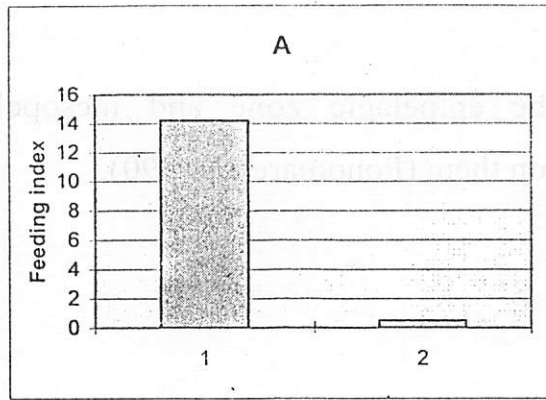


Fig. 7. Seasonal dynamics of feeding indices of *S. nannochir* in the Bering Sea.  
 A - summer, B - autumn, C - winter. 1- upper mesopelagic zone  
 2 - lower mesopelagic zone

density in the epipelagic zone and mesopelagic fishes can successfully forage on them (Ponomareva, 1990).

# Stable carbon and nitrogen isotope ratios of mesopelagic micronekton and their prey.

Dhugal J. Lindsay, Masao Minagawa\*, Kouichi Kawaguchi

Plankton Research Division, Ocean Research Institute, University of Tokyo, Tokyo, Japan. 164.

\*Division of Geoscience, Hokkaido University, Sapporo, Japan. 060.

e-mail: dhugal@jamstec.go.jp

This paper should not be cited without permission from authors.

## Introduction

Stable isotope ratios of nitrogen and carbon have been used in recent times to determine organism trophic positions and overall food web structures in both terrestrial and aquatic environments. The relative percentages of the heavy isotopes in animal tissues have been found to increase with increasing trophic level due to the higher reaction speeds of the lighter isotopes leading to preferential excretion in bodily wastes such as ammonia (Minagawa & Wada 1984, Checkley & Miller 1989), urea (Steele & Daniel 1978) and carbon dioxide (De Niro & Epstein 1978). These isotope ratios are expressed as delta values with the standard for nitrogen ( $\delta^{15}\text{N}$ ) being air and the standard for carbon ( $\delta^{13}\text{C}$ ) being PeeDee Belemnite. The  $\delta^{15}\text{N}$  of an organism has been found to increase by 3-4‰ per trophic level (De Niro & Epstein 1981, Minagawa & Wada 1984) and the  $\delta^{13}\text{C}$  to increase by 0-2‰ per trophic level (De Niro & Epstein 1978, Fry & Sherr 1984). We decided to use the stable isotope technique to investigate trophic links in mesopelagic food webs and to elucidate the extent and form of nutrient exchange between surface waters and the deep sea. To this end we determined the  $\delta^{15}\text{N}$  and  $\delta^{13}\text{C}$  values of both vertically migrating organisms such as myctophids, vertically segregated non-migrants such as bristlemouths of the genus *Cyclothone* and possible prey items.

## Materials and Methods

Samples were collected by IKMT trawls on the 14 May 1994 and by IKMT, MTD and ORI nets in the last week of May 1995 at point P (34°35'N, 139°20'E) in Sagami Bay. Vertical distributions were determined from these and previous net samples and from reports found in the literature. Particulate organic matter (POM) was obtained from water samples that were taken from discrete depths using a rosette sampler with an

attached CTD meter and filtered through a filter of 1.2 $\mu$ m pore size. All samples were frozen at -20°C until ready for analysis, whereupon they were thawed and sorted. After wet weight determination and length measurement, samples were rinsed quickly with distilled water and the stomach contents were dissected out of all fish and shrimp. Organisms taken on 14 May 1994 were analyzed whole. Apart from for copepods or unless otherwise indicated, only the muscle tissue was used for analyses in all organisms taken in late May 1995. In both years material from several individuals was pooled to give an average value for each species and size class. Samples were desiccated in a dry oven at 60°C and ground to a fine powder. To avoid artifactual variance in  $\delta^{13}\text{C}$  due to fluctuation in lipid content levels the solvent-extractable lipid fraction was removed from a subsample by regrinding with a mixture of chloroform:methanol (2:1), filtration onto a Whatman GF/C glass fibre filter, rinsing with the chloroform/methanol solution several times and subsequent redrying at 60°C overnight for  $\delta^{13}\text{C}$  analyses. Samples were converted to  $\text{CO}_2$  and  $\text{N}_2$  gas by the quartz combustion method of Minagawa *et al.* (1984). These gases were cryogenically separated and the %N, %C and C:N ratios of the samples determined volumetrically using a mercury manometer. The carbon ( $^{13}\text{C}/^{12}\text{C}$ ) and nitrogen ( $^{15}\text{N}/^{14}\text{N}$ ) ratios were analyzed by a FINNIGAN MAT 251 isotope ratio mass spectrometer and converted to delta values relative to the international standards; PDB (Peedee Belemnite) and atmospheric  $\text{N}_2$ , respectively, by using working amino acid laboratory standards (Aspartate and Histidine) that were ground and combusted in the same way. Analytical reproducibility was better than  $\pm 0.1\%$  for both  $\delta^{15}\text{N}$  and  $\delta^{13}\text{C}$ .

## Results

### Non-migratory fish

Three *Cyclothone* species occurred in large numbers in Sagami Bay and they were segregated vertically by species with *C. alba* being shallowest with an abundance maximum between 300 and 500m, then *C. pseudopallida* between 500 and 700m and with *C. atraria* occurring at the greatest depths (500-700m for smaller and below 700m for larger individuals). There was a trend for the larger fish of each species to live deeper than the smaller individuals of that species. No evidence of extensive diel vertical migration was found. The  $\delta^{15}\text{N}$  increased with increasing depth of the abundance maximums of the *Cyclothone* individuals involved, while  $\delta^{13}\text{C}$  remained relatively stable for samples taken in both 1994 and 1995 (Fig. 1).

To determine the amount of spread around each data point, whole *Cyclothone* individuals taken in late May 1995 were analyzed separately and both their isotope

ratios and chemical compositions compared. The  $\delta^{15}\text{N}$  of each was significantly different to at least the 5% confidence level as was the  $\delta^{13}\text{C}$  for all but *C. alba* and *C. atraria* (Fig. 2). The percentage of dry weight composed of nitrogen was low at between 9.5 and 11% for all three species and the percentage of dry weight composed of carbon was greatest for *C. atraria* at 42-43% compared to 35-38% for the other two species.

Other samples that were analyzed from the 1995 samples include the myctophid *Lampanyctus jordani* (11.6‰, -19.2‰), which does not migrate in Sagami Bay, the surface-dwelling larvae of the Japanese anchovy (9.5‰, -17.1‰) and the snipe eel *Avocettina infans* (11.9‰, -19.3‰) (Fig. 3).

### Vertical Migrants

A comparison of the chemical composition of the vertical migrant *Maurolicus muelleri* with the non-migratory *Cyclothone* species showed that the percentage of dry weight composed of nitrogen was significantly higher for *M. muelleri* and that the percentage composed of carbon was greatest for both *M. muelleri* and *C. atraria*. (Fig. 2). The delta positions of midwater vertical migrants in Sagami Bay seemed to fall into two groups (Fig. 3). Members of the first group include fish such as *Diaphus garmani* (10.0‰, -18.5‰), small (9.5‰, -18.7‰) and large (10.3‰, -18.1‰) *Diaphus kuroshio* and the squid *Eucleoteuthis luminosa* (10.9‰, -17.6‰). Members of the other group included the fish *Ceratoscopelus warmingii* (9.2‰, -17.0‰), medium-size individuals of *Diaphus kuroshio* (10.4‰, -15.9‰), *Maurolicus muelleri* (10.0‰, -16.1‰) and *Diaphus suborbitalis* (10.1‰, -16.0‰) as well as the shrimp *Sergia prehensilis* (8.1‰, -17.4‰). The shrimp *Sergestes similis* (9.5‰) and two individuals of the shrimp *Acanthephyra quadrispinosa* (8.4‰, 8.8‰) also had  $\delta^{15}\text{N}$  values within this range although  $\delta^{13}\text{C}$  values are not available at this time. The  $\delta^{15}\text{N}$  values of midwater migrants on the whole fell between those values for deep-living non-migrants and non-migrants inhabiting the 300-500m layer. The euphausiid, *Euphausia similis*, which has a shallower daytime abundance maximum at around 350m (Hirota *et al.* 1984), had a  $\delta^{15}\text{N}$  of 7.0‰.

### Non-migratory Crustaceans

Non-migratory shrimp with an abundance maximum below 700m had high  $\delta^{15}\text{N}$  values (Fig. 3). These included *Bentheogennema borealis* (11.0‰, -19.4‰), small (11.7‰, -18.7‰) and larger (11.3‰, -18.8‰) individuals of *Hymenodora frontalis* and small

individuals of *Hymenodora gracilis* (11.6‰, -18.2‰). The  $\delta^{15}\text{N}$  of *Sergia japonica* (10.1‰) was less so but was still higher than that of migrant shrimp.

The carbon and nitrogen stable isotope ratios of some possible prey items, the copepods, were determined. Deep-living copepods such as *Lucicutia wolfendeni*, *Cornucalanus indicus*, *Arietellus simplex* and *Paraeuchaeta rubra* all clustered at high  $\delta^{15}\text{N}$  and more negative  $\delta^{13}\text{C}$  values (11.4 to 12.4‰, -18.4 to -19.4‰) (Fig. 3). Although only the  $\delta^{13}\text{C}$  of *Bathycalanus richardi* is available it was also highly negative (-20.4‰). Surface-living copepods such as *Calanus sinicus* (9.3‰, -17.0‰) and *Eucalanus attenuata* (9.0‰, -16.2‰) had less negatively-skewed  $\delta^{13}\text{C}$  values and median  $\delta^{15}\text{N}$  values. The  $\delta^{15}\text{N}$  and  $\delta^{13}\text{C}$  values of *Neocalanus cristatus*, which is a surface-dwelling subarctic copepod in diapause at depth in Sagami Bay, were 8.0‰ and -19.4‰, respectively.

#### Particulate Organic Matter

The stable nitrogen and carbon isotope values for POM from 0m, 100m, 200m and 300m in depth were 8.5‰ and -18.1‰, 10.3‰ and -20.8‰, 9.4‰ and -21.3‰, non-available and -21.1‰, respectively. The  $\delta^{13}\text{C}$  of POM decreased with depth while  $\delta^{15}\text{N}$  seemed to increase with a peak at 100m. The C/N ratio of POM also peaked at 100m where a density profile reveals the presence of a pycnocline.

#### Samples from other years

Delta values for whole organisms taken at Point P, Sagami Bay, on 14 May 1994 also follow the pattern seen in muscle tissue samples from late May 1995 of  $\delta^{15}\text{N}$  increasing and  $\delta^{13}\text{C}$  decreasing with depth for the non-migratory fish *Cyclothone alba* (6.6‰, -18.0‰), *C. pseudopallida* (7.5‰, -18.2‰; 8.5‰, -17.9‰) and *C. atraria* (10.8‰, -18.7‰; 11.9‰, -18.5‰), the non-migratory shrimp *Hymenodora frontalis* (9.7‰, -18.9‰) and *Bentheogennema borealis* (10.2‰, -18.9‰) and the non-migratory copepod *Euchaeta* sp. (10.3‰, -19.8‰). Again *Neocalanus cristatus* (6.1-8.3‰, -19.0‰) had a delta position not in compliance with its vertical distribution maximum in Sagami Bay and vertical migrants, including *Maurolicus muelleri* (8.5‰, -16.6‰), *Acanthephyra quadrispinosa* (8.3‰, -16.8‰) and the copepod *Pleuromamma xyphias* (8.4‰, -17.5‰; 8.9‰, -17.5‰), clustered together with median  $\delta^{15}\text{N}$  and more positive  $\delta^{13}\text{C}$  values. *Euphausia similis* once again had  $\delta^{15}\text{N}$  values at the lowest end of the scale (6.3-6.9‰). This overall pattern is exactly the same as was seen for the the



delta positions of samples taken in late May 1995. Values found in the literature for the muscle tissue of mesopelagic organisms were fairly stable (Table 1.)

### Discussion

Delta values seem to be determined on a large scale by the depths at which the animals live and this is thought to be due to the structure of the food web. There is an anomaly however in that organisms living in the surface layers had higher  $\delta^{15}\text{N}$  values than non-migrating Cyclothone that live between 300 and 500m in depth (Fig. 3). We believe this can be explained because the spring bloom in Sagami Bay had just finished at the time our samples were collected. Both the concentration of heavy nitrogen in phytoplankton due to the paucity of nutrients towards the end of a bloom and the existence of large numbers of carnivorous microplankton such as flagellates and ciliates towards the end of blooms have been reported previously. The high  $\delta^{15}\text{N}$  of surface POM collected on the 25th May 1995 is likely a consequence of the period in which the samples were collected. The delta values of surface-dwelling copepods and anchovy larvae have also been affected by the high  $\delta^{15}\text{N}$  values of late and post-bloom POM due to these organisms' short generation times and high growth rates. The delta values of mesopelagic organisms however, are more stable temporally due to lower growth and metabolic rates.

Both the C/N and  $\delta^{15}\text{N}$  of POM peaked at 100m depth. We propose that particles below a certain density built up at the pycnocline and the high  $\delta^{15}\text{N}$  reflects the degradation of POM by endemic bacteria and the higher C/N ratio a build-up of refractile carbon particles. Particles of higher densities continued their descent through the water column without a large build-up of degradation products and therefore the  $\delta^{15}\text{N}$  and C/N values at depth are lower than at the pycnocline although still higher than at the surface.

Although the abundance maximum for the copepod *Neocalanus cristatus* is found below 700m in Sagami Bay this copepod is invariably in diapause, having been swept down the eastern seaboard of Japan by the Oyashio subsurface current from its feeding grounds in the subarctic north, where it is a surface dweller that feeds mainly on phytoplankton and other suspended organic matter. Its delta position is understandably different than would be expected from its present habitat. The stable isotope ratios of the flesh from a megamouth shark caught off Japan were similar to those of vertical migrants and for this reason we speculate that it too is a vertical migrant.

Delta values obtained by the analysis of separate individuals of the same species were significantly different from each other (Fig. 2) and therefore the pooling of sample material from several individuals before isotopic analysis was determined to be meaningful. The comparatively higher percentage of nitrogen per unit of dry weight in *M. muelleri* is thought to reflect the more developed musculature in the vertical migrant. The high C/N ratio and high percentage of carbon in *C. atraria* suggests higher lipid levels, as previously reported in other deep-living fish, while the low C/N ratio and high carbon content of *M. muelleri* suggests a more highly developed musculature.

Organisms with trophic habits as different as the snipe eel, which eats only sergestid shrimps, *Lampanyctus jordani*, a large myctophid, and several detritivorous and/or carnivorous copepods all had similar delta values. This suggests that the distribution of delta values is determined more by the overall structure of the food chain than by individual differences in prey type preferences. When food chain structure is simple with predator/prey relationships only, both  $\delta^{15}\text{N}$  and  $\delta^{13}\text{C}$  values increase with trophic level. This was however not the case for the samples from 1994 or 1995. Although  $\delta^{15}\text{N}$  increases the  $\delta^{13}\text{C}$  actually decreases slightly. The negative shift in the  $\delta^{13}\text{C}$  values of organisms with increasing depth may be explained by the increasing importance of detritus or POM, that has highly negative  $\delta^{13}\text{C}$  values, in the food web at depth. The deeper one goes, the more important detritus or POM becomes as an energy source, whether ingested directly or when transformed into the body mass of a prey organism.

### Conclusions

The  $\delta^{15}\text{N}$  of non-migrating bristlemouths of the genus *Cyclothone* increased while  $\delta^{13}\text{C}$  decreased with the depth of their distribution maximums. This pattern mirrors that of POM  $\delta^{15}\text{N}$  and  $\delta^{13}\text{C}$  with depth and was found in May of both 1994 and 1995. Midwater migrants could be classified into two groups on the basis of their delta positions. This was true regardless of taxonomic group. Non-migrants, whether fish, shrimps or copepods, exhibited high  $\delta^{15}\text{N}$  values for deep-living species and lower  $\delta^{15}\text{N}$  for shallower living species. Decreasing  $\delta^{13}\text{C}$  of organisms with depth points to the increasing importance of POM-derived matter as a food source further from the surface. The overall structure of the food chain seemed to be conserved regardless of the year with higher trophic levels and more detritivory in the deeper layers.

### Acknowledgements

Samples were collected by the R/V Tanseimaru, Tokyo University. Associate Professor T. Kikuchi, Yokohama National University, identified the shrimps and Associate Professor S. Nishida, University of Tokyo, identified the copepods. M. Moku and H. Watanabe, University of Tokyo, provided assistance in the identification of the fish.

## Bibliography

- Checkley DM, Miller CA (1989) Nitrogen isotope fractionation by oceanic zooplankton. *Deep Sea Res* 36:1449–1456
- DeNiro MJ, Epstein S (1978) Influence of diet on the distribution of carbon isotopes in animals. *Geochim Cosmochim Acta* 42: 495–506
- DeNiro MJ, Epstein S (1981) Influence of diet on the distribution of nitrogen isotopes in animals. *Geochim Cosmochim Acta* 45: 341–351
- Fry B, Sherr EB (1984)  $\delta^{13}\text{C}$  measurements as indicators of carbon flow in marine and freshwater ecosystems. *Contr Mar Sci* 27: 13–47
- Hirota Y, Nemoto T, Marumo R (1984) Vertical distribution of larvae of *Euphausia nana* and *E. similis* (Crustacea: Euphausiacea) in Sagami Bay and Suruga Bay, Central Japan. *Mar Biol* 81: 131–137
- Minagawa M, Wada E (1984) Stepwise enrichment of  $^{15}\text{N}$  along food chains: Further evidence and the relation between  $\delta^{15}\text{N}$  and animal age. *Geochim Cosmochim Acta* 48:1135–1140
- Minagawa M, Winter DA, Kaplan IR (1984) Comparison of Kjeldhal and combustion method for measurement of nitrogen isotope composition in natural organic matters. *Anal Chem* 56: 1859–1861
- Steele KW, Daniel RM (1978) Fractionation of nitrogen isotopes by animals: A further complication to the use of variations in the natural abundance of  $^{15}\text{N}$  for tracer studies. *J Agric Sci Camb* 90: 7–9

## Figure Legends

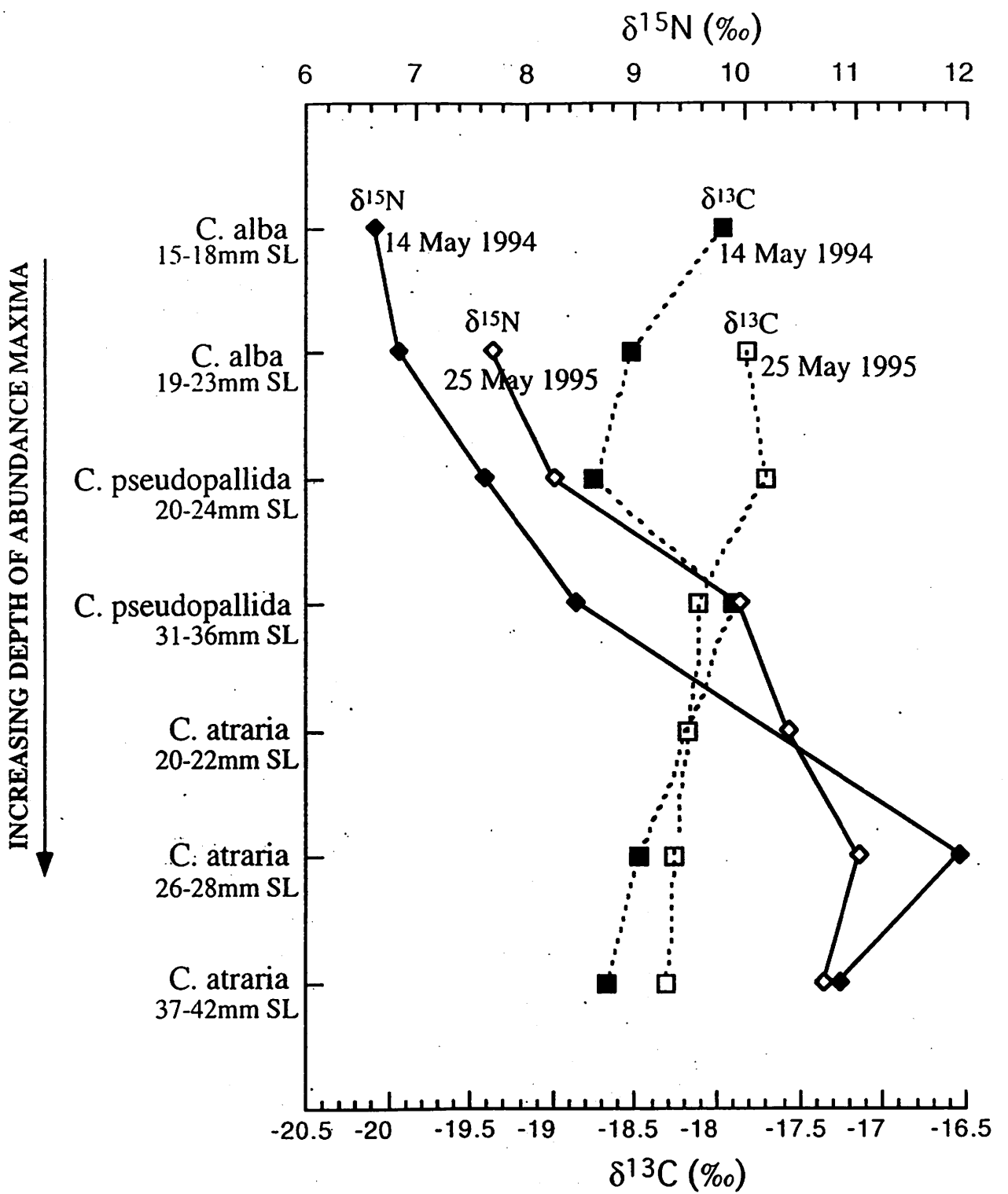
Fig. 1. Change in delta values with depth of distribution maxima for *Cyclothone* taken in 1994 and 1995. Samples from 14 May 1994 are whole animal values while those from 25 May 1995 are for muscle tissue.

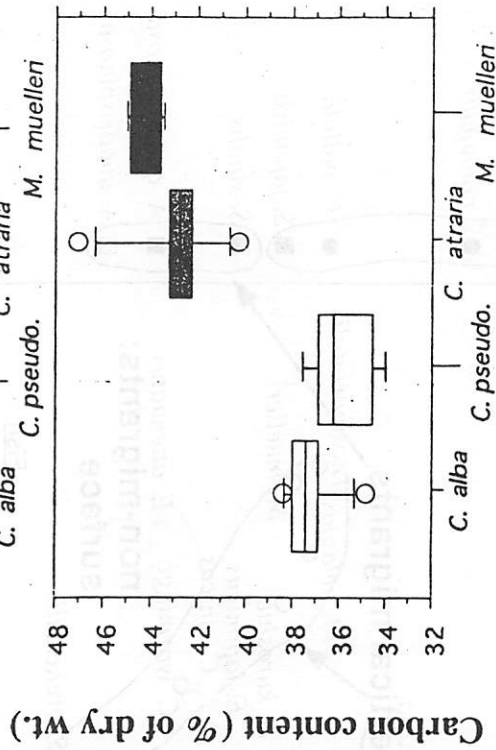
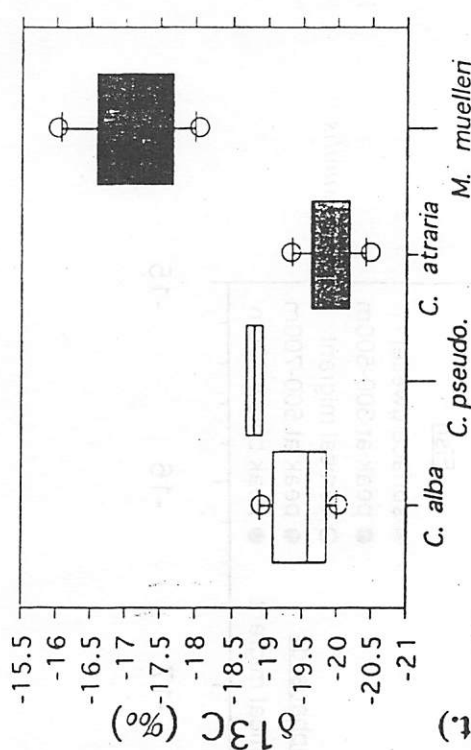
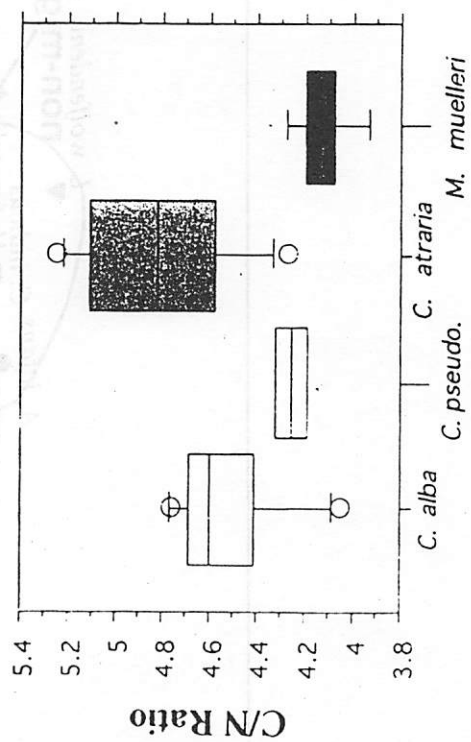
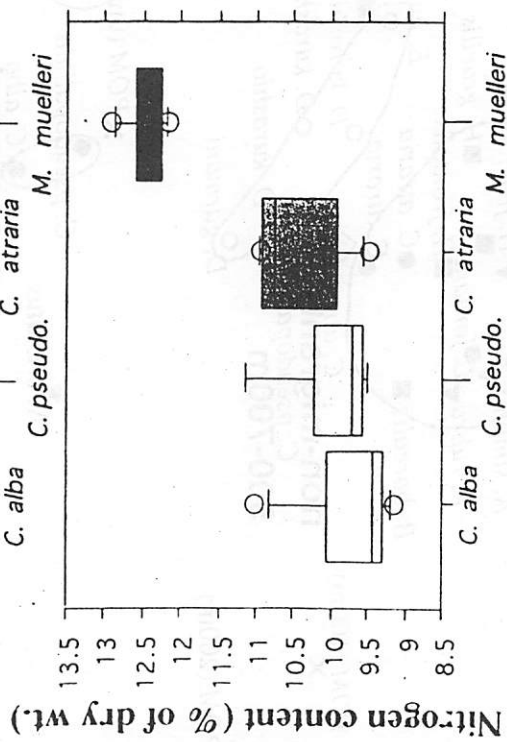
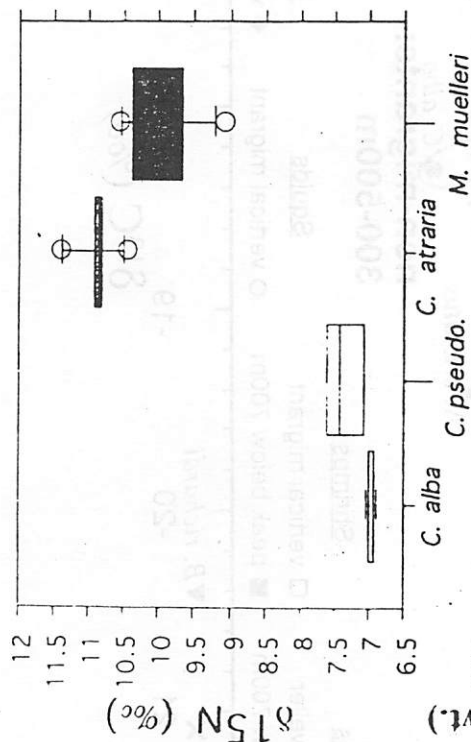
Fig. 2. Comparison of the delta values and chemical compositions of fish taken from Sagami Bay on the 25 May 1995 and analyzed as whole individuals.

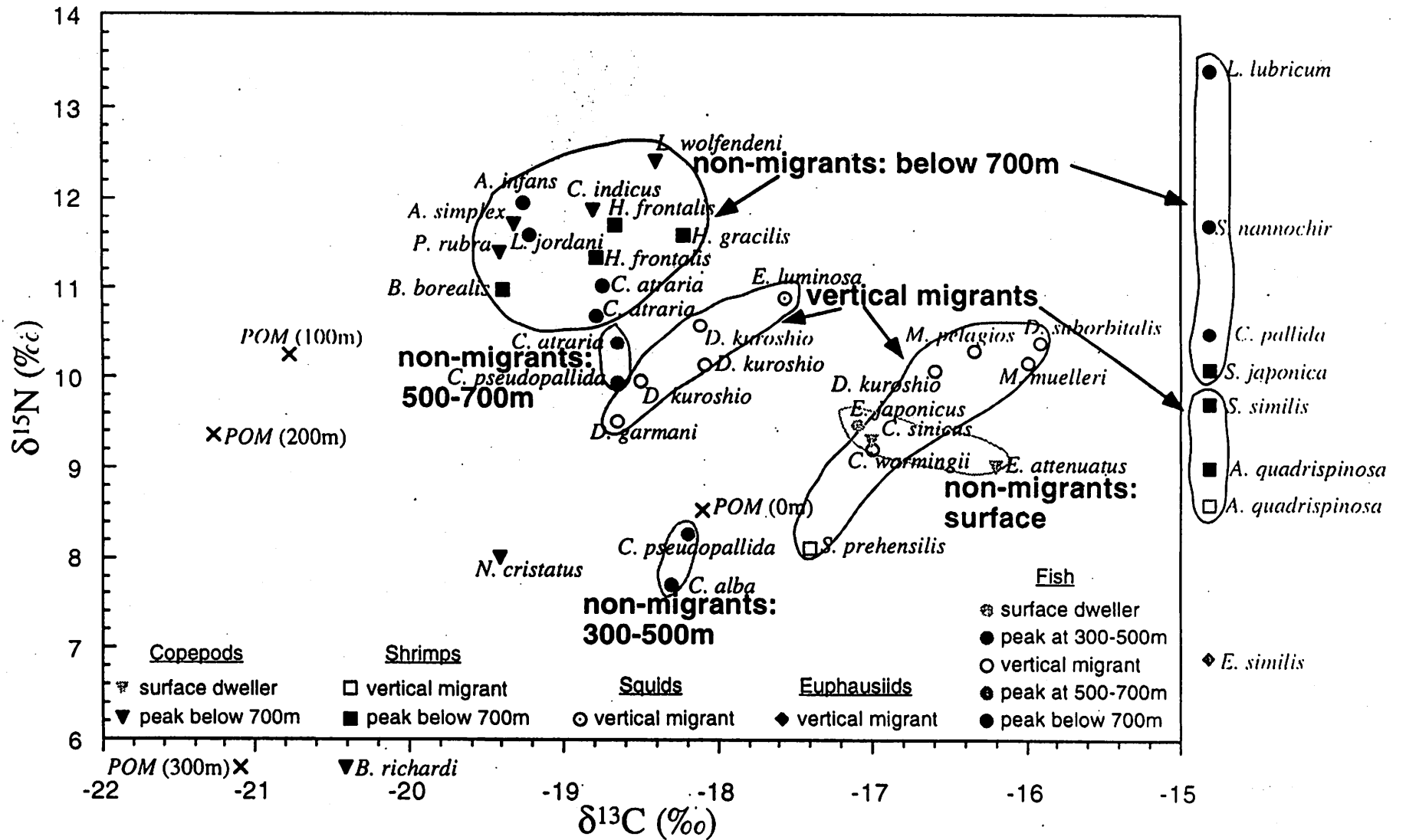
Fig. 3. Plot of nitrogen vs carbon delta values of POM and organisms taken from Sagami Bay on the 25 May 1995. Copepods were analyzed whole while only the flesh of shrimp, fish, squid, euphausiids and the megamouth shark was measured.

Organism	<i>N. cristatus</i>	<i>C. pseudopallida</i>	<i>C. atraria</i>	<i>S. japonica</i>	<i>H. frontalis</i>	<i>S. nanochir</i>	<i>L. jordani</i>	<i>L. lubricum</i>
Present Study	8.0	9.9	10.7-11.0	10.1	11.3	11.7	11.6	13.2
Sugisaki & Tsuda 1995	8.2	9.6	10.6-11.7	-	-	11.2-12.1	11.6-12.1	-
Terazaki <i>et al.</i> 1994	-	-	-	10.7	9.9	12.6	11.5	14.2

Table 1. Comparison of  $\delta^{15}\text{N}$  values of mesopelagic organisms determined in this study and found in the literature. Samples in Terazaki *et al.* were from Sagami Bay, August 1983. Samples in Sugisaki and Tsuda were from the Western North Pacific and were probably also collected in the early 1980s. Values for the present study refer to samples from late May 1995.









# Feeding habits and diel vertical migration patterns of the three dominant myctophid fishes in the western subarctic and transitional Pacific

Masatoshi Moku, Hikaru Watanabe, Akinori Ohno\*, Kouichi Kawaguchi  
Ocean Research Institute, University of Tokyo  
\*Japan Marine Fishery Resource Center

e-mail: moku@ori.u-tokyo.ac.jp

This paper should not be cited without permission of authors.

## Introduction

Myctophid fishes are one of the most dominant fishes in mesopelagic zone and are composed of about 250 species belonging to the 30 genera in the world. It has been estimated that the biomass of mesopelagic fishes including myctophids may be more than 16 million tons in the western north Pacific (Gjøsaeter and Kawaguchi, 1980), suggesting their important role in the oceanic ecosystem. As the most of them take place diel vertical migration to feed on zooplankton, especially small crustaceans, they are thought to compete for preys with small pelagic fishes, like Japanese sardine, mackerel, and saury which migrate to Oyashio and transitional areas off northern Japan in summer, and play important roles as transporters of organic matter from surface to deep-sea system (Merret and Roe, 1974; Hopkins and Baird, 1977). Myctophid fishes are also major preys of larger sized fishes, like salmon, tunas and squids, marine mammals, and sea birds (Mead and Taylor, 1953; Percy et al., 1988).

Ecological informations of these fishes including diel vertical migration pattern and feeding habits have not been well documented in the western north Pacific compared with the eastern north Pacific mainly due to the lack of suitable sampling methods. This study aimed to examine the feeding habits of the 3 dominant myctophid species, *Diaphus theta*, *Stenobrachius leucopsarus* and *S. nannochir* were presented in relation to their diel vertical migration patterns based on the time series samples collected by big commercial otter trawl in the western subarctic and transitional Pacific.

## Materials and Methods

Samples were collected off northern Japan by the commercial trawler "Marusada-maru" chartered by Japan Marine Fishery Resource Center in August 1994, July 1995, and July 1996. Collections were made in 6 layers in the daytime and 8 layers at night from 20 to 700m at 14 stations.

Standard length, body weight, and wet weight of stomach contents were measured for 3 species. After the identification of stomach contents to higher taxa, and frequency of occurrence of each food item in the total stomachs examined (F), percentage of each food items in the total number of identifiable food items (Cn) and percentage of each food items in the total wet weight of identifiable food items (WW) were calculated as follows.

$$F(\%) = (\text{number of stomachs including each food item} / \text{total number of stomachs examined except for empty stomachs}) \times 100$$

$$Cn(\%) = (\text{total number of each food item} / \text{total number of items identified}) \times 100$$

$$WW(\%) = (\text{total wet weight of each food item} / \text{total wet weight of food items identified}) \times 100$$

Using the above 3 indices, index of relative importance (IRI) was calculated based upon the following equation:

$$IRI = (Cn + WW) \times F \text{ (Pinkas et al., 1971)}$$

which is represented by the area of a rectangle defined by plotting the three values on a three-way graph.

Stomach contents index (SCI) was calculated as follows.

$$SCI = (\text{wet weight of stomach contents} / \text{wet weight of fish body}) \times 100$$

The digestion state of food items was staged by the modified method of Percy et al. (1979) as

follows ; stage1 = fresh prey, not digested; stage2 = shape of prey preserved, but a part of appendages or carapace are separated; stage3 = shape of prey deformed, but identifiable to higher taxa.

Analyzing the above indexes, feeding rhythms of *D. theta*, *S. leucopsarus* and *S. nannochir* were studied and their feeding strategies were discussed.

## Results

**Species composition and vertical migration pattern :** A total of 1020 g myctophid fishes of the 23 species belonging to the 12 genera were captured in the 52 tows in 1995. Of the 23 species collected, the 3 species, *Diaphus theta* (migratory species), *Stenobranchius leucopsarus* (semi-migratory) and *Stenobranchius nannochir* (non-migratory) accounted for 52 % of the total catch in wet weight in 1995.

These fishes can be grouped into the 4 types based on vertical migration patterns; Type 1, migratory species; Type 2, most of population migratory, but a part of population sometimes remain in the daytime habitat at night; Type 3, the upper limit of depth distribution shifts to the shallower layer at night than daytime habitat; Type 4, non-migratory species.

**Feeding habits :** *D. theta*, which is typical vertical migrant, mainly fed on euphausiids, copepods and amphipods, and index of relative importance (IRI) of each food items were 4549, 9255 and 740 respectively. *S. leucopsarus* showed similar feeding habit to that of *D. theta*, although digestive condition of stomach content were different between migratory and non-migratory population at night as stated later. Their stomach contents were mainly composed of euphausiids, copepods and amphipods and IRI of each food item were 7832, 5555 and 866 respectively. Non-migratory *S. nannochir* mainly fed on copepods, and IRI of copepods was 14592, while total IRI value of the other food items was only 142. This suggest that diet of *S. nannochir* were different from those of *D. theta* and *S. leucopsarus*, although they depend on the variety of small crustaceans.

**Feeding rhythm :** A total of 415 stomachs of *D. theta* collected in 1994 and 1996 were analyzed to examine the feeding rhythm. SCI of *D. theta* changed from 1.2 to 2.7% on the average, and the percentage of empty stomachs was very low, less than 3% throughout 24 hours. To depict the feeding rhythm, digestion stage of euphausiids, copepods and amphipods in stomachs were examined in relation to sampling time. The percentage of fresh euphausiids at digestion stage1 was observed at higher frequency at 1300 (27.3%), and from 2100 to midnight (11.7 to 18.2%). The frequency of stage 1 copepods showed no change all through the day. The percentage of stage 1 of amphipods was relatively high (46.7 to 71.1%) when *D. theta* was in the upper 100m at night, but below 20.0% during the daytime. These results indicate that *D. theta* feeds on euphausiids, mainly composed of *Euphausia pacifica*, from dusk to midnight and also around the noon, copepods throughout 24 hours and amphipods at night.

A total of 506 stomachs of *S. leucopsarus* were analyzed. As a part of population sometimes remains in the daytime habitat at night, samples collected at night were separated into migrant and non-migrant, and separately analyzed. Stomach content index showed no remarkable change from 0.6 to 1.3% on the average and lower than *D. theta*. Percentage of empty of stomachs was 0 to 6% during the daytime, as observed in *D. theta*. Stomach content index values of migratory population were 1.0 to 1.4% at night, and percentage of empty stomach was 0 to 2%, but SCI of non-migratory population collected below 400m depth at night was 0.6% and significantly lower than those of migratory population. Their percentage of empty stomach was 21.4% and significantly higher than those of migratory one. Fresh euphausiids at digestion stage 1 showed higher percentage of 12.5 to 23.3% from dusk to midnight than in the daytime (0 to 11.8%). Similar tendencies were also observed on copepods and amphipods. The percentage of stage 1 of each food items of non-migratory individuals were very low compared with those of migratory population, 12.5% vs. 23.3% for euphausiids, 6.5% vs. 26.6% for copepods and 0% vs. 72.2% for amphipods. These results suggest that vertical migratory population of *S. leucopsarus* had a clear diel feeding rhythm for euphausiids, copepods and amphipods, and the feeding activity was high from dusk to midnight, and non-migratory population of *S. leucopsarus* had low feeding activity at night.

A total of 365 stomachs of non-migratory *S. nannochir* were analyzed. They showed

no remarkable diel change in the feeding activities. Stomach content index showed no diel change, but was much lower compared with the two migratory species (0.07 ~ 0.14% vs. 1.2 ~ 2.7% in *D. theta*; 0.75 ~ 1.4% in *S. leucopsarus*). The percentage of fresh copepods at digestion stage I did not show a conspicuous change throughout 24 hours. Frequency occurrence of the empty stomach was very high compared with the other two migratory species (11.5 ~ 44.0% vs. 0 ~ 2.9% in *D. theta*; 0 ~ 6.0% in *S. leucopsarus*).

### Discussion

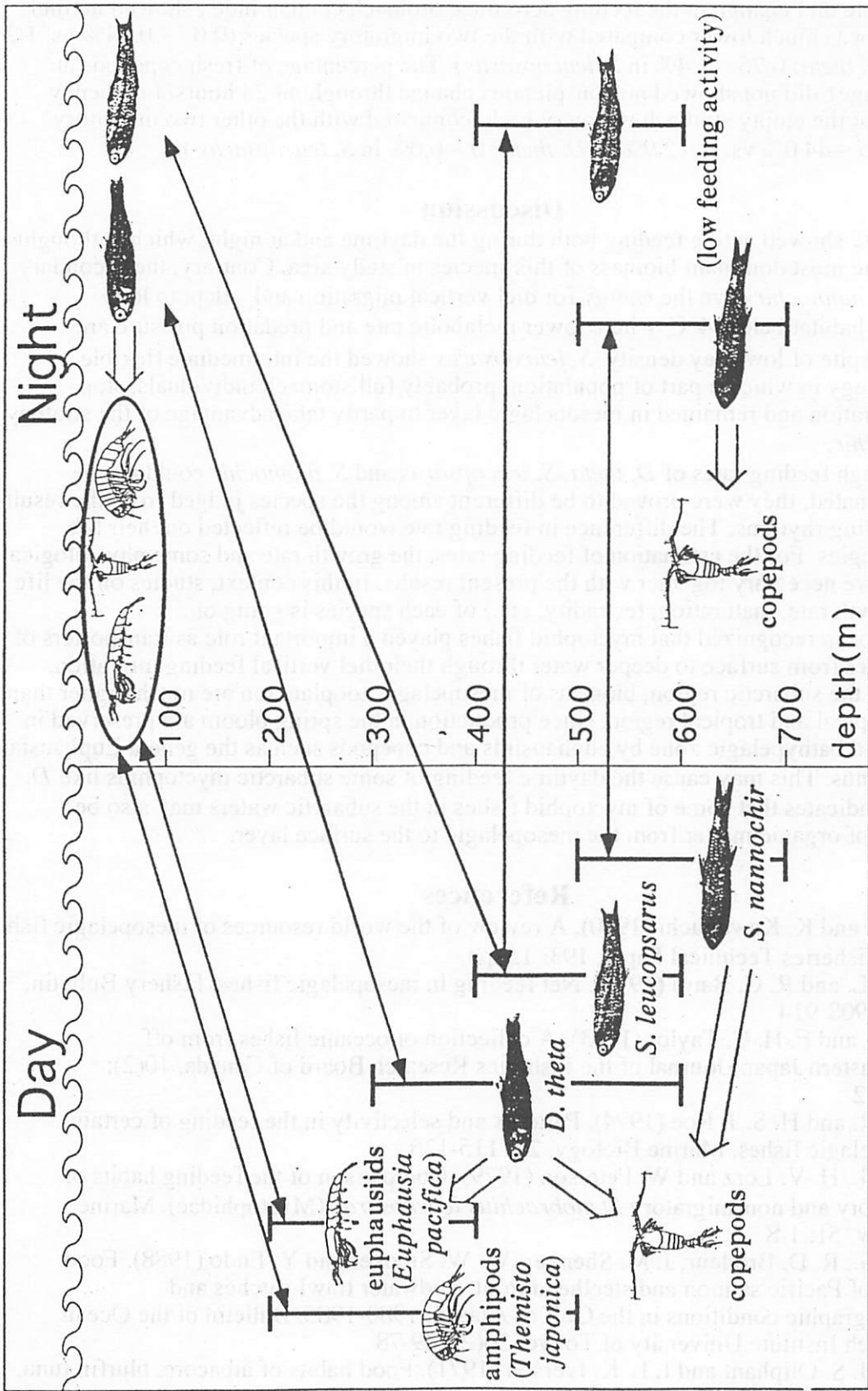
*D. theta* showed active feeding both during the daytime and at night, which is thought to support the most dominant biomass of this species in study area. Contrary, the secondary dominant *S. nannochir* save the energy for diel vertical migration and adapt to low temperature habitat below 4°C where lower metabolic rate and predation pressure are expected in spite of low prey density. *S. leucopsarus* showed the intermediate flexible feeding strategy in which a part of population, probably full stomach individuals, stop vertical migration and remained in mesopelagic layer to partly take advantage of the strategy of *S. nannochir*.

Although feeding rates of *D. theta*, *S. leucopsarus* and *S. nannochir* could not be directly estimated, they were proved to be different among the species judged from the results on their feeding rhythms. The difference in feeding rate would be reflected on their life history strategies. For the estimation of feeding rates, the growth rate and some physiological parameters are necessary together with the present results. In this context, studies on the life history (growth rate, maturation, fecundity, etc.) of each species is going on.

It has been recognized that myctophid fishes played an important role as transporters of organic matter from surface to deeper water through their diel vertical feeding migration. However, in the subarctic region, biomass of mesopelagic zooplankton are much higher than in the subtropical and tropical region, since production in the spring bloom are preserved in the meso- and bathypelagic zone by euphausiids and copepods such as the genera *Euphausia* and *Neocalanus*. This may cause the daytime feeding of some subarctic myctophids like *D. theta*. This indicates that some of myctophid fishes in the subarctic waters may also be transporters of organic matter from the mesopelagic to the surface layer.

### References

- Gjøsaeter, J. and K. Kawaguchi (1980). A review of the world resources of mesopelagic fish. FAO Fisheries Technical Paper, 193: 151pp.
- Hopkins, T. L. and R. C. Baird (1975). Net feeding in mesopelagic fishes. *Fishery Bulletin*, 73(4): 908-914
- Mead, G. W. and F. H. C. Taylor (1953). A collection of oceanic fishes from off northeastern Japan. *Journal of the Fisheries Research Board of Canada*, 10(2): 560-582
- Merrett, N. R. and H. S. J. Roe (1974). Patterns and selectivity in the feeding of certain mesopelagic fishes. *Marine Biology*, 28: 115-126
- Pearcy, W. G., H. V. Lorz and W. Peterson (1979). Comparison of the feeding habits of migratory and non-migratory *Stenobrachius leucopsarus* (Myctophidae). *Marine Biology*, 51: 1-8
- Pearcy, W. G., R. D. Brodeur, J. M. Shenker, W. W. Smoker and Y. Endo (1988). Food habits of Pacific salmon and steelhead trout, midwater trawl catches and oceanographic conditions in the Gulf of Alaska, 1980-1985. *Bulletin of the Ocean Research Institute University of Tokyo*, 26(2): 29-78
- Pinkas, L., M. S. Oliphant and I. L. K. Iverson (1971). Food habits of albacore, blurfin tuna, and bonito in California waters. *Fish Bulletin*, 152: 1-105



The relationship between vertical distribution of main zooplankton and the three myctophid fishes.

**Stomach contents of Dall's porpoises in the North Pacific  
Ocean.**

Hiroshi Ohizumi<sup>1</sup>, Toshiaki Kuramochi<sup>2</sup> and Nobuyuki  
Miyazaki<sup>1</sup>

<sup>1</sup>Otsuchi Marine Research Center, Ocean Research Institute,  
The University of Tokyo. 2-106-1, Akahama, Otsuchi, Iwate  
028-11, Japan.

<sup>2</sup>Department of Zoology, the National Science Museum. 3-23-  
1, Hyakunincho, Shinjuku, Tokyo, 169 Japan.

E-mail: oizumi@wakame.ori.u-tokyo.ac.jp, for H. Ohizumi  
kuramoti@kahaku.go.jp, for T. Kuramochi  
miyazaki@wakame.ori.u-tokyo.ac.jp, for N. Miyazaki

**Introduction**

Dall's porpoises are distributed in a wide range of the northern North Pacific and adjacent waters. Their total population was estimated as over ~~200~~ million, and they are thought to be one of the most numerous species among dolphins and porpoises that are distributed in borealic zone in the North Pacific. Major preys of Dall's porpoises vary among populations and local habitats. Mizue and Yoshida (1965) and Mizue et al. (1966) noted that squids were main prey around the Aleutian Islands. Crawford (1981) reported that gonatid squids were major prey followed by myctophid fishes which were mainly *Protomyctophum thompsoni* around the Aleutian Islands. Kuramochi et al. (1993) reported from the Bering Sea that they fed on many

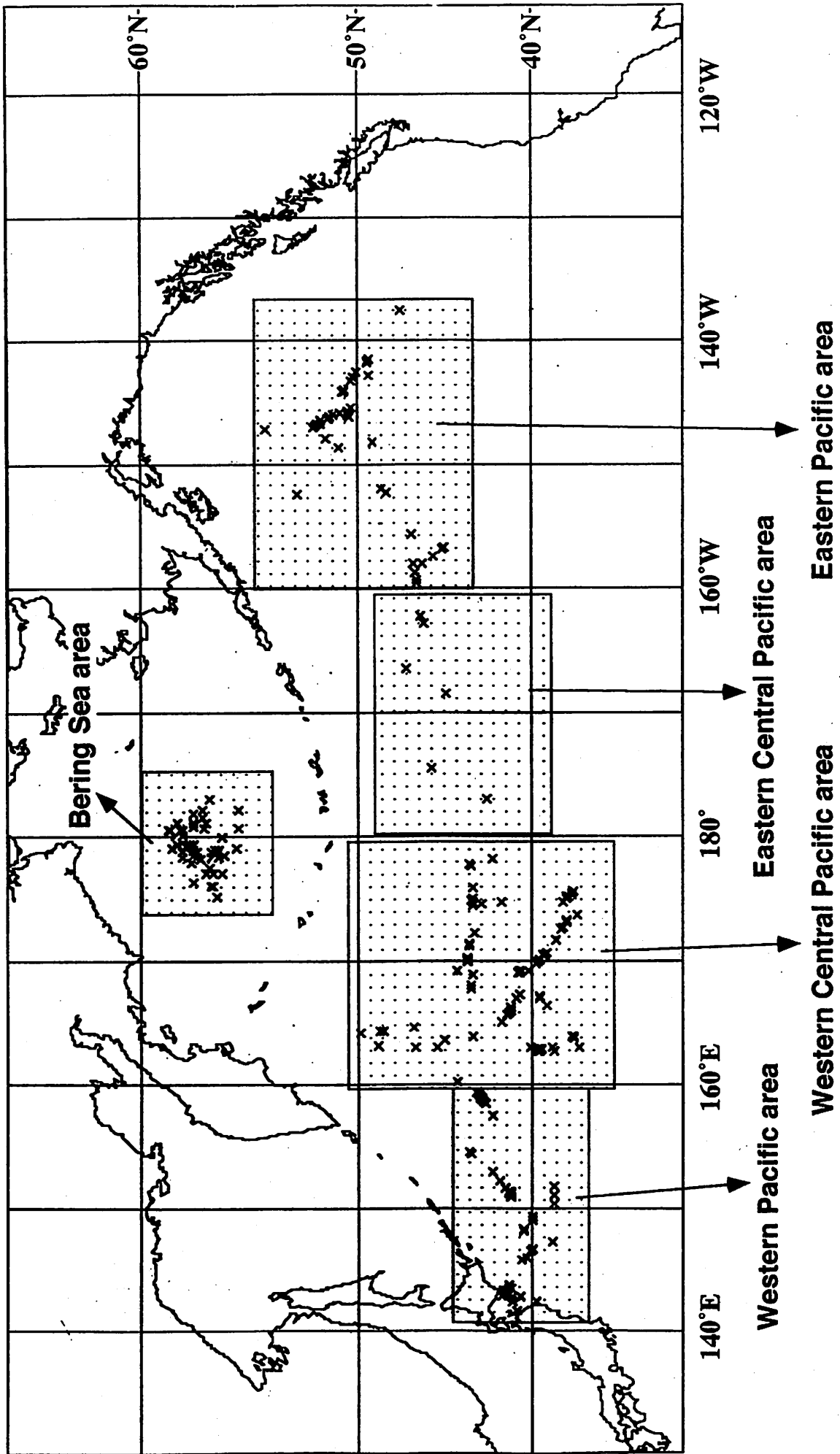


Fig. 1 Sampling locations of Dall's porpoises during 1984 to 1988

incidentally by drift gill nets, and hunted under scientific survey cruises. In the Sea of Japan and Sea of Okhotsk, six sampling surveys were conducted on board the vessels of hand harpoon fishery operated in coastal waters around Hokkaido during 1988 to 1996. Fore stomach contents were sorted into taxonomic groups by referring to the senior author's otolith collection, lower beak collection of the National Science Museum, and Clarke (1986).

For the samples taken in the Sea of Okhotsk and Sea of Japan, body weights of each prey species were estimated from otolith lengths or standard length for fishes; lower rostral lengths or dorsal mantle length for squids. These estimated weights were converted into calorific value.

Five geographical areas in the Pacific were set in order to examine prey variation (Fig.1). The North Pacific was divided into four areas at each about 20° longitudinal lines from 140°E to 140°W. These four areas were named as the Western Pacific area, the Western Central Pacific area, the Eastern Central Pacific area, and the Eastern Pacific area. In addition, the Bering Sea area was defined as fifth area. The latitudinal widths were different among areas, and the Western Central Pacific area was covered widest latitudinal area. Latitudinal prey variation was examined in this area. Calorific contributions were not analyzed for the samples taken in the Pacific and the Bering Sea. We did not examine all stomach specimens for the squids prey in the Pacific and in the Bering Sea, and these are preliminary results.

composition of squid preys was diversified, and most of the Dall's porpoises became to feed on squids. *Berryteuthis magister* was the most predominant calorific contributor among squids (43% and 70% in 1994 and 1995, respectively) followed by *Gonatus* species (Table 1B).

Japanese pilchards were not important prey item also in the Sea of Japan in the mid 1990's. Walleye pollocks were main calory resources in 1995, which occupied 81% of total calory from fishes. In 1996, walleye pollock's calorific contribution decreased to 55% and fish prey items were diversified (Table 2A). Squid prey items varied among years in the Sea of Japan. Japanese common squid (*Todarodes pacificus*) was predominant species for calorific contribution from squids in 1995, and *B. magister* was the main prey squid in 1996 (51% and 42%, respectively) (Table 2B).

The population of Japanese pilchards around Japan believed to have decreased drastically after 1989 (Watanabe 1995), and there were little yields in Hokkaido in the mid 1990's. The prey shift from Japanese pilchards to walleye pollock, Japanese anchovies and *B. magister* may reflect this population decline of Japanese pilchards.

#### *Geographical variation of prey in the Pacific*

Fish prey items were dominated by myctophid fishes in all areas for numerical contribution (Table 3).

*Notoscopelus japonicus* was the most dominant species which occupied 32% of contribution followed by *Diaphus theta* (20%) and *Protomyctophum thompsoni* (14%) in the Western



correlation between net sampling results and stomach contents results (Kendall's  $\tau$  test; Alaska Gyre:  $\tau=0.6$ ,  $P=0.09$ ; Western Transition Zone:  $\tau=0.333$ ,  $P=0.5$ ; Bering Sea  $\tau=0.2$ ,  $P=0.62$ ). These statistical results seemed to be caused by discrepancy in lower ranked fishes.

In the area of Western Central Pacific, latitudinal variation of prey fishes was found. *Bathylagus ochotensis*, *Electrona rissoi*, *Ceratoscopelus warmingi* and *Ichthyococcus* sp. (probably *I. elongatus*) occupied large portion of numeric contribution as food in 36°N-37°N. These fishes except for *Ichthyococcus* sp. were reduced their contribution in higher latitudinal areas, and cold water species such as *D. theta*, *Lampanyctus jordani*, *P. thompsoni*, *S. leucopsarus* and *Symbolophorus californiensis* increased (Fig 3). These variations probably reflected geographical distribution of prey species.

Although the results taken by net sampling was not always consistent with results obtained by stomach content analyses, Dall's porpoises seemed to feed on abundant fishes in the local habitat in the North Pacific and the Bering Sea. Many fish species found in the stomach were mesopelagic fishes, but most of them are thought to migrate to the shallower waters during the night (Moku et al. presented to PICES this meeting). *Protomyctophum thompsoni* is an exception. This species does not migrate to the surface and inhabits 300-400m layer in both day and night (Moku et al. presented to PICES this meeting). Because there were rare example of fresh fishes in the stomach taken in the daylight hours, most of the fish prey was

Major prey squids such as *G. borealis* and *G. onyx* migrate to the surface at night, and *O. borealijaponica* is surface resident. Same as the case of fish prey, Dall's porpoises seemed to feed on squids at night when squids were distributed in the surface layer.

In the Pacific, numbers of prey squids per one porpoise varied from 2.7 in the Western Pacific to 22.7 in the Eastern Central Pacific. These are lower than 61.6 in the Bering Sea. On the other hand, number of prey fishes per one porpoise in the Bering Sea was 32.2, while those varied from 65.2 in the Western Pacific to 201 in the Eastern Pacific. Number of squids per one porpoise in the Sea of Japan and Sea of Okhotsk in the mid 1990's varied from 96.7 to 127.9. Dall's porpoises in marginal adjacent waters of the Pacific fed on many squids as well as fishes, but in the Pacific, they fed mainly on fishes.

#### References

- Clarke, M. R. ed. (1986) A handbook for the identification of cephalopod beaks. Clarendon Press, pp 273.
- Crawford, T. W. (1981) Vertebrate prey of *Phocoenoides dalli*, (Dall's porpoise), associated with the Japanese high seas salmon fishery in the North Pacific Ocean. Ph. D. thesis University of Washington. pp 72.
- Kuramochi, T., T. Kubodera and N. Miyazaki (1993) Squids eaten by Dall's porpoises, *Phocoenoides dalli* in the northwestern North Pacific and in the Bering Sea. in T. Okutani, R. K. O'Dor, and T. Kubodera (eds.) Recent

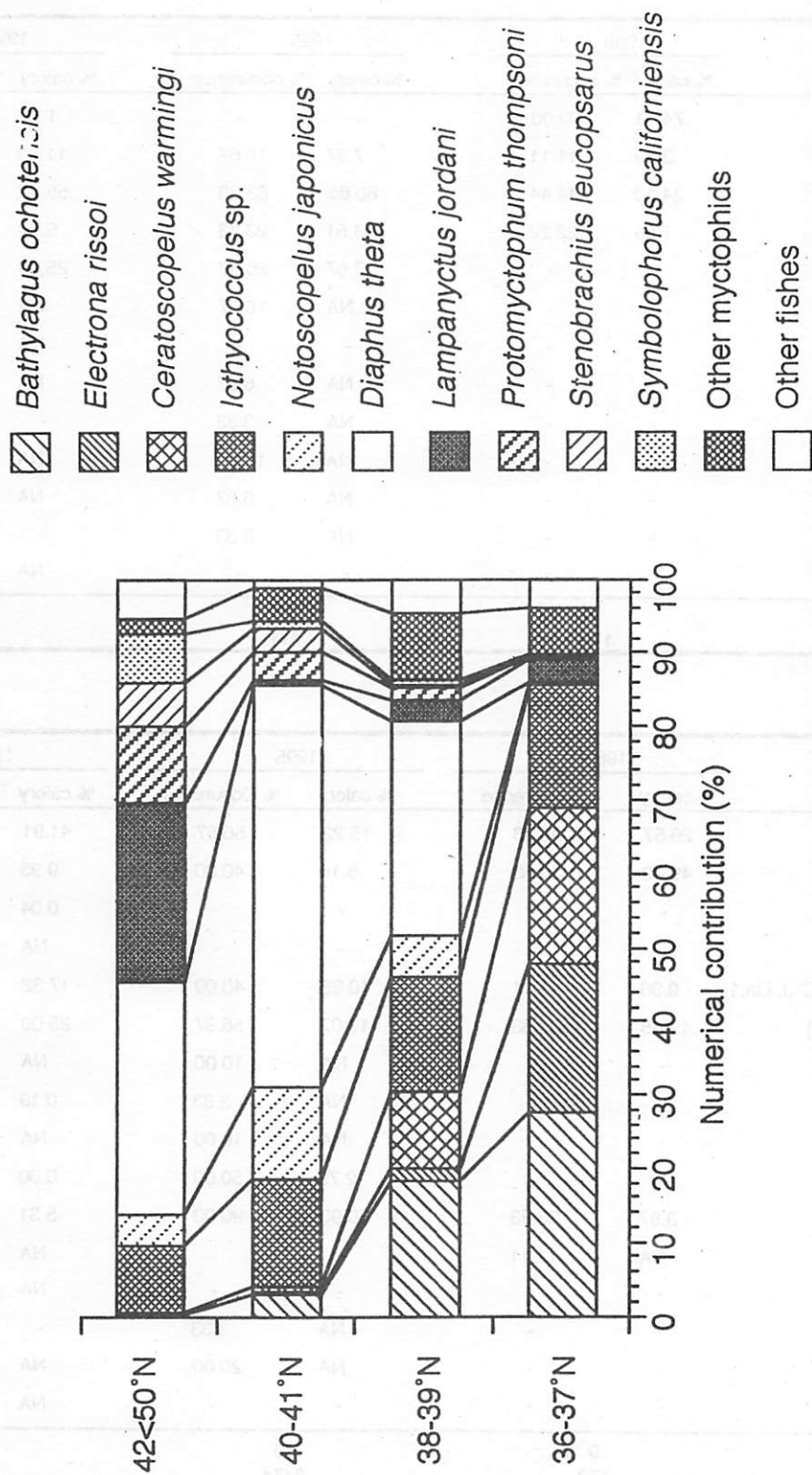


Fig. 3 Latitudinal variation of prey fishes in the Western Central Pacific area (160-180°E)

Table 2. Variation of the prey items in the Sea of Japan

(A) Fishes

Prey fishes	1989		1995		1996	
	% calory	% occurrence	% calory	% occurrence	% calory	% occurrence
<i>Sardinops melanostictus</i>	74.11	100.00	-	-	1.20	13.33
<i>Engraulis japonicus</i>	0.19	11.11	7.97	16.67	11.60	53.33
<i>Theragra chalcogramma</i>	24.10	44.44	80.85	83.33	55.42	66.67
<i>Ammodytes personatus</i>	1.59	22.22	3.51	23.33	5.78	16.67
<i>Pleurogrammus azonus</i>	-	-	7.67	26.67	25.99	46.67
<i>Maurolicus muelleri</i>	-	-	NA	16.67	NA	30.00
Pleuronectidae sp.	-	-	-	-	NA	3.33
Zoarcidae sp.	-	-	NA	6.67	NA	3.33
Type 82	-	-	NA	3.33	-	-
Type 85	-	-	NA	10.00	NA	10.00
Type 86	-	-	NA	6.67	NA	23.33
Type 87	-	-	NA	3.33	-	-
Type 96	-	-	-	-	NA	3.33
Number of porpoises	9		30		30	
Number of fishes	177		711		1483	

(B) Squids

Prey squids	1989		1995		1996	
	% calory	% Occurrence	% calory	% Occurrence	% calory	% Occurrence
<i>Beryteuthis magister</i>	26.57	33.33	15.22	56.67	41.91	46.67
<i>Gonatus middendorffi</i>	49.03	33.33	8.14	40.00	9.93	53.33
<i>Gonatus onyx</i>	-	-	-	-	0.04	3.33
<i>Gonatus berryi</i>	-	-	-	-	NA	6.67
Unidentified <i>Gonatus</i> sp. (G-C'-J, Un.1)	0.96	11.11	10.93	40.00	17.32	50.00
<i>Gonatus</i> spp. juvenile (G-A-1)	19.48	33.33	12.07	56.67	25.00	76.67
<i>Gonatus</i> spp.	-	-	NA	10.00	NA	3.33
<i>Gonatopsis borealis</i>	-	-	NA	3.33	0.19	3.33
<i>Enoploteuthis chuni</i>	-	-	NA	10.00	NA	3.33
<i>Watasenia scintillans</i>	-	-	2.75	50.00	0.30	40.00
<i>Todarodes pacificus</i>	3.97	33.33	50.90	90.00	5.31	53.33
<i>Loligo japonica</i>	NA	11.11	-	-	NA	23.33
<i>Loligo bleekeri</i>	-	-	-	-	NA	6.67
<i>Rossia pacifica</i>	-	-	NA	3.33	-	-
<i>Euprymna morsei</i>	-	-	NA	20.00	NA	13.33
Octopoda sp.	-	-	-	-	NA	6.67
Number of porpoises	9		30		30	
Number of squids	172		3474		2902	

NA: Not available

Table 4 Numerical contribution by squids in the Pacific and Bering Sea

Prey squids	Western Pacific	Western Central Pacific	Eastern Central Pacific	Eastern Pacific	Bering Sea
<i>Gonatopsis borealis</i>	10.42	32.68	44.65	44.97	22.43
<i>Beryteuthis magister</i>	-	0.65	-	0.22	-
<i>Beryteuthis anonycus</i>	-	-	27.67	7.61	34.75
<i>Gonatus onyx</i> (including small type)	37.50	33.99	3.14	21.25	30.59
<i>Gonatus berryi</i>	4.17	2.61	0.63	1.34	1.09
<i>Gonatus middendorffi</i>	-	-	-	0.22	0.71
<i>Gonatus madokai</i>	-	-	-	0.22	0.33
<i>Gonatus pyros?</i>	10.42	1.96	-	0.22	0.94
<i>Gonatus</i> spp. juvenile (G-A-1)	6.25	0.65	3.14	3.80	5.85
<i>Gonatus</i> sp. (G-C)	-	-	-	-	1.75
<i>Enoploteuthis chuni</i>	6.25	-	-	-	-
<i>Watacena scintillans</i>	12.50	-	-	-	-
<i>Abraliopsis</i> sp. ( <i>A. felis?</i> )	-	11.11	4.40	0.22	-
<i>Galliteuthis</i> sp.	2.08	-	-	0.67	0.42
<i>Taonius pavo</i>	2.08	1.31	4.40	6.04	1.13
Cranchiidae sp.	-	0.65	-	0.22	-
<i>Onychoteuthis borealijaponica</i>	8.33	13.73	10.06	11.86	-
Octopoteuthidae sp.	-	-	1.26	0.22	-
Unknown total	-	0.65	0.63	0.89	-
Number of porpoises	18	28	7	38	36
Number of squids	48	153	159	447	2118

Unit: Percent

# Distribution and stomach contents of *Maurolicus muelleri* in the Japan Sea (East Sea)

Seiji OHSHIMO

(Seikai National Fisheries Research Institute, 49 Kokubu-machi Nagasaki, 850, Japan)

E-mail: oshimo@snf.affrc.go.jp

## Abstract

The mesopelagic fish *Maurolicus muelleri* is a key species acting as a trophic link between zooplankton and higher carnivorous fishes and mammals in the Japan Sea. In the present study, the distribution pattern and density of this mesopelagic fish was estimated using a quantitative echo sounder (Furuno, FQ-70; 50kHz), and the stomach contents and stomach weight were measured in the early summer of 1993, 1994 and 1995. *M. muelleri* was distributed in the waters off the shelf edge, and its horizontal distribution was restricted by the cold water masses. In addition, *M. muelleri* was distributed above the Japan Sea Proper Waters. The density of the mesopelagic fish in the distribution area was estimated to be about 30 tons/km<sup>2</sup> using TS=-58.9dB/individual and body weight estimated as 1.2 g. Most of the stomach contents of *M. muelleri* were zooplankton (Euphausia, Copepoda and Cladocera) and fish larvae. The somatic stomach index (stomach weight / body weight) at immediately after sunset was higher than that during the daytime or at nighttime, and a single *M. muelleri* consumed at least 0.02g of zooplankton over a 24 hour period.

## Introduction

The Japan Sea is surrounded by Russia, North Korea, South Korea and Japan and is about 130 km<sup>2</sup> in area. Fisheries catches are at a very high level, especially the mackerels, jack mackerel and tunas are caught by the large powered purse seine nets in the western part of the Japan Sea. These middle or large pelagic carnivorous fishes feed on the small pelagic fish and micronekton. The dominant micronekton species in the Japan Sea is *Maurolicus muelleri*, however the other micronekton, such as Myctophidae, are not present (Nishimura, 1959; Okiyama, 1971). Okiyama (1981) reported 3.3 x 10<sup>6</sup> metric tons of *M. muelleri* in the Japan Sea.

*M. muelleri* is known to be distributed off the shelf edge (Okiyama, 1971), and their biomass is huge. *M. muelleri* feed on zooplankton (Ikeda et al., 1994), and is fed a by upon larger fishes, mammals, sea birds and squids (Nishimura, 1959). Therefore, *M. muelleri* is a key species in the midwater layer in the Japan Sea. However, there are few reports of the quantitative assessment of *M. muelleri* (Hamano, 1993).

In the present study, the density and distribution pattern of *M. muelleri* was investigated using a quantitative echo sounder, and also the consumption quantity of zooplankton for *M. muelleri* was estimated by the stomach weight and contents.

## Methods

Acoustic surveys were conducted using an echo sounder (Furuno FQ-70; frequency 50 kHz) in the western area off Kyushu and western part of the Japan Sea in the early summer of 1993, 1994 and 1995 (Fig. 1). The research vessel (Yoko-maru, 499 tons) surveyed along parallel transect lines at about 10 knots, and automatically logged SV (spontaneous back-scattering volume) data on a floppy disk for each 0.5 nautical miles. The water temperature and salinity were observed by CTD (Niel Brown MK3B).

Fishing was directed at the pelagic layer by a midwater trawl net with a 60 mm cod end, and a 20 mm cover net. The trawling sets were made at 20 sites. In order to monitor net conditions, Scanmar transducers (Scanmar catch control system) were mounted on both sides of the net as well as at the top and bottom near the net mouth. Also, a Furuno FNR-200 II net recorder was mounted on the top of the net mouth for monitoring the net depth. The midwater trawl net was towed for times ranging from 30 to 110 minutes. The warp length of the trawl net and towing speed were target in order to adjust the net opening at the

strata of fish schools. The towing speed ranged from 2 to 3 knots during the trawl surveys.

The samples caught were sorted on board by species, and part of the sample was immediately frozen or fixed by 10 % formaldehyde. *M. muelleri* was measured for standard length (mm), body weight (g) and stomach weight (g) (from the pharyngeal to the cardiac orifice). The somatic stomach index (SSI) was calculate as follows;

$$\text{SSI} = \text{stomach weight} \times 100 / \text{body weight.}$$

After the measurements, the stomach contents were placed in small petri-dishes and dispersed in a small amount of water. The stomach contents were observed, the prey species and the degree of digestion were examined under a dissecting microscope, and were weighed.

## Results

### 1) Midwater trawling catches and biological characters of *M. muelleri*

Midwater trawlings were executed at 20 sites. *M. muelleri* was caught at 6 sites in the Japan Sea, and most of this catch was *M. muelleri*. *M. muelleri* was also caught in the western area off Kyushu, but the quantity was very small (< 0.1 kg). The other fish species caught were anchovy (*Engraulis japonicus*), sardine (*Sardinops melanostictus*), jack mackerel (*Trachurus japonicus*) and others (Table 1).

The sampled *M. muelleri* was about 41 mm in standard length and 1.2 g in body weight (Table 2). The SSI changed over a 24 hour period (ANOVA,  $F(2,59)=4.478$ ,  $p=0.0155$ ), and the SSI in the twilight time was higher than that in the daytime and nighttime (Fisher's PLSD test,  $p=0.0052$ ) (Fig. 2). The weight of stomach contents were estimated as at least 0.02 g (range: empty to 0.09 g) in wet weight over a day. The stomach contents of *M. muelleri* comprised zooplankton (Euphausia, Copepoda and Cladocera) and fish larvae. The contents in the stomach at the twilight was fresh (Fig. 3A), but the contents in the daytime was digested (Fig. 3B).

### 2) Distribution pattern and density of *M. muelleri*

All of the results from midwater trawling of *M. muelleri* was dense echogram (Fig. 4) in the midwater layer (surface to 150m depth layer). In this study, the dense echogram was assumed to be *M. muelleri*. *M. muelleri* was distributed in the eastern area off Tsushima Island, and particularly distributed off the shelf edge (Fig. 5). *M. muelleri* was observed on the continental shelf (< 200 m depth). *M. muelleri* was restricted by the cold water mass at 150 m depth. The school of *M. muelleri* was rapidly diffused and moved to the surface layer after sunset. *M. muelleri* was distributed above the Japan Sea Proper Waters as a result of low temperature and salinity. This distribution pattern was similar to that reported by Noda and Moriwaki (1996).

Target strength (TS: dB/individual) of *M. muelleri* is was quoted from Hamano (1993) as follows;

$$\text{TS} = 17.4 \log \text{BL} - 69.6$$

where BL is standard length (cm). As results of the biological characteristics of *M. muelleri*, TS was assumed to be -58.9 dB/individual using 4.1 cm as standard length. The density (D: indiv./m<sup>3</sup>) of *M. muelleri* was calculated as follows;

$$D = V \times 10^{((\text{SV} - \text{TS})/10)}$$

where V is water volume of integration interval (0.5 n.m. x 1852 m x 190 m).

The density of *M. muelleri* in the distributed area was about 30 g/m<sup>3</sup> (=25 indiv./m<sup>3</sup>) using 1.2 g as estimated body weight (Table 3).

## Discussion

### 1) Problems

It is well known that the micronekton in the ocean is a very high quantity, and play an important role in circulation of materials between the surface and deep layers by their vertical migration. However, their stock size assessment is difficult, because there are no data from fisheries catch. In the present study, the density of *M. muelleri* as dominant micronekton in the Japan Sea was estimated using a quantitative echo sounder.

The density of *M. muelleri* is estimated using a quantitative echo sounder around the Oki island (Hamano, 1993) in the Japan Sea, in waters off Norway (Gjøsæter, 1978), and the

Red Sea (Armstrong and Prosch, 1991). Hamano (1993) and Gjøsaeter (1978) estimated the density as 30.9 g/m<sup>2</sup> and 10-35 g/m<sup>2</sup> in the Japan Sea and waters off Norway, respectively. However, Armstrong and Prosch (1991) estimated the density as ranging from 4 to 10 g/m<sup>2</sup>. In addition, the density of *M. muelleri* was estimated by egg surveys, and the density ranged from 26 to 56 fish/m<sup>2</sup> in a fjord off Norway (Lopes, 1979). The estimation of density in the present study was about 30 g/m<sup>2</sup> (=25 indiv./m<sup>2</sup>), so this estimation and other estimations are comparable. However, there are several problems in the present study for estimating the density of *M. muelleri*.

TS of *M. muelleri* in the present study used a regression from Hamano (1993), but his regression was calculated using a frequency of 88 kHz. Therefore, it is possible that TS of my estimation (50 kHz) might differ from his regression. Next problem was diel vertical migration of *M. muelleri*. In the daytime, *M. muelleri* shoaled densely in the midwater layer, but diffused and moved to the surface layer after sunset in the present study. The density of *M. muelleri* decreased at night (Uchida et al., 1992; Hamano, 1993). This diel distribution pattern could affect biomass estimation of *M. muelleri*. In this study, the density was selected the area of high intensity and calculated using only daytime data.

## 2) Plankton consumption by *M. muelleri*

In the present study, the density of *M. muelleri* was estimated to be about 30 g/m<sup>2</sup> (25 indiv./m<sup>2</sup>). *M. muelleri* fed on zooplankton (Euphausia, Copepoda and Cladocera) and fish larvae totalling at least 0.02 g (range: empty to 0.09 g) over a 24 hour period. The SSI after sunset was significantly higher than that in the daytime and nighttime (Fisher's PLSD test). This results suggest that *M. muelleri* fed on zooplankton during diffusion and moving to the upper layer. There are reports of the time of feeding of *M. muelleri*, but it is not clear whether *M. muelleri* is nocturnal (Ikeda et al., 1994; Young and Blaber, 1986; Rasmussen and Giske, 1994) or opportunistic (Dalpadado and Gjøsaeter, 1987). In the present study, the degree of digestion in the stomach in the nighttime and daytime was more than that in the twilight time.

On the other hand, the secondary production of zooplankton in the Japan Sea ranged from 120 to 160 g/m<sup>2</sup>/year (Morioka, 1980). The life-span of *M. muelleri* is about 20-22 months (Yuuki, 1984), and two types were found as spring brood and autumn brood (Yuuki, 1984). In the present study, most of *M. muelleri* were 1 year-old adult fish of the spring brood (Yuuki, 1984). Maturing time of *M. muelleri* of the spring brood was 8 months (Yuuki, 1984), and all adults died after spawning. Then, the consumption quantity (Q g/m<sup>2</sup>) of zooplankton for *M. muelleri* was calculated as follows;

$$Q = S \times D \times 240 \text{ days}$$

where S is stomach contents weight (present value = 0.02 g), and D is density of *M. muelleri* (25 indiv./m<sup>2</sup>). The calculated Q is 120 g/m<sup>2</sup>/240 days. This value is nearly equal to the secondary production of zooplankton in the Japan Sea (Morioka, 1980). Therefore, most of the secondary production of zooplankton was consumed by *M. muelleri* in the Japan Sea. However, the density of the *M. muelleri*, might decrease with natural mortality, thus the consumption quantity of zooplankton might be overestimated. In addition, the Q should be estimated over the whole distribution area of *M. muelleri*, and the Q would be more accurate the understanding of the distribution and density of *M. muelleri* in the Japan Sea. The secondary production of zooplankton in the Japan Sea should be also assessed in the near future.

## References

- Armstrong, M. J. and Prosch, R. M. (1991) Abundance and distribution of the mesopelagic fish *Maurollicus muelleri* in the southern Benguela system. *S. Afr. J. Mar. Sci.*, 10, 13-28.
- Dalpadado, P. and Gjøsaeter, J. (1987) Observations on mesopelagic fish from the Red Sea. *Mar. Biol.*, 96, 173-183.
- Gjøsaeter, J. (1978) Resource study of mesopelagic fish. PhD thesis. University of Bergen, Bergen, p 203.
- Hamano, A. (1993) Studies on the acoustic method for estimating biomass of micronektonic



- fish. *J. Shimonoseki Univ. Fish.*, **41**, 85-165 (in Japanese with English abstract).
- Ikeda, T., Hirakawa, K. and Kajihara, N. (1994) Diet composition and prey size of the mesopelagic fish *Maurollicus muelleri* (Sternoptycidae) in the Japan Sea. *Bull. Plankton Soc. Japan*, **41**, 105-116.
- Lopes, P. C. (1979) Eggs and larvae of *Maurollicus muelleri* (Gonostomatidae) and other fish eggs and larvae from two fjords in western Norway. *Sarsia*, **64**, 199-210.
- Morioka, Y. (1980) Nihonkai no doubutsu plankton. *Kaiyo Kagaku*, **12**, 646-653 (in Japanese).
- Nishimura, S. (1959) Observations on the spawning and the early life history of the pearlsides in the adjacent waters to Noto peninsula in the Japan Sea. *Ann. Rept. Jap. Sea Reg. Fish. Res. Lab.*, **5**, 61-75 (in Japanese with English abstract).
- Noda, K. and Moriwaki, S. (1996) Acoustic survey of distribution and abundance of micronektonic fish, *Maurollicus muelleri*, in the southwestern Japan Sea. *Bull. Jap. Soc. Fish. Oceanog.*, **60**, 1-6 (in Japanese with English abstract).
- Okiyama, M. (1971) Early life history of the Gonostomatid fish, *Maurollicus muelleri* (GMELIN), in the Japan Sea. *Bull. Jap. Sea Reg. Fish. Res. Lab.*, **23**, 21-53 (in Japanese with English abstract).
- Okiyama, M. (1981) Abundance and distribution of eggs and larvae of a Sternoptychid fish, *Maurollicus muelleri*, in the Japan Sea, with comments on the strategy for successful larval life. *Rapp. P.-v. Réun. Cons. int. Explor. Mer.*, **178**, 246-247.
- Rasmussen, O. I. and Giske, J. (1994) Life-history parameters and vertical distribution of *Maurollicus muelleri* in Masfjorden in summer. *Mar. Biol.*, **120**, 649-664.
- Uchida, K., Hamano, A., Takeda, Y. and Tatsumi, S. (1992) The daily rhythmic change in the distribution of *Maurollicus muelleri*, off Oki islands in the Japan Sea, measured by using the 88 kHz quantitative echo sounder. *J. Shimonoseki Univ. Fish.*, **40**, 163-172 (in Japanese with English abstract).
- Young, J. W. and Blaber, S. J. M. (1986) Feeding ecology of three species of midwater fishes associated with the continental slope of eastern Tasmania, Australia. *Mar. Biol.*, **93**, 147-156.
- Yuuki, Y. (1984) Age and growth of Sternoptychid fish *Maurollicus muelleri* in the south western waters of the Sea of Japan. *Bull. Jap. Soc. Sci. Fish.*, **50**, 1849-1854 (in Japanese with English abstract).

Table 1 Total catches from midwater trawl

Site	Date	Towing Time (min)	Towing Layer (m)	Total Catch	Anchovy	Sardine	Round Herring	Jack Mackerel	<i>M. Muelleri</i>	Others
1	1993/Jun. 6	30	?	0.3	0.0	0.0	0.0	0.0	0.3	0.0
2	1993/Jun. 7	30	?	84.4	38.1	0.0	0.4	42.2	0.0	3.7
3	1994/May 17	52	80-90	0.1	0.0	0.0	0.0	0.0	0.1	0.0
4	1994/May 17	66	20-30	3.2	0.0	0.0	0.0	0.0	3.2	0.0
5	1994/May 18	43	30-40	0.0	0.0	0.0	0.0	0.0	0.0	0.0
6	1994/May 18	110	10-20	0.1	0.0	0.0	0.0	0.0	0.1	0.0
7	1994/May 18			0.0	?	?	0.0	0.0	0.0	0.0
8	1994/May 20	80	45-65	7.5	6.0	0.0	0.0	0.0	0.0	1.5
9	1994/May 21	44	10-30	42.5	27.0	6.8	0.0	0.1	0.0	8.6
10	1994/May 21	40	20-40	16.0	6.6	8.9	0.0	0.1	0.0	0.4
11	1994/May 22	65	10-30	7.0	0.0	4.2	1.0	0.1	0.0	1.7
12	1995/Jun. 10	70	60-80	0.1	0.0	0.0	0.0	0.0	0.0	0.1
13	1995/Jun. 10	32	90-110	1.0	0.0	0.0	0.0	0.0	1.0	0.0
14	1995/Jun. 10	30	70-90	1.9	0.0	0.0	0.0	0.0	1.7	0.2
15	1995/Jun. 12	30	15-35	3.5	0.0	0.0	0.0	0.8	0.0	2.7
16	1995/Jun. 12	30	20-40	6.3	0.0	0.0	0.0	4.2	0.0	2.1
17	1995/Jun. 12	30	15-35	0.5	0.0	0.0	0.0	0.1	0.0	0.4
18	1995/Jun. 13	30	15-35	3.4	0.6	0.0	0.0	0.0	0.0	2.8
19	1995/Jun. 14	30	8-28	212.3	63.2	23.6	85.5	34.7	0.0	5.3
20	1995/Jun. 14	30	8-28	19.0	6.3	0.3	3.5	3.3	0.0	5.6
21	1995/Jun. 15	60	7-27	24.1	15.7	2.6	3.7	1.5	0.0	0.6

Table 2 Biological characteristics of *M. muelleri*

Site	SL(mm)	BW(g)	Sample Num.
4	41.4 ± 1.7	1.2 ± 0.2	44
13	47.0 ± 2.4	1.25 ± 0.37	12
14	42.6 ± 3.8	0.86 ± 0.28	27

Table 3 Biomass estimation of *Maurolicus muelleri*

	Distribution area (km <sup>2</sup> )	Biomass (tons)	Density (tons/km <sup>2</sup> )
1993 Transect III	2655.4	83,270	31.36
Transect IV	2585.6	47,935	18.54
Transect V	1747.0	18,889	10.81
Transect VI	1607.2	38,076	23.69
Transect VII	1257.8	42,895	34.10
Transect VIII	1467.5	43,302	29.51
Transect IX	1257.8	15,252	12.13
Transect X	1537.4	82,405	53.60
Sub Total	14115.8	372,024	
Average		46,503	26.72
	Distribution area (km <sup>2</sup> )	Biomass (tons)	Density (tons/km <sup>2</sup> )
1994 Transect C1	244.7	1,763	7.20
Transect C2	69.9	742	10.62
Transect C3	139.8	1,143	8.18
Transect C4	209.7	1,539	7.34
Transect D2	272.6	7,839	28.76
Transect D3	7.0	139	19.89
Transect D4	69.9	1,405	20.10
Transect D5	139.8	23,399	167.37
Transect D6	349.5	2,380	6.81
Sub Total	1502.9	40,349	
Average		4,483	30.70
	Distribution area (km <sup>2</sup> )	Biomass (tons)	Density (tons/km <sup>2</sup> )
1995 Transect C4	1048.2	13,954	13.31
Transect C6	559.0	19,801	35.42
Transect C7	349.4	259	0.74
Transect C8	349.4	2,867	8.21
Transect D1	139.8	394	2.82
Transect D2	28.0	326	11.64
Transect D5	335.5	28,113	83.79
Transect D6	237.7	28,106	118.26
Sub Total	3047.0	93,820	
Average		11,728	34.27

Fig.1 Acoustic transect lines and trawling sites (1 to 21) in 1993, 1994 and 1995. Broken lines were acoustic transects in 1993, and solid lines were acoustic transects in 1994 and 1995. Numbers were trawling sites.

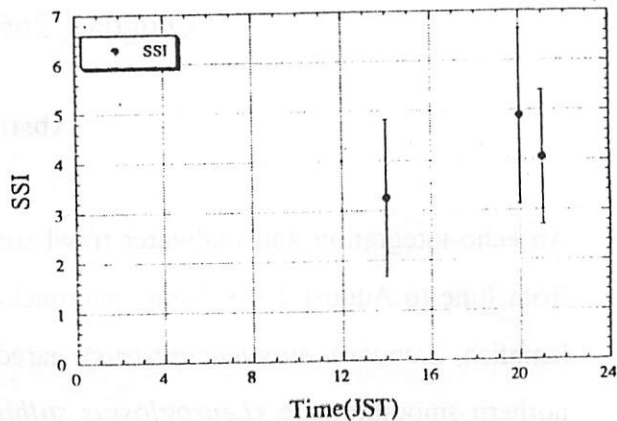
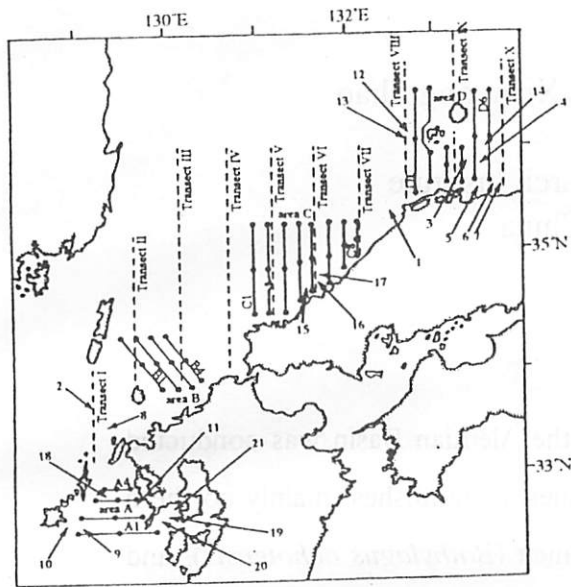


Fig. 2 Change of Somatic stomach index (SSI) of *M. muelleri*. The SSI was changed over a 24 hour period (ANOVA,  $F(2,59)=4.478$ ,  $p=0.0155$ ), and the SSI in the twilight was higher than that in the daytime and nighttime (Fisher's PLSD test,  $p=0.0052$ ).

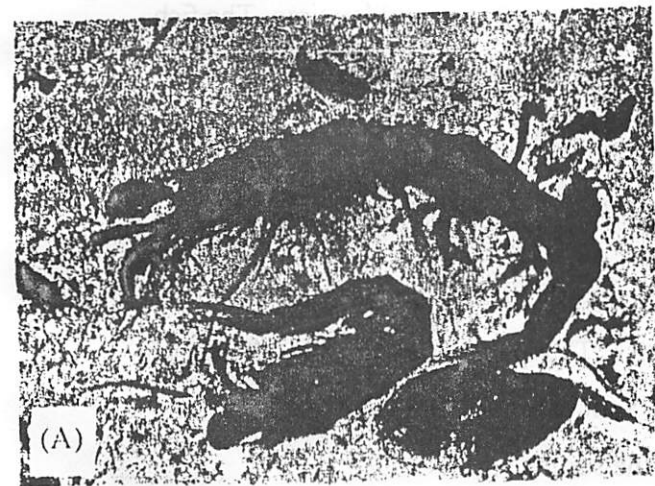


Fig. 3 Photographs of the stomach contents of *M. muelleri*. Most of the stomach contents of *M. muelleri* were zooplankton and fish larvae. Most of the stomach contents in the twilight were not digested (A; SSI=4.64), but digested contents were observed in the daytime (B; SSI=1.71).

# Distribution and Relative Abundance of Some Micronektonic Fishes in the Aleutian Basin

Qisheng Tang, Xianshi Jin and Xianyong Zhao

Yellow Sea Fisheries Research Institute  
Qingdao, 266071, China

## Abstract

An echo-integration and midwater trawl survey in the Aleutian Basin was conducted from June to August 1993. Some micronektonic fishes, lanternfishes (mainly northern lampfish, *Stenobrachius leucopsarus*), eared blacksmelt (*Bathylagus ochotensis*), and northern smoothtongue (*Leuroglossus stilbius schmidti*) were observed in the Basin. Large concentrations of northern lampfish were found in the waters between the Bowers Ridge and the Aleutian Islands and very small quantity in the central and northern part of the Basin. Northern lampfish which was presented in fine sands shape on the echogram, showed a distinct diurnal vertical migration. They were distributed in the water layer between surface and 100 m depth at midnight, and below 200 m at midday time. The fish from the catch was 4.9-9.0 cm in fork length and 3.3 g in average weight.

## 1. Introduction

An echo-integration and midwater trawl survey in the Aleutian Basin was carried out by R/V "Bei Dou" from June 28 to August 2, 1993. This paper presents the results of geographic distribution, vertical migration and relative abundance of some micronektonic fishes in the Aleutian Basin from the survey.

## 2. Materials and Method

The transects and stations occupied for pelagic trawling and environmental observations are shown in Figure 1. The distance between transects was 22 n.mi near Bogoslof Island, and 44 n.mi. in other areas. The acoustic survey covered the main part of the Aleutian

Basin. A pelagic trawl with 400 cm mesh and 4-cm mesh codend was used to collect samples. The acoustic data were collected with a scientific echo sounding-integrating system (SIMRAD EK400/38 KHz echo sounder with a hull-mounted SIMRAD ES38 transducer and a SIMRAD QD digital echo integrator). All data were logged onto a personal computer. The SIMRAD EK400 (120 KHz) echo sounder was also used to help identify different echo signs in the upper 100-m layer. The integration value was given for each 5-m section of the transect for a set of successive depth intervals and was regarded as a relative abundance index for the detected fish. The acoustic system was all calibrated with a standard target at a frequency of 38 KHz (Foote et al., 1987) at the beginning and end of the cruise.

Water temperature, salinity, and dissolved oxygen (DO) at the surface and at 25, 50, 100, 150, 200, 300, and 500 m were measured at predetermined stations.

### 3. Results and Discussion

#### 3.1 Geographic distribution and relations with biological environment

During the survey, some micronektonic fishes were found in the southern part of the Aleutian Basin along the Aleutian Islands (Fig.2), including lanternfishes (mainly northern lampfish, *Stenobrachius leucopsarus*), eared blacksmelt (*Bathylagus ochotensis*), and northern smoothtongue (*Leuroglossus stilbius schmidti*). Large concentrations of northern lampfish were found in the waters between the Bowers Ridge and the Aleutian Islands and very small quantity in the central and northern parts of the Basin. Northern lampfish was presented in fine sands shape on the echogram (Fig. 3). By sampling, there were mostly northern lampfish, and the other two species very few. Therefore, the relative abundance of northern lampfish was obtained from the integration values (Fig. 2). The densest distributional area was at the northern part of the Near Islands with the highest integration value of around 100, with temperatures at the surface of 7°-8°C, salinities of 32.8-33.0, and a DO level of 10 mg/l. The lower density was in the southeastern part of the basin with the integration value of 10-30 with temperatures at the surface of 8°-9°C, salinities of 32.6-32.8, and a DO level of 10 mg/l (Fig.4 and 5).

There was relatively low concentration of zooplankton distribution in the high density area of lampfish (Fig. 6), but high concentration of phytoplankton distribution (Fig. 7).

### **3.2 Vertical migration**

A distinct diurnal vertical migration of northern lampfish was observed during the survey (Fig. 3 and 8). Northern lampfish were mostly distributed below 200 m depth with temperature of around 4 °C, salinity of around 33.5, and DO level of 3-6 mg/l and few in the water layer between 100 m and 200 m during daytime hours (0600-1800) with temperature of around 3 °-4 °C, salinity of around 33.2, and DO level of 5-10 mg/l. After 1800, they gradually migrated to upper waters, and all were concentrated in the upper 100 m from 2200 to 0200. Thereafter, the species descended to deeper water, mainly in the 100-200 m depth layer (Fig. 9 and 10).

### **3.3. Biological status**

The northern lampfish caught in the southwestern part of the basin ranged from 4.9-9.0 cm in fork length, with a mean weight of 3.3 g. The micronektonic fishes were eaten by yellowtail rockfish and salmon (Hart, 1973), and not found in the stomach of walleye pollock.

### **Reference**

- Foote, K.G., H.P.Knudsen, G. Vestnes, D.N. MacLennan, and J. Simmonds. 1987. Calibration of acoustic instruments for fish density estimation: a practical guide. Coop. Res. Rep. Int. Counc. Explor. Sea 144: 1-69.
- Hart, J.L. 1973. Pacific fishes of Canada. Fish. Res. Bd. Canada Bull. 180: 198-199.

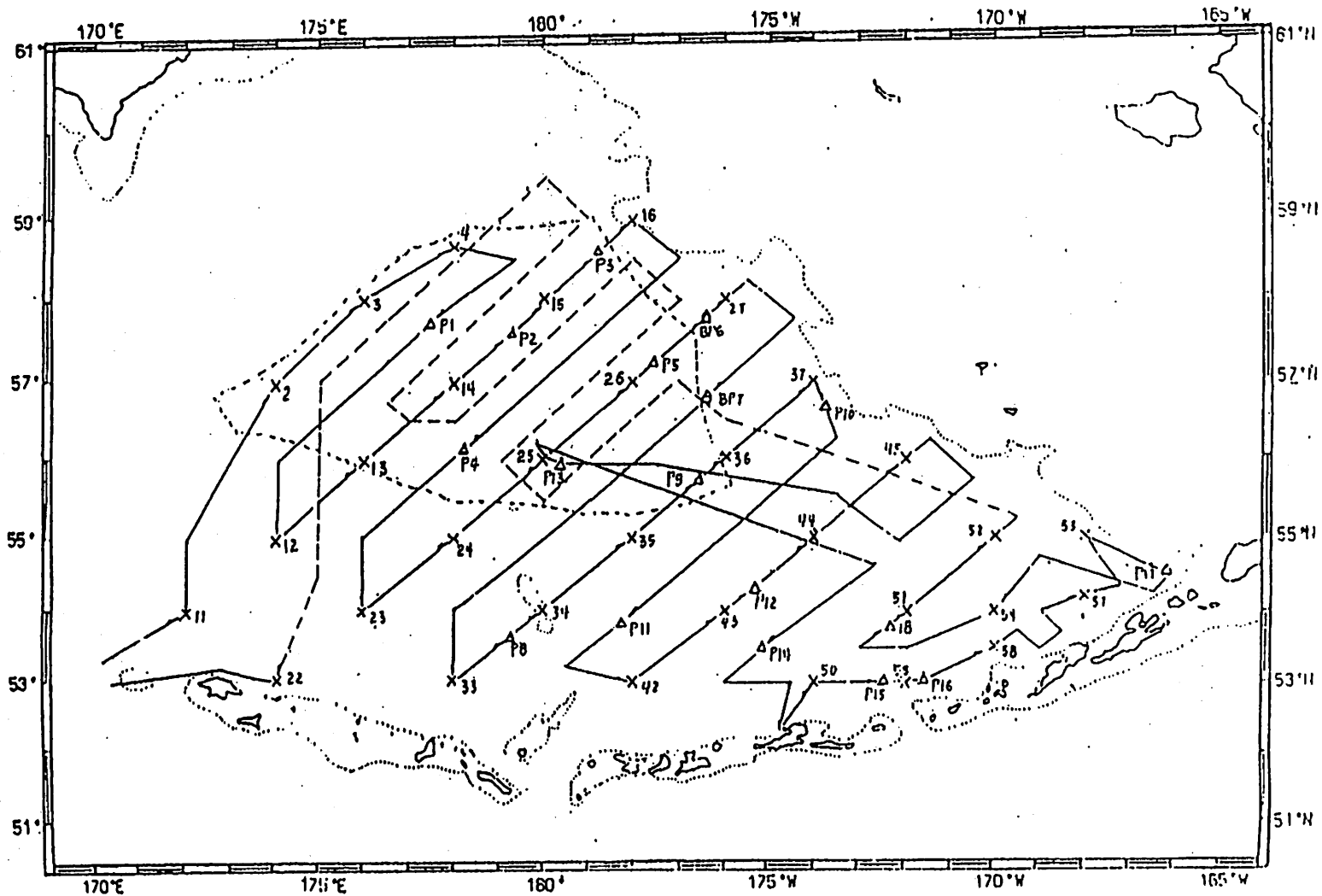


Fig. 1. Track line and positions of midwater trawl ( $\Delta$ ) and hydrography (X) operations in the acoustic/midwater trawl survey for walleye pollock in the Aleutian Basin.

Solid line: June 28-July 24, 1993;  
Dotted line: July 25-August 2, 1993

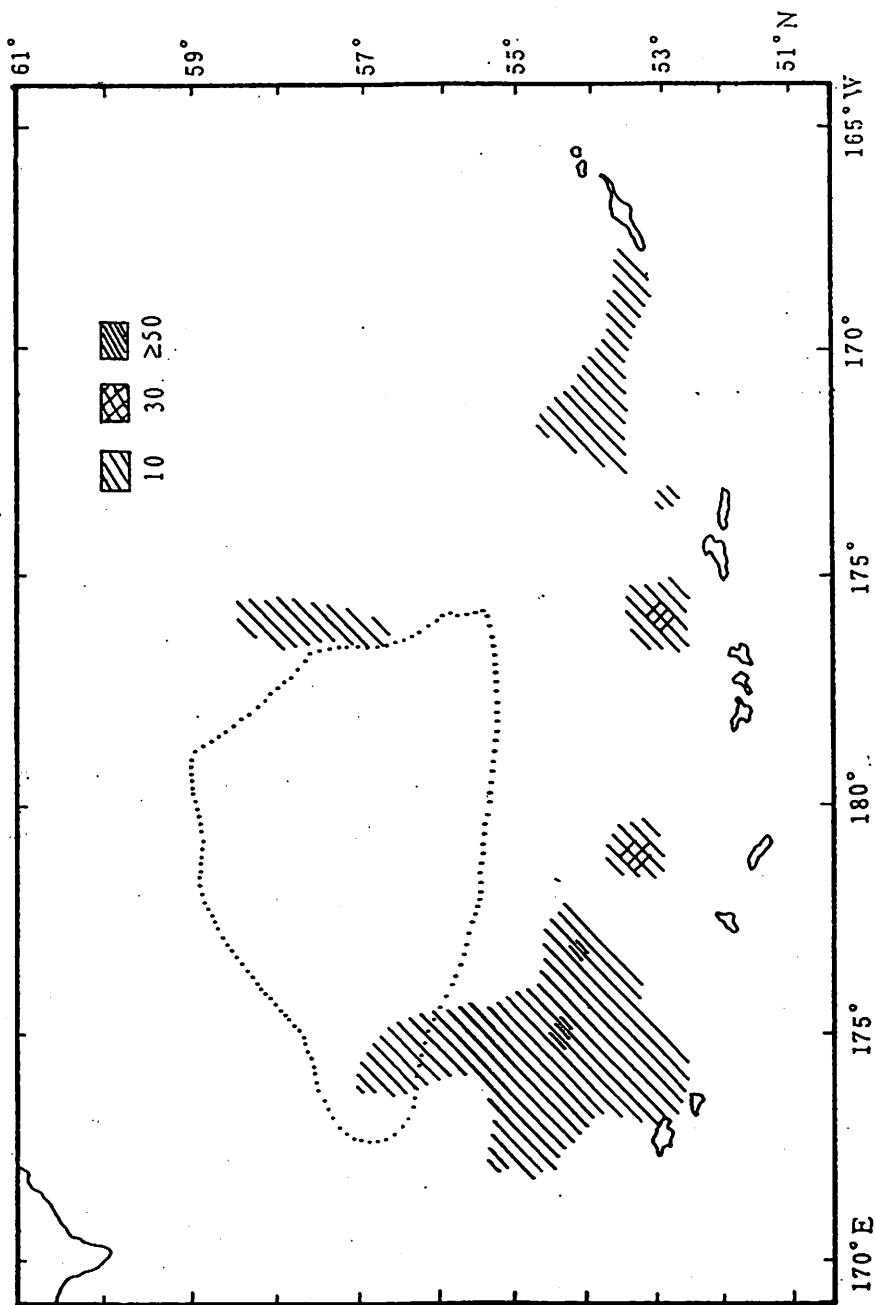


Fig. 2. Distribution and relative density (integration value) of northern lampfish in the Aleutian Basin (June 28-August 2, 1993)



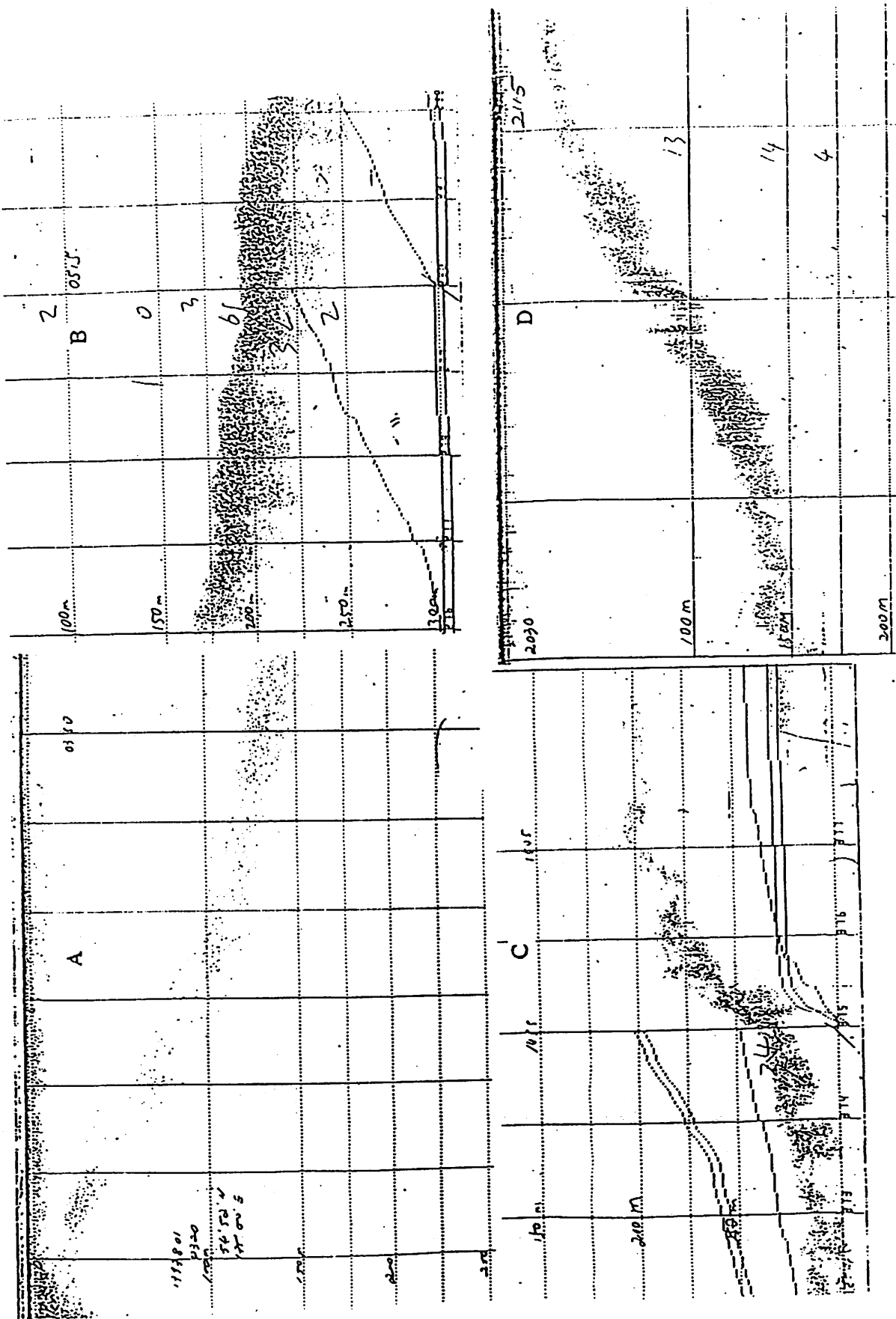


Fig. 3. Echograms of vertical distribution of northern lampfish in the southwestern part of the Aleutian Basin.  
Local time: A, 0320-0350; B, 0455-0525; C, 1440-1510; D, 2030-2120.

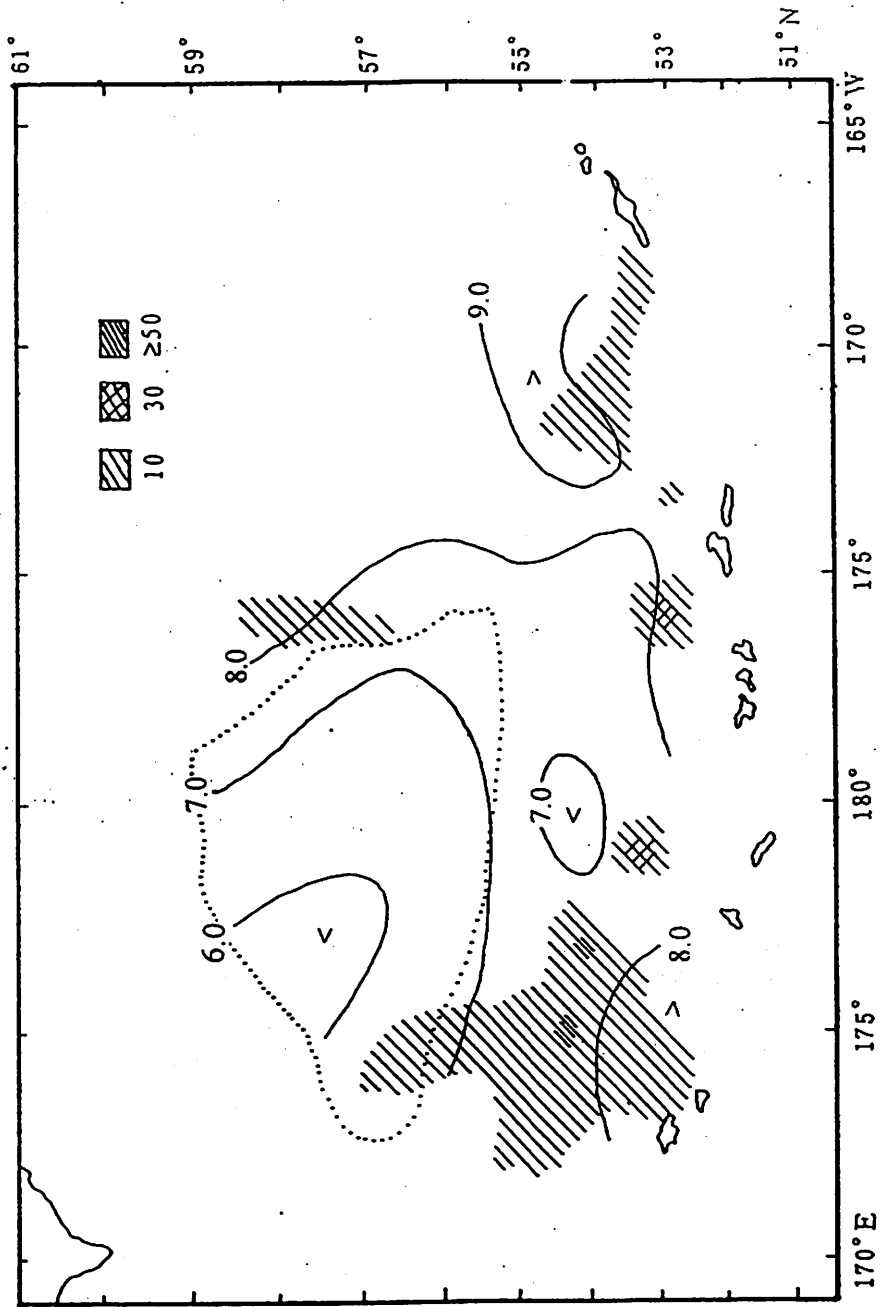


Fig. 4. Relation between the distribution area of lampfish and temperature ( $^{\circ}\text{C}$ ) at surface.

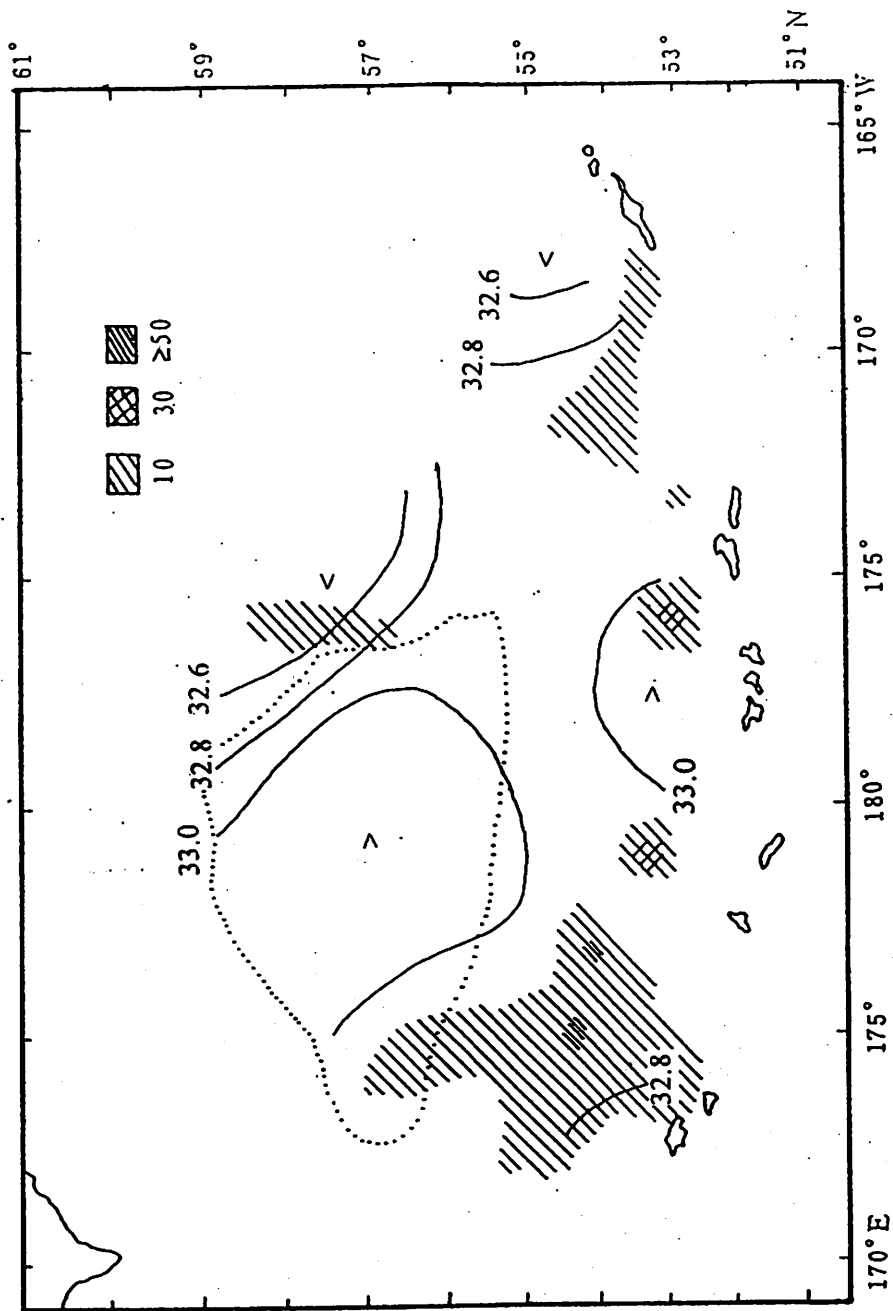


Fig. 5. Relation between the distribution area of lampfish and salinity at surface.

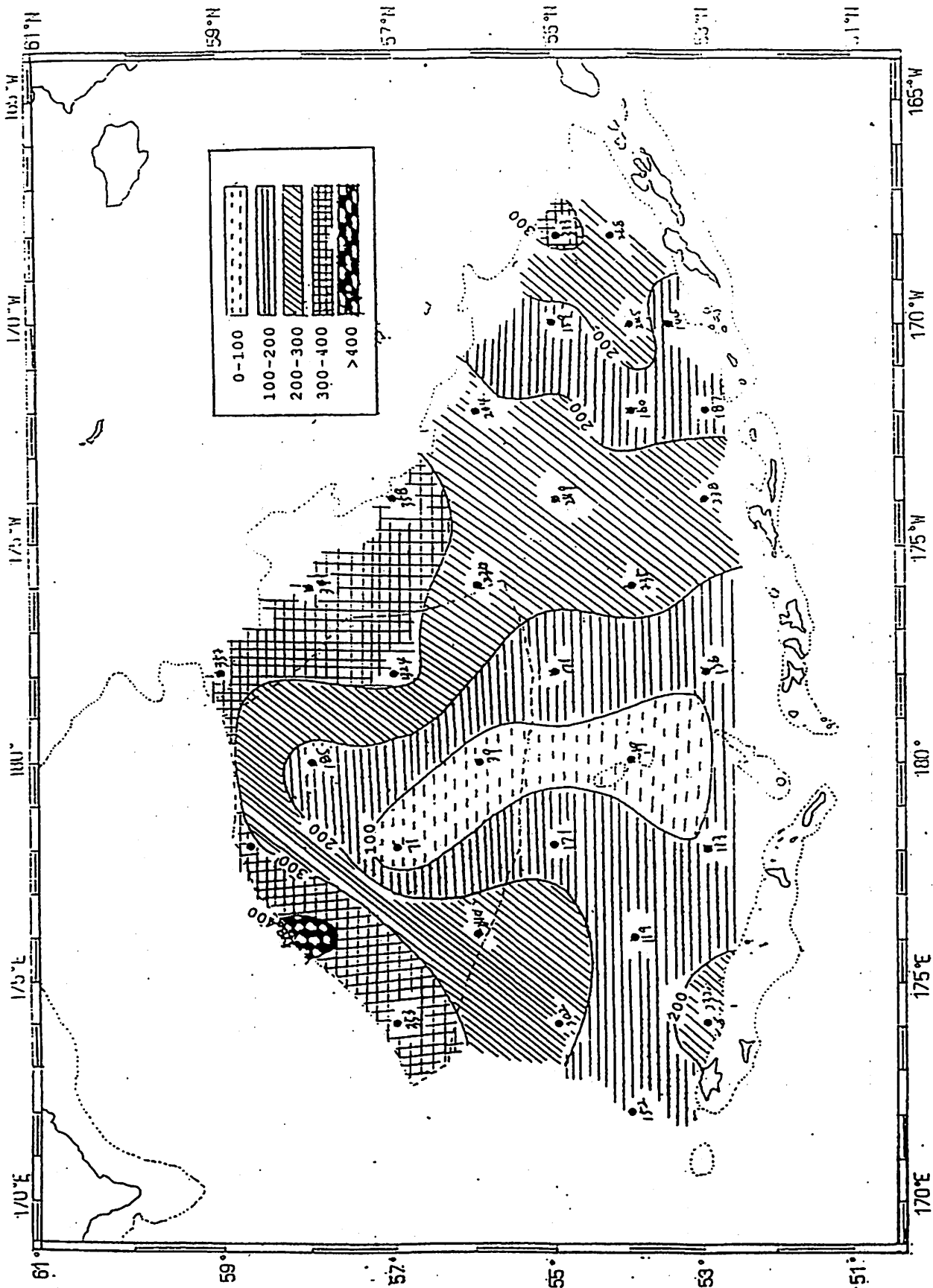


Fig. 6. Total biomass distribution of zooplankton (mg/m<sup>3</sup>)

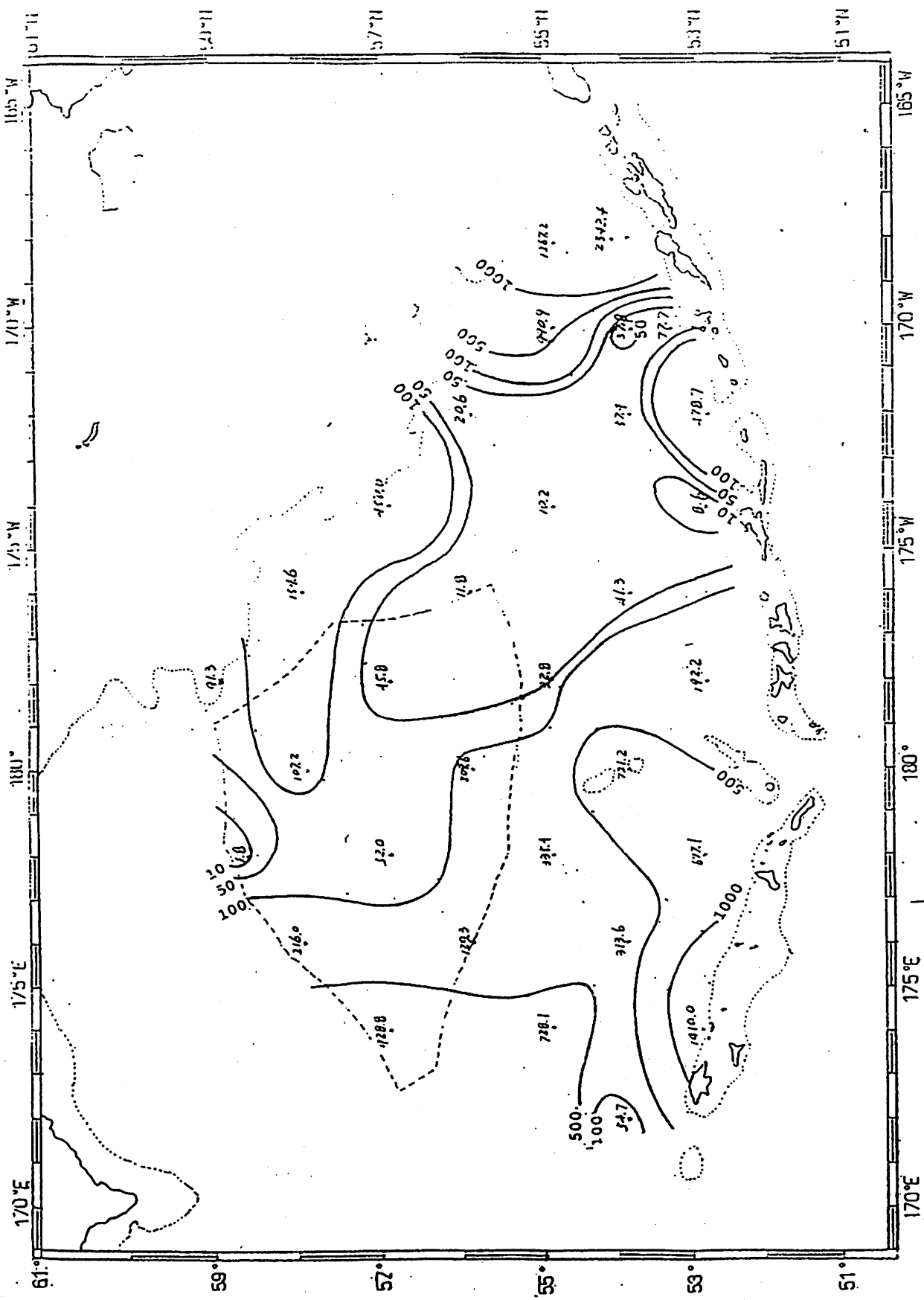


Fig. 7. Distribution of total phytoplankton ( $\times 10^6$  cell/ $m^3$ )

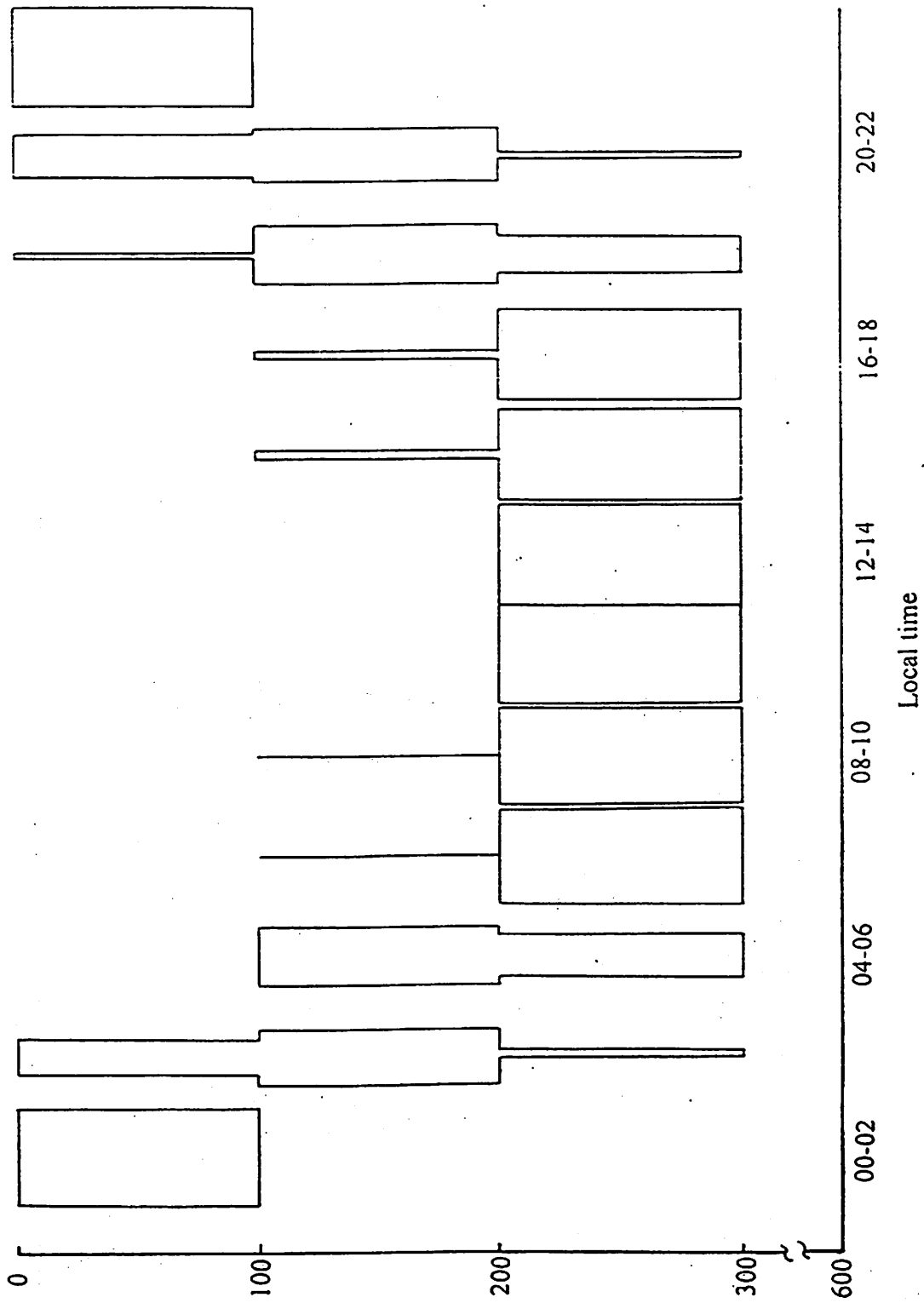


Fig.8. Day and night variation in distribution of lampfish in the southern part of the Aleutian Basin

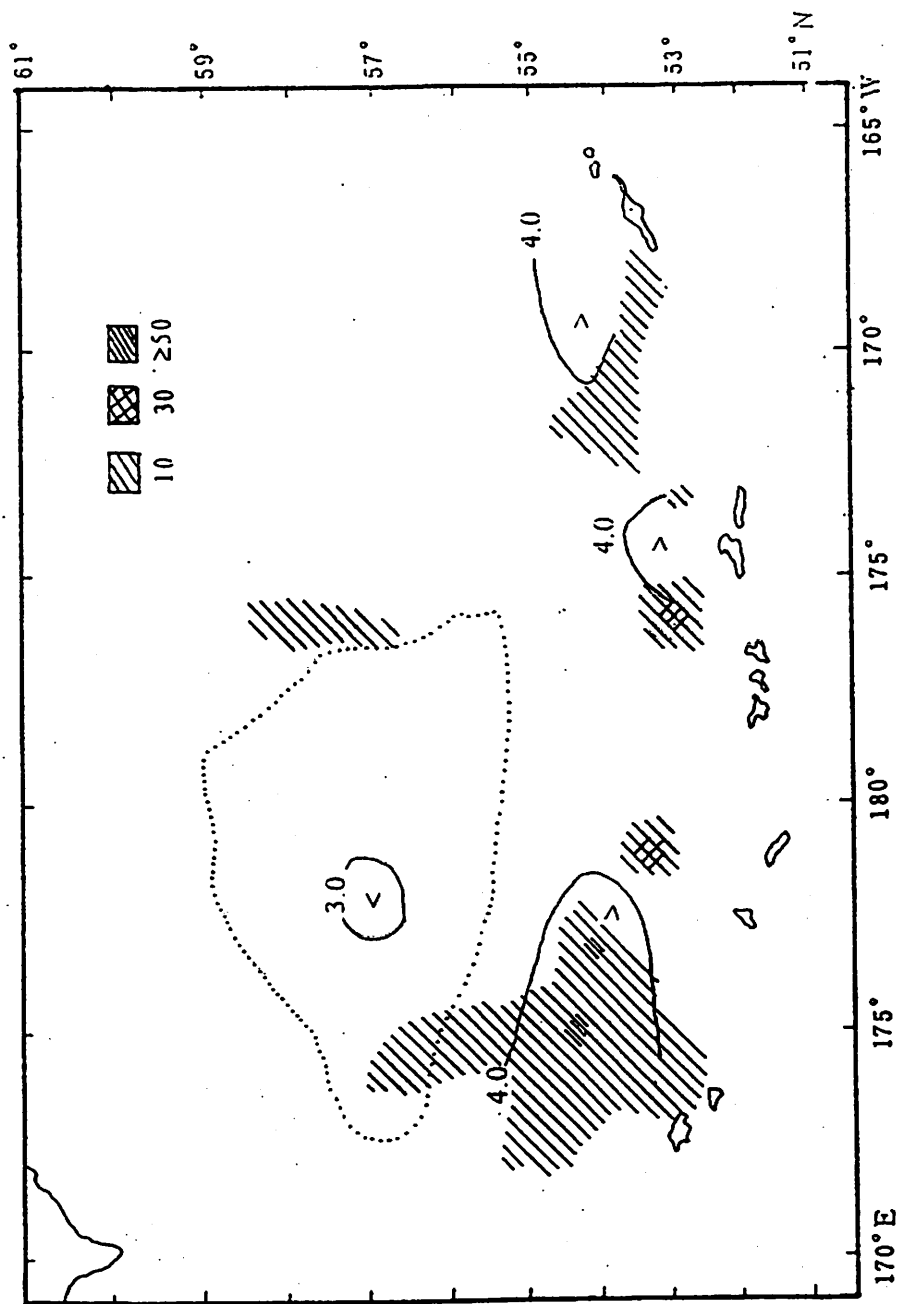


Fig. 9 Relation between the distribution area of lampfish and temperature ( $^{\circ}\text{C}$ ) at 250 m depth.

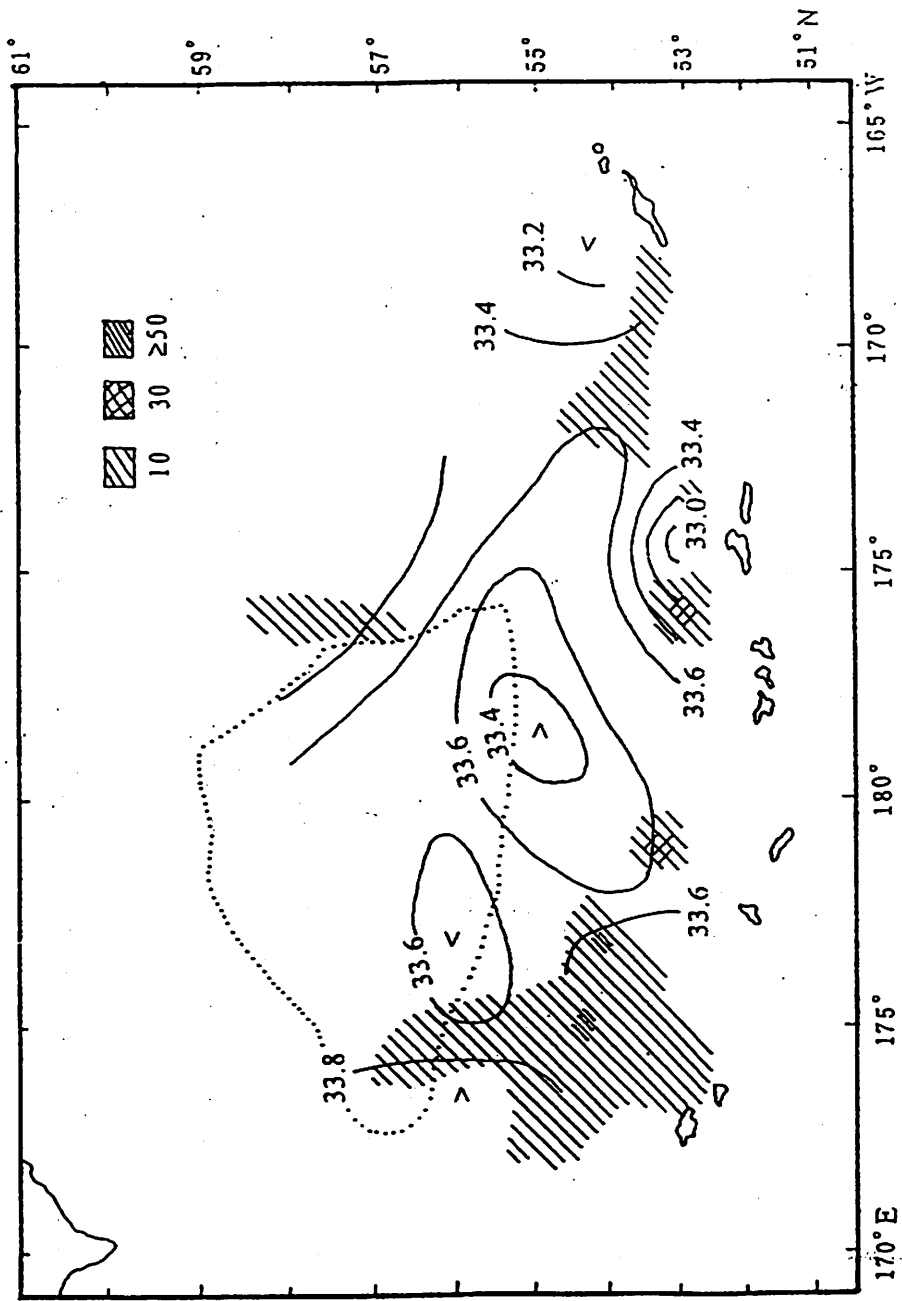


Fig.10 Relation between the distribution area of lampfish and salinity at 250 m depth.



Community ecology of juvenile pollock (*Theragra chalcogramma*) and other midwater taxa in the eastern Bering Sea during August-October, 1987

Matt Wilson  
NOAA/NMFS/AFSC  
7600 Sand Point Way NE, Bldg 4  
Seattle, Washington 98115-6349  
phone: (206) 526-6522  
fax: (206) 526-6723  
email: mwilson@afsc.noaa.gov

## Introduction

Climate change, ecosystem considerations, and essential fish habitat are popular fisheries management issues due to their supposed effect on the distribution and production of fish. Before we can go too far with these concepts, however, we need some baseline descriptive information about large-scale distribution patterns of fish and environmental variability. Community ecologists have long-since been interested in gradients of species composition arguing that such gradients reflect environmental influences. Interpreting a compositional gradient may be accomplished by relating it to known environmental variability. Because fish distribution data is often collected for many species simultaneously, for example trawl surveys, it seems logical to first use all of this information and conduct a community analysis to describe general fish-environment associations evident at the time the data were collected. Subsequent analyses can then examine associations between the environmental variables and species of particular interest with some specific knowledge of biotic and abiotic associations, throughout the study area during the time of collection.

For walleye pollock (*Theragra chalcogramma*) in the Bering Sea, production is largely affected by variations in recruitment as a result of inter-annual losses during the early life history stage. Although the mechanisms responsible for this loss can only be guessed, it is likely that processes operating during the early juvenile or age-0 stage influence year-class strength. Defining associations between the distribution of young fish and their environment may help reveal which environmental parameters are more likely to affect production. For example, if the juveniles of a particular species are most common in areas of relatively warm water then, it stands to reason, that they may flourish during warm rather than cold years. Although useful for illustration, this example is overly-simplistic because other interacting environmental factors and density-dependant effects are ignored. In the Bering Sea, age-0 pollock are one of the most common members of the micronekton. They are of interest to the National Marine Fisheries Service due to the commercial value of walleye pollock (*Theragra chalcogramma*) and the potential of age-0 abundance estimates as a management tool to predict year-class strength. Also, age-0 pollock occur regularly in the diet of marine mammals, birds, and fishes making them an important consideration in ecosystem studies and multi-species management programs in the Bering Sea.

The purpose of this study is to use field data to describe the structure of midwater communities in the eastern Bering Sea and to determine if any of the evident structure is associated with available environmental measurements. Special attention is focused on determining associations between the distribution of age-0 pollock and the environment due to the commercial importance of the pollock resource and the importance of this stage in

recruitment dynamics.

### Materials and Methods

Data from a U.S.-Russia cooperative survey of age-0 pollock during 22 August - 8 October, 1987 are uniquely well-suited for developing this hypothesis. The survey area was extensive, limited to U.S. waters of the Bering Sea south of St. Lawrence Island and deeper than about 40 m. Sampling stations were pre-determined to be along half-degree lines of latitude and degree lines of longitude (Figure 1). Operations were conducted 24 hrs. The available information from this survey includes midwater trawl catch data, hydrological data, and estimates of plankton biomass. For this study, however, use is made only of the trawl catch composition data, and temperature, salinity, and dissolved oxygen measurements.

Collections of micronekton and associated species was accomplished using the Soviet pelagic trawl 77.4. This is a rope trawl constructed of mesh sizes ranging from 1200 mm near the mouth down to the 10 mm mesh-sized codend liner. The operational mouth opening of the trawl is about 20 m vertical and 40 m horizontal. The trawl was fished over a stepped-oblique path, the total water depth was divided into two or three intervals, depending on depth, and the net was positioned such that it spent an equal amount of time at each depth. The shallowest depth was with the headrope at the surface. The duration of each tow was 1 hr and the target towing speed was 4 - 4.5 kts.

All taxa were processed but the taxonomic level of identification varied and is reflected in the analysis. At sea, the catch weights and numbers for each group were measured using the standard procedures of the Alaska Fisheries Science Center. According to these procedures, pollock juveniles ( $\leq 20$  cm) and adults ( $> 20$  cm) were processed separately. Fork lengths were measured to the nearest centimeter on all or a subsample ( $\geq 200$  fish) of each pollock group. To separate the juveniles into an age-0 and age-1 component, the size composition from each trawl haul and pollock group was standardized to catch per unit effort (number of fish per hour trawled). These size compositions were then combined to give one size composition for each haul which was then divided into three categories by eye based on minima in the length frequency distribution. These categories are assumed to represent age-0, age-1, and age-2+ (age-2 and older) pollock. This manipulation made it necessary to estimate the catch weight for each of these three groups in order to compare biomass and mean individual weights among all groups collected. To do this, the size composition for each haul was converted to a weight composition using length-weight relationships and then summing the frequency-weighted weights.

Hydrographic casts were made to a depth comparable to that fished with the trawl. Collection of water samples and temperatures measurements was accomplished at select depths. Salinity and dissolved oxygen were measured at sea using an electronic salinometer and the titration method, respectively. Only measurements made at the sea surface, 45 m ( $\pm 5$  m), and at the maximum depth sampled were used in this study, thus there were nine environmental variables.

Analysis of community-level patterns in the data was accomplished using cluster and ordination techniques on log<sub>e</sub>-transformed catch data ( $\ln(\text{no/hr} + 1)$ ). Cluster techniques are useful for detecting marked dissimilarities among samples or taxa but ordination techniques will likely be more useful if the change in composition is more continuous. For cluster analysis, station dissimilarities were based on the Bray-Curtis index of dissimilarity. Station clusters were generated using the algorithm in SYSTAT which is a hierarchical, polythetic

clustering technique. Cluster amalgamation was accomplished using Euclidean distance and average linkage. Since there was no obvious level of dissimilarity at which to choose station clusters, the choice was made on the basis of geographic cohesiveness of member stations. One-way ANOVA were used to detect differences among the cluster groups for each environmental variable. Because the ordination results were similar to the cluster results, I will only include one ordination diagram, produced using detrended correspondence analysis (DCA), for the express purpose of showing how each of the 18 taxonomic groups relate to each station cluster. DCA uses a two-way weighted averaging algorithm, assuming a bell-shaped response curve, to order the samples and taxa to reveal underlying gradients. Distances along the ordination axes indicate similarities among taxa (with regard to distribution) or stations (with regard to catch composition). The axes are scaled so that if taxa differ by 4 or more units they are unlikely to co-occur within the same sample.

Associations between the distribution of age-0 pollock and each of the nine environmental variables over all 149 stations were tested using the procedure of Perry and Smith (1994). This procedure tests the hypothesis of no association between the distribution of fish density (fish/hr) and the environmental variable being tested. Interactions between environmental variables were not accounted for in these tests. Plots were constructed showing the cumulative proportion of fish caught and the cumulative proportion of samples collected, as a function of each variable. The proportion of fish or samples within any range of the environmental variable is then easily estimated from these plots.

## Results

Eighteen groups occurred at 15 or more of the 149 stations at which midwater trawl samples were collected (Table 1). Five of these groups were above the species taxonomic level due to difficulties in separating member species. For nine groups, the average weight per individual was less than 100 g. Thus, except for sturgeon poachers (*P. acipenserinus*) which is typically benthic, these nine groups might be considered micronekton. Mean catch density indicated that pollock and jellyfish (cnidaria) comprised more than 90% of the catch whether by number or weight per hour. Although age-0 pollock had the lowest individual mean weight, their extreme abundance allowed them to place third in terms of highest mean biomass.

The fork length intervals, 12 and 20 cm, appeared to be reasonable sizes at which to separate the three pollock age groups. For a few of the earliest and latest samples, size compositions from individual hauls indicated that 12 cm was too large or too small, respectively, so this breakpoint was altered but by no more than 2 cm.

Five clusters were chosen based on geographic cohesiveness of the member stations (Figure 2). The first cluster contained only one station at which the catch of cnidarians and chum salmon (*O. keta*) was high, this cluster is hereafter disregarded. The second cluster, comprised of 75 stations, was largely restricted to the basin. Clusters 3, 4, and 5 were mostly restricted to distinct regions of the shelf but there were some individual exceptions, these clusters were comprised of 34, 26, and 13 stations, respectively. Cluster 3 occupied the northern inner shelf but extended southwest enough to include the Pribilof Islands. Cluster 4 occupied the southeast shelf with a branch extending north along the outer shelf up to Cluster 5. Cluster 5 occupied the northern outer shelf.

Catch composition of each cluster is perhaps best indicated in the DCA ordination diagram on which the station cluster membership is indicated (Figure 3). Myctophids,

bathylagids, and cephalopods are closely associated with Cluster 2. Sturgeon poachers, capelin (*M. villosus*), Pacific cod (*G. macrocephalus*), and shrimps (*Natantia*) are characteristic of Cluster 3. The groups most closely associated with Cluster 4 are age-0 pollock, jellyfish, and prowfish (*Z. silenus*). Older age groups of pollock and Pacific herring are characteristic of Cluster 5.

Significant differences among clusters was detected for almost all of the environmental variables examined (Table 2). Clusters 3, 4, and 5 were significantly shallower in bottom depth than Cluster 2, and this was also reflected in the maximum sample depth. Cluster 2 was characterized as having low temperature at the surface but warm at depth, high salinity, and low dissolved oxygen. Cluster 3 stations had a warm mean temperature at the surface, cold at depth, low salinity, and high dissolved oxygen. Cluster 4 had mean temperatures that were cold at the surface but warm at depth, intermediate salinity and dissolved oxygen. Cluster 5 had warm mean surface temperatures but was cold at depth, intermediate salinity and dissolved oxygen.

Most age-0 pollock were found on the shelf and although they occurred with some regularity over the Aleutian Basin (Cluster 2 samples) the densities were low. On the shelf, these fish were conspicuously absent from the stations belonging to Cluster 5.

The hypothesis of no association between the number of age-0 pollock was rejected ( $p < 0.05$ ) for each environmental variable depending on the depth at which the measurement was made (Figure 4 and 5). For salinity, however, an association existed regardless of depth. This is not surprising given the high correlation among salinity measurements ( $r > 0.92$ ) and their association with midwater community structure. When measured at 45 m, a salinity range of 31.8 to 32.5 ppt encompassed only 27% of the samples but 86% of the fish. Temperature and dissolved oxygen, both measured at the maximum depth sampled, were also significantly associated with the distribution of age-0 pollock. A temperature range of 4 - 8 degrees C encompassed 25% of the samples and 67% of the fish. For dissolved oxygen, a range of 4.0 - 5.6 ml/L included 28% of the samples and 63% of the fish. Dissolved oxygen, measured at 45 m, was also significantly associated with the distribution of age-0 pollock.

#### Discussion/Conclusions

Correspondence between the structure of midwater communities in the Bering Sea and some of the environmental variables considered in this study indicates that biophysical differences existed among different midwater regions of the Bering Sea. The distribution of age-0 pollock was also associated with these gradients. Because these fish were included in the community analysis, their low densities in the basin and NW shelf undoubtedly helped shape the regional community differences but the distributions of other taxa were also responsible. For instance, myctophids and bathylagids were present only over the basin; whereas, older pollock and Pacific herring were particularly abundant over the NW shelf. With regard to specific mechanisms responsible for the observed species-environment associations, it is difficult to conclude any direct causal effect. In fact, the variables included in this study may simply covary with other more complicated or direct effects (e.g., plankton productivity). The list of variables examined in this study is certainly by no means exhaustive and other perhaps more complex environmental parameters are likely to emerge as important determinants of fish distribution in the Bering Sea.

## Figures

Figure 1. Map of stations sampled during 22 August - 8 October, 1997 during the U.S.-Russia cooperative survey of midwater taxa and hydrographic variables.

Figure 2. Map of stations sampled during the R/V Darwin survey of 1997 showing cluster membership. Each station belongs to one of five station clusters based on catch composition similarity (Bray-Curtis) and geographic cohesiveness.

Figure 3. Ordination diagram from detrended correspondence analysis shows which taxonomic groups are most closely associated with each of four station clusters. Station coordinates are shown as dots, the lines and numbers indicate cluster membership. See Figure 2 for geographic location of station clusters.

Figure 4. Map of age-0 pollock midwater densities throughout the area surveyed during 22 August - 8 October, 1997.

Figure 5. Cumulative distribution plot of the proportion of age-0 pollock caught (fish/hr) and the number of samples collected as a function of the maximum depth sampled.

Figure 6. Cumulative distribution plots showing the proportion of age-0 pollock caught (fish/hr) and the number of samples collected as a function of each of nine environmental variables.

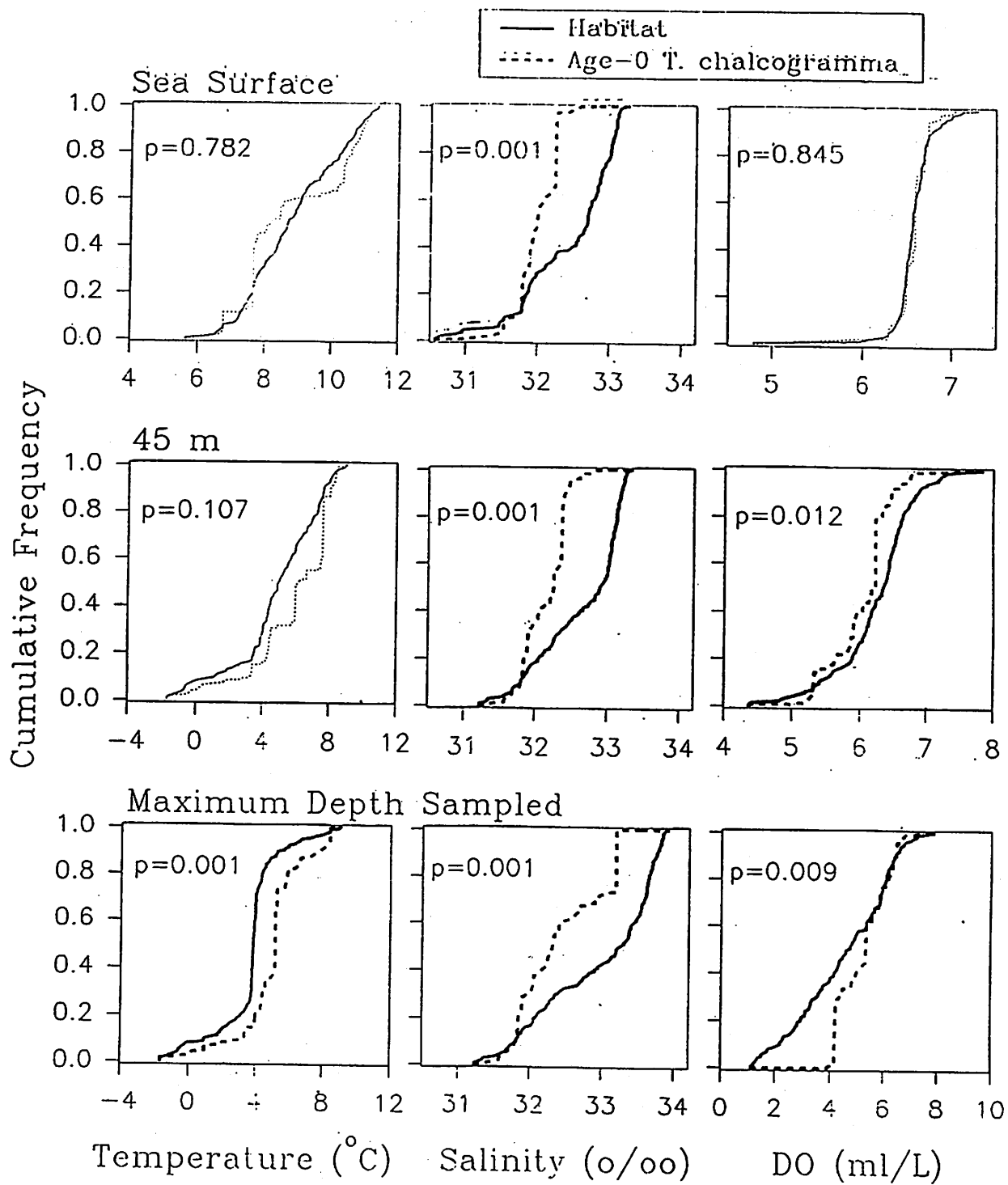


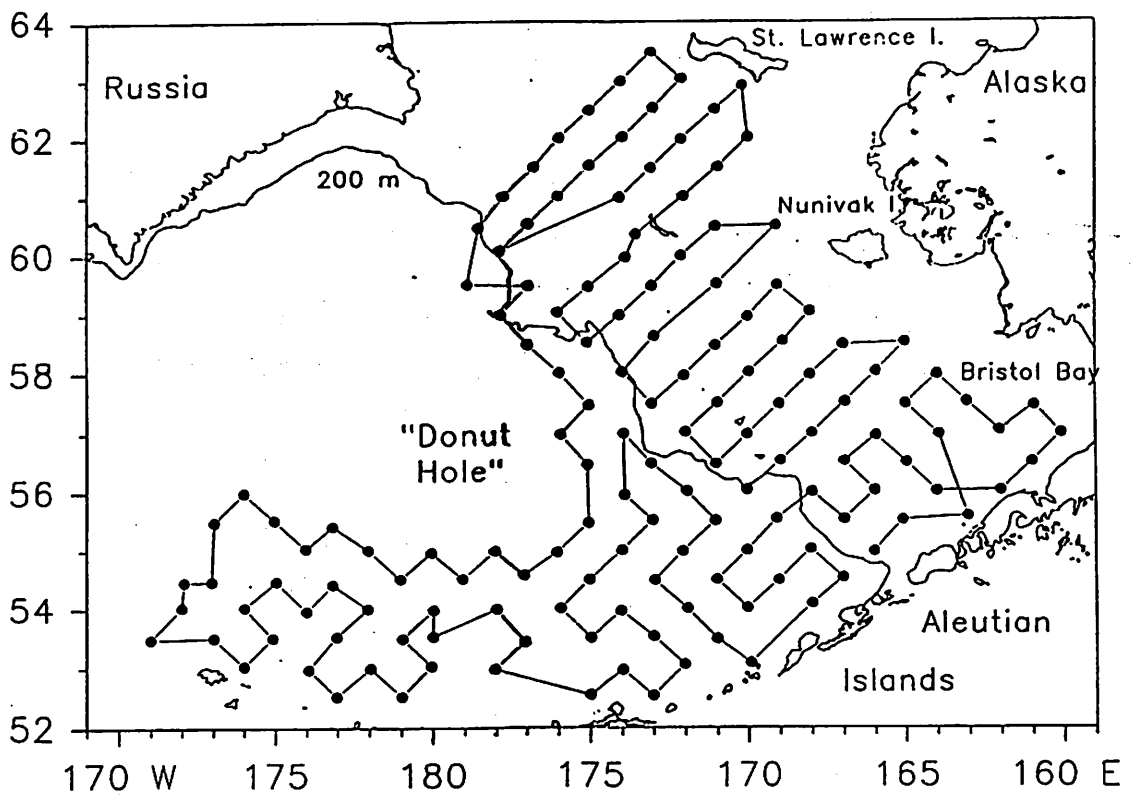
Table 1. Catch summary table from the U.S-Russia cooperative survey of midwater taxa during 22 August - 8 October, 1997. The frequency of occurrence, catch per hour (number and weight), and mean individual weight by taxonomic group for those occurring in at least 15 of the 149 stations.

## CATCH SUMMARY TABLE

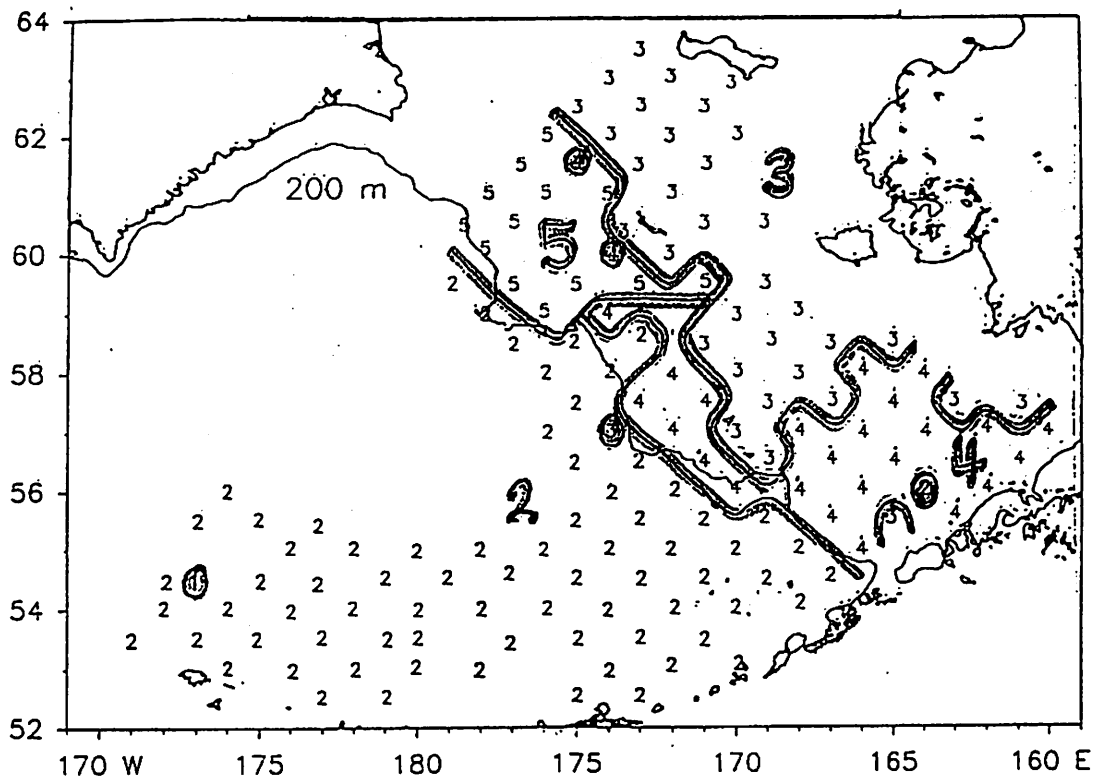
Taxonomic Group	FO	Average		Individ.
		No./hr	Kg/hr	Wt (g)
Cnidaria	139	72.6	43.72	757
<i>Theragra chalcogramma</i> (age 2+)	120	701.8	166.68	764
<i>Theragra chalcogramma</i> (age 0)	100	9471.8	41.82	3
<i>Oncorhynchus keta</i>	85	12.8	11.50	1147
<i>Zaprora silenus</i>	84	6.0	0.29	87
Cephalopoda	67	61.1	1.39	32
<i>Gadus macrocephalus</i>	48	29.9	1.95	1510
<i>Pleurogrammus monoptyerygius</i>	45	24.4	2.45	70
<i>Clupea pallasii</i>	40	7.6	1.59	194
<i>Mallotus villosus</i>	35	76.6	0.60	15
Myctophidae	32	252.6	0.78	7
<i>Theragra chalcogramma</i> (age 1)	28	715.3	25.20	35
<i>Pleuronectes aspera</i>	25	4.1	1.49	327
Bathylagidae	23	13.2	0.18	24
<i>Blepsius bilobus</i>	22	0.3	0.03	133
Natantia	20	17.0	0.04	25
<i>Podothecus acipenserinus</i>	20	1.6	0.08	71
<i>Oncorhynchus tshawytscha</i>	16	0.7	0.37	1329

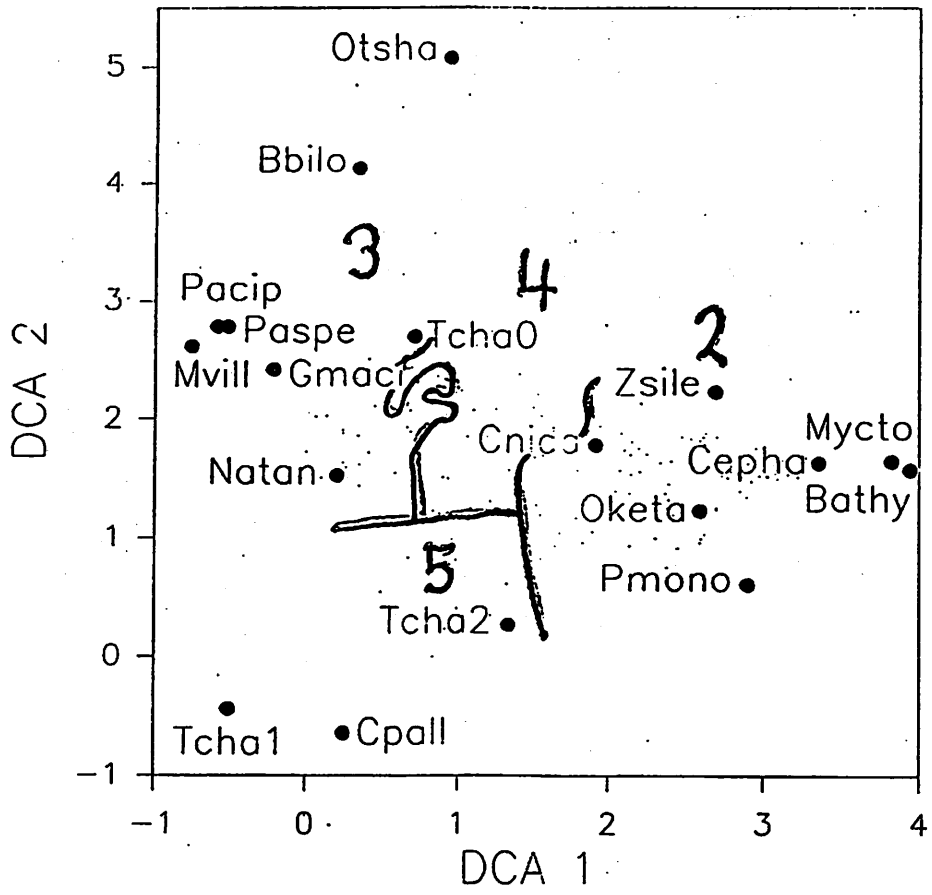
Table 2. Averages of temperature, salinity, and dissolved oxygen by sample depth and cluster group. Cluster group refers to the station clusters shown in Figure 2. Heavy vertical lines connect means not significantly different.

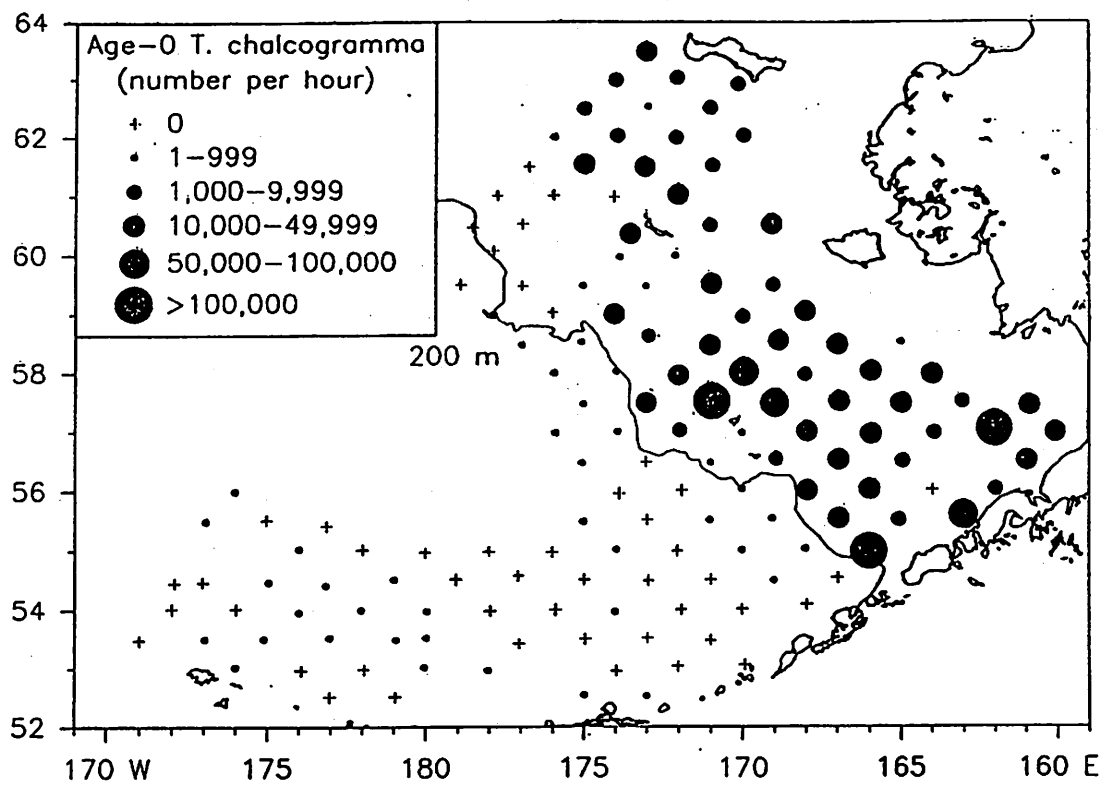
Bray-Curtis Cluster	Average Max. Sample Depth (m)	Average Temperature (C)			Average Salinity (o/oo)			Average Dissolved Oxygen (ml/L)		
		0 m	45 m	Max. m	0 m	45 m	Max. m	0 m	45 m	Max. m
2	221	8.31	5.83	3.89	32.50	33.07	33.57	6.56	6.30	3.32
4	85	8.80	5.74	5.11	32.04	32.21	32.41	6.56	5.97	5.26
5	113	9.89	3.16	2.41	32.74	32.83	32.90	6.46	6.48	6.04
3	62	9.73	2.87	2.74	31.63	31.99	32.03	6.63	6.29	6.17

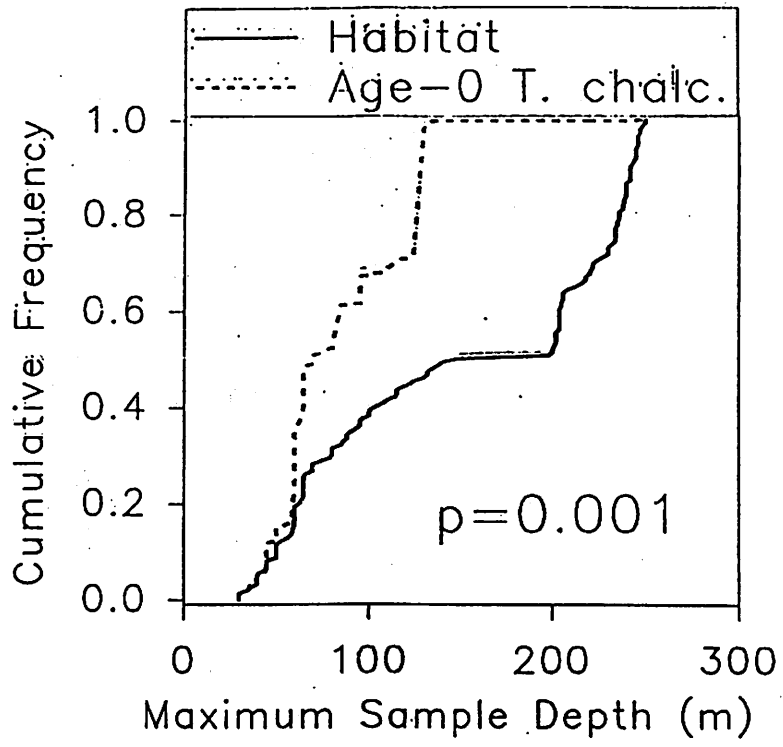


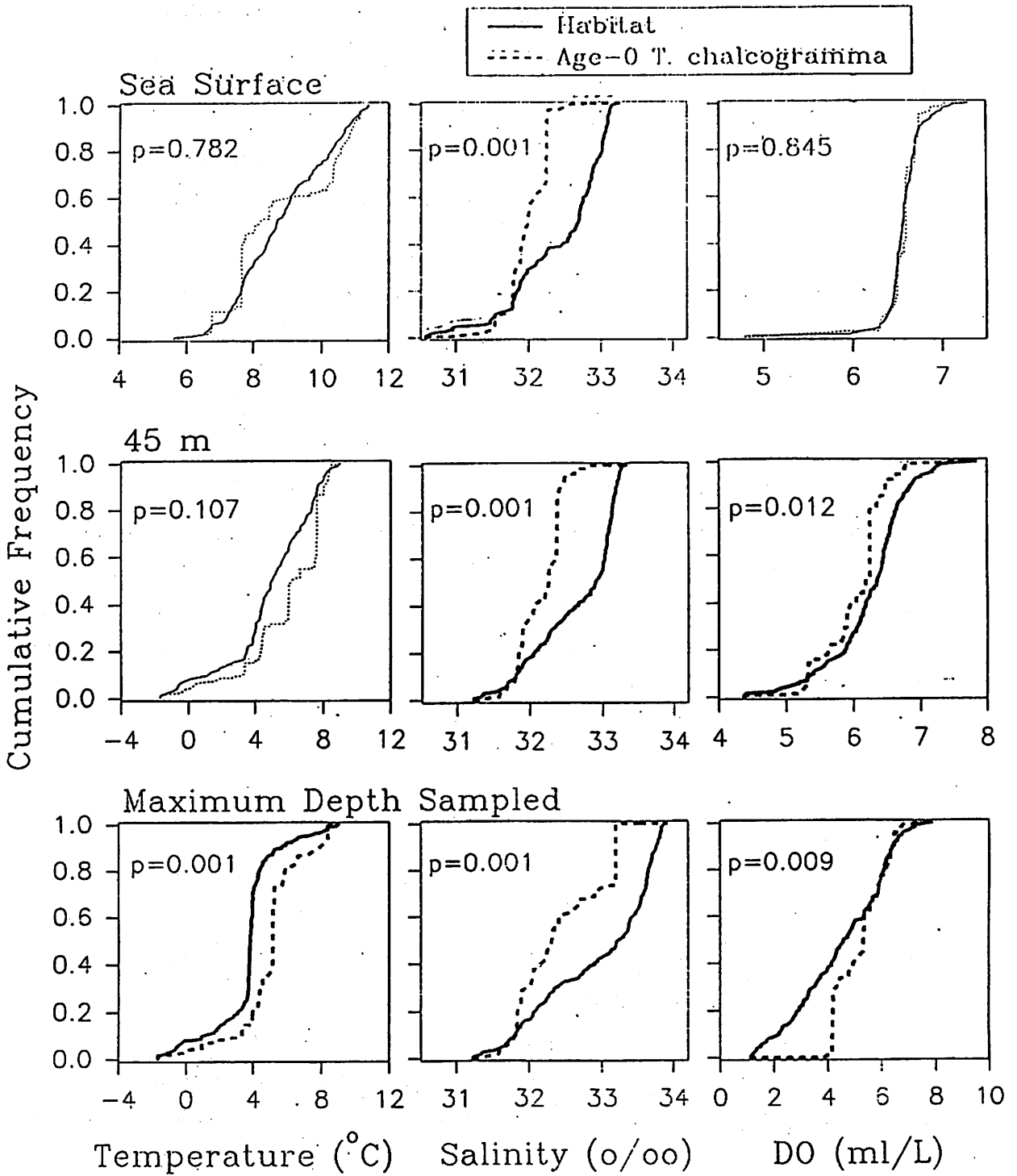












# Predation on micronekton by demersal fishes

Orio Yamamura

Hokkaido National Fisheries Research  
Institute, Kushiro, 085 Japan

## Introduction

Micronektonic organisms have been believed to take important roles in marine ecosystems due to their vast biomass. In fact, various animals, extending from fish to seabirds and marine mammals utilize micronekton as food. Although such utilization has been reported by many authors, there have been no study evaluating the importance of micronektonic organism quantitatively as prey in a specific community. In this paper, the analysis evaluating the importance of micronektonic organisms for the total diet of bottom fish community, using data from more than 8,000 fish stomach examination is presented.

## Materials and methods

The samples used in study was collected during the eight cruises made during May and November, 1989-1992. The area surveyed was the lower continental shelf and upper continental slope off Sendai Bay, northern Japan. During each cruises, about 30 stations were trawled. From each trawling station, catch composition of fish was recorded, and 20 or less stomachs were sampled from each fish species for examination at the laboratory.

The contribution of micronektonic organisms to the total diet was calculated. A total of 255 trawling samples were included in the analysis. They were classified into eight assemblages of different year, month and depths. Since previous studies clarified that the fish assemblage in the present study area shows distinct change of fauna across the 300 m contour during May and across the 200 m contour

during November, respectively, the trawling samples were classified according to the depths.

The contribution to the total diet of was expressed by the following formula:

$$W = \sum diwi \times 10^{-2},$$

where  $W$  is the percent contribution of micronekton to the diet of the total fish species in a fish assemblage,  $di$  is the percent relative abundance of the species  $i$  in an assemblage, and  $wi$  is the percent contribution of micronektonic organism in the diet of species  $i$ . In calculating  $di$ , catch data obtained by different research vessels were standardized by average wing spreads of trawling nets. The calculation was made separately for lantern fish (myctophidae), non-myctophid mesopelagic fish (mainly gonostomatidae and bathylagidae), the enoplotheuthid pelagic squid *Watasenia scintillans* and the pelagic shrimp *Sergestes similis*.

## Results and Discussion

Although more than a total of 80 species of demersal fishes were included in the analysis, the bulk of the fish biomass (generally >70%) was represented by Pacific cod, walleye pollock, brown hake (*Physiculus maximowiczi*) and threadfin hake (*Laemonema longipes*) (Fig. 1).

The contribution of micronektonic organisms to each of the fish assemblages is shown in Fig. 2. The contribution ranged from zero to 57% with differences by month, depth and year. The almost of the contribution was made by firefly squid and lantern fish, except for the two assemblages, in which *Sergestes similis* was important.

During November, the contribution of micronekton was scarce in the shallow where the bottom water temperature was high (>10°C) due to the prevalence of the warm Kuroshio Current water.

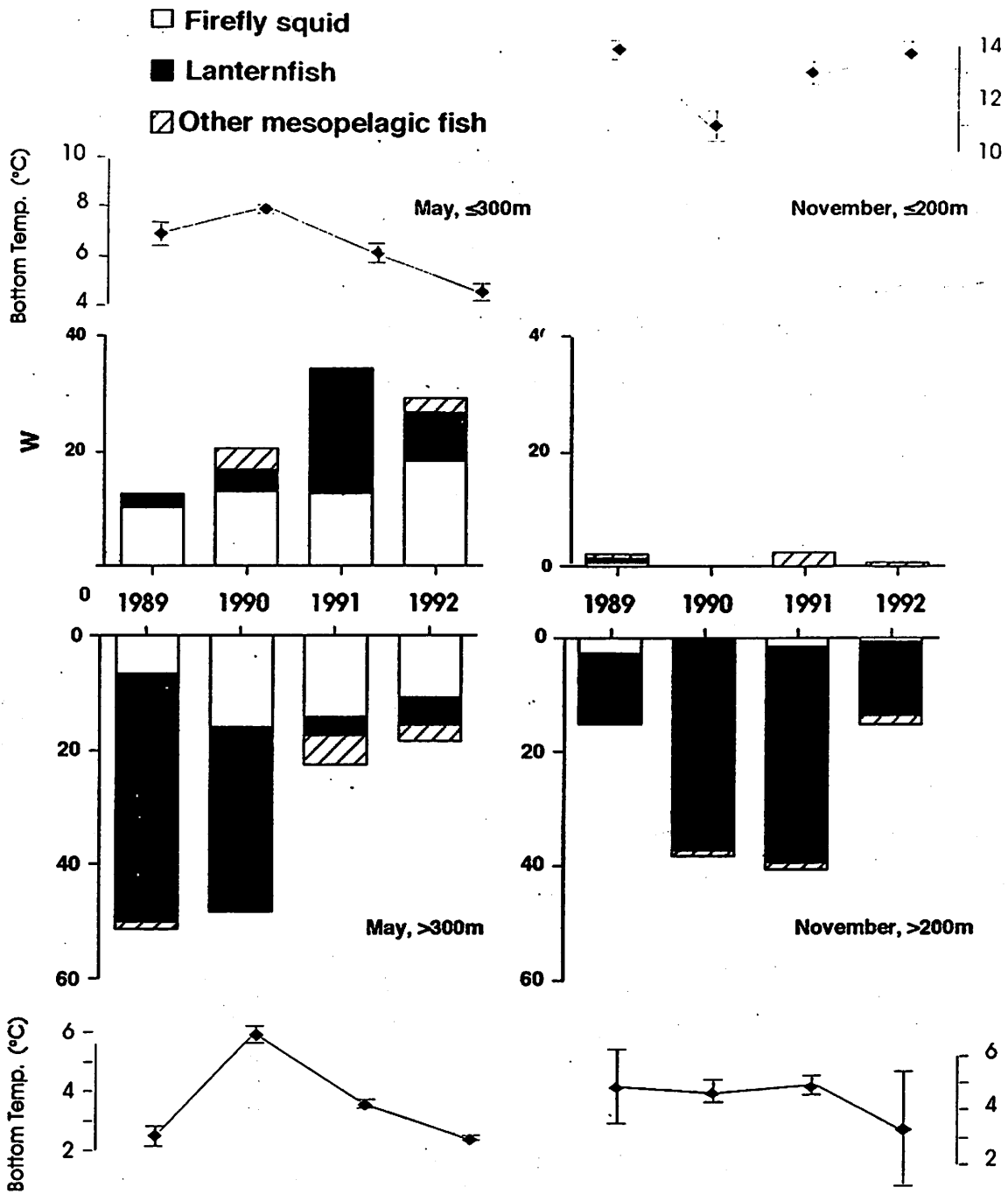
The contribution of firefly squid was remarkable both in the shallow and deep during May ranging 10-18% during May, however, it decreased abruptly through November. This decrease was not explained by the change of the water temperature, because there was no

considerable seasonal difference of water temperature in the area deeper than 200m.

On the other hand, our result of stomach contents analysis of walleye pollock from southeastern Hokkaido, about 1,000 km north from the present study area showed the reverse seasonal pattern compared to the present study area: no firefly squid was found from pollock stomach during June, but it was the most important prey for walleye pollock during November. This opposite seasonal pattern between the present study area and the southeastern Hokkaido area suggests that firefly squid undertake a northward migration between these months.

All of the micronektonic prey undertake diurnal vertical migration, and they have larger body size and longer lifespan compared to the major zooplankton prey such as *Euphausia pacifica* and *Neocalanus cristatus*. It is therefore concluded that the micronektonic prey benefit demersal fish assemblage as 1) vertical food transporter, 2) food concentrator and 3) food storage.





2  
 Fig. 4. Percentage contribution in total diet of demersal fishes caught at different depths, months and years, calculated by the formula  $W = \sum D_i w_i \times 10^2$ . Mean bottom water temperature, weighted by the catch (kg) at each trawling station is also given. Error bars are  $\pm 1$  S.E.

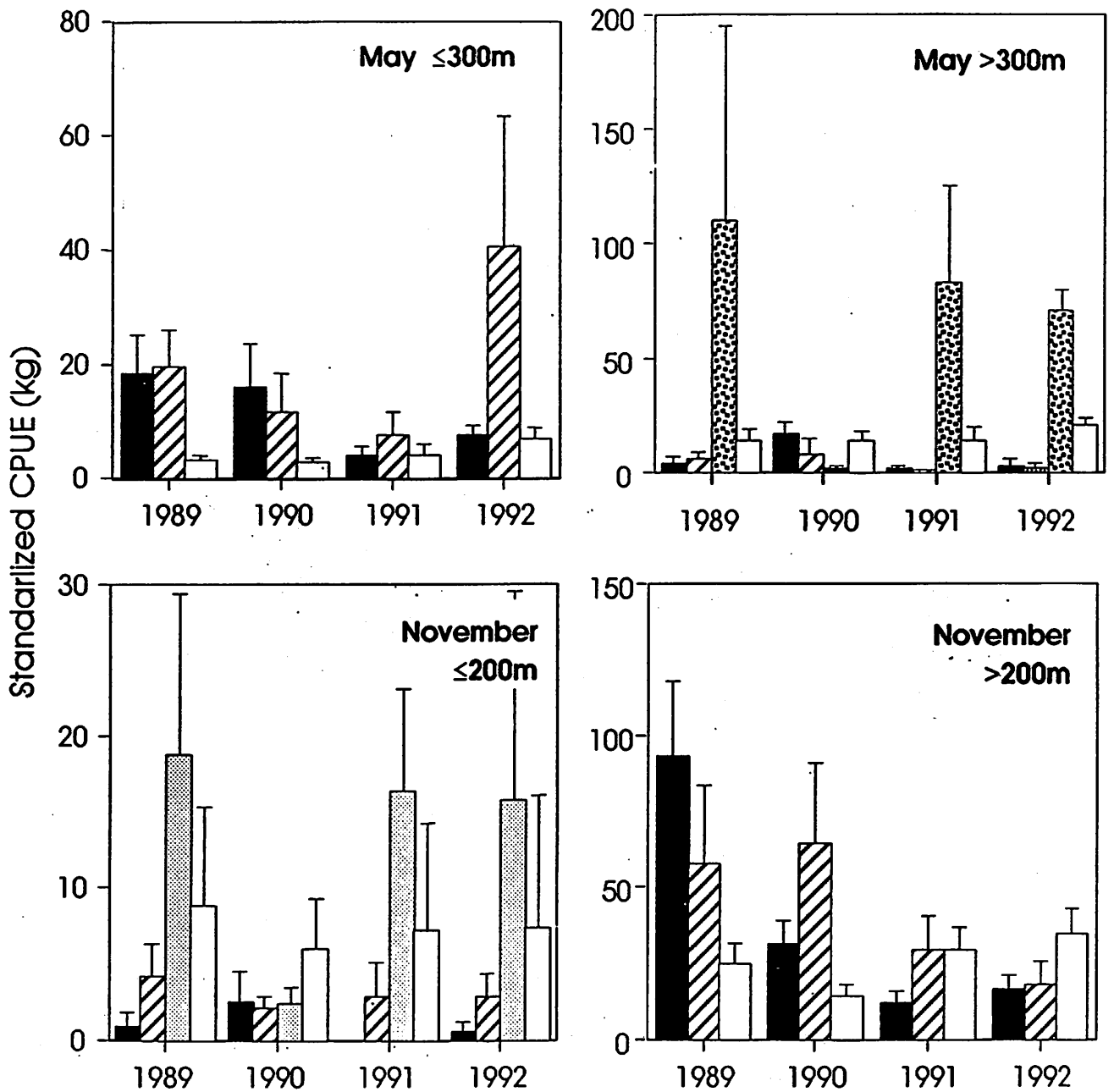
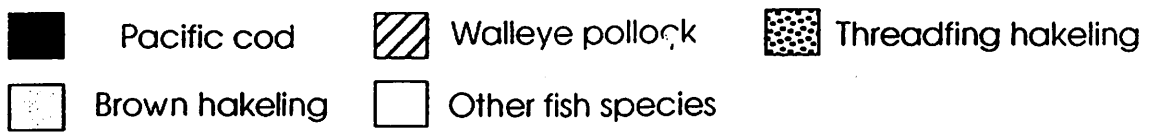


Fig.1. Abundance of demersal fishes in the study area for each year, month and depth. Abundance is expressed as CPUE standardized by the mean wing spread of trawling nets of research vessels. Error bars are  $\pm 1$  S.E.

## 5. BIO Papers(생물해양분과)

- Distributional characters of salps in relation to oceanographic condition in the Korean waters(한반도 주변의 해양환경에 따른 살파(salps)의 분포 특징) ..... 221
- Long-term change in zooplankton biomass in the Korean waters(한반도 수괴에서 동물플랑크톤 생물량의 장기 변동 조사) ..... 229
- The effect of changing environmental regimes on japanese commonsquid, *Todarodes pacificus* populations : a possible scenario(일본 오징어 (*Todarodes pacificus*)군집에 미치는 환경 변화 효과 예측) ..... 238
- Comparison of zooplankton communities between the central and western subarctic Pacific Ocean(중앙 태평양과 서부 아북극 태평양 사이의 동물플랑크톤 군집 구조 비교) ..... 247
- Interannual-interdecadal variations in zooplankton biomass, chlorophyll concentration and physical environment in the subarctic Pacific and Bering Sea(아북극 태평양과 베링해의 물리 환경과 동물플랑크톤 생물량, 엽록소 농도의 시간에 따른 변화 조사) ..... 254
- West-east comparison of seasonal variation in phytoplankton biomass in the subarctic North Pacific Ocean(아북극 북태평양의 서부와 동부에서 식물플랑크톤 생물량의 비교) ..... 264
- Life cycles of *Neocalanus flemingeri* and *N. plumchrus*(Calanoida, Copepoda) in the western subarctic Pacific(서부 아북극 태평양에 서식하는 *Neocalanus flemingeri*와 *N. plumchrus*의 생활사) ..... 269

## Distributional Characters of Salps in relation to Oceanographic Condition in the Korean waters

Young Shil Kang, Yeong Jo Jo, Woo Jin Go, Soung Soo Kim and  
Kyeong Am Jeon.

National Fisheries Research and Development Institute  
Shirang-ri, Kijang-up, Kijang-gun, Pusan city, 619-900, Korea

Salps are filter-feeding pelagic tunicates with a world-wide distribution in oceanic and some coastal waters. A zooplankton community dominated by large grazers like salps can produce a very different fate for primary production than one composed mainly of microzooplankton and copepods. Also they affect the change of marine ecosystem.

We examine factors related to distributional patterns of salps in the South Sea of Korea. We also try to find, in particular, trends in phytoplankton as an indicator of changes in productivity in this marine ecosystem.

Salps were vertically collected by NORPAC net (mesh size, 330  $\mu\text{m}$ ; diameter, 0.45 m) in the South Sea of Korea in February and April, 1997. Temperature, salinity,  $\text{O}_2$  and chlorophyll-a were estimated at five different depths, 0, 10, 20, 30, 50 m.

The dramatic increase and change in distribution of salps occurred in the South Sea of Korea in April, 1997 (Fig. 1).

Salps were, in particular, densely populated at the offshore of the South

Sea with densities of 150~934 inds./haul (0.159 m<sup>3</sup>).

Surface temperature and chlorophyll-a showed the detectable characteristics in April, 1997. The temperature was *ca.* 2°C higher than 1996 and mean of the 1961~1983 (Fig. 5). Chlorophyll-a in April, 1997 was less than February, 1997 and April and February, 1996 (Fig. 6).

Salps showed positive relationship with surface salinity but negative relationship with surface O<sub>2</sub> (Figs. 10, 11).

Considering high temperature and positive relationship between salinity and abundance of salps in April, 1997, salps distributed in the South Sea of Korea are transported by the Kuroshio Warm Current. Regarding the low chlorophyll-a in April, 1997, it was assumed that salps consumed a lot of chlorophyll-a in ecosystem and caused the competition with the other herbivorous zooplankton on food. The increased salps also affected O<sub>2</sub> concentration in the marine ecosystem.



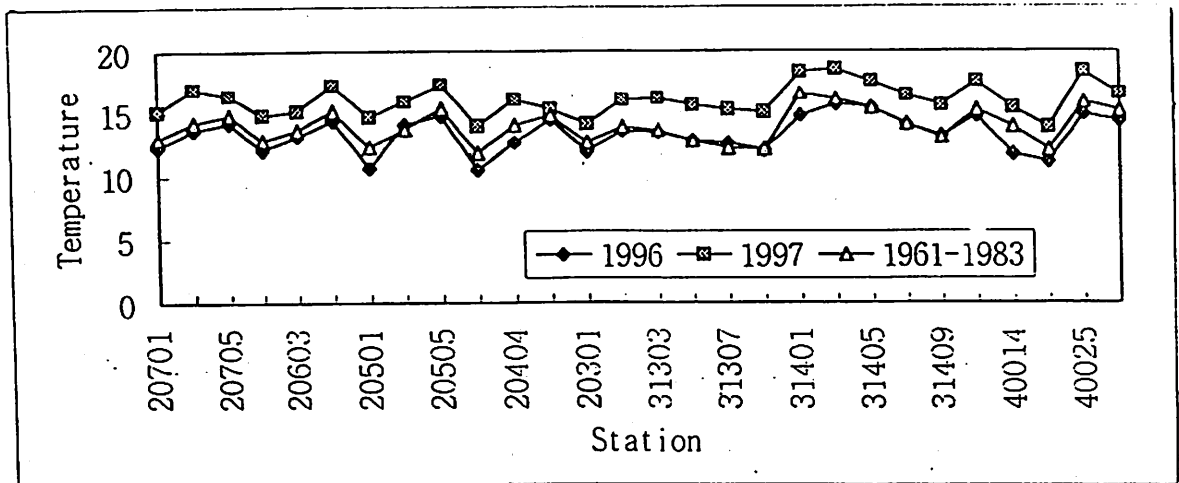


Fig. 5-a. Comparing surface temperatures in April, 1997 with April, 1996 and mean of 1961~1983.

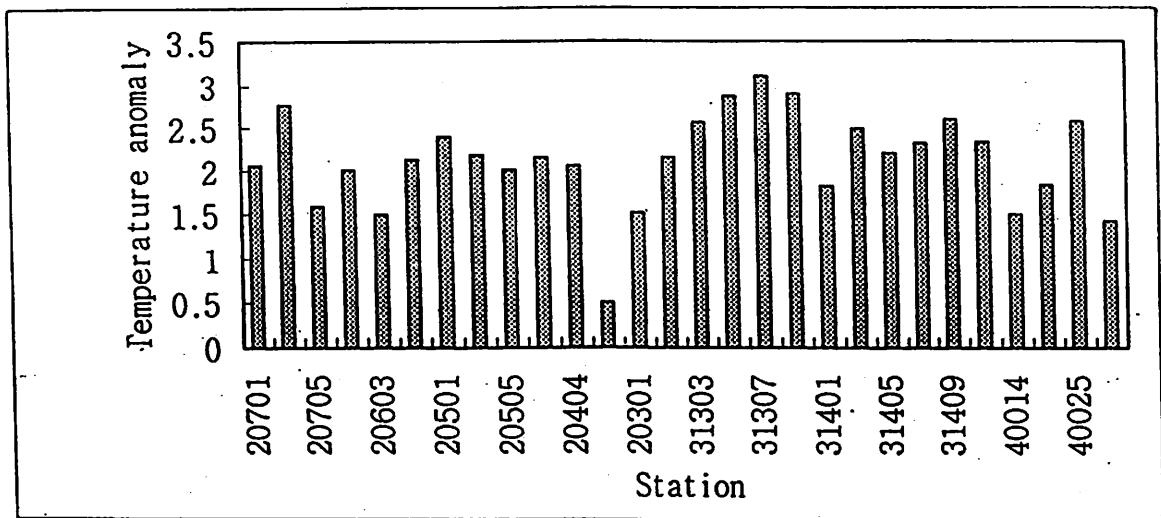


Fig. 5-b. Anomaly of surface temperature in April, 1997 based on the mean in April, 1961~1983.

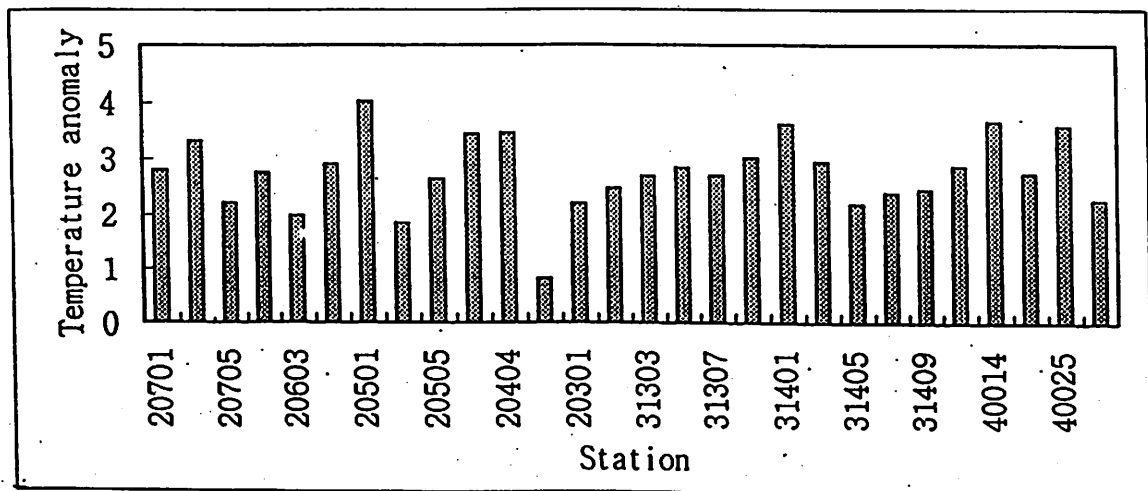


Fig. 5-c. Anomaly of surface temperature in April, 1997 based on April, 1996.

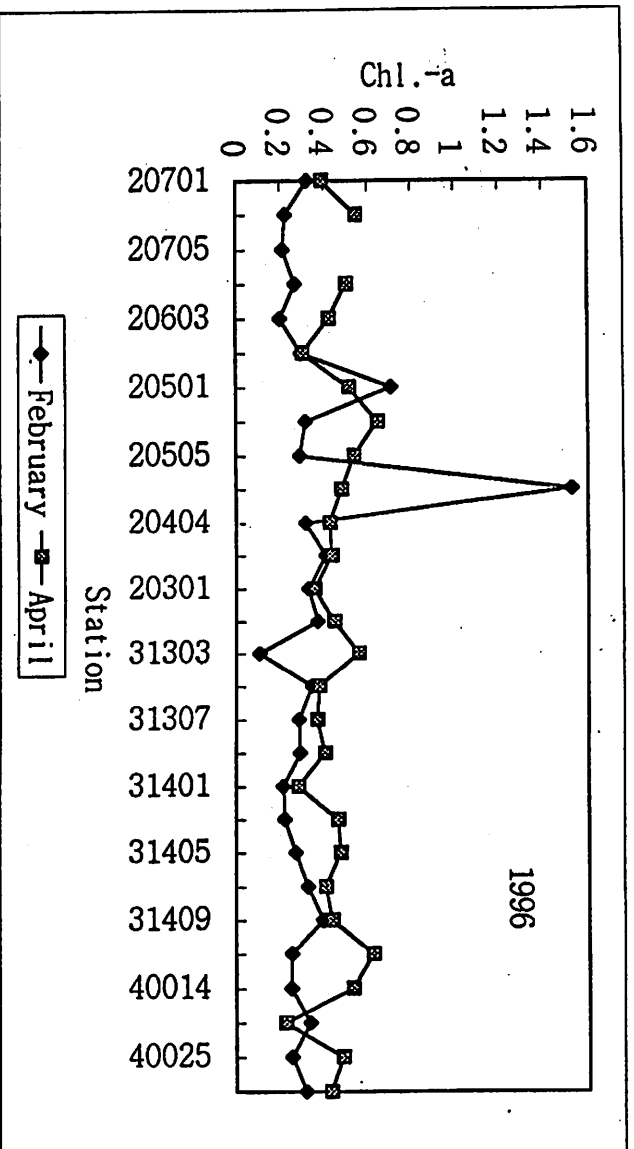
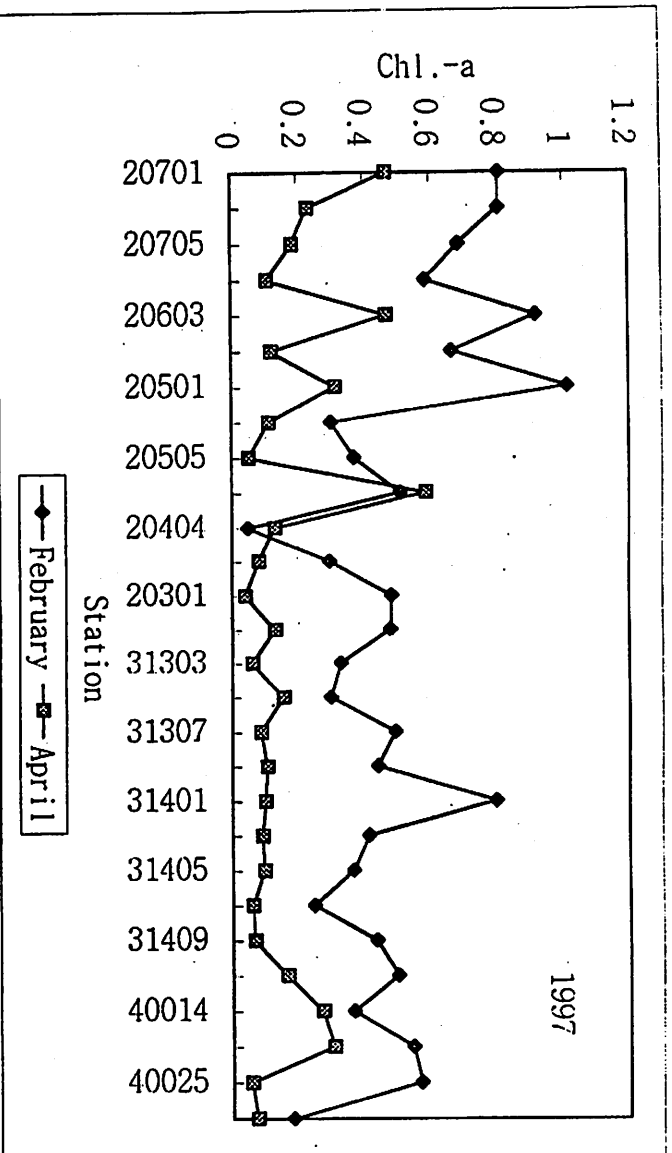


Fig. 6. Comparing mean of chlorophyll-a in April with February, 1997 and April with February 1996.



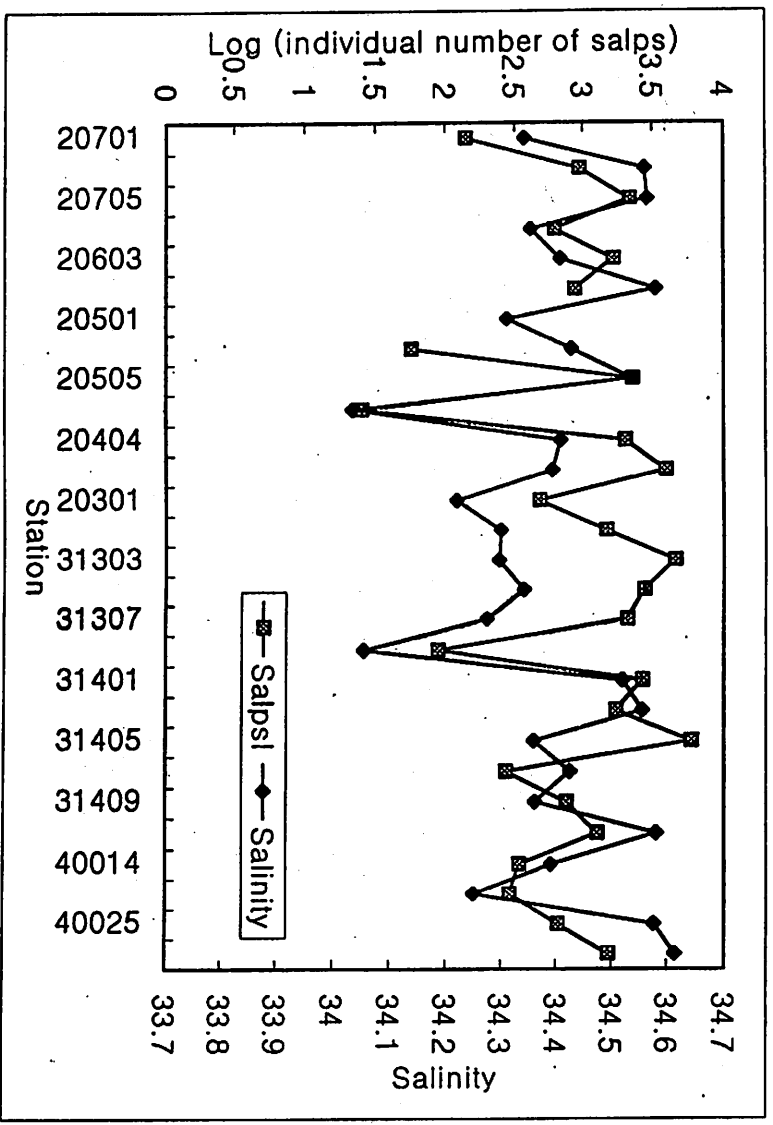
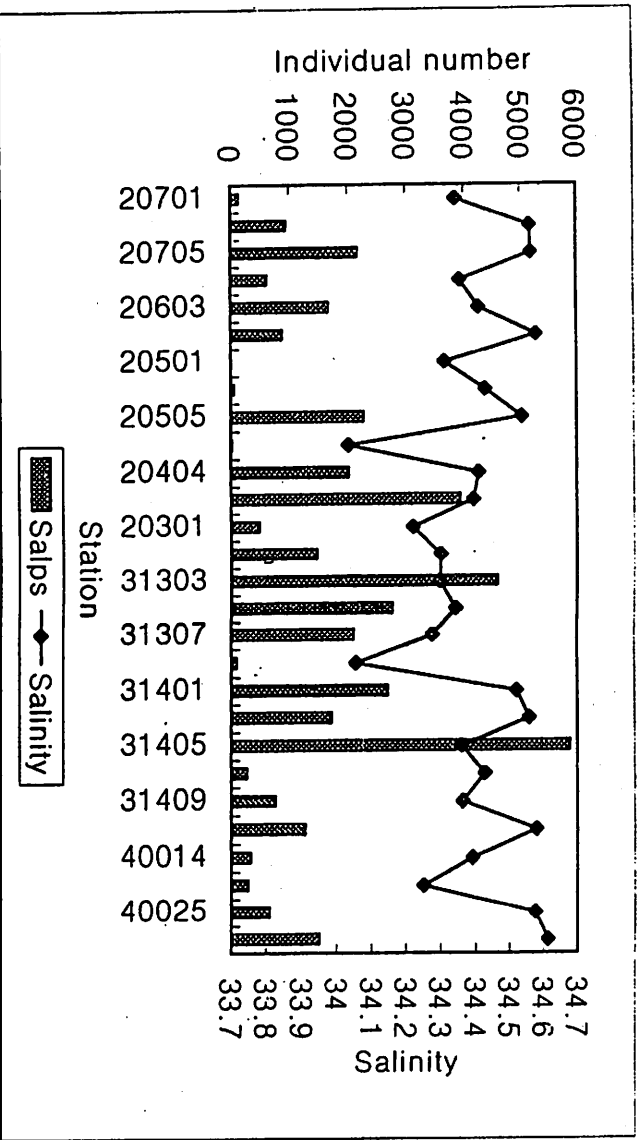


Fig. 10. Comparing the surface salinity with abundance of salps (inds. no.) and log-transformed data in April, 1997.

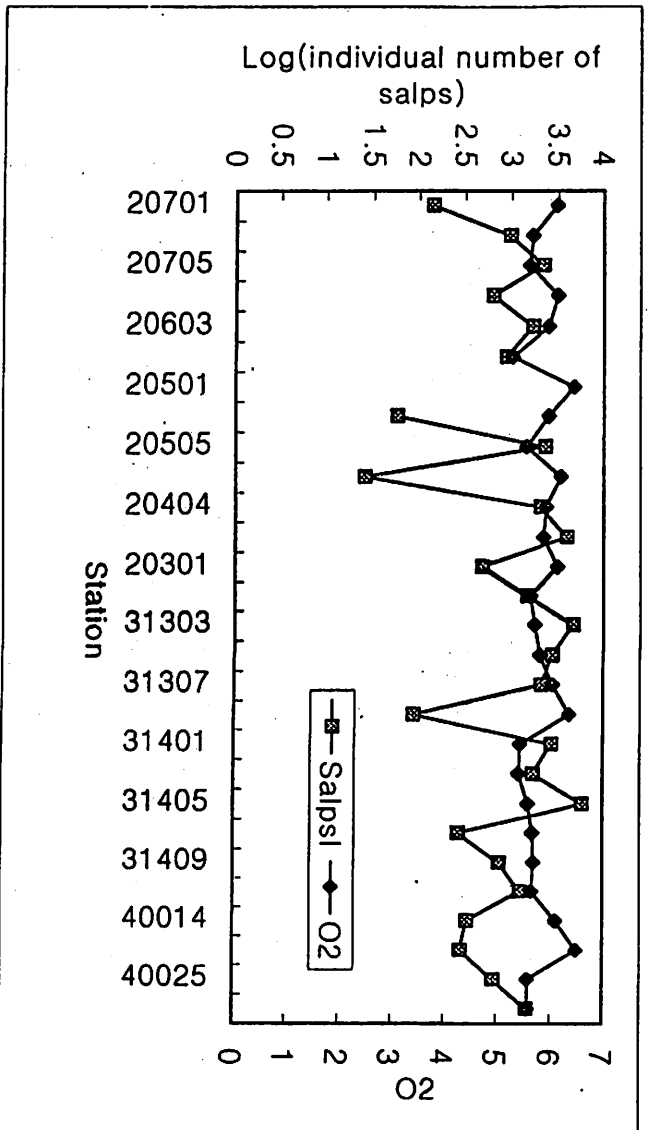
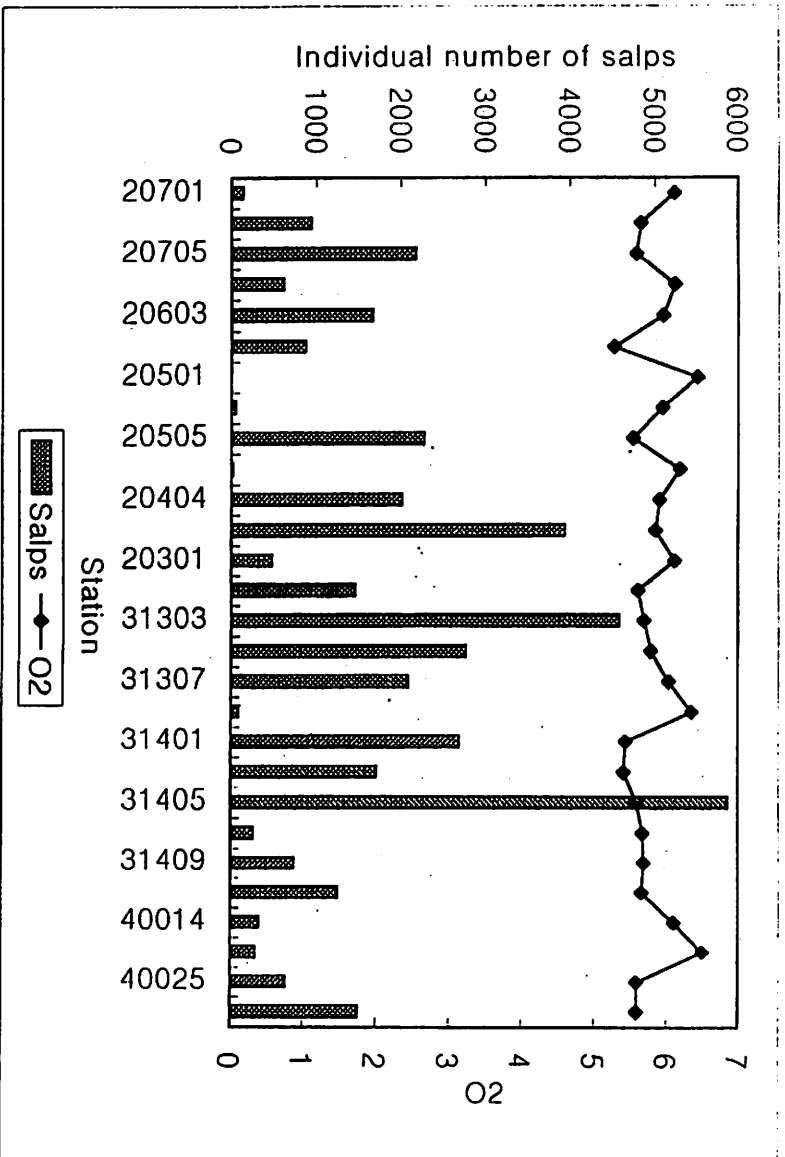


Fig. 11. Comparing the surface O<sub>2</sub> with abundance of salps (inds. no.) and log-transformed data in April, 1997.

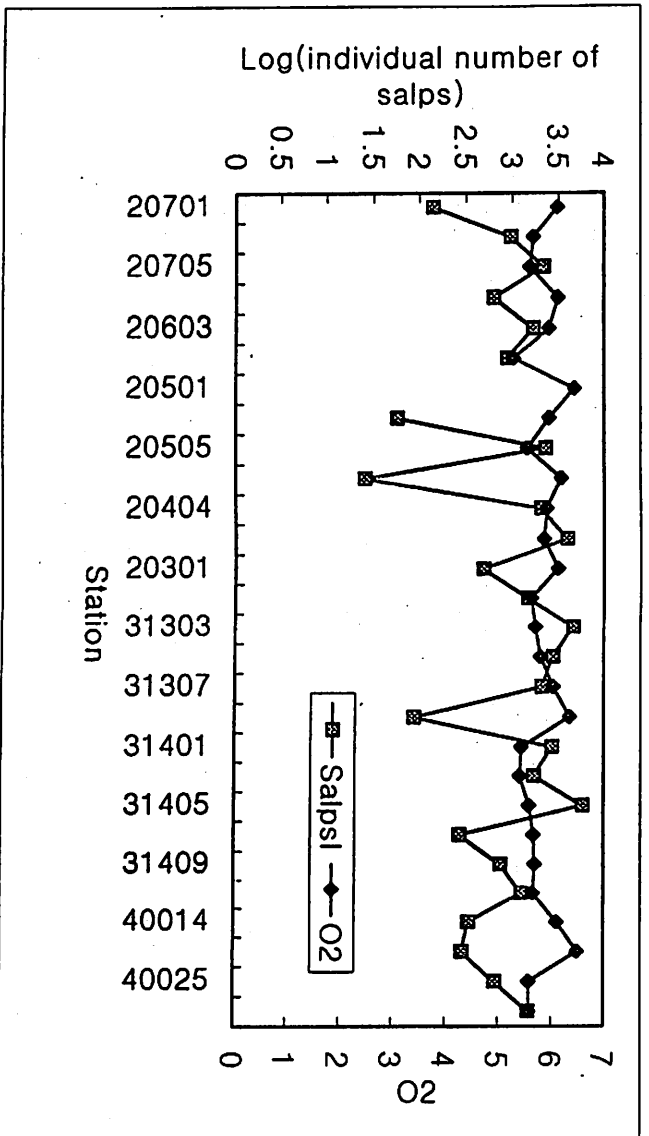
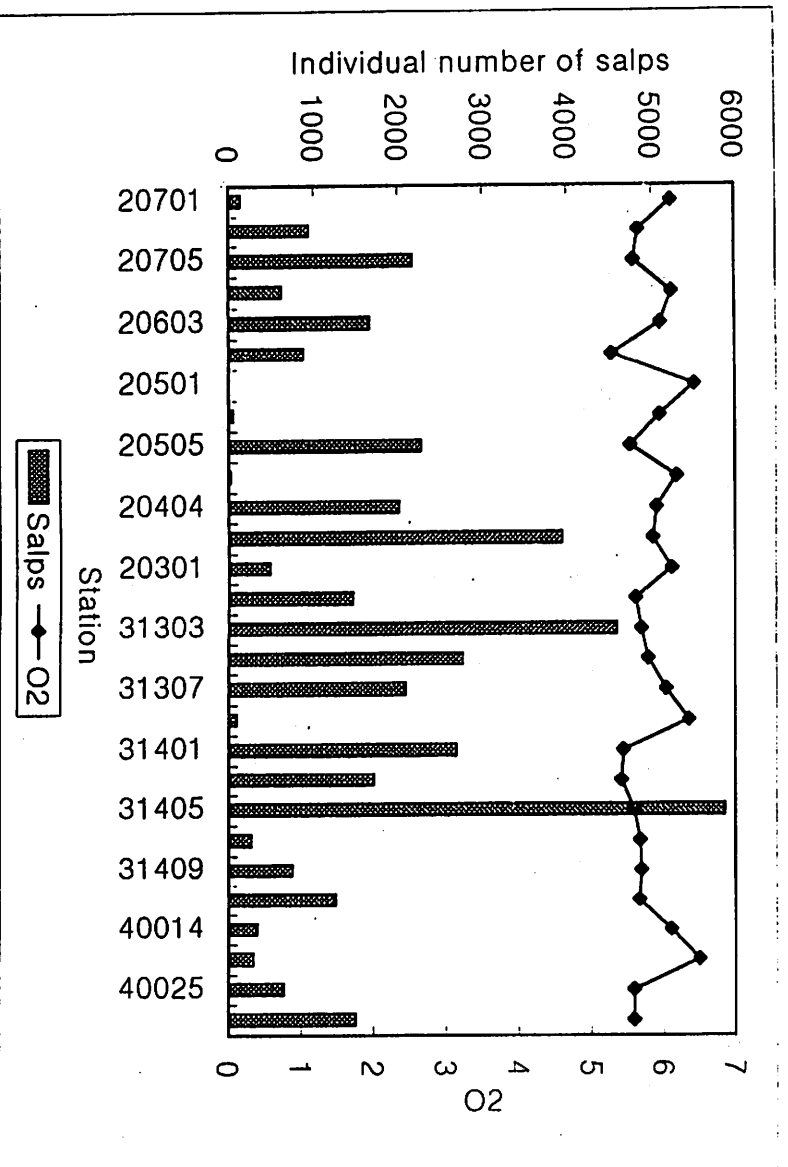


Fig. 11. Comparing the surface O<sub>2</sub> with abundance of salps (inds. no.) and log-transformed data in April, 1997.

## Long-term change in zooplankton biomass in the Korean waters

Young Shil Kang

National Fisheries Research & Development Institute, Shirang-ri,  
Kijang-up, Kijang-kun, Pusan city, 619-900, Korea  
e-mail: yskang@haema.nfrda.re.kr

Large scale climatic and oceanographic conditions affect the productivity of oceanic ecosystems. The change of large scale ecosystem can be recognized by understanding on the long-term change in ecosystem.

The objective of this study is to examine the long-term changes of zooplankton biomass in the Korean waters, which was sampled regularly using similar methodology during 1965~1995. I also examine the large scale distributional pattern of zooplankton biomass and how the these zooplankton biomass responded to long term changes in climate with surface temperature.

Zooplankton biomass data from 31 years (1965~1995) of vertical net sampling at 79 stations in the Korean waters used in this study (Fig. 1). Sampling was conducted bimonthly, February, April, June, August, October and December. Hauls were mainly done during daytime, and were vertically from 100 m depth in East and bottom in West and South to surface with NORPAC net (0.45 m diameter; 330  $\mu$ m mesh size).

Zooplankton biomass was estimated based on wet weight. Sampling frequency ratio varied from 0.021 to 0.996 based on total sampling number (474) in a year. The year showed sampling frequency ratio

less than 0.2 were not used to analyze the trend of long-term change.

Surface temperature also measured at same stations during 31 years (1965~1995).

I used coefficient of variation.  $(SD/x)$  (McGowan et al., 1996) to smooth the data and percentage anomaly  $[(X-x)/x*100]$  (Mullin, 1994) to trace the trend of year to year changes.

The annual mean of zooplankton biomass during 1965~1995 was  $88.82 \text{ mg/m}^3$  with peaks in April, June and October (Fig. 10). The high biomass over than  $100 \text{ mg/m}^3$  occurred mainly in the middle part of West Sea, inshore and offshore areas of South Sea and the upper middle part of East Sea (Fig. 3). The lower biomass less than  $50 \text{ mg/m}^3$  appeared very spot in the coastal area of East Sea and the central part of West Sea. Those distributional patterns showed the seasonal variations with north-south and inshore-offshore gradients.

The annual coefficient of variation  $(SD/x)$  showed the high spatial variability in the inshore-offshore area of middle part of East Sea, the southeastern area of South Sea and the inshore area of middle part of West Sea (Fig. 5). This revealed the states that the range is large in February, April and June with the mean over than about 1.5 but is small in August, October and December with the mean less than about 1.0 (Fig. 7).

Annual anomaly showed the year to year changes, and it was distinct that anomaly is positively increased from 1990 to 1995 (Fig. 8). Of these years, 1993 revealed the highest positive anomaly. It was caused by the high zooplankton biomass in the offshore area of the southeastern part of South Sea in April when temperature was about  $1^\circ\text{C}$  higher than the other years (Fig. 14).

From this study, I could find an important facts. Zooplankton biomass showed the increasing trend since 1990. It is mainly caused by very limited areas where appeared the complex hydrogratical conditions, such as polar front in the middle part of the East Sea, the main area of Kuroshio Warm Current in the South Sea and the coastal area of West Sea.

Zooplankton biomass revealed the typical seasonal variation. But it is impossible to trace the relationship between fluctuation of zooplankton biomass and surface temperature in the long-term series.

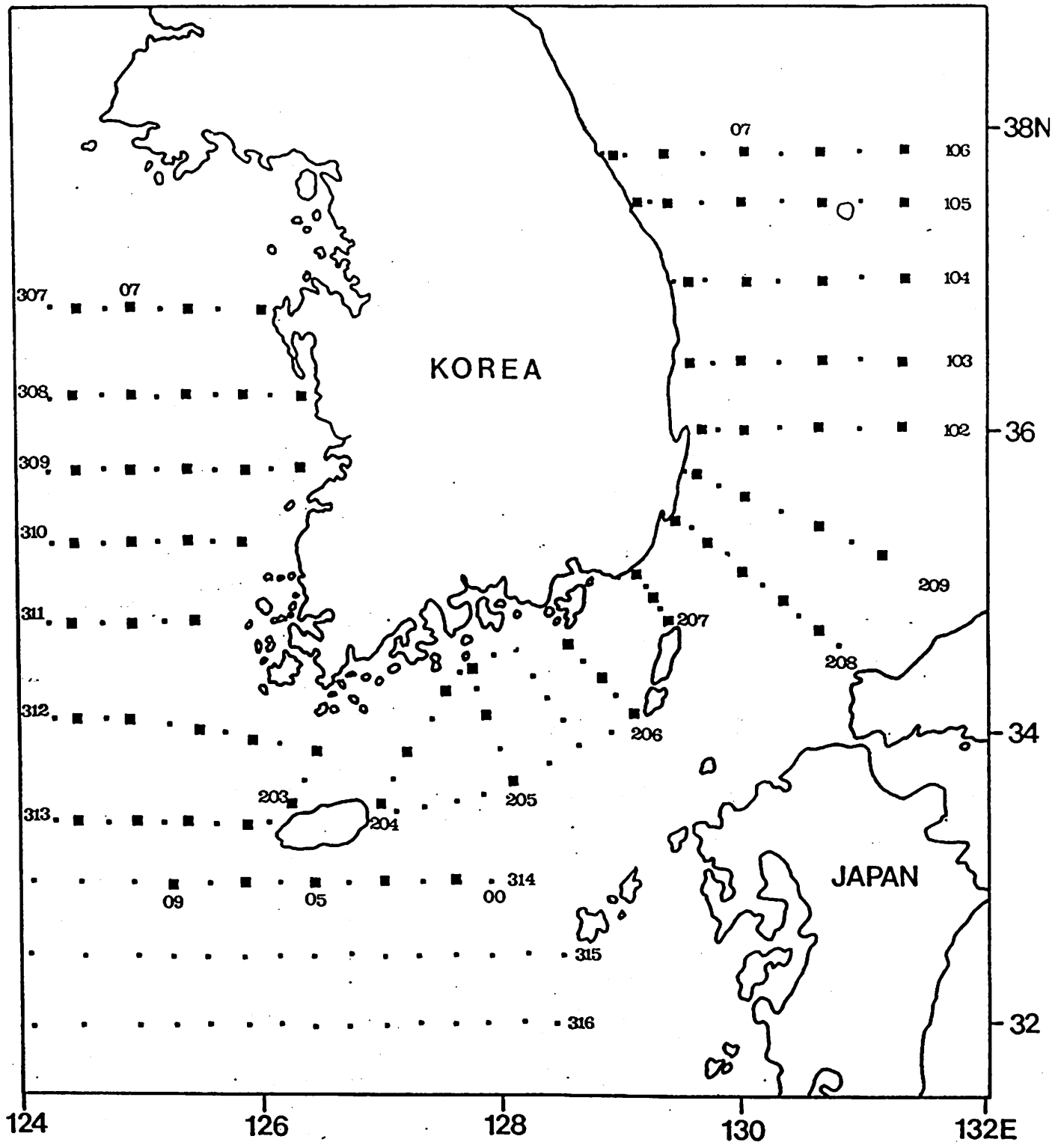


Fig. 1. Map showing the study area and sampling sites.

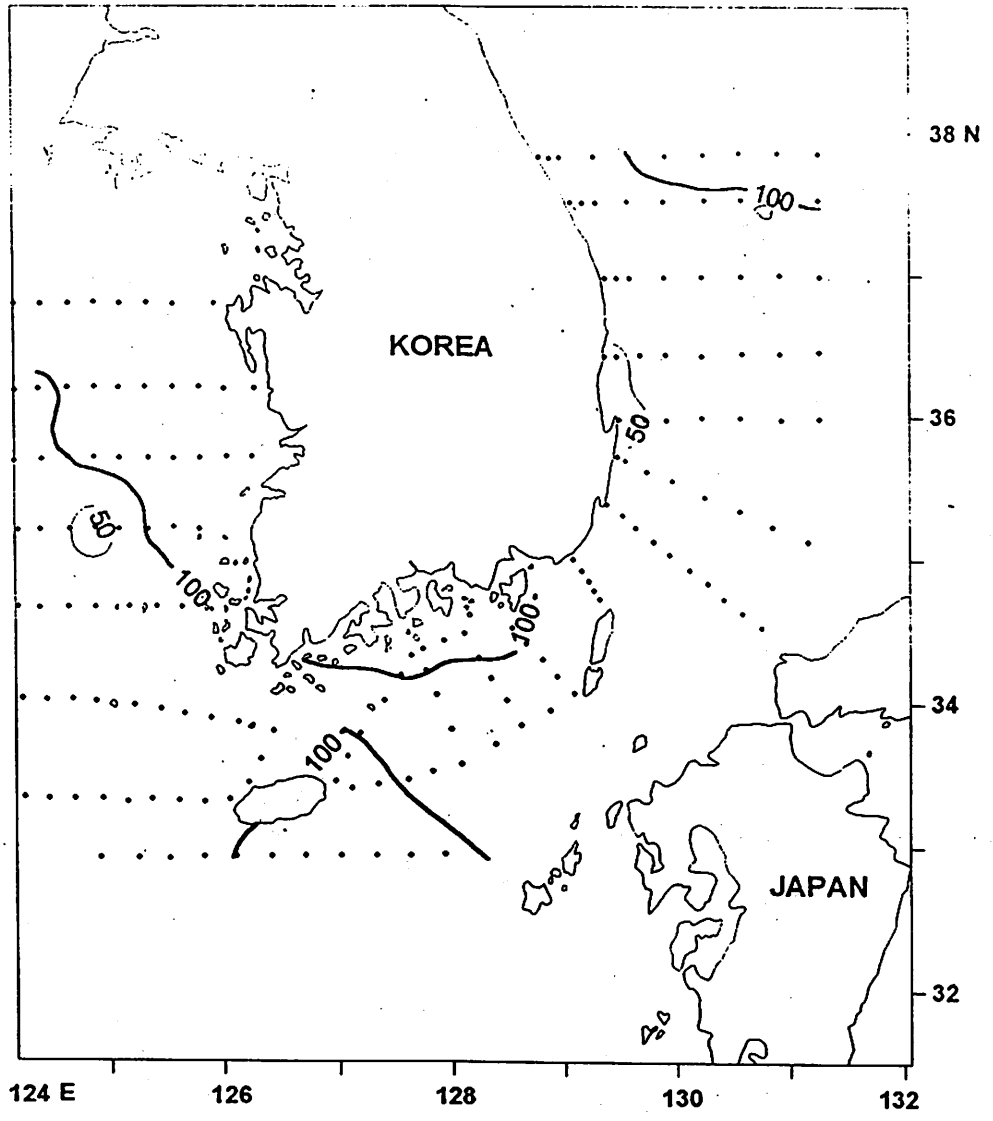


Fig. 3. Distribution of the long term annual mean of zooplankton biomass (mg/m<sup>3</sup>).

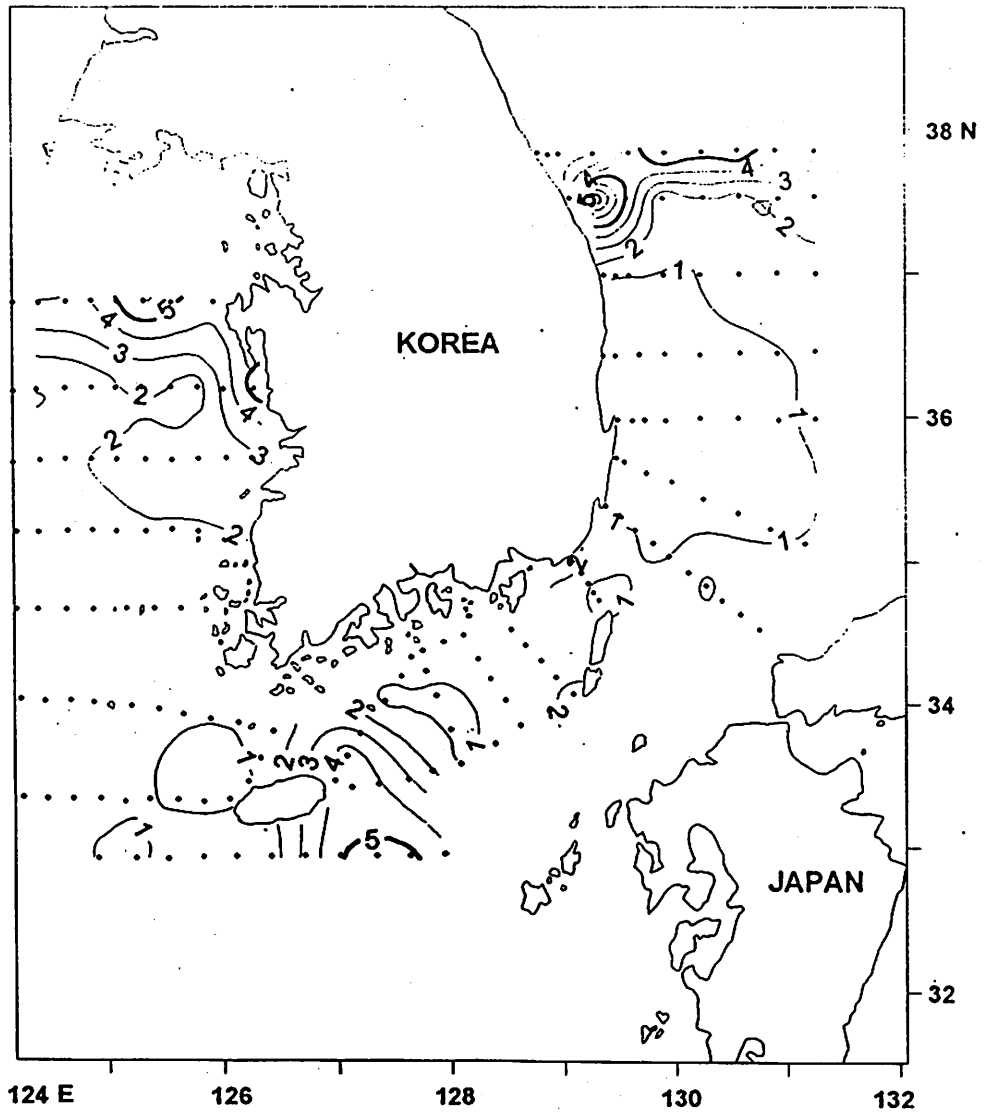


Fig. 5. Distribution of the annual coefficient of variation ( $SD/\bar{x}$ ) of zooplankton biomass based on the mean ( $\bar{x}$ ) of all over stations.



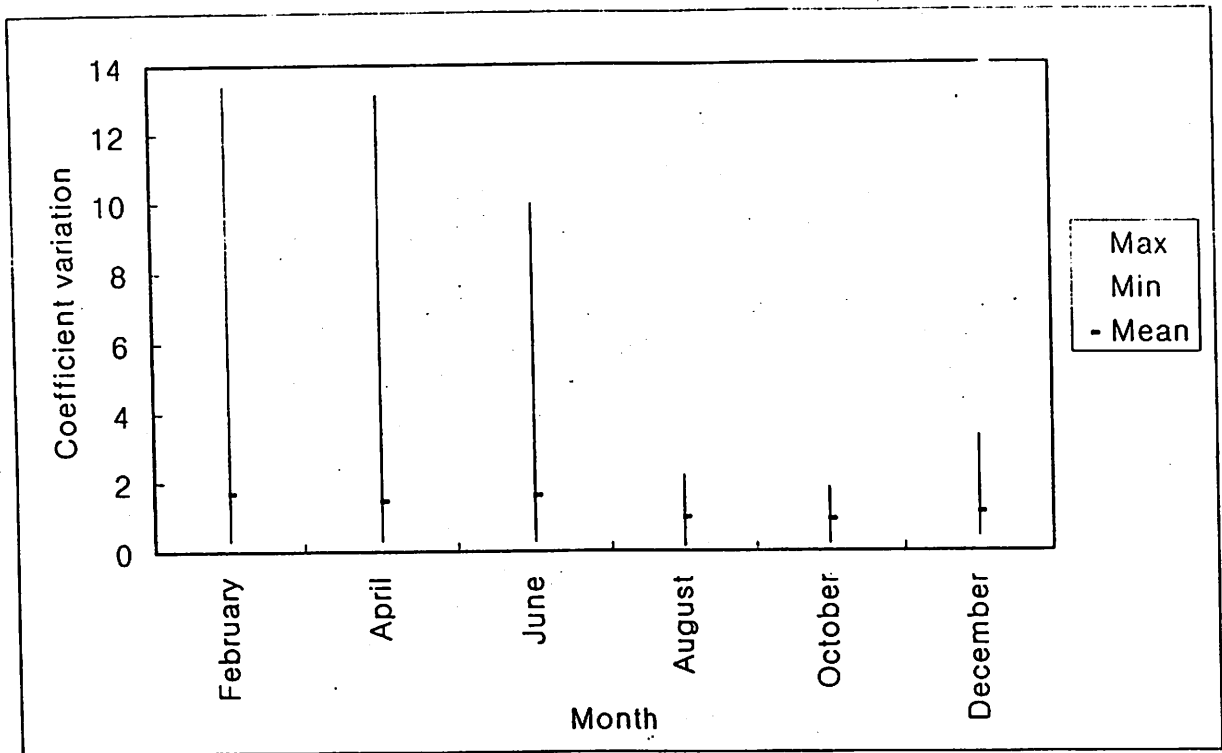


Fig. 7. Mean and ranges of the coefficient of variation (SD/x) based on the mean (x) of all over stations in February, April, June, August, October and December.

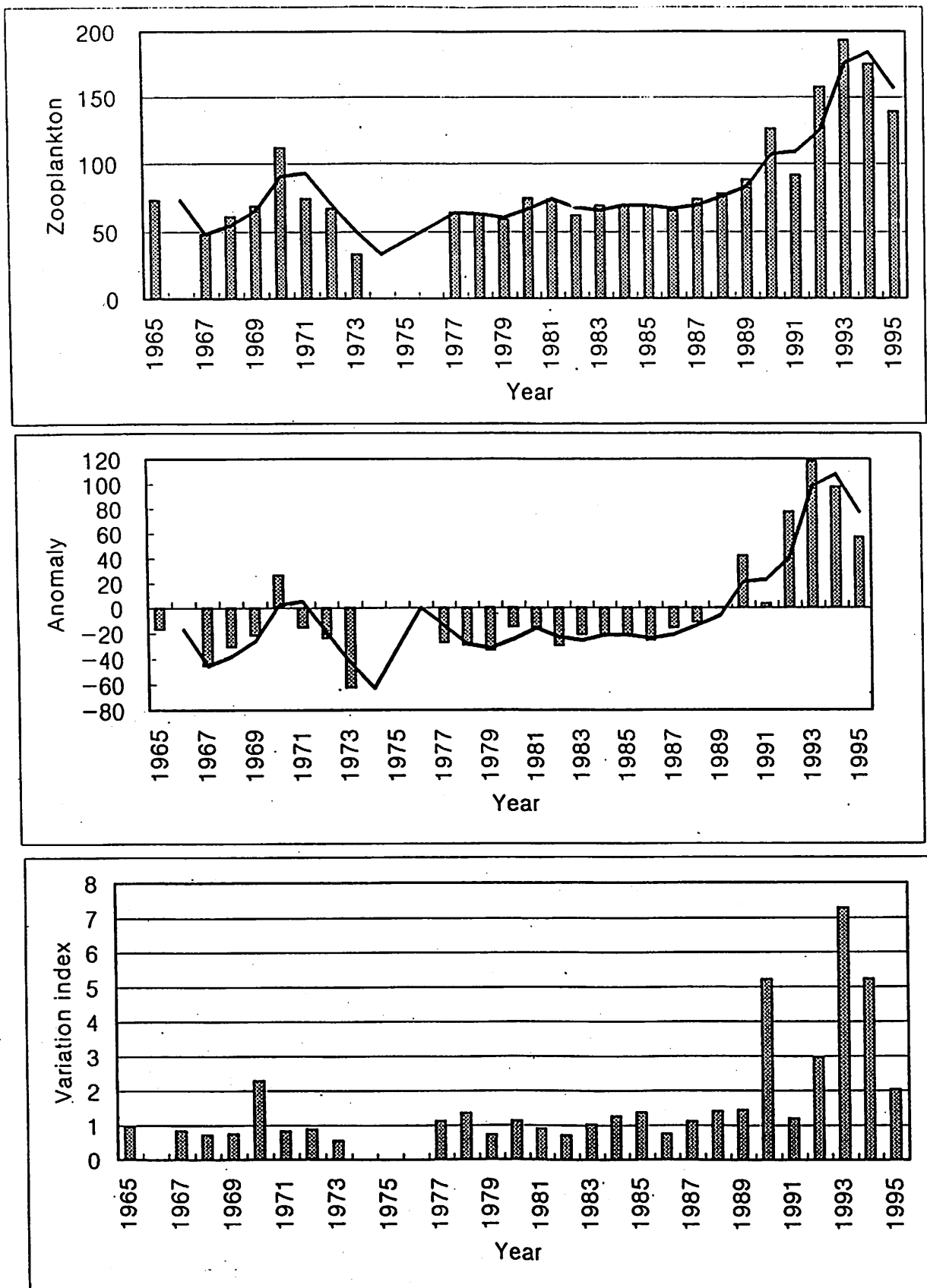


Fig. 8. Long term changes in annual mean (A), anomaly (B) and the coefficient of variation ( $SD/x$ ) of zooplankton biomass from 1965 to 1995.

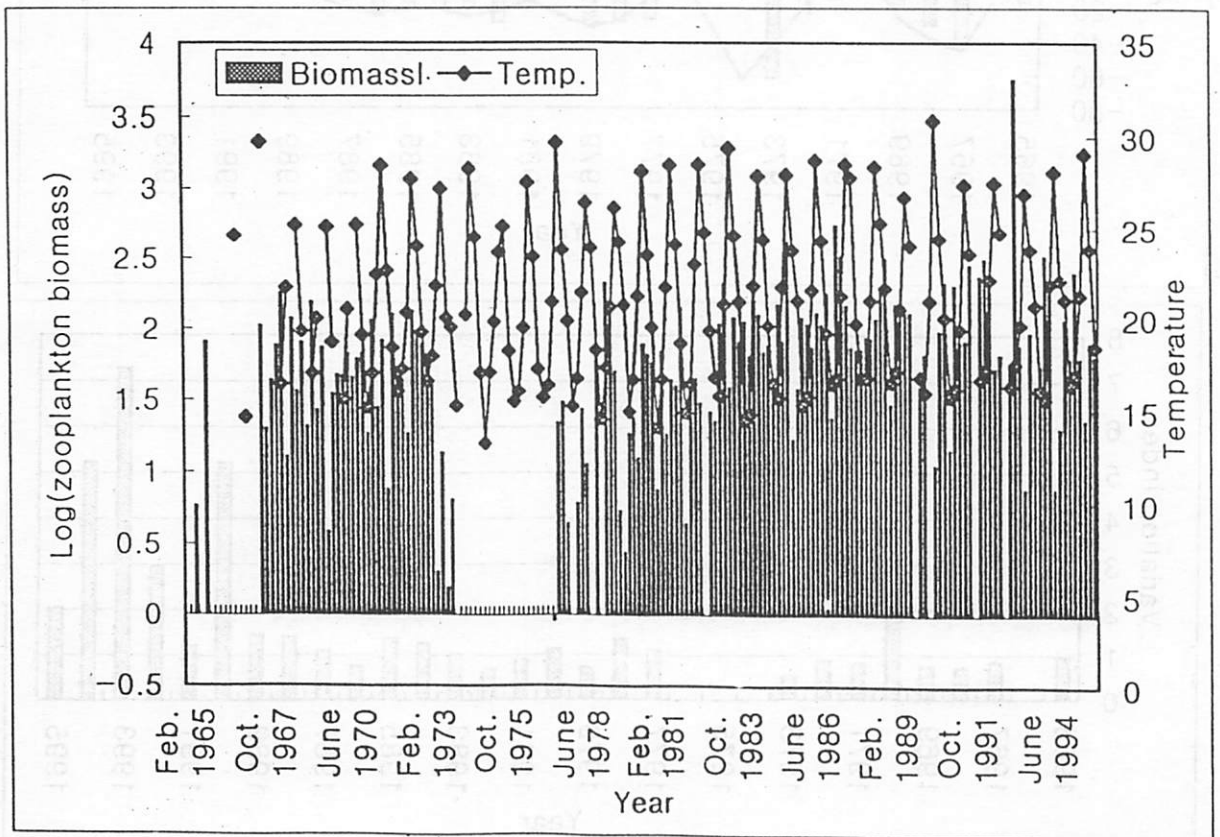
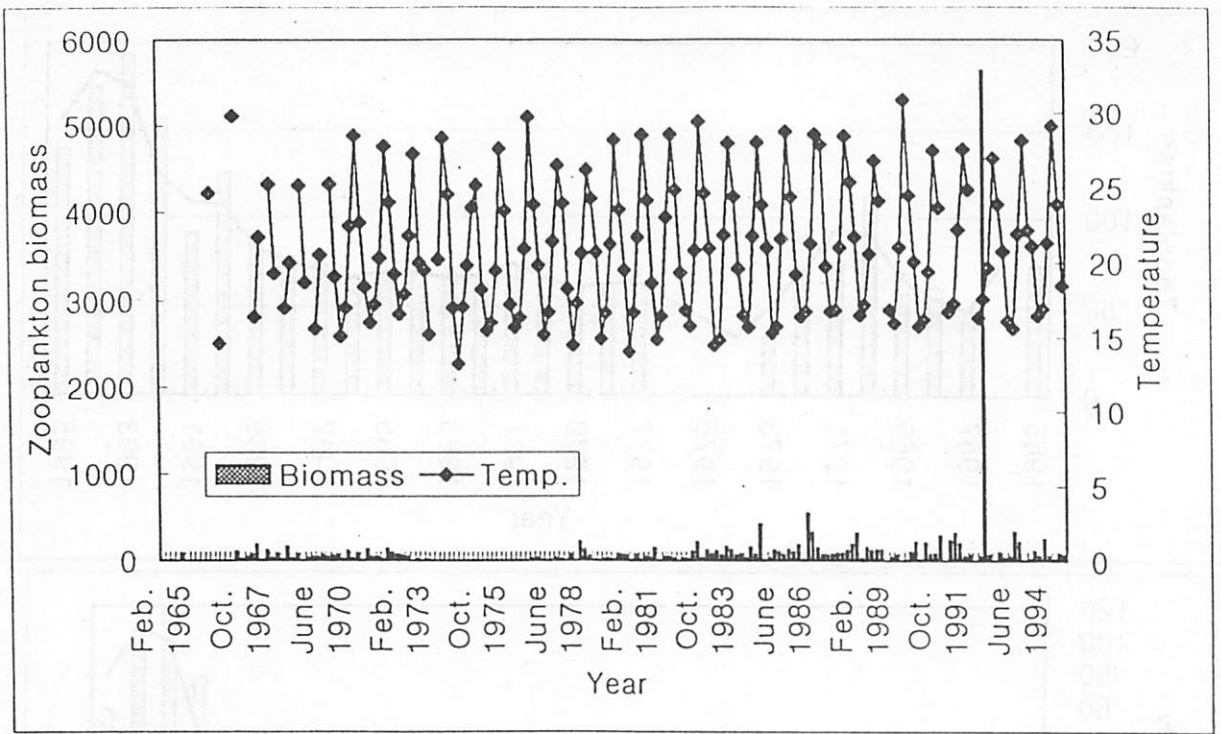


Fig. 13. Long term changes in zooplankton biomass (A) and  $\log_{10}$ -transformed zooplankton biomass (B) and surface temperature at station 31401.

McGowan, J.A., D.B. Chetton and A.A. Conversi. 1996. Plankton patterns, climate, and change in the California current. CalCOFI Rep., 37, 45~68.

Mullin, M.M., 1994. Distribution and reproduction of the planktonic copepod, *Calanus pacificus*, off southern California during winter-spring of 1992, relative to 1989~1991. Fish. Oceanogr., 3/2, 142~157.

## The effect of changing environmental regimes on Japanese common squid, *Todarodes pacificus* populations: a possible scenario

Yasunori Sakurai, Hidetoshi Kiyofuji and Sei-ichi Saitoh

Faculty of Fisheries, Hokkaido University, Hakodate, Hokkaido, 041 Japan

### Introduction

The Japanese common squid, *Todarodes pacificus* (Ommastrephidae), performs seasonal migrations in waters near Japan and Korea, with spawning occurring at the southern end of its distribution (Murata, 1990). On the basis of the spawning seasons, growth types, and migratory patterns, three groups of winter, fall and summer spawning groups are believed to exist in their waters. However, these spawning grounds are overlapped through the seasons. Many ommastrephid squid populations show large fluctuations in abundance and catch. The catches of *T. pacificus* have fluctuated during 20<sup>th</sup> century. The annual catch rate near Japan has gradually increased since 1987 to about 400,000 tons in the last year, 1996, which is close to the catch rates during the 1950s and 1970s. These fluctuations naturally depend on the development of fishing efforts, including size of fleets, acoustic and fishing gear, and lighting fixture.

In the western North Pacific, interdecadal regime shifts in water temperature occurred from a warming regime in the mid 1940s, to a cooling regime in the mid 1970s, and back to a warming regime in the late 1980s (e.g. Kodama *et al.*, 1995). The catch fluctuation looks like to fit to their environmental regimes, particularly the 1980s decreasing phase and the increasing phase of catch rates. The abundance of paralarvae in fall after 1989 has been higher than during the late 1970s to the mid 1980s (Goto, pers. comm.). These fluctuations may occur related with long-term regime shifts in water temperature around Japan more than that of catch rates of adult squids.

In the present study, therefore, we proposed a possible scenario about the effects of changing environmental regimes on *T. pacificus* populations, based on two working hypotheses: the catch rates in the western North Pacific increase with a shift to a warm regime, and a warm regime will create an favorable environmental conditions for reproduction and recruitment of the squid. Finally, we examined the relationship between the recent annual and decadal changes of the optimum spawning grounds of *T. pacificus* and the water temperature around southern Japan.

## Materials and Methods

We examined the possible spawning sites of *Todarodes pacificus* around Japan, using the following information from laboratory and field studies. *T. pacificus* produces gelatinous and nearly neutrally buoyant egg mass, which would be maintained in the warm surface layer, where temperatures are adequate for normal embryonic development (Bower *et al.*, 1996). The optimum temperatures for survival of embryos and paralarvae are between 15 and 23°C (Sakurai *et al.*, 1996). The most hatchlings occur where the sea temperature range from 18 to 23°C (Bower, 1997). The females sit on the bottom just before spawning (Bower *et al.*, 1996), suggesting that spawning occurs near or above the continental shelf.

Based on these information, we estimated that the favorable spawning sites of *T. pacificus* will be formed in the warm surface layers of temperature range from 15 to 23°C near or above the continental shelf around Japan. The optimum temperature range of normal development will seasonally delimit the timing and location of spawning of this squid, and the location of egg masses in nature. Therefore, we tried to detect the possible spawning area of *T. pacificus* using both of their information and the seasonal changes of mean monthly temperature at 50m depth between 1900 and 1972, and the position of the continental shelf near the Japanese Archipelago (JODC, 1978).

For detecting the relationship between the recent annual and decadal changes of spawning grounds of *T. pacificus* and water temperature around the southern Japan between 1982 and 1994, we selected four study areas in the adjacent waters of Noto Peninsula, Iki Island, Goto Islands and continental shelf water of East China Sea. For each study area, mean sea surface temperature in each 5×5 pixels was calculated by the equation for each pixels from temperature at the depth of 0m and 50m of Levitus Data, which was produced by the NDOC (National Oceanographic Data Center). By this equation, we calculated monthly mean temperature at the depth of 50m for each area during the periods of 1982 and 1994 was calculated, when the monthly global MCSST was set to the 0m temperature. The MCSST was derived from the NOAA Advanced Very High Resolution Radiometer (AVHRR).

## Results and Discussion

We estimated monthly possible spawning sites of *T. pacificus* around Japan during a year, which were only made by information of optimum temperature for reproduction of this squid, not catch data of adult squid

and distribution data of paralarvae (Fig.1 and 2). All of shaded areas and dark-shaded areas in Figures indicate spawning sites of favorable temperature for embryonic development between 15°C and 23°C (Sakurai *et al.*, 1996), and occurrence temperature of many hatchlings between 18°C and 23°C at 50m depth (Bower, 1997) above the continental shelf surrounded by 100m and 200m isobaths around Japan, respectively. In this study, we used temperature at 50m depth, not at sea surface or more deeper depth, because the squid egg mass would be maintained in the warm surface layer (Bower *et al.*, 1996; Sakurai, pers. comm.) and hatchlings are concentrated in waters from 25m to 50m depth (Watanabe, 1965). Also, we estimated that spawning sites of *T. pacificus* will be above the continental shelf around Japan, because the females always sit on the bottom just before spawning at the captive observation (Bower *et al.*, 1996; Sakurai, pers. obs.) and many exhausted spent females in nature are caught by commercial bottom trawl net at the continental shelf (e.g. Hamabe and Shimizu, 1966), suggesting that spawning occurs near or above the continental shelf.

Main spawning sites in winter are widely formed along the continental shelf of the East China Sea from Kyushu to Taiwan, and small spawning areas occur in the western and the southwestern coast waters of Kyushu and Pacific coast water along Shikoku (Fig. 1). Most of paralarvae hatched in winter will be transported to Pacific side in the inshore water masses of Kuroshio. During spring to summer, possible spawning areas gradually move to northwards along the both continental shelves of the Sea of Japan and Pacific side. In fall, main spawning grounds will be formed around the Tsushima Strait and Noto Peninsula (Fig. 2). Small areas for spawning will occur along the coast of northern Japan. Throughout the year, spawning sites along the coast of Pacific side will be limited. For this reason, spawning grounds of *T. pacificus* will mainly occur around the Tsushima Strait in fall, and the East China Sea in winter (Murata, 1990), but these spawning sites may be not segregated seasonally. Thus, we could reproduce the seasonal shifts of possible spawning sites of this squid by temperature changes. It was suggested that the success of spawning strategy of *T. pacificus* will be strongly related to changing environmental regimes in waters around Japan.

For detecting the environmental effects to *T. pacificus* populations, we examined the relationship between the recent annual and decadal changes of optimum spawning grounds of *T. pacificus* and water temperature around the southern Japan. Fig. 3 shows the recent trend of water temperature at surface and 50m depth of selected 4 stations in February, when peak of spawning in winter, during 1982 to 1994 (Murata, 1990). After 1987 when catch rates of *T. pacificus* and abundance of paralarvae increased (Goto, pers. comm.), both of SST and temperature of 50m depth at off

Goto Islands have increased over 15°C, which are in optimum temperature of spawning and embryonic development of *T. pacificus*. Also, temperature changes at two stations in waters around Iki Island and off Noto Peninsula show that spawning sites were not formed in the Sea of Japan during winter.

We compared the seasonal changes of temperature at 50m depth between 1984 as a cold year and 1994 as a warm year (Fig.4). In 1984, possible spawning areas occurred at St. 1, 2 and 3 in fall, and St.4 in winter. However, in 1994, possible spawning grounds were formed at St.1 and 2 in the Sea of Japan in fall, and St.3 in fall and winter and St.4 in winter. These results mean that spawning area in a cold year will be limited in the Sea of Japan during fall and in the East China Sea in winter. However, spawning area in a warm year will be overlapped in the water off Goto Islands during fall and winter.

It was suggested that *T. pacificus* population reduction phase with a cooling regime will occur with reduction of spawning area and season to the southwestern Japan Sea during fall, and population increase phase with a warming regime will occur with extension of spawning area and season to the Sea of Japan, East China Sea, and sometimes to Pacific side during fall and winter. Further investigations of life cycle strategy of ommastrephid squids is needed, especially in the case of population dynamics of *Todarodes pacificus* related to environmental regimes in the past and present.

**Acknowledgments.** We thank Drs. John Bower and Yutaka Isoda for valuable discussion.

## References

- Bower, J. R. and Y. Sakurai, Laboratory observations on *Todarodes pacificus* (Cephalopoda: Ommastrephidae) egg masses. *Amer. Malaco. Bull.*, 13, 65-71, 1996.
- Bower, J. R., A biological study of egg masses and paralarvae of the squid *Todarodes pacificus*. Ph. D. Thesis, Hokkaido University, 1997.
- Hamabe, M. and T. Shimizu, Ecological studies on the common squid, *Todarodes pacificus* Steenstrup, in the southeastern waters of the Japan Sea. *Bull. Jap. Sea Reg. Fish. Res. Lab.*, 16, 13-55, 1966. (in Japanese with English summary)
- Japan Oceanographic Data Center [JODC]. Marine Environmental Atlas. Northwestern Pacific Ocean II (Seasonal and Monthly). Japan Hydrogr. Association, Tokyo, 147pp., 1978. (in Japanese with English summary)
- Kodama, J., H. Nagashima, and Y. Izumi, Long-term variations in the "Mang ku herring", *Clupea pallasii valenciennes* resources in relation to



- the ocean environments in the waters off Sanriku and Joban. *Bull. Miyagi Pref. Fish. Res. Dev. Center*, 14, 17-36, 1995. (in Japanese)
- Murata, M., Ocean resources of squids. *Mar. Behav. Physiol.*, 18, 19-71, 1990.
- Sakurai, Y., J. R. Bower, Y. Nakamura, S. Yamamoto, and K. Watanabe, Effect of temperature on development and survival of *Todarodes pacificus* embryos and paralarvae. *Amer. Malaco. Bull.*, 13, 89-95, 1996.
- Watanabe, T., Ecological distribution of rhynchoteution larva of common squid, *Todarodes pacificus* Steenstrup, in the southeastern waters off Japan during the winters, 1959-1962. *Bull. Tokai Reg. Fish. Res. Lab.*, 43, 1-12, 1965. (in Japanese with English summary)

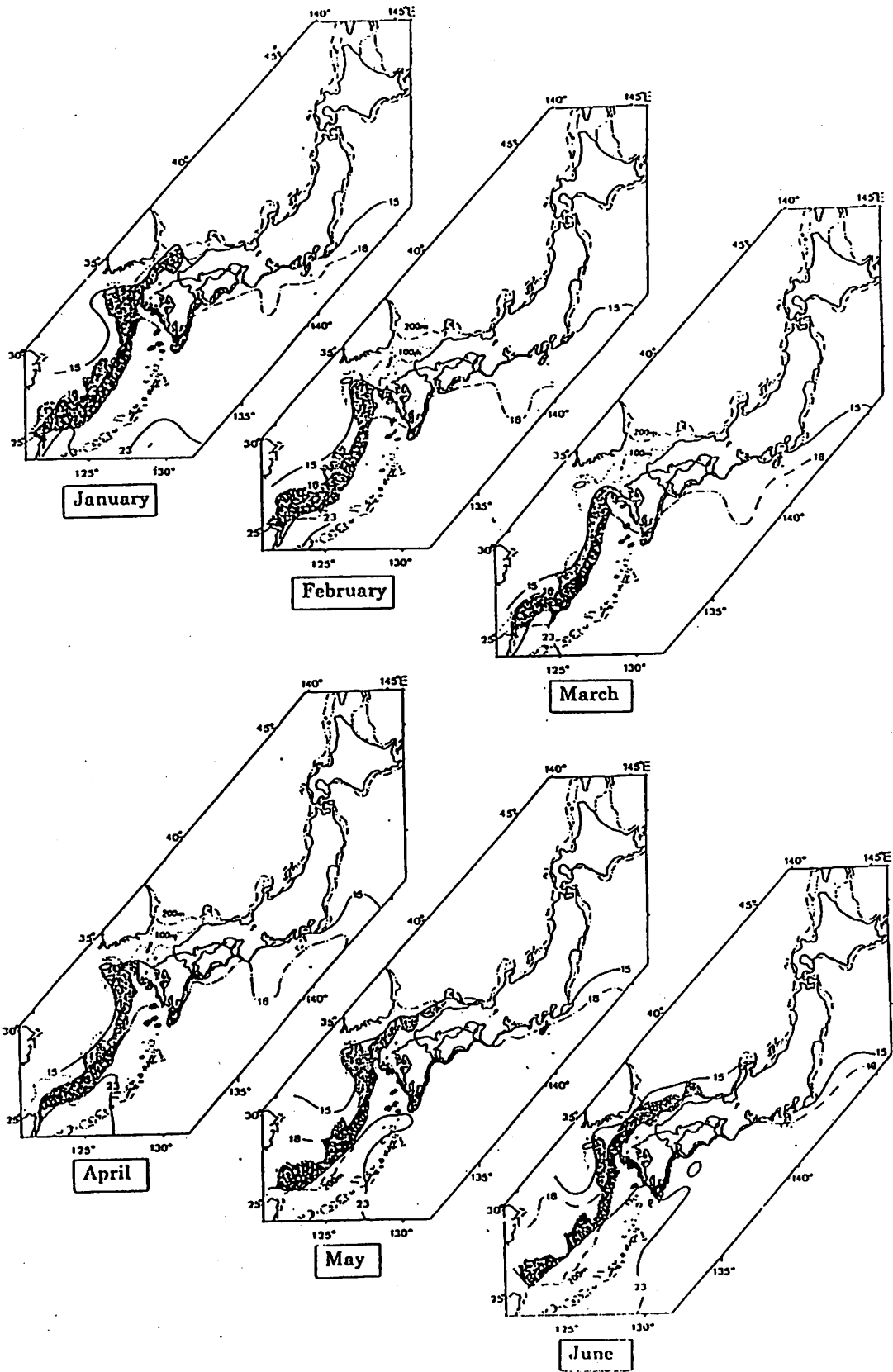


Fig. 1 Monthly possible spawning sites of *T. pacificus* around Japan during January to June, based on mean temperature at 50m depth between 1900 and 1972 (JODC, 1978). All of shaded areas and dark-shaded areas in Figures indicate spawning sites of favorable temperature at 50m depth for embryonic development between 15°C and 23°C (Sakurai *et al.*, 1996), and occurrence temperature of many hatchlings between 18°C and 23°C at 50m depth (Bower, 1997) above the continental

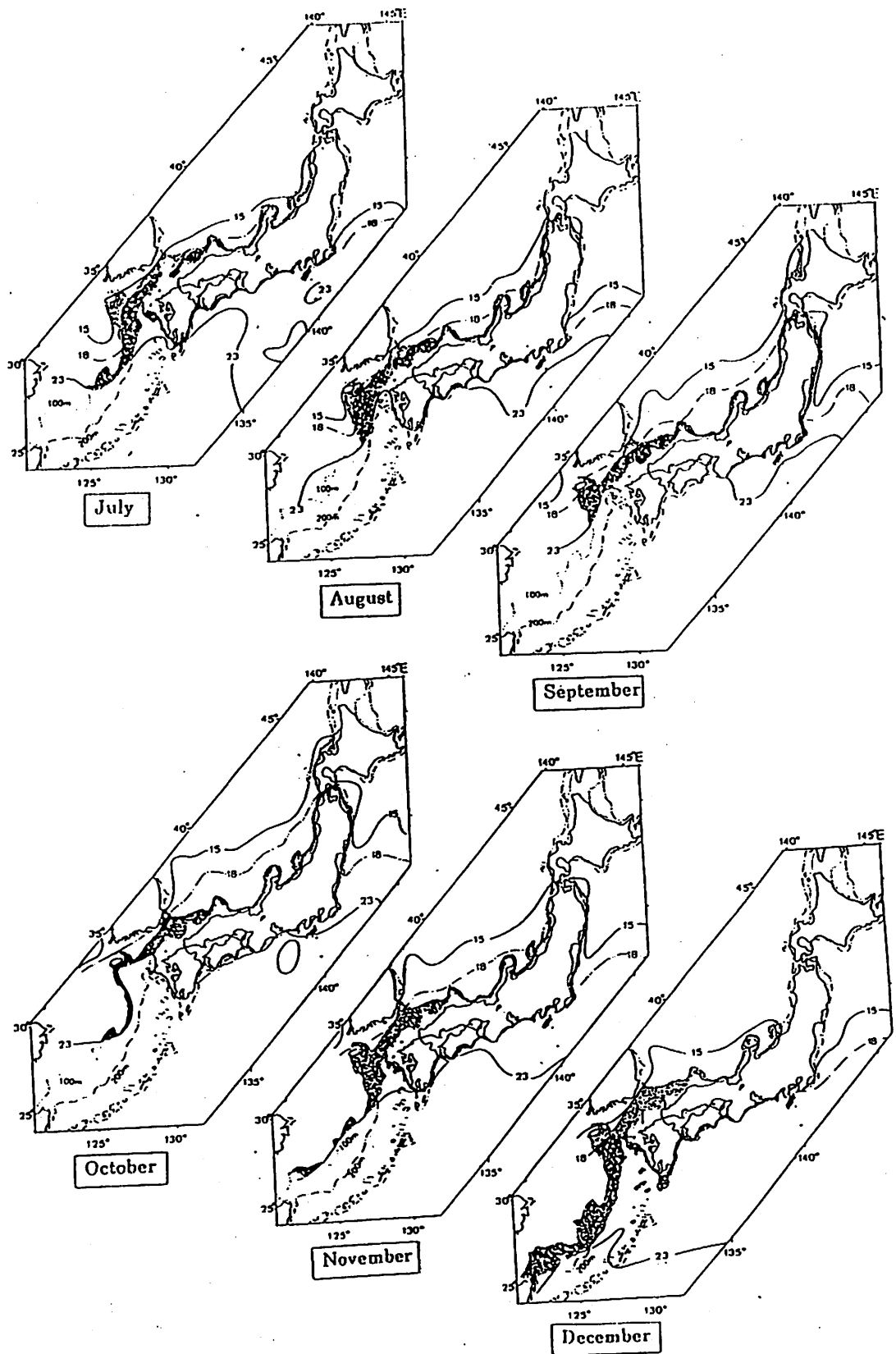


Fig. 2 Monthly possible spawning sites of *T. pacificus* around Japan during July to December, based on mean temperature at 50m depth between 1900 and 1972 (JODC, 1978).

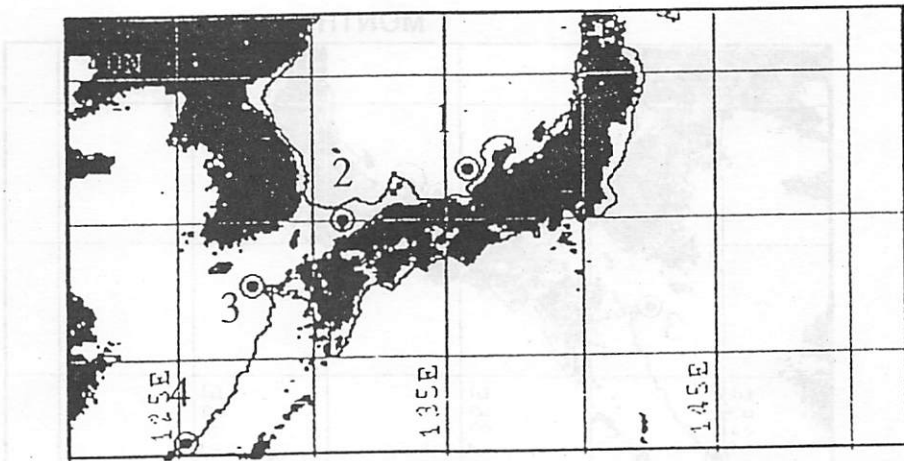
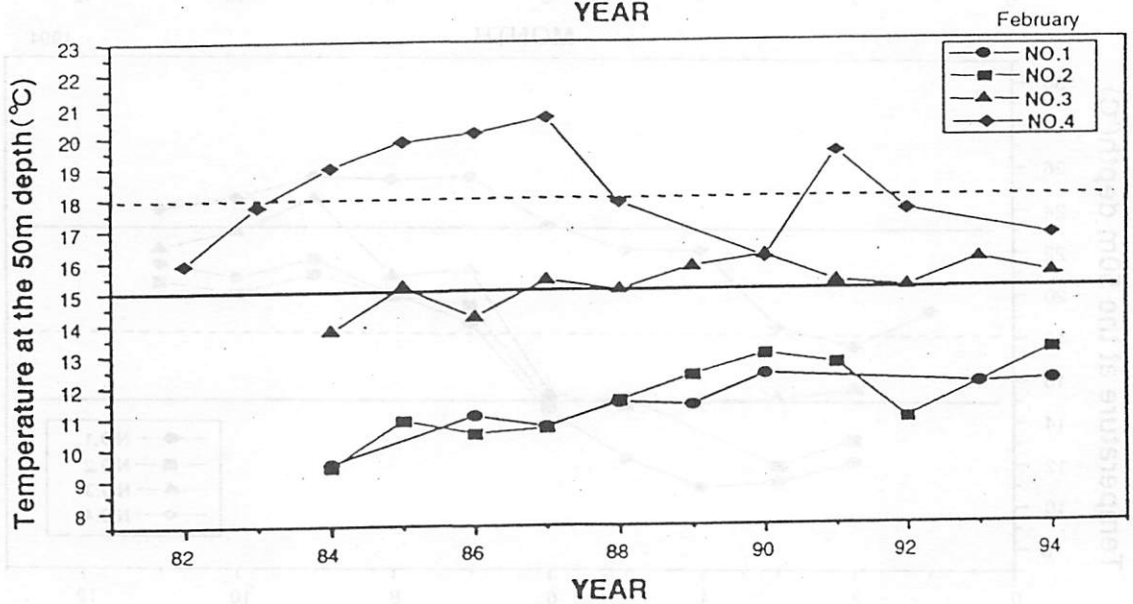
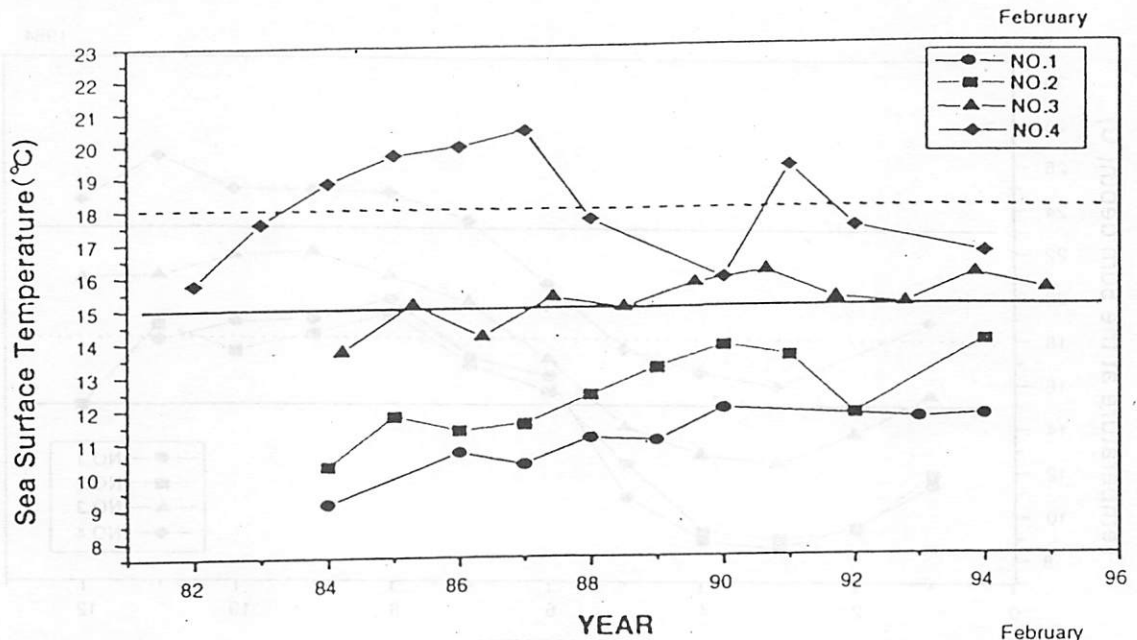


Fig. 3 Recent changes of water temperatures at the sea surface and 50m depth in February around the southern Japan between 1982 and 1994. For detecting the favorable spawning grounds of *T. pacificus*, we selected four study areas in the adjacent waters of Noto Peninsula (St.1), Iki Island (St.2), Goto Islands (St.3) and continental shelf water of East China Sea (St.4).

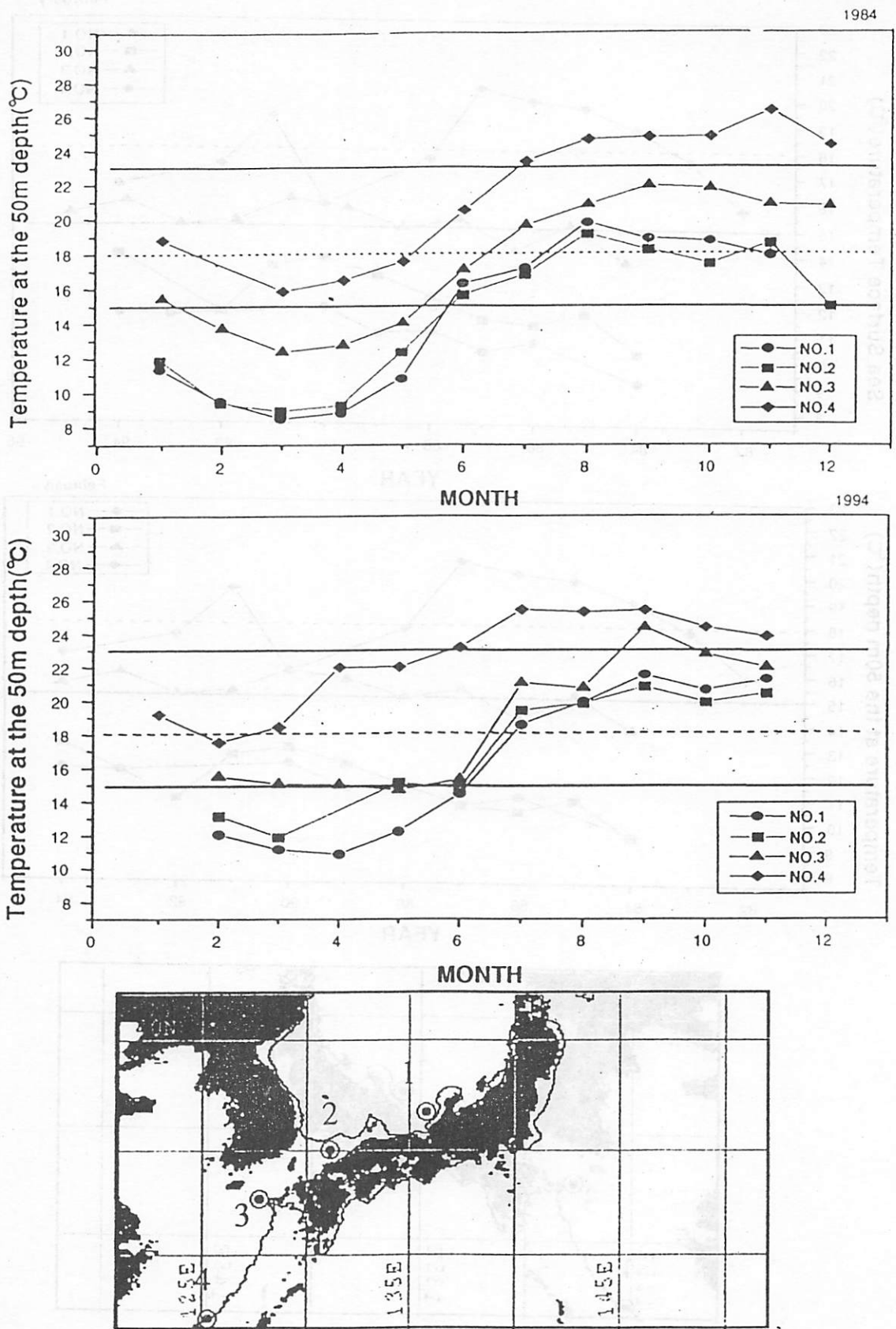


Fig.1 Comparison the seasonal changes of temperature at 50m depth between 1984 as a cold year and 1991 as a warm year.

# Comparison of zooplankton communities between the central and western subarctic Pacific Ocean

Naonobu Shiga and Koh Nishiuchi  
(Faculty of Fisheries, Hokkaido University)

## Introduction

The subarctic Pacific Ocean is occupied by two large gyre systems; eastern part is the Gulf of Alaska Gyre and west one is the Western Subarctic Gyre. Our understanding of structure and function in the lower trophic level have been accumulated largely from the Gulf of Alaska Gyre, especially from Station P which is the most famous fixed station for long-term monitoring biological and physical environment in the North Pacific.

There is no assurance that the pelagic ecosystem in the Gulf of Alaska would be equal to that in the Western Subarctic Gyre. Recently, it has been pointed out the discrepancy in lower trophic structure between these two gyre systems.

We are analyzing not only biomass but also community structure of zooplankton, using samples collected from the subarctic Pacific Ocean. This task is very time-consuming and need to many experts for identification of zooplankton. In this paper we report the comparison of the community structure of two animal groups; appendicularians and chaetognaths between the central and western subarctic Pacific Ocean. Preliminary results indicate that the community structure of zooplankton in the central subarctic Pacific Ocean is similar to that in the Gulf of Alaska Gyre.

## Materials and Methods

Zooplankton samples were collected by the Oshoro Maru and the Hokusei Maru of Hokkaido University at two fixed north-south transects located in the northwestern and central regions of the North Pacific Ocean from 1986 to 1996 (Fig. 1). The transect along 155°E were occupied by the Hokusei Maru in early and late June. The stations at which hydrographic casts and plankton net tows were made, were set up at intervals of 45 miles from 35°N to 44°N along 155°E (hereafter call as "western" region). Stations set up at 30 mile-intervals from 36°N to 51°N along the 180° meridian ("central" region) were occupied by the Oshoro Maru during early to middle June. All cruises were carried out in June. Total number of sampling stations varied from 10 to 34 per cruise and all the samples were not always used for this study.

Vertical tows with a NORPAC net (45 cm in diameter, 330-350  $\mu$ m mesh) were made from 150 m to the surface at each station. The amount of water filtered by each net was recorded by a flowmeter suspended in its mouth. After chaetognaths and appendicularians in these tows had been identified and enumerated, the number of individuals per 1000 cubic meters

were calculated. Hydrographic measurements with a CTD were made at the same stations.

## Results

### Hydrographic condition

In the subarctic Pacific Ocean, the transition domain intervenes between the subarctic and subtropical domains. According to previous oceanographic studies, the southern boundary of the transition domain is the subarctic front at which the 34.0 isohaline intersects the surface. The northern boundary of the transition domain is the latitude at which the permanent halocline located at 125-150 m breaks down and/or the 4°C isotherm abruptly deepens to about 100 m.

These water masses were clearly distinguishable in the T-S diagrams. All of the stations could be partitioned into one of these three domains by the T-S diagrams. Temperature and salinity in the surface layer of the subtropical and transition domains were slightly higher at the western region than at the central region.

### Appendicularia

A total of 27 appendicularian species belonging to 9 genera were identified in the whole areas (Table 1). Number of species ranged from 2 in the central region of the subarctic domain to 25 in the western region of the subtropical domain. It is clear that the number of species in the western region was much more than that in the central region within the same domain. In the transition domain, cold water species and warm water species cooccurred. In addition to warm water species, *Oikopleura dioica*, which is the typical neritic species, occurred in the subtropical domain.

Fig. 2 shows mean abundance and species composition in each domain of both regions (155°E and 180°). As indicated by S.D., total abundance varied considerably among samples. While appendicularians were less abundant in the subarctic domain, they are abundant in the subtropical domain. Highly significant difference between western and central regions was observed in the transition domain. In this domain, individuals at the central region was minimum (3,480 inds/1000m<sup>3</sup>), whereas individuals at the western region was maximum (45,510), having the difference with a factor of 15. Species composition, as well as number of individuals was different between two regions. *Fritillaria pellucida* and *O. longicauda* occupied overwhelmingly at the western, central regions respectively. Both species are low in frequency of occurrence. Nevertheless, the fact that mean abundance of these two species was high suggesting their sporadic and local vast occurrence in the transition domain. The maximum abundance of 916,240 was recorded for *F. pellucida*. Species diversity was high in the subtropical domain. This tendency was prominent at the western.

### Chaetognatha

A total of 22 chaetognath species belonging to 4 genera were identified in the whole areas (Table 3). Number of species varied between 2 at the western region in the subarctic domain and 22 at the central region in the subtropical domain. As similar to appendicularians, the number of chaetognath species in the western region was more than that in the central region of the subtropical domain. On the contrast to appendicularians, cold water species (*Sagitta elegans* and *Eukrohnia hamata*) occurred all areas, even in the subtropical domain. *S. nageae*, which is the neritic species, occurred at western region in the subtropical and transition domains.

Fig. 3 shows mean abundance and species composition in each domain of both regions. The largest discrepancy of abundance was observed in the subtropical domain; the maximum of 28,774 was at the western region and the minimum of 2,897 was at the central region. The difference in abundance is a factor of 10. Species composition in subtropical and transition domains were different between two regions. Especially composition difference in the subtropical domain reflects large difference in abundance.

## Conclusion

(1) Community structures of appendicularians and chaetognaths at the western and central regions in the subarctic domain were simple and no difference each other. The community was composed of *Fritillaria borealis* f. *typica*, *Oikopleura labradoriensis*, *Eukrohnia hamata* and *Sagitta elegans*.

(2) In the transition domain, appendicularian community is widely different between two regions. *F. pellucida* was overwhelming at the western region. Chaetognath community was also different; *S. elegans* and *E. hamata* were predominant at the western, central regions respectively.

(3) Relative to appendicularians, chaetognath community was much more different between two regions in the subtropical domain. Chaetognaths at the western region exceeded that at the central region both in abundance and number of species. *S. nageae*, neritic species, was predominant at the western region.

(4) In the east-west comparison of appendicularian and chaetognath community, there is no approvable difference in the subarctic domain. However, a large difference was found in the transition and subtropical domains. Number of species of both taxa at the western region was much more than at the central one. This increase in species diversity is due to an increase in the abundance of its members in the Kuroshio extension, where the water appears to be "enriched" along the subarctic front.

In this study only two kinds of zooplankton were analyzed; appendicularians and chaetognaths. The lack of data on the most abundant animals, copepods, is a serious deficiency. We would like to obtain data on another animal groups, such as Euphausiacea, Amphipoda, Doliolida, Salpida and Cladocera, as well as Copepoda. And after that we would like to analyze recurrent groups to clarify the characteristics of zooplankton community in both regions.



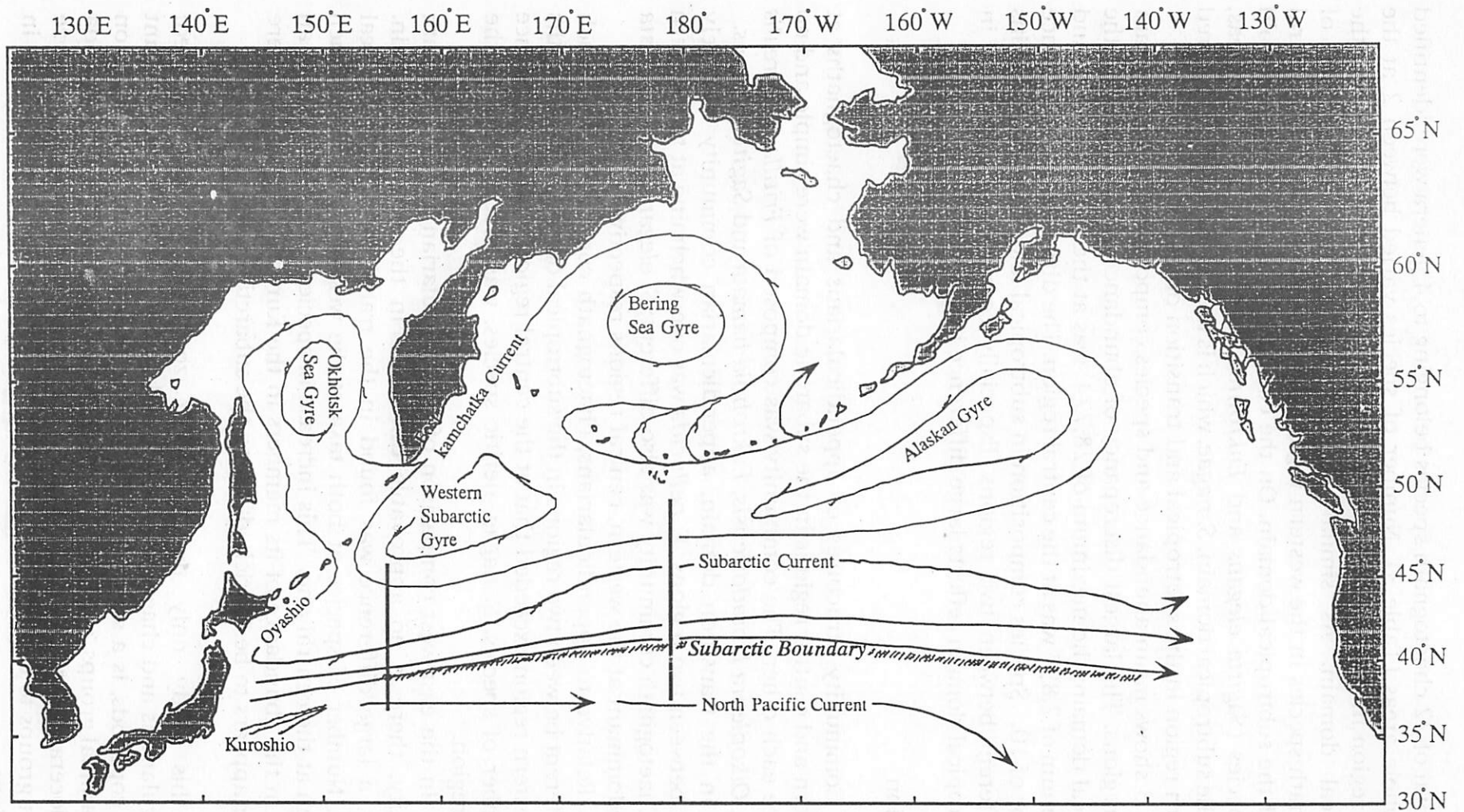


Fig. 1. Schematic representation of the surface water masses in the northern North Pacific Ocean (redrawn from Dodimead et al., 1963) and two transects at which the plankton samplings were carried out on the "Oshoro Maru" and "Hokusei Maru" cruises in early summer.

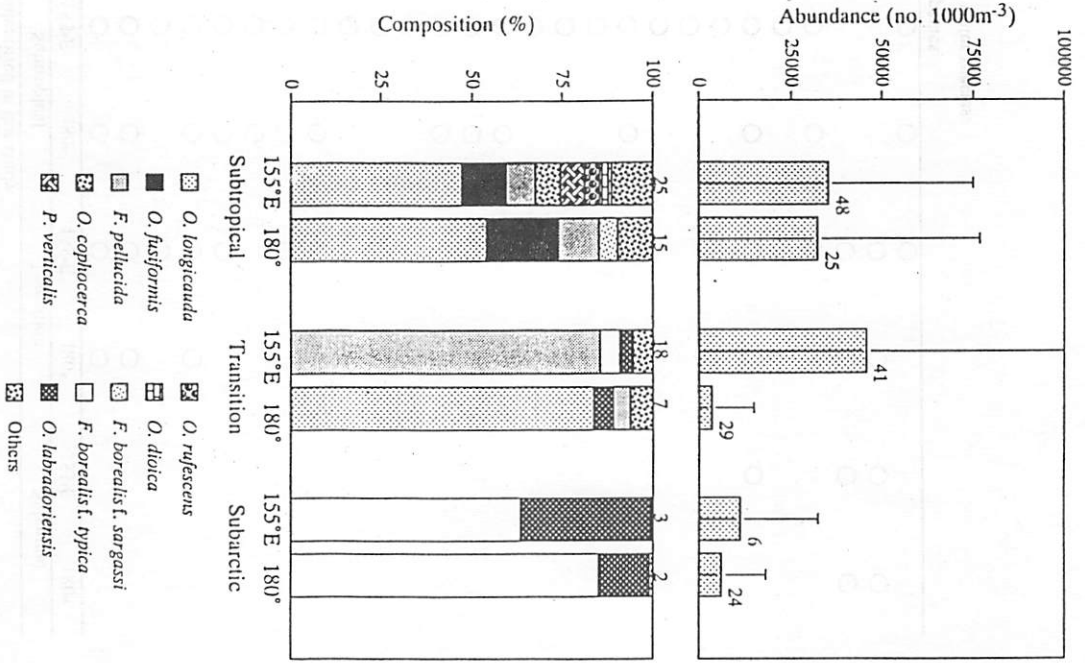


Fig. 2. Mean abundance and specific composition of Appendicularia. Vertical bars show standard deviation. Numbers above histograms are number of samples for upper panel and number of species for bottom panel.

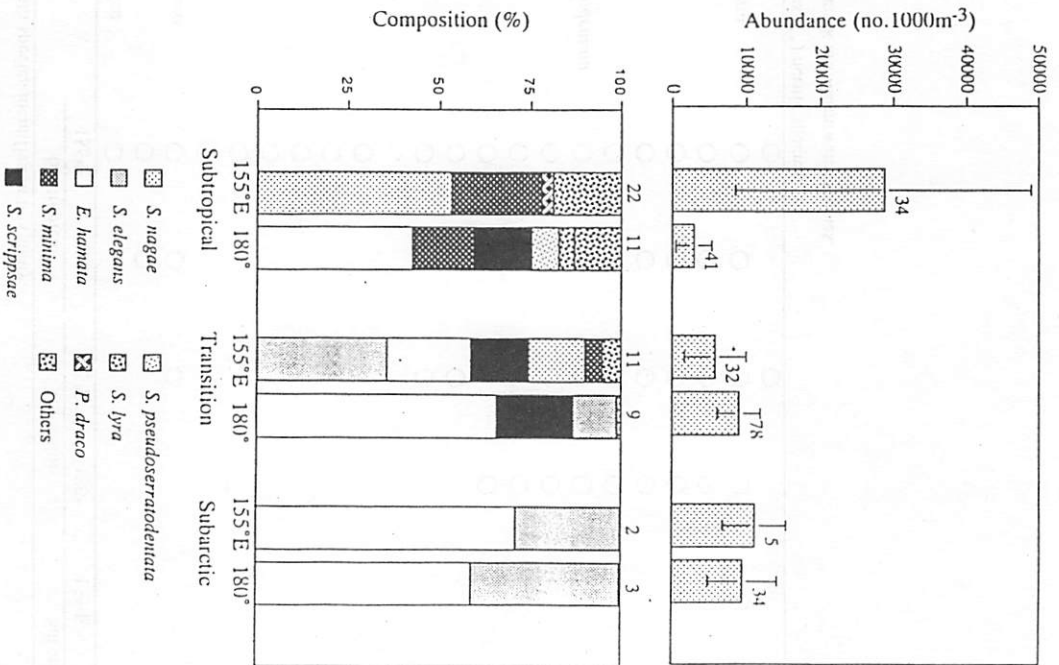


Fig. 3. Mean abundance and specific composition of Chaetognatha. Vertical bars show standard deviation. Numbers above histograms are number of samples for upper panel and number of species for bottom panel.

Table 1. Appendicularian species identified in this study.

Species	Subtropical		Transition		Subarctic	
	155°E	180°	155°E	180°	155°E	180°
<i>Okopleura gracilis</i>	○	○	○	○		
<i>O. longicauda</i>	○	○	○	○		
<i>O. intermedia</i>	○		○			
<i>O. fusiformis</i>	○	○	○	○		
<i>O. albicans</i>	○	○	○			
<i>O. rufescens</i>	○	○				
<i>O. parva</i>	○	○	○			
<i>O. cophocerca</i>	○	○	○			
<i>Folia gracilis</i>	○					
<i>Stegosoma magnum</i>	○		○			
<i>Sinisteroffia scrippsi</i>	○					
<i>Megalocercus huxleyi</i>	○	○				
<i>Pelagopleura verticalis</i>	○	○	○			
<i>Fritillaria formica</i>	○	○				
<i>F. haplostoma</i>	○		○			
<i>F. gracilis</i>	○		○			
<i>F. aberrans</i>	○		○			
<i>F. borealis f. surgassi</i>	○	○	○	○		
<i>F. messanensis</i>	○					
<i>F. megacheli</i>	○					
<i>F. tenella</i>	○					
<i>F. pellucida</i>	○	○	○	○	○	
<i>Tectillaria fertillis</i>	○					
<i>Appendicularia sicula</i>	○	○	○			
* <i>O. labradoriensis</i>			○	○	○	○
* <i>F. borealis f. typica</i>			○	○	○	○
** <i>O. divica</i>	○	○	○			

\*) cold water species, \*\*) neritic species.

Species without asterisk are warm water species.

Table 2. Chaetognath species identified in this study.

Species	Subtropical		Transition		Subarctic	
	155°E	180°	155°E	180°	155°E	180°
<i>Krohnitta pacifica</i>	○					
<i>K. subtilis</i>	○	○				
<i>Pterosagitta draco</i>	○	○	○			
<i>Sagitta bedoti</i>	○					
<i>S. robsta</i>	○					
<i>S. ferox</i>	○					
<i>S. bipunctata</i>	○					
<i>S. neglecta</i>	○					
<i>S. regularis</i>	○					
<i>S. pacifica</i>	○					
<i>S. decipiens</i>	○			○		
<i>S. neodecipiens</i>	○	○		○		
<i>S. zetesios</i>	○	○			○	
<i>S. enflata</i>	○				○	○
<i>S. hexaptera</i>	○	○		○	○	○
<i>S. pseudoserratodentata</i>	○	○		○	○	○
<i>S. minima</i>	○	○		○	○	○
<i>S. lyra</i>	○	○		○	○	○
* <i>S. scrippsae</i>	○	○		○	○	○
* <i>S. elegans</i>	○	○		○	○	○
* <i>Eukrohnia hamata</i>	○	○		○	○	○
** <i>S. nagae</i>	○			○		

\*) cold water species, \*\*) neritic species.

Species without asterisk are warm water species.

Table 1. Appendicularian species identified in this study.

Species	Subtropical		Transition		Subarctic	
	155°E	180°	155°E	180°	155°E	180°
<i>Oikopleura gracilis</i>	○	○	○	○		
<i>O. longicauda</i>	○	○	○	○		
<i>O. intermedia</i>	○		○			
<i>O. fusiformis</i>	○	○	○	○		
<i>O. albicans</i>	○	○	○			
<i>O. rufescens</i>	○	○				
<i>O. parva</i>	○	○	○			
<i>O. cophocerca</i>	○	○	○			
<i>Folia gracilis</i>	○					
<i>Stegosoma magnum</i>	○		○			
<i>Sinisteroffia scrippsi</i>	○					
<i>Megalocercus huxleyi</i>	○	○				
<i>Pelagopleura verticulis</i>	○	○	○			
<i>Fritillaria formica</i>	○	○				
<i>F. haplostoma</i>	○		○			
<i>F. gracilis</i>	○		○			
<i>F. aberrans</i>	○		○			
<i>F. borealis f. surgassi</i>	○	○	○	○		
<i>F. messanensis</i>	○					
<i>F. megacheli</i>	○					
<i>F. tenella</i>	○					
<i>F. pellucida</i>	○	○	○	○	○	
<i>Tectillaria fertillis</i>	○					
<i>Appendicularia sicula</i>	○	○	○			
* <i>O. labradoriensis</i>			○	○	○	○
* <i>F. borealis f. typica</i>			○	○	○	○
** <i>O. dioica</i>	○	○	○			

\*) cold water species, \*\*) neritic species.

Species without asterisk are warm water species.

Table 2. Chaetognath species identified in this study.

Species	Subtropical		Transition		Subarctic	
	155°E	180°	155°E	180°	155°E	180°
<i>Krohnitta pacifica</i>	○					
<i>K. subtilis</i>	○	○				
<i>Pterosagitta draco</i>	○	○	○			
<i>Sagitta bedoti</i>	○					
<i>S. robusta</i>	○					
<i>S. ferox</i>	○					
<i>S. bipunctata</i>	○					
<i>S. neglecta</i>	○					
<i>S. regularis</i>	○					
<i>S. pacifica</i>	○					
<i>S. decipiens</i>	○			○		
<i>S. neodecipiens</i>	○	○	○			
<i>S. zetesios</i>	○	○				○
<i>S. enflata</i>	○					○
<i>S. hexaptera</i>	○	○	○	○	○	○
<i>S. pseudoserratodentata</i>	○	○	○	○	○	○
<i>S. minima</i>	○	○	○	○	○	○
<i>S. lyra</i>	○	○	○	○	○	○
* <i>S. scrippsae</i>	○	○	○	○	○	○
* <i>S. elegans</i>	○	○	○	○	○	○
* <i>Eukrohnia hamata</i>	○	○	○	○	○	○
** <i>S. nagae</i>	○			○		

\*) cold water species, \*\*) neritic species.

Species without asterisk are warm water species.

# Interannual–interdecadal variations in zooplankton biomass, chlorophyll concentration and physical environment in the subarctic Pacific and Bering Sea

TAKASHIGE SUGIMOTO<sup>1</sup>  
AND KAZUAKI TADOKORO

Ocean Research Institute, University of Tokyo, 1-15-1,  
Minamidai, Nakanoku, Tokyo 164, Japan

## ABSTRACT

Interannual, decadal and interdecadal variations in summer plankton biomass during 1954–1994 in the whole subarctic Pacific and Bering Sea were compared among regions as well as with climatic and oceanographic conditions. The zooplankton biomass and chlorophyll concentration during the mid 1960s to early 1970s in the central and western subarctic Pacific were a few times higher than those in the preceding and following decades. The values in the eastern Bering Sea and eastern subarctic Pacific also increased in the mid 1960s, but remained at an elevated level until the end of the 1980s. These decades of higher and mid plankton biomass levels during the mid 1960s to early 1970s and mid 1970s to late 1980s correspond to the period of positive and negative values of the Northern Hemisphere zonal index (NHZI), respectively. In the decadal scale, one can see a significant positive correlation between the summer plankton biomass and the wind speed during winters in the eastern Bering Sea. The effect of grazing by biennially fluctuating Asian pink salmon on zooplankton biomass and its effect on chlorophyll concentration in the central subarctic Pacific is also significant.

**Key words:** chlorophyll concentration, climate change, interannual variation, interdecadal variation, pink salmon, subarctic Pacific, zooplankton biomass

## INTRODUCTION

Zooplankton biomass in the Alaskan gyre in the 1980s was estimated to have increased to as much as twice

the levels found in the late 1950s to early 1960s, as reported by Brodeur and Ware (1992). The phenomenon was thought to be caused by the increase of upward flux of micronutrients due to intensification of the wind-induced upwelling or vertical mixing associated with an intensified Aleutian Low in winter after the mid 1970s' climatic regime shift. Pelagic nekton populations, such as salmon and squid, also increased during the same time (Beamish and Bouillon, 1993; Francis and Hare, 1994; Brodeur and Ware, 1995).

The levels of zooplankton biomass during summer in the Kuroshio Extension and in the Kuroshio–Oyashio transition regions in the decades of the 1970s and 1980s were higher than those of the 1950s and 1960s (K. Odate, 1994). However, in Oyashio water in the south-western subarctic Pacific, zooplankton biomass in the summer of the late 1970s and in the early 1980s was lower than that of the mid 1960s to late 1970s (K. Odate, 1994). In the early and mid 1980s, the southward intrusion of the primary (first) branch of the Oyashio water rich in nutrients was intensified (Sekine, 1988; Hanawa, 1995), whereas the water temperature and zooplankton biomass in the Oyashio water decreased (Tomosada and Odate, 1995).

Polovina *et al.* (1995) calculated seasonal variation in mixed layer depth (MLD) in the North Pacific and obtained its spatial variation in winter and spring between 1960–1976 and 1977–1988. The MLD became deeper during the latter period in the subtropical–subarctic transition region of the central North Pacific and in the offshore areas of the Kuroshio south of Japan, but it became shallower in the surrounding regions off the west coast of North America and northern subarctic Pacific. Obata *et al.* (1996) have obtained similar results, and globally confirmed Sverdrup's critical depth theory by using the observed water temperature and satellite ocean-colour data.

Venrick *et al.* (1987) showed that the chlorophyll-a concentration in the central part of the subtropical gyre north of Hawaii has doubled twice after the mid 1970s. This was believed to be caused by stronger winter mixing associated with the intensification of the Aleutian Low after the mid 1970s. In the northern half of the subtropical gyre south of Japan, however, chlorophyll concentrations in winter during the 1980s

Received for publication 20 July 1996

Accepted for publication 4 December 1996

<sup>1</sup>Corresponding author. (Fax: +81-3-5351-6506

e-mail: sugimoto@ori.u-tokyo.ac.jp)

and *Hokusei-Maru*, a CTD (Neil Brown Ltd) was used instead of Nansen casts after 1984 and 1988, respectively. Transparency depth (*TD*), measured with a Secchi disc, was converted to a measure of chlorophyll *a* concentration, by using the statistical relationship after Falkowski and Wilson (1992):

$$\text{Chl } a = 457 \text{ TD}^{-2.37} \quad (1)$$

where Chl *a* values are in  $\text{mg m}^{-3}$  and *TD* is in metres. This relationship was verified with data seasonally obtained in the western subarctic Pacific by R/V *Kofu-Maru* of the Japan Meteorological Agency, as shown in Fig. 2. Values of *TD* less than 5 m were approximated to 5 m. Values of equation 1 are 1.3–1.7 times higher than the values of the best-fit line (Fig. 2), although the standard deviation is large. This relation might be attributed to the season as shown in Fig. 2 by different symbols and to water masses containing different species and size composition of phytoplankton. Nagata (1996) suggested that this relationship is applicable only in spring and summer for the Oyashio water.

For obtaining zooplankton samples, a NORPAC net with 0.33–0.35 mm mesh size, 180 cm in length and with a mouth ring diameter of 45 cm, was towed vertically from 150 m depth to the sea surface. Before 1979, zooplankton biomass was measured excluding large organisms such as salps and jellyfish. However,

during and after 1979, zooplankton biomass was measured including these large organisms. Hence, for the present analysis, the data for samples that contain salps, jellyfish or a considerable volume of phytoplankton were omitted and those which exceed  $5 \text{ mg m}^{-3}$  in wet weight were approximated as  $5 \text{ mg m}^{-3}$ . Sometimes, the standard sampling depth of 150 m is not sufficient when the upper mixed layer depth becomes deeper and a large amount of cold-water species of zooplankton occurs below 150 m (N. Shiga, personal communication). The difference between day and night sampling was not significant in this high-latitude area in summer, and is ignored here.

Table 1 shows the number of stations sampled and the mean date for zooplankton sampling (day of the year) in each subarea and year, with mean wet weight of zooplankton and standard deviation. Mean values of chlorophyll *a* concentrations calculated from transparency depth (*TD*) are also shown in Table 2. To nullify the error caused by year-to-year seasonal variations in phytoplankton and zooplankton biomass peaks of late spring and early summer in the subarctic Pacific (Anderson *et al.*, 1977; Fulton, 1983; Miller *et al.*, 1984; Brodeur and Ware, 1992; K. Odate, 1994; Tseytlin *et al.*, 1994; Brodeur *et al.*, 1996; C.W. Brown, personal communication), the data from June and July were used; however, there is still some error depending on year-to-year fluctuation in the peak and mean observation date.

Figure 2. Relationship between transparency depth and chlorophyll *a* concentration observed seasonally by R/V *Kofu-Maru* in the western subarctic Pacific. Solid curve shows equation 1; dashed curve is the best fit.

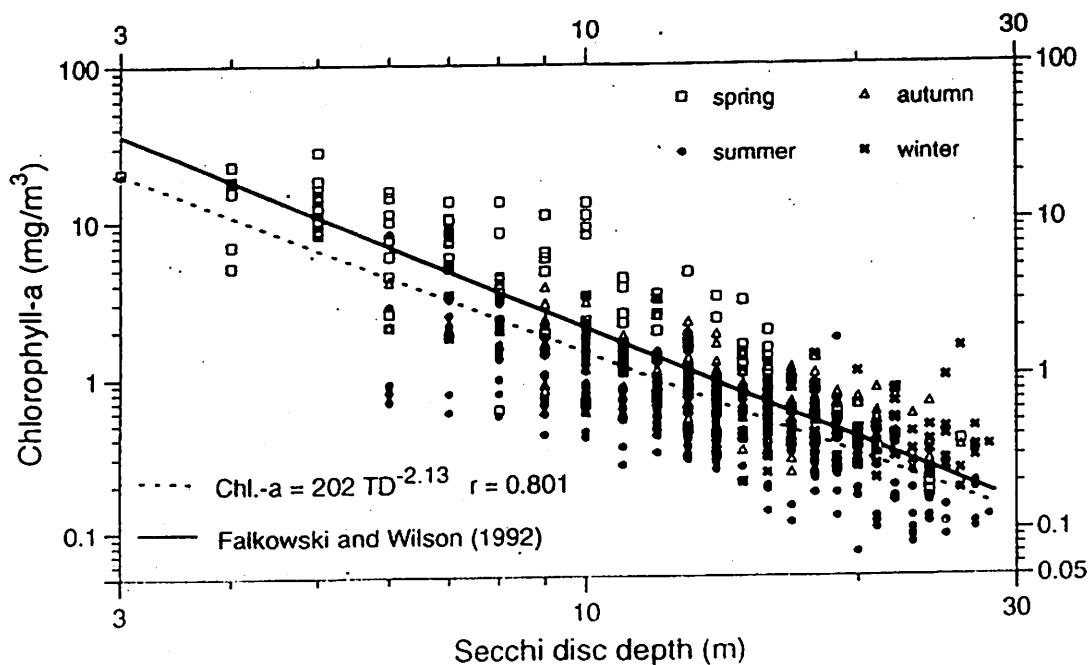


Table 2. Mean values and standard deviations (SD) of chlorophyll concentration ( $\text{mg m}^{-3}$ ), total number of samplings ( $N$ ) and mean sampling day (J. day) for each subarea of the subarctic Pacific (WP, CP and EP) and eastern Bering Sea (EB) in June and July from 1954–1994.

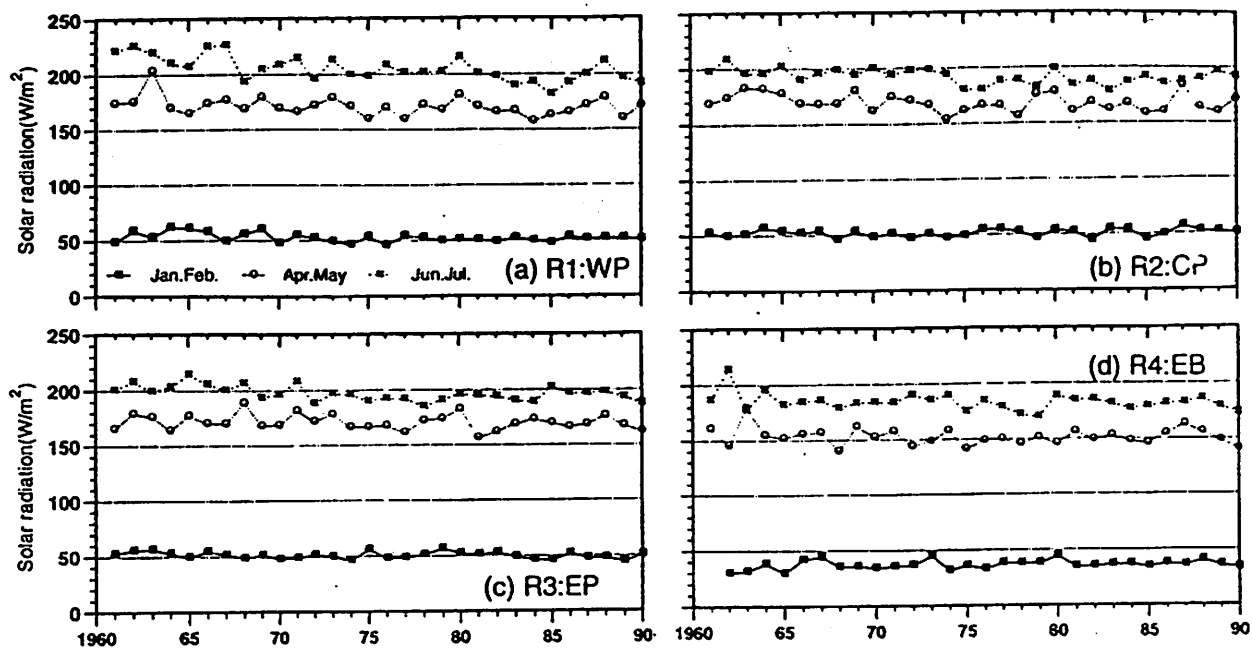
Year	WP			CP			EP			EB						
	Mean	SD	$N$	J. day	Mean	SD	$N$	J. day	Mean	SD	$N$	J. day	Mean	SD	$N$	J. day
1954	1.03	0.45	13	175	0.88		1	170					1.31	1.00	9	161
1955			0				0								0	
1956			0		0.87	0.46	4	205					1.03	0.67	5	209
1957	2.58	3.14	8	184	1.99	1.74	12	183					0.79	0.18	4	190
1958	1.24	0.87	10	169	2.56	3.73	6	168					1.89	1.07	7	166
1959	2.47	2.05	31	177	1.27	0.80	11	174					0.70	0.35	6	182
1960	2.98	3.26	11	168	1.36	0.74	13	178	0.61	0.15	5	198	1.76	1.95	18	185
1961	1.53	1.44	58	184	1.59	0.94	17	183					0.70	0.52	7	186
1962	1.96	1.98	23	171	1.21	0.52	8	155					1.89	2.91	10	162
1963	1.29	0.83	33	180	0.83	0.43	5	164					1.60	1.29	36	183
1964	1.70	2.43	21	163	0.87	0.59	13	171					1.19	1.06	40	184
1965	1.09	0.30	4	153	2.14	3.51	7	168					2.39	1.90	57	182
1966			0				0						2.73	2.19	50	185
1967			0		1.13	0.75	3	162					2.88	2.09	48	181
1968	3.33	1.13	5	165	6.29	5.36	2	162	1.83	1.39	8	197	1.82	1.79	49	178
1969	5.65	3.68	7	165	1.90	2.29	3	163					2.73	2.42	81	186
1970	1.12	0.97	4	159	0.99	0.52	5	169	4.37	3.35	10	198	2.72	2.96	30	173
1971	3.29	3.04	11	164	1.76	0.93	8	202					2.51	2.74	37	183
1972	5.32	2.35	9	165			0						1.73	1.09	51	182
1973	3.33	2.83	8	165			0						2.26	2.01	95	186
1974	2.90	1.37	10	174	3.63	4.35	4	165					2.12	2.45	101	183
1975	5.05	2.58	18	167	1.25	0.71	8	186	2.50		1	188	2.89	2.32	43	177
1976	4.39	2.73	29	168	4.13	4.02	8	165					2.37	2.33	56	179
1977			0		1.07	0.21	5	163					1.29	1.18	56	182
1978	3.21	0.96	4	202	1.24	0.54	18	203					2.12	1.43	40	173
1979	0.55		1	201	0.79	0.85	36	190					2.58	2.60	33	198
1980	1.10	0.49	5	201	1.42	1.30	29	187	0.73	0.19	5	193	4.01	3.26	22	179
1981	2.43	1.20	6	199	1.22	0.67	31	185	1.49	1.19	17	199	3.90	2.45	29	178
1982	2.78	2.36	18	181	0.84	0.57	30	186	1.18	1.45	17	201	2.40	1.83	25	180
1983	1.52	0.88	12	184	0.88	0.66	25	188	1.17	0.54	17	186	2.75	1.91	20	203
1984	2.74	3.02	13	178	0.93	0.46	28	188	2.44	2.70	32	196	1.99	1.22	23	172
1985	1.10	0.63	16	182	1.95	1.56	23	188	2.15	1.46	19	189	2.86	2.95	22	174
1986	2.52	2.31	15	183	1.01	0.62	28	189					2.21	2.41	46	183
1987	2.15	2.38	14	188	1.43	1.24	29	182	1.14	0.65	25	199	1.18	0.90	28	182
1988	3.08	2.23	24	172	0.92	0.54	31	185	0.98	0.68	27	197	3.16	2.65	16	179
1989	1.73	2.10	22	185	1.97	1.88	31	182	1.13	0.48	32	191	3.63	3.16	15	175
1990	0.89	0.59	12	173	1.72	2.10	39	185	0.95	0.43	24	188	2.00	1.70	17	173
1991	1.59	1.14	10	182	1.16	0.66	35	180	2.13	1.73	21	186	3.02	2.50	15	173
1992	1.34	0.85	18	184	1.02	0.61	27	182	1.02	0.54	16	182	1.75	0.23	4	197
1993	1.06	0.67	23	185	1.10	0.65	34	185	0.90	0.37	17	182	1.75	1.15	13	194
1994	1.75	1.24	28	191	0.78	0.35	23	170	1.47	1.27	38	184	1.45	0.61	15	199

into consideration its rate of increase between June and July and the mean observation date.

To analyse the relationships among the time changes of the wind intensity, chlorophyll concentration, macrozooplankton biomass and pink salmon population, the time series data were separated into

three different time scales by calculating running means of 3 and 11 years. Anomalies from the 3-year running mean (a high-pass filter), 3-year running mean minus 11-year running mean (like a 10-year pass filter) and 11-year running mean (a low-pass filter), which represent the time scale for interannual varia-

Figure 4. Year-to-year variations of mean solar radiation flux ( $W m^{-2}$ ) during winter, spring and summer in areas R1 (a) to R4 (d) (Fig. 1) from 1961 to 1990.



1970s. In the eastern Bering Sea (R4) and western subarctic Pacific (R1), SST in winter, spring and summer was higher after the mid 1970s, whereas in the eastern subarctic Pacific (R3), SST increased in the late 1970s but decreased after the late 1980s.

Table 3 shows variations in physical factors during winter, spring and summer, before and after the climatic regime shift occurred in the mid 1970s. The table shows mean values for 1961–1990, and mean anomaly and standard deviation for 1961–1975 and

Figure 5. Year-to-year variations of sea surface wind speed (1 knot =  $0.44 ms^{-1}$ ) during winter, spring and summer in areas R1 (a) to R4 (d) from 1961 to 1990.

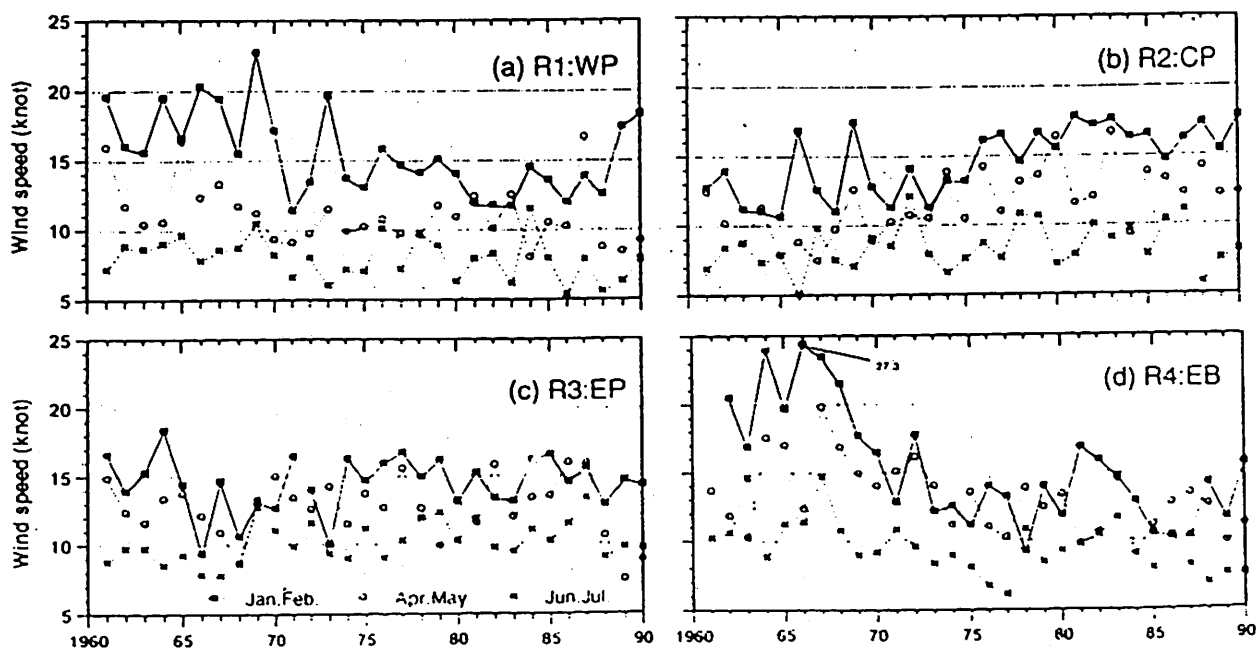




Table 3. Mean values of insolation, wind speed and SST for 1961-1990 in each subarea R1-R4, and mean anomaly and standard deviation (SD) for 1961-1975 and 1976-1990.

Variable	Subarea	Jan.-Feb.						Apr.-May						Jun.-Jul.					
		1961-1990		1961-1975		1976-1990		1961-1990		1961-1975		1976-1990		1961-1990		1961-1975		1976-1990	
		Mean <sup>1</sup>	Anomaly SD	Anomaly	SD	Anomaly	SD	Mean <sup>1</sup>	Anomaly	SD	Anomaly	SD	Mean <sup>1</sup>	Anomaly	SD	Anomaly	SD		
Insolation (W)	R1	52.6	1.8	5.1	-1.8	2.2* <sup>2</sup>	170.8	2.7	9.9	-2.7	6.8	205.1	6.1	11.3	-6.1	8.8*			
	R2	51.5	-0.2	3.1	0.2	3.8	168.5	2.3	8.2	-2.3	7.8	192.1	4.3	6.2	-4.3	5.5*			
	R3	50.5	1.0	3.2	-1.0	3.2	170.7	2.2	7.0	-2.2	6.6	196.9	3.7	7.3	-3.7	4.4*			
	R4	36.4	-0.3	4.8	0.3	2.9	152.2	1.8	10.0	-1.8	5.6	183.4	3.1	9.2	-3.1	5.5*			
Wind speed (knots) <sup>3</sup>	R1	15.4	1.4	3.2	-1.4	2.0*	11.0	0.5	2.2	-0.5	2.1	7.9	0.2	1.2	-0.2	1.7			
	R2	14.6	-1.8	2.1	1.8	1.0*	11.6	-1.4	1.8	1.4	1.9*	8.4	-0.4	1.6	0.4	1.5			
	R3	14.4	-0.4	2.6	0.4	1.3	12.7	0.1	1.7	-0.1	2.6	10.1	-0.5	1.4	0.5	1.3			
	R4	15.4	2.7	5.0	-2.5	2.3*	13.1	1.4	2.6	-1.4	1.7*	9.5	0.9	2.0	-0.9	1.6*			
SST <sup>4</sup> (°C)	R1	2.2	-0.1	0.5	0.1	0.3	2.6	-0.1	0.4	0.1	0.4	6.8	-0.1	0.4	0.1	0.6			
	R2	4.0	0.1	0.4	-0.1	0.4	4.3	0.0	0.4	0.0	0.4	7.3	-0.1	0.5	0.1	0.5			
	R3	6.3	-0.3	0.5	0.3	0.5*	6.5	-0.2	0.5	0.2	0.6*	9.8	-0.1	0.8	0.1	0.6			
	R4	3.3	-0.4	0.7	0.4	0.3*	3.4	-0.5	0.7	0.5	0.4*	6.7	-0.3	0.7	0.3	0.6*			

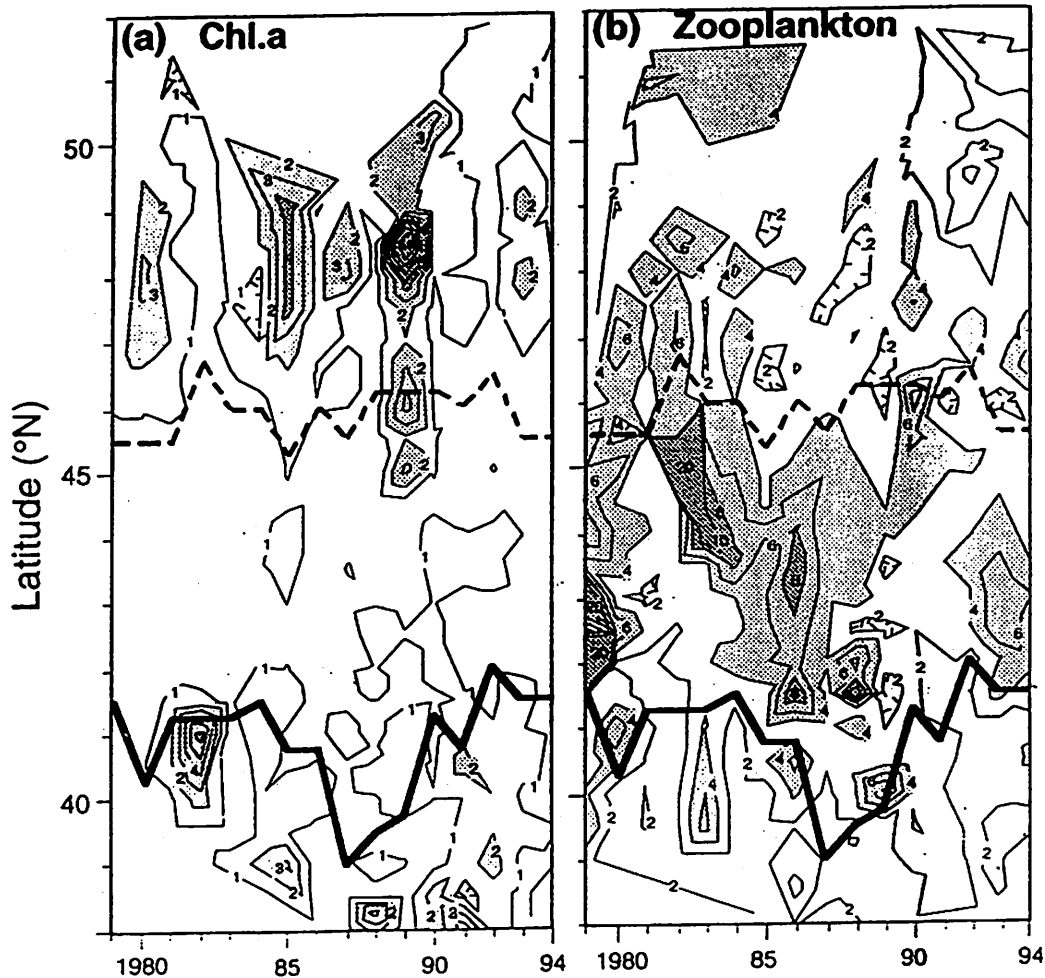
<sup>1</sup> Mean: mean for 1961-1990.

<sup>2</sup>\*, Significantly different at 5% level.

<sup>3</sup> 1 knot = 0.44 m s<sup>-1</sup>.

<sup>4</sup> Sea surface temperature.

Figure 8. Year-to-year variations in the latitudinal distributions of (a) chlorophyll concentration ( $\text{mg m}^{-3}$ ) (b) zooplankton biomass, ( $\text{mg m}^{-3}$ ), along the meridian date line observed by T/S *Oshoro-Maru* during 1979–1994. Thick solid lines indicate the northern boundary of the subtropical water identified by 34.0 psu isohaline at the sea surface (Favorite *et al.*, 1976), and dashed lines indicate northern boundary of the subarctic transition water identified by  $4.0^\circ\text{C}$  at 100 m depth.



In the eastern subarctic Pacific, including St. P, the level of the zooplankton biomass was as low as about half of the values of the central subarctic Pacific and eastern Bering Sea. Although the temporal variation at St. P is similar to that in the eastern Bering Sea, the biomass in the eastern subarctic Pacific is  $300\text{--}400 \text{ mg m}^{-3}$  during the 1960s, which is much higher than in the 1980s (Fig. 10b).

## DISCUSSION

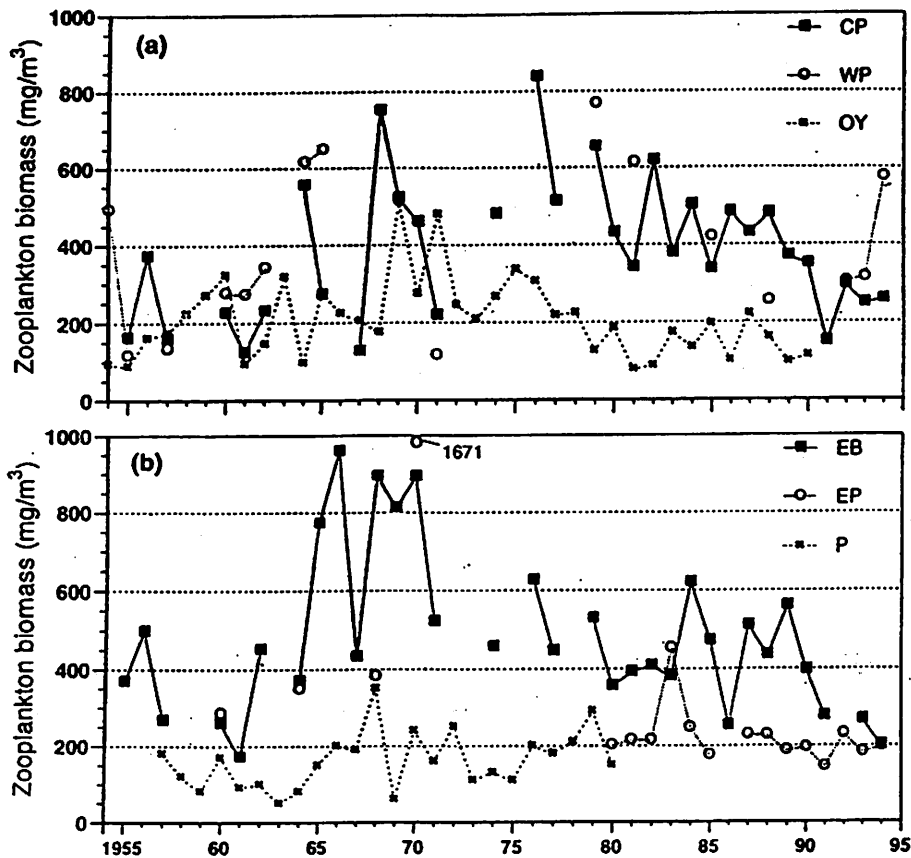
*Regional comparison: of the decadal–interdecadal variations in the plankton biomass*

Comparing the regional mean chlorophyll concentrations in each year of Fig. 9(a) and (b), some similarity and dissimilarity may be attributed to the spatial coherence of the variations in the regional meteorolog-

ical and oceanographic conditions as shown in Figs 4–6 and Table 3. On the interdecadal time scale, the chlorophyll concentration was low in the mid 1950s to mid 1960s and in the early 1990s, but high in the mid 1960s to mid 1970s or until the late 1980s throughout the entire subarctic Pacific. The higher levels continued until the end of the 1980s in the eastern Bering Sea and western subarctic Pacific, although they decreased after the mid 1970s in the central and eastern subarctic Pacific, including Ocean Weather Station Papa (St. P).

Comparing Fig. 10(a) and (b), the macrozooplankton biomass was also low in the mid 1950s to mid 1960s and the early 1990s. The decrease of biomass in the early 1990s was evident in the central subarctic Pacific and eastern Bering Sea. In the eastern Bering Sea shelf region (not shown here) as well as the

Figure 10. Year-to-year variations in the mean macrozooplankton biomass in each subarea (Fig. 1b) during 1954–1994. (a) Central subarctic Pacific and western subarctic Pacific; (b) eastern Bering Sea and eastern subarctic Pacific. Data for Oyashio (OY) and Ocean Weather Station Papa (P) are shown by crosses, after K. Odate (1994) and Brodeur and Ware (1992), respectively.



mid 1970s in R2 (CP) significantly and in R3 (EP) slightly, but weakened in R1 (WP) and R4 (EB) significantly. Chlorophyll concentration after the mid 1970s decreased in the windy CP and EP regions of the subarctic Pacific, but remained at higher levels in the less windy EB and WP regions. However, we cannot find any remarkable change in the wind speed in each region (Fig. 5) relating to the abrupt increase of zoo- and phytoplankton biomass in the mid 1960s.

On the decadal scale, the chlorophyll concentration in the EB changed with three peaks in 1965–1971, 1980–1983 and 1988–1991, corresponding well with the periods of strong winter wind (1964–1970, 1981–1983 and 1988–1990). The peak chlorophyll concentration in the late 1960s is considered to have been reduced due to strong grazing by high biomass of zooplankton (Fig. 10b) or stronger wind intensity. In the WP, the wind speed during winter decreased after the mid 1970s until the late 1980s and chlorophyll concentration decreased, corresponding positively to

the wind speed. But in case of CP, strong wind in winter of the late 1970s to mid 1980s separates the years of lowest chlorophyll concentrations. In EP the relationship between wind speed of winter and the chlorophyll concentration of the summer is not clear, but there seems to be positive correlation in the decadal scale after the mid 1970s.

On the other hand, Fig. 10 shows that the zooplankton biomass in the late 1970s was high not only in the EB and WP, but also in the CP and EP. This discrepancy of interdecadal-scale variation in chlorophyll concentration and zooplankton biomass, can be explained as follows:

In Fig. 8(a), we notice higher chlorophyll concentrations in the subarctic current system (SCS) than in the subarctic transition domain (STD), whereas zooplankton biomass (Fig. 8b) follows an opposite tendency in the north–south distribution. Hence, intensification of the northward advection after the mid 1970s might maintain a high zooplankton abun-

upper layer of the subarctic water during summer is determined not only by the vertical profile of water temperature caused by winter cooling and summer heating, but also salinity profile, caused by net precipitation and horizontal advection of the fresh water from the coast. The figure shows that the density stratification during the mid 1960s to mid 1970s was only two-thirds of that in the following decade. This suggests the importance of the effect of decrease in fresh water supply (Fig. 11b). These features are still qualitative, but correspond well to the interdecadal-scale variations in the fresh water supply (Royer, 1982) and also NHZI shown in Fig. 3.

The relative effect of the variation in silicate and iron supply on primary production (Miller *et al.*, 1991) due to changes in the atmospheric transport (Duce and Tindale, 1991) or wind-induced turbulent mixing, and change in density stratification caused by fresh water supply, should be verified through field observation in the future. In the Bering Sea, the silicate concentration is much higher than in the subarctic Pacific, and the effect of this regional difference on the biological production needs further explanation.

*Bottom-up control or top-down control?*

Comparing Fig. 9 with Fig. 10, the interdecadal variation of the zooplankton biomass in the different subarctic regions is generally similar among regions (low in the decade around 1960 and in the early 1990s), and positively correlated with chlorophyll concentration. In order to elucidate correlations between the mean chlorophyll concentration and zooplankton biomass on the decadal and interannual scales, anomalies of 3-year running means and differences between the 3-year running means and 11-year running means were considered. Those in the central subarctic Pacific and the eastern Bering Sea are shown in Fig. 12 (a) and (b), respectively. On the decadal scale, positive correlations were observed between the wind intensity and chlorophyll concentration in the EB and between the zooplankton biomass and chlorophyll concentration both in the CP and EB as shown also in Fig. 13 (a) and (b), respectively. However, on a biennial period, a negative correlation is evident in CP (Fig. 13c). In the subarctic North Atlantic, zoo- and phytoplankton biomasses were obtained by towing a CPR (continuous plankton recorder, Colebrook, 1986), which varied from year to year with a negative correlation in the decade of the 1960s and with a

Figure 12. Anomalies of chlorophyll concentration and zooplankton biomass from the 3-year running means (thin line with open circle) and differences between the 3-year running means and 11-year running means (thick line) in the central subarctic Pacific (a) and eastern Bering Sea (b).

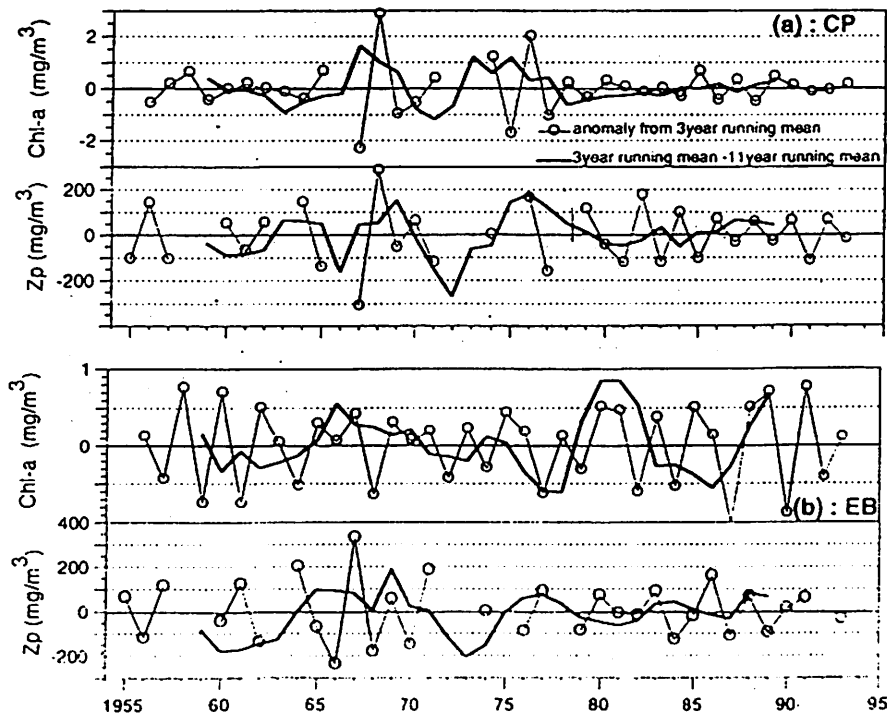
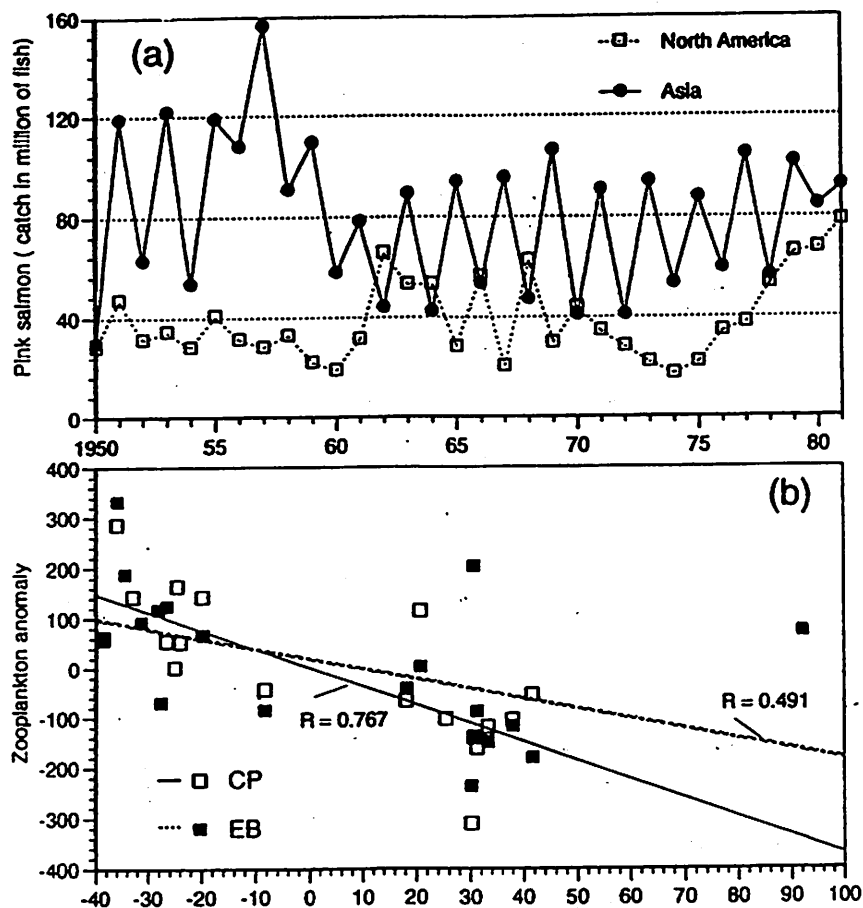


Figure 14. (a) Interannual variations in the catch of Asian pink salmon (closed circles with solid line) and North American pink salmon (open squares with dotted line) during 1950–1981 after Takagi (1981). (b) Correlations between Asian pink salmon catch and zooplankton biomass anomalies in the central subarctic Pacific and eastern Bering Sea on a biennial scale.



based on field observations during the summers of 1985–1994 in the central subarctic Pacific. Cooney (1988) also indicated the grazing effect of the North American pink salmon on zooplankton biomass at St. P.

We examined the effect of biennial fluctuation of Asian pink salmon abundance on the grazing strength of the zooplankton biomass by using the data of 1954–1981. Fig. 14 (a) shows the odd/even years fluctuation of the Asian pink salmon abundance clearly (Takagi *et al.*, 1981). Asian pink salmon migrates for feeding to the central subarctic Pacific and Bering Sea during summer. Fig. 14 (b) shows a significant negative correlation between anomalies of the zooplankton biomass from the 3-year running mean in the central subarctic Pacific and eastern Bering Sea and those of the Asian pink salmon catch. This suggests that predation pressure of Asian pink salmon controls the zooplankton biomass in the year-to-year variation,

even though the bottom-up control is more influential than top-down control on the decadal and interdecadal time scales.

Shiga *et al.* (1995) showed that warming of the upper mixed layer in summer induces northward intrusions of transitional water species of zooplankton, such as salps, which increase zooplankton biomass in the subarctic region. Similar northward intrusions of pelagic nekton associated with northward shift of the subtropical and subarctic fronts were reported by Percy (1991) and Percy *et al.* (1996). Hence, the higher grazing pressure on phytoplankton by salps and on zooplankton by nekton in the subarctic region may be suppressing the chlorophyll concentration and zooplankton biomass, respectively.

It would be useful to examine the effects of variations in the size (T. Odote, 1994) and community structure on the biomass associated with the warmer and colder periods as well as different water masses: It

## ACKNOWLEDGEMENTS

The authors would like to express sincere thanks to the scientists and crews of Hokkaido University, who devoted more than 40 years to monitoring the zooplankton biomass by T/V *Oshoro-Maru* and T/V *Hokusei-Maru* and for their published data. We thank Dr N. Shiga of Hokkaido University for providing useful unpublished information on the community structures of zooplankton in the subarctic Pacific. The authors also thank Dr Y. Ishida of the Japan National Research Institute of Far Seas Fisheries (JNRIFSF), who gave us an opportunity to study the interannual variations in the subarctic Pacific. Thanks are also extended to Japan Meteorological Agency for their long-term statistical published data, used in this paper. Comments from Drs T. R. Parsons, A. Tomosada, K. Hanawa, M. Endoh, R. D. Brodeur, B. W. Frost and J. J. Polovina were useful and encouraging. We also extend thanks to Mr K. Ishikawa, Dr P. Mishra and Ms Y. Ueno of Ocean Research Institute, University of Tokyo, for arranging the meteorological data, correcting the English and typing the manuscript, respectively.

## REFERENCES

- Anderson, G.C., Lam, R.K., Booth, B.C. and Glass, J.M. (1977) A description and numerical analysis of the factors affecting the processes of production in the Gulf of Alaska. *Univ. of Washington, Dept. of Oceanogr., Special Rep. No. 76*, 1–231, pp.
- Anma, G., Masuda, K., Kobayashi, G., Yamaguchi, H., Meguro, T., Sasaki, N. and Ohtani, K. (1990) Oceanographic structures and changes around the transition domain along 180° longitude, during June 1979–1988. *Bull. Fac. Fish., Hokkaido Univ.* 41:73–88.
- Aoki, I., and Komatsu, T. (1996) Analysis of the response of sardine and zooplankton biomass to climate and ocean environmental change. In: *Response of Marine Living Resources to the Earth Environmental Change – its Modeling and Application for Fisheries Resources Management*. T. Sugimoto (ed.). Tokyo: Ocean Research Institute, University of Tokyo, pp. 54–60. (In Japanese.)
- Beamish, R.J., and Bouillon, D.R. (1993) Pacific salmon production trends in relation to climate. *Can. J. Fish. Aquat. Sci.* 50:1002–1016.
- Brodeur, R.D., and Ware, D.M. (1992) Long-term variability in zooplankton biomass in the subarctic Pacific Ocean. *Fish. Oceanogr.* 1:32–38.
- Brodeur, R.D., and Ware, D.M. (1995) Interdecadal variability in distribution and catch rates of epipelagic nekton in the Northeast Pacific Ocean. In: *Climate change and northern fish populations* (ed. by R.J. Beamish), *Can. Spec. Publ. Fish. Aquat. Sci.* 121:329–356.
- Brodeur, R.D., Frost, B.W., Hare, S.R., Francis R.C. and Ingraham, W.I. (1996) Interannual variations in zooplankton biomass in the Gulf of Alaska and covariation with California Current zooplankton biomass. *U.S. OFI Rep.* 37:52–99.
- Colebrook, J.M. (1986) Environmental influences on long-term variability in marine plankton. *Hydrobiologia* 142, 309–325.
- Cooney, R.T. (1988) Distribution and ecology of zooplankton in the Gulf of Alaska: a synopsis. *Bull. Ocean Res. Inst. Univ. Tokyo.* 26:27–41.
- Duce, R.A., and Tindale, N.W. (1991) Atmospheric transport of iron and its deposition in the ocean. *Limnol. Oceanogr.* 36:1715–1726.
- Faculty of Fisheries, Hokkaido University (1956–1995) Data record of oceanographic observations and exploratory fishing, Nos 1–37.
- Falkowski, P.G., and Wilson, C. (1992) Phytoplankton productivity in the North Pacific ocean since 1900 and implications for absorption of anthropogenic CO<sub>2</sub>. *Nature* 358:741–743.
- Favorite, F., Dodimead, A.J., and Nasu, N. (1976) Oceanography of the subarctic Pacific region, 1960–71. *INPFC Bull.* 33:1–48.
- Francis, R.C., and Hare, S.R. (1994) Decadal-scale regime shifts in the large marine ecosystems of the North-east Pacific: a case for historical science. *Fish. Oceanogr.* 3:279–291.
- Frost, B.W. (1987) Grazing control of phytoplankton stock in the open subarctic Pacific ocean: a model assessing the role of mesozooplankton, particularly the large calanoid copepods *Neocalanus* spp. *Mar. Ecol. Prog. Ser.* 39:49–68.
- Fulton, J.D. (1983) Seasonal and annual variations of net zooplankton at Ocean Station P, 1956–1980. *Canadian Data Rep. Fish. Aquat. Sci.* 374:1–65.
- Hanawa, K. (1995) Southward penetration of the Oyashio water system and the winter time condition of mid latitude west-erlies over the North Pacific. *Bull. Hokkaido Natl. Fish. Res. Inst.* 59:103–120.
- Ishida, Y. (1992) Salmon research and carrying capacity in the North Pacific. *Fisheries Res.* 11:48–55. (In Japanese.)
- Japan Meteorological Agency (1989) Abnormal Weather Report '89. 146–149. (In Japanese)
- Japan Meteorological Agency (1994a) Ocean surface fluxes in the North Pacific. 1–40. (In Japanese.)
- Japan Meteorological Agency (1994b) Abnormal Weather Report '94. 4–5. (In Japanese.)
- Japan Meteorological Agency (1994c) Ten-day mean 500 hPa high and anomaly charts for the northern hemisphere (1951–1992). (In Japanese.)
- Kawamiya, M., Kishi, M.J., Yamanaka, Y., and Sugino-hara, N. (1995) An ecological-physical coupled model applied to station Papa. *J. Oceanogr.* 51:635–664.
- van Loon, H., and Labitzke, K. (1988) Association between the 11-year solar cycle, the QBO, and the atmosphere. Part 2: Surface and 700 mb in the northern hemisphere in winter. *J. Climate* 1: 905–920.
- Miller, C.B., Frost, B.W., Batchelder, H.P., Clemons, M.J., and Conway, R.E. (1984) Life histories of large, grazing copepods in a subarctic ocean gyre: *Neocalanus plumchrus*, *Neocalanus cristatus* and *Eucalanus bungii* in the Northeast Pacific. *Prog. Oceanogr.* 13:201–243.
- Miller, C.B., Frost, B.W., Wheeler, P.A., Landry, M.R., Welschmeyer, N., and Powell, T.M. (1991) Ecological dynamics in the subarctic Pacific, a possibly iron-limited ecosystem. *Limnol. Oceanogr.* 36:1600–1615.
- Nagata, H. (1996) Relationship between chlorophyll-a concentration and water transparency in the seas adjacent to Japan. *Bull. Japan Sea Natl. Fish. Res. Inst.* 40:25–43.

# West-east comparison of seasonal variation in phytoplankton biomass in the subarctic North Pacific Ocean.

K. Tadokoro<sup>1</sup> and T. Sugimoto<sup>2</sup>

1: National Research Institute of Far Sea Fisheries, 5-7-1 Orido  
Shimizushi Shizuoka 424 Japan. E-mail, [denden@ss.enyو.affrc.go.jp](mailto:denden@ss.enyو.affrc.go.jp)

2: Ocean Research Institute, University of Tokyo  
1-15-1 Minamidai Nakano Tokyo, 164 Japan. E-mail, [sugimoto@ori.u-tokyo.ac.jp](mailto:sugimoto@ori.u-tokyo.ac.jp)

## Abstract

To make clear the limiting factor for the biological processes in the subarctic North Pacific, we compared seasonal variations in physical and biological processes in the Oyashio and Western North Pacific Ocean. Oceanographic data in the Oyashio water were analyzed by using "the results of oceanographic observations" No.6-85 (Japan Meteorological Agency, 1949-1994). Meteorological data were furnished by Japan Meteorological Agency (1994).

Chl-a concentration of the eastern North Pacific Ocean is generally low in the four seasons (MacAllister, 1969; Parsons and Lalli 1988). In contrast, the Oyashio water shows prominent Chl-a concentration in spring season (April-May) due to diatom. In the western subarctic Pacific, timing of seasonal pycnocline formation in April was earlier than in the eastern subarctic by about one month. In the Oyashio water, the earlier timing of spring blooming was coincident with the earlier start of seasonal halocline formation.

## Introduction

In Gulf of Alaska, Phytoplankton biomass does not show considerable seasonality during year (McAllister, 1969). Nitrate concentration in the upper layers does not show seasonality (Anderson *et al.*, 1969). So, it is considered that the macro-nutrients does not limit for the primarily productivity in Gulf Alaska. In last decade, the two hypothesis were suggested and progressed for the phytoplankton none seasonality in Gulf of Alaska. One is the grazing effect of micro-zooplankton (Miller & SUPER Group 1988), other one is the lack of micro-nutrients (Martin & Fitzwater, 1988).

The Oyashio is also important part of the subarctic Pacific circulation. In spite of extensive and long term survey have carried out, there was few study on phytoplankton seasonality in the Oyashio water. Therefore we investigated the phytoplankton seasonality in the Oyashio water and limiting factor for the primarily production in the subarctic North Pacific comparing the Oyashio and Gulf of Alaska.

## Materials and Methods

Two data sets which were "The results of oceanographical observations" No. 6-85. (1949-94) and "Ocean surface fluxes in the North Pacific" (1994) published by Japan Meteorological Agency were used for this study. We analysis the data on Chl-a, plankton cell number, nutrients, transparency depth, temperature, and salinity from the first data set. Also, we analyze the second data set of the SST, wind speed, and insolation. The analyzed area was 36-56°N, 155°W, and Pacific side coastal line of Japan and 141°W (Fig. 1a). We used data only collected at stations belong to the Oyashio water in this area. Although, subarctic water including the Oyashio water is classified as the surface salinity lower than 34.0 psu isohaline in the North Pacific Ocean (Dodimead *et al.* 1963), The

Therefore, it is considered that formation of the seasonal pycnocline triggered the phytoplankton blooming in spring, and exhaustion of the nutrients led to the decreasing of phytoplankton biomass in early summer.

#### ***West-east Comparison of phytoplankton biomass***

The Oyashio water shows large seasonal variation in Chl-a concentration, whereas the seasonal variation is quite small at St. P (Fig. 8; Mcallister, 1969), in spite of the both water belong to the same subarctic circulation. It is considered that the differences in physical environment for primary production or grazing pressure by zooplankton induce to the differences in Chl-a concentration and its seasonality.

Although, nitrate is exhausted from June to September in the Oyashio water (Fig. 9a), it does not change much at St. P during the year (Anderson *et al.*, 1969). So, nitrate may not limit primary production at St. P. Furthermore, sea surface temperature at St. P remains the higher values during spring (Fig. 9b), which may cause smaller amplitude of seasonal variation. Timing of formation of the seasonal pycnocline determines the timing of phytoplankton growth. Although, seasonal pycnocline formed during April in the Oyashio water, at St. P, seasonal pycnocline formed in May delayed by one month (Fig. 9d).

Comparing zooplankton biomass, it is considered that the potential grazing pressure on macro-zooplankton in the Oyashio water is higher than at St. P (Fig. 10), but the delay makes its efficiency low.

### **Discussion**

#### ***Start for seasonal pycnocline formation***

Seasonal pycnocline (halocline) formed during April in the Oyashio due to decrease of the sea surface salinity. It was reported that the western subarctic Pacific has higher precipitation in winter and higher evaporation in summer (Jacobs, 1951). In the eastern subarctic, however, precipitation is higher than evaporation during the whole year (Jacobs, 1951). So, there is possibility that diluting the surface water by precipitation is trigger of the seasonal pycnocline formation.

The effect of horizontal advection is another possibility for a cause of the seasonal pycnocline formation in the Oyashio water. Horizontal advection from the northern part of the Pacific and Okhotsk sea were enhanced in April. The water which have diluted water may intrude into the observation area and may be cause of seasonal pycnocline formation.

We considered that the delay of seasonal pycnocline formation led to the none seasonality of phytoplankton at St. P. Calanoid copepods, *Neocalanus* spp. dominated in macro-zooplankton community in west and east subarctic Pacific (Omori, 1965). The copepods have a generation cycle by one year, and migrates into upper layer from February to April, and heavily fed on the phytoplankton on May. Zooplankton had similar seasonality in the both water. Although, substantial feeding pressure may be higher in the Oyashio water than in St. P, delaying the phytoplankton blooming at St. P, phytoplankton may match the considerable copepods feeding. :

#### ***Phytoplankton composition***

Another possibility were also considered. In the Oyashio water, diatom was dominant phytoplankton, and increase of diatom cell number led to the spring blooming. Productivity of diatom for irradiance condition is more sensitive than dinoflagellata. So, the timing of diatom cell increase and a peak is earlier than dinoflagellata. It is reported that the diatom is dominant phytoplankton in Gulf of Alaska (Odate, 1996) same as the Oyashio water. But, size distribution of west and east waters were somewhat different. Pico (<2 $\mu$ m) sized phytoplankton dominated in Gulf



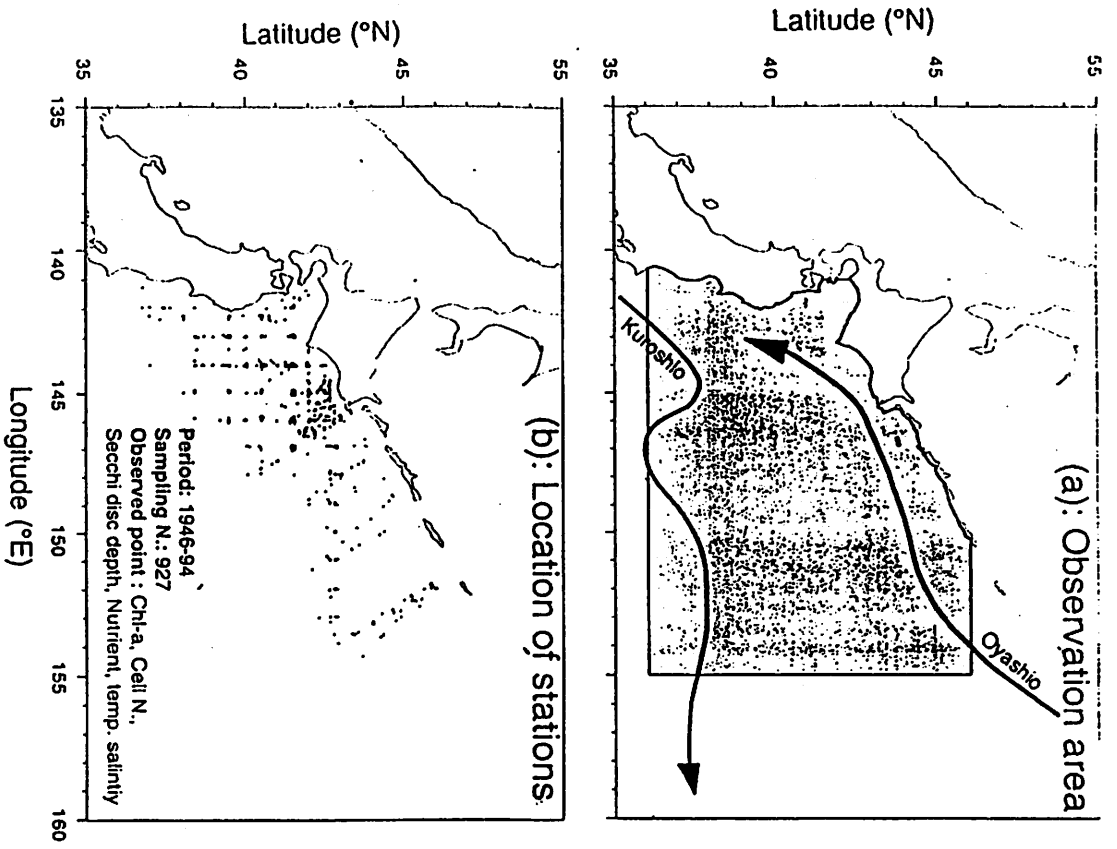


Fig. 1 Observation area and location of stations

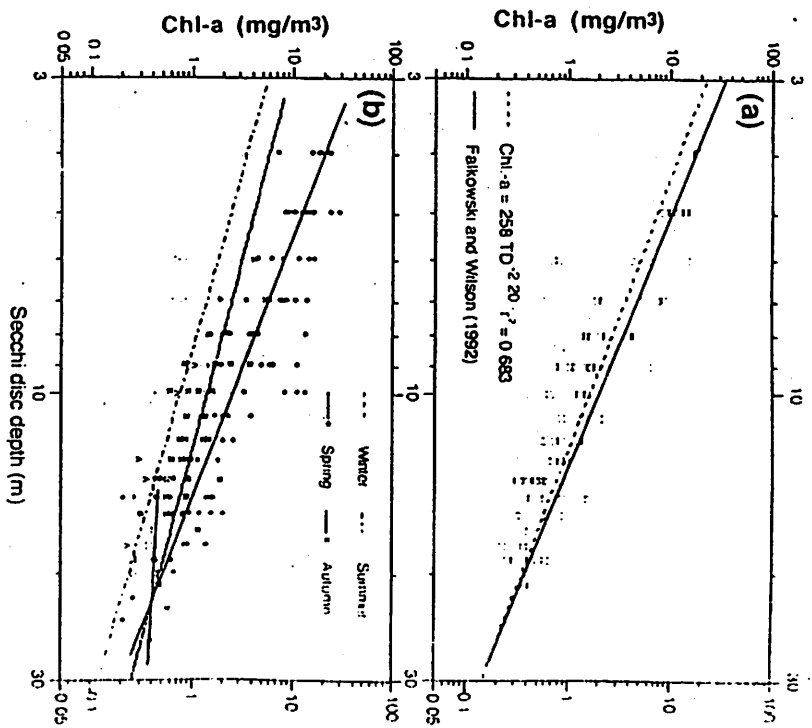


Fig. 2 (a): Solid line was calculated from the equation (1), and the dashed line was calculated from the best fit equation found by the annual relationship between transparency and chlorophyll-a. (b): Seasonal relationship between transparency and chlorophyll-a concentration. Winter: February, Chl-a = TD<sup>-0.414</sup>,  $r^2=0.026$ . Spring: March, April and May, Chl-a = 55 · TD<sup>-2.33</sup>,  $r^2=0.807$ . Summer: June, July, and August, Chl-a = 38 · TD<sup>-1.65</sup>,  $r^2=0.521$ . Autumn: September, October, and November, Chl-a = 52 · TD<sup>-1.57</sup>,  $r^2=0.563$

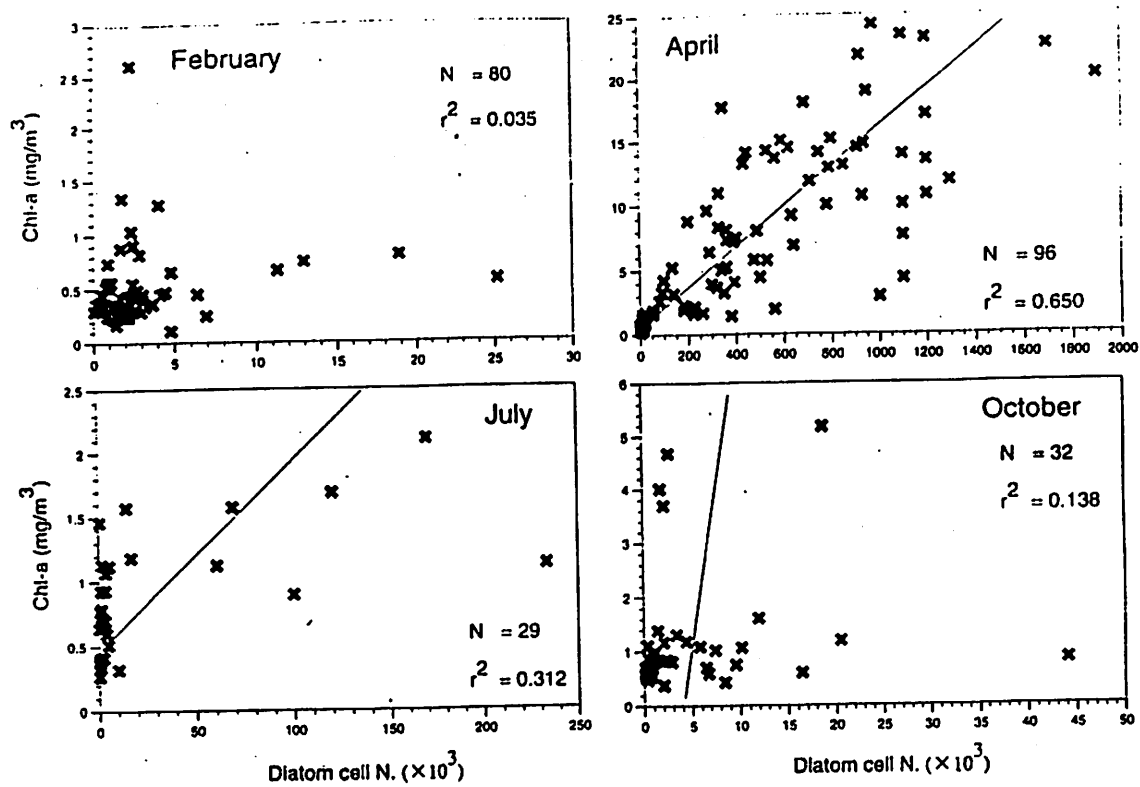


Fig. 5 The monthly relationship between Chl-a (mg/m<sup>3</sup>) and diatom cell N. at sea surface.

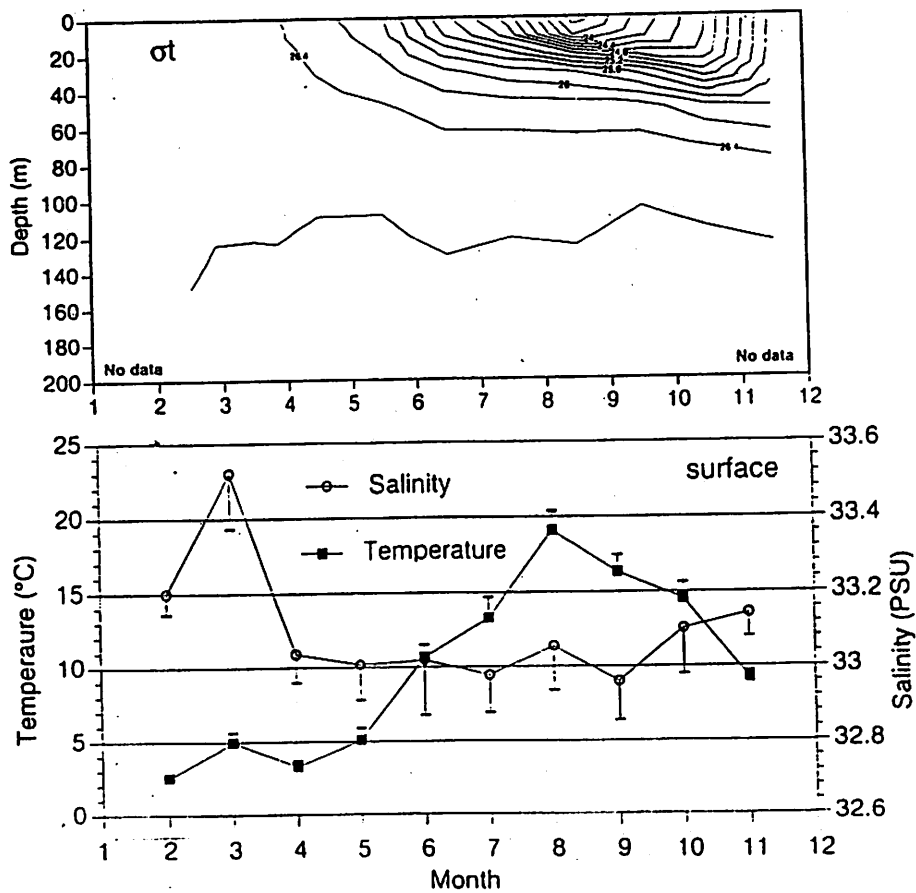
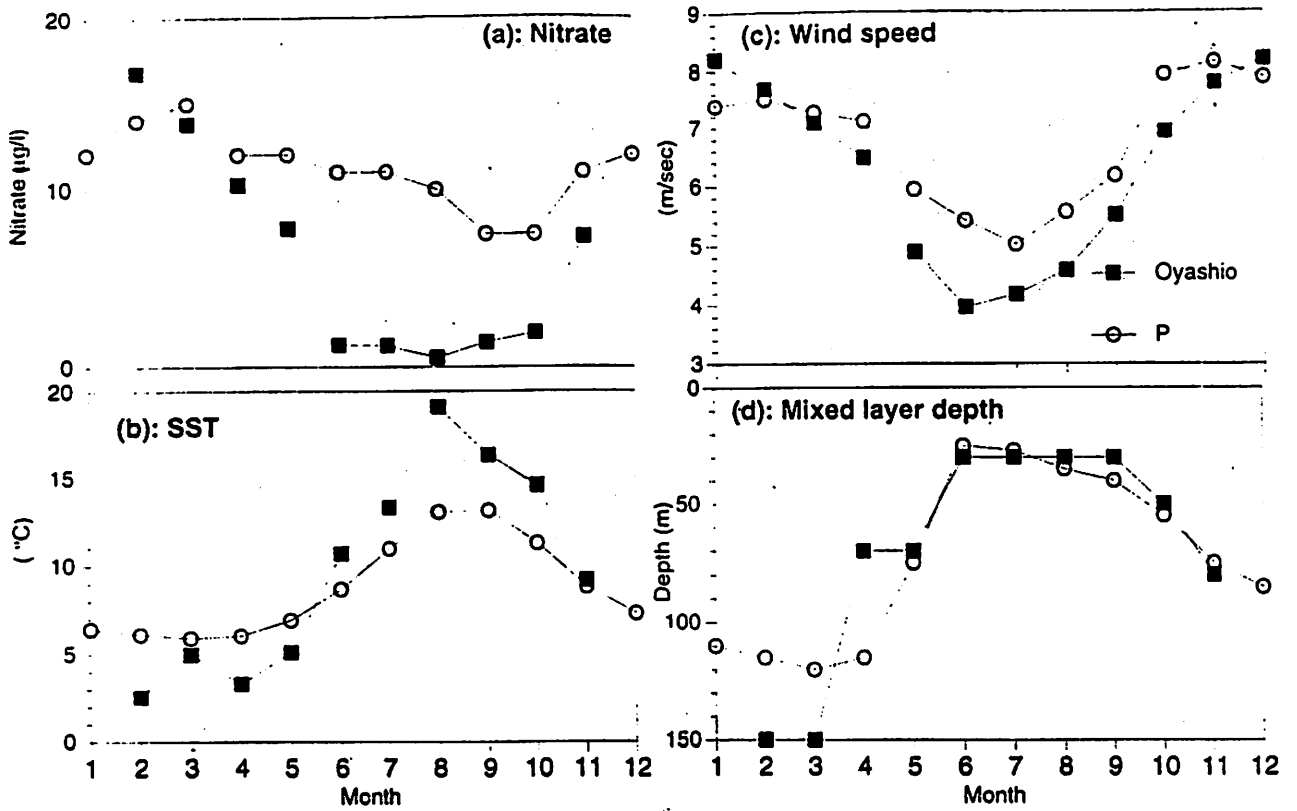
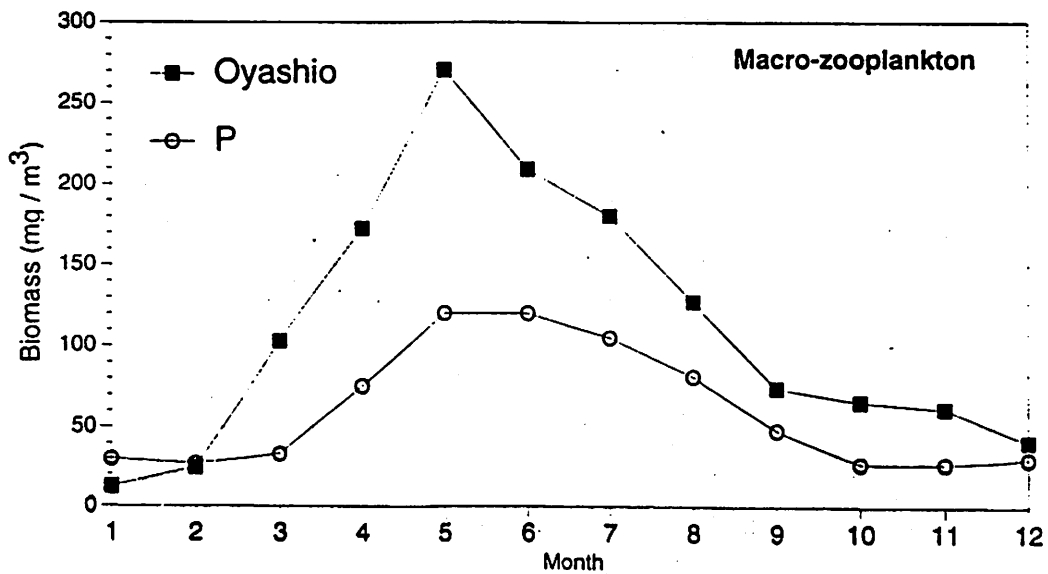


Fig. 6 Seasonal variation of  $\sigma_t$ , SST, and SSS in Oyashio region



**Fig. 9** Comparison of the environmental factor between Oyashio and ST. Papa. Nitrate, and Mixed layer depth in ST. Papa, is referred from Anderson et al. (1969), and Parsons and Lalli (1988), respectively.



**Fig. 10** Comparison of the seasonal variation in macro-zooplankton biomass between Oyashio and ST. Papa. Data on Oyashio and St. Papa are referred from Odate (1994) and Parsons and Lalli (1988), respectively.

Life cycles of *Neocalanus flemingeri* and *N. plumchrus* (Calanoida, Copepoda) in the western subarctic Pacific

Atsushi Tsuda, Hiroaki Saito and Hiromi Kasai  
Hokkaido National Fisheries Research Institute  
116 Katsurakoi, Kushiro, Hokkaido 085, Japan  
e-mail tsuda@hnf.affrc.go.jp

**Abstract**

Life cycles of large suspension-feeding copepods were investigated at the western subarctic gyre (Oyashio area). Two populations were recognized in *N. flemingeri* by the body size, life cycle and timing of ontogenetic migration. Small forms (same size as original description; ca 3.5 mm in prosome length at adult female) have one-year life cycle and occurred at surface between January and June. Large forms (3.9-5.2mm in prosome length at adult female) have two-years life cycle with winter dormancy at C4 and adult female. The young copepodites of the large forms occur at the surface water later than the small forms, then grow to C4 with full deposition of lipid. The next year, the C4s start grazing from January, and sink to deep layer at the same timing as the small forms. The life cycle of *N. plumchrus* was identical to original description by Miller et al. (1989), but the surface occurrence was later in season than eastern gyre. Temporal partitioning of the surface habitat utilization was clearly established between *N. plumchrus* and small forms of *N. flemingeri*, but overlap was observed between *N. plumchrus* and the large forms of *N. flemingeri*. Another difference in life cycle strategy among the two species of copepods was lipid deposition.. *Neocalanus plumchrus* showed almost no lipid deposition until C5, in the contrast, both forms of *N. flemingeri* started lipid deposition as early as C1.

## Introduction

*Neocalanus flemingeri* was described by Miller (1988), and the life histories of the species and sibling species (*N. plumchrus*) were re-examined by Miller and Clemons (1988). These works were mainly based on the samples collected in the western subarctic gyre of the North Pacific. The goal of the present study is comparison of the life histories of the two copepods between the eastern and western subarctic gyre of the North Pacific.

## Materials and Methods

### Samplings

Samplings were carried out at the stations roughly located first and second branches of Oyashio current (Fig. 1) by *FRV Hokkou Maru* and *Tankai Maru*, Hokkaido National Fisheries Research Institute, 6 to 10 times a year from July 1996. The samplings are still going. Copepods were collected oblique tows with a bongo net (mouth opening 70 cm x 2, mesh opening 330  $\mu$ m) from about 500 m-depth during night. The net was equipped with a depth meter and flow meters. Samples were preserved with neutralized formalin seawater.

### Identification

Miller (1988) suggested characters such as body color in unpreserved specimen, morphology of mandible gnathobase and length of maxilla for the identification of C5 of *Neocalanus flemingeri* from *N. plumchrus*. We applied width of mandible gnathobase and length of maxilla for younger copepodite stages. Two species were clearly separated by the 2 morphological characters until C2 (Fig. 2) The following analysis of the life history were mainly based on the data of C2 to C6.

## Results

### Two populations (or forms) of *N. flemingeri*

Bimodal distribution was observed in the length frequency distribution of *Neocalanus flemingeri* for each developmental stage (Fig. 3). Smaller individuals ranged same size range of that reported from eastern subarctic gyre, but larger individuals were same size range of *N. plumchrus* or even larger. The largest adult female was 5.1 mm in prosome length. In October sample, it was dormant season of *N. flemingeri*, adult female and C4 occupied the population (Fig. 4), and these C4 individuals were the large forms (Fig. 3). In January, both forms of C4 occurred but large forms showed higher lipid content than small forms. These results suggest that small forms have a year life cycle as the population of eastern subarctic gyre, large forms have 2-year life cycle as

the population of Japan Sea.

#### Life cycles of *Neocalanus flemingeri* and *N. plumchrus*

*Neocalanus flemingeri* showed the spawning peak at January (Fig. 6), which agrees with eastern population. Difference of spawning season was not clear between both forms of *N. flemingeri*. Although spawning peak of *N. flemingeri* was January, C4 and younger copepodites were observed at the same time (Fig 4). The C4 individuals were occupied by both large and small forms as mentioned earlier, and younger copepodites were occupied by small forms. This suggest that copepodites of small forms were brought from the early spawner, because small numbers of spawning females were observed in October sample. Although the population of *N. flemingeri* increased from January to May and C4 was observed from January, C5 appeared from April, which suggest that C4 has longer duration than other copepodite stages. Although younger copepodite of small forms appeared from January, those of large forms appeared later in season which was almost same timing of *N. plumchrus*. Dormant females and male appeared July and August in both forms, and many females with spermatophore were observed, indicating mating season of *N. flemingeri* is summer as eastern gyre.

Spawning females of *N. plumchrus* were collected except July (Fig. 6), spawning season was not clear, may be caused by shallow sampling. However, it should be certain that *N. plumchrus* have long spawning period from fall to spring as eastern gyre. Although very small number of younger copepodites were observed from March to May, the population much increased between May (5/12) and July (7/6) and increased population was dominated by C5 (Fig. 5), which strongly suggest that major part of the population appeared at the surface layer and grow to C5 within one and half months at most. Schematic illustration is presented in Fig. 8.

Then, replacement from *N. flemingeri* (small form) to *N. plumchrus* took place during June. It is about a month later in season than that of eastern subarctic gyre. Separation of season utilizing the surface layer was not clear between the large forms of *N. flemingeri* and *N. plumchrus*.

#### Lipid accumulation

Lipid accumulation pattern was different between *N. flemingeri* and *N. plumchrus*. *N. flemingeri* showed higher lipid content throughout a year (Fig. 7). This phenomenon was most obvious at abundant season for each species, *N. flemingeri* in May and *N. plumchrus* in July. Over 60 % of C3 and C4 of *N. flemingeri* were partly filled by lipid and even C2 showed lipid accumulation, on the contrary, younger copepodites (C2 to C4) of *N. plumchrus* rarely showed lipid accumulation (Fig. 7). Obvious lipid

accumulation by *N. plumchrus* was observed at only C5 and the accumulation progressed from early summer to winter.

## Discussion

Large form of *Neocalanus flemingeri* have 2-year life span which indicate that large forms suffer roughly 2 times higher predation mortality than small forms. However, the large forms have about 1.4 times larger in length (2.7 times in volume), then if we assume egg production is proportional to body volume, we may expect 2.7 times higher egg production rate in large forms than small forms. Disadvantage of long duration of life span in large forms may be compensated by high egg production rates. The younger copepodites appeared different season at the surface layer, but the both forms progressed C4 to C5 and then adult stage mainly May to July, and adult male were observed July and August. Therefore, genetic separation between both forms was not suggested from our sampling. Moreover, the origin of the large form of *N. flemingeri* is not clear at the present study.

*Neocalanus* species have been thought to be spring grazers. However, abundant species (in biomass), *N. plumchrus* migrate to the surface layer, graze and grow from June to August. In the studied area, spring bloom dominated by diatom take place March to May then phytoplankton community changes to non-diatom dominated community. Thus, *N. plumchrus* population must be supported by primary production in summer. It is also curious that *Neocalanus* species succession and phytoplankton community succession take place at the same timing. Moreover, the timing was a month later in season than eastern subarctic gyre. We can not propose the causes of the difference, but environmental factors such as food and temperature will be examined near future.

Difference in lipid accumulation strategy was observed between two species. *N. flemingeri* showed slow growth (several months to C5) with lipid accumulation, and *N. plumchrus* showed fast growth (within 1.5 month) without lipid accumulation. *N. flemingeri* grow winter to spring, in which period primary production is generally low but some time high production occur (spring bloom) by wind and radiation induced water column stratification. Therefore, *N. flemingeri* can meet good food environment some time but must stand tough condition for unpredictable period. Then, a pessimistic strategy of *N. flemingeri*, small investment for feeding appendages (maxilla), slow growth with lipid accumulation should be adaptive for spring weather condition. In contrast, phytoplankton are small size compared with spring but high and constant primary production can be expected in summer. Then, an optimistic strategy of *N.*

*plumchrus*, heavy investment for feeding appendage, fast growth without lipid accumulation should be adaptive for summer condition.

#### References

- Miller, C.B. (1998) *Neocalanus flemingeri*, A new species of calanidae (Copepoda: Calanoida) from the subarctic Pacific Ocean, with a comparative redescription of *Neocalanus plumchrus* (Marukawa) 1921. Prog. Oceanogr., 20: 223-274
- Miller, C.B. and M.J. Clemons (1988) Revised life history analysis for large grazing copepods in the subarctic Pacific Ocean. Prog. Oceanogr., 20: 293-313



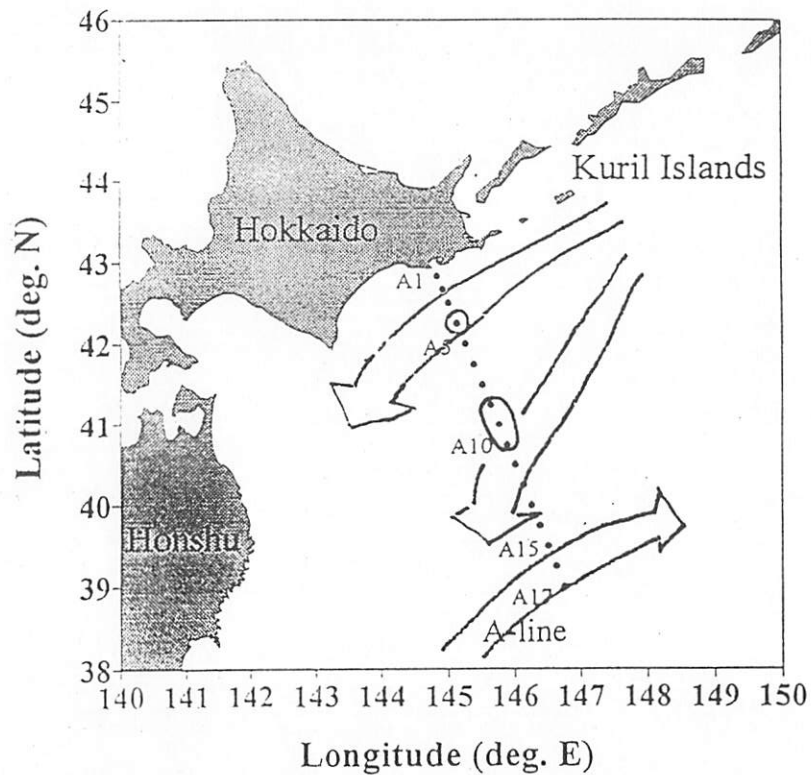


Fig. Sampling location (red circles) and schematic flow pattern of Oyashio

①

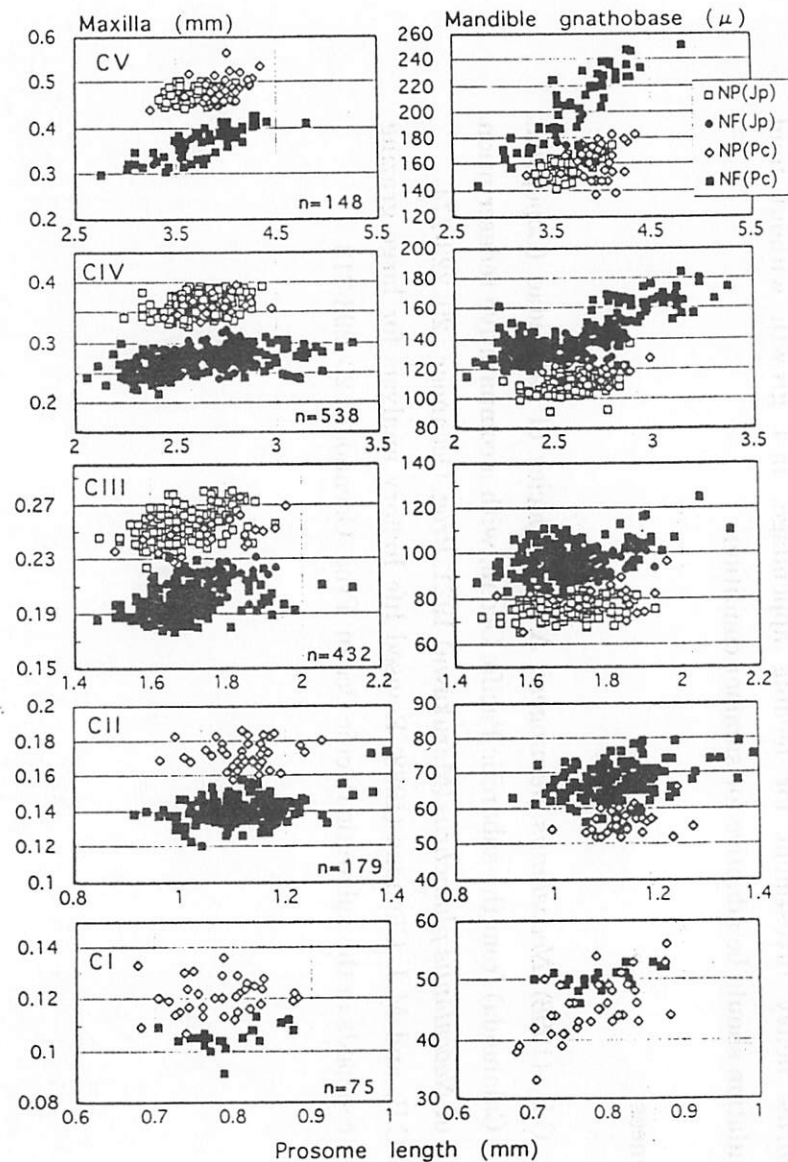


Fig. Plots of prosome length versus maxilla length and mandible gnathobase width of *Neocalanus plumchris* (open symbols) and *N. flemingeri* (filled symbols). Samples were collected from the western North Pacific and Japan Sea

②

*Neocalanus flemingeri*

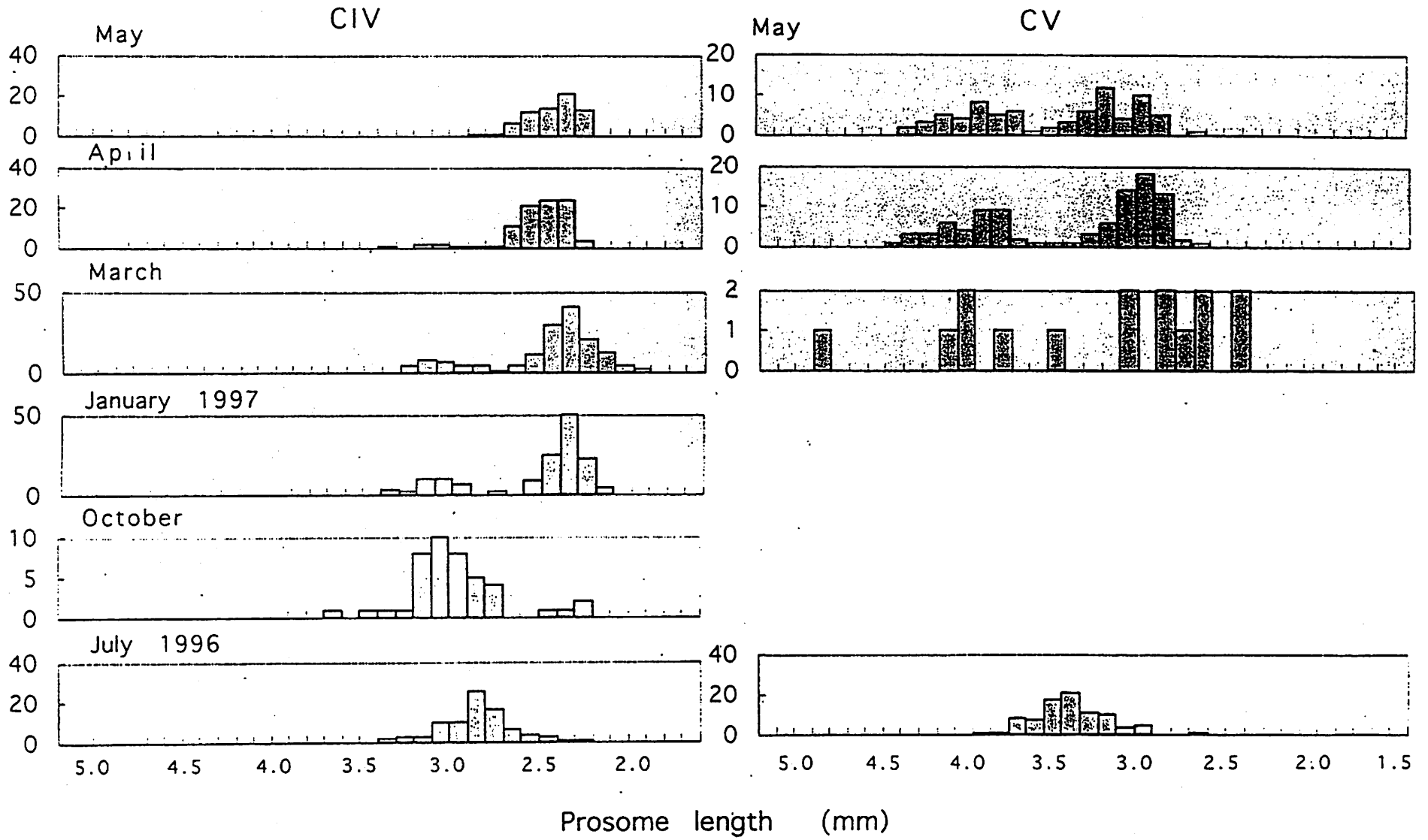


Fig. *Neocalanus flemingeri*. Prosome length distribution of C4 and C5

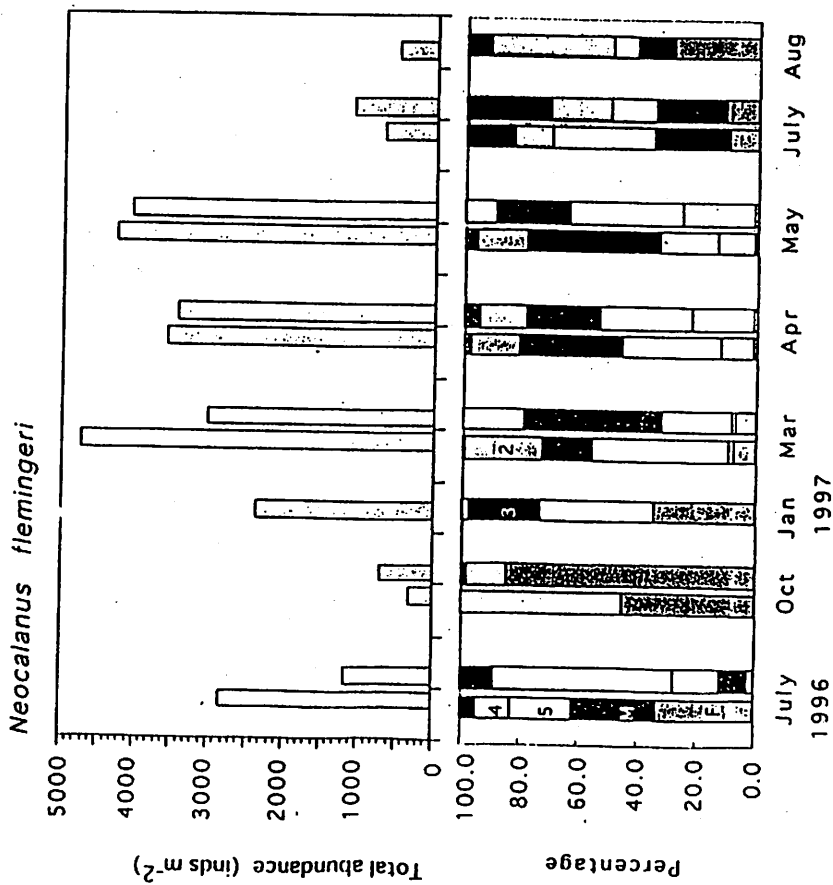


Fig. *Neocalanus flemingeri*. Numerical abundance (upper) and stage composition (lower) from 1996 July to 1997 August

④

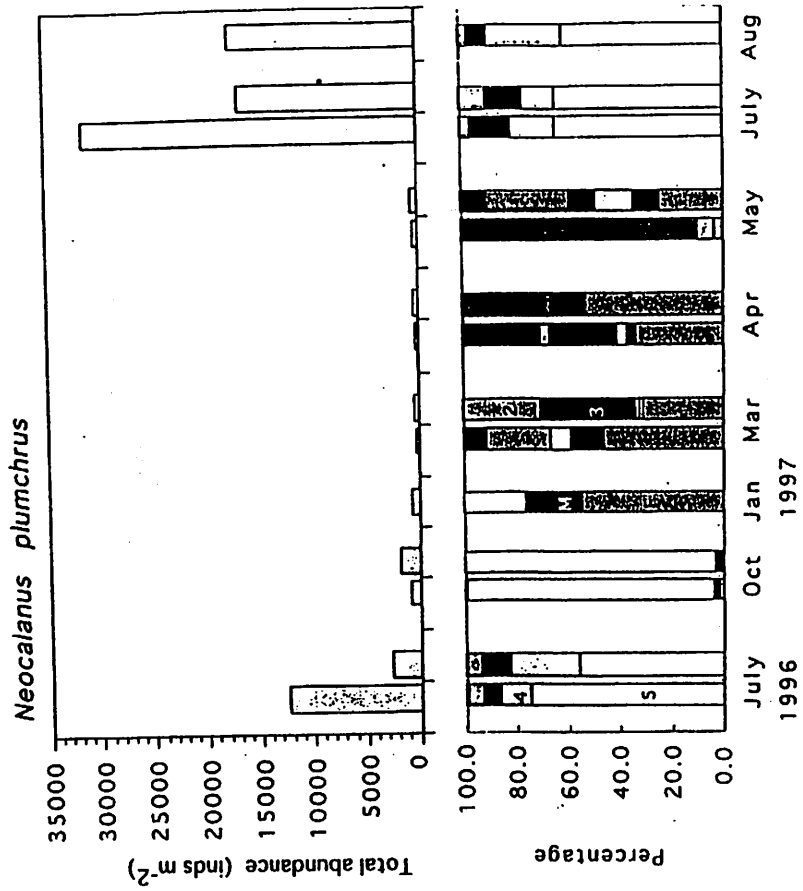


Fig. *Neocalanus plumchrus*. Numerical abundance (upper) and stage composition (lower) from 1996 July to 1997 August

⑤

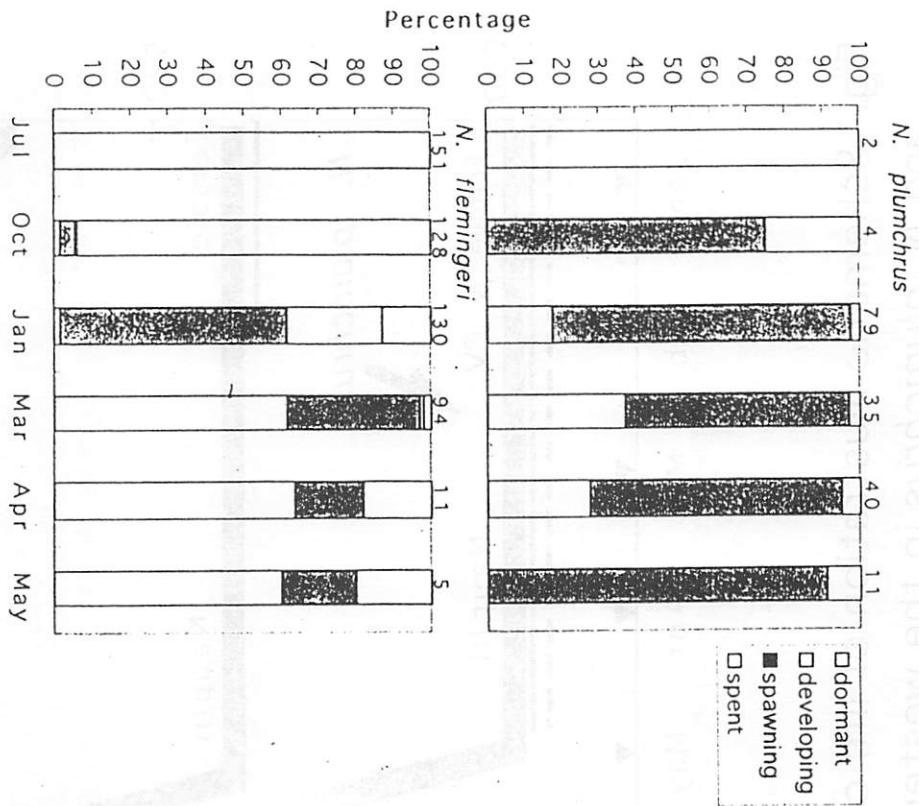


Fig. Time series of cumulative percentages of *Neocalanus flemingeri* and *N. plumchrus* in the 4 ovarian stages

(6)

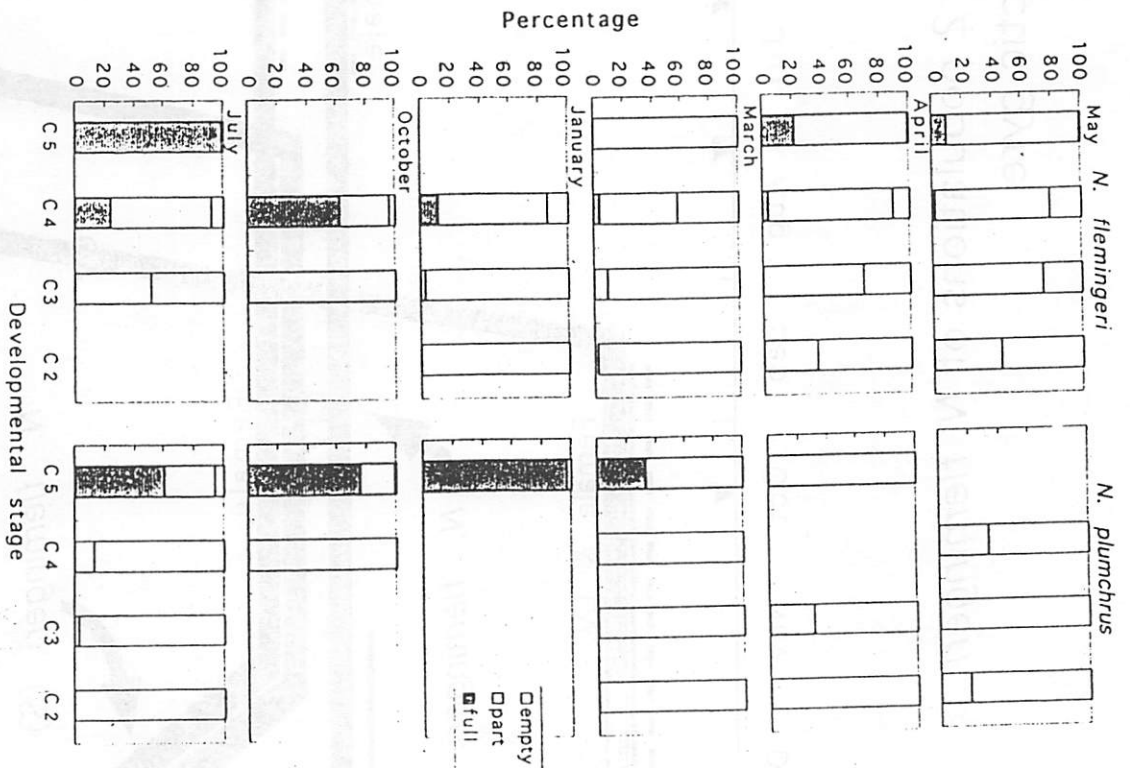


Fig. Lipid accumulations by copepodite stages of *Neocalanus plumchrus* and *N. flemingeri*; lipid accumulation was categorized 3 level, full, partly, empty

(7)

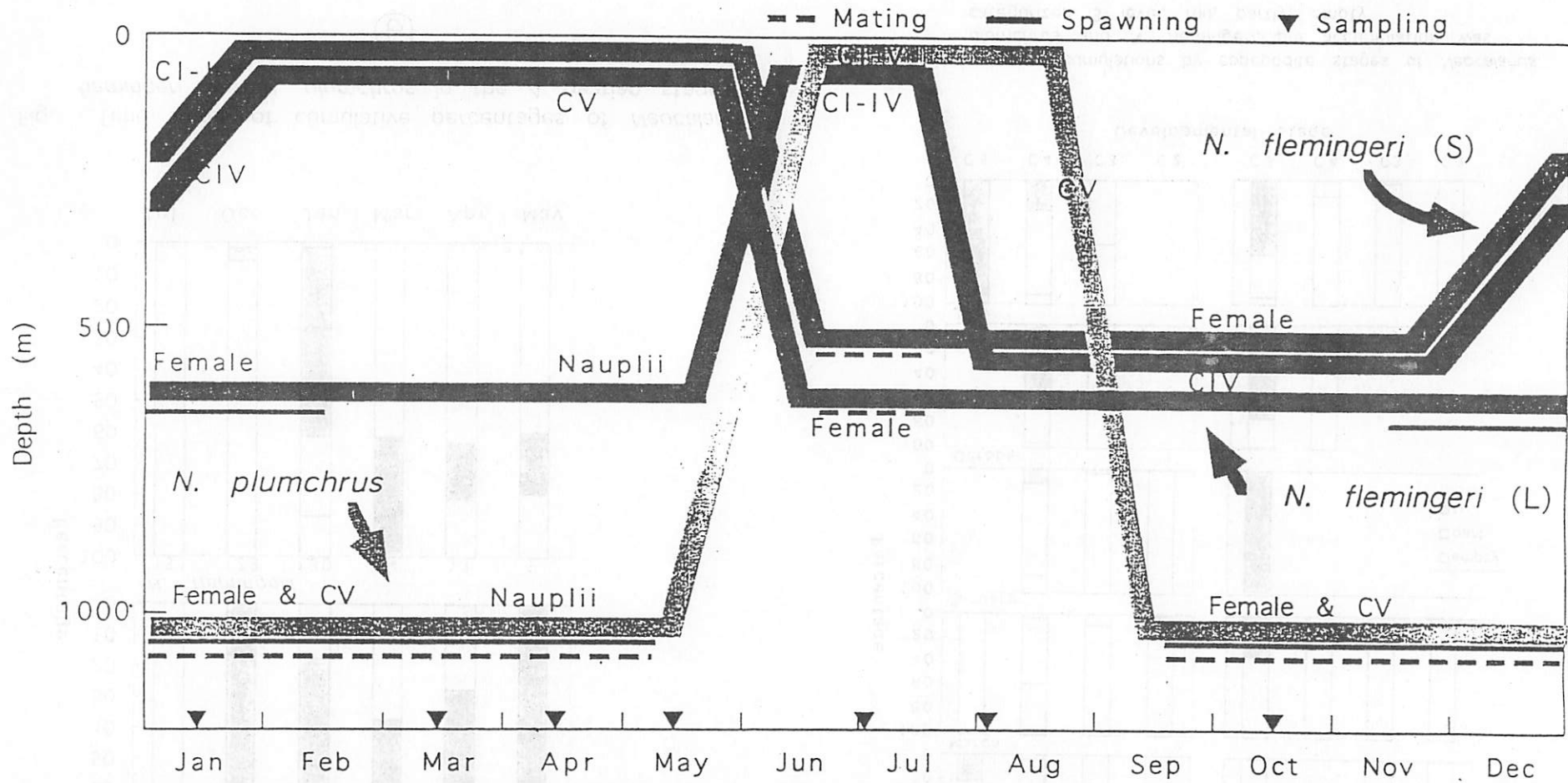


Fig. Schematic illustration of life cycles of 2 populations of *N. flemingeri* and *N. plumchrus* in the western subarctic gyre